31st iapri

MEMBERS' CONFERENCE

Mumbai | May 22-25, 2023

RESPONSIBLE PACKAGING FOR A BETTER FUTURE

Conference Proceedings

The 31st IAPRI
World Conference on Packaging

EDITED BY Prof. Prasad Balan Iyer
Dr. Vivek Sudhir Parab

HOSTED BY

SIES
RISE WITH EDUCATION
School of Packaging
Packaging Technology Centre

First online edition, 25th May, 2023 .

ISBN (e-book) 978-81-963392-0-3

SIES School of Packaging - Packaging Technology Centre

Plot No. D388, MIDC TTC Industrial Area, Kukshet Village,

Next to IOCL Vashi Terminal, Navi Mumbai – 400 705.

Email: iaprimumbai@sies.edu.in, sopdirector@sies.edu.in

Website: www.siessop.edu.in

CONTENTS

31st IAPRI Member Conference on Packaging

CONFERENCE PROGRAMME

May 22-25, 2023

Monday 22nd May — Hotel Four Points by Sheraton, Navi Mumbai

9:00 – 12:00	IAPRI Board Meeting	Unison 1
12:00 – 13:00	Lunch Break	Pre-function Area
13:00 – 14:00	IAPRI Communities of Practice - University Education CoP	Unison 3 **Led by**: Edward A. Church
14:00 – 15:00	IAPRI Communities of Practice - Distribution Packaging CoP	Unison 1 **Led by**: Edward A. Church
15:00 – 16:00	IAPRI Communities of Practice - Sustainable Packaging CoP	Unison 3 **Chair:** Carlos Diaz-Acosta
16:00 – 17:00	IAPRI Communities of Practice - Packaging & Consumers CoP and Active & Intelligent CoP	Unison 1 **Chair**: Selcuk Yildirim
18:00 – 20:00	Registration	Pre-function Area
19:00 – 22:00	Welcome reception	Unison Hall

Tuesday 23rd May — Hotel Four Points by Sheraton, Navi Mumbai

09:00 – 09:30	Registration	Pre-function Area
09:30 – 11:00	Conference Opening / Inauguration Chief Guest *Mr. Piyush Goyal,* *Minister of Commerce & Industry, Consumer Affairs &* *Food & Public Distribution and Textiles* *Government of India*	Unison Hall
11.00 – 11:30	Beverage Break	Pre-function Area
11:30 – 12:00	Keynote Lecture - 1 "Coup d'oeil - The Indian Packaging & Printing Industry" *Ramu Ramanathan, Editor,* *PrintWeek India & WhatPackaging?, India*	Unison Hall
12:00 – 12:30	Keynote Lecture - 2 "EU Packaging Regulations – forward regulatory insight update" *Diana Schiffer, Packaging Regulatory Advisor,* *The LCA Centre, Netherlands*	Unison Hall

12:30 – 13:30	Lunch break	Pre-function Area
13:30 – 15:00	**Oral Presentations** **Session 01 - Distribution Packaging** **Session 02 - Packaging sustainability**	**Chair** **Session 01 -** Jay Singh **Session 02 -** Eric Martine
13.30 – 13:55	**1.1** Effect of Wooden Pallets Characteristics on the Compression Strength of Palletized Plastic Pails with Double Overhang. *Mary Paz Alvarez Valverde - Virginia Tech - Center for Packaging and Unit Load Design/United States* **2.1** Life cycle assessment of multiple dispensing systems used for cosmetic product packaging. *Shambhavi Rathore - Toronto Metropolitan University /Canada*	Session Room **1.1** Unison 1 **2.1** Unison 3
14:00 – 14:25	**1.2** Predicting the Effect of Pallet Overhang on the Box Compression Strength. *Saewhan Kim - Virginia Tech - Center for Packaging and Unit Load Design/United States* **2.2** Microfibrillated cellulose as reinforcement in PLA-based packaging materials: Dry or wet addition in extrusion processes. *Soraya Sánchez - ITENE/Spain*	Session Room **1.2** Unison 1 **2.2** Unison 3
14:30 – 14:55	**1.3** Evaluation of Maximum Pallet Deflection Under Dynamic Forklift Handling Conditions. *Seth Capizzi - Virginia Tech - Center for Packaging and Unit Load Design/United States*	**1.3** Unison 1
15:00 – 15.15	Beverage Break	Pre-function Area
15:15 – 17:15	**Oral Presentations** **Session 03** – **Packaging Materials** **Session 04 – Active & Intelligent Packaging**	**Chair** **Session 03 -** Yves Wyser **Session 04 -** Selcuk Yildirim
15:15 – 15:40	**3.1** Effect of food simulants on CuONP stability in bionanocomposite food packaging film. *Nattinee Bumbudsanpharoke - Kasetsart University/Thailand* **4.1** Evaluation of the Antimicrobial Activity of Sodium Alginate Films Integrated with Cinnamon Essential Oil and Citric Acid. *Nadine Rüegg - Zurich University of Applied Sciences/Switzerland*	Session Room **3.1** Unison 1 **4.1** Unison 3
15:45 – 16:10	**3.2** Seal materials in flexible plastic food packaging: A review. *Bram Bamps - Uhasselt/Belgium* **4.2** Barrier Properties of PLA/PBAT Films Incorporating Titanium Dioxide. *Uruchaya Sonchaeng - Kasetsart University/Thailand*	Session Room **3.2** Unison 1 **4.2** Unison 3
16:15 – 16:40	**3 3** Effect of Consecutive Extrusion Process on the Properties of Recycled Polyethylene Terephthalate (rPET). *Busarin Chongcharoenyanon - Kasetsart University/Thailand*	Session Room **3.3** Unison 1 **4.3** Unison 3

	4.3 Ethylene Colorimetric Ink for Monitoring Fruit Ripening. *Jesus Palenzuela - ITENE/Spain*	
16:45 – 17:10	**4.4** Mechanical properties of PBAT/TPS nanocomposites under UV exposure. *Thitiporn Kaewpetch - Kasetsart University/Thailand*	Session Room **4.4** Unison 3
19:00 – 22:00	Official Dinner with Musical Performance	Skygrill – Open Terrace

Wednesday 24th May — Hotel Four Points by Sheraton, Navi Mumbai

08.30 – 09.00	Registration	Pre-function Area
08.30 - 09.00	Keynote Lecture - 3 "Latest research & developments in the area of food packaging" *Dr. Kirtiraj Gaikwad, Asst. Professor (Packaging Tech), Indian Institute of Technology, Roorkee, India*	Unison Hall
09.00 - 09.30	Keynote Lecture - 4 "Innovation at Scale: Regenerative Packaging for a cleaner Planet" *Dr. Ramjee Subramanian, Business Head, Pakka Impact Ltd., Bengaluru, India*	Unison Hall
09.30 - 10.00	Presentation by Student Scholarship Award Winner *Marije Linders from the University of Twente, The Netherlands*	Unison Hall
10.00 - 10.30	**Poster Presentations**	Unison Hall
10.00 - 10.05	**Pitch 1** - Estimation of the degradation of strawberries during Rail transport from knowledge and experiences made on Roads trips by *Jean-Baptiste NOLOT and Philippe DELLOQUE - Universite de Reims Champagne-Ardenne/ France*	
10.05 - 10.10	**Pitch 2** - Understanding silver nanoparticle leaching behavior from active biobased nanocomposites by *Mieke Buntinx - Hasselt University - MPR&S Institute for Materials Research/Belgium*	
10.10 - 10.15	**Pitch 3** - Sustainable Development of Single-Use Paper Cups for Beverage Packaging in Thailand by *Supawadee Theerathammakorn - Sukhothai Thammathirat Open University/Thailand*	
10.15 - 10.20	**Pitch 4**- Release of Vanillin, trans-Cinnamaldehyde, and Citral from Poly(butylene succinate) Films Containing Lignin Nanoparticles by *Pathtamawadee Nuamduang - Kasetsart University/Thailand*	
10.20 - 10.25	**Pitch 5**- Novel Temperature-sensitive label based on thermochromic ink for hot food packaging and	

	serving applications by *Prachi Jain, Indian Institute of Technology Roorkee / India*	
10.25 - 10.30	**Pitch 6**- Natural pH sensors as a quality monitoring smart label for poultry packaging by *Akhila Konala, Indian Institute of Technology Roorkee / India*	
10.30 – 11.00	Beverage Break	Pre-function Area
11.00 – 12.30	**Oral Presentations** **Session 05** – **Distribution Packaging** **Session 06 – Packaging Materials**	**Chair** **Session 05 -** Damien Erre **Session 06 –** Carmen Sanchez
11.00 – 11.25	**5.1** Transport stresses in e-commerce logistics and its effects on corrugated board packaging. *Astrid Odeberg Glasenapp - RISE Bioeconomy/Sweden* **6.1** Biochar composites for sustainable thermal packaging applications. *Carlos Diaz-Acosta - Rochester Institute of Technology/United States*	Session Room **5.1** Unison 1 **6.1** Unison 3
11.30 – 11.55	**5.2** Optimal selection of the percentage of recycled material in plastic according to the risks of distribution cycle. *Marta Garrido García - ITENE/Spain* **6.2** Effect of wrapping parameters and transport constraints on stretch film properties for freight transport applications. *Elora Leguebe - Metropack/France*	Session Room **5.2** Unison 1 **6.2** Unison 3
12.00 – 12.25	**5.3** Understanding how vertical and multi-axial vibrations affects the load stability. *Manuel García-Romeu - Safe Load Testing Technologies/Spain* **6.3** Sugarcane as a source to produce paper in Mexico. Study to evaluate the feasibility for Mexican Industry. *Cristina Guzman - Universidad de Monterrey/Mexico*	Session Room **5.3** Unison 1 **6.3** Unison 3
12.30 – 13.30	Lunch Break	Pre-function Area
13.30 – 15.30	**Oral Presentations** **Session 07** – **Novel packaging** Packaging for hazardous & dangerous goods **(7.3, 7.4)** **Session 08 – Packaging sustainability** Active & Intelligent Packaging **(8.4)**	**Chair** **Session 07 –** Yves Wyser **Session 08 –** Cristina Guzmán
13.30 - 13.55	**7.1** Fluorescent markers for bioplastics from encapsulated algae chlorophyll. *Soraya Sánchez - ITENE/Spain* **8.1** The position of refill systems in the future of supermarkets. *Roland ten Klooster - University of Twente/ The Netherlands*	Session Room **7.1** Unison 1 **8.1** Unison 3

14.00 - 14.25	**7.2** Pilot-scale processing and functional properties of compostable thermoplastic gliadin/poly(ε-caprolactone) blend films. *Alejandro Aragón-Gutiérrez - ITENE/Spain* **8.2** Research after an innovative way to determine designs of squeeze bottles with the least leftovers. *Zoë Menting - University of Twente/The Netherlands*	Session Room **7.2** Unison 1 **8.2** Unison 3
14.30 - 14.55	**7.3** Improved criteria for evaluating impact targets in regulative drop tests of dangerous goods packagings. *Nikolaos Lengas - BAM Federal Institute for Materials Research and Testing/Germany* **8.3** A review of sustainable packaging trends globally and in India with changes in regulatory & consumer requirements. *Saurabh Narawade - SIES School of Packaging/India*	Session Room **7.3** Unison 1 **8.3** Unison 3
15.00 - 15.25	**7.4** How to measure the angle of repose of hazardous substances in the test centres for dangerous goods packagings. *Eva Schlick-Hasper - Federal Institute for Materials Research and Testing (BAM)/ Germany* **8.4** Centrifugal fiber spinning to fabricate polyhydroxyalkanoate/zinc oxide nanocomposite films: structure-property analysis. *Chris Vanheusden - Hasselt University - MPR&S/Belgium*	Session Room **7.4** Unison 1 **8.4** Unison 3
15.30 – 15.45	Beverage Break	Pre-function Area
15.45 – 17.15	**Oral Presentations** **Session 09** – **Logistics & Supply Chain** **Session 10 – Packaging machinery & systems** Packaging for Food & Agriculture **(10.2, 10.3)**	**Chair** **Session 07 –** Jay Singh **Session 08 –** Roland Klooster
15.45 - 16.10	**9.1** How grocery retailers can utilize learnings from meal kit delivery services to optimize their supply chain. *Jay Singh - Cal Poly State University, Industrial Tech. and Packaging/United States* **10.1** Developing a design method and tool for producing customizable forming shoulders. *Roland ten Klooster - University of Twente/ The Netherlands*	Session Room **9.1** Unison 1 **10.1** Unison 3
16.15 – 16.40	**9.2** Logistical Challenges to Deliver in the Last Mile for Consumer, Furniture, and Military including White Glove Services. *Kevin Smith and Paul Singh – Packaging Forensic Associates/United States* **10.2** Use of waxes and rubbers to create SUPD-compliant coated packaging. *Akansha Singh - VTT/Finland*	Session Room **9.2** Unison 1 **10.2** Unison 3
16.45 - 17.10	**10.3** Microperforated PBAT/PLA Film with Enhanced Gas Transmission Rate for Packaging of Fresh Produce. *Pichamon Sungdech - Kasetsart University/Thailand*	Session Room **10.3** Unison 3
19.00 – 22.00	Social Dinner with Cultural Show	Unison Hall

Thursday 25th May — Hotel Four Points by Sheraton, Navi Mumbai

09:00 – 11.00	**Oral Presentations** **Session 11** – **Distribution Packaging** Active & Intelligent Packaging **(11.4)** **Session 12 – Packaging sustainability**	**Chair** **Session 11 – Cristina Guzman** **Session 12 – Rafael Auras**
09.00 – 09.25	**11.1** High-speed camera analysis of load/pallet interface behavior in logistics unit submitted to impact. *Charles Tissandie - Institut Clément Ader Université de Toulouse/France* **12.1** New Sustainable Inks For The Packaging Printing Industries. *Jesus Palenzuela - ITENE/Spain*	Session Room **11.1** Unison 1 **12.1** Unison 3
09.30 – 09.55	**11.2** Statistical study on acceleration value data recorded on roundabout, curve, during a road trip to classify then in funct. *Baptiste Boutrige - Metropack/France* **12.2** Recycled Polymers: Improving recycled high density polyethylene properties through reactive extrusion. *Alejandro Aragón-Gutiérrez - ITENE/Spain*	Session Room **11.2** Unison 1 **12.2** Unison 3
10.00 – 10.25	**11.3** Case studies for optimization and standardization of packaging references improving its environmental behaviour. *Marta Garrido García - ITENE/Spain* **12.3** A trend-based analysis of packaging material amounts per capita per day in The Netherlands. *Roland ten Klooster - University of Twente/The Netherlands*	Session Room **11.3** Unison 1 **12.3** Unison 3
10.30 – 10.55	**11.4** Shelf-life extension of fresh-cut pineapple by sodium alginate-based active edible coating with lemongrass essential oil. *Darylle Ortiz - DOST-Packaging Technology Division/Philippines* **12.4** Accelerating the biodegradation of poly(lactic acid) at mesophilic conditions by biostimulation. *Rafael Auras - Michigan State University, School of Packaging/ United States*	Session Room **11.4** Unison 1 **12.4** Unison 3
11.00 – 11.30	Beverage Break	Unison Hall
11.30 – 12.30	Conference Closure	
12.30 – 13.30	Lunch Break	Pre-function Area
13.30 – 14.30	IAPRI General Meeting	Unison Hall

SCIENTIFIC COMMITTEE

Alexander Bardenshtein	Danish Technological Institute	Denmark
Gregory Batt	Clemson University	USA
Laura Bix	Michigan State University	USA
Vanee Chonhenchob	Kasetsart University	Thailand
Silvia Dantas	CETEA	Brazil
Damien Erre	ESIReims	France
Changfeng Ge	Rochester Institute of Technology	USA
Cristina Guzmán	Universidad de Monterrey	Mexico
Daniel Hellström	Lund University	Sweden
Eric Martine	HEIG-VD	Switzerland
Vincent Rouillard	Victoria University	Australia
Susan Selke	Michigan State University	USA
David Shires	Department for Business, Energy and Industrial Strategy (BEIS)	UK
Jay Singh	Cal Poly State University	USA
Zhi-Wei Wang	Jinan University	China
Yves Wyser	Nestlé Research Centre	Switzerland
Renee Wever	Linköping University	Sweden
Selcuk Yildirim	ZHAW	Switzerland
Roland ten Klooster	University of Twente	Netherlands
Javier Zabaleta	ITENE	Spain
Frank Welle	Fraunhofer Institute for Process Engineering and Packaging	Germany
Maria Jose Galotto	University of Santiago de Chile	Chile
Eva Schlick-Hasper	BAM	Germany
Hiroaki Kitazawa	NARO	Japan

ORGANIZING COMMITTEE

PATRONS

Dr. V. Shankar

Mr. M. V. Ramnarayan

CHAIR

Prof. Prasad Balan Iyer

COMMITTEE

Mr. Suresh Kunjan

Prof. Sanghamitra Shahal

Ms. Manjula Gohil

Ms. Sandhya Satyaraj

Ms. Manisha Chaukekar

Mr. Durai B.

Mr. Prakash Singh

Ms. Siddhi Panchal

Mr. Prasad Deshmukh

Mr. S. Gurumurthy

Ms. Radha Palanikumar

Mr, S. Venkatraman

Mr. Vilas Nagane

Ms. Poornakala K.

CONFERENCE SECRETARY

Dr. Vivek Sudhir Parab

CONFERENCE PROCEEDINGS

KEYNOTE SPEAKERS

Dr. Kirtiraj Gaikwad	Latest research & developments in the area of food packaging
Mr. Ramu Ramanathan	Coup d'oeil - The Indian Packaging & Printing Industry
Ms. Diana Schiffer	EU Packaging Regulations – forward regulatory insight update
Dr. Ramjee Subramanian	Innovation at Scale: Regenerative Packaging for a cleaner Planet

Dr. Kirtiraj Gaikwad

Keynote Lecture on ***"Latest research & developments in the area of food packaging"***

Dr. Kirtiraj K. Gaikwad, PhD, is an Assistant Professor in the Packaging Technology Division, Department of Paper Technology, IIT Roorkee, India. He received his PhD in Packaging Technology from Yonsei University, Seoul, South Korea; MS in Packaging Technology from Michigan State University,

Lansing, USA, and B.Tech. in Food Technology from Dr. Panjabrao Deshmukh Agriculture University, India. He is a fellow of the Linnean Society of London, UK. Before joining IIT Roorkee, he worked as a postdoctoral fellow at Chemical Engg Department, Ecole Polytechnic de Montreal, Canada. He has mainly worked in the field of plastic packaging technology and biopolymers.

Dr. Gaikwad received several national and international awards, including a FSSAI Research Award; DST INSPIRE Faculty Award from DST Govt. of India; Young Scientist Award from the International Association for Food Protection (IAFP), USA; and A J Bank Research Award from the Society of Chemical Industries (SCI), London, UK. Dr. Gaikwad has published more than 75 research papers in SCI-indexed journals, four international patents, and he authored two books, with CRC press USA. He has successfully received high impact research projects valued more than 11 million Indian rupees from DST, SERB.

He is dynamically involved in teaching (graduate and doctorate students) and research, and he has proved himself as an active scientist in sustainable polymeric packaging. Presently he is guiding 8 PhD student in the area of Food Packaging

Mr. Ramu Ramanathan

Keynote Lecture on ***"Coup d'oeil - The Indian Packaging & Printing Industry"***

Ramu Ramanathan is editor of magazines, PrintWeek and WhatPackaging? Ramanathan has been associated with the print + packaging industry for 30 years. Like his hero Alois Senefelyder, he is also a playwright whose plays have performed in multiple languages in India and overseas.

Ramanathan has three books to his credit. 3, Sakina Manzil and Other Plays which is a collection of eight plays. And, two collections of poems, My Encounters with a Peacock and To Sit on A Stone - And Other Shorts. Currently, he is working on his fourth book which is based on theatre in Mumbai. In addition, he regularly pens columns for newspapers.

He has also co-edited Book Binding with Adhesives and Babri Masjid, 25 Years. He is most likely to be cheering for Fulham Football Club in his free time

Ms. Diana Schiffer

Keynote Lecture on ***"EU Packaging Regulations – forward regulatory insight update"***

With an education in environmental policy and environmental systems analysis at Wageningen University & Research (Netherlands) and food technology at the University of Technology in Munich (Germany), Ms. Diana Schiffer has a 2-year background working as packaging technologist and LCA practitioner at The LCA Centre (Netherlands). The LCA Centre focuses on forensic Life Cycle Assessment (LCA) of packaging systems, reverse engineering of packaging, packaging innovation, and (future) packaging legislation.

The regulatory landscape related to packaging is fast-changing and becomes increasingly complex. In her current role as Packaging Regulatory Advisor, it is Ms. Schiffer's mission to bring together (packaging) science, business realities and policy.

Dr. Ramjee Subramanian

Keynote Lecture on ***"Innovation at Scale: Regenerative Packaging for a cleaner Planet"***

Name: Dr. Ramjee Subramanian

Home Town: Tiruchirappalli**,** Tamil Nadu

With over 20 years of experience in the Paper, Materials & Packaging industry, Dr. Ramjee joined Pakka Impact in December 2022 as Business Head.

Dr. Ramjee has over 20 years of experience, including ten years at ITC and ten years at the Helsinki University of Technology. He was a Research and Development Specialist at Xamk, South-Eastern Finland University of Applied Sciences in Finland before joining Pakka Impact. He completed his doctoral dissertation on “Engineering fine paper by utilizing the structural elements of the raw materials”. He has an extensive knowledge in Agri and wood value chain raw materials, processes, and products and expertise in technology transfer.

Driving "Concept to Commercialization" in global companies for mass-scale productions with more than two decades of experience in European & Asian markets through strategic leadership and agile delivery.

Dr. Ramjee feels thrilled to be a part of Yash Pakka and hope to learn from each one of them. He is determined to work on developing Sustainable Packaging Solutions with his team, fulfilling all their expectations.

CONFERENCE PROCEEDINGS

ACTIVE

AND

INTELLIGENT PACKAGING

ORAL PRESENTATION

GENERAL STREAM

AI-GO01	Ethylene Colorimetric Ink for Monitoring Fruit Ripening
AI-GO02	Shelf-life extension of fresh-cut pineapple by sodium alginate-based active edible coating with lemongrass essential oil
AI-GO03	Barrier Properties of PLA/PBAT Films Incorporating Titanium Dioxide
AI-GO04	Centrifugal fiber spinning to fabricate polyhydroxyalkanoate/zinc oxide nanocomposite films: structure-property analysis
AI-GO05	Mechanical properties of PBAT/TPS nanocomposites under UV exposure

PEER-REVIEWED

AI-GP01	Evaluation of the Antimicrobial Activity of Sodium Alginate Films Integrated with Cinnamon Essential Oil and Citric Acid

POSTER PRESENTATION

AI-PP01	Understanding silver nanoparticle leaching behavior from active biobased nanocomposites
AI-PP02	Novel temperature-sensitive label based on thermochromic ink for hot food packaging and serving applications.
AI-PP03	Natural pH sensors as a quality monitoring smart label for poultry packaging

AI-GO01

Ethylene Colorimetric Ink for Monitoring Fruit Ripening

Inmaculada Lorente[*1], Ana Maria Tone[1], Maria Monedero[1], Jesus Palenzuela[1]

[1]Centro Tecnológico del Embalaje, Transporte y Logística (ITENE), Paterna 46980, España.

[*]***Correspondence to:*** *Inmaculada Lorente Gómez, Project Manager, ITENE.*
E-mail: inmaculada.lorente@itene.com

ABSTRACT: Ethylene is a gaseous plant hormone that plays an important role in inducing the ripening process for many fruits. Some fruits, after been harvested and prior to be commercialized, are exposed to ethylene gas in a ripening chamber. The objective is to homogenize appearance and state of maturity of the fruit. Although the concentration of ethylene gas is monitored and automatically regulated, the concentration that can reach the fruits may be conditioned by their location in the chamber or on the pallet. Additionally, there are other fruits that, after reaching their ideal point of maturity, are harvested for marketing. In this case, the effects of ethylene are no longer positive, causing them to rot and age.

This work aims to assess and develop an optimal combination of non-thermal sanitization, preservation, and stabilization methods to improve the safety, while preserving the nutritional quality and prolonging the shelf-life of minimally fruits and vegetable products. ITENE in the framework of the UE financed SHEALTHY project has developed an ink that detects the concentration of external ethylene and changes it colour according to the time and the ethylene concentration to which it is exposed. The lower sensitivity limit of the ink is 20 ppm. Its initial colour is light brown, and it changes to dark blue when ethylene is present. The effect of the concentration of the different compounds, as well as addition of different binders, and the use of different materials as printing substrates has been evaluated. Additionally, its colour change has been monitored according to different ethylene concentrations.

This ink has been found to be a promising tool for improving the management and the control of fruits prior to be commercialized in other to reduce losses and improve its quality over the supply chain.

Keywords: intelligent packaging, indicator, ethylene, freshness, colour change.

INTRODUCTION

After harvesting, fruit and vegetables (F&V) continue with their respiratory activity, and enzymatic and biochemical reactions, which leads to important changes in the organoleptic and nutritional properties of these products and thus, to its senescence. The respiratory activity degrades the acids, carbohydrates, proteins, and lipids generating volatile organic compounds (VOCs) during F&V ripening. VOCs are gradually synthesised via different pathways. In general, F&V produce terpenes, aldehydes, carboxylic acids, sulphur compounds and ammonia[1]. Additionally, some fruits produce ethylene, a hormone capable to stimulate the fruit ripening.

Ethylene is a gaseous plant hormone that plays an important role in inducing the ripening process for many fruits, together with other hormones and signals. Fruits that respond to ethylene are called "climacteric" and include apples, avocados, bananas, figs, mangoes, papayas, peaches, pears and tomatoes. Generally speaking, climacteric fruits continue to ripen after they've been picked, and the ripening process can be manipulated by exposing them to ethylene. This could be interesting for distributors, whose can modulate the ripening rate of these products according to their interest.

Commercial fresh produce companies rely on the process of ripening to meet the demands of buyers. In order to do this, many use artificial ripening processes by introducing excess amounts of ethylene to speed up ripening. Ethylene gas detection is essential in this industry to ensure that the right amount of ethylene concentration is introduced. Different products require different concentrations and time for optimal ripening. The use of ethylene gas detectors is extended in the industry. They enable the correct amount of ethylene to be added to produce to ripen them quickly without over-ripening them, but their use has some constraints. Ethylene gas detectors are not cheap, require periodic calibration and have a limited lifetime [2].

ITENE in the framework of the UE financed SHEALTHY project has developed an ink that detects the concentration of external ethylene and changes its colour according to the time and the ethylene concentration to which it is exposed. This indicator can be used as a label, to detect ambient ethylene concentration and improve the management of climacteric fruits at the supply chain.

According to the information compiled from literatura [3, 4, 5], molybdate was selected for the formulation of the freshness indicator. Molybdenum chromophores change under the impact of ethylene from white/yellow to blue because of partial reduction of Mo (Vl) to Mo (V). To accelerate the redox reaction of molybdate with ethylene, a catalyst can be used. Different relations indicating compound – catalyst have been studied. Additionally, in this paper we present the effect of different substrates, as well as the effect of different binders / polymers on its sensitivity.

MATERIAL AND METHODS

Effect of the relation catalyst – molybdate. Ammonium molybdate tetrahydrate (Sigma Aldrich) is diluted and stirred overnight. On the other hand, a catalyst is dissolved in water and used freshly. Both dilutions are mixed. Then ethylene is burbled in the liquid and colour change is visually evaluated. This is done to assess that the reaction takes place. Once it has been checked that the reaction takes place, the relation molybdenum – catalyst is optimised. Five different molar relations were studied. Additionally, for this optimization, the shelf life of the molybdate dissolution was also studied. One dissolution was freshly prepared. The other one was prepared 2 weeks before. Gaseous ethylene is burble inside the indicating solution and colour change is visually evaluated after 5 minutes.

Substrate study. Additionally, to select the appropriate substrate on which to deposit the formulation, different substrates have been tested. Tested substrates were four types of filter paper: Whatman 540, VWR paper, Albet, and fiberglass. Thin layer chromatography (TLC) substrate was also evaluated. Indicators were prepared by drop casting.

Those that allowed the development of stable indicators, were exposed to ethylene to evaluate their sensitivity. To develop the indicators, a drop of each indicator solution was

deposited on the substrate, with a Pasteur pipette. The indicators were stored in darkness until they were completely dry. Once the indicators were properly dried, they were cut (1 x 2.5 cm) and introduced inside 20 mL vials and hermetically sealed. Indicators were exposed to different concentrations of ethylene, from 200 to 1,200 ppm. Finally, for evaluating the colour change of the indicators over the time at low ethylene concentration (20 ppm), a chamber was developed in which ethylene is injected and the concentration of this gas is monitored by means of a sensor. Colour change was again visually evaluated over the time.

Binder study. Once the best molybdate: catalyst relation was selected, different polymers were added to the selected relation to increase the solution viscosity for being printed by flexography. 1) Polyvinyl alcohol (PVA) from Kuraray, 2) PVA Mowiol 4 – 88 from Sigma Aldrich, 3) chitosan from Sigma-Aldrich, and 4) polyurethane dispersion (DispercollU XP 2643, from Covestro) have been evaluated as binders for the formulation of the ethylene indicating ink. PVA solutions of 3.5% (w/v) in water was prepared mixing using a magnetic stirrer for 30 minutes at 80°C. Chitosan solution was prepared at 3% (w/v) in acetic acid and the mixing conditions were 60 min at 50°C using a magnetic stirrer. No dilution was needed for Dispercoll U XP 2643. The sensitivity to ethylene of those inks that remained stable was studied. Indicators were prepared by drop casting and different concentrations of molybdate: catalyst were evaluated.

RESULTS AND DISCUSSION.

Effect of the relation catalist – molibdate

Few drops of the catalyst are added to the dilution of molibdate and the mix is exposed to ethylene. The reaction takes place. The initial colour of the liquid is light yellow and it changes to dark blue. Initial and final colour are shown in Figure 1.

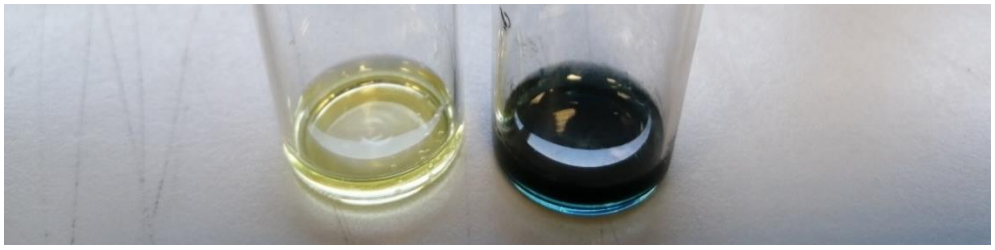

Figure 1. Indicating solution. Left: initial colour. Right: final colour

The next step was to optimize the molybdenum – catalyst relation. Ammonium molybdate tetrahydrate was diluted and stirred overnight. Then, different quantities of catalyst are added. The sensitivity of a dissolution of ammonium molybdate prepared 2 weeks before was also evaluated.

Table 1 shows the final colour of the ink after 5 minutes to have been exposed to ethylene. Initial colour was light yellow. All tested relations changed the colour and this colour change was easily perceptible to the naked eye. Although all relations changed their colour, not all shown the colour change from yellow to blue, that was observed in the first trial and that is described in literature. When freshly prepared molibdate dissolution was prepared, only relation A shown this colour change. The other tested relations shown a colour change from

light yellow to brown. When molibdate disolution prepared two weeks before was evaluated, the indicating solution changed to green and this colour evolve to a greener – coffee colour as higher the concentration of the catalyst in the indicating ink was. After 2 hours, only relation A remained blue, independently to when ammonium molybdate dissolution was prepared. A possible one reason why the formulation turns brown and not blue could be due to the excess of catalyst.

	Relation A	**Relation B**	**Relation C**	**Relation D**	**Relation E**
Freshly prepared molibdate disolution					
Molibdate disolution prepared two weeks before					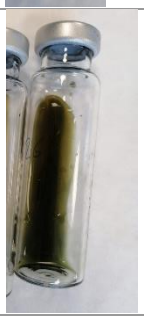

Table 1. colour change of the different tested formulations

Substrate study

To select the appropriate substrate on which to deposit the formulation, different substrates have been tested. Albet substrate did not show good results. Albet substrate did not absorb the formulation and it turned to blue colour. The other substrates (Whatman, fiberglass and thin layer chromatography substrate) did not react with the freshness ink and remained yellow. Nevertheless, the freshness indicating ink on the Whatman substrate shown a light colour after several hours and it was discarded as printing substrate for developing the freshness indicator. Fiberglass and TLC did not change the color of the indicating ink. The colour of the indicating ink on the different substrates is shown in Figure 2.

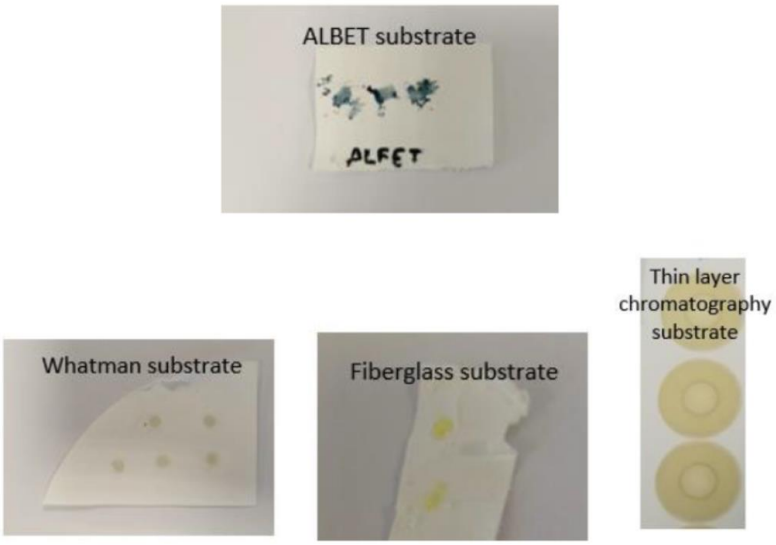

Figure 2. Freshness ink on Albet, Whatman, fiberglass and thin layer chromatography substrates

As for the same quantity of indicating formulation, the sensor area on the TLC substrate is higher, this substrate was selected for further trials. Freshness indicators done using TLC as substrate were exposed to different concentrations of ethylene. Those concentrations range from 200 ppm to 1,200 ppm. Figure 3 shown the different colours that the indicator presents when it is exposed to different concentrations of ethylene. A clear colour evolution and proportional to the ethylene concentration, was observed. The initial colour of the indicators was colourless. It changed to cian when the concentration was increased to 200 ppm until a cobalt blue when the concentration was 800 ppm or higher.

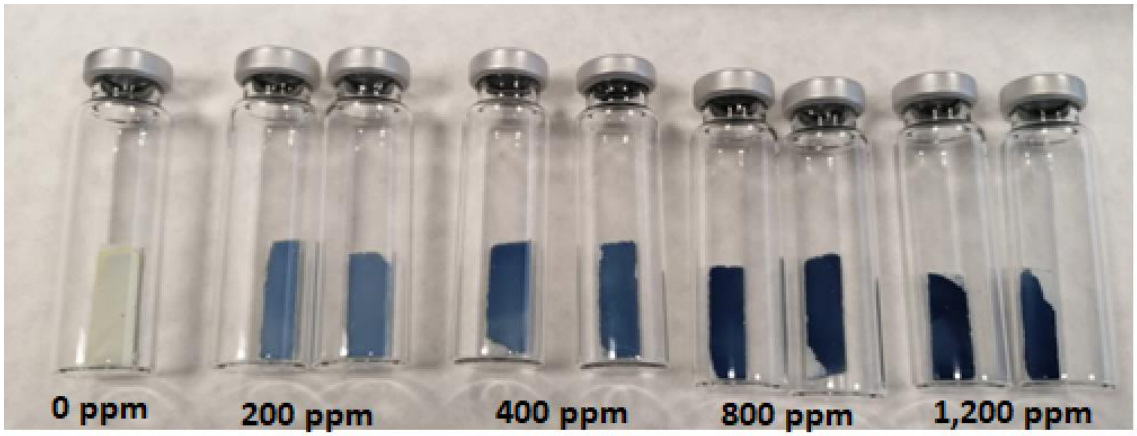

Figure 3. Ethylene indicator exposed to different amount of ethylene

Finally, indicators were introduced inside a chamber and ethylene was injected. Ethylene concentration was 20 ppm. Indicators colour change was visually monitored over 6 hours. Colour evolution is shown in Table 2. Five minutes after ethylene has been injected, indicators show a clear blue colour. This colour change is increased over the time until a darker colour is reached.

5 minutes	60 minutes	240 minutes	360 minutes
			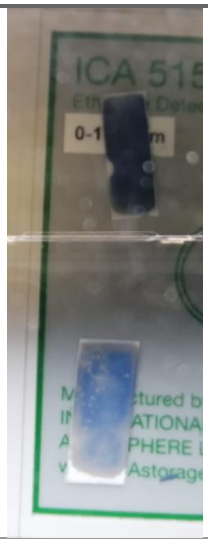

Table 2. colour evolution of the indicator when it is exposed to 20 ppm of ethylene

Binder study

The stability of the indicating solution (molybdate + catalyst) when it is mixed different binder has been evaluated. Three different matrix solutions were formulated, and their appearance was evaluated to choose the best matrix to develop the ethylene sensitive ink. The different matrix obtained with indicator solution (Mo)can be in Figure 4.

Figure 4. Appearance of the different evaluated binders

Regarding the formulation based on PVA as binder, when 0.1 mL of Mo were added to PVA Mowiol, the formulation presented a light-yellow colour. When this quantity was increased to 0.5 mL of Mo, the final dissolution adopts a more yellowish hue and the formulation remained clear over the time. When PVA from Kurray was used, molybdate was difficult to disperse.

When 0.1 mL of Mo was added, no yellow colour was observed. Quantity had to be increased to 0.5 mL in order to observe a light-yellow hue. Formulations based on the chitosan matrix, when Mo was added, a precipitate was generated, more pronounced when 0.5 ml of Mo was added. Formulations based on Dispercol matrix solution, when adding 0.1 mL of the indicator solution has a white colour, when this quantity was increased, a precipitated was generated. According to these results, PVA was selected for evaluating the sensitivity to ethylene of an ink made up of PVA, molybdate and a catalyst. Indicators were prepared on TLC substrate by drop casting. Different quantities, ranged from 0,25 ml to 1 ml of molybdate: catalyst, were added to 1 ml of PVA dissolved in water at 3.5% wt. Indicators without PVA were also evaluated. Indicators were prepared by drop casting and let dry at room temperature overnight. The indicators sensitivity could not be evaluated because the indicators formulated with PVA did not remain stable. After 18 hours at room conditions, their colour changed from colourless to dark yellow or blue, depending on the concentration of molybdate: catalyst in the formulation. Indicators prepared without PVA remained colourless (see Figure 5).

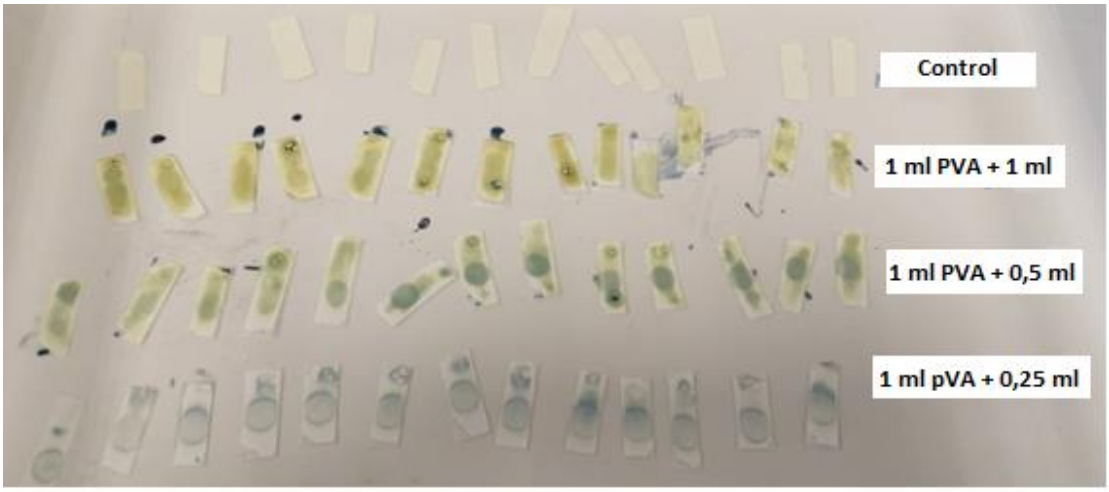

Figure 5. Colour of the indicators after 18 hours at room temperature

CONCLUSIONS

An ethylene indicating ink based on ammonium molybdate and a catalyst has been developed. The relation molybdenum : catalyst determinates the sensitivity of the indicator and also its colour change. The best relation has been selected. This formulation can detect 20 ppm of ethylene and its colour change is gradual and proportional to the time that the indicator has been exposed to ethylene. In order to fabricate it as a printed indicator, the effect of different substrates and binders has been evaluated. TLC was selected as substrate. It did not react with the ink, so indicators prepared on this substrate are stable over the time at room conditions. Regarding the binder, different options have been evaluated. When the indicating compounds are added to the formulation of chitosan and polyurethane, the binders react and produce a precipitate. Only PVA produce stable inks but when this ink in applied on the substrate, the indicators are not stable and change their colour at room conditions.

This investigation demonstrates that visual colour changing indicators for monitoring the exposure time of fruits to low concentrations of ethylene can be developed by drop casting.

This indicator is a promising tool for improving the management of climacteric fruits at the supply chain.

REFERENCES

1. Chen, X., Fedrizzi, B., Kilmartin, P. A., & Quek, S. Y. (2021). Development of volatile organic compounds and their glycosylated precursors in tamarillo (Solanum betaceum Cav.) during fruit ripening: A prediction of biochemical pathway. *Food Chemistry*, 339, 128046.
2. https://www.forensicsdetectors.com/blogs/articles/ethylene-gas-detector-produce
3. Lang, C. & Hübert, T. (2011). A Colour Ripeness Indicator for Apples. *Food and Bioprocess Technology*. 5. 10.1007/s11947-011-0694-
4. Putri, VJ &Warsiki, Endang & Syamsu, Khaswar & Iskandar, A. (2019). Application Nano Zeolite-Molybdate For Avocado Ripeness Indicator. *IOP Conference Series: Earth and Environmental Science*. 347. 012063. 10.1088/1755-1315/347/1/012063.
5. Jin-Ho Kim&Seimei Shiratori. (2006). Fabrication of Color Changeable Film to Detect Ethylene Gas. *Japanese Journal of Applied Physics*, Vol. 45, No. 5A, pp. 4274–4278

AI-GO02

Shelf-life extension of fresh-cut pineapple by sodium alginate-based active edible coating with lemongrass essential oil

Darylle Jerome Ortiz*[1], Ray Anne Grace Garalde[1], Cynthia Bihis[1], and Dane Archibald Balanon[1]

[1]*Industrial Technology Development Institute, Department of Science and Technology Taguig City, Metro Manila, 1630 Philippines*

[*]***Correspondence to:*** *Industrial Technology Development Institute, Department of Science and Technology*
E-mail: djiortiz@itdi.dost.gov.ph

Abstract: Fresh-cut fruits offer a healthier choice to consumers for a better well-being. While minimal processing provides convenience, it consequently speeds up fruit deterioration-damaging the tissues and increasing its surface area which amplifies respiration and promotes microbial growth, respectively. This leads to faster senescence thus, higher food loss. To address this issue, an active edible coating solution was developed and applied on fresh-cut Queen pineapples (Ananas comosus var. Formosa) to potentially extend its shelf-life. The base coating solution was prepared using sodium alginate (SA) and distilled water using a magnetic mixer. For improved plasticity, glycerol was added at 1% w/w concentration. Suitable solution thickness was identified at 1% w/w SA with a viscosity of approximately 484.3 cP. Lemongrass essential oil (LEO) was then incorporated at various amounts (0.3%, 0.2%, 0.1%, and 0.05% w/w) to SA-based coating solution as active compound using sonication technique. The active edible coating with varying LEO levels were applied by dipping method followed by cross-linking using calcium lactate solution. The effect of LEO to the viscosity of coating solution was measured. More so, its acceptable amount mixed in the solution was also evaluated through sensory evaluation of fresh-cut pineapples applied with the developed active edible coating. The addition of LEO resulted to slight decrease in viscosity of the solution to 453.1 cP. Maximum acceptable LEO limit was also identified at 0.1% (w/w). The final formulation was further applied to fresh-cut pineapples and the physicochemical indexes (visual quality, weight loss, color values, pH, TSS, and firmness), sensory quality, and microbiological parameters were measured during storage at 10°C. Non-coated and pure SA-coated fresh-cuts served as control. Results showed that 0.1% LEO exhibited a slightly higher weight and firmness compared to other samples. Parameters such as glossiness, juiciness, sweet-sour taste, and texture were promisingly improved. In addition, the coating evidently reduced total plate and yeast and mold count of fresh-cut pineapples which demonstrates its antimicrobial property. With active edible coating applied, the shelf-life of fresh-cut pineapples was extended from 4 up to 8 days-100% increase compared to control sample. The results revealed the effectiveness of developed active edible coating in maintaining quality, safety and extending the shelf-life of fresh-cut pineapples. The active edible coating can be possibly further developed for application to other fresh-cut fruit types.

Keywords: Edible coating, active packaging, essential oil, alginate, shelf-life, antimicrobial, cross-linking

INTRODUCTION

Edible coating (EC) has reimagined the context of food packaging and led to research studies on effectively extending the shelf life of perishables. From its first commercial form as wax[1] being applied on the surface of intact fruits, it shifted to a direct film layer on pulps, particularly fresh-cuts. This classifies edible coatings as primary packaging[2]. Sodium alginate (SA), a good base for a polysaccharide coating, has a very distinct colloidal property.
Its remarkable thickening and film-forming characteristics are good prerequisites for a coating solution. On the other hand, it also has great stabilizing, suspending, and emulsifying properties, which make it a good carrier material for active compounds for improved coating functionality[3]. In this context, essential oils (EOs) are used as antimicrobial constituents for edible coatings, considering their effectiveness, sustainability, and safety over chemical additives[4,5].

Its remarkable thickening and film-forming characteristics are good prerequisites for a coating solution. On the other hand, it also has great stabilizing, suspending, and emulsifying properties, which make it a good carrier material for active compounds for improved coating functionality[3]. In this context, essential oils (EOs) are used as antimicrobial constituents for edible coatings, considering their effectiveness, sustainability, and safety over chemical additives[4,5].

Lemongrass essential oil (LEO) is of high interest as an active component in edible coatings due to its high citral content as its active compound, which comprises about 75% of its total composition[6]. Yousuf and Srivastava[7] incorporated LEO (0 ppm, 200 ppm, 500 ppm, and 800 ppm) via flaxseed gum EC into ready-to-eat pomegranate arils for 12 days at 5°C. The study focused on the potential of the coating to reduce microbial populations as well as its possible effect on total soluble solids, pH, titratable acidity, and color over the storage period. In 2007, Raybaudi-Massilia et al.[8] used SA as a base coating material to carry different essential oils, including LEO (0.3% and 0.7%), to improve the shelf life and safety of fresh-cut melon. In the subsequent year, he focused on LEO (0.3%, 0.5%, and 0.7% v/v) alone in SA edible coating to possibly preserve the microbial and physicochemical quality of fresh-cut Fuji apples[9]. Similarly, Azarakhsh et al.[10] utilized SA with LEO at even decreased concentrations (0.1%, 0.3%, and 0.5% w/v) in fresh-cut pineapple. The study investigated the effect of the edible coating on respiration rate, physicochemical, microbiological, and sensory quality during 16 days of storage at 10°C and 65% RH.

The aforementioned literature suggests the applicability of LEO as an active compound in edible coating solutions. Results from these studies provided a desirable effect on shelf life among different commodities. However, these also revealed that higher LEO concentrations negatively affect the sensory quality of the fresh-cut fruits.
In this work, we decided to further lower the concentration of the LEO included in the SA-based edible coating solution. The study aims to initially establish the appropriate amount of essential oil based on sensory evaluation. Moreso, the study aims to further determine the effect of the identified optimum LEO concentration on the physicochemical, sensory, and microbial quality of fresh-cut pineapple.

METHODOLOGY

Preparation of SA-base coating solution

The edible coating solution was prepared by dissolving 1.0% w/w food sodium alginate (SA) (Marine Resources Development Corporation, Philippines) in distilled water using a magnetic stirrer. Food-grade glycerol (Chemline Scientific Corp., Philippines) was further added at 1.0% w/w as a plasticizer. The viscosity of the base coating solution was then measured using a viscometer (Brookfield LVDV-11+, USA). Three replicates of approximately 400 mL of edible coating solution were poured into a 500 mL beaker. Each was measured three (3) times and mean viscosity was expressed in centipoise (cP).

Determination of viscosity of SA edible coating with LEO

Different LEO (Hi-Q Commercial Inc., Philippines) concentrations (0.1%, 0.2%, and 0.3% w/w) were mixed into the coating solution by sonication (Ney® ULTRAsonik sonicator Model 28H, USA) for 20 minutes. Occasional manual mixing was also done to aid the incorporation. The same procedure on viscosity measurement done to pure SA coating solution was employed to coating solutions incorporated with LEO.

Determination of acceptable LEO concentration

Similar active edible coating formulations were tested for overall acceptability through sensory evaluation. Application of coating was carried out by dipping fresh-cut pineapple pieces in SA-LEO coating solution for 1 min. The excess coating was allowed to drip off for 1 min followed by drenching into food grade calcium lactate (Dalkem Corporation, Philippines) solution (2% w/w) for 1 min following Azarakhsh et al.'s[10] method. Coated pineapples were air dried for 1 h at 25°C then subsequently packed by ten (10) pieces each in self-locking polystyrene trays. Non-coated and pure SA-coated (without LEO) fresh-cut pineapples served as controls. Samples were rated using a 9-point hedonic rating scale.

Determination of quality and shelf-life of SA-LEO coated fresh-cut pineapple

The identified acceptable LEO level was further assessed for its visual, physicochemical, and microbial qualities and shelf life of fresh-cut pineapple. Non-coated and pure SA-coated pineapples served as controls. A summary of treatments is shown in Table 1. Samples were stored at 5°C and 85% RH and monitored for up to 8 days.

Molecules	Formulation
No coating (Control)	No edible coating applied
Pure SA coating	1% sodium alginate (w/w)
SA + 0.1% LEO	1% sodium alginate + 0.01% lemongrass essential oil (w/w)

Table 1 Treatments for determination of effect of edible coating solution

Visual Quality. Fresh-cut pineapples were photographed from day 1 to day 8 of sample monitoring. Images were captured upon pulling samples from storage using a smart phone (iPhone SE, Canada).

Weight loss. Five (5) trays containing ten (10) pieces of fresh-cut pineapple packed were weighed every sampling schedule using a table-top balance. The loss in weight was calculated using the given formula below:

Equation 1

$$\%\, Weight\ Loss = \frac{Wt_i - Wt_f}{Wt_i} x100$$

Color values. Ten (10) pieces of fresh-cut pineapples were randomly selected per treatment and measured for color using a portable chromameter (Konica Minolta Inc., Model CR-20, Japan). Results were expressed in terms of *L* (lightness), *a* (green to red chromaticity), and *b* values (yellow to blue chromaticity). Total color difference (TCD) will be calculated using these values to quantify the visible color difference between samples [12]. Total color space between storage days was calculated using the equation below:

Equation 2

$$Total\ Color\ Difference\ (\mathrm{TCD}) = \sqrt{(L_1 - L_2)^2 + (a_1 - a_2)^2 + (b_1 - b_2)^2}$$

Total soluble solids and pH. Juice extracted from samples was used to measure acidity using a Laqua pH meter PH1100 (Horiba Ltd., Japan) based on the procedure described in AOAC 981.12. On the other hand, the Atago pocket refractometer PAL-3 (Atago Co., Ltd., Japan) was used to measure TSS.

Firmness. The firmness of the pineapple pieces was evaluated during storage using a Shimadzu EZ-SX texture analyzer with Trapezium X Material Testing Operation Software Ver. 1.4.0 (Shimadzu Corp., Japan). Analysis was carried out by measuring ten (10) pineapple pieces using a 7.9 mm diameter stainless cylindrical pointed probe at 1 mm/sec speed. Results were expressed in Newtown (N), which is the average of all the measured forces per treatment.

Sensory evaluation. Fresh-cut pineapples were subjected to sensory analysis for 8 days. Ten (10) trained panelists assessed the samples based on appearance, odor, texture, juiciness, sweetness, sourness, and overall quality. Samples were individually packed in polypropylene and uniquely coded. Quality parameters were rated using a 5-point scale, whereas overall acceptability was assessed using a 9-point hedonic rating scale.

Microbiological analysis. Aerobic plate count (APC) and mold and yeast count (MYC) were tested on all treatments from Day 0 to Day 8 of storage at 5°C. Both tests were carried out using the pour-plate method. The APC plates were inoculated with prepared fresh-cut fruit samples and incubated for 48 h at 35 °C, while the MYC plates were incubated for 5 to 7 days at 25°C. Both tests were conducted in duplicate for each treatment. Results were expressed as log10 colony-forming units per gram (CFU/gram).

Statistical analysis

Results from each parameter were evaluated using one-way analysis of variance (ANOVA)and *t*-test. Significant results from ANOVA were further tested using the least significant difference (LSD). Both analyses were conducted at $p \leq 0.05$ using Microsoft Excel. All experiments were done in triplicate.

RESULTS AND DISCUSSION

Viscosity of SA-LEO active edible coating solution

Viscosity is an important factor for edible coating application on fresh-cut fruit surfaces. The possible effect of LEO on the viscosity (centipoise, cP) of SA-base coating solutions was investigated. As illustrated in Figure 1, the results obtained showed that the SA edible coating decreased in viscosity upon successive additions of LEO (0.1%, 0.2% and 0.3% w/w) to the solution; hence, the solution became thinner. A decrease from 484.3 cP to 419.5 cP was noted for pure SA coating solution and SA+LEO 0.3%, respectively. Based on the statistical analysis ($p<0.05$), the observed decrease in viscosity among treatments is significant. Similar behavior was observed by Cofelice et al[13] wherein they investigated the rheological behavior of alginate-essential oil nanodispersions with increasing oil concentration.

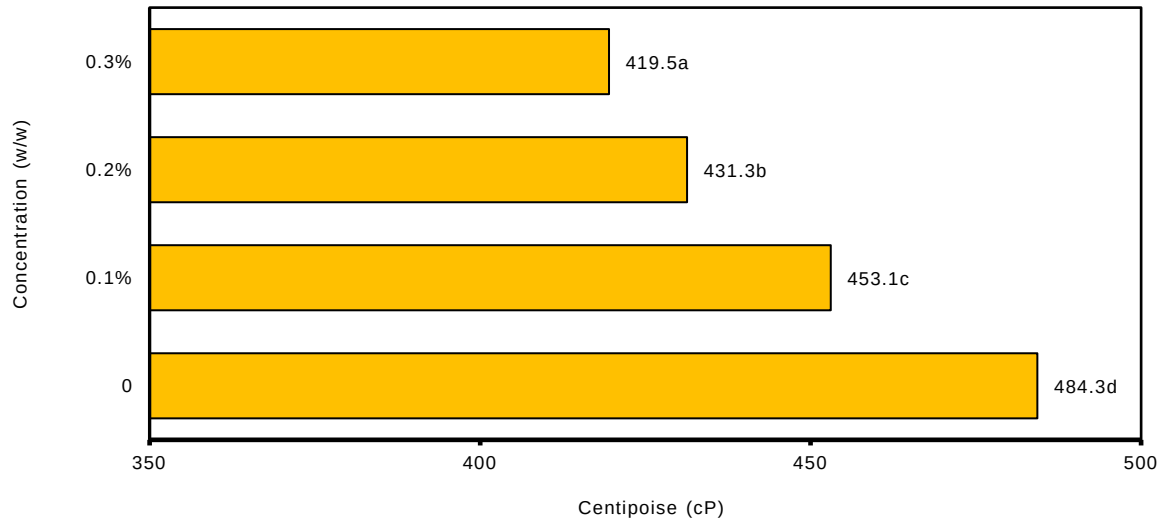

Figure 1 Effect of LEO on the viscosity of SA-based edible coating solution. Means sharing the same letter are not significantly different according to least significant difference ($p > 0.05$).

Acceptable LEO concentration

The acceptable level of LEO incorporation was determined based on the overall acceptability of fresh-cut pineapple applied with active edible coating through sensory evaluation. The test was carried out on the same treatments used in assessment of viscosity of SA-edible coating. The results show that among coated pineapples, those with 0.1% w/w LEO obtained the highest acceptability (Table 2). Its mean score was also found to have no significant difference a

compared to those without coating and with pure SA coating. In contrast, significant difference was identified between the mean scores of samples with 0.2% and 0.3% (w/w) LEO versus the other samples. These results suggest that the incorporation of at least 0.1% (w/w) LEO imparts none to minimal slight alteration to odor and taste given that LEO has strong flavor[14]. Fresh-cut pineapples coated with 0.1% LEO edible coating garnered a mean score which corresponds to like moderately (7.3), while 0.2% (6.6) and 0.3% (5.9) LEO edible coating both obtained scores equivalent to like slightly.

Treatment	Overall acceptability	Remarks
No coating (Control)	7.2a	Dry
Pure SA coating (Control)	7.2a	Glossy
SA + 0.1% LEO	7.3a	Glossy, slight LEO odor & taste
SA + 0.2% LEO	6.4b	Glossy, strong LEO odor & taste
SA + 0.3% LEO	5.9c	Glossy, strong LEO odor & taste

Remarks: Means sharing the same letter are not significantly different according to least significant difference ($p > 0.05$).
9: Extremely acceptable; 5: Neither like nor dislike; 1: Dislike extremely

Table 2 Overall acceptability of fresh-cut pineapple with different amounts of LEO.

Quality and shelf-life of SA-LEO coated fresh-cut pineapple

The effect of SA-LEO active edible coating on the different quality indices of fresh-cut pineapple. The assessed parameters directly related to the marketability of fresh-cut fruits in general.

Visual quality

Figure 2 illustrates the visual quality of fresh-cut pineapple at different treatments. Non-coated fresh-cut pineapples were found dry after 5 days of storage at 5±1°C and 85±10% RH. In contrast, coated samples appeared glossy after 8 days of storage under the same conditions. These observations can be attributed to the loss of moisture in fruits during storage. Based on the results, it can be inferred that the application of an edible coating effectively improved the appearance of fresh-cut pineapple.

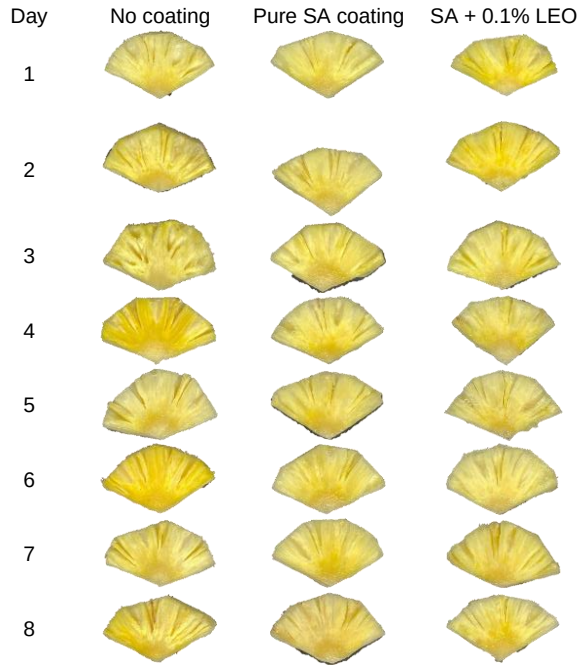

Figure 2 Visual quality of fresh-cut pineapple with and without edible coating.

Weight loss

Weight loss is an essential parameter to evaluate the quality of fresh-cut fruits[7]. At the end of the storage test, a notable difference was observed between coated and non-coated samples. Based on the graph in Figure 3, the weight loss of all coated samples is lower compared to non-coated fresh-cut pineapple, especially on day 8 of storage. On the other hand, a slight difference in weight loss was only observed in samples with and without LEO. This conforms to the results of the study conducted by Azarakhsh et al[10], wherein the addition of LEO (0.1%, 0.3%, and 0.5%) into an edible coating solution demonstrated no significant effect in terms of weight loss reduction. Also, Draget et al.[11] indicated that the coating significantly prevents moisture loss in fresh-cut fruits. In general, the application of an edible coating to fresh-cut pineapple showed an improvement in weight retention.

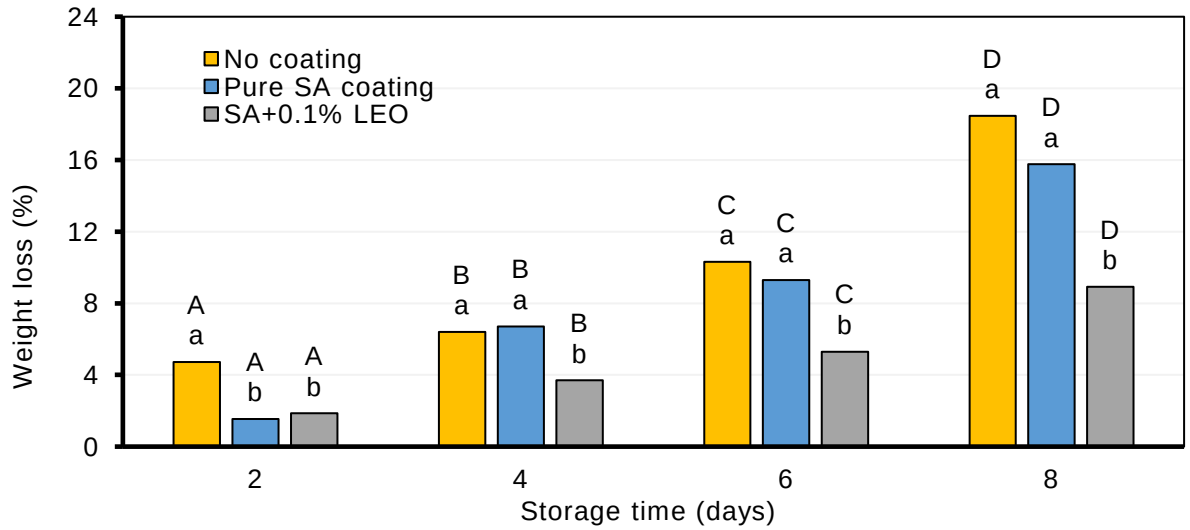

Figure 3 Weight loss of fresh-cut pineapples with and without edible coating during storage at 5±1°C and 85±10% RH for 8 days. Means sharing the same letter are not significantly different according to least significant difference (p >0.05).

Color values

Color change in fresh-cut fruit is a critical factor in its marketability, related to its visual quality. The b values (blue to yellow chromaticity) of pineapples from different treatments are shown in Figure 3. As observed, all treatments decreased in yellowness during storage. However, control and pure SA-coated samples showed a higher b value from day 6 to day 8 compared to those with LEO. Pineapples with 0.1% (w/w) LEO were found to be less yellow compared to other values at the end of the test (b = 25.5).

Although no trend was observed on L and a (data not presented), these were used in the calculation of the total color difference (TCD). Figure 4 shows the progressive color change of all fresh-cut pineapples during storage with continuous increase in TCD from day 2 to day 8. Non-coated and pure SA-coated pineapples expressed lower TCD scores than those with LEO. This implies that the perception of color change among samples with LEO is more obvious than that of the other treatments. Moreso, the TCD score of pineapples with LEO was noted to be higher from day 6 up to day 8 of the storage test. This supports the observation of a decrease in yellowness (b value) in samples with the same treatment and similar storage duration. Based on these results, the addition of LEO to the edible coating solution has an effect on the color of fresh-cut pineapples.

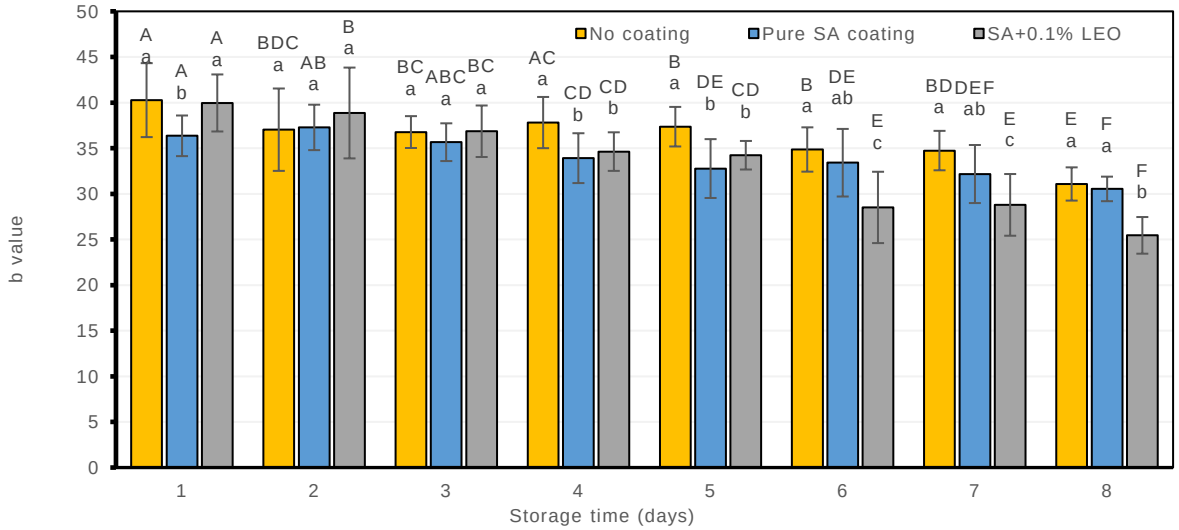

Figure 4 b value of fresh-cut pineapples with and without edible coating during storage at 5±1°C and 85±10% RH for 8 days. Means sharing the same letter are not significantly different according to least significant difference (p >0.05).

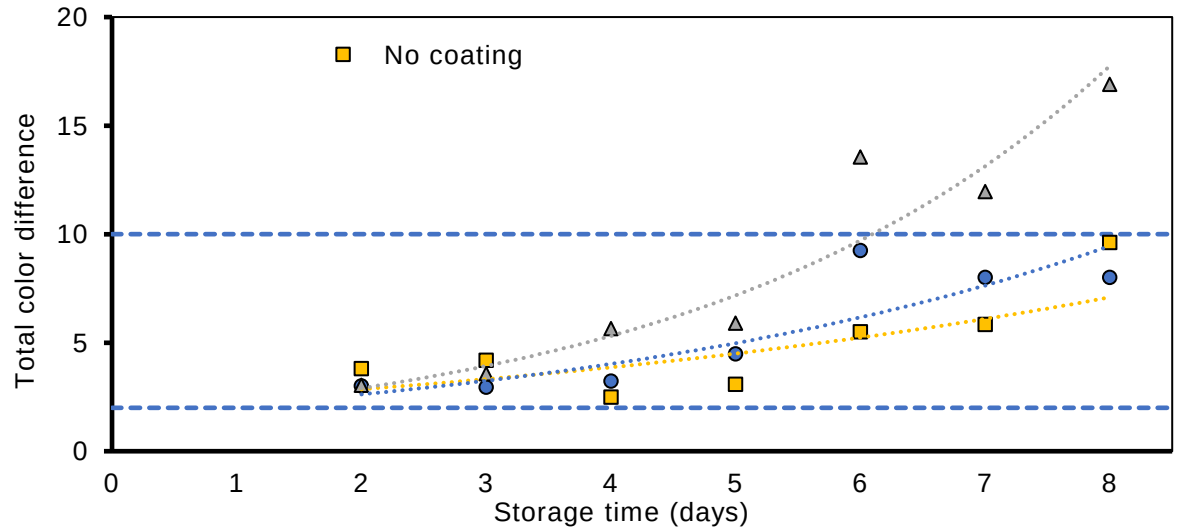

Figure 5 Total color difference of fresh-cut pineapples with and without edible coating during storage at 5±1°C and 85±10% RH for 8 days. Means between 2 and 10 are perceptible at glance. Means above 10 are different but similar than opposite (Xrite, 2005).

Total soluble solids and pH

pH and TSS are intrinsic qualities of fruits that dictate taste, particularly sweet-sour balance. In Figure 6, the pH of fresh-cut pineapples at different treatments is illustrated. Based on the results, the coating lessened the acidity of fresh-cut pineapples throughout storage, particularly those with LEO. Fresh-cut pineapples coated with 0.1% LEO have a higher pH compared to pineapples coated with pure SA coating from days 4 to 8. On the other hand, the pH of control samples slightly decreased during storage, from 3.62 at Day 1 to 3.42 at Day 8. The difference

in pH among fresh-cut pineapples may be attributed to the pH of the LEO at 5.6, which is higher compared to that of pineapple[15].

On the other hand, the edible coating affected the TSS of the fresh-cut pineapples. As shown in Figure 7, non-coated samples have a higher TSS compared with edible coatings. The decreased TSS value observed on coated samples suggests a delay in the metabolic process (ripening) among fresh-cut pineapples as an effect of edible coating application. Although hampered, it can also be determined that TSS gradually increased from Days 2 to 7. Moreover, among coated pineapples, those with 0.1% LEO had the highest TSS value. The results on pH and TSS clearly express that the edible coating could slow down the process of converting sugar and acid that occurs among fresh-cut fruits and, hence, retard the degradation.

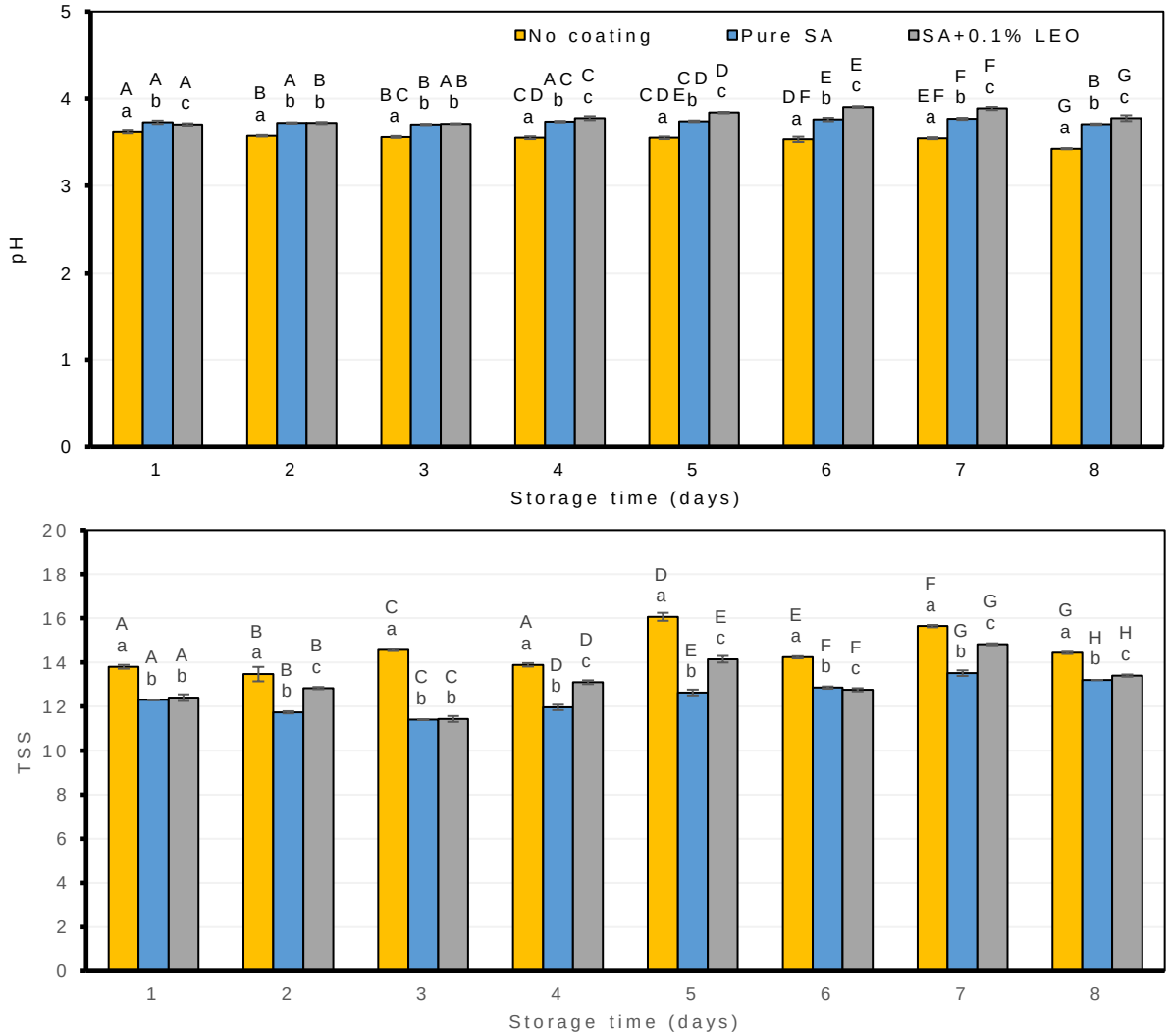

Figure 6 pH and TSS of fresh-cut pineapples with and without edible coating during storage at 5±1°C and 85±10% RH for 8 days. Means sharing the same letter are not significantly different according to least significant difference ($p > 0.05$).

Firmness

Fruits naturally lose their firmness as they approach their end of life. This happens on intact fruits and is hastened in fresh-cut fruit as its respiration apparently speeds up due to cutting, disrupting fruit tissues. Figure 7 shows the effect of edible coating application on the texture of fresh-cut pineapples. After 8 days of storage, coated pineapples with 0.1% LEO significantly retained a higher texture (4.15 N) compared to control (3.34 N) ($p>0.05$). This result could be related to the use of calcium lactate in the cross-linking process, which could possibly aid firmness retention. Related studies by Raybaudi-Massilia et al.[8] experimented with using a calcium-containing compound (calcium chloride) and found that it was effective in preserving the firmness of fresh-cut melon. Studies by Rojas–Graü[16] on alginate-based coatings and calcium chloride as crosslinking solutions also revealed that they were effective in minimising the softening of apple wedges.

On the other hand, the observed effect of LEO on texture can be related to Azarakhsh et al.[10] findings. In their work, the addition of LEO at 0.5% (w/v) resulted in a significant decrease in firmness. Raybaudi–Massilia[8] incorporated LEO at a relative lower concentration of 0.7% (w/v) but was still found to significantly decrease the firmness of fresh-cut melon. He concluded that active compounds of the essential oil, such as citral and geraniol, had a reaction with the cell tissues of the fruit, which induced structural change. In the case of the present research, 0.1% (w/w) LEO incorporated in an alginate-based coating was identified to have no undesirable effect on firmness. Therefore, an appropriate amount must be considered in addition to essential oil as an active agent in an edible coating solution.

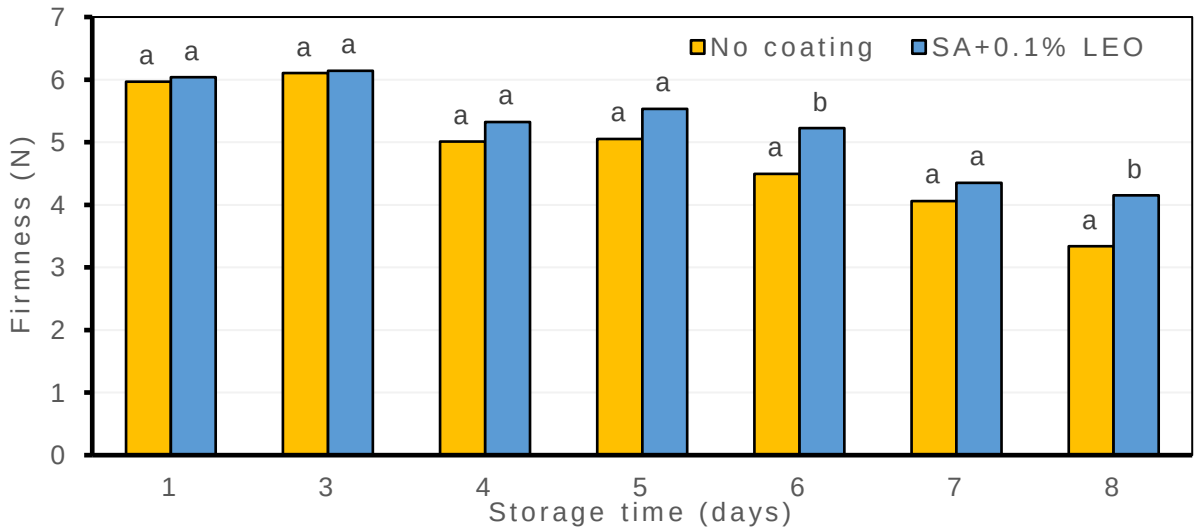

Figure 7 Firmness of fresh-cut pineapples with and without edible coating during storage at storage at 5±1°C and 85±10% RH for 8 days. Means sharing the same letter are not significantly different according to least significant difference ($p >0.05$).

Sensory evaluation

The t-test (Figures 8-A, B, and C) between day 1 and day 8 of the sample storage test revealed that non-coated fresh-cut pineapples exhibited changes on all parameters except sourness

(p>0.05). On the other hand, appearance, overall taste, texture, and juiciness significantly changed on both coated samples. However, even with these observations, there were differences between all treatments based on the sensory parameters measured (Figure 8 D) (p>0.05).

The highest mean scores for texture were noted on pineapples coated with SA+LEO coating, which agrees with the result obtained from the firmness test. It was also slightly less juicy and glossy compared to pure SA-coated pineapples but a bit sweeter and more aromatic. Additionally, the presence of LEO did not alter the overall taste of the fresh-cut pineapples since there was no significant difference with other treatments. The developed coating was meant to be consumed while on the surface of a fresh cut; hence, this result has an impact on the acceptability of LEO incorporation into the edible coating solution. It has a comparable sweetness to other samples but also maintains a higher level of sourness. Moreso, no significant difference was also determined in terms of the overall acceptability of all treatments (Figure 9). Hence, the LEO in the edible coating had no adverse effect on the sensory quality of fresh-cut pineapple.

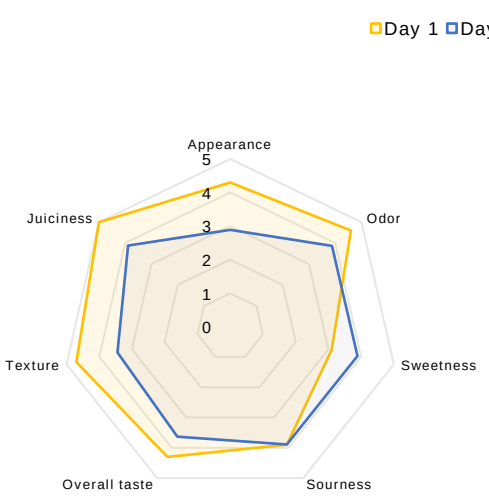

A. No coating
Day 1 vs Day 8

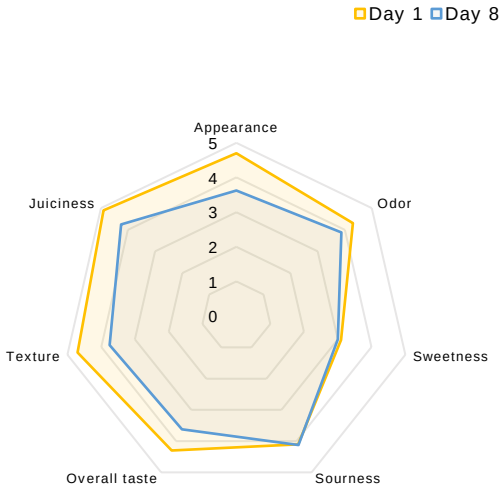

B. Pure SA coating

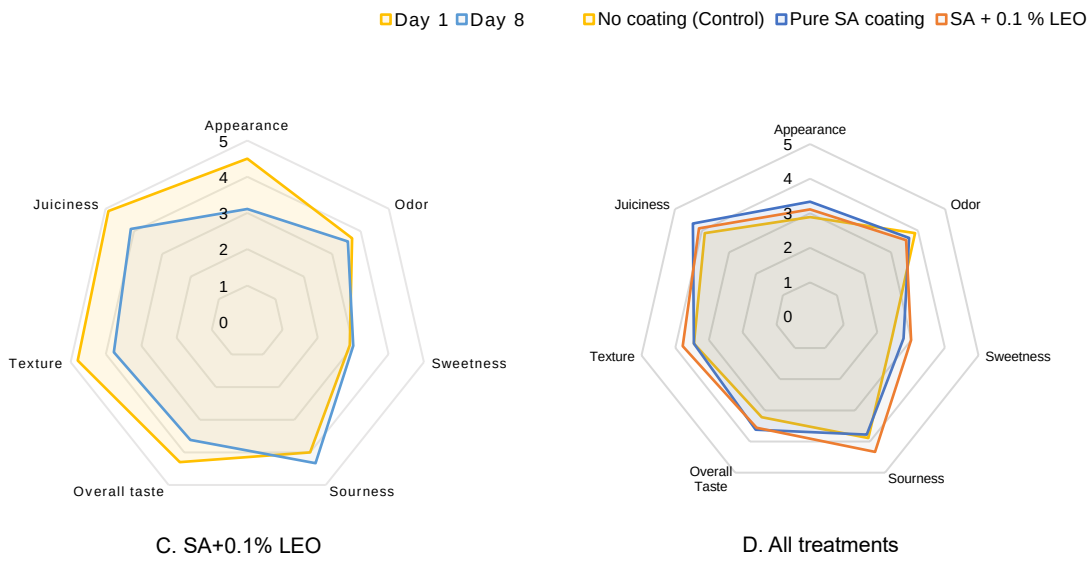

Figure 6 Sensory evaluation results of fresh-cut pineapples with and without edible coating during storage at storage at 5±1°C and 85±10% RH for 8 days. (A, B, and C: Day 1 vs Day 8 of the treatments; D: all treatments at Day 8).

Microbiological quality

Figure 10 shows the results obtained from microbiological testing of fresh-cut pineapple treatments. Although slightly erratic, the APC and MYC of the non-coated samples were higher than the coated ones during 8 days of storage at 5°C. A declining trend in load was observed for both tests. This could be due to the inhibitory effect of lemongrass essential oil on microbial growth, hence the decrease in APC and MYC.

Azaraskhsh et al.[10] utilised the same concentration of the active agent and were found to significantly decrease the load of the same microorganisms after 8 days of storage at 10°C. Raybaudi-Massilia et al. (2008) also successfully tested the microbial inhibitory effect of an alginate-based edible coating with lemongrass essential oil (0.3% and 0.5% v/v). This resulted in the shelf-life extension of fresh-cut Fuji apples. In other studies, lemongrass oil incorporation at higher concentrations (1.0 and 1.5% w/w) also significantly inhibited the growth of psychrophilic aerobes, yeast, and molds on fresh-cut apples when incorporated in an apple-puree-alginate edible coating, but induced severe texture loss[17]. Based on the results of the microbiological test, the incorporation of lemongrass essential oil in an alginate-based edible coating was effective in controlling microbial growth when combined with low-temperature storage.

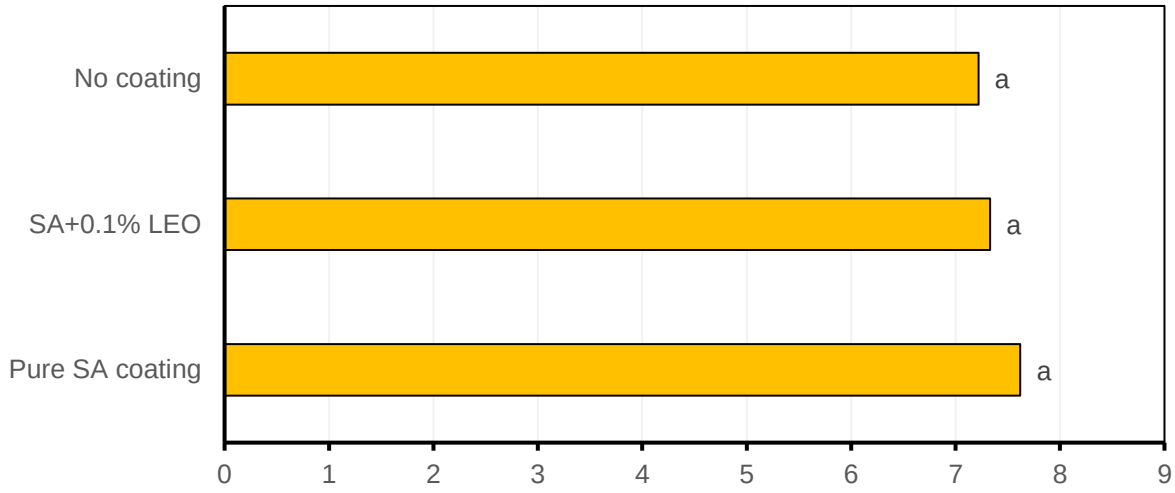

Figure 7 Overall acceptability of fresh-cut pineapples with and without edible coating during storage at storage at 5±1°C and 85±10% RH for 8 days. Means sharing the same letter are not significantly different according to least significant difference (p >0.05).

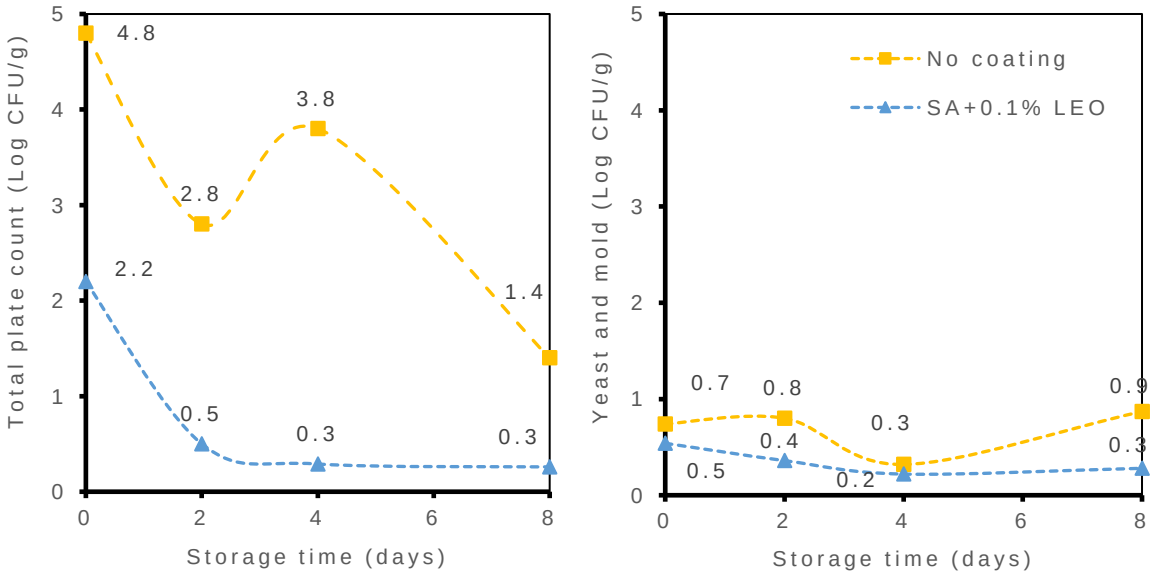

Figure 8 Total plate and yeast and mold counts of fresh-cut pineapples (Log CFU/g) with and without edible coating during storage at storage at 5±1°C and 85±10% RH for 8 days.

CONCLUSION

An active edible coating developed using sodium alginate and lemongrass essential oil was tested for its potential for quality preservation and shelf life extension on fresh-cut pineapples. The results suggest that lemongrass essential oil has a significant effect on the viscosity of the edible coating solution. Additionally, the active edible coating largely affected the overall acceptability of the fresh-cut pineapples upon application. Therefore, the optimum amount of

essential oil incorporation could be determined by its effect on the sensory quality of the fresh-cut fruit. Results also revealed that the active edible coating preserved the physicochemical properties as well as the visual and sensorial qualities of fresh-cut pineapple. Thus, it can be inferred that the developed edible coating has an effective preservation property for maintaining the quality and extending the shelf life of fresh-cut pineapples. In addition, 0.1% (w/w) LEO was found effective in decreasing the total plate count and yeast and mold counts of fresh-cut pineapple during low-temperature storage. This clearly suggests that LEO could be a potent antimicrobial agent even at low concentrations.

REFERENCES

[1] P. Saee, Z. Nafiseh, T. RezaM, K. Maryam, E. Shima, S. Nadia, & M. Sayyed. (2021). Edible coating and films as promising packaging: a mini review. Journal of Food Measurement and Characterization. 15. 10.1007/s11694-021-00979-7.

[2] K. Priya, N. Thirunavookarasu & D.V. Chidanand, (2023). Recent advances in edible coating of food products and its legislations: A review. Journal of Agriculture and Food Research. Volume 12 100623. ISSN 2666-1543. https://doi.org/10.1016/j.jafr.2023.100623.

[3] A.Steinbüchel & S. K.Rhee. (2005). Polysaccharides and polyamides in the food industry. Properties, production, and patents. ISBN: 978-3-527-31345-7.

[4] M. Mastromatteo, M. Mastromatteo, A. Conte, M. A. Del Nobile. (2010). Combined effect of active coating and MAP to prolong the shelf life of minimally processed kiwifruit (Actinidia deliciosa cv. Hayward). Food Research International. Vol. 44, pp. 1224-1230. https://doi.org/10.1016/j.foodres.2010.11.002.

[5] Burt, S., 2004. Essential oils: their antibacterial properties and potential applications in foods – a review. Int. J. Food Microbiol. 94, 223-253. https://doi.org/10.1016/j.ijfoodmicro.2004.03.022.

[6] Hanaa, A.R., Sallam, Y.I., El-Leitht, A.S., & Aly, S.E. 2012. Lemongrass (Cymbopogon citratus) essential oil as affected by drying methods. Ann. Agric. Sci. 57, 113-116. https://doi.org/10.1016/j.aoas.2012.08.004.

[7] B.Yousuf, A. K.Srivastava. (2017). Flaxseed gum in combination with lemongrass essential oil as an effective edible coating for ready-to-eat pomegranate arils. International Journal of Biology Macromolecules. Vol. 104, pp. 1030–1038. https://doi.org/10.1016/j.ijbiomac.2017.07.025.

[8] R.M. Raybaudi-Massilia, M.A. Rojas-Graü, Mosqueda-Melgar, J. Martín-Belloso, O. (2007). Edible alginate-based coating as carrier of antimicrobials to improve shelf-life and safety of fresh-cut melon. International Journal of Food Microbiology. Vol. 121 (3), pp. 313-327. https://doi.org/10.1016/j.ijfoodmicro.2007.11.010.

[9] R.M. Raybaudi-Massilia, M.A. Rojas-Graü, Mosqueda-Melgar, J. Martín-Belloso, O. (2008). Comparative Study on Essential Oils Incorporated into an Alginate-Based Edible Coating to Assure the Safety and Quality of Fresh-Cut Fuji Apples. Journal of Food Protection. Vol. 71 (6), pp.1150-1161. ISSN: 0362-028X. http://agris.fao.org/agris-search/search.do?recordID=US201300906814.

[10] N. Azarakhsh, A. Osman, H. M.Ghazali, C. P. Tan, & N. M.Adzahan. (2013). Lemongrass essential oil incorporated into alginate-based edible coating for shelf-life extension and

quality retention of fresh-cut pineapple. Postharvest Biology and Technology Vol. 88, pp. 1-7. https://doi.org/10.1016/j.postharvbio.2013.09.004.

[11] Draget, K.I., Smidsrod, O., & Skjak-Braek, G. 2005. Polysaccharides and polyamides in the food industry. Properties, production, and patents. 1-30.

[12] Xrite, Incorporated (2005). The Color Guide and Glossary. Retrieved from https://www.xritephoto.com/documents/literature/en/L11-029_color_guide_EN.pdf.

[13] Cofelice, M., Cuomo, F., & Lopez, F. (2018). Rheological Properties of Alginate–Essential Oil Nanodispersions. Colloids and Interfaces. Vol 2 (48). doi:10.3390/colloids2040048.

[14] Jalali-Heravi, M., Parastar, H., & Sereshti, H. (2010). Towards obtaining more information from gas chromatography-mass spectrometric data of essential oils: an overview of mean field independent component analysis. J. Chromatogr. A. 1217, 4850-4861.

[15] Abera, A. (2020). Extraction and physicochemical analysis of essential oils in lemongrass leaves grown in Arbaminch, Ethiopia. International Journal of Engineering Research and Technology (IJERT) ISSSN: 2278-0181. Vol. 9. Issue 10.

[16] Rojas–Grau M., Tapia M., & Martin–Belloso O. (2007). Using polysaccharide-based edible coating to maintain quality of fresh-cut Fuji apples. ScienceDirect. www.elseview.com.locate/lwt.

[17] Rojas–Grau M., Raybaudi–Massilia R., Soliva–Fortuny R., Avena–Bustillos R., McHugh T., Martin–Belloso O. (2007). Apple puree-alginate edible coating as carrier of antimicrobial agents to prolong shelf-life of fresh-cut apples. Postharvest Biology ang Technology. Vol. 45 Issue 2. pp. 254-264.

AI-GO03

Barrier Properties of PLA/ PBAT Films Incorporating Titanium Dioxide

Uruchaya Sonchaeng[1,3], Busarin Chongcharoenyanon[1,3], Piyawanee Jariyasakoolroj[1,3], Ubonrat Siripatrawan[2,3], and Panuwat Suppakul[1,3*]

[1]*Department of Packaging and Materials Technology, Kasetsart University, Bangkok, 10900, Thailand*
[2]*Department of Food Technology, Faculty of Science, Chulalongkorn University, Bangkok, 10330, Thailand*
[3]*Research Unit on Smart Packaging Technology for Foods, Kasetsart University Research and Development Institute (KURDI), Kasetsart University, Bangkok, 10900, Thailand*

***Correspondence to:** Panuwat Suppakul, Department of Packaging and Materials Technology, Kasetsart University, Bangkok, 10900, Thailand.*
E-mail: panuwat.s@ku.ac.th

ABSTRACT: Demand for biodegradable polymers, especially for those used as packaging materials, is growing with increasing environmental awareness around the world. Films from poly(lactic acid) (PLA), poly(butylene adipate-*co*-terephthalate) (PBAT), and PLA/PBAT blends are biodegradable. PLA/PBAT blend films have improved processability and mechanical properties over the based PLA or PBAT film. Our previous research demonstrated that incorporating titanium dioxide (TiO_2) 1 and 3 wt% improved visible light and ultraviolet (UV) shielding properties of PLA/PBAT blend films. Good UV-shielding and optical properties make PLA/PBAT/TiO_2 film a candidate for food packaging applications to extend shelf life of UV-sensitive products. However, adding TiO_2 can alter barrier properties of the base films and affect or limit the applications of the films. Therefore, this research aimed to investigate the barrier properties of the PLA/PBAT films and PLA/PBAT films incorporating TiO_2 1 and 3 wt%. The oxygen permeability (OP), water vapor permeability (WVP), and water contact angle (CA) of the films were measured. The results showed that by adding TiO_2 1 and 3 wt% to PLA/PBAT films, the OP (tested at 25°C and 0% RH, according to ASTM D3985) did not significantly differ from the OP of the base film, while the WVP (tested at 37.8°C and 90% RH according to ASTM F1249) slightly decreased. The OP values were in the range of 2.8E-18 to 3.5E-18 kg.m/(m^2.s.Pa) and the WVP values were in the range of 0.9E-14 to 1.2E-14 kg.m/(m^2.s.Pa). Adding TiO_2 1% to PLA/PBAT film slightly decreased the base film CA (tested at ambient conditions) from 81° to 75°. However, TiO_2 3% did not affect the CA of the film.

Keywords: Smart packaging, Barrier film, PLA, PBAT, titanium dioxide

INTRODUCTION

The increasing demand for sustainable packaging solutions has accelerated the development of biodegradable films as an alternative to traditional petroleum-based films. The commercially available poly(lactic acid) (PLA) and poly(butylene adipate-*co*-terephthalate) (PBAT) are alternatives to conventional non-biodegradable plastics. According to the European Bioplastics [1], the total global production capacities of bioplastics in 2021 were 2.42 million tons. Among them, PBAT had the highest production capacity (at 19.2%) and PLA came second (at 18.9%). Both PLA and PBAT are biodegradable polyesters, which means that they will turn into food sources for microorganisms under suitable environmental conditions [2,3]. Moreover, after their biodegradation, only natural and non-harmful residues remain [4]. In general, PLA is brittle and has poor toughness. PBAT, on the other hand, is ductile and flexible with low transparency. When PLA is combined with PBAT through a process such as blending, their properties can complement each other [5–7] and the PLA/PBAT product is still biodegradable [8,9]. Chemical structures of PLA and PBAT are shown in Figure 1.

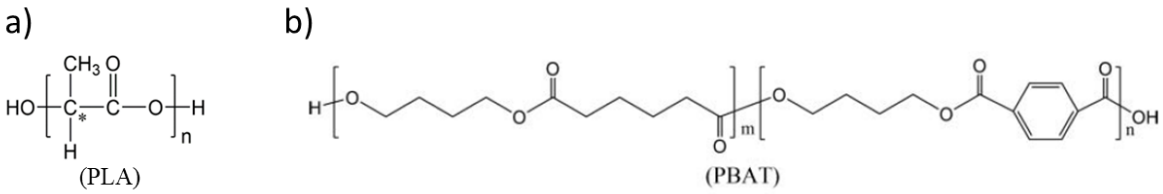

Figure 9. Chemical structures of a) poly(lactic acid) (PLA) and b) poly(butylene adipate-*co*-terephthalate) (PBAT) repeating units. * indicates a chiral carbon atom in PLA.

Our previous research[10] confirmed the ultraviolet (UV)-shielding properties of 85:15 (wt%) PLA/PBAT film incorporating inorganic compounds such as zinc oxide (ZnO) and titanium dioxide (TiO_2). The film incorporating TiO_2 was found to be more effective in UV-shielding than the film incorporating ZnO. Therefore, TiO_2 was chosen over ZnO for our study. However, more investigation on other properties of PLA/PBAT/TiO_2 was required to assess potential use as a packaging film. One of the major concerns for polymeric packaging is the barrier properties to gases and small molecules. In food packaging, the barrier properties can affect food safety and food quality. Thus, in this study, we aimed to evaluate the barrier properties of the PLA/PBAT/TiO_2 film with 1 wt% and 3 wt% of TiO_2.

MATERIALS AND METHODS

Materials

The PLA/PBAT blend was made using PLA Ingeo™ 4043D (NatureWorks LLC, Minnesota, USA) and PBAT Ecoflex® F Blend C1200 (BASF Corporation, Ludwigshafen, Germany) resins. The resins of PLA and PBAT were mixed in a Labtech Engineering twin-screw extruder (Labtech Engineering LTE, Samutprakarn, Thailand) with a fixed ratio of 85% PLA:15% PBAT by weight. The ratio of 85:15 was decided upon the previously reported optimum ratio for

PLA:PBAT blends [6,7]. Rutile TiO_2 micro particles (Chemipan Corporation Co., Ltd., Bangkok, Thailand) 1 and 3 wt % were added into the 85:15 PLA/PBAT blend. The mixed compounds were then pelletized and made into blown films with a Labtech Engineering LE-25-30/C single-screw extruder equipped with a Labtech Engineering LF-400 blown film unit. Blown film processing was based on the settings from our previous work [10], with extruder temperature range of 160–175 °C, annular die temperature of 160 °C, and nip-roll speed of 2.7 m/min. A digital hand-held micrometer (Hahn & Kolb, Stuttgart, Germany) was used for measuring film thickness. The average thickness of the samples was in the range of 0.048-0.054 mm. The film samples used in this study are summarized in Table 1.

Sample	PLA (%wt)	PBAT (%wt)	TiO_2 (%wt)
PLA/PBAT	85.00	15.00	-
PLA/PBAT/TiO_2 1 %	84.15	14.85	1.00
PLA/PBAT/TiO_2 3 %	82.45	14.55	3.00

Table 1. Blending ratios of the film samples

Methods

The measurements of barrier properties were performed at least in duplicate for each film sample.

Oxygen Barrier Measurement

The oxygen transmission rate (OTR) of each film was measured by an Oxygen Analyzer (Systech Illinois, Massachusetts, USA) as described by ASTM D3985 at 25°C and 0% relative humidity (RH). The oxygen permeability (OP) was calculated from (1):

$$OP = OTR \times \text{Film thickness} / (\text{Area} \times \Delta p_{\text{Oxygen}}) \quad (1)$$

where Δp_{Oxygen} is partial pressure difference of oxygen gas across the two sides of the test film, which was 1 atm in this study

Water Vapor Barrier Measurement

The water vapor transmission rate (WVTR) of each film was measured by a Permatran-W Model 398 (Mocon, Minnesota, USA) as described by ASTM F1249 at 37.8°C and 90% RH. The water vapor permeability (WVP) was calculated from (2):

$$WVP = WVTR \times \text{Film thickness} / (\text{Area} \times \Delta p_{\text{Water vapor}}) \quad (2)$$

where $\Delta p_{\text{Water vapor}}$ is partial pressure difference of water vapor across the two sides of the film, which was derived from the saturated water vapor pressure at the test conditions (i.e., temperature and relative humidity) in this study.

Contact Angle (CA) Measurement

CA of each film was determined using an optical contact angle goniometer (DataPhysics Instruments, Filderstadt, Germany) at ambient temperature. All measurements were preformed using the sessile drop method, used for the determination of hydrophobicity, and made with drops of 1 µL distilled water after about 15 s.

Statistical Analysis

Statistical analysis was conducted using SAS OnDemand for Academics software (SAS Institute Inc., North Carolina, USA).

RESULTS AND DISCUSSION

Oxygen and Water Vapor Permeabilities

The OP of the film samples is shown in Figures 2. The OP values were close to the reported OP[11] of low-density polyethylene (LDPE), slightly higher than OP of polystyrene (PS), and lower than OP of other commercial packaging films such as high-density polyethylene (HDPE) and polypropylene (PP). Adding TiO_2 did not significantly change the OP of the base PLA/PBAT film. While TiO_2 did not help to reduce the OP of the PLA/PBAT, it did not increase the OP. Improvement in oxygen barrier may be required for packaging of oxygen sensitive product. Adding montmorillonite to PLA/PBAT blend film was reported to reduce OP of the film [12].

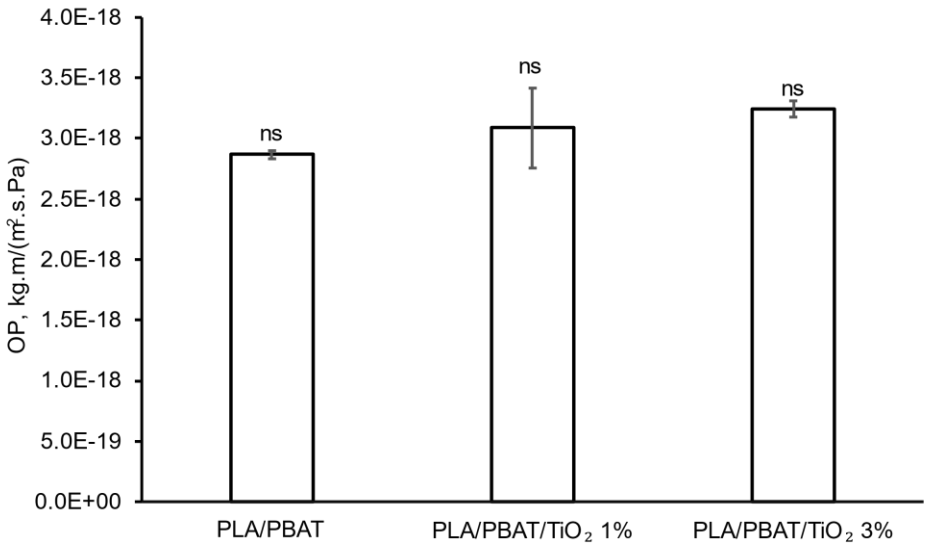

Figure 2. Oxygen permeability (OP) of the PLA/PBAT film and PLA/PBAT film incorporating TiO_2 %1 and 3%. The label "ns" indicates not significant difference (Tukey's HSD, $p < 0.05$).

The water vapor permeability (WVP) of the film samples is shown in Figure 3. The WVP values of the film samples are higher than the reported WVP[11] of most commercial packaging films such as LDPE, HDPE, PP, and PS. Adding TiO_2 1% and 3% to the PLA/PBAT reduced the WVP of the film by 17% and 18%, respectively. The incorporation of TiO_2 might create a more tortuous path for the water vapor molecules resulting in a lower diffusion rate. However, the WVP values of the PLA/PBAT/TiO_2 1% and PLA/PBAT/TiO_2 3% were not significantly different. The PLA/PBAT/TiO_2 film might not be a good choice for water vapor sensitive products but could be used for products that require moderate to high WVP such as fresh produce.

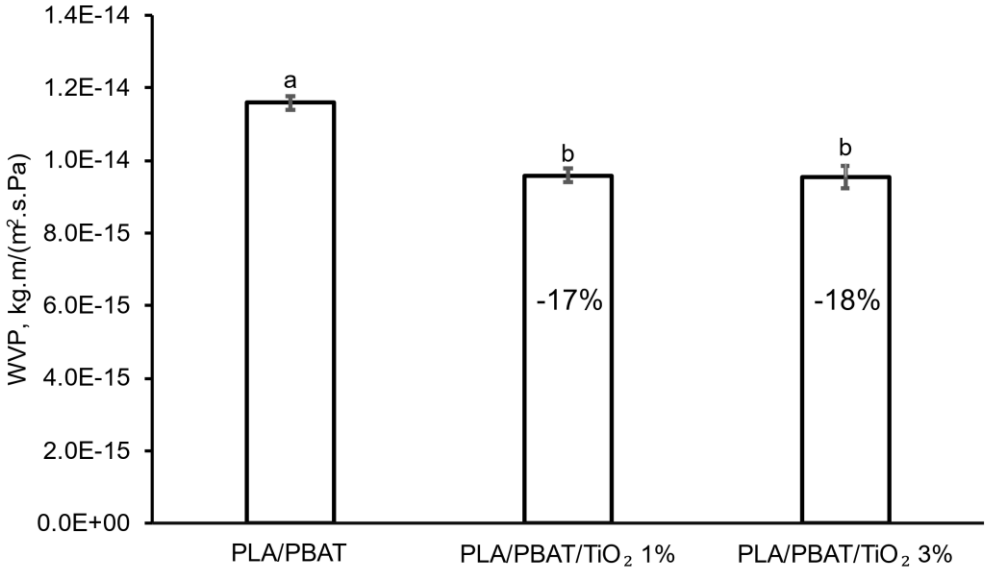

Figure 3. Water vapor permeability (WVP) of the PLA/PBAT film and PLA/PBAT film incorporating TiO_2 %1 and 3%. Different letter labels indicate significant differences between groups (Tukey's HSD, $p < 0.05$). Percentages shown are changes in WVP of PLA/PBAT/TiO_2 films compared to the PLA/PBAT film.

Surface Hydrophobicity

The CA results are shown in Table 2. The result for PLA/PBAT is close to the reported CA of neat PLA film at 81° [13], but different from the reported CA values of PLA/PBAT at 67.5° [14] and 74.3° [15]. The difference could be due to different blend ratios and film processing methods. Incorporation of TiO_2 1% into PLA/PBAT film slightly decreased the base film CA. The smaller CA, which implied that the surface tension of PLA/PBAT/TiO_2 1% was higher than that of PLA/PBAT and PLA/PBAT/TiO_2 3%. The low CA (i.e., < 90°) for the PLA/PBAT and PLA/PBAT/TiO_2 films indicated high surface wetting and low hydrophobicity. TiO_2 nanoparticle was reported to increase hydrophobicity of cassava starch-based biodegradable film [16]. However, the effect of TiO_2 on the CA of PLA/PBAT in this study is still unclear. Further investigations such as on morphology of the blend film might help to clarify the results.

Samples	Water contact angle (°) *	Representative images
PLA/PBAT	81.28±1.45 [a]	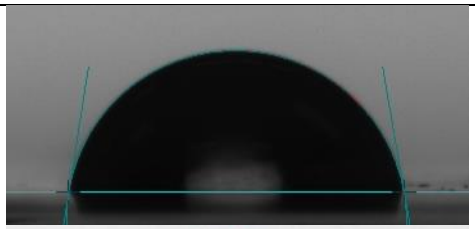
PLA/PBAT/TiO_2 1%	74.59±1.52 [b]	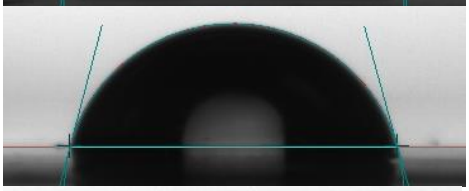
PLA/PBAT/TiO_2 3%	79.21±2.68 [a]	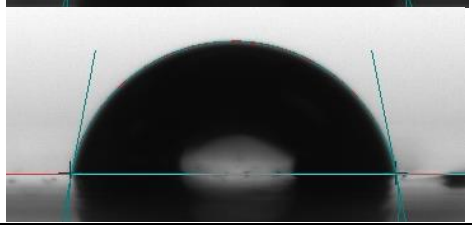

* Values shown as mean ± standard deviation. Different superscript letters indicate significant differences between groups (Tukey's HSD, $p < 0.05$).

Table 2. Contact angle results of the PLA/PBAT film and PLA/PBAT film incorporating TiO_2 %1 and 3%.

CONCLUSION AND REMARKS

TiO_2 1 wt% and 3 wt% were added to 85:15 PLA/PBAT blend film to improve the film's UV-shielding properties. The WVP of the PLA/PBAT film decreased up to 18% when TiO_2 was incorporated into the film. However, the OP of the PLA/PBAT film was not affected by TiO_2. The CA decreased when adding TiO_2 1% to the PLA/PBAT film, but the CA was not different when adding TiO_2 3%. Overall, incorporating TiO_2 contributed to improved UV-shielding properties without compromising barrier properties of the base PLA/PBAT film. Further investigation on morphology of the film samples might contribute to better understanding of the film properties.

ACKNOWLEDGEMENT

This research was supported by Kasetsart University Research and Development Institute (KURDI) FF(KU) 25.64.

REFERENCES

[1] European Bioplastics. Bioplastic market development update 2021. Press Release. https://www.european-bioplastics.org/global-bioplastics-production-will-more-than-triple-within-the-next-five-years/. Published 2021. Accessed September 26, 2022.

[2] Deshoulles Q, Gall M Le, Benali S, et al. Hydrolytic degradation of biodegradable poly(butylene adipate-co-terephthalate) (PBAT) - Towards an understanding of microplastics fragmentation. *Polym Degrad Stab*. 2022;205(August):110122. 10.1016/j.polymdegradstab.2022.110122

[3] Iñiguez-Franco F, Auras R, Burgess G, et al. Concurrent solvent induced crystallization and hydrolytic degradation of PLA by water-ethanol solutions. *Polymer (Guildf)*. 2016;99:315-323. 10.1016/j.polymer.2016.07.018

[4] Folino A, Karageorgiou A, Calabrò PS, Komilis D. Biodegradation of Wasted Bioplastics in Natural and Industrial Environments: A Review. *Sustainability*. 2020;12(15):6030. 10.3390/su12156030

[5] Farsetti S, Cioni B, Lazzeri A. Physico-Mechanical Properties of Biodegradable Rubber Toughened Polymers. *Macromol Symp*. 2011;301(1):82-89. 10.1002/masy.201150311

[6] Deng Y, Yu C, Wongwiwattana P, Thomas NL. Optimising Ductility of Poly(Lactic Acid)/Poly(Butylene Adipate-co-Terephthalate) Blends Through Co-continuous Phase Morphology. *J Polym Environ*. 2018;26(9):3802-3816. 10.1007/s10924-018-1256-x

[7] Teamsinsungvon A, Ruksakulpiwat Y, Jarukumjorn K. Mechanical and morphological properties of poly (lactic acid)/poly (butylene adipate-co-terephthalate)/calcium carbonate composite. *ICCM Int Conf Compos Mater*. 2011:1-5.

[8] Hamad K, Kaseem M, Ayyoob M, Joo J, Deri F. Polylactic acid blends: The future of green, light and tough. *Prog Polym Sci*. 2018;85:83-127. 10.1016/j.progpolymsci.2018.07.001

[9] Ma P, Cai X, Zhang Y, et al. In-situ compatibilization of poly(lactic acid) and poly(butylene adipate-co-terephthalate) blends by using dicumyl peroxide as a free-radical initiator. *Polym Degrad Stab*. 2014;102:145-151. 10.1016/j.polymdegradstab.2014.01.025

[10] Sonchaeng U, Chongcharoenyanon B, Jariyasakoolroj P, Siripatrawan U, Suppakul P. UV-shielding Properties of Poly(lactic acid) (PLA)/Poly(butylene adipate-co-terephthalate) (PBAT) Films Incorporating Metal Oxides. In: *The 23rd IAPRI World Conference on Packaging*. Thailand Institute of Scientific and Technological Research; 2022:60-67. https://www.iapribangkok.com/conferenceproceedings.

[11] Selke SEM, Culter JD. Mass Transfer in Polymeric Packaging Systems: Sorption, Diffusion, Permeation, and Shelf Life. In: *Plastics Packaging*. München: Carl Hanser Verlag GmbH & Co. KG; 2016:353-393. 10.3139/9783446437197.014

[12] Ludwiczak J, Frąckowiak S, Leluk K. Study of Thermal, Mechanical and Barrier Properties of Biodegradable PLA/PBAT Films with Highly Oriented MMT. *Materials (Basel)*. 2021;14(23):7189. 10.3390/ma14237189

[13] Lizundia E, Ruiz-Rubio L, Vilas JL, León LM. Poly(<scp>l</scp> -lactide)/ZnO nanocomposites as efficient UV-shielding coatings for packaging applications. *J Appl Polym Sci*. 2016;133(2):42426. 10.1002/app.42426

[14] Kim H-J, Lee C-L, Yoon K-S, Rhim J-W. Synergistic effect of UV-C LED irradiation

and PLA/PBAT-based antimicrobial packaging film on fresh-cut vegetables. *Food Control*. 2022;138(April):109027. 10.1016/j.foodcont.2022.109027

[15] Shankar S, Rhim J-W. Preparation of antibacterial poly(lactide)/poly(butylene adipate-co-terephthalate) composite films incorporated with grapefruit seed extract. *Int J Biol Macromol*. 2018;120:846-852. 10.1016/j.ijbiomac.2018.09.004

[16] Iacovone C, Yulita F, Cerini D, et al. Effect of TiO2 Nanoparticles and Extrusion Process on the Physicochemical Properties of Biodegradable and Active Cassava Starch Nanocomposites. *Polymers (Basel)*. 2023;15(3):535. 10.3390/polym15030535

AI-GO04

Centrifugal fiber spinning to fabricate polyhydroxyalkanoate/zinc oxide nanocomposite films: structure-property analysis

Chris Vanheusden[1]*, Jan Vanminsel[1], Pieter Samyn[2], Naveen Reddy[1], Anitha Ethirajan[3], Roos Peeters[1], Mieke Buntinx[1]

[1]Materials and Packaging Research & Services, Institute for Materials Research (IMO-IMOMEC), Hasselt University, Wetenschapspark 27, 3590 Diepenbeek, Belgium
[2]SIRRIS, Department Circular Economy and Renewable Materials, Gaston Geenslaan 8, 3001 Leuven, Belgium
[3]Nano-Biophysics and Soft Matter Interfaces (NSI) Group, Institute for Materials Research (IMO-IMOMEC), Hasselt University, Wetenschapspark 1, 3590 Diepenbeek, Belgium

***Correspondence to**: Chris Vanheusden. [1]Materials and Packaging Research & Services, Institute for Materials Research (IMO-IMOMEC), Hasselt University, Wetenschapspark 27, 3590 Diepenbeek, Belgium*
E-mail: chris.vanheusden@uhasselt.be

ABSTRACT: Polyhydroxyalkanoates (PHAs) show great potential as packaging materials due to t heir bio-based and biodegradable nature. The copolymer poly(3-hydroxybutyrate-co-3-hydroxyhexanoate) (PHBHHx) is very promising because of its flexibility and intermediate barrier properties. However, novel processing techniques and development of PHBHHx as active packaging material remain relatively unexplored. Adding zinc oxide (ZnO) nanoparticles (NPs) to the polymer matrix is a known approach to introduce functional properties, such as UV barrier and antimicrobial activity, but optimal dispersion of the nanoparticles remains precarious. Therefore, we aim to incorporate ZnO NPs into PHBHHx fibers via centrifugal fiber spinning (CFS) and subsequently deposit the fiber mats on top of PHBHHx film substrates. First, centrifugal fiber spinning of PHBHHx fibers was optimized before ZnO NPs were added to the chloroform dispersions under controlled conditions (4000 rpm, 0.6 mm nozzle diameter). The average PHBHHx fiber diameter (ø=0.50-4.62 µm) and morphology (from beads-on-a-string to continuous) are mainly dependent on the concentration and rheology of the respective solutions (4-12 wt. % PHBHHx). Based on thorough physical, thermal and chemical characterization, 10 wt. % PHBHHx (ø=3.58 µm) was chosen to fabricate nanocomposite fibers. The PHBHHx/ZnO fibers show a predominantly continuous morphology with decreasing diameter (ø=3.50-2.99 µm) and some bead formation upon addition of ZnO (1-10 wt.%), though no chemical interactions were observed. Subsequently, fiber mats were deposited as 10-20 µm continuous layers onto 160 µm-tick PHBHHx substrates by post-process annealing at 160°C in a hot press. The films show good ZnO dispersion quality, they effectively block UVC, UVB, and a major part of the UVA wavelength region, and show suitable hydrophobicity for packaging of food products (water contact angles above 95°). We

conclude that this novel incorporation method of ZnO NPs in PHBHHx is a promising approach for the development of packaging films with an active top layer.

Keywords: poly(3-hydroxybutyrate-co-3-hydroxyhexanoate), PHBHHx, zinc oxide, ZnO, centrifugal fiber spinning, nanocomposites, active layer

INTRODUCTION

Plastic packaging has the advantage of being low-cost, lightweight, flexible and efficient to process, while providing protection against several environmental factors. Contemporary packaging materials can provide barriers to gases, protect food from UV light or more passively increase food quality and shelf life by maintaining the desired atmosphere around the product [1]. However, in 2020, food waste in the EU was still measured to be around 59 million tons of fresh mass, with a 53% share for household food waste [2]. In addition, the widely used traditional oil-based plastics such as polyethylene (PE), polypropylene (PP) or polystyrene (PS) are accumulating in soils, waters, coastlines and the human body, with geophysical and biological impacts as a result [3].

Due to this increasing plastic pollution and the depletion of fossil-fuels, bioplastics have gained significant attention as replacement for conventional plastics. Among bioplastics, polyhydroxy-alkanoates (PHAs) have emerged as scalable solutions with production possibilities from various biomass substrates, including waste streams [4]. Biobased and biodegradable PHAs also show great promise for (food) packaging applications [5]. The copolymer poly(3-hydroxybutyrate-co-3-hydroxyhexanoate) (PHBHHx) is very promising because of its increased flexibility [6] and intermediate barrier properties, compared to the more stiff and brittle poly(3-hydroxybutyrate) (PHB) and poly(3-hydroxybutyrate-co-3-hydroxyvalerate) (PHBV). Having medium oxygen barrier, slow crystallization rate, relatively low strength and poor heat resistance, PHBHHx needs to be further functionalized to broaden its application in packaging areas. In addition, more studies regarding PHA-based (multilayer) films and active packaging, using innovative processing techniques are required [7].

PHAs can be functionalized into (active) packaging films with superior properties by incorporating fillers like zinc oxide (ZnO) nanoparticles (NPs). ZnO NPs are commonly used in a variety of applications (including packaging) due to their low cost, relative safe nature [8], UV and antimicrobial characteristics [9], [10]. Previous studies have shown that the incorporation of inorganic nanoparticles like ZnO by extrusion or solvent casting techniques in PHB [11], PHBV [12], [13] and PHBHHx [14], [15] can increase the mechanical, thermal and crystallization properties, while adding functionalities like oxygen barrier, UV resistance and antimicrobial properties. However, current challenges associated with the production of these nanocomposites are to obtain a uniform ZnO NP dispersion quality and to select and develop efficient processing techniques to regulate the level of ZnO NP dispersion [16].

For these reasons, the innovative centrifugal fiber spinning (CFS) technique shows promise to develop high-quality ZnO nanocomposite fibers as previously shown for PHB and PLA [17], [18]. In addition, the post-processing of these fibers into films or multi-layer structures has shown promise [19]–[21]. Therefore, the aims of this study are (i) to incorporate

ZnO NPs in PHBHHx with good dispersion quality using the CFS technique and to study the fiber morphology and (ii) to assess the feasibility of post-processing these nanocomposite fibers as an active top-layer for packaging applications.

MATERIALS AND METHODS

Materials

PHBHHx pellets under trade name KANEKA Biodegradable Polymer Green Planet™ (10.5 mol% 3HHx and M_w=3.3 × 10^5 g/mol) were kindly provided by Kaneka (Westerlo-Oevel, Belgium). Rod-like ZnO NP powder (Tenray Z2P) with a diameter of ~10-30 nm and length of ~100 nm was supplied by EverCare (Eijsden, The Netherlands). The Tenray Z2P was subjected to silane surface treatment with respectively triethoxy caprylyl silane (TEOS) (± 4%). Chloroform ($CHCl_3$, AnalaR NORMAPUR) was purchased from VWR Chemicals (Leuven, Belgium) and was used without further purification.

Centrifugal fiber spinning

PHBHHx solutions were prepared by dissolving PHBHHx in chloroform (2-14 wt.%) by stirring for 1h at 55°C in sealed glass vials until all polymer dissolved. The PHBHHx/ZnO solutions were prepared by dispersing ZnO NPs in chloroform in sealed glass vials and sonicating for 30 min in a water bath before PHBHHx was added and stirred for 1h at 55°C until all polymer dissolved. The solution was then sonicated again for 30 min. ZnO NPs were added in ratios of 1-10 wt.% (relative to PHBHHx) and the solid content of the dispersions (PHBHHx + ZnO NPs) was 10 wt.%. All the solutions were cooled to room temperature prior to spinning. A custom-built CFS setup with an aluminum arm-style spinneret and two aluminum nozzles [19], [22], [23] was used to produce PHBHHx/ZnO nanocomposite fibers. The fibers were spun at a spinneret speed of 4000 rpm, with a nozzle diameter of 0.6 mm and a collector distance of ± 10-12 cm. The solutions were added via a syringe pump to the center of the rotating spinneret to ensure a continuous liquid flow. CFS experiments were done at room temperature under a fume hood. After CFS, fibers were collected using a homemade fork for analysis and further processing.

Fabrication of top-layer films

Centrifugally spun PHBHHx and PHBHHx/ZnO fiber mats were annealed onto PHBHHx substrates in order to fabricate continuous top-layer films. An overview of the production process is shown in Figure 1. First, PHBHHx substrate films (10 cm × 10 cm) of ±160–170 µm thickness were fabricated via compression molding using a hot-press PCH-600DG (Henan Chuanghe Laboratory Equipment Co. Ltd., Zhengzhou, China). PHBHHx pellets were dried for ±3 days at 65 °C and approximately 2.1 g was placed in a stainless-steel mold, sandwiched between Teflon sheets and aluminum plates. The pellets were preheated for 4 min at 145 °C

without pressure, followed by pressure cycles of 3 and 15 MPa at 145 °C (both for 2 min) and water cooling for 10 min at 5 MPa pressure.

Secondly, small amounts of centrifugally spun PHBHHx and PHBHHx/ZnO fiber mats (±0.01–0.03 g) were placed onto PHBHHx film substrates (cut to ±2.5 cm × 2.5 cm) and both materials were dried at 65 °C for 24 h in an opened petri-dish. The thin fiber layers were then attached to the virgin substrates by annealing in the hot press for 6 min at 160 °C (upper plate) and 40 °C (lower plate) without pressure [19]. The resulting films were cooled to room temperature. The top-layer films are further denoted in this study as 'substrate//top-layer', e.g. PHBHHx//PHBHHx and PHBHHx//PHBHHx/ZnO.

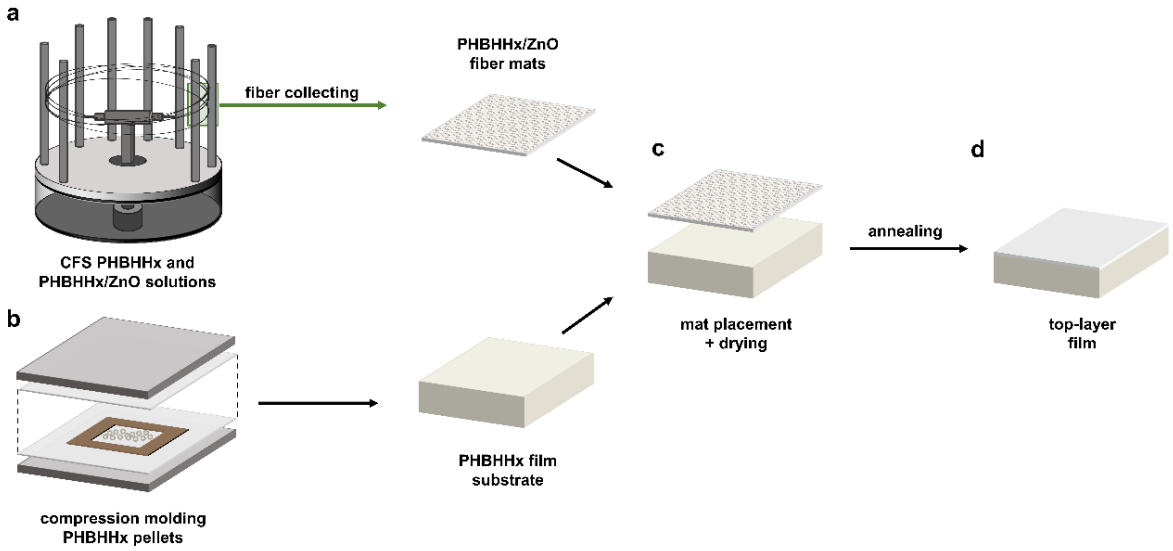

Figure 10. Schematic overview of top-layer film production. (a) centrifugal fiber spinning of PHBHHx and PHBHHx/ZnO solutions into fiber mats, (b) compression molding of PHBHHx pellets into substrate films, (c) placement of spun fiber mats onto substrate and (d) formation of top-layer films after the annealing process.

Characterization of fibers and films

Scanning Electron Microscopy (SEM)

The morphology of the fibers and films was analyzed via SEM images acquired using a Zeiss 450 FEGSEM with Gemini 2 optics (ZEISS, Zaventem, Belgium) at 10 kV under high vacuum. The fibers and films were sputtered with a thin layer of gold-palladium before analysis to reduce charging. The distribution in fiber diameters was measured from SEM images using ImageJ software (Maryland, United States). At least 132 fibers were measured for PHBHHx and PHBHHx/ZnO samples and evenly divided over two to four SEM images.

Fourier transform infrared spectroscopy (FTIR)

The chemical composition of PHBHHx and ZnO-PHBHHx interactions were analyzed by attenuated total reflectance Fourier transform infrared spectroscopy (ATR-FTIR) using a Vertex 70 instrument (Bruker, Massachusetts, United States).

UV-VIS spectrophotometry

The UV barrier properties of the PHBHHx/ZnO deposition systems were determined with a Carry 5000 UV/VIS/NIR spectrophotometer (Agilent Technologies, Santa Clara, USA). The UV/VIS spectra were recorded in the wavelength range of 200-800 nm and expressed as a percentage of transmission. Air was used as the blank reference.

Contact angle measurements (CAM)

Water contact angle measurements (Sessile drops) were performed with a DataPhysics instrument (Filderstadt, Germany) and SCA 20 software. Distilled water was used as the testing liquid and deposited as 0.5 µl droplets on the PHBHHx, PHBHHx//PHBHHx and PHBHHx//PHBHHx/ZnO top-layer films using a Hamilton syringe and software-controlled dosing system. The contact angle at time zero was obtained by extrapolating the linear part of the contact angle versus time curve by linear regression. The contact angles are reported as the average of 10 measurements at different locations on the sample.

RESULTS AND DISCUSSION

PHBHHx and PHBHHx/ZnO fiber morphology

The CFS process of PHBHHx was investigated thoroughly [19], in order to acquire effective process conditions (polymer concentration, rotational speed, collector distance etc.) to develop continuous fibers with minimal defects (e.g. beads). The polymer concentration was identified as the main parameter, influencing fiber diameter and fiber morphology. The fiber diameter distributions of centrifugally spun PHBHHx fibers are shown in Figure 2a. The average fiber diameter increases with polymer concentration, from 0.50 ± 0.37 µm at 4 wt.% to 4.62 ± 1.84 µm at 12 wt.%. The increased solution viscosity at higher PHBHHx concentrations (10-12 wt.%) prevents the elongation of the polymer jet, resulting in larger fiber diameters [19]. In addition, the rise in viscosity with increasing polymer concentration also changes the fiber morphology from beaded and beads-on-a-string (4 wt.% PHBHHx) to continuous (12 wt.% PHBHHx), as shown in Figure 3. The visco-elastic forces are sufficient to counteract capillary breakup of the polymer jet, forming more continuous fibers. These results suggest that a polymer concentration of around 10 wt.% is effective to form smooth and continuous fibers and is applicable to the development of PHBHHx/ZnO nanocomposite fibers.

Based on these data, PHBHHx/ZnO solutions with a solid content (PHBHHx + ZnO) of 10 wt.% and different ZnO loadings (1-10 wt.%) were centrifugally spun into fibers. This

study mainly focuses on the use of silanized (TEOS) ZnO NPs, because they showed increased dispersion quality and polymer compatibility in previous studies [24], [25]. The diameter distributions of PHBHHx/ZnO fibers are shown in Figure 2b. The fiber diameter decreases upon ZnO loading and ranges between 3.50 ± 1.69 µm at 1 wt.% ZnO and 2.20 ± 1.03 µm at 5 wt.% ZnO. The decrease in fiber diameter is mainly attributed to the slight decrease in polymer concentration (solid content calculation). The diameter of the PHBHHx/ZnO fibers is situated between those of 8 and 10 wt.% PHBHHx fibers, respectively 1.61 and 3.58 µm. A rather continuous fiber morphology is formed at all ZnO loadings, but bead formation slightly increases at higher loadings as shown in Figure 4.

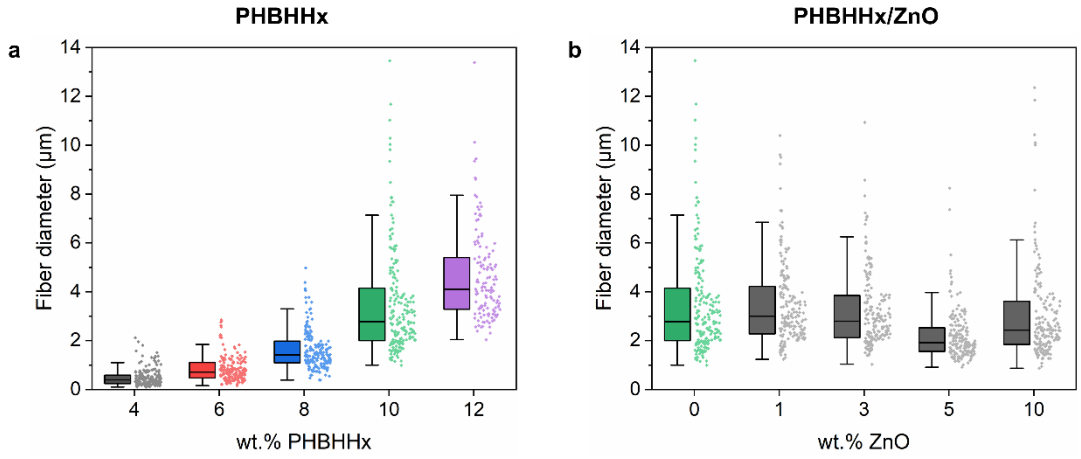

Figure 11. Diameter distributions of (a) PHBHHx fibers spun with different polymer concentrations (4-12 wt.%) [19] and (b) PHBHHx/ZnO fibers with a solid content (PHBHHx + ZnO) of 10 wt.% with different ZnO loadings (1-10 wt.%). The box is determined by the 25th and 75th percentiles together with the median fiber diameter (horizontal solid line).

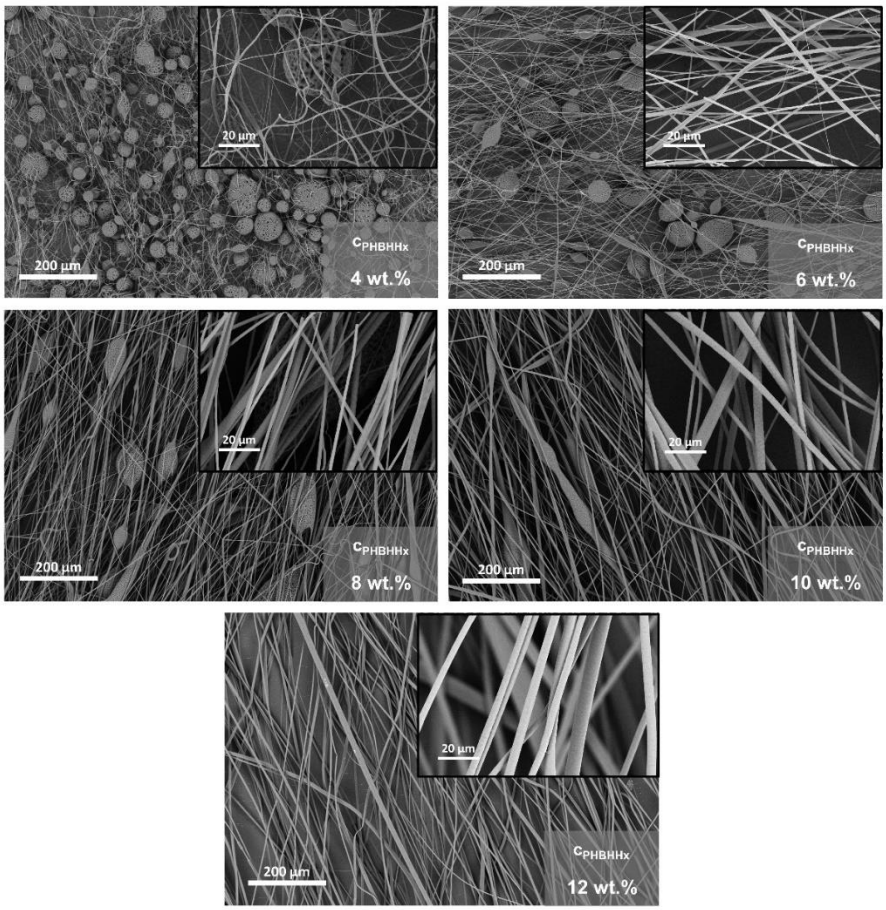

Figure 12. SEM images showing the fiber morphology of PHBHHx fibers spun from 4, 6, 8, 10 and 12 wt.% solutions [19].

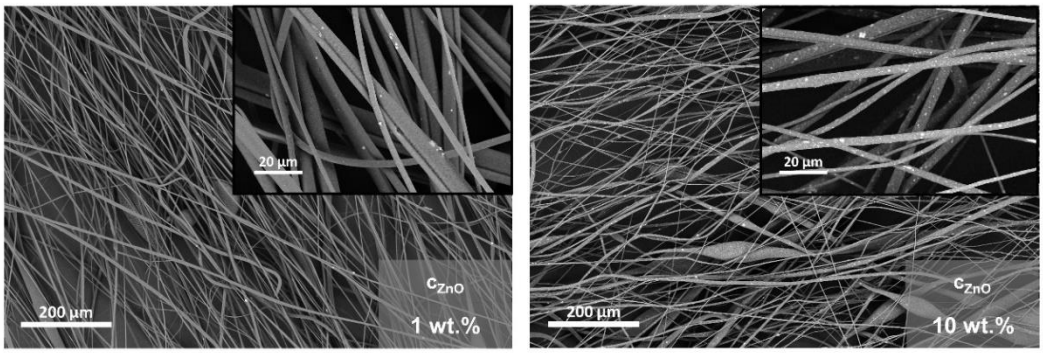

Figure 4. SEM images showing fiber morphology and ZnO dispersion of PHBHHx/ZnO fibers with 1 and 10 wt.% ZnO loading, spun from 10 wt.% ZnO + polymer solutions.

PHBHHx/ZnO interactions

The final properties of centrifugally spun fibers are determined by several factors such as the diameter, morphology (continuous vs. beads), porosity etc. For nanocomposite fibers, the surface treatment of the nanoparticles can influence the interaction with the polymer matrix and the final fiber properties (e.g. mechanical, thermal and antimicrobial properties). Therefore, the interactions between ZnO and PHBHHx (spun from 10 wt.% (PHBHHx + ZnO) solutions) were investigated with FTIR. The FTIR spectra of 10 wt.% PHBHHx fibers and PHBHHx/ZnO nanocomposite fibers with 5 wt.% ZnO are shown in Figure 5. The FTIR spectrum of PHBHHx (Figure 5a) is clearly characterized by an ester function (C=O) at 1720 cm^{-1} [26], [27]. The observed peaks at 1130 cm^{-1}, 1178 cm^{-1}, 1226 cm^{-1}, 1379 cm^{-1} and 1453 cm^{-1} arise from C-O-C symmetric stretching, C-O-C asymmetric stretching, conformational band of helical chains, CH_3 symmetric wagging, and CH_3 asymmetric bending respectively [26], [27]. Figure 5b confirms that the ZnO NPs are incorporated in the PHBHHx matrix, because the absorbance intensity at wavelengths of 400-500 cm^{-1} (ZnO-stretching) is higher than that of neat PHBHHx. Figure 5b also shows that no matrix-filler interactions (hydrogen bonding) occur between ZnO and the PHBHHx matrix, because no shift occurs in the peak at 1720 cm^{-1}. A lowering of the C=O stretching band by approximately 10 to 30 cm^{-1}, can be indicative of hydrogen bonding between the available hydroxyl groups of ZnO and PHAs, as previously shown for PHB [11], PHBV [13] and PHBHHx [14]. Further research should include the investigation of other ZnO surface functionalization on interaction effects and fiber properties.

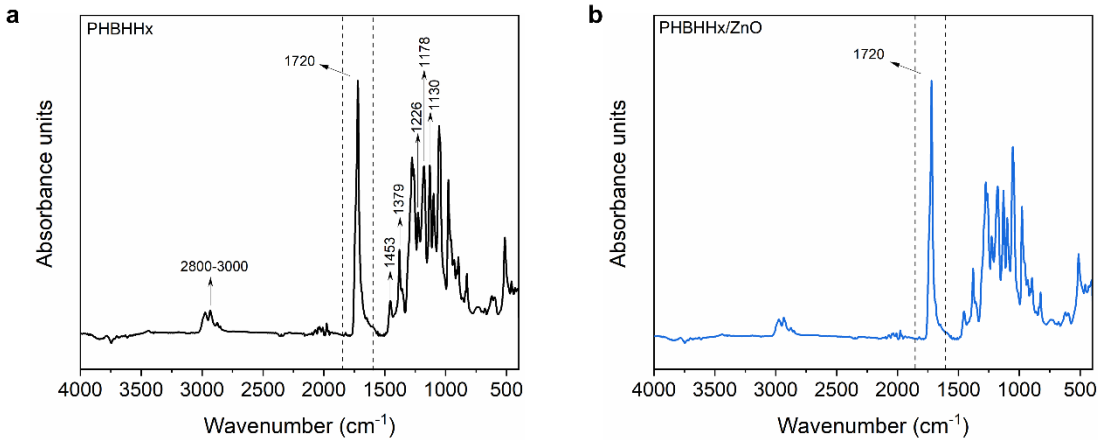

Figure 5. (a) FTIR spectrum of PHBHHx fibers (spun from 10 wt.% solutions) and (b) comparison with 5 wt.% PHBHHx/ZnO nanocomposites fibers, showing no matrix-filler interaction.

PHBHHx and PHBHHx/ZnO top-layer film morphology

The main objective of this study is to assess the feasibility of developing well dispersed PHBHHx// PHBHHx/ZnO nanocomposite films via the CFS technique. Therefore,

centrifugally spun PHBHHx and PHBHHx/ZnO fiber mats were collected and subsequently deposited onto virgin PHBHHx film substrates (S) as top-layers (TL) of 10-20 µm by annealing in a hot press at 160°C without pressure for 6 min to form continuous layers, based on our previous research [19]. Figure 6 shows cross-sectional SEM images of the surface depositions for PHBHHx (Figure 6a-b) and PHBHHx/ZnO fibers (Figure 6c-d). It is apparent that the ZnO NPs are homogeneously dispersed in the top-layer. The ZnO NPs are contained in the top-layer, indicating that no ZnO NPs are transferred from the fiber mat to the substrate by possible melting effects. Some smaller aggregates can be discerned in the top-layer.

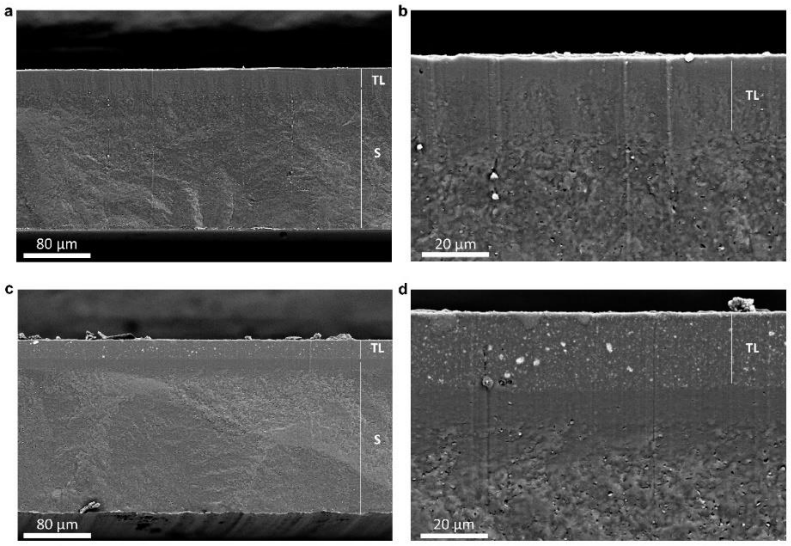

Figure 6. Cross-sectional SEM images of a PHBHHx//PHBHHx fiber deposition film (a-b) [19] and a PHBHHx// PHBHHx/ZnO (5 wt.% ZnO) fiber deposition film (c-d), showing the substrate (S) and the top-layer (TL) with and without ZnO incorporation.

Functional properties of PHBHHx/ZnO top-layer films

UV-barrier properties of PHBHHx/ZnO top-layer films

UV/VIS measurements were performed to study the UV barrier effect of the deposited PHBHHx/ZnO fibers. The UV/VIS transmission spectra of the PHBHHx substrate, PHBHHx//PHBHHx and PHBHHx//PHBHHx/ZnO top-layer films are shown in Figure 7. These results show that the PHBHHx/ZnO top-layers can effectively act as a UV barrier. Similar UV barrier effects were also observed for ZnO NP ultrasonic spray-coated PHBHHx [28]. The UV barrier effect of ZnO NPs can be explained by the combination of bandgap absorption and light scattering [29].

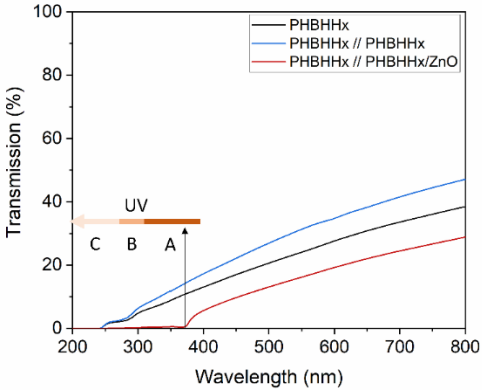

Figure 7. UV/VIS spectra of the PHBHHx film substrate, PHBHHx//PHBHHx and PHBHHx//PHBHHx/ZnO (5 wt.% ZnO) top-layer films.

Wettability properties of PHBHHx/ZnO top-layer films

The wettability properties of the top-layer films are important for application as (food) packaging materials, because hydrophobicity can prevent fouling and contamination of food packages while ensuring the convenient sliding of food [30]. Therefore, water contact angle measurements were performed to determine the hydrophobicity of the top-layer films. The results of the CAM are shown in Table 1. The PHBHHx substrate and top-layer films exhibit similar contact angles (>90°), indicating a hydrophobic nature (low wettability) [31]. The PHBHHx//PHBHHx/ZnO (5 wt.% ZnO) film shows a slightly larger contact angle of approximately 103°, which could be attributed to the more hydrophobic ZnO NPs (silane surface functionalization) that are present on the sample surface.

Sample	**Contact angle (°)**
PHBHHx substrate	98.1 ± 5.1
PHBHHx // PHBHHx	97.7 ± 3.3
PHBHHx // PHBHHx/ZnO	103.0 ± 2.3
Other biomaterials	
PBS	84.2[a]
PLA	80.0 [a]
PLA/PBAT blend	102.2 [a]
PHBV/PBAT/mineral filler blend	95.2 [a]
PBS/PBSA blend	104.6 [a]
Starch/PBAT blend	105.0 [a]
PHBV	78.2-85.6 [b]
PHB/PHBV nanocellulose coated	75-85 [c]
Conventional plastics	
PP	104.9 [e]
PET	66.3-91.3 [d, e]

Water contact angles retrieved from [a] [32], [b] [12], [c] [33], [d] [34], [e] [35]

Table 3. Water contact angles of the PHBHHx film substrate, PHBHHx//PHBHHx and PHBHHx/ZnO (5 wt.% ZnO) top-layer films (n = 10, ± 1 SD). Indicative water contact angles of other (commercial) biomaterials and conventional plastics are included for comparative purposes.

A comparison of the reported contact angles with biomaterials and conventional food packaging plastics is shown in Table 1. The water contact angles of the PHBHHx substrate and top-layer films are in line with, but rather on the higher end compared to the other reported materials. Based on these results and comparison with available literature, the PHBHHx//PHBHHx and PHBHHx//PHBHHx/ZnO top-layer films seem suitable for use as (food) packaging applications.

CONCLUSIONS

This study shows the development of PHBHHx and PHBHHx/ZnO fibers via the novel centrifugal fiber spinning (CFS) technique. We show that the polymer concentration of the spinning solutions changes the fiber morphology from a beaded to a continuous morphology, with an increase of the fiber diameter from 0.50 to 4.62 µm (4-12 wt.% PHBHHx). The incorporation of ZnO NPs (1-10 wt.%) into PHBHHx results in fibers with diameters in the range of 3.50 µm (1 wt.% ZnO) and 2.20 µm (5 wt.% ZnO), with a slight increase of bead formation. No interactions between the ZnO NPs and the PHBHHx matrix were detected.

As application potential, we successfully attached the developed PHBHHx and PHBHHx/ZnO fiber mats to PHBHHx substrates as ~10-20 µm top-layers by an annealing process. The ZnO top-layer films show effective UV blocking and hydrophobic properties for use as packaging material.

Future research will investigate the influence of solution rheology on the fiber morphology in combination with thermal, crystallization and mechanical properties of the nanocomposite fibers. In addition, the influence of ZnO type on structure and end-properties (UV barrier and antimicrobial effects) will be investigated.

ACKNOWLEDGEMENTS

The authors acknowledge Prof. Louis Pitet (Advanced Functional Polymers, IMO-IMOMEC, UHasselt) for use of the hot-press equipment, Prof. Wouter Marchal (Analytical and Circular Chemistry, IMO-IMOMEC, UHasselt) for access to FTIR and Prof. Jan D'Haen (Analytical & Microscopical Services, IMO-IMOMEC, UHasselt) for access to SEM. This research was funded by the Special Research Fund (BOF) of Hasselt University, grant number BOF20DOC06.

REFERENCES

[1] SJ Risch, "Food Packaging History and Innovations," *J. Agric. Food Chem.*, 57, 18, 8089–8092, 2009.

[2] "Food waste and food waste prevention - estimates." Eurostat. Accessed: Apr. 23, 2023. [Online]. Available: https://ec.europa.eu/eurostat/statistics-explained/index.php?title=Food_waste_and_food_waste_prevention _-_estimates

[3] M MacLeod, HPH Arp, MB Tekman and A Jahnke, "The global threat from plastic pollution," *Science*, 373, 6550, 61–65, 2021.

[4] NI Ibrahim, FS Shahar, MTH Sultan, AUM Shah, SNA Safri, and MH Mat Yazik, "Overview of Bioplastic Introduction and Its Applications in Product Packaging," *Coatings*, 11, 11, 1423, 2021.
[5] P. Ragaert, M. Buntinx, *et al.*, "Polyhydroxyalkanoates for Food Packaging Applications," in *Reference Module in Food Science*, Amsterdam: Elsevier, 2019. doi: 10.1016/B978-0-08-100596-5.22502-X.
[6] Vanheusden C, Samyn P, Goderis B, Hamid M, Reddy N, Ethirajan A, Peeters R, Buntinx M, "Extrusion and Injection Molding of (PHBHHx): Influence of Processing Conditions on Mechanical Properties and Microstructure," *Polymers*, 13, 22, 4012, 2021, doi: 10.3390/polym13224012.
[7] AZ Naser, I Deiab, and BM Darras, "Poly(lactic acid) (PLA) and polyhydroxyalkanoates (PHAs), green alternatives to petroleum-based plastics: a review," *RSC Adv.*, vol. 11, no. 28, pp. 17151–17196, 2021.
[8] "Safety assessment of the substance zinc oxide, nanoparticles, for use in food contact materials," *EFSA Journal*, p. 8, 2016.
[9] PJP Espitia, et.al., "Zinc Oxide Nanoparticles for Food Packaging Applications," in *Antimicrobial Food Packaging*, Elsevier, 2016, pp. 425–431. doi: 10.1016/B978-0-12-800723-5.00034-6.
[10] W Zhang, et al., "High performance biopolymeric packaging films containing zinc oxide nanoparticles for fresh food preservation: A review," *International Journal of Biological Macromolecules*, 230, 123188, 2023.
[11] A Díez-Pascual and A Díez-Vicente, "Poly(3-hydroxybutyrate)/ZnO Bionanocomposites with Improved Mechanical, Barrier and Antibacterial Properties," *IJMS*, 15, 6, 10950–10973, 2014.
[12] B Melendez-Rodriguez *et al.*, "Preparation and Characterization of Electrospun Food Biopackaging Films of PHBV Derived From Fruit Pulp Biowaste," *Front. Sustain. Food Syst.*, 2, 38, 2018.
[13] AM Díez-Pascual and AL Díez-Vicente, "ZnO-Reinforced Poly(3-hydroxybutyrate-co-3-hydroxy-valerate) Bionanocomposites with Antimicrobial Function for Food Packaging," *ACS Appl. Mater. Interfaces*, 6, 12, 9822–9834, 2014.
[14] AM Díez-Pascual, "Poly(3-hydroxybutyrate-co-3-hydroxyhexanoate) with zinc oxide nanoparticles for food packaging," *J Food Process Eng*, 2021, doi: https://doi.org/10.1111/jfpe.13814.
[15] I Berrabah *et al.*, "A bionanocomposite of poly(3-hydroxybutyrate-co-3-hydroxyhexanoate)/ZnO-nanoparticles intended for food packaging," *IJBM*, 238, 124162, 2023.
[16] M Abbas, M Buntinx, W Deferme and R Peeters, "(Bio)polymer/ZnO Nanocomposites for Packaging Applications: A Review of Gas Barrier and Mechanical Properties," *Nanomaterials*, 9, 10, 1494, 2019.
[17] V Padilla-Gainza *et al.*, "Processing-structure-property relationships of biopolyester/zinc oxide fibrous scaffolds engineered by centrifugal spinning," *Polym Adv Technol*, 4987, 2020, doi: 10.1002/pat.4987.

[18] V. Padilla-Gainza *et al.*, "Development of zinc oxide/hydroxyapatite/poly(D,L-lactic acid) fibrous scaffold for tissue engineering applications," *Biomaterials Advances*, 133, 112594, 2022.
[19] C Vanheusden C, Vanminsel J, Reddy N, Samyn P, D'Haen J, Peeters R, Ethirajan A, Buntinx M, "Fabrication of poly(3-hydroxybutyrate-co-3-hydroxyhexanoate) Fibers Using Centrifugal Fiber Spinning: Structure, Properties and Application Potential," *Polymers*, 15, 5, 1181, 2023, doi: 10.3390/polym15051181.
[20] JL Castro-Mayorga, MJ Fabra, AM. Pourrahimi et al., "The impact of zinc oxide particle morphology as an antimicrobial and when incorporated in poly(3-hydroxybutyrate-co-3-hydroxyvalerate) films for food packaging and food contact surfaces applications," *Food and Bioproducts Processing*, 101, 32–44, 2017.
[21] C Zhang, Y Li, P Wang, and H Zhang, "Electrospinning of nanofibers: Potentials and perspectives for active food packaging," *Compr. Rev. Food Sci. Food Saf.*, 19, 2, 479–502, 2020, doi: 10.1111/1541-4337.12536.
[22] Merchiers J, Meurs W, Deferme W, Peeters R, Buntinx M, Reddy NK. Influence of Polymer Concentration and Nozzle Material on Centrifugal Fiber Spinning. *Polymers*. 2020; 12, 3, 575.
[23] J Merchiers *et al.*, "Centrifugally spun poly(ethylene oxide) fibers rival the properties of electrospun fibers," *J. Polym. Sci.*, p. 9, 2021, doi: https://doi.org/10.1002/pol.20210424.
[24] M Murariu *et al.*, "High-Performance Polylactide/ZnO Nanocomposites Designed for Films and Fibers with Special End-Use Properties," *Biomacromolecules*, 12, 5, 1762–1771, 2011, doi: 10.1021/bm2001445.
[25] A Anžlovar, M Primožič, I Švab, M Leitgeb, Ž Knez and E Žagar, "Polyolefin/ZnO Composites Prepared by Melt Processing," *Molecules*, 24, 13, 2432, 2019, doi: 10.3390/molecules24132432.
[26] J Xu, B-H. Guo, R Yang, Q Wu, et al., "In situ FTIR study on melting and crystallization of polyhydroxyalkanoates," *Polymer*, 43, 25, 6893–6899, 2002, doi: 10.1016/S0032-3861(02)00615-8.
[27] H-X Yang, M Sun, Y Zhang and P Zhou, "Degradable PHBHHx Modified by the Silk Fibroin for the Applications of Cardiovascular Tissue Engineering," *ISRN Materials Science*, 2011, 1–11, 2011.
[28] M Abbas, M Buntinx, W Deferme, N Reddy and R. Peeters, "Oxygen Gas and UV Barrier Properties of Nano-ZnO-Coated PET and PHBHHx Materials Fabricated by Ultrasonic Spray-Coating Technique," *Nanomaterials*, p. 14, 2021.
[29] S Kwon, A Orsuwan, N Bumbudsanpharoke, et al., "A Short Review of Light Barrier Materials for Food and Beverage Packaging," *Korean. J. Packag. Sci. Technol.*, 24, 3, 141–148, 2018.
[30] M Ruzi, N Celik and MS Onses, "Superhydrophobic coatings for food packaging applications: A review," *Food Packaging and Shelf Life*, 32, 100823, 2022, doi: 10.1016/j.fpsl.2022.100823.
[31] G Bracco and B Holst, Eds., "Contact Angle and Wetting Properties," in *Surface Science Techniques*, in Springer Series in Surface Sciences, 51. Berlin, Heidelberg: Springer Berlin Heidelberg, 2013, pp. 3–34.

[32] Bamps B, Guimaraes RMM, Duijsters G, Hermans D, Vanminsel J, Vervoort E, Buntinx M, Peeters R. "Characterizing Mechanical, Heat Seal, and Gas Barrier Performance of Biodegradable Films to Determine Food Packaging Applications," *Polymers*, 14, 13, 2569, 2022, doi: 10.3390/polym14132569.
[33] A Cherpinski, S Torres-Giner, J Vartiainen, MS Peresin, P Lahtinen, and JM Lagaron, "Improving the water resistance of nanocellulose-based films with polyhydroxyalkanoates processed by the electrospinning coating technique," *Cellulose*, 25, 2, 1291–1307, 2018, doi: 10.1007/s10570-018-1648-z.
[34] T Homola, LYL Wu and M Černák, "Atmospheric Plasma Surface Activation of Poly(Ethylene Terephthalate) Film for Roll-To-Roll Application of Transparent Conductive Coating," *The Journal of Adhesion*, 90, 4, 296–309, 2014, doi: 10.1080/00218464.2013.794110.
[35] H-J Choi, MS Kim, D Ahn, SY Yeo and S Lee, "Electrical percolation threshold of carbon black in a polymer matrix and its application to antistatic fibre," *Sci Rep*, 9, 1, 6338, 2019, doi: 10.1038/s41598-019-42495-1.

AI-GO05

Mechanical Properties of PBAT/TPS Nanocomposites under UV exposure

Thitiporn Kaewpetch, Tanaporn Purasata, Millapat Chamnandoo, and Nattinee Bumbudsanpharoke*

Department of Packaging and Materials Technology, Kasetsart University, Bangkok, 10900, Thailand

__Correspondence to:__ Nattinee Bumbudsanpharoke. Department of Packaging and Materials Technology, Kasetsart University, Bangkok, 10900, Thailand.
Email: nattinee.bu@ku.ac.th

ABSTRACT: Blends of biodegradable poly(butylene adipate-co-terephthalate) (PBAT) and thermoplastic starch (TPS) have been extensively developed to obtain cost-effectiveness and superior properties in biopolymer packaging applications. Incorporation of nanoparticles into PBAT/TPS matrices enhanced properties of bioplastics, such as mechanical properties, physical properties, barrier properties, and antimicrobial properties. However, the properties of PBAT/TPS nanocomposites could be potentially influenced by external factors during storage, such as UV light, temperature, and humidity. This work aimed to primarily study changes of mechanical properties of PBAT/TPS nanocomposite films after the films were exposed to UV light. The polymer matrices were incorporated with copper and zinc nanoparticles separately and manufactured using blown film extrusion process. UV irradiation of the films is up to 168 hours using QUV accelerated weathering tester. Young's modulus, tensile strength, and elongation at break, were determined at exposure time of 48, 96, 144, and 168 hours. The results showed a film discoloration and a reduction of mechanical properties of PBAT/TPS nanocomposites over exposure time. This could be possibly caused by the degradation of either polymer matrices or nanoparticles themselves, or the degradation of both polymers and nanoparticles.

Keywords: bioplastics, nanocomposites, UV exposure, mechanical properties, degradation

INTRODUCTION

Biodegradable plastics have been increasingly demanded in packaging industries. They are ubiquitously known as alternative materials that could be used to replace conventional plastics to solve global environmental issues from growing plastic waste. Biodegradable plastics can be derived from both renewable and petroleum-based resources[1-3]. They have been developed to improve their physical and mechanical properties to be equivalent to the properties of traditional polyolefins that have dominated in packaging applications.

Poly(butylene-adipate-*co*-terephthalate) (PBAT), a developed novel biodegradable plastic, is an aromatic-aliphatic co-polyester produced from fossil resources of 1,4-butanediol, adipic acid, and terephthalic acid. A combination of aromatic and aliphatic units of polyesters provides excellent mechanical properties and good biodegradability[4, 5]. PBAT has similar mechanical
properties to polyethylene. It shows more flexibility and higher elongation at break than most biodegradable polyesters, making it more suitable for food packaging and agricultural films[6]. However, PBAT market is restrictively limited due to high production cost. An addition of thermoplastic starch (TPS), which is abundant renewable materials, could potentially reduce the cost while maintaining the material properties.

PBAT/TPS films have been developed to obtain more compatibility between two polymer matrices, leading to an improvement of mechanical and barrier properties[7, 8]. Moreover, these properties can be reinforced by incorporating nanoparticles into polymer matrix[9, 10]. Besides the reinforcement, the nanoparticles, such as CuO, ZnO, and TiO_2, could be served as antimicrobial agents[11-14], antioxidants[15, 16], and UV blocking agents[17, 18]. Nevertheless, during storage of materials, storage conditions are crucial to the material stability. External factors including UV light, temperature, and humidity could potentially influence the properties of the nanocomposites, especially mechanical properties. Under UV exposure the materials could undergo two mechanisms of degradation; photolysis and photo-oxidative degradation[19]. In photolysis materials absorb energy from light source and decomposed to smaller molecules through chemical reactions. On the other hand, the photo-oxidative degradation causes the formation of radicals that induce oxidation in the materials[20]. These processes do not have only chain scission but also crosslinking of degraded polymer molecules. A competition between chain scission and crosslinking leads to a change in polymer molecular weight; the molecular weight decreases when chain scission dominates but increases due to crosslinking[21]. A reduction of average molecular weight deteriorates mechanical properties of the materials. Besides the mechanical properties, damages from UV exposure could also be discoloration of dyes and pigments, burnt surfaces, and yellowing of plastics[22].
The degradation of materials under UV light has a strong impact on the packaging industry. Understanding the changes of the material stability, especially for biodegradable materials, would be helpful for the industry to improve the properties of the materials in the future. In this work, mechanical properties of biodegradable PBAT/ TPS nanocomposite films with different nanoparticles were studied after the films are exposed to UV light. Film microstructure and color changes were also discussed.

MATERIALS AND METHODS

Materials

Commercial Polybutylene adipate-co-terephthalate (Ecoflex®F Blend C1200, BASF, Germany) with density of 1.25-1.27 g/cm^3, and thermoplastic starch prepared from acetylated cassava starch with degree of substitution of 0.01-0.03 (KREATION® SS, SMS Corp., Thailand) were prepared as polymer matrix. Commercial glycerol (P. Wai Co., Ltd., Thailand),

was used as plasticizer in the film forming process. Copper oxide nanospheres with average diameter of 40 nm and spherical Zinc oxide nanofillers with average diameter of 35 nm were purchased from US Research Nanomaterials Inc. (USA) and Kawa compay, Ltd. (Japan), respectively.

Film preparation

Preparation of PBAT/TPS nanocomposite pellets

Prior to the film formation, PBAT/TPS nanocomposite pallets were prepared by compounding commercial PBAT resins and TPS pellets along with CuO or ZnO nanoparticles through a twin-screw extruder (LTE-20-40, Labtech Engineering, Samut Prakan, Thailand). Firstly, TPS pellets were produced using a twin-screw extruder to mix and extrude a mixture of acetylated cassava starch powder and glycerol with a ratio of 70:30. The heating profile and screw speed were set at 90-150°C and 180 rpm, respectively. The TPS extrudates were then air cooled and cut using a pelletizer (Labtech Engineering, Thailand).

A masterbatch of TPS/CuO or ZnO pellets were then prepared by primarily compounding extruded TPS pellets with each type of nanoparticles and extruding through a twin-screw extruder. The final masterbatch composition would contain 20wt% nanoparticles.

TPS pellets were then mixed with commercial PBAT resins with a 30:70 ratio to produce PBAT/TPS control films. To manufacture nanocomposite films, a mixture of PBAT and TPS pellets were combined with the prepared masterbatch of nanoparticles and then extruded through a twin-screw extruder at 90-150°C heating profile and 180 rpm screw speed. Finally, compounded pallets of PBAT/TPS, PBAT/TPS-CuO1%, and PBAT/TPS-ZnO3% were obtained. Note that 1% CuO and 3% ZnO were used because they exhibited the most effective performance on antimicrobial activity in a previous study.

Preparation of PBAT/TPS nanocomposite films by blown film extrusion

The prepared PBAT/TPS-CuO or ZnO pellets were dried at 60°C overnight and blown using a blown film extruder. The blown film extruder contains two main parts; one is a single-screw extruder (LE-25-30/C, Labtech Engineering) with screw diameter of 25 mm and four controlled temperature zones of barrel, and another is a film-blowing attachment (LF-400, Labtech Engineering) which is connected to an annular die from the first part. The barrel temperature zones were set at 160/170/180/180°C. Speeds of screw and nip roll were adjusted to 30-40 and 3 rpm, respectively. An extrudate was blown into a vertical tubular bubble which is then squeezed into thin films.

UV irradiation of PBAT/TPS nanocomposite films

Neat PBAT/TPS films and PBAT/TPS nanocomposites were cut into small pieces with the size of 23.5×11 cm. The films were exposed to UVA at 0.68 and 1.10 W/m^2 UV intensity and at

60°C up to 168 hours using an accelerated weathering tester with eight UVA-340 lamps (QUV, Q-Lab Corporation, USA). The films were then collected at 0, 48, 96, 144, and 168 hours.

Film morphology

Film samples with the dimension of 1×1 cm were fixed on metal stubs and coated with gold by sputter coater (Quorum Technology Polaron Range SC7620, East Sussex, UK). Surface microstructure of the films after exposed to the UV light was visualized by scanning electron microscopy (SEM, FEI Quanta 450, Thermo Fisher Scientific, Waltham, MA, USA) at 2500X magnification and 15 kV beam current.

Mechanical characterizations of nanocomposite films

Mechanical testing including tensile strength, Young's modulus, and elongation at break followed the ASTM D882 standard. The procedure started from cutting the UV exposed films to the size of 15×2.5 cm. Then the films were dried for 24 hours prior to the mechanical characterization. For each film condition, 12 specimens were characterized the mechanical properties using the universal testing machine (Instron 5965, Instron®, USA) with the tension mode. A clamp distance was 5 cm and a deformation rate was 200 mm/min.

RESULTS AND DISCUSSION

Film color

Prior to UV exposure, color of neat PBAT/TPS and PBAT/TPS films containing ZnO nanoparticles was originally white but PBAT/TPS with CuO showed a dark brown color which was primarily a result of CuO nanoparticles (Fig. 1a). However, figure 1b shows that the colors started to change apparently after the films were exposed to UV light for 96 hours. Over exposure time the original white color of the neat films and the films with ZnO was faded. The white shade became more yellowish. For PBAT/TPS/CuO films, the brown shade of the films became lighter after 96-hour UV exposure. This suggested that film degradation had occurred and affected the film appearance.

Surface microstructure

Since the film appearance changed after UV irradiation, the UV light could possibly influence film morphology causing the deterioration of the film structure. Figure 2 shows the microstructure of film surface using scanning electron microscopy before and after the films were exposed to UV light at two different UV intensities. The control films of neat PBAT/TPS and PBAT/TPS nanocomposites without UV exposure exhibited rough surface with large amount of TPS starch granules. The size of the starch granules was larger for the neat PBAT/TPS films (Fig. 2a) but the granules size reduced after the films were incorporated with CuO and ZnO nanoparticles (Fig. 2b, c). Incorporation of nanoparticles led to a higher degree

of starch gelatinization which improved the material processability and reduced the size of starch granules[23, 24].

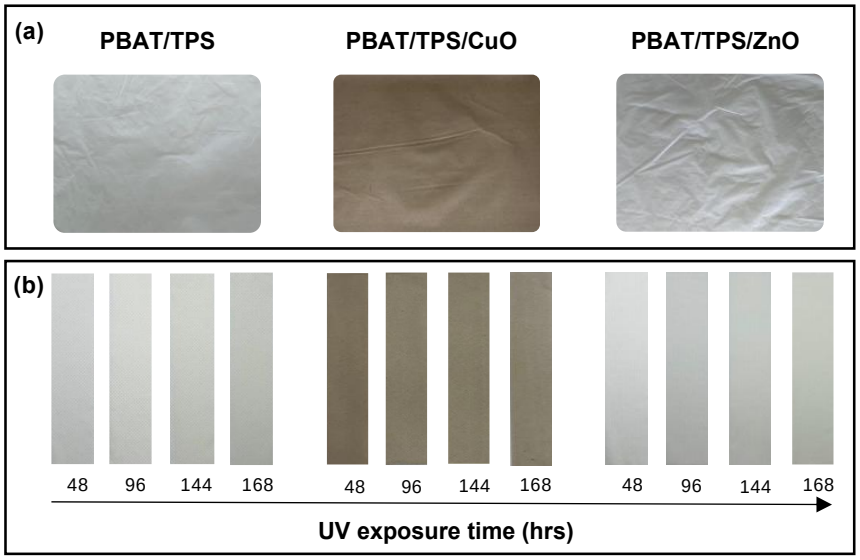

Figure 1. Color change of PBAT/TPS films and PBAT/TPS films containing CuO and ZnO nanoparticles (a) before and (b) during UV exposure at UV intensity of 1.10 W/m^2.

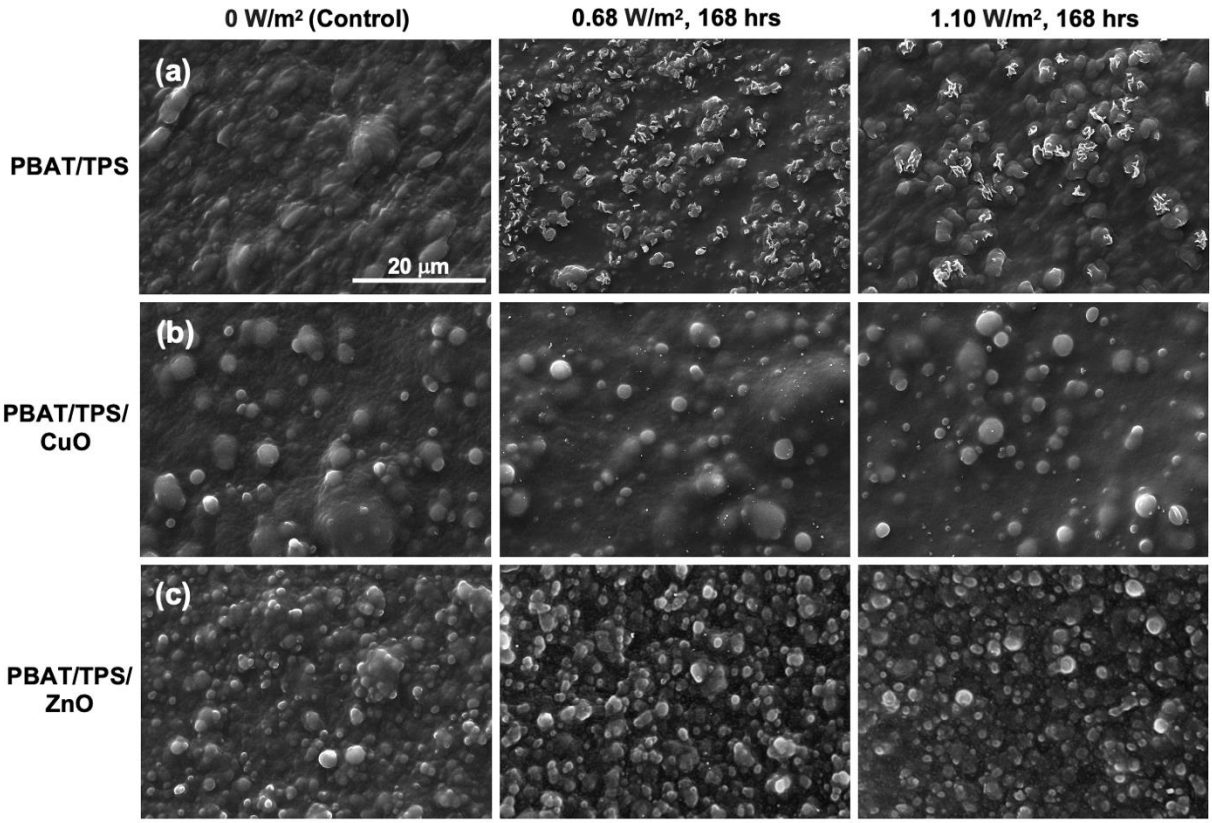

Figure 2. Scanning electron microscopy (SEM) micrographs of (a) PBAT/TPS films without nanoparticle and PBAT/TPS films containing (b) CuO or (c) ZnO nanoparticles after UV exposure at UV intensity of 0, 0.68, and 1.10 W/m^2.

After the films were exposed to the UV for 168 hours, the microstructure of PBAT/TPS films at both UV intensities was deteriorated. The deterioration visibly appeared at the area of TPS granules on the film surface. The surface of the granules was feasibly burnt from the UV light, leading to a large area of flake-like deformation of the TPS granules. For PBAT/TPS/CuO films, the starch granules started to deform, exhibiting small number of tiny flakes on the granule surface compared to the neat PBAT/TPS films. However, there was no obvious change on the surface microstructure of the PBAT/TPS/ZnO films.

Mechanical characterization

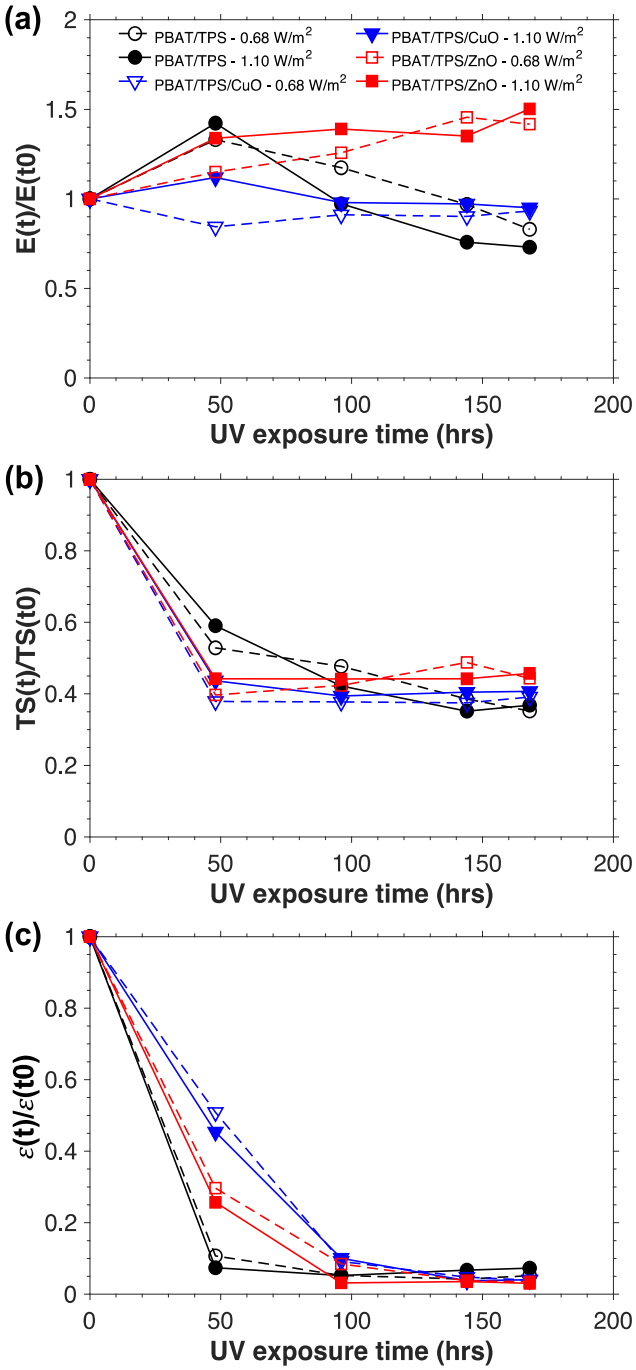

Figure 3. Mechanical properties including normalized (a) Young's modulus, (b) ultimate tensile strength, and (c) elongation at break of neat PBAT/TPS and nanocomposite films.

As mentioned above, storage conditions, particularly UV light, could affect the stability of polymeric materials. The degradation of materials during storage is a challenge for the manufacturer to minimize, especially for biodegradable materials. Figure 3 shows mechanical properties, including tensile strength (TS), Young's modulus (E), and elongation at break (ε), of pure PBAT/TPS and its nanocomposite films over UV exposure time. These properties were reported in terms of the values at a certain exposure time (t) over that of the time before UV irradiation starts (t0).

For Young's modulus (Fig. 3a), most films had higher E ($E(t)/E(t0) > 1$) at the exposure time of 48 hours for both UV intensities, suggesting that the materials were stiffer. An increase in E could be affected by crosslinking in an amorphous phase of PBAT due to the photo-oxidative degradation process[25]. Also, E of PBAT/TPS films was larger than the films containing ZnO and CuO, respectively. After 48 hours the film properties behaved differently. For neat PBAT/TPS films, E decreased after 48 hours and tended to get below an initial value of PBAT/TPS films at the end of exposure. This could be a result of chain scission from material degradation. In case of PBAT/TPS/CuO, the films exhibited a slightly lower E after 48 hours and remained constant near $E(t)/E(t0) = 1$. On the other hand, E of PBAT/TPS/ZnO increased over entire UV exposure time, indicating that PBAT/TPS/ZnO films became stronger and were likely to withstand higher stress before the films started to deform, compared to the other types of films. However, within the same types of materials, different UV intensity did not significantly alter the material properties.

In terms of tensile strength, figure 3b shows that the ultimate TS of PBAT/TPS and its nanocomposite films decreased drastically at 48 hours, explaining that photo-oxidation caused the materials to degrade and resist less stress before breaking. However, at this period PBAT/TPS films had a slightly higher TS than the other two nanocomposites, indicating more brittleness of PBAT/TPS films. After 48 hours of UV exposure, TS of the films with CuO and ZnO remained constant at $TS(t)/TS(t0) \sim 0.4\text{-}0.5$. In contrast, TS of pure PBAT/TPS gradually decreased to the same level of the nanocomposite films. Interestingly, after 96-hour UV exposure TS values of all films reached the same plateau, suggesting a complete degradation of the materials.

For elongation at break (figure 3c), all materials had a sharp drop at the exposure time of 48 hours. Pure PBAT/TPS dropped around 90% which was larger than PBAT/TPS/ZnO (70% drop) and PBAT/TPS/CuO (50% drop) films, respectively. This confirmed that neat PBAT/TPS films became stiffer and more brittle than the nanocomposite films after exposed to UV light so they were harder to be stretched. This result was correlated to the results of Young's modulus and Tensile strength reported above. This could also suggest that incorporating nanoparticles into polymer films could sustain the material stability after exposed to UV. However, when the films were exposed to the UV light for longer time (>96 hours), the mechanical properties of materials degraded completely and elongation at break decreased to near $\varepsilon(t)/\varepsilon(t0) = 0$, indicating a brittle failure.

CONCLUSION

Mechanical stability is a desirable property of materials that industries expect. Typically, polymeric materials degrade over time due to their internal factors including chain structure, chemical components, and impurities. However, the degradation can be accelerated by external stimulus such as UV radiation. Biodegradable plastics (e.g. PBAT/TPS) have raised a concern over stability and durability of the materials if they are subjected to the external factors. In terms of biodegradable PBAT/TPS and PBAT/TPS nanocomposites, after the films were exposed to UV light, the photo-degradation caused the film discoloration. Also, microstructure of PBAT/TPS film was deteriorated but the incorporation of nanoparticles could reduce the extent of photo-degradation, decelerating the degradation of mechanical properties.

REFERENCES

[1] Flieger M, Kantorova M, Prell A, Řezanka T, Votruba J. Biodegradable plastics from renewable sources. Folia microbiologica 2003; 48, pp. 27-44.
[2] Rujnić-Sokele M, Pilipović A. Challenges and opportunities of biodegradable plastics: A mini review. Waste Management & Research 2017; 35(2), pp. 132-140.
[3] Havstad MR. Biodegradable plastics. In Plastic waste and recycling, Elsevier 2020; pp. 97-129.
[4] Jian J, Xiangbin Z, Xianbo H. An overview on synthesis, properties and applications of poly (butylene-adipate-co-terephthalate)–PBAT. Advanced Industrial and Engineering Polymer Research 2020; 3(1), pp. 19-26.
[5] Müller R-J, Kleeberg I, Deckwer W-D. Biodegradation of polyesters containing aromatic constituents. Journal of biotechnology 2001; 86(2), pp. 87-95.
[6] Bordes P, Pollet E, Avérous L. Nano-biocomposites: biodegradable polyester/nanoclay systems. Progress in Polymer Science 2009; 34(2), pp. 125-155.
[7] Bai J, Pei H, Zhou X, Xie X. Reactive compatibilization and properties of low-cost and high-performance PBAT/thermoplastic starch blends. European Polymer Journal 2021; 143, pp. 110198.
[8] Katekhong W, Wongphan P, Klinmalai P, Harnkarnsujarit N. Thermoplastic starch blown films functionalized by plasticized nitrite blended with PBAT for superior oxygen barrier and active biodegradable meat packaging. Food Chemistry 2022; 374, pp. 131709.
[9] Wang C, Gong C, Qin Y, Hu Y, Jiao A, Jin Z, Qiu C, Wang J. Bioactive and functional biodegradable packaging films reinforced with nanoparticles. Journal of Food Engineering 2022; 312, pp. 110752.
[10] Arshian M, Estaji S, Tayouri MI, Mousavi SR, Shojaei S, Khonakdar HA. Poly (lactic acid) films reinforced with hybrid zinc oxide-polyhedral oligomeric silsesquioxane nanoparticles: Morphological, mechanical, and antibacterial properties. Polymers for Advanced Technologies 2023; 34(3), pp. 985-997.
[11] Phothisarattana D, Wongphan P, Promhuad K, Promsorn J, Harnkarnsujarit N. Blown film extrusion of PBAT/TPS/ZnO nanocomposites for shelf-life extension of meat packaging. Colloids and Surfaces B: Biointerfaces 2022; 214, pp. 112472.

[12] Zhai X, Zhou S, Zhang R, Wang W, Hou H. Antimicrobial starch/poly (butylene adipate-co-terephthalate) nanocomposite films loaded with a combination of silver and zinc oxide nanoparticles for food packaging. International Journal of Biological Macromolecules 2022; 206, pp. 298-305.
[13] Yakdoumi FZ, Hadj-Hamou AS. Effectiveness assessment of TiO2-Al2O3 nano-mixture as a filler material for improvement of packaging performance of PLA nanocomposite films. Journal of Polymer Engineering 2020; 40(10), pp. 848-858.
[14] Wang Y, Zhang J, Li W, Xie X, Yu W, Xie L, Wei Z, Guo R, Yan H, Zheng Q. Antibacterial poly (butylene succinate-co-terephthalate)/titanium dioxide/copper oxide nanocomposites films for food packaging applications. Food Packaging and Shelf Life 2022; 34, pp. 101004.
[15] Xiao L, Yao Z, He Y, Han Z, Zhang X, Li C, Xu P, Yang W, Ma P. Antioxidant and antibacterial PBAT/lignin-ZnO nanocomposite films for active food packaging. Industrial Crops and Products 2022; 187, pp. 115515.
[16] Kalia A, Kaur M, Shami A, Jawandha SK, Alghuthaymi MA, Thakur A, Abd-Elsalam KA. Nettle-leaf extract derived ZnO/CuO nanoparticle-biopolymer-based antioxidant and antimicrobial nanocomposite packaging films and their impact on extending the post-harvest shelf life of guava fruit. Biomolecules 2021; 11(2), pp. 224.
[17] Badry R, El-Nahass MM, Nada N, Elhaes H, Ibrahim MA. Structural and UV-blocking properties of carboxymethyl cellulose sodium/CuO nanocomposite films. Scientific Reports 2023; 13(1), pp. 1123.
[18] Channa IA, Ashfaq J, Gilani SJ, Shah AA, Chandio AD, Jumah MNb. UV blocking and Oxygen Barrier Coatings based on polyvinyl alcohol and zinc oxide nanoparticles for packaging applications. Coatings 2022; 12(7), pp. 897.
[19] Yang R. Chapter 7 - Polymer degradation and stability. In Polymer Science and Nanotechnology, Narain, R Ed.; Elsevier 2020; pp. 125-148.
[20] Gijsman P, Diepens M. Photolysis and photooxidation in engineering plastics. In Polymer Degradation and Performance Oxford University Press 2009; pp. 287-306.
[21] Shyichuk A, White J. Analysis of chain-scission and crosslinking rates in the photo-oxidation of polystyrene. Journal of Applied Polymer Science 2000; 77(13), pp. 3015-3023.
[22] Yousif E, Haddad R. Photodegradation and photostabilization of polymers, especially polystyrene. SpringerPlus 2013; 2(1), pp. 1-32.
[23] Phothisarattana D, Harnkarnsujarit N. Migration, aggregations and thermal degradation behaviors of TiO2 and ZnO incorporated PBAT/TPS nanocomposite blown films. Food Packaging and Shelf Life 2022; 33, pp. 100901.
[24] González Seligra P, Eloy Moura L, Famá L, Druzian JI, Goyanes S. Influence of incorporation of starch nanoparticles in PBAT/TPS composite films. Polymer International 2016; 65(8), pp. 938-945.
[25] Titone V, La Mantia FP, Mistretta MC. The Effect of Calcium Carbonate on the Photo-Oxidative Behavior of Poly (butylene adipate-co-terephthalate). Macromolecular Materials and Engineering 2020; 305(10), pp. 2000358.

AI-GP01

Evaluation of the antimicrobial activity of sodium alginate films integrated with cinnamon essential oil and citric acid on sliced cooked ham

Melissa Lee[1], Nadine Rüegg[1], Selçuk Yildirim*[1]

[1]*Life Sciences and Facility Management, Zurich University of Applied Sciences, Waedenswil, Switzerland*

***Correspondence to**: Selçuk Yildirim, Life Sciences and Facility Management, Zurich University of Applied Sciences, Campus Reidbach, Waedenswil 8820, Switzerland.*
Email: selcuk.yildirim@zhaw.ch

ABSTRACT: Bio-based antimicrobial films have been developed using sodium alginate and 6 wt% of cinnamon essential oil (CEO) as a volatile antimicrobial substance and 4 and 6 wt% of citric acid (CA) as a non-volatile antimicrobial substance. Antimicrobial activity of the films was tested in in vitro tests against Escherichia coli and Listeria innocua by disc diffusion or vapour diffusion assay. Sodium alginate films containing CA exhibited a zone of inhibition between 30.86 ± 2.55 and 45.87 ± 1.90 against E. coli and L. innocua in the disc diffusion assays. Films containing CEO also showed significant antimicrobial activities in the vapour diffusion assays that resulted in a log reduction of 5.3 for E. coli and 3.2 for L. innocua after 6 days. Antimicrobial activities of all films were also tested against L. innocua on sliced cooked ham. Films containing CEO did not prevent the growth of L. innocua inoculated on ham. On the other hand, sodium alginate films with CA fully inhibited the growth of L. innocua on ham during storage at 7.5_C for 12 days resulting in a bacterial count below the detection limit after 12 days. The addition of antimicrobial substances in sodium alginate films resulted in a slight colour change (but significant) and reduced the tensile strength of the films significantly. Adding CA to sodium alginate films increased the moisture content (from 24.81% to 35.41–48.02%) as well as the elongation at break (from 11.3% to 22.6–33.2%) of the films.

Keywords: active films, active packaging, antimicrobial packaging, essential oils, food packaging

AI-PP01

Understanding silver nanoparticle leaching behavior from active biodegradable nanocomposites

Mieke Buntinx[*1], Dries Hermans[1], Muhammet Gücyetmez[2], Wouter Marchal[2]

[1]*Materials and Packaging Research & Services (MPR&S), Institute for Materials Research (imo-imomec), Hasselt University, Diepenbeek, Belgium*
[2]*Analytical & Circular Chemistry (ACC), Institute for Materials Research (imo-imomec), Hasselt University, Diepenbeek, Belgium*

[1] ***Correspondence to**: Mieke Buntinx, University Hasselt, MPR&S, Institute for Materials Research imo-imomec,*
E-mail: mieke.buntinx@uhasselt.be

ABSTRACT: Biobased and biodegradable polyhydroxyalkanoates (PHAs) can be seen as polymers of the future, which can replace fossil equivalents in a circular bioeconomy. Indeed, PHAs can be produced in bacteria from various biomass feedstocks. PHA biopolymers can be used in packaging, agricultural and medical applications, and they fit at least six end-of-life (EoL) scenarios. Incorporation of silver nanoparticles (NP) in bioplastic food contact materials (FCM) shows great potential as active packaging with antimicrobial performance, which can contribute to reduce food waste, as targeted by SDG 12.3. However, the lack of knowledge regarding NP release, associated risks on human health and accumulation in the environment leads to restricting legislation. Before investigating NP migration from biodegradable PHAs, the first objective is to update the dynamic European legislation regarding biobased and biodegradable packaging materials, FCM and active packaging.
In Nov 2022, the European Commission proposed the new Packaging and Packaging Waste Regulation to put the packaging sector on track for climate neutrality by 2050 in line with the European Green Deal's Circular Economy Action Plan. The new rules will clarify how bioplastics can be part of a sustainable future. In the meantime, the Commission also intends to modernize the rules on FCM (Regulation 1935/2004) to ensure food safety, while taking account of the latest science and technology, and supporting innovation and sustainability by promoting safe reusable and recyclable solutions. Two PHAs are on the Union List of permitted substances but authorisations for nanomaterials must be assessed on a case-by-case basis.
The PHA value-chain from design through manufacture, value enhancement and disposal should be strategic, considering safety and legislation. Therefore, our research will focus on elucidating mechanisms of silver NP migration from PHAs in consumer as well as specific EoL scenarios to estimate the safety and application potential of bio-nanocomposites as active packaging material.

Keywords: silver nanoparticles – biodegradable packaging materials – food contact materials – active packaging material – migration – polyhydroxyalkanoates

INTRODUCTION

Polyhydroxyalkanoates are promising circular plastics

In light of the current concerns about environmental problems caused by the excessive use of fossil resources, the transition to a sustainable and circular economy is increasingly coming to the fore. Bioplastics are promoted as eco-friendly plastics that could help to solve the problem of plastic pollution. Among the bioplastics, biobased and biodegradable **polyhydroxyalkanoates** (PHAs) definitely meet the criteria of **sustainable circular plastics**.

First, PHAs can be produced from various **biomass** substrates, including edible biomass, non-edible biomass from waste streams, algal biomass and electrical driven-fermentation processes, which are respectively classified as first, second, third and fourth-generation feedstocks [1].

Second, these **bacterially produced polyesters** offer a spectrum of possible applications, such as packaging materials, daily-use objects, agricultural films, medical devices or implantable objects [2]. Indeed, PHAs show great promise for use in food packaging applications with medium gas barrier properties. The copolymer poly(3-hydroxybutyrate-co-3-hydroxyhexanoate) (PHBHHx) is useful for flexible (food) packaging applications [3,4], whereas the stiffer and more brittle copolymers poly(3-hydroxybutyrate) (PHB) and poly(3-hydroxybutyrate-co-3-hydroxyvalerate) (PHBV) are better suitable for rigid applications [5].

Finally, the PHA family is outstanding among current polymers that can fully fit all end-of-life scenarios in the bioplastics industry. PHA postconsumer products have **six basic end-of-life alternatives (EoL)**. PHA plastics can be either i) reused, ii) mechanically recycled, iii) chemically recycled to its monomers, iv) composted, v) burned, or vi) biodegraded. Of course, the end-of-life pathway varies greatly depending on the use of PHA products. [6]

Mechanical recycling has a relatively low environmental impact due to the low energy usage and raw materials reliance. However, recycled PHA suffers from polymer breakdown during usage or heat deterioration during extrusion and pelletization. Although recycling appears to be more energy-efficient than composting, sorting and cleaning are critical to preventing contamination.

Chemical recycling is possible via: i) depolymerization of polymer chains into monomers and ii) pyrolysis to recover high-value chemicals/monomers such as organic vapors, char and gases using thermal methods, which are processed into oil through condensation. A greener alternative is **biodegradation**, where microorganisms break down the biopolymer chains into CO_2 or CH_4, water and biomass. PHAs biodegrade both aerobically and anaerobically. PHAs are the only fully biosynthesized materials that are biodegradable and compostable in soil, freshwater and saltwater when compared to other biopolymers [7]. In

addition, **anaerobic digestion** has emerged as a critical EoL alternative for PHA waste. Finally, **incineration** of PHA waste with energy recovery is another EoL strategy, because of the relatively high calorific value of bioplastics. However, due to the increase of greenhouse gases in the atmosphere, energy recuperation is the least preferred end-of-life option for PHAs compared to recycling, composting and anaerobic digestion.

Using bioplastics such as PHAs, could address various Sustainable Development Goals (SDGs), although **cost, processability and thermal/mechanical performance** remain crucial factors to compete with fossil-based plastics.

To improve their competitiveness, a promising and popular strategy is to incorporate 'nano' particles/fibres/platelets, creating **advanced nanocomposite materials**.

Nanocomposite materials for use as active packaging materials

Plenty of literature is available on how **incorporating metal(oxide) nanoparticles (NPs)**, such as Ag, Cu, ZnO, TiO2, SiO2, Al2O3 NPs in a biopolymer network positively affects a multitude of physical, mechanical, barrier and antimicrobial properties [8].

Ag NPs have been hosted in durable polymers, such as polyvinyl chloride (PVC), polyethylene (PE), and polypropylene (PP) among others, as well as in biodegradable polymer matrices such as polylactic acid (PLA), PHBHHx, PHBV, starch, etc. Due to the Ag NP incorporation, these nanocomposites show enhanced **antimicrobial, mechanical and barrier properties** [9-12].

The antimicrobial action of Ag NPs against a wide range of micro-organisms is explained by the potential appearance of both Ag_0 and Ag^+ species. Ag NPs can cause cell death by accumulating in the bacterial cell membrane via reactive oxygen species (ROS) generation or binding to enzymes and DNA. Another contribution to the bactericidal effect is the release of potentially very reactive Ag^+ ions, which may react with the negatively charged cell membrane [13].

Ag NPs are already widely found in **many applications** ranging from healthcare (covid masks), water treatment, printing inks, coatings, sensors, cosmetics, pharmacy and (food) packaging [14]. As a consequence of their biocompatibility and easy functionalization, AgNPs can be applied in different products and give them bactericidal capacity [13]. Incorporation of Ag NPs in packaging materials results in active packaging.

Active packaging concepts interact with the packaged product or the atmosphere inside the packaging to protect the valuable nutritional components, prevent spoilage or loss of quality, and prolong shelf life [15]. They are designed to deliberately incorporate components that would release or absorb substances into or from the packaged food or the environment surrounding the food; e.g. modified atmosphere, scavengers, absorbers, emitters or adaptors, which can be coated on or integrated in the packaging material, sachets, pads, etc. [16].

Antimicrobial active packaging materials can contribute to tackle **SDG 12.3**. Goal 12 is about ensuring sustainable consumption and production patterns, which is key to sustain the livelihoods of current and future generations. Today, the world wastes or loses around a third of the food it produces while almost 690 million people go hungry. SDG 12.3 aims to significantly reduce food waste and food loss [17].

Safe use of nanocomposite materials

Apart from the widely-reported advantages which inevitably will result in an increase of nanotechnology-based products over the coming years, many studies do not systematically address **NP release mechanisms** from these advanced NCs. **Public concern about the potential risks related to the release of NPs** from packaging into food is associated with insufficient knowledge about their safety and toxicity, especially if the host material is a biodegradable polymer.
This drives authorities to use precautionary principles and handle the issue conservatively. To be used as an active FCM in the EU, compliance with Regulations (EC) 1935/2004, (EC) 10/2011 and (EC) 450/2009 is required, resulting in a Union List of permitted substances. Biobased polymers such as PHBV and PHBHHx are currently on the Union List ((EC) 2019/37). However, authorisations for **nanomaterials must be assessed on a case-by-case basis,** leading to complex situations: Ag NPs intended for surface biocide use are only authorised up to 0.025% w/w in polar polymers, such as polyolefins that do not swell in contact with aqueous foods [18].

Goal of the research

The final goal of this starting PhD project is to develop more generalist insights into the possible leaching mechanisms of Ag NPs from biodegradable polymers, which can contribute to more widely-applicable decision-making in nanocomposite risk assessment. The first objective is to update the dynamic European legislation regarding biobased and biodegradable packaging materials, food contact materials and active packaging.

RESULTS

Bioplastic packaging materials in a circular EU

In November 2022, the European Commission proposed the **new Packaging and Packaging Waste Regulation** to stop the trend of the constantly growing source of packaging waste [19].

The new EU-wide rules must put the packaging sector on track for **climate neutrality by 2050**, as aimed by the European Green Deal's Circular Economy Action Plan [20]. In brief, unnecessary packaging will be banned, overpackaging will be limited, more reusable packaging options will be offered and clear labels will be provided to support correct recycling. While these actions will be visible to consumers, the rules must also create new business opportunities for the industry and decrease the need for virgin materials. The latter will boost Europe's recycling capacity as well as make Europe less dependent on primary resources and external suppliers.

Alternatives to conventional plastics, such as biobased, biodegradable and compostable plastics are emerging everywhere, not only in packaging, but also in consumer goods, textiles, automotive, transport, agriculture, horticulture, electrics, electronics and other sectors. In 2022,

packaging occupied the largest field of application of the total bioplastics market (1 million tons, 48%). The global bioplastics production capacity is set to increase significantly from around 2.23 million tons in 2022 to 6.3 million tons in 2027 [21].

However, these **bioplastics** must meet a number of conditions to have positive environmental impacts, rather than exacerbating plastic pollution, climate change and biodiversity loss. The Commission's new framework has clarified **how these bioplastics can be part of a sustainable future** by setting out for which applications such plastics are truly environmentally beneficial and how they should be designed, disposed of and recycled.

An initially proposed partial ban on **compostable plastic packaging** was eventually lifted, because compostable packaging solutions can have environmental benefits, when they do not negatively affect the quality of the compost. They are especially useful when there is a proper biowaste collection and treatment system in place. Moreover, they can reduce the contamination of (organic) waste streams [22]. According to the new rules, bags for the separate collection of biowaste, very lightweight plastic carrier bags, tea bags, filter coffee pods and pads, fruit and vegetable stickers, must be compostable in industrial composting facilities [20]. The use of compostable plastics for other packaging is still possible if it allows material recycling [22]. Compostable products must always specify that they are certified for industrial composting, in line with EU standards, and explain the way to dispose of them.

In addition, **biodegradable plastics** also have their place in a sustainable future, but they need to be directed to specific applications where their environmental benefits and value for the circular economy are proven (e.g. agricultural mulch film). They must be labelled to show the timeframe for biodegradation under specified circumstances and environments (excluding a license to litter).

It is also emphasized that biomass used to produce **biobased plastics** must be sourced sustainably, without harm to the environment, and that producers must prioritize the use of organic waste and by-products as raw materials [20].

And finally, the share of biobased plastic content should be disclosed, whereas greenwashing and confusing claims on biodegradation of litter-prone products should be banned at all times [20].

Revision of the rules on food contact materials

In the meantime, the Commission intends to modernize the rules on food contact materials (currently under framework Regulation (EC) 1935/2004) to ensure food safety, while taking account of the latest science and technology, and **supporting innovation and sustainability** by promoting safe reusable and recyclable solutions and help reduce the sector's environmental impact [23]. The framework Regulation was already amended in 2009 to enable active and intelligent packaging and in 2022 to allow safe recycled plastics in food packaging.

Legislation on food contact materials (FCM) is relevant for the success of key Commission policies under the EU Green Deal. The 'farm to fork' strategy commits to revise the FCM legislation in order **to improve food safety and public health**, in particular by reducing the use of hazardous chemicals, support packaging solutions using environmentally-friendly, re-usable and recyclable materials, and **contribute to food waste reduction**. A new

initiative is therefore also critical to support the Circular Economy Action Plan including a follow-up to the 2018 Plastics Strategy. It is also necessary to contribute to the ambitions of the Chemicals Strategy for Sustainability towards a toxic-free environment and action related to the most hazardous chemicals as well as considering their cumulative and combinative effects [24].

After a roadmap open for feedback in 2021 and a public consultation in the fourth quarter of 2022, the Commission is expected to announce its proposal in the second quarter of 2023 [23].

Active packaging on the EU market

The development of active food packaging to prolong product freshness and slow down spoilage can be promising to tackle SDG target 12.3, which specifically aims to reduce global food waste at the retail and consumer levels. The current trends of reduced food processing and using fewer food additives stimulate research on active packaging. If such **packaging innovations are allowed to advance**, their impact could be of benefit, not only in reducing food waste but also in improving food safety.

In the EU, active and intelligent packaging intended for food contact is regulated pursuant to Regulation (EC) No 450/2009. This regulation establishes a **premarket approval system** in which active and intelligent materials may not be marketed unless the individual substances responsible for the active or intelligent function are evaluated and included on the **European Community list** of eligible substances, with some limited exceptions. The safety of such substances must be evaluated by the European Food Safety Authority (EFSA) before their use in food packaging in the EU can be authorized.

EFSA's Panel on Food Contact Materials, Enzymes, Flavourings and Processing Aids (CEF) initially published guidelines on **submitting a dossier for safety evaluation** in 2009. A revision was endorsed in 2020, and the revised version of the guidelines was implemented in March 2021. The guidelines explain that safety assessments focus on the risks related to the dietary exposure to chemicals due to: i) migration of the active or intelligent substance, ii) migration of their degradation and/or reaction products and iii) their toxicological properties [25].

Active substances **behind a functional barrier** do not need a safety evaluation, provided that they are not mutagenic, carcinogenic, toxic to reproduction, or deliberately engineered to the nanoparticle size. The use of **nanoparticles** in food contact materials is assessed and eventually authorized on a case-by-case basis by EFSA. In 2021, EFSA has updated its Guidance on risk assessment of the application of nanoscience and nanotechnologies in the food and feed chain, human and animal health, which also cover the application area of food contact materials [26]. Both guidance documents on nano risk assessment and technical requirements elaborate on physicochemical characterization, key parameters that should be measured, methods and techniques that can be used for characterization of nanomaterials and their determination in complex matrices.

As new active packaging technologies find their way **into global markets**, legislative and regulatory issues must be considered. While Regulation (EC) No 450/2009 officially came into

force in 2009, the provisions relating to composition will not take effect until the **Community list of eligible substances** is published. Until then, the relevant national provisions will continue to apply [27].

CONCLUSION AND RECOMMENDATION

Research into PHAs is growing exponentially. Thanks to their broad physicochemical features, including biodegradability and biocompatibility, PHAs can be seen as circular polymers of the future, replacing traditional petrochemical equivalents. Given the duality of long-term features and degradation needs, the value-chain of PHA products from design through manufacture, value enhancement, and disposal should be strategic, considering safety and current legislation. In this PhD research, methodologies are being optimized to elucidate the potential mechanisms of Ag nanoparticle migration from biodegradable PHAs both in consumer and specific end-of-life scenarios in order to estimate the safety and application potential of bio-nanocomposites as active packaging materials. In this way, we aim to contribute to the implementation of sustainable, active, and above all safe bioplastic packaging materials.

REFERENCES

[1] Gutschmann B et al. Native feedstock options for the polyhydroxyalkanoate industry in Europe: A review. Microbiological Research. **2022**; 264: 127177, ISSN0944-5013. https://doi.org/10.1016/j.micres.2022.127177.

[2] Guzik MW. Polyhydroxyalkanoates, bacterially synthesized polymers, as a source of chemical compounds for the synthesis of advanced materials and bioactive molecules. Appl Microbiol Biotechnol. **2021**; 105(20): 7555-7566. doi: 10.1007/s00253-021-11589-0.

[3] Vanheusden C, Samyn P, Goderis B, Hamid M, Reddy N, Ethirajan A, Peeters R and Buntinx M. Extrusion and Injection Molding of (PHBHHx): Influence of Processing Conditions on Mechanical Properties and Microstructure. Polymers. **2021**; 13(22): 4012. https://doi.org/10.3390/polym13224012.

[4] Vanheusden C, Vanminsel J, Reddy N, Samyn P, D'Haen J, Peeters R, Ethirajan A and Buntinx M. Fabrication of poly(3-hydroxybutyrate-co-3-hydroxyhexanoate) Fibers Using Centrifugal Fiber Spinning: Structure, Properties and Application Potential. Polymers. **2023**; 15(5):1181. https://doi.org/10.3390/polym15051181

[5] Ragaert P, Buntinx M, Maes C, Vanheusden C, Peeters R, Wang S, et al. Polyhydroxyalkanoates for Food Packaging Applications in Reference Module in Food Science, Amsterdam: Elsevier, **2019**.

[6] Muiruri JM, Chuan JC et al. Poly(hydroxyalkanoates): Production, Applications and End-of-Life Strategies – Life Cycle Assessment Nexus. ACS Sustainable Chemistry & Engineering. **2022**; 10 (11), 3387-3406. https://doi.org/10.1021/acssuschemeng.1c08631.

[7] Meereboer KW et al. Review of recent advances in the biodegradability of polyhydroxyalkanoate (PHA) bioplastics and their composites. Green Chem. **2020**; 22: 5519, https://doi.org/10.1039/D0GC01647K

[8] Tan C et al. Novel bio-based materials and applications in antimicrobial food packaging: recent advances and future trends. Int J Mol Sci. 2021; 22: 9663. https://doi.org/10.3390/ijms22189663

[9] Couto C & Almeida A. Metallic Nanoparticles in the Food Sector: A Mini-Review. Foods. **2022**; 11: 402.

[10] Relinque J et al. Development of surface-coated PLA/PHA nanocomposites. Polymers. **2019**; 11:

400.
[11] Kraśniewska K et al. Biopolymers-Based Materials Containing Silver Nanoparticles as Active Packaging for Food Applications. A Review. Int J Mol Sci. **2020**; 21: 698.
[12] Istiqola A & Syafiuddin A. A review of silver nanoparticles in food packaging technologies: Regulation, methods, properties, migration, and future challenges. JCCS. **2020**; 67, 1942–1956.
[13] Bruna T, Maldonado-Bravo F, Jara P, Caro N. Silver Nanoparticles and Their Antibacterial Applications. Int J Mol Sci. **2021**; 22(13):7202. https://doi.org/10.3390/ijms22137202.
[14] Zahoor M et al. A Review on silver NPs: classification, various methods of synthesis, and their potential roles in biomedical applications and water treatment. Water. **2021**; 13: 2216.
[15] Tiekstra S, Dopico A, Koivula H, Lahti J and Buntinx M. Holistic Approach to a Successful Market Implementation of Active and Intelligent Food Packaging. Foods. **2021**; 10(2):465. https://doi.org/10.3390/foods10020465.
[16] Yildirim S et al. Active Packaging Applications for Food. Compr Rev Food Sci Food Saf. **2018**; 17: 165–199.
[17] FAO. Sustainable development goals. https://www.fao.org/sustainable-development-goals/goals/goal-12/en/
[18] Lambré C et al. Safety assessment of the substance silver NPs for use in food contact materials. EFSA Journal, **2021**; 19.
[19] Proposal for a revision of EU legislation on Packaging and Packaging Waste, Nov **2022**. Accessed April 2023 https://environment.ec.europa.eu/publications/proposal-packaging-and-packaging-waste_en
[20] European Green Deal: Putting an end to wasteful packaging, boosting reuse and recycling. Accessed April 2023 https://ec.europa.eu/commission/presscorner/detail/en/ip_22_7155
[21] Global bioplastics production defies challenges by showing significant increase, Dec **2022**, Accessed April 2023 https://www.european-bioplastics.org/global-bioplastics-production-defies-challenges-by-showing-significant-increase/
[22] EUBP's response on the proposal for rules on packaging and packaging waste. Accessed April 2023 https://www.european-bioplastics.org/policy/revision-of-the-packaging-and-packaging-waste-directive/
[23] Revision of EU rules on food contact materials. Accessed April 2023 https://ec.europa.eu/info/law/better-regulation/have-your-say/initiatives/12497-Revision-of-EU-rules-on-food-contact-materials_en
[24] Katsarova I. Members' Research Service. Proposal for a regulation revising EU legislation on Food Contact Materials In "A European Green Deal". Accessed April 2023 https://www.europarl.europa.eu/legislative-train/theme-a-european-green-deal/file-revision-of-eu-legislation-on-food-contact-materials
[25] EFSA. Administrative guidance for the preparation of applications on substances to be used in active and intelligent materials and articles intended to come into contact with food. EFSA Journal. **2021**: 18(3): EN-6513. 32 pp. doi: 10.2903/sp.efsa.2021.EN-6513.
[26] EFSA Scientific Committee. Guidance on risk assessment of nanomaterials to be applied in the food and feed chain: human and animal health. EFSA Journal. **2021**;19(8):6768. https://doi.org/10.2903/j.efsa.2021.6768
[27] Misko GG. The Regulation of Active and Intelligent Food Packaging in the U.S. and the EU. Food Safety Magazine. April/May **2022**.

AI-PP02

Novel temperature-sensitive label based on thermochromic ink for hot food packaging and serving applications

Prachi Jain[*1], *Kirtiraj K. Gaikwad*[1]

[1]*Department of Paper Technology, Indian Institute of Technology Roorkee, 247667, India*

[*]***Correspondence to:*** *Kirtiraj K. Gaikwad, Indian Institute of Technology Roorkee, E-mail: kirtiraj.gaikwad@pt.iitr.ac.in*

ABSTRACT: Changes in the lifestyle of the millennials have started a revolution in the food industry. They started preferring to have effortless ready-to-eat or cook meals (RTE) or fast-food chains and restaurants, and at the same time, they expect the food to be served hot. Nonetheless, it is impossible to know whether the desired temperature has been maintained in the RTE pouches or delivered food. Employing thermochromic materials as temperature indicators on the packaging can communicate the temperature of food inside. This work proposes a thermochromic coating composed of silver tetraiodomercurate (STIM) and cellulose acetate in the form of a coated label as a temperature indicator. From the thermochromism property of STIM, it was observed that the phase transition occurs at temperatures between 323 to 333 K. Colorimetric analysis of the labels revealed that the color changes from yellow to orange to red, indicating normal temperature and higher temperatures, respectively. Microstructural analysis of the label via FESEM reveals a uniform coating formation with traces of STIM agglomerates. Rub resistance and adhesion test proved that the solid particles have good adhesion with substrate and no scuffing traces. Hence, silver tetraiodomercurate-based thermochromic pigment can be used as a temperature indicator label for hot beverages, ready-to-cook retort pouches, and hot-served food delivered through apps for better communication of products' temperature.

Keywords: Thermochromic ink; Intelligent packaging; Food**;** Distribution

INTRODUCTION

The food packaging industry has been growing exponentially, and one of the major reasons is customer convenience. The growth of food delivery apps and fast-food chains has skyrocketed in recent times, largely due to the changing lifestyle of millennials. Therefore, the focus on customer convenience has increased like never before. These so-called food delivery apps are based on fulfilling customer needs with the utmost ease. But a practical problem that exists in these kinds of systems is that the final consumers are absolutely ignorant about the condition of the food being served. The term 'condition of food' focuses on the freshness of the food and some inquiries, such as whether the food that was delivered was actually prepared fresh when

the order was placed or if it was stale. In addition, if the food is not served hot, the customer who pays for hot food is let down and cheated.

Therefore, we have developed thermochromic ink to address these straightforward issues that arise frequently in the food chain systems. A suitable temperature indicator for hot-delivered foods not only tackles the above-mentioned issues efficiently but also prevents any chances of malpractices from restaurants or food chains and increases customer loyalty.

GOAL OF THE RESEARCH

- To develop a reliable temperature indicator that changes color instantly when exposed to different temperatures,
as shown in Fig. 1.
- To apply it as a coating on a paper substrate with adhesive backing.
- To help the consumer identify the state or temperature of delivered food or ready-to-eat foods.
- To avoid any case of malpractice from the fast-food chains.
- To ensure the food safety of the delivered food.

Figure 1. Shows the color change from yellow to orange-red of the thermochromic label when a hot liquid is poured into a cup.

EXECUTION OF THE RESEARCH

The research was executed in two steps, mainly the preparation of thermochromic pigment and coating solution, followed by testing procedures and results interpretations.
The methodology related to the preparation of thermochromic pigment and coating solution is described below.

Preparation of thermochromic pigment

The thermochromic pigment was prepared using a simple precipitation reaction. Initially, the silver nitrate solution was prepared by dissolving 7.8 g of silver nitrate in 100 mL of distilled water. 60 mL of Nessler's reagent was measured and kept for stirring at 323 K. Once it reached the desired temperature, 50 mL of the prepared silver nitrate solution was added while mixing. After 30 minutes of continuous stirring at low speeds, a yellow precipitate of silvertetraiodo mercurate was formed and kept undisturbed for the next 4 hours. Finally, the deposit was filtrated using Whatman filter paper to separate the settled solid particles, followed by drying at 333 K to obtain dry pigment. It is further stored in airtight containers till the coating solution is prepared.

Preparation of thermochromic coating solution

The coating solution was prepared in a cellulose acetate emulsion with varying concentrations of thermochromic pigment. Initially, 10 wt.% cellulose acetate (CA), i.e., 4g, emulsion was prepared in 40 g of acetone and stirred at room temperature for 2 h. Glycerol, as a plasticizer, was added to the CA solution at a constant 1 wt% concentration based on solvent mass and continued to stir for another 10 minutes. For uniform dissolution of glycerol, the solution was subjected to sonication for 10 minutes using a bath sonicator. Now, the mass concentrations of thermochromic pigment were considered as 0%, 50%, 60%, 70%, and 80 wt% of CA, and they are added to the CA solutions followed by stirring for 20 mins and are stored in air-tight containers till further use.

Thermochromic coating on a paper sheet

The prepared solution was coated onto an adhesive back paper of GSM 150 using an automatic bar coater (Sheen Automatic Film Applicator-113N). A single layer was coated using a Meyer rod of a thickness of 50 µm. The traverse speed of the machine was maintained at 100 mm/sec. Drying was carried out at room temperature for 2 h. The samples were named Neat CA, CA/STIM 50, CA/STIM 60, CA/STIM 70, and CA/STIM 80 according to the mass percentage of STIM added.

RESULTS AND CONCLUSIONS

Solid content test

Strict laws follow for the utilization and emission of volatile organic compounds, so the coating industry constantly reduces the ink's volatile content and increases solid content (Huang et al., 2017). A solid content of 16.93% in the organic-based thermochromic ink was observed. The higher solid content of the coating influences the viscosity, which can affect the drying rate, shades, and printing speed.

Field emission scanning electron microscopy:

The microstructure of the coated surface was captured under field emission scanning electron microscopy at a magnification of 100 µm and represented in Fig. 2. As seen in the figure, the coating of cellulose acetate has formed a smooth and fine coating on the paper's surface. This confirms that the cellulose acetate has formed a homogenous coating solution that can adhere to the surface without any phase separation. With the addition of thermochromic pigment to the base solution, the density of solids settled on the surface has gradually increased. The coating with 80% (w/w) of STIM has maximum aggregated particles on the surface. This could either be because of the non-uniform dispersion of STIM in CA solution leading to observable micro-clusters or the etched top most layer due to the plasma sputtering. The conductive nature of STIM could be responsible for the latter phenomenon. Our result was similar to (Hameed et al., 2018), who characterized Ag_2HgI_4 films. From the micrographs, it can be concluded that, although there is the micro aggregation of STIM particles, the surface hasn't had any phase separation; instead seems to be having excellent adhesion despite agglomerates.

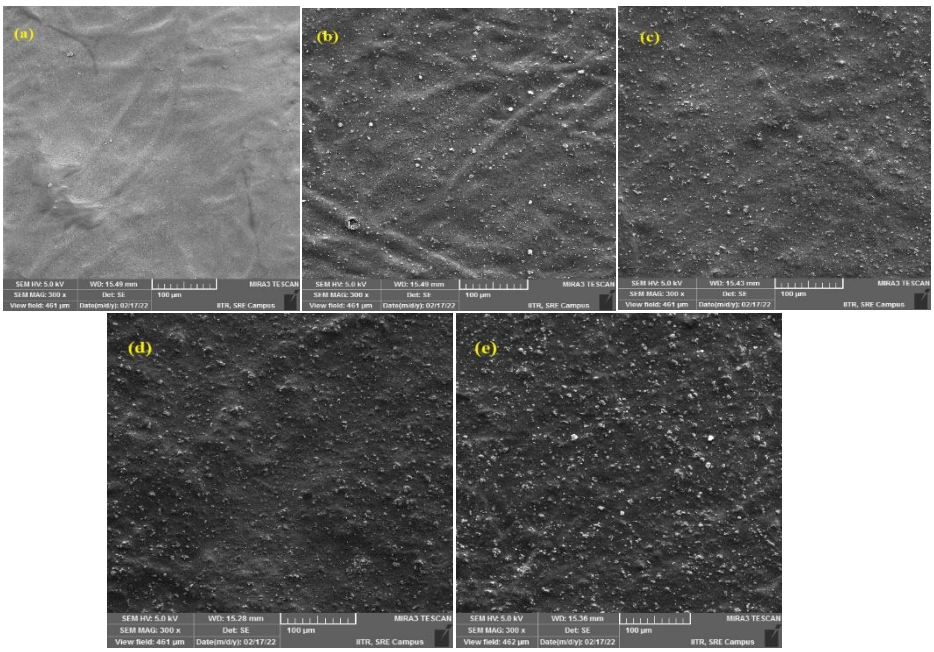

Figure 2. Surface morphology of thermochromic pigment coated labels (a) Neat cellulose acetate, (b) cellulose acetate/ silver tetraiodomercurate 50, (c) cellulose acetate/ silver tetraiodomercurate 60, (d) cellulose acetate/ silver tetraiodomercurate 70 and (e) cellulose acetate/ silver tetraiodomercurate 80

Thermal analysis

The thermal degradation pattern of Neat CA and CA STIM with different loadings of STIM Pigment was shown in Fig. 3. The thermal degradation of Neat CA and CA STIM-50, 60, 70,

and 80 occurs in three different regions, as illustrated in DTG curves. The loss in mass below 200 °C was due to the evaporation of volatile materials like moisture and solvent residues from the coated paper. The main degradation takes place in the range of 270-350 °C, which was the disintegration of the macromolecular polymeric chain of cellulose acetate and the evaporation of HgI_2 impurities. The last stage of loss in mass was due to the carbonization of the left-out products into ash at ~600 °C (Arthanareeswaran et al., 2004). There was a decrement in Neat CA's thermal stability, as seen in Fig. 3. This may be a result of an increase in the loading of STIM. It was depicted from the DTG curve, Fig.3, that the T_{max} for the Neat CA, CA STIM-50, 60, 70, and 80 was 340 °C, 330 °C, 328 °C, 330 °C, 332 °C, respectively. The T_{max} was slightly modified with the addition of thermochromic ink. These results illustrated that the T_{max} for the CA STIM-50 and CA STIM-60 was decreased and for CA STIM-70 and CA STIM-80 increased, but the value of T_{max} for different loadings of STIM was less than Neat CA, which implies that thermal stability decreased. Similar results were found by (Bruna et al., 2014), where the thermal stability of cellulose acetate decreased by the presence of $MtCu^{2+}$.

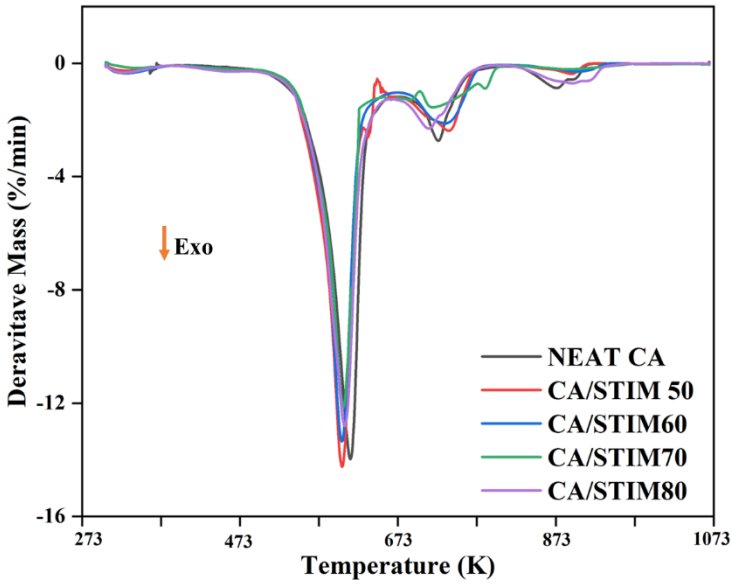

Figure 3. Differential thermogravimetric curves of neat cellulose acetate coated label and labels with varying concentrations of silver tetraiodomercurate. Arrow indicates Exo (exothermic) direction on the DTG scale.

Rub resistance test

Rub resistance is an essential characteristic of ink that ensures the clarity of printed objects or even the visibility of any flaws in printing design. They are subjected to exposure to vibration, impacts, abrasion, continuous interaction with one another, and rubbing inside the printed roll itself during the shipping of the products. Coated label adhered to the package must be durable in all conditions. A digital camera was used to take photographs of the rubbed paper surface of the thermochromic coating on a paper sheet after 20 rub cycles. The change in colour in the

rubbed surface area of the thermochromic coated test sample can be used to demonstrate the rub resistance of the coated paper sheet, which can be analysed by the images given in Fig. 4. The obtained results indicate no significant signs on the rubbed thermochromic ink-coated paper sheet, demonstrating the produced inks' outstanding rub resistance property. Our finding are similar to Sharma et al., 2021 and Nielsen et al., 2015, in their study of Waterborne acrylic copolymer resin preparation as a binding agent to develop water-based inks in the printing application and silica films on glass surfaces.

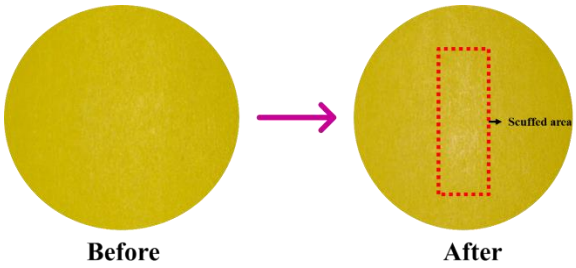

Figure 4. Rub resistance analysis performed on cellulose acetate and silver tetraiodomercurate 70 coated label before and after 20 cycles of testing

Adhesion test

The primary cause of organic solvent-based thermochromic ink failure is poor printability toward paper-based substances and polymeric films due to the large surface energy gap between paper-based polymeric films and ink. It is challenging to maintain sufficient adhesion between the polymeric film and ink. Various additives are also responsible for the ink's excellent adhesion properties. Winder, also known as resin, is important in imparting ink and dye adhesion properties. Because of the high surface energy of organic solvent acetone used as a vehicle for ink transfer, it is tough to maintain the variation in surface energy. The adhesion significance for yellow colour thermochromic inks coated on the paper sheet was 86 %, indicating that the developed inks had good adhesion properties to the paper sheet. The enhanced intermolecular interactions among the cellulose acetate resin chain might have improved the adhesion property. The surface irregularity of the paper sheet and the low surface energy difference between the paper sheet and the produced ink may also work as anchoring between ink and surface. Lee and Choa, 2012 depicts a similar test result and method in their study of adhesion enhancement of ink-jet printed conductive copper patterns on a flexible substrate.

Colorimetric analysis

Color values are extremely important in the customer's acceptance of a packaging product. L, a, and b values can quantify the color of any ink. The color of coated labels before and after exposure to varying temperatures was analyzed using Spectro-colorimeter (CIE Lab Values). The color of the labels at room temperature is determined as yellow by visual examination. But

with the increasing concentration of STIM, it was presumed that the yellow color's intensity would also increase. The neat CA label has the highest L value of 89.77, and the label with 80% STIM has the lowest of 67.26. As the concentration of thermochromic ink increased, the yellowness (+b value) was seen to be increasing from 0.37 to 62.95. Surprisingly, CA/STIM 70 has the highest b value, possibly because of the increased coat mass as understood from the thermogravimetric analysis. When exposed to increasing temperature, there was a noticeable change in a^* values as the color changed from yellow to orange or reddish-orange. It has gradually increased with temperature for all the samples. As seen from Fig. 5., at every temperature, the sample with 70% STIM has shown the highest +a value. The graphs conclude that the coated samples were changing their color gradually from yellow to orange when exposed to higher temperatures and that change was significant enough to know whether the packaging had reached a temperature of more than 323 K if applied on ready-to-eat retard pouches.

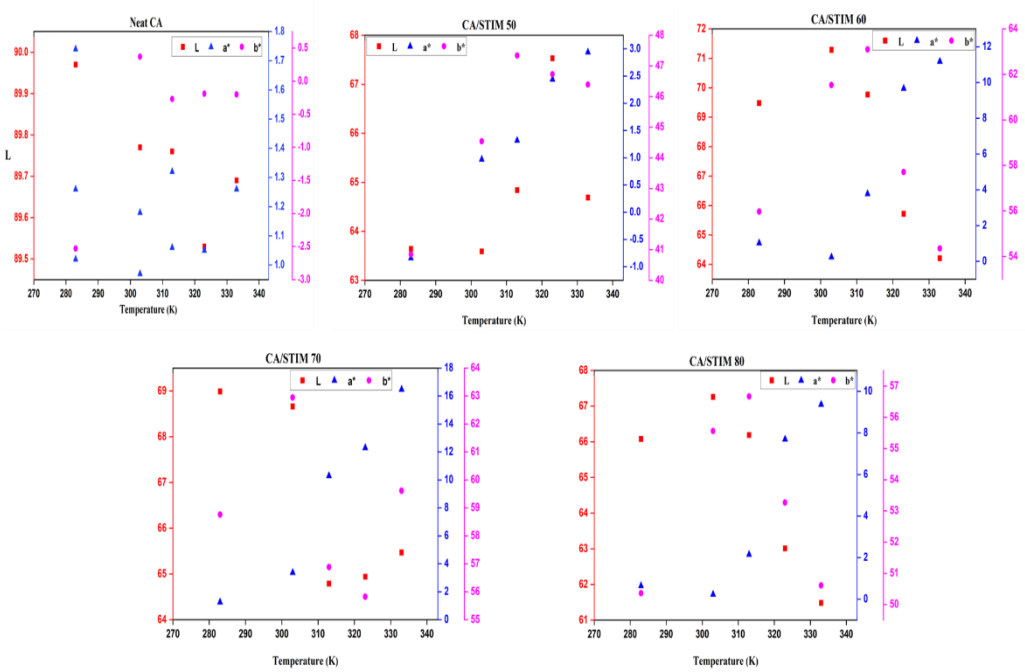

Figure 5. Colorimetric analysis for observed change in color of neat cellulose acetate coated label and labels coated with different silver tetraiodomercurate loading solutions when exposed to varying temperatures ranging between 283 and 333 K

Thermochromism of coated label

As seen in Fig. 6., it is clear that the coated label changes its color when exposed to different temperatures, and its intensity has varied by the concentration of STIM. As discussed, the initial color of all coated samples was yellow, and the intensity of the yellow color is maximum for 80% STIM. At room temperature, the sample with 50% STIM was more greenish-yellow in color, and at 80%, yellow was prominently visualized. With the increase in temperature, the

sample with 70% STIM has shown reddish-brown color at 313 K and the highest a^* value indicating the dominant reddish-orange color. The reason behind this color change is the change in the crystal lattice structure of STIM accompanied by electrical and ionic conductivities when exposed to elevated temperatures. The structure of STIM has a huge number of interstitial spaces which are connected tridimensionally and allow the movement of cations for ionic conductivity. At lower temperatures, STIM has an ordered tetragonal shape called β- the phase, and at high temperatures, it turns into a disordered pseudo-cubic α- phase. The thermochromic transition occurs as a consequence of the order-disorder transition. This change occurs at a particular temperature called phase change temperature, typically 323 K for STIM (Chocolatl-Torres et al., 2020). This change is reversible in nature, and the color changes from yellow to orange to red. These images confirm that STIM in a coated label form changes its color and can be used as a thermochromic label for smart packaging applications.

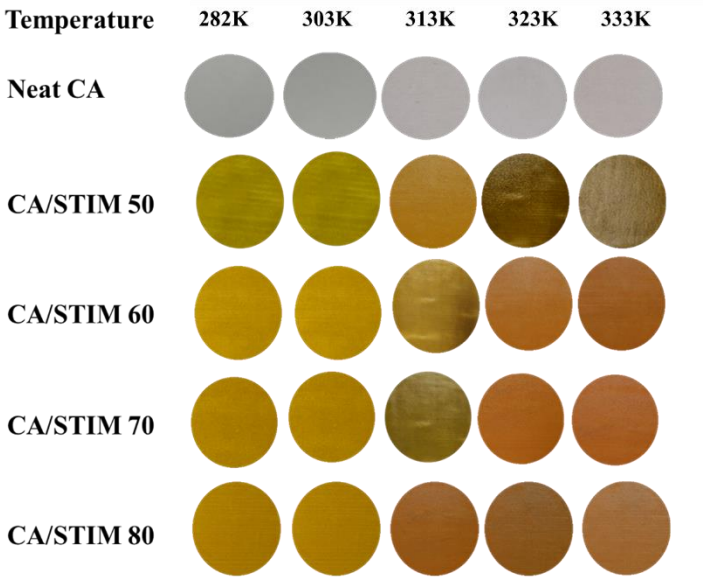

Figure 6. Thermochromism observed in cellulose acetate and silver tetraiodomercurate (varying concentrations) coated labels when exposed to 283, 303, 313, 323, and 333 K

CONCLUSION

Advanced packaging with effective communication regarding the state of the packed product is highly convenient for consumers. These days, ready-to-eat or cooked meals and snacks are being preferred alongside ordering from restaurants. Also, consumers wish to know the freshness of the food ordered just by looking at the packaging. A simple temperature indicator will visually channel the temperature of food inside by a simple mechanism of thermochromism. Such an indicator label was developed using silver tetraiodo mercurate pigment by coating it on paper with the help of a cellulose acetate binder. The performed characterization techniques on examining the thermochromism of the prepared label concluded

that the developed indicator is efficient to use in monitoring the temperatures. The colorimetry has proved that STIM has changed its color from yellow to orange when exposed to temperatures greater than 313 K and will remain the same till 333 K. Such types of indicators can be used on foods that are preferred to be eaten and served hot such as hot beverages, primary packaging of food ordered through food delivery apps, and read to cook or eat retort pouches just to indicate whether the food is at the desired temperature or not. By performing adhesion and rub resistance tests, it is understood that this coating can further be developed for printing ink which can be even more convenient.

RECOMMENDATIONS

- The developed novel color-changing system based on temperature is a kind of advanced packaging that communicates the state of the product to consumers. It focuses on customer convenience.
- Thermochromic ink can not only communicate about the food's temperature but may also communicate about the freshness of the food.
- All the tests performed on the ink produced positive results, such as colorimetry tests proving the change in color with a change in temperature from 39.8 ºC to 59.8 ºC.
- By performing adhesion and rub resistance tests, it is understood that this coating can further be developed for printing ink which can be even more convenient.

REFERENCES

1. Arthanareeswaran, G., Thanikaivelan, P., Srinivasn, K., Mohan, D., Rajendran, M., 2004. Synthesis, characterization and thermal studies on cellulose acetate membranes with additive. Eur. Polym. J. 40, 2153–2159.
2. Bruna, J.E., Galotto, M.J., Guarda, A., Rodríguez, F., 2014. A novel polymer based on MtCu2+/cellulose acetate with antimicrobial activity. Carbohydr. Polym. 102, 317–323.
3. Chocolatl-Torres, M., Franco-Bacca, A.P., Ramírez-Rincón, J.A., Gómez-Heredia, C.L., Cervantes-Alvarez, F., Alvarado-Gil, J.J., Silva-Gonzalez, R., Toledo, M., Salazar-Kuri, U., 2020. Study of structural and optical properties of the thermochromic silver and copper tetraiodomercurates (Ag 2, Cu 2) HgI 4 ceramics. Appl. Phys. A 126, 1–9.
4. Hameed, T.A., Radaf, I.M. El, Sakr, G.B., 2018. Synthesis and characterization of thermochromic Ag 2 HgI 4 thin films. Appl. Phys. A 124, 1–9.
5. Huang, S., Xiao, J., Zhu, Y., Qu, J., 2017. Synthesis and properties of spray-applied high solid content two component polyurethane coatings based on polycaprolactone polyols. Prog. Org. Coatings 106, 60–68.
6. Lee, Y.-I., Choa, Y.-H., 2012. Adhesion enhancement of ink-jet printed conductive copper patterns on a flexible substrate. J. Mater. Chem. 22, 12517–12522.
7. Nielsen, K.H., Karlsson, S., Limbach, R., Wondraczek, L., 2015. Quantitative image analysis for evaluating the abrasion resistance of nanoporous silica films on glass. Sci. Rep. 5, 1–10.
8. Sharma, B., Sauraj, S., Kumar, B., Pandey, A., Dutt, D., Negi, Y.S., Maji, P.K., Kulshreshtha, A., 2021. Synthesis of waterborne acrylic copolymer resin as a binding agent for the development of water-based inks in the printing application. Polym. Eng. Sci. 61, 1569–1580.

AI-PP03

Natural pH sensors as a quality monitoring smart label for poultry packaging

Konala Akhila[1], Dakuri Ramakanth[2], Kirtiraj K. Gaikwad[1*]

[1]Department of Paper Technology, Indian Institute of Technology Roorkee, Roorkee, Uttarakhand, 247667
[2]Department of Polymer and Process Engineering, Indian Institute of Technology Roorkee, Roorkee, Uttarakhand, 247667

***Correspondence to**: Kirtiraj K. Gaikwad, Indian Institute of Technology Roorkee, E-mail: kirtiraj.gaikwad@pt.iitr.ac.in*

ABSTRACT: With enormous amounts of food being wasted at every level of consumption, the future of food security is in jeopardy. The confusion aroused due to "best before" or "use by" can be eliminated by intelligent colorimetric indicators which communicate the quality of food. pH indicators have gained their attention because they are simple and visually informative. Using natural pigments to fabricate pH indicators can help reducing use of carcinogenic chemicals in packaging. In this work, anthocyanins extracted from a novel flower source named Ipomoea coccinea (ICE) were added to polyvinyl alcohol (PVA) and guar gum (GG) matrix in varying amounts and was applied as antioxidant and intelligent pH indicator film to monitor the freshness of chicken fillets and to visually communicate the quality of chicken. The pH indicator was characterized for halochromism, antioxidant activity, thermogravimetry, water solubility, water contact angle, surface morphology, colorimetry and X-ray diffractograms. The color change of the extract was observed from orange to red to yellow. Film with highest amount of anthocyanin extract has increased thickness of 150.5±17.86a (µm), decreased water vapor transmission rate of 4.95±0.29a (mg day-1 cm-2) and has a crystallinity of 52.35%. Anthocyanins started to degrade at 65°C according to thermogravimetric analysis. The film with 20% ICE showed an excellent color change in pH solutions and the highest antioxidant activity of ~ 91%. The food study results suggested that the developed film has the potential to be employed as an active and intelligent visual indicator in poultry packaging.

Keywords: pH indicator; Guar gum; Ipomea coccinea extract; Antioxidant; Intelligent Packaging;

INTRODUCTION

Due to its high moisture content, meat that is fresh is a perishable food item that is rich in nutrients. The smallest amount of meat deterioration cannot be seen with the naked eye, and the conventional way of determining spoiling is a time-consuming procedure that is not

practical for the consumer. Food can be guarded from environmental dangers by packaging, which also makes marketing and distribution easier and lowers financial losses. Research progress has resulted in the creation of pH indicators that can forecast changes in the physiological properties of food. A pH sensor or indicator typically consists of two elements: dye and solid support. Generally, natural dyes such as curcumin, anthocyanin, and betacyanin are preferred over synthetic dyes because the latter has carcinogenic behavior and toxicity(Akhila et al., 2022; Friedman & Jürgens, 2000; Kunam et al., 2022)

The most popular natural pigments for making pH indicators to check the freshness of food are anthocyanins. It comes in six different forms, including cyanidin, peonidin, pelargonidin, malvidin, delphinidin, and petunidin, and is made up of anthocyanidins with colors ranging from red to blue. Ipomoea, a genus with thousands of species in the family Convolvulaceae, is one of the sources. It is a genus that is significantly expanding. Fewer Ipomoea flowers have yellow petals because of carotenoids, and most of their petals are red because of anthocyanins. One species of Ipomoea coccinea has red-colored flowers and is abundant in pelargonidin(Cui et al., 2022; Khoo et al., 2017; Yong & Liu, 2020).

Polyvinyl alcohol is one of the widely studied materials. It is biodegradable thermoplastic and has good chemical resistance, non-toxic behavior, good barrier characteristics, and high flexibility. Various studies have used a combination of polyvinyl alcohol with natural polysaccharides to improve the mechanical strength of the film, such as polyvinyl alcohol blended with okra mucilage polysaccharide. Guar gum (GG) is a non-ionic natural polysaccharide obtained from Cyamopsis tetragonolobus. The addition of guar gum to the packaging matrix is desirable due to its good film-forming ability, biodegradability, water solubility, wide range pH stability, and emulsifying ability, which helps in improving the intrinsic characteristics of the packaging matrix(Deshmukh et al., 2022; Mohammadi et al., 2018; Mustafa et al., 2021; Pieczykolan & Kurek, 2019; Tanwar et al., 2021).

To the best of our knowledge, a study on anthocyanins extracted from Ipomoea coccinea as pH indicator films has not been investigated so far. The purpose of this study is to develop a pH indicating film using Ipomoea coccinea extract (ICE) and a biodegradable matrix made up of polyvinyl alcohol and guar gum which monitors the shelf life of chicken fillets.

GOAL OF THE RESEARCH

- Using natural pigments to fabricate a pH indicator
- Exploring novel sources for anthocyanins
- Monitoring the dynamic shelf life of poultry meat
- To develop a food contact safe, potentially biodegradable and non-carcinogenic pH sensitive freshness indicator
- Analyzing the compatibility of two biodegradable polymers namely guar gum and PVA

EXECUTION OF THE RESEARCH

Extraction of Anthocyanins from Ipomoea Coccinea

Extraction was carried out according to (Boonsiriwit et al., 2021) with slight modifications. In brief, fresh flowers were sun-dried until the petals turned brittle. Dried flower petals were powdered and weighed to 6 g. Solvent (90 mL) was prepared using 80% of ethanol (v/v) and 20% deionized water (v/v). Then the pH of the solvent was adjusted to 2 using 1M HCl to facilitate efficient extraction from the dried powder. The powdered flower was immersed in solvent for 12 h under constant stirring at 350 rpm. The obtained mixture was filtered using Whatman filter paper 1 followed by centrifugation at 7000 rpm for 10 min. The obtained supernatant was stored under refrigeration (4°C) until further use.

Preparation of pH indicator films

The solvent casting method was used to develop the films. 4 g of PVA was dissolved in 100 mL of deionized water at 90 °C with continuous stirring at a speed of 350 rpm for 120 min with the help of a hot plate magnetic stirrer. Then 0.25 g of guar gum was weighed and incorporated into the aqueous PVA solution. To improve the flexibility of the film, glycerol 2 % (v/v) was added to the solution. Different concentrations (5, 10, and 20%) of Ipomoea coccinea extract were added to the film forming solutions. Then solutions were homogenized at 5000 rpm for 10 min to obtain homogenous solutions. The compositions of the films with varying concentrations of the flower extract are mentioned in Table T_1 (Supplementary data).

The prepared solutions were cast onto the polypropylene petri dishes (9 cm diameter) and dried at 40°C for 12 h. The dried films were peeled off, and the films without the incorporation of flower extract were labeled as neat and considered as control. The films with flower extract concentrations of 5%, 10%, and 20% were labeled as PVA/GG/ICE5, PVA/GG/ICE10 and PVA/GG/ICE20, respectively.

RESULTS AND CONCLUSIONS

Thickness

The bio composite films developed using polyvinyl alcohol and guar gum were able to be peeled off from petri dishes and showed homogenous morphology without bubbles and brittle areas. The thickness of the film is a critical characteristic for evaluating physical properties and is associated with mechanical attributes, water vapor transmission rate, oxygen transmission rate, and light permeability (Kanatt et al., 2012; Kumar et al., 2021). The thickness of films with and without extract ranged between 139.0 ± 14.86^{a} to 152.5 ± 21.63^{a} µm, as shown in Table 1. Compared with the neat films, films with Ipomoea Coccinea extract showed a slight increment in thickness. The PVA/GG films were incorporated with ethanolic extract of flower and dried at elevated temperatures, which caused the complete volatilization of the solvent. The residual solid content might have contributed to the increase in film thickness. In a previous

study, Qin and co-workers reported that the addition of extract contributed to an increment in film thickness (Qin et al., 2019).

Samples	Thickness (µm)
Neat	139.0±14.86[a]
PVA/GG/ICE5	152.5±21.63[a]
PVA/GG/ICE10	147.5±18.14[a]
PVA/GG/ICE20	150.5±17.86[a]

Table 1. Thickness and tensile strength of the neat and active/intelligent film samples

The values displayed are as Mean ± Standard deviation obtained through triplicate (n = 3) analysis. The a, b, c within the same column is significantly different at a 95% confidence interval ($p < 0.05$)

Field Emission Scanning Electron Microscope (FESEM)

A qualitative analysis to understand the geometrical hierarchy of developed films was carried out with the help of FESEM, and the images were represented in Fig. 1. A homogenous clean surface was observed for the neat film with sparse particles. Due to homogenization, the guar gum particles were well dispersed in the solution; hence no significant clusters were seen, which indicates that the film has good interaction between PVA and guar gum with better integrity. With the addition of ICE to the neat film, increased agglomerates were found, which could be formed due to altered interactions between the biopolymer network of GG and PVA (Alizadeh-Sani et al., 2021). The magnified image in PVA/GG/ICE 10 shows the clustered particle of guar gum. Although there was not any notable increase in agglomerates with further addition of ICE, slightly bigger clumps could be seen in PVA/GG/ICE 20. Moreover, a further increased number of hydroxyl groups in the film might have been an added advantage to GG in retaining its hydrogen bonding with PVA and might help control additional agglomeration (Koosha & Hamedi, 2019). Comparatively, PVA/GG/ICE 10 seems rough, which might be the reason for its increased water contact angle.

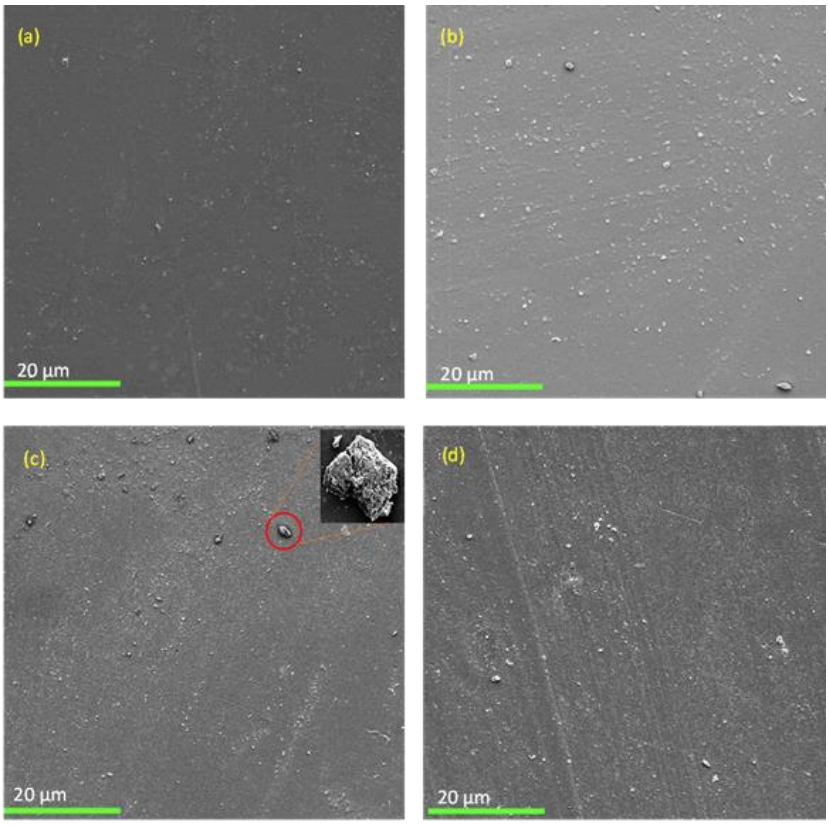

Figure 1. Surface morphology analysis of (a) Neat, (b) poly vinyl alcohol and guar gum matrix with 5% Ipomoea Coccinea extract, (c) poly vinyl alcohol and guar gum matrix with 10% Ipomoea Coccinea extract, and (d) poly vinyl alcohol and guar gum matrix with 20% Ipomoea Coccinea extract; The Magnified image in (c) is guar gum agglomerate taken at 5µm

UV–Vis Spectra of ICE in Different pH Solutions

Fig. 2 (a). represents the color variation of ICE in different pH solutions ranging from 2 to 12. The red color was observed at pH 2; red to orange at pH 3-6; orange to yellow at pH 7-10; and purple to brown at pH 11-12. The corresponding UV-vis spectra of ICE in pH solutions are shown in Fig. 2(b). At pH 2, the maximum absorption of ICE was observed at 504 nm, suggesting that the increase in anhydrous bases and the red flavylium ion predominates possessed red color. When the pH increased from 3 to 6, the maximum absorbance of the ICE was decreased, and the color was changed from red to orange, which might be due to the predominant form (pelargonidin) of anthocyanins (Castañeda-Ovando et al., 2009). Upon increasing the pH from 7 to 9, the maximum absorbance was shifted to 577 nm. The shift might be due to the transformation of anthocyanins which results in the formation of apigeninidin (3-desoxypelargonidin), a yellow pigment. The absorption maxima for pH 10, 11, and 12 were recorded at 580 nm, 595 nm, and 605 nm suggesting the shift in absorbance. It might be due to the transformation of anthocyanins to cyanidin, which might have possessed purple-brown

color. When the extract is exposed to changing pH from acidic to alkaline medium, a bathochromic shift was observed due to the structural changes in anthocyanins (Harborne, 1993).

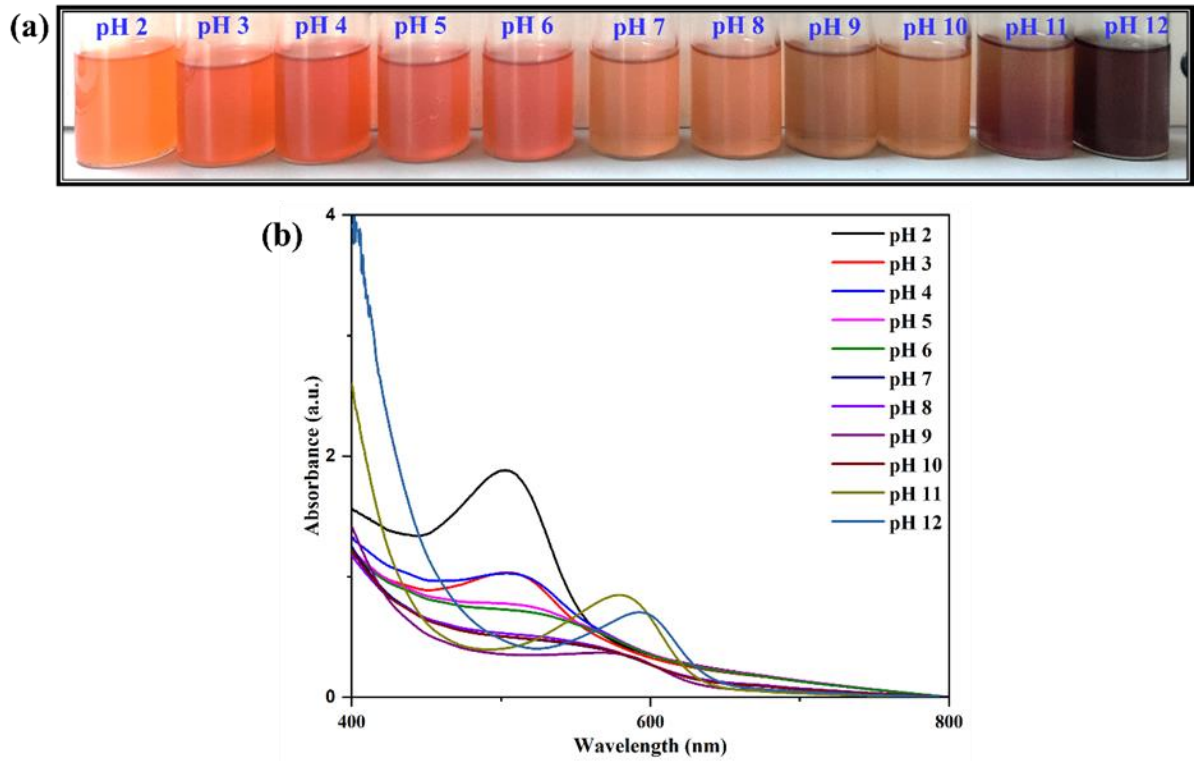

Figure 2. (a) Color change of Ipomoea Coccinea extract in different pH solutions ranging between 2 to 12, and (b) corresponding UV–Visible spectra observed between 400 to 800nm

Colorimetric Response of The Films to Different pH Solutions

The color response and the UV-vis spectra revealed that the color of the ICE was strongly pH-dependent. To understand the visual color variation of PVA/GG/ICE20 films, it was immersed in different pH solutions, as shown in Fig. 3. The variation in the color of anthocyanin at different pH is due to a change in the chemical structure of anthocyanin (Castañeda-Ovando et al., 2009). The color of the film was red at pH 2, possibly due to a higher number of flavylium cations. This color changed to light violet upon increasing the pH. The color intensity was enhanced at pH 9-11, and it might be due to the emergence of carbinol pseudo-bases or quinonoidal bases (Mohammadalinejhad et al., 2020). At pH 12, yellowish-green color was observed, which further intensified to yellow at pH 13. This could be possibly due to the formation of yellow chalcone (Brouillard, 1982).

The pH-induced color change in PVA/GG/ICE20 is different from the color change of the ICE. This could be possibly due to the difference in phase, which might have been attributed to the different changes in the structural formation of anthocyanins. The evaporation of the

solvent incorporated into the film with ICE might have also contributed to the change in pH response, which was reported in previous studies on pH indicators (Luchese et al., 2017; Wei et al., 2017; Yong et al., 2019). FTIR results also revealed shifting in bonds, which might have contributed to the difference in color change between ICE and film in response to the pH.

Fig. 4 (a)., shows the ΔL, Δa, Δb, and ΔE values. The lightness values of the films at pH 2 and 13 were recorded as 81.12 and 81.67, respectively, showing no significant difference, with an erratic fluctuation between the pH solutions. The Δa value of the films between pH 3-7 was lesser than the value at pH 2 (8.43). From pH 8-10, the Δa value increased and then further decreased. The Δb value didn't show a significant difference between pH 2 and 11, but at pH 12, a greenish-yellow color was observed (Prietto et al., 2018). Yellowness was increased upon the further increase in pH to 13 (17.65). Generally, ΔE values above 5 are considered to be perceivable by the naked eye, and if above 12, it has an absolute color change which is more prominent (Moradi et al., 2019). Our results suggest that except for the pH 8 (4.40), all are higher than 5, which can be visually observed in Fig. 4(b). Therefore, PVA/GG/ICE20 had good color-changing properties; thus, it can be used as a pH indicator to monitor the freshness of meat-based food products.

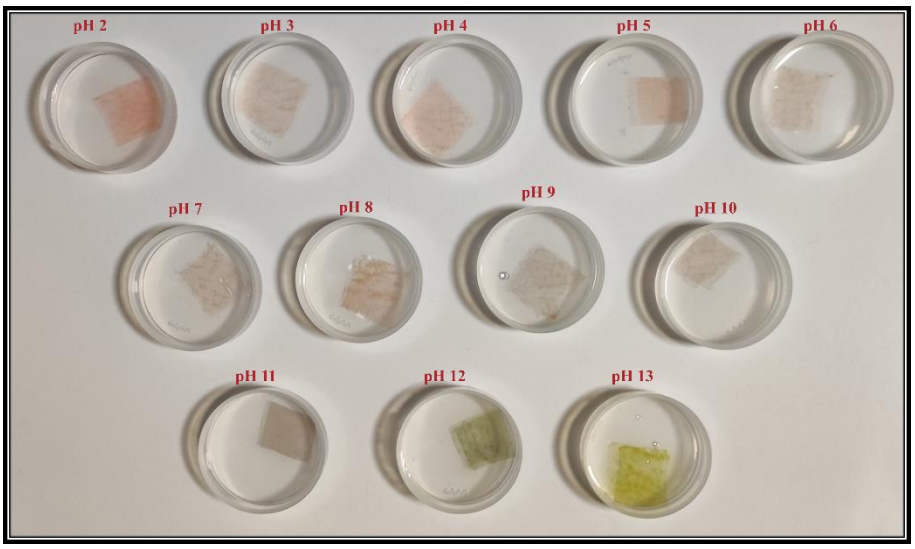

Figure 3. Color change observed in poly vinyl alcohol and guar gum matrix incorporated with 20% Ipomoea Coccinea extract samples when immersed in different pH solutions ranging between 2 to 13

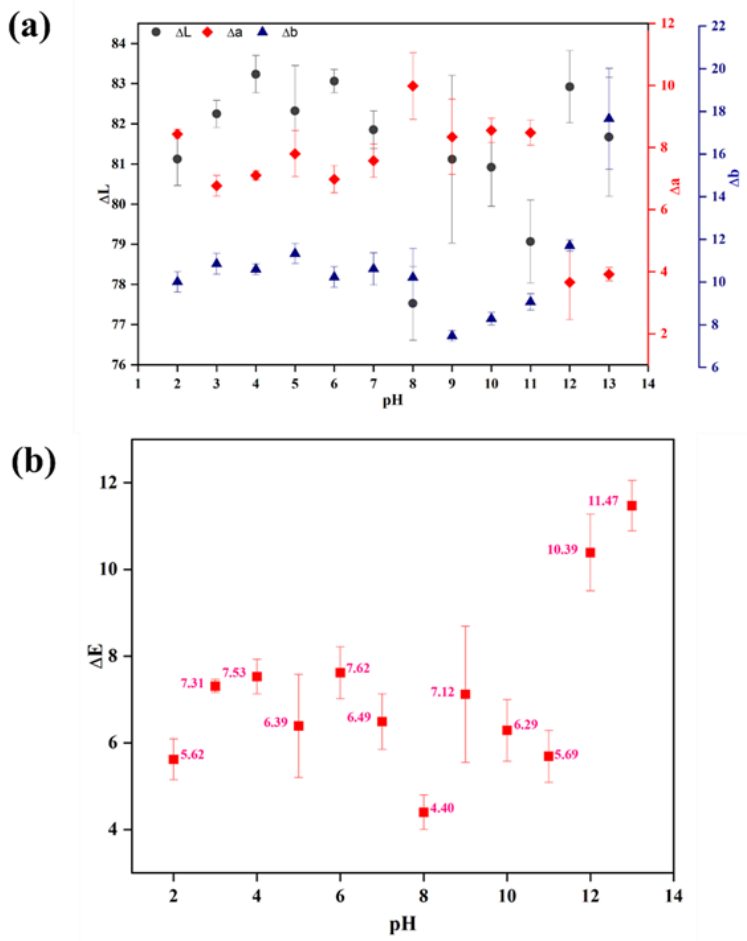

Figure 4. The plot of lightness, redness, and yellowness (a) ΔL, Δa & Δb Vs. pH (b) ΔE Vs. pH values of active/intelligent films after exposure to different pH solutions

Samples	WVTR (mg day^{-1} cm^{-2})	Contact Angle (º)
Neat	5.59±0.08^{b}	37.63±0.95^{b}
PVA/GG/ICE5	5.24±0.14^{ab}	31.54±2.58^{b}
PVA/GG/ICE10	5.17±0.26^{ab}	34.20±4.65^{b}
PVA/GG/ICE20	4.95±0.29^{a}	23.15±3.22^{a}

The values displayed are as Mean ± Standard deviation obtained through triplicate (n = 3) analysis. The a, b, c within the same column is significantly different at a 95% confidence interval ($p < 0.05$).

Table 2. Water solubility, WVTR, and contact angle of the neat film and the PVA/GG films with 5, 10, and 20% Ipomoea Coccinea extract concentrations

Water Contact Angle

The water contact angle value helps predict the hydrophobicity of the samples; the greater the angle, the more is the hydrophobicity and vice-versa. The contact angles of film samples are shown in Table 2. The decrease in contact angle was observed with an increase in ICE concentration, and the neat film showed the contact angle of 37.63±0.95º. Water droplet spreads more widely on soluble surfaces than insoluble ones. It can be observed from the water solubility results that the water solubility of films with ICE was higher than the neat film (Monjazeb Marvdashti et al., 2017; Phan et al., 2005). Thus, this could be the conceivable reason for the increase in contact angle. The contact angle results were consistent with the water solubility of the films. These results do not follow the same trend observed in the water vapor transmission rate. Therefore it needs to be considered that there are other factors affecting wettability apart from affinity to water (da Silva Filipini et al., 2020). For PVA/GG/ICE10 film samples, the contact angle was 34.20±4.65, which could be due to the formation of strong intermolecular interactions of ICE components with the base matrix, increasing crystallinity of the film.

Water Vapor Transmission Rate

The water vapor transmission rate of food packaging material is an important factor because it impacts the shelf life. Therefore, it is desirable to have a low water vapor transmission rate of the film (Chen et al., 2019; Gasti et al., 2021). Table 2 represents the WVTR value of the neat film and films with ICE. The WVTR of films followed a decreasing trend with increasing the ICE concentration, and the neat film showed the highest transmission rate (5.59 ± 0.08^{b}). The lowest water vapor transmission rate was recorded by PVA/GG/ICE 20 film. As observed from the FTIR results, hydrogen bonds were formed between hydrophilic groups of PVA/GG matrix and ICE, which reduced the free hydroxyl groups hence, resulting in a better water-resistant property (Alizadeh-Sani et al.,2021; Mustafa et al., 2021). Thus, the decrease in water vapor transmission rate might be due to the increase in the formation of new bonds between ICE and matrix, which enhances the potential of the developed film to apply in packaging applications.

Antioxidant Activity of Developed Films

The antioxidant activity of PVA/GG/ICE films was studied by using DPPH radical scavenging assay. The active antioxidant agents help decelerate lipid oxidation, thus enhancing the shelf life of packed food. Therefore, it's crucial to determine the DPPH radical scavenging property of the film samples. The color-changing ability of DPPH into yellow color depends on the potency of the proton donating active antioxidant agent incorporated in the films. Antioxidant activity of the developed neat, PVA/GG/ICE5, PVA/GG/ICE10, and PVA/GG/ICE20 films was represented in Fig. 5. The outcomes show that the DPPH scavenging activity of prepared films significantly increased with the addition of ICE. The film PVA/GG/ICE 20 had shown an antioxidant activity of 90.62%, which is a 98.3% improvement when compared to neat films, which have shown 1.55% activity which is almost negligible compared to films containing

active antioxidant agents, i.e., ICE. With the addition of small amounts of ICE, the antioxidant activity of pH indicating films has improved to 39.15 % further, with the addition of 10% ICE, the DPPH radical scavenging activity has increased to 86.12 %, which is very high compared to neat films. The high antioxidant activity of ICE might be due to the presence of high amounts of phenolics and flavonoids present in it. Previously, researchers have explored the antioxidant activity of other species of genus Ipomoea (Koncic et al., 2013; Parekh et al., 2012), but the antioxidant activity of Ipomoea Coccinea has not been reported in the literature to the best of our knowledge.

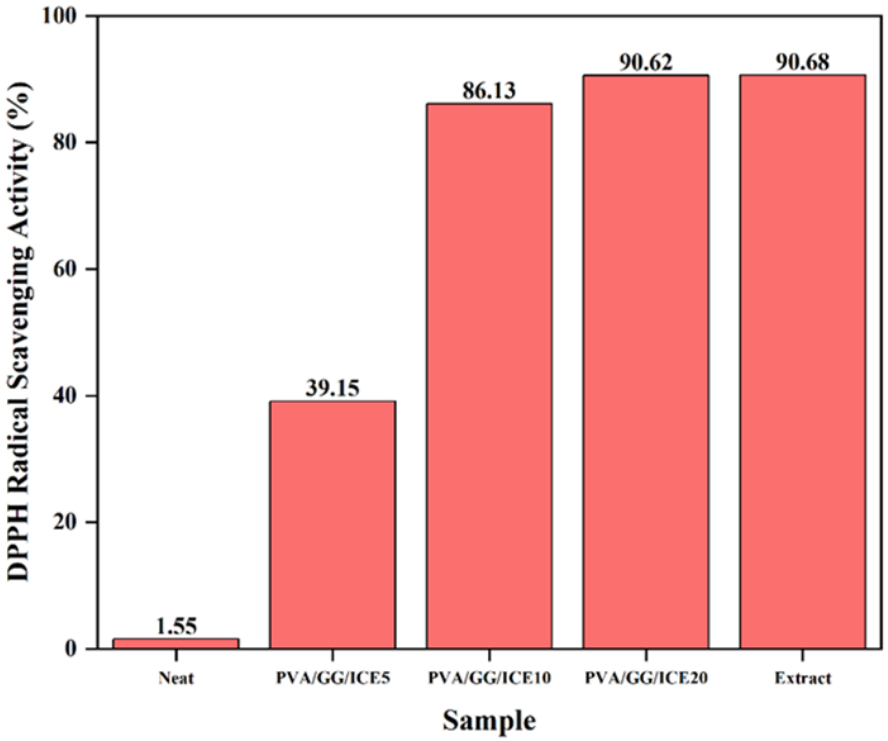

Figure 5. Antioxidant DPPH radical scavenging activity of poly vinyl alcohol and guar gum films with varying concentrations of Ipomoea Coccinea extract and Ipomoea Coccinea extract

Application of pH indicator for monitoring the freshness of chicken fillets

To study the potentiality of the developed indicator films, PVA/GG/ICE20 was applied to fresh chicken meat packed in a transparent container, as shown in Fig. 6. The film's sensitivity was studied at two temperatures, i.e., 8°C and 15°C. The fresh chicken sample showed a pH of 6.03, which is similar to the previously reported results (Javaherzadeh et al., 2020). On the 0^{th} day, the color of the pH indicator film was observed as reddish-pink. After 10 days of storage at 8±2°C, the pH increased to 6.94, and the film's color has changed to violet. At the other temperature (15±2°C), the pH of the chicken was recorded as 7.44 on the 4^{th} day of storage, and the color of the film was observed as violet. These results were consistent with the color change observed in the colorimetric response of the extract at different pH conditions. The pH

of fresh chicken is usually around 5.5, and if it increases above 6, it is considered as spoiled. The authors ((Kanatt, 2020); Kurek et al. (2019) studied the freshness of chicken meat using a pH-sensitive film developed from chitosan/carboxymethyl cellulose-based incorporated with blueberry and red grape skin pomace. They observed a change in pH from 5.9 to 6.5 during 48 h of storage which resulted in a change in color of the film (Kurek et al., 2019). It is well known that microbial deterioration and lipid oxidation are the main reasons for fresh meat spoilage. These spoilage processes change the pH and appearance of the meat and further causes structural component degradation. This degradation hence releases biogenic amines and volatile organic compounds, due to microbial decarboxylation of amino acids, into the headspace, which comes in contact with the anthocyanins and results in its color change. Hence, it is presumed that the visible color change is an indirect measurement of pH. The resulted color change suggests that the developed films can be efficiently used as pH indicators for poultry meat (Alessandroni et al., 2022; Nassar & Emam, 2002).

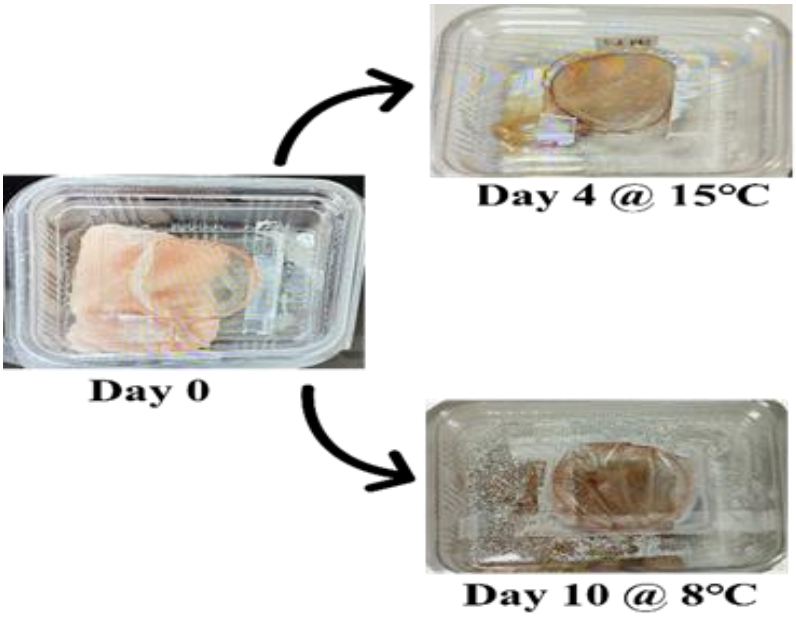

Figure 6. Chicken meat samples packed in a polypropylene tray with pH indicator films and stored at 8±2°C and 15±2°C

RECOMMENDATIONS

- The intensity of color change observed in labels is low when compared to that of extract which must be increased for better visualization
- The mechanical properties of fabricated labels need to be analyzed and improved for better strength
- Biodegradability and migration studies has to be performed

REFERENCES

1. Akhila, K., Ramakanth, D., & Gaikwad, K. K. (2022). Development of novel gallic acid- and cellulose acetate-coated paper as pH-responsive oxygen indicator for intelligent food packaging. Journal of Coatings Technology and Research, 19(5), 1493–1506. https://doi.org/10.1007/S11998-022-00622-0/
2. Alessandroni, L., Caprioli, G., Faiella, F., Fiorini, D., Galli, R., Huang, X., Marinelli, G., Nzekoue, F., Ricciutelli, M., Scortichini, S., Silvi, S., Tao, J., Tramontano, A., Turati, D., & Sagratini, G. (2022). A shelf-life study for the evaluation of a new biopackaging to preserve the quality of organic chicken meat. Food Chemistry, 371, 131134. https://doi.org/10.1016/j.foodchem.2021.131134
3. Alizadeh-Sani, M., Tavassoli, M., Mohammadian, E., Ehsani, A., Khaniki, G. J., Priyadarshi, R., & Rhim, J. W. (2021). pH-responsive color indicator films based on methylcellulose/chitosan nanofiber and barberry anthocyanins for real-time monitoring of meat freshness. International Journal of Biological Macromolecules, 166, 741–750. https://doi.org/10.1016/j.ijbiomac.2020.10.231
4. Boonsiriwit, A., Lee, M., Kim, M., Inthamat, P., Siripatrawan, U., & Lee, Y. S. (2021). Hydroxypropyl methylcellulose/microcrystalline cellulose biocomposite film incorporated with butterfly pea anthocyanin as a sustainable pH-responsive indicator for intelligent food-packaging applications. Food Bioscience, 44, 101392. https://doi.org/10.1016/J.FBIO.2021.101392
5. Castañeda-Ovando, A., Pacheco-Hernández, M. de L., Páez-Hernández, M. E., Rodríguez, J. A., & Galán-Vidal, C. A. (2009). Chemical studies of anthocyanins: A review. In Food Chemistry (Vol. 113, Issue 4, pp. 859–871). https://doi.org/10.1016/j.foodchem.2008.09.001
6. Chen, W., Ding, J., Yan, X., Yan, W., He, M., & Yin, G. (2019). Plasticization of cottonseed protein/polyvinyl alcohol blend films. Polymers, 11(12), 2096. https://doi.org/10.3390/polym11122096
7. colors, R. B.-A. as food, & 1982, U. (1982). Chemical Structure of Anthocyanins. In Anthocyanins As Food Colors (pp. 1–40). https://doi.org/10.1016/b978-0-12-472550-8.50005-6
8. Cui, H., Si, X., Tian, J., Lang, Y., Gao, N., Tan, H., Bian, Y., Zang, Z., Jiang, Q., Bao, Y., & Li, B. (2022). Anthocyanins-loaded nanocomplexes comprising casein and carboxymethyl cellulose: stability, antioxidant capacity, and bioaccessibility. Food Hydrocolloids, 122, 107073. https://doi.org/10.1016/J.FOODHYD.2021.107073
9. da Silva Filipini, G., Romani, V. P., & Guimarães Martins, V. (2020). Biodegradable and active-intelligent films based on methylcellulose and jambolão (Syzygium cumini) skins extract for food packaging. Food Hydrocolloids, 109, 106139. https://doi.org/10.1016/j.foodhyd.2020.106139
10. Deshmukh, R. K., Akhila, K., Ramakanth, D., & Gaikwad, K. K. (2022). Guar gum/carboxymethyl cellulose based antioxidant film incorporated with halloysite

nanotubes and litchi shell waste extract for active packaging. International Journal of Biological Macromolecules, 201, 1–13. https://doi.org/10.1016/j.ijbiomac.2021.12.198
11. Friedman, M., & Jürgens, H. S. (2000). Effect of pH on the stability of plant phenolic compounds. Journal of Agricultural and Food Chemistry, 48(6), 2101–2110. https://doi.org/10.1021/jf990489j
12. Gasti, T., Hiremani, V. D., Kesti, S. S., Vanjeri, V. N., Goudar, N., Masti, S. P., Thimmappa, S. C., & Chougale, R. B. (2021). Physicochemical and Antibacterial Evaluation of Poly (Vinyl Alcohol)/Guar Gum/Silver Nanocomposite Films for Food Packaging Applications. Journal of Polymers and the Environment, 29(10), 3347–3363. https://doi.org/10.1007/s10924-021-02123-4
13. Harborne, J. B. (1993). J. B. Harborne. In Introduction to Ecological Biochemistry.
14. Javaherzadeh, R., Tabatabaee Bafroee, A. S., & Kanjari, A. (2020). Preservation effect of Polylophium involucratum essential oil incorporated poly lactic acid/ nanochitosan composite film on shelf life and sensory properties of chicken fillets at refrigeration temperature. LWT, 118, 108783. https://doi.org/10.1016/j.lwt.2019.108783
15. Kanatt, S. R. (2020). Development of active/intelligent food packaging film containing Amaranthus leaf extract for shelf life extension of chicken/fish during chilled storage. Food Packaging and Shelf Life, 24, 100506. https://doi.org/10.1016/j.fpsl.2020.100506
16. Kanatt, S. R., Rao, M. S., Chawla, S. P., & Sharma, A. (2012). Active chitosan-polyvinyl alcohol films with natural extracts. Food Hydrocolloids, 29(2), 290–297. https://doi.org/10.1016/j.foodhyd.2012.03.005
17. Khoo, H. E., Azlan, A., Tang, S. T., & Lim, S. M. (2017). Anthocyanidins and anthocyanins: Colored pigments as food, pharmaceutical ingredients, and the potential health benefits. In Food and Nutrition Research (Vol. 61). Taylor & Francis. https://doi.org/10.1080/16546628.2017.1361779
18. Koncic, M. Z., Petlevski, R., & Kalodera, Z. (2013). Antioxidant activity of ipomoea batatas L. Lam. Leaf Grown in continental croatia and its effect on glutathione level in glucose-induced oxidative stress. International Journal of Food Properties, 16(5), 964–973. https://doi.org/10.1080/10942912.2011.573117
19. Koosha, M., & Hamedi, S. (2019). Intelligent Chitosan/PVA nanocomposite films containing black carrot anthocyanin and bentonite nanoclays with improved mechanical, thermal and antibacterial properties. Progress in Organic Coatings, 127, 338–347. https://doi.org/10.1016/j.porgcoat.2018.11.028
20. Kumar, P., Tanwar, R., Gupta, V., Upadhyay, A., Kumar, A., & Gaikwad, K. K. (2021). Pineapple peel extract incorporated poly(vinyl alcohol)-corn starch film for active food packaging: Preparation, characterization and antioxidant activity. International Journal of Biological Macromolecules, 187, 223–231. https://doi.org/10.1016/j.ijbiomac.2021.07.136
21. Kunam, P. K., Ramakanth, D., Akhila, K., & Gaikwad, K. K. (2022). Bio-based materials for barrier coatings on paper packaging. Biomass Conversion and Biorefinery, 1, 1–16. https://doi.org/10.1007/S13399-022-03241-2/FIGURES/7
22. Kurek, M., Hlupić, L., Ščetar, M., Bosiljkov, T., & Galić, K. (2019). Comparison of Two pH Responsive Color Changing Bio-Based Films Containing Wasted Fruit

Pomace as a Source of Colorants. Journal of Food Science, 84(9), 2490–2498. https://doi.org/10.1111/1750-3841.14716

23. Luchese, C. L., Sperotto, N., Spada, J. C., & Tessaro, I. C. (2017). Effect of blueberry agro-industrial waste addition to corn starch-based films for the production of a pH-indicator film. International Journal of Biological Macromolecules, 104, 11–18. https://doi.org/10.1016/j.ijbiomac.2017.05.149
24. Mohammadalinejhad, S., Almasi, H., & Moradi, M. (2020). Immobilization of Echium amoenum anthocyanins into bacterial cellulose film: A novel colorimetric pH indicator for freshness/spoilage monitoring of shrimp. Food Control, 113. https://doi.org/10.1016/j.foodcont.2020.107169
25. Mohammadi, H., Kamkar, A., & Misaghi, A. (2018). Nanocomposite films based on CMC, okra mucilage and ZnO nanoparticles: Physico mechanical and antibacterial properties. Carbohydrate Polymers, 181, 351–357. https://doi.org/10.1016/j.carbpol.2017.10.045
26. Monjazeb Marvdashti, L., Koocheki, A., & Yavarmanesh, M. (2017). Alyssum homolocarpum seed gum-polyvinyl alcohol biodegradable composite film: Physicochemical, mechanical, thermal and barrier properties. Carbohydrate Polymers, 155, 280–293. https://doi.org/10.1016/j.carbpol.2016.07.123
27. Moradi, M., Tajik, H., Almasi, H., Forough, M., & Ezati, P. (2019). A novel pH-sensing indicator based on bacterial cellulose nanofibers and black carrot anthocyanins for monitoring fish freshness. Carbohydrate Polymers, 222. https://doi.org/10.1016/j.carbpol.2019.115030
28. Mustafa, P., Niazi, M. B. K., Jahan, Z., Rafiq, S., Ahmad, T., Sikander, U., & Javaid, F. (2021). Improving functional properties of PVA/starch-based films as active and intelligent food packaging by incorporating propolis and anthocyanin. Polymers and Polymer Composites, 29(9), 1472–1484. https://doi.org/10.1177/0967391120973503
29. Nassar, A. M., & Emam, W. H. (2002). Biogenic amines in chicken meat products in relation to bacterial load, pH value and sodium chloride content. Nahrung - Food, 46(3), 197–199. https://doi.org/10.1002/1521-3803(20020501)46:3<197::AID-FOOD197>3.0.CO;2-1
30. Parekh, K. K., Patel, A. M., Modi, A. J., & Chandrashe, H. R. (2012). Antioxidant and Cytotoxic Activities of Few Selected Ipomoea Species. Pharmacologia, 3(9), 377–386. https://doi.org/10.5567/pharmacologia.2012.377.386
31. Phan, T., Debeaufort, F., … D. L.-J. of A. and, & 2005, U. (2005). Functional properties of edible agar-based and starch-based films for food quality preservation. Journal of Agricultural and Food Chemistry, 53(4), 973–981. https://doi.org/10.1021/jf040309s
32. Pieczykolan, E., & Kurek, M. A. (2019). Use of guar gum, gum arabic, pectin, beta-glucan and inulin for microencapsulation of anthocyanins from chokeberry. International Journal of Biological Macromolecules, 129, 665–671. https://doi.org/10.1016/J.IJBIOMAC.2019.02.073
33. Prietto, L., Pinto, V. Z., El Halal, S. L. M., de Morais, M. G., Costa, J. A. V., Lim, L. T., Dias, A. R. G., & Zavareze, E. da R. (2018). Ultrafine fibers of zein and

anthocyanins as natural pH indicator. Journal of the Science of Food and Agriculture, 98(7), 2735–2741. https://doi.org/10.1002/jsfa.8769

34. Qin, Y., Liu, Y., Yong, H., Liu, J., Zhang, X., & Liu, J. (2019). Preparation and characterization of active and intelligent packaging films based on cassava starch and anthocyanins from Lycium ruthenicum Murr. International Journal of Biological Macromolecules, 134, 80–90. https://doi.org/10.1016/j.ijbiomac.2019.05.029
35. Tanwar, R., Gupta, V., Kumar, P., Kumar, A., Singh, S., & Gaikwad, K. K. (2021). Development and characterization of PVA-starch incorporated with coconut shell extract and sepiolite clay as an antioxidant film for active food packaging applications. International Journal of Biological Macromolecules, 185, 451–461.
36. Wei, Y. C., Cheng, C. H., Ho, Y. C., Tsai, M. L., & Mi, F. L. (2017). Active gellan gum/purple sweet potato composite films capable of monitoring pH variations. Food Hydrocolloids, 69, 491–502. https://doi.org/10.1016/j.foodhyd.2017.03.010
37. Yong, H., & Liu, J. (2020). Recent advances in the preparation, physical and functional properties, and applications of anthocyanins-based active and intelligent packaging films. In Food Packaging and Shelf Life (Vol. 26, p. 100550). Elsevier. https://doi.org/10.1016/j.fpsl.2020.100550
38. Yong, H., Wang, X., Bai, R., Miao, Z., Zhang, X., & Liu, J. (2019). Development of antioxidant and intelligent pH-sensing packaging films by incorporating purple-fleshed sweet potato extract into chitosan matrix. Food Hydrocolloids, 90, 216–224. https://doi.org/10.1016/j.foodhyd.2018.12.015

CONFERENCE PROCEEDINGS

DISTRIBUTION PACKAGING

ORAL PRESENTATION

GENERAL STREAM

DP-GO01	Transport stresses in e-commerce logistics and its effects on corrugated board packaging
DP-GO02	Understanding how vertical and multi-axial vibrations affects the load stability
DP-GO03	High-speed camera analysis of load/pallet interface behavior in logistics unit submitted to impact
DP-GO04	Statistical study on acceleration value data recorded on roundabout, curve, during a road trip to classify then in function of their impact on load stability
DP-GO05	Case study for optimisation and standardization of packaging references improving its environmental behaviour
DP-GO06	Optimal selection of the percentage of recycled material in plastic according to the risks of distribution cycle
DP-GO07	Evaluation of Maximum Pallet Deflection Under Dynamic Forklift Handling Conditions
DP-GO08	Effect of Wooden Pallets Characteristics on the Compression Strength of Palletized Plastic Pails with Double Overhang

PEER-REVIEWED

DP-GP01	Predicting the Effect of Pallet Overhang on the Box Compression Strength

POSTER PRESENTATION

DP-PP01	Estimation of the degradation of strawberries during Rail transport from knowledge and experiences made on Roads trips

DP-GO01

Transport stresses in e-commerce logistics and its effects on corrugated board packaging

Thomas Trost[*1], Astrid Odeberg Glasenapp[1], Maria Sundin[1]

[1] *RISE Bioeconomy and Health, SE-164 40, Stockholm-Kista, Sweden*

***Correspondence to**: Thomas Trost. RISE Bioeconomy and Health, SE-164 40, Stockholm-Kista, Sweden*
Email: thomas.trost@ri.se

ABSTRACT: In the Research program "Improving corrugated board performance" at RISE several case studies on transport packaging in e-commerce were conducted. Field tests with e-commerce packages with mixed products and laboratory tests with the same products were compared. Laboratory transport tests have been carried out using the standard ISTA 6 Amazon – Over boxing. The field study was carried out through sending packages between two cities in Sweden. All packaging were equipped with field data recorders during each trial, which captured the data relevant to compare transport simulation and the real environment during the e-commerce logistics. A comparison between Amazon testing and reality was made. Similarities between the field studies and laboratory tests are identified.
When comparing the results with this and other studies, it was concluded that the ISTA 6 Amazon Ship-in-own-container (SIOC) and ISTA 6 Amazon Over boxing (OB) are demanding tests and this especially concerning the drop tests.

Keywords: e-commerce, logistics, packaging design, transport stresses, corrugated board

INTRODUCTION

The latest years the e-commerce has been under steady growth. The problems with oversized boxes, return sending's etc are well known to everybody. Broodh (2018) have studied the concerns regarding packaging design, logistics and environmental aspects. There also exists guidelines, e.g. Coles (2015) or Walmart (2016) authored by the large retailers aimed for visibility etc. However, very few measurements of the physical distribution environment are reported for e-commerce cargo.

Before the e-commerce era there were also distributions of single packages, often in test standards denoted as single parcel delivery systems. Looking at sorting centers and distribution terminals it becomes clear that the digitalization, tracking of cargo etc have undergone a large change or development, e.g. some packages are scanned at incoming and outbound of each hub passed, but the physical handling has in some places not changed as much, compare e.g. Trost

(1986) and ISTA (2018a). Therefore, it is relevant to also look at earlier monitoring activities of single parcel delivery systems.

Garcia-Romeu-Martinez et al. (2007) compared DHL and FedEx, two of the largest international parcel carriers, when transporting single parcels between Europe and North America. The aim was to gather data for drop heights that can be used for package testing. They focused on measuring and analyzing the international shipping environment for midsized (0.36 m × 0.34 m × 0.34 m) and lightweight (6.5 kg) packages. Statistics from six round trips with each carrier showed on 95 % occurrence level that the package is likely to experience an average of 27 drops with and with 95 % occurrence have at least one drop of around 0.6 m.

Lately, in the light of the increased e-commerce, there have also been an increased interest in "the last mile delivery", i.e. the distribution out to customer or a service point. Böröcz and Singh (2018) measured the vibration levels that occur in parcel delivery shipments from pickup to delivery, especially the sections involving delivery vans and small vehicles over ground road transportation in Hungary. Among the findings towards better test programs were that the highest vibrational energy levels occurred in vertical axis between 2 to 3 Hz and 13 to 16 Hz, and not between 3 to 5 Hz and 15 to 24 Hz as shown in ASTM D7386/ISTA 3A pick and delivery vehicle test methods for shipments. Also, lateral forces generated by the pitch and roll vibratory motion of relatively small delivery vehicles due to road surface unevenness have recently been measured by Rouillard et al. (2018). One can suspect that the influence of multi-axial vibrations is larger at smaller delivery vans.

Dunno et al. (2019) evaluated the drop heights dependence on the packaged size and weight in the small parcel supply chain by following several instrumented packages in the United States. They found among other that the mean drop height was fairly constant with respect to the packages weight, but that smaller dimensions of the package caused a higher mean drop height.

Mojzes et al. (2018) pointed out the new practice that courier express operators transport dangerous goods as single package. This parcel delivery method means a higher risk for all kind of logistics participants. Therefore, e.g. well-defined drop heights for qualifying tests is quite important. Some interesting results showed that for some types of packages, the height of drop is not the strongest influencing factor of the damages, rather the number of drops. This is probably explained by the fact that a minor damage occurring at the first drop escalates by increasing the number of drops. The conclusion from this study is that important factors to consider/understand are the damage mechanisms, which are different for different materials and package constructions, as well as transport conditions.

METHOD

Four loggers were packed in four boxes with identical content, see Figure 1-2. Two loggers were SAVER™ 3X90, denoted A and B, one SAVER™ 9X30, denoted C and one SAVER™ 3M30 Plus, denoted D (Lansmont Corp., Monterey, CA). The boxes used was box size nr 3 chosen by the Office Depot software based on the content (except the logger volume). The dimensions of the box with cover were 41x30x28 cm^3 (volume of 34.4 litres). The weights of the boxes varied from 5.55 kg to 6.25 kg depending on the logger inserted in the package.

The content of the boxes was considered to be 'typical' for the office customers of Office Depot, i.e. contained four common products; Yes detergent, a box of cookies, a box with coffee milk and a chocolate package.

The parcels were sent from Office Depot's logistic centre in Strängnäs, following their normal distribution flow, on consecutive days starting with parcel A (containing logger A) in March 2019 and so on. All single parcels from Strängnäs go to PostNord's sorting terminal in Segeltorp outside Stockholm before being spread out, see Figure 3. Thereafter the four parcels were sent to the sorting terminal Växjö-Väster for delivery out to the 'customer', a private person in Växjö. This means a total travelling distance of about 550 km for each parcel.

Also, laboratory tests with two new boxes and content were performed in March 2019 with logged boxes and the test standard ISTA 6 Amazon - Over boxing.

The tests were carried out on two packages labelled E and F. They were packed identically to packages A-D. One deviation from the standard was that the testing was done with the four actual products. The standard prescribes using one product together with several dummies.

According to the standard, a package of less than 15 kg and containing fragile products (such as liquids) requires five samples, of which two should be single item test. Only two samples were tested, both multiple items. The decision was based on the aim of comparing the stresses occurring on the transport package during field trials and laboratory tests, rather than determining the properties of the individual primary packages. On the same grounds, the integrity test (leakage test) for the detergent was omitted.

The reason for using ISTA Amazon tests is its more 'mandatory' approach, i.e. if an Amazon customer wants smooth treatment the product/package need to be tested according to ISTA Amazon.

The packages were equipped with loggers with the same settings and placement as during the field trials, see Table 1. The same type of corrugated box and the same content as in the field trials were used. The packages were packed in the testing laboratory.

Figure 1. Overview of the four mixed cargo e-commerce boxes.

Figure 2. Example of box at arrival.

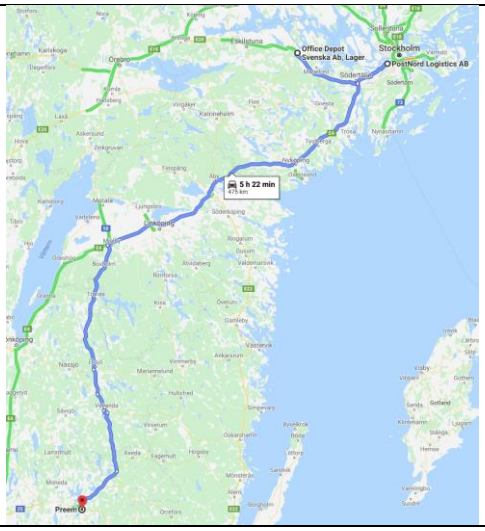

Figure 3. Route for the field trials according to Google maps.

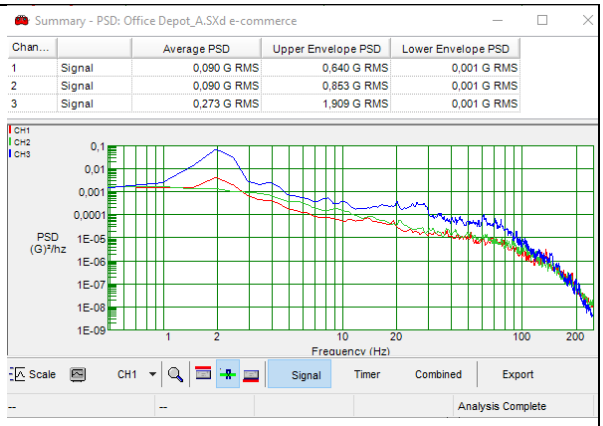

Figure 4. Typical average PSD spectrum from signal triggered events (Parcel A).

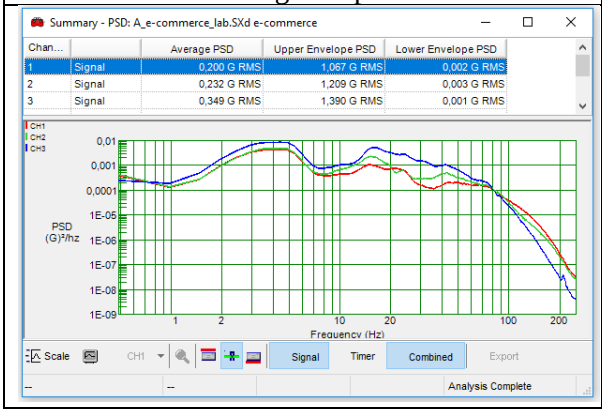

Figure 5. Average PSD spectrum for the laboratory tests of Parcel E.

Figure 6. Parcel E – corrugated board buckled. Glue released on top lid side 2-6.

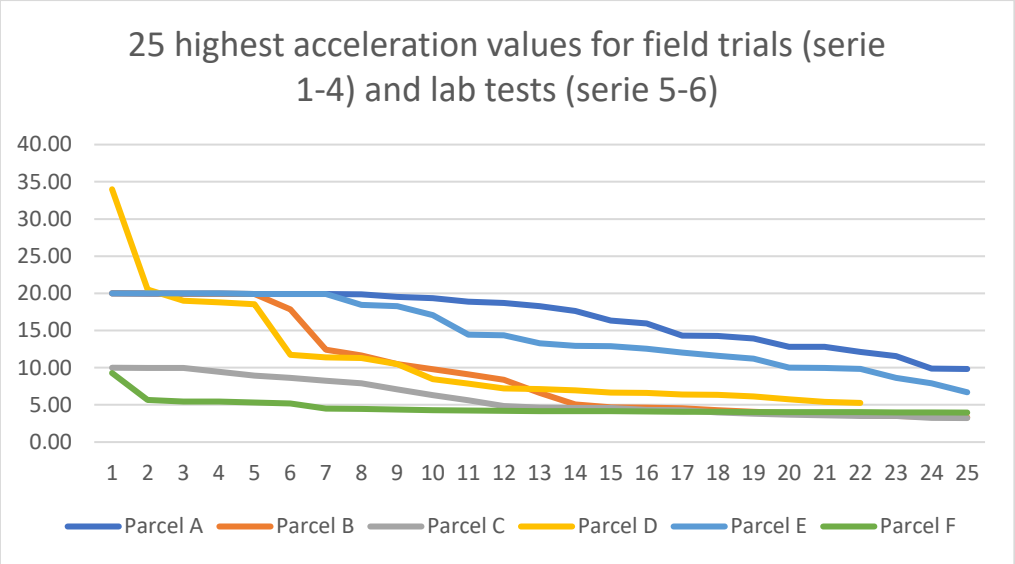

Figure 7. The 25 highest acceleration values for field trials and lab tests

RESULTS

Field trials

All four parcels have the same principal look regarding the PSD behaviour with most energy around two Hertz, see Figure 4.

One of the parcels (Parcel C) has probably laid on one side instead of the having the top lid upward, which is the intended direction. Thus, one of the lateral channels had the highest PSD summary. It was noted that Parcel C had severe leakage from the liquid Yes detergent, most probably as a result from being transported with one not intended side up.

Laboratory tests

The total number of signal triggered events for the Amazon test were 3830 using Saver 3X90 for Parcel E. The large number of events at lab is due to that vibration testing is performed at a higher, time accelerated, Grms level than during the real transport. Laboratory tests were performed at 0.53 Grms, while the field test vibrations typically were 0.27 Grms. The logger's threshold level was set to 0.50 g.

An overview of the Grms values and the PSD spectrum for the whole laboratory test of Parcel E is shown in Figure 5. It should be noted that there is a mix of vibration sequences and sometimes high drop sequences. This is illustrated in the figure header as quite high upper envelope Grms values. Since the package is different orientated during the drop sequence the x-, y- and z- directions are not differing too much. One example of the box behaviour is shown for parcel E in Figure 6 where the top lid cracked during the second series of drops.

The e-commerce typically includes more "touch points" (sorting/storage/transit events) and therefore expose the cargo to an elevated number of potential physical harmful elements

and an increased risk of damage (Singh and Saha, 2018). This was indicated by comparing the field data with the quite demanding test levels according to ISTA 6 Amazon Over Boxing test method. This means that horizontal shocks (x- and y-direction) are more common than during the transport phase of the distribution. It is considered that the ISTA 6 Amazon Over Boxing test method is a too tough test method for the e-commerce package investigated, also concluded by ten Klooster et al. (2020).

Table 1 shows some overview numbers of parcel in field tests as well as parcel in laboratory tests. Figure 7 shows the 25 highest acceleration values for the field trials and laboratory tests respectively. Note that Parcel C and the corresponding laboratory test had lower full-scale value (10 g versus 20g for the other cases, except Parcel D with 100 g).

Table 1 also shows the number and percentage of threshold triggered events and how they are characterized; either as vibrations or shocks/drops/tosses. The largest difference between field trials and laboratory tests occurs when it comes to number of triggered vibration events. The vibration tests shall in a shortened time reflect the stresses during a real transport which occurs over a longer time duration. In this case the transport that lasted for around 7 h without traffic jam is compared with 2 h vibration test at higher vibration levels than the actual transport has. That also means that the loggers get triggered much more often during the vibration tests than during the actual transport. The number of triggered events characterized as shocks is lower than the vibration ones but in general has higher acceleration levels. That is particularly true for the laboratory tests where most of the drops occur at 460 mm drop height.

	Parcel A, field	Parcel E, laboratory
Number of signal triggered events	550	3830
Number of shocks - % of total number of events	87 - 16	284 - 7
Number of vibrations - % of total number of events	463 - 84	3546 - 93
Average X Grms	0.090	0.200
Average Y Grms	0.090	0.232
Average Z Grms	0.273	0.349
Max Grms	1.726	0.653
Mean of 10 highest events (Grms)	1.322	0.631
Mean of 10 highest acceleration levels (g)	19.84	19.35

Table 1. Overview comparison between field studies and laboratory studies

DISCUSSION AND CONCLUSIONS

The four parcels sent on four consecutive days could be seen as a snapshot of the e-commerce distribution. The outcome of the four trips were quite different with results from no damage to

severe leakage. This illustrates the spread between different shipments. According to e.g. ISTA's Data collection standards (2018c) a minimum of 30 one-way trips are recommended for each set of variables used. Although this number could be questioned as unnecessary high, four trips are only four trips.

The lightweight e-commerce packages (around 6 kg) studied here are subjected to many shocks, tosses, tumbling etc during the delivery chain. This has been illustrated here with time records of the acceleration signals.

It is notable that compared to the field trial, the outer packaging was more damaged and that the damage looked quite different. In the lab trial, the corrugated board suffered a too high load and was dented. In the field trial, several of the dents were on the lid, showing signs of a heavy top load with a smaller base area.

The content of the box also showed traces of the different treatments. The leakage was also dissimilar in the lab trial and the field study. In the lab, one of the bottles stayed intact while the other leaked in an explosive way, covering most of the contents in the corrugated box with Yes detergent. In the field trial, the detergent seemed to leak in a more sedated way. On the other hand, the leakage had longer to seep through the board and damage the material of the outer box.

The vibrations seem to be unnecessarily high in the testing program, since a wide majority of the cookies were in crumbs afterwards. In the field trial, only a thin layer of crumbs was covering the bottom of the plastic container and most of the cookies were still intact. But it's worth mentioning that the field trials were relatively short in distance, only around 550 km.

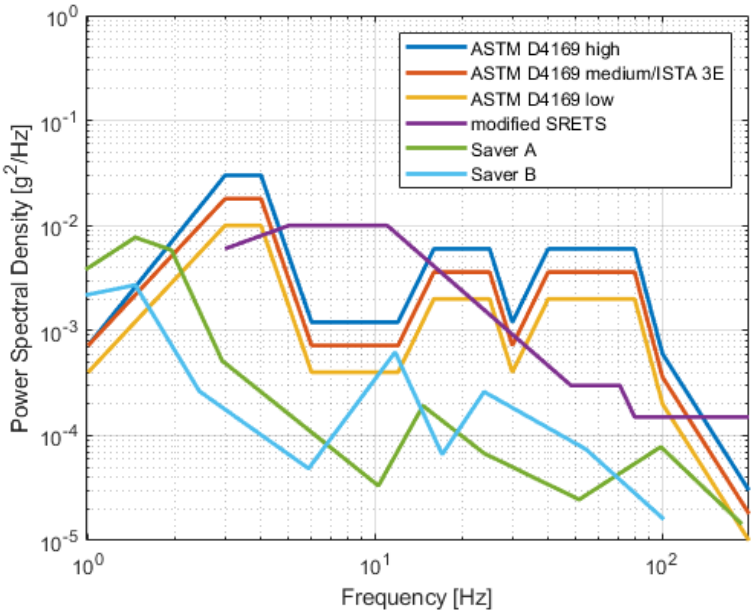

Figure 8. Average level random test spectra for different transport modes according to ASTM D4169, ISTA 3E and modified SRETS spectrum. The average measured PSD spectra from Saver A and B, during a long European truck transport of pallets with cargo, are added for comparison

Figure 8 shows the average level random test spectra for different transport modes according to ASTM D4169, ISTA 3A together with the SRETS-spectrum (Braunmiller, 1999), later modified to a not too demanding spectrum. As expected, the test spectra has higher energy content than measured spectra, since the aim is to time-compress the random vibration tests in comparison with the real transport duration.

ACKNOWLEDGEMENT

The transport logging study was performed within the Bioeconomy Research program of RISE, RP18 Improving corrugated board performance. Participants and financiers of this studies were ABInBev, MetsäBoard and Stora Enso. Their contribution is highly acknowledged.

REFERENCES

1. ASTM D4169: Standard practice for performance testing of shipping containers and systems.
2. Braunmiller, Ulrich (editor) (1999); Source reduction by European testing schedules (SRETS) - Final report; Packforsk Report No: 189.
3. Broodh, Anna (2018); Literature study on topics or concerns on packaging intended for e-commerce logistics. RISE Bioeconomy Report No 35.
4. Böröcz, Péter; Singh, Paul (2018); Measurement and analysis of delivery van vibration levels to simulate package testing for parcel delivery in Hungary. Packaging Technology and Science, 2018; 31: 342-352.
5. Coles (2015); Shelf Ready Packaging. Suppliers Guide. www.supplierportal.coles.com.au. June 2015
6. Dunno, Kyle; Klingshirn, Theresa; Helenek, Amy (2019); Effect of packaged product size, weight and shipping location on mean drop heights in the small parcel shipping environment. International Journal of Advanced Packaging Technology 2019, Volume 7, Issue 1, pp. 292-299.
7. Garcia-Romeu-Martinez, Manuel-Alfredo; Singh, Paul; Cloquell-Ballester, Vicente-Agustin; Saha, Koushik (2007); Measurement and analysis of international air parcel shipping environment for DHL and FedEx between Europe and United States. Packaging Technology and Science, 2007; 20: 421–429.
8. ISTA 3E: Similar packaged products in unitized loads for truckload shipment.
9. ISTA (2018a) Touchpoints – E-retailer fulfilment. Version 1, July 2018.
10. ISTA 6 Amazon.com - Over Boxing (2018b): e-commerce fulfilment for parcel delivery shipment.
11. ISTA Data collection standards (2018c). ISTA´s requirements for measuring Atmospheric, shocks/impacts and drops, Vehicle vibration.
12. Mojzes, Ákos; Trost, Thomas; Vörösköi, Kata (2018); Drop performance of dangerous goods packages in the aspect of parcel delivery standards. 21st IAPRI World Conference on Packaging, Zhuhai, China, 19-22 June 2018.

13. Rouillard Vincent; Lamb, Matthew J.; Losk, Yevgeni (2018); Developing test schedules for simulating multiaxial vibratory motions of delivery vehicles. 21st IAPRI World Conference on Packaging, Zhuhai, China, 19-22 June 2018.
14. Singh, Jay; Saha, Koushik (2018); Ecommerce retail: Challenges and opportunities for CPG related distribution packaging. 21st IAPRI World Conference on Packaging, Zhuhai, China, 19-22 June 2018.
15. ten Klooster, Roland; de Koeijer, Bjorn; Huijben, Corné (2020); Analysis to develop a packaging engineering model for e-commerce in the grocery market. 22nd IAPRI World Packaging Conference, University of Monterrey, Mexico 2020.
16. Trost, Thomas (1986); Stresses at handling - Study of Swedish terminals. Packforsk Report No 106 (in Swedish).
17. Walmart (2016); Retail Ready Packaging, 2016 Guidelines (North America).

DP-GO02

Understanding how vertical and multi-axial vibrations affect load stability

Enrique de la Cruz Navarro MSc[1], Manuel García-Romeu Martínez PhD[2]*

1 R&D manager, Safe Load Testing Technologies, Paterna 46980, Spain
2 Product Development Manager, Safe Load Testing Technologies, Paterna 46980, Spain
Safe Load Testing Technologies, Paterna 46980, Spain,

***Correspondence to**: Manuel García-Romeu Martínez, PhD. Safe Load Testing Technologies, Paterna, 46980, Spain,*
Email: manuel.garcia-romeu@safeloadtesting.com

ABSTRACT: A common way of simulating the stress that a unit load undergoes during transport is by performing a sequence of different stresses, such as compression, vibration, and horizontal shocks or accelerations.
The study focused on field data measurement where a unit load was monitored inside a truck during transport until the failure or lack of stability occurs. The vibrations and accelerations of the truck were recorded, and the data collected was processed to obtain the necessary PSD to simulate in the lab different vibration test methods, like the single-axial vertical vibration and the multi-axial vibrations (vertical + pitch + roll).
Subsequently, in order to study the stability and failure mode of the unit load in the laboratory, both the loads subjected to transport and new unit loads were subjected to different monoaxial and multiaxial vibration test methods extracted from the field data collection. After submitting the unit loads to each vibration method, these were subjected to an increasing horizontal acceleration test sequence from 0.1 g until the failure mode occurs, to evaluate if there is any difference in the value of acceleration or deformation obtained during the stability test assessment.
This presentation provides attendees with an opportunity to understand how real-world vibration affects the load stability during transport. The aim of this study is to show different results at the stability test when the samples are preconditioned using different random vibration methods.

Keywords: transport simulation, load stability, sustained acceleration, horizontal acceleration, multi-axial vibration, random vibration.

INTRODUCTION

The reason of the transport simulation is to reproduce whatever happens on the real distribution cycle under controlled conditions in a laboratory. Its main target is to reproduce the same stress and damages that the load suffers at the distribution chain.

Nowadays, stability test methods are coming more demanding as effect of the safety on road requirements of several governments, and its legislation. The main standard method types are statics and dynamics. The main dynamic standard methods for checking the load stability are US FMCSA [1] and EUMOS 40509 [2].

In general Standard laboratory testing methods for transport simulation like ASTM [3] and testing procedures like ISTA [4] concatenates different tests to the same sample to know if it will survive to the distribution cycle or not. The mission of some of the test methods applied is preconditioning the sample for the next test. The procedures only have sense if all the tests are done.

The aim of this paper is to find out if preconditioning the samples by vibration tests as other testing procedures do, improves or not the stability test results, as well as to determine which is the most appropriate method to reproduce the stress the load suffers.

The deflection of the load on a transport is a reference of its strength. For the same kind of unit load as less deflection steadiest is it. So, this document studies the stability of different samples comparing its deflection in order to know which samples have a defection closer to the one studied on road.

Five load samples were studied. Every load sample consisted of a Europallet of 1,5L water bottles. The pallet was packed with a stretch film and formed by four layers of bottles. Every layer had 14x9 bottles, and the bottles were packed with shrink film in 3x2 format. A sample for monitoring on transport, a sample as reference without precondition, 3 samples for preconditioning, and a sample more as reference. As the target of this study is reproducing the damages on transport, the sample was installed without the possibility of leaning on against the truck walls, and it was the same at the laboratory simulation.

The pallet sample was monitoring the transport of a palletized load until it fails. Analyzing the recorded data to extract the transport PSDs and testing multiple samples using vibration test machines to study the behavior of different PSDs.

TRANSPORT MONITORING

A route was selected for the transport. The main reason to select this route is because it is well known as a hazardous one. The palletized load was monitored through its distribution cycle using Safe Load DR4-01 and DR4-02 [5] data-recorders and a camera mounted inside the truck. Table 1 shows the monitoring data and the applied sampling frequency for each channel.

Parameter	DR4-01 (Hz)	DR4-02 (Hz)
2000G accel.	4000	4000
40G accel.	1000	1000
Rotation	200	200
GNSS (Positioning)	0.8	n.a.

Table 1: Sampling frequencies of the sensors

Normally the data recorders are fixed on the backwards wheels as PhD. V. Rouillard recommends [6] for testing complete loaded trucks, because it is the strongest signal. In this case the DR04-02 was fixed on the pallet and the DR04-01 was fixed under the pallet because what the study wants to test which is exactly what the sample is suffering. Channel 1 records the driving direction, channel 2 records the lateral movements and channel 3 records the vertical accelerations.
Additionally, a video of the sample movement was recorded in order to understand how the sample moves, detecting when the sample fell and to study its stability in front lateral accelerations.

MONITORED DATA ANALYSIS

Before 41 minutes of route the sample fell. The collected data on boar was processed two points of view, what the truck transmit to the sample, and how the sample reacts to, from the stability point of view.
The truck dynamic which produces the sample damages was studied from two points of view: vibrations and the extraordinary accelerations, considering the 6dof, 3 lineal movements (x, y and z) and 3 angular movements (pitch, roll and yaw).
The sample response is studied from its stability point of view. The sample stability is quantified according to its deflection and which acceleration produces. The stability was measured applying an Artificial Intelligence app (innVision), over onboard the recorded video.

Truck dynamics: Extraordinary accelerations

In order to identify the trip's extraordinary accelerations, data was processed in search of events exceeding 0,3s of duration and 0,2gG or more during the transport. The Table 2 shows the criterium and the quantity of events found by channel according this criterium.

Event selection criterium	**Channel 1**	**Channel 2**	**Channel 3**
Event time duration	0,3s	0,3s	0,3s
Event G level	>0,2G	>0,2G	>0,2G
Number of identified events	7	20	5

Table 2. Detection criteria for acceleration processing

Next graphs represent a point for every single identified point. The points are positioned at the graph according to their intensity and duration.

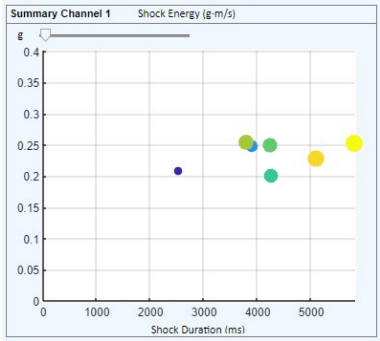

Graph 1. Shock energy graph of the detected acceleration events ch 1

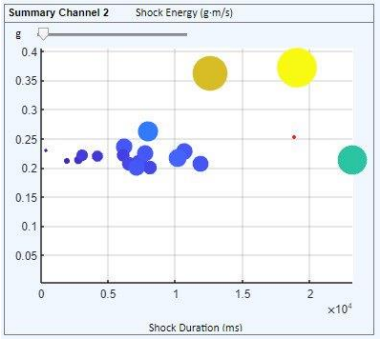

Graph 2. Shock energy graph of the detected acceleration events ch 2

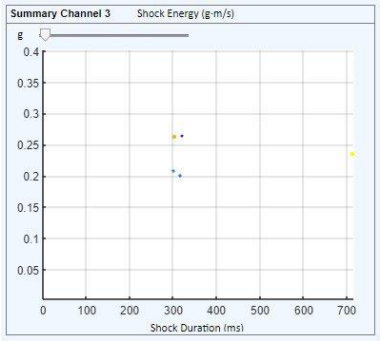

Graph 3. Shock energy graph of the detected acceleration events ch 3

Graph 4 shows the acceleration pulse recorded at channel 2when the load sample fell during the transport. Its parameters are 0.36G peak and holds close to 0.3G for 3 seconds.

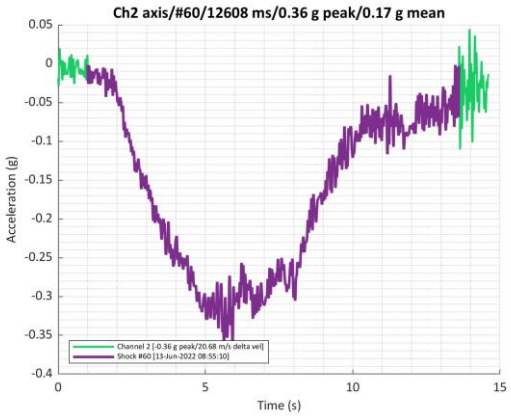

Graph 4. Acceleration event during the fall of the test sample

The sample fell after 41 minutes on road. Graph 4 shows the pulse, and this pulse corresponds to the ocher point at the graph 2. At graph 2 even it is possible to see (in yellow) a rudest previous pulse (from 25minutes after the trip starts). This means the failure was not an effect of reaching the pallet breaks point, because the yellow point was 16 minutes before the failure. It breaks as an effect of the stress of the road.

Truck dynamics: Power Spectral Distribution (PSD)

The application Analyze App was used for removing the gaps when the truck was stopped, and for calculating the following PSDs. To calculate the vibration's PSD, registered accelerations and rotations were processed, based on ISTA's guidelines [7] for PSDs processing and design. The following table shows the parameters used for calculating the PSDs.

	Heave	Pitch	Roll
Event time duration	10s	10s	10s
event selection level	> 0,01 G_{rms}	> 0,5º/s_{rms}	> 0,5º/s_{rms}

Table 3. Detection criteria for PSD processing

After obtaining the PSD, it is necessary to reduce its resolution for applying it to a vibration machine. Since the test machines have physical limits in stroke, bandwidth and others, it is necessary to apply those limits to the PSD. A tool for performing test profiles included in Analyze App was used for creating the vertical PSD. For reducing the PSD resolution, a tool that allows to select PSD graph's points was used, as well as to join them with straight lines. Once the points are defined, it exports the simplified PSD.

Vertical		Pitch		Roll	
Fr (Hz)	**G/Hz²**	**Fr (Hz)**	**°/Hz²**	**Fr (Hz)**	**°/Hz²**
0,5	4,209E-05	0,4	0,166	0,4	0,789
1,2	9,631E-05	0,6	0,212	0,5	0,989
1,7	0,000362	0,8	0,190	0,7	1,778
2	0,000373	1,1	0,224	0,8	2,793
2,6	0,00028	1,4	0,256	0,9	2,552
6,6	9,206E-06	1,7	0,333	1	1,625
7,9	2,762E-05	2,8	0,0258	1,6	0,0945
9,3	1,656E-05	4,4	0,00108	2,8	0,0145
12,1	0,000121	5,2	0,000765	3,7	0,00299
15,7	4,403E-05	7,1	0,000128	4,7	0,0166
19,4	0,000119	8,8	0,000262	7,7	0,000689
29,3	6,040E-06	10,5	0,000293	11,7	0,00279
44,4	9,345E-05	15,5	0,00308	14	0,00139
50,5	1,137E-05	21,5	0,00102	17,4	0,0118
61	5,687E-05	24,3	0,000340	20,9	0,00142
166,8	1,207E-05	28,3	0,000293	22,6	0,00124
192,2	2,933E-06	33,2	0,000104		

Table 4. Calculated PSDs of the transport.

The sample response

An artificial vision app call innVision analyzed the onboard images. The maximum deflection measured in transport was 372mm, without considering when the sample fell. It happened during a turn of 20s and its intensity reaches 0,38G. It was the rudest lateral recorded pulse.

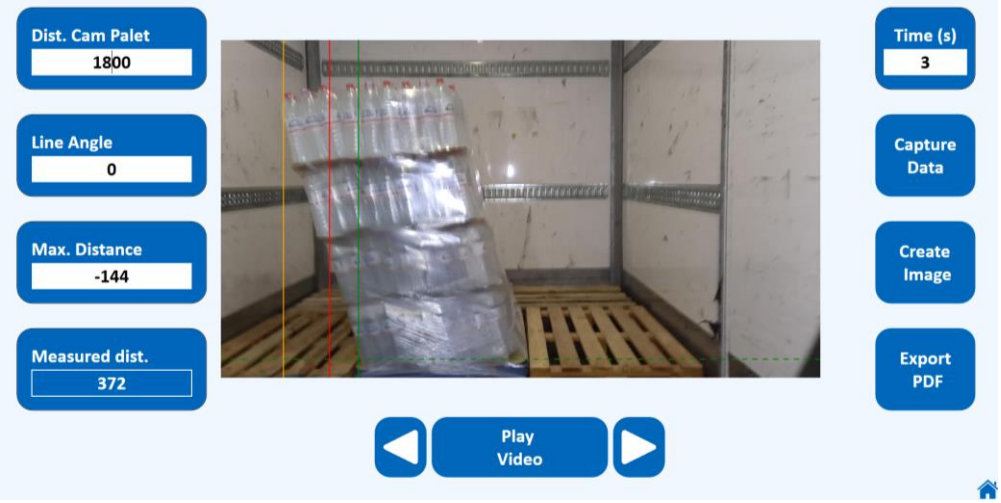

Graph 5. Max deflection on transport identified and measured by artificial vision system.

TEST DESIGN

The aim of the test is to compare the response of a test sample in front of different stability tests intensities for different preconditioning methods.

- Sample preconditioning: Vibration test for 40 minutes using the following methods:
  - Method ASTM 4169 Truck level 2 [3]
  - Method ISTA Pickup and delivery [7]
  - Method multy-axial PSDs testing from recorded data.
  - No tested reference sample.

The standard methods of ASTM and ISTA only contemplate vertical vibration tests, so they only specify vertical PSDs. On the other hand, the multy-axial processed data PSDs include vertical (or heave) and pitch & roll PSDs. Graphs 6 and 7 show the test PSDs:

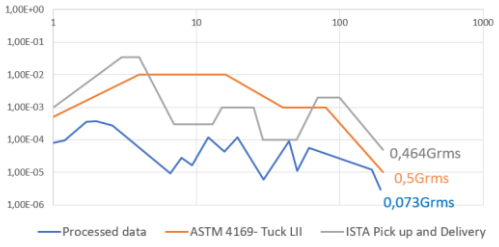

Graph 6. Vertical PSDs of each method

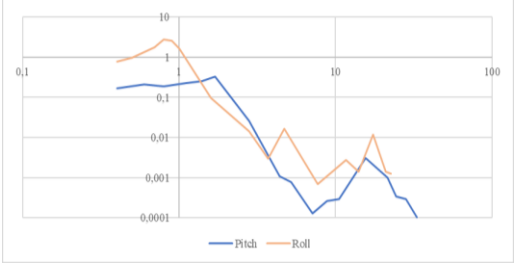

Graph 7. Pitch & Roll PSDs of the processed data

An innWave SF-PR90, vibration testing system, was used for random vibration test, for vertical testing and for vertical plus pitch and roll testing.

- Stability test: Horizontal stability test performed increasing the intensity 0.1g until fatal fail or reaching the machine limit and measuring the dynamic and static deflection for every test. The stability test is performed on a Safe Load HSB1000 type machine.

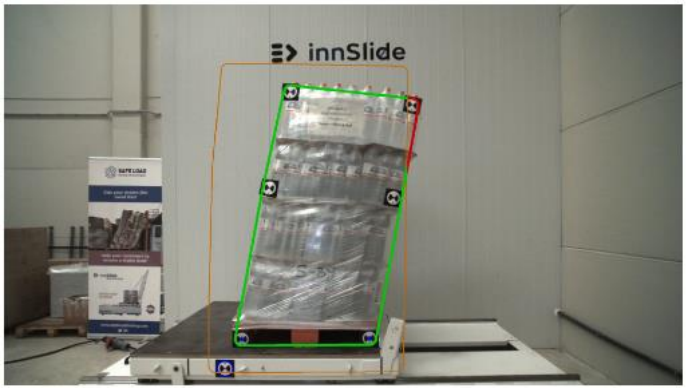

Graph 8. Max deflection instant identified and measured by artificial vision system

The response of every sample for every test is evaluated measuring the maximum dynamic deflection during the test and the permanent deflection after testing. The deflections are measured with an artificial vision system (Safe Load's innVision [5]). This is the same app used for studying the sample stability on boar.

TEST RESULTS

The sample without preconditioning and the samples preconditioned with standard vibration tests fall at the 0.5G stability test. The sample preconditioned by multy-axial random vibration test from the recorded data falls at the 0.4G stability test.

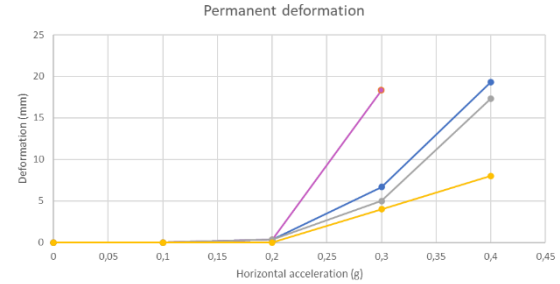

Graph 9. Permanent deformation after stability test.

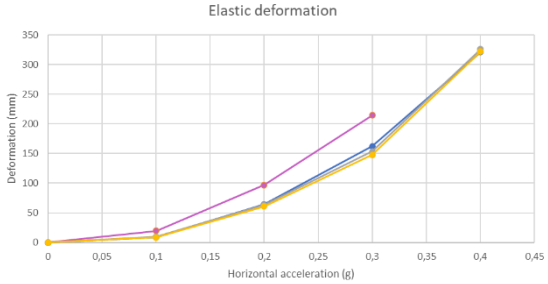

Graph 10. Elastic deformation during stability test.

An artificial vision system was used during the stability tests for measuring the maximum elastic deformation and the permanent deformation after every single stability test. It is worth mentioning that the sample conditioned with heave pitch and roll has a point less than the others because it fell one test before the others.

ANALYSIS

Next graph shows in blue the area where the deflection overpasses the maximum deflection recorded (372mm), the limit is the horizontal red line. The area where the acceleration overpasses the acceleration when the sample dropped (0.36G), the limit is the vertical black line. The purple area is where accomplishes both conditions.

The load fails when its deflection overpasses its breakpoint. When the sample is in transit, the acceleration is what creates the force which produces the load deflection. The deflection is a function of the applied force, so it is a function of the acceleration. This is easy to appreciate on the elastic deformation curves, as all the samples increase its deflection when the acceleration goes up.

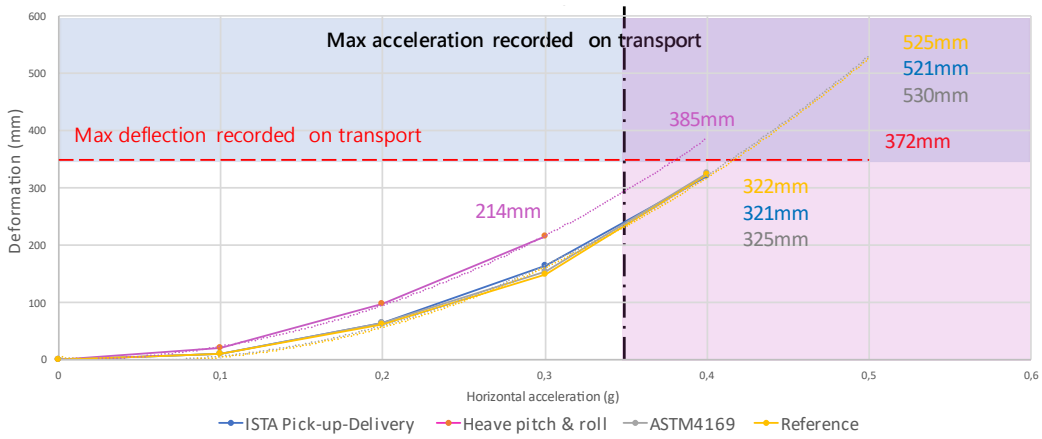

Graph 11. Test deflection vs transport maximum deformation including an extrapolated point by curve

The study does not produce any reference regarding the load defection breaking point, but it is well-know which acceleration breaks it. Extrapolating the deflection vs acceleration curves an extra point is added for the values when the sample did fall. The added points for all the curves came into the purple area where the load on road failed. According to the purple curve (Multy-axial H, P&R preconditioning), the sample broke when it passes the acceleration of 0,36G which broke the sample on road. For this preconditioned test and on road the fails are produced by the accumulative effect of the stress.

Comparing the deflection curve responses from the sample without preconditioning, and the samples preconditioned by the standard vertical random vibrations, we can say these are practically the same. Also comparing the tested vertical component PSDs, the one from the multi-axial is smaller to the standard test for all the bandwidth. So, the necessary stress for

preconditioning the sample for stability testing is not a question of the vertical random intensity or bandwidth.

Then multi-axial testing gives the same response we recorded and reproduced at the laboratory, but using vertical vibration preconditioning is practically the same as no preconditioning.

CONCLUSIONS

Results from the present study can be summarized as follows:

- Preconditioning by multi-axial random vibration improves the stability test results.
  - Laboratory testing gives the same result as the distribution chain using the proper preconditioning method.
  - Preconditioning with classical vertical vibration test for stability testing is the same as not preconditioning the samples.
  - Preconditioning with multi-axial test prepares the sample for approaching the result to the on road responses of the samples.
- The load stability strength decreases as effect of the mechanical stress produced on road in transport.
  - This stress can be done by preconditioning the sample using multi-axial random vibration test methods.

However, this study is limited since the same procedure should be applied to more loads.
Thus further studies could focus on more accurate stability steps, and the same procedure should be applied to other loads. Besides, some issues to apply are the impact of this methodology over packaging redesign., costs improvement and environmental waste reduction.

REFERENCES

[1] United States Department of Transportation, "Federal Motor Carrier Safety Administration," [Online]. Available: https://www.fmcsa.dot.gov/.

[2] EUMOS, *EUMOS 40509*, 2020.

[3] *ASTM D4003-98 ((Reapproved 2003), Standard Test Methods for Programmable Horizontal Impact Test for*.

[4] International Safe Transit Association, "ISTA," 2023. [Online]. Available: https://ista.org/.

[5] Safe Load TT, "Horizontal Stability Tester," [Online]. Available: https://www.safeloadtesting.com/. [Accessed 20 04 2023].

[6] L. M. Rouillard V, "On the effects of sampling parameters when surveying distribution vibrations," *Packaging Technology and Science,* no. 21, pp. 467-477, 2008.

[7] International Safe Transit Association, "ISTA.org," [Online]. Available: https://ista.org/docs/ISTA_Data_Collection_Standards.pdf.

DP-GO03

High-speed camera analysis of load/pallet interface behavior in logistics unit submitted to impact

Charles Tissandie*[1,2], Samuel Rivallant[1]

1 Institut Clément Ader, Université de Toulouse, UMR CNRS 5312, INSA - ISAE-SUPAERO - UPS - IMT Mines Albi. 3 rue Caroline Aigle, Toulouse 31400, France
2 ILIPACK, Avenue Georges Pompidou - CS 20258 - 81104 Castres

***Correspondence to**:* Charles Tissandie. *Institut Clément Ader, Université de Toulouse, UMR CNRS 5312, INSA - ISAE-SUPAERO - UPS - IMT Mines Albi. 3 rue Caroline Aigle, Toulouse 31400, France*
Email: charles.tissandie@iut-tlse3.fr

ABSTRACT: The study presented here highlights the phenomena involved in the load-pallet link during an impact, the role of each of the elements and their impact: speed, load-pallet adhesion, stretch film. This is the beginning of a larger study which should lead to the implementation of a model of pallet behavior in dynamics.
We present here the results of a test campaign, during which we carried out inclined plane impacts on logistics units with a clearance between the load and the edge of the pallet, which made it possible to observe their movements during the impact with a high-speed camera. This study therefore shows the evolution of the displacements and speeds of the load in relation to the pallet during the different phases of the movement, during an inclined plane impact. This study allows us to better understand the influence of friction and stretch film in the shock resistance of logistics units.

Keywords: load/pallet connection, Impact, Stretch film

INTRODUCTION

The general objective of our study is to work on the behavior of products, their packaging and conditioning under mechanical stress during transport. The overall aim is to provide tools to improve the consideration of transport-related constraints from the product design and packaging phase. We will focus here on the analysis of the load-pallet link thanks to a high-speed camera, by analyzing the behavior of the load during an impact on the inclined plane. We will highlight the impact of the various factors that can influence this behavior: adhesion, friction, stretch film…

Film wrapping is the most common way of holding loads on pallets, as it is an inexpensive system that can be automatically installed. Its main function is to hold the load in

place without crushing it during the storage and transport phases. The stretch film ensures the connection of the load to the pallet without tearing, thus ensuring the cohesion of the logistics unit. Several experimental studies have been carried out on the impact of stretch film on the load and the logistics unit, but none has yet studied the behavior of the stretch film in the load-pallet connection.

Indeed, several studies on the role of the stretch film in maintaining the cohesion of the load have been published and models of behavior have been proposed.

Bisha[1] measured the force when the stretch film is placed on the load and established a correlation between the properties of the stretch film and the force on the load. He showed that the static behavior of the stretch film can be modelled by springs on each face, which makes it possible to deduce, from the mechanical characteristics of the stretch film, the forces on the load. *Veneshuck*[2], after an experimental study, proposed a model for determining the number of stretch film turns necessary to maintain the load as a function of the mechanical characteristics of the stretch film in the case of sliding and tilting of the columns.

During the stretch film wrapping of logistics units, two parameters are important and influence the performance of the unit: the pre-stretching of the stretch film (elongation of the stretch film by the stretch film machine just before application), which uses the plastic characteristics of the stretch film, and the application tension (force exerted at the time of stretch film application), which uses the elastic characteristics of the stretch film. The impact of these characteristics on the distribution and transmission of forces between the elements of the logistics unit has been the subject of experimental studies.

Singh et al.[3] carried out an experimental study which showed the impact of the number of turns on the forces generated on the boxes during the stretch film wrapping phase and during a transport test simulation (ISTA 3E protocol). *Wyns et al*[4] conducted an experimental study on stretch film and the evolution of the load force as a function of the application tension, the application area and the type of stretch film.

Other studies have focused on the load-pallet connection and the impact of wrapping on the behavior of the logistics unit, particularly on load distribution. An experimental study presented by *Park et al.*[5] showed that in addition to ensuring load cohesion, wrapping minimizes pallet deformation by modifying the load distribution. A study of the behavior of a logistics unit was proposed by *Matyja*[6,7] in which he proposed a model for determining the number of wrapping turns to ensure load cohesion during a static and a dynamic tilt test.

The load/pallet connection and the behavior of the stretch film in it have not yet been studied or modelled, yet it is an important part of the behavior of logistics units, especially as it presents a clearance between the load and the edge of the pallet (Figure 1). This is the type of phenomenon that is reproduced by the inclined plane impact. Before a model can be created, it is important to understand the behavior of each of the elements. This is why in the study presented here we will observe the movement of the load in relation to the pallet, we will analyze the effect of the stretch film on the total sliding of the load and its behavior in dynamics in the load-pallet link, which will allow us to identify the important elements to be considered in the modelling of this case.

MATERIAL AND METHOD

Sample

Constitution

The logistics unit consisted of 40 boxes and the palletization is columnar (figure 1) with a theoretical maximum cumulative clearance in the direction of the test of 184 mm. This clearance is large but was chosen to allow a good analysis of the movement after the impact, as a larger clearance would have caused difficulties in maintaining the load-pallet connection (stretch film dislodgement).

Some tests were performed with stretch film to ensure the load/pallet connection, some without. For the tests with stretch film, the logistics unit was wrapped in the standard way. For the tests without stretch film at the load/pallet connection, the boxes were however wrapped together in order to minimize their relative movements during the test, our aim not being to study the cohesion of the load but to study the sliding of the load on the pallet

The wrapping operations were carried out on an automatic stretch film machine (ROBOPLAT 708). This wrapping machine allows the application tension and pre-stretching to be adjusted. This type of application is currently the most widely used.

Wooden pallet

- Europe model
- Mass [Kg]: 25

Stretch film: BARSTRETCH

- 9 layers cast
- Thickness [µm]: 20
- Width: [mm]: 500

There are two main families of palletizing stretch film. Here we chose a cast stretch film which is the most used due to its lower cost, and we took a 20 µm stretch film in order to be able to pre-stretch it to different values. The same stretch film was used for load wrapping and load/pallet connection.

Boxes

- Dimensions [mm]: 380 * 256 * 225
- Mass [Kg]: 8,5

Logistics Unit

- Palletization: Columnar

- Dimensions [mm] 1200 * 800 * 1150
- Total Actual Mass [Kg]: 364
- Theoretical Mass of the load [Kg]: 340

Means of testing

The tests were performed on an inclined plane (10° angle). The inclined plane test is the test in the standardized ISTA 3E transport qualification protocol that causes the load to slip on the pallet if the clearance between the load and the edge of the pallet is sufficient.

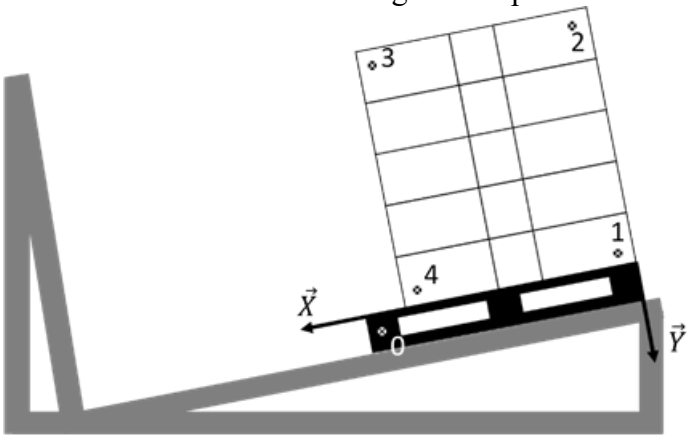

Figure 1. Logistics unit on the inclined plane with indication of the test patterns and the marker used.

For this study we worked with reference axes linked to the inclined plane (figure 1) and we placed test patterns on the logistics units. For the analyses, point 0 is a point taken on the pallet (generally at the front), and points 1 to 4 are taken on the boxes as indicated on figure 1. The logistics unit represented here corresponds to the cases of the study without stretch film, indeed for this one in order to have the largest possible observation area the load was placed at the edge of the pallet. For the wrapped logistics unit tests, the load was placed at the center of the wooden pallet.

Means of measurement

Photron high-speed camera:

- Resolution of 1024*1024 pixels
- 1000 frames /s.
- Accuracy in the case of our study: 2.225 mm/pixel

Camera control software: Photon FASTCAM Viewer.

Analysis software: Photron FASTCAM Analysis. This software allows the tracking of targets by contrast detection (in this case: test patterns). It allows the position of each test pattern to be known on each of the images taken and thus to deduce the displacement and speed of the 5 points.

Test

- The pallet is placed on the platform of the inclined plane (Figure 2a),
- The tray rises at the desired height, which triggers the system,

- The plateau gets down,
- The pallet hits the wall: the analysis phase begins (Figure 2b),
- The load slides on the pallet,
- The top of the load hits the wall: end of the useful measurements (figure 2c)
- The bottom of the load hits the wall

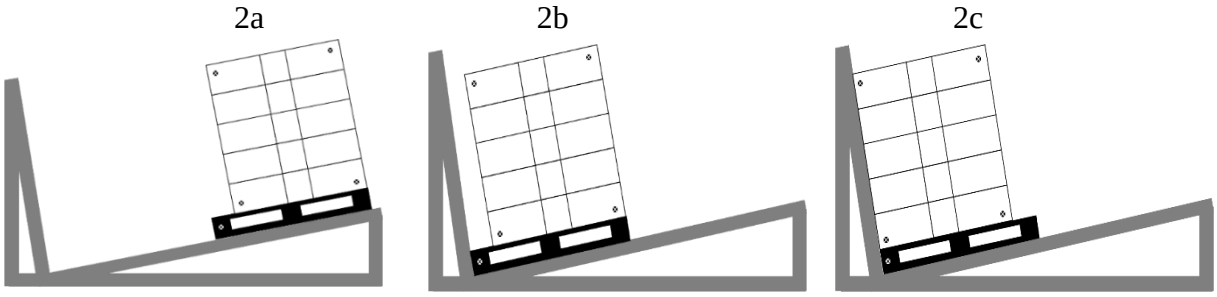

Figure 2. Inclined test, schematic of pallet and load movement

Figure 3. Photo of the test facility

Table Of Tests

For the tests we used two different logistics units P1 and P2. The tests were carried out in the longitudinal direction of the pallet.
The following table shows the different tests presented, indicating the pallet used, the presence or absence of anti-slip between pallet and load and the parameters used for the logistics unit wrapping.

N° Test	Anti-slip	Unit load	Presstressing	Laying tension	Numbers of turns down
	(nue : non)		%	%	
1	Non	P1			
2	Non	P1			
3	Non	P1			
4	Non	P1			
5	Oui	P2			
6	Oui	P2			
7	Oui	P2			
8	Oui	P2			
9	Non	P1	150	2	4
10	Non	P1	300	2	4
11	Non	P1	150	30	4
12	Non	P1	250	2	4
13	oui	P2	250	2	4
14	Non	P1	250	2	8
15	Non	P1	150	30	8
16	Non	P1	150	30	8
17	Non	P1	250	2	4

In all tests the pallet stretch film did not come loose and the pallet load connection was maintained.

RESULTS AND ANALYSIS OF PALLET WITHOUT PALLET WRAPPING

The objective being to study the load-pallet connection, we began by carrying out load tests (coherent box unit) on a pallet without wrapping of the logistics unit and anti-slip material between the two. These tests allowed us to analyze the behavior of the load during impact.

Analysis of the behavior of the load without pallet wrapping.

Note: On all the following graphs in the legend, the curves are labelled A-BCD, where A is the number of the test used, B is the type and C is the point and D is the treatment of the curve. Example 4-Vx1rm is the X-axis component of the average relative velocity (between the load and the pallet) of point 1 of test 4.

Motion graphs

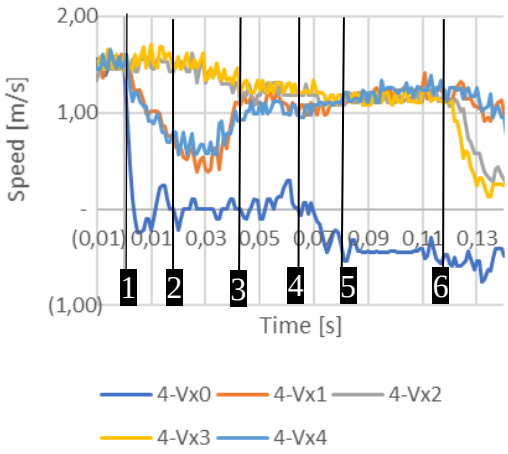

Figure 4: Plot of measured velocities in x direction

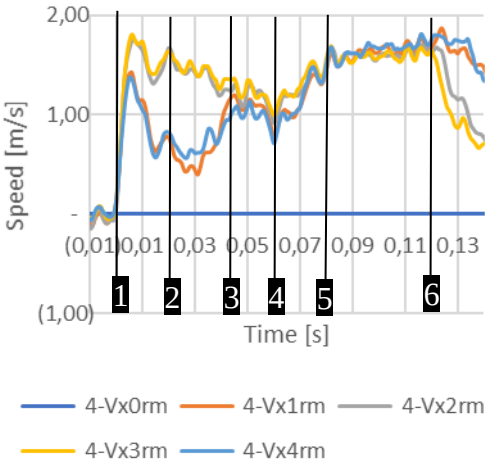

Figure 5: Plot of relative velocities with respect to the pallet in x direction, smoothed by 3 points averaging.

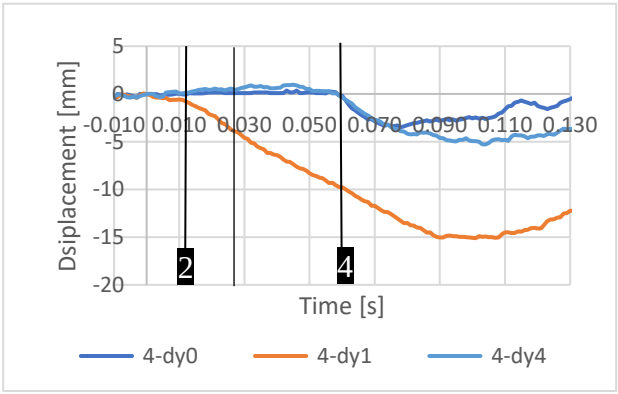

Figure 6: Displacement graph in y direction.

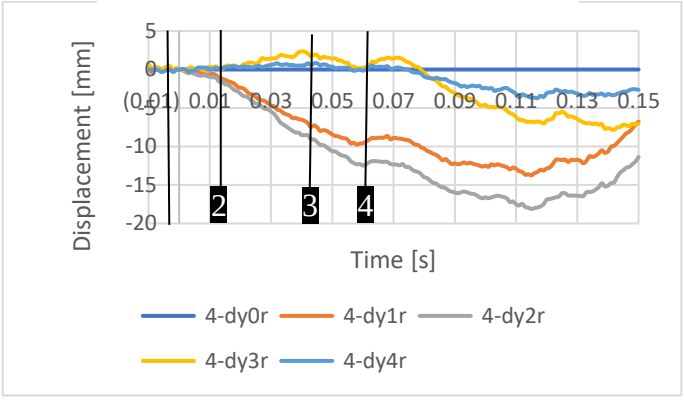

Figure 7: Plot of the relative displacement with respect to the pallet in y direction.

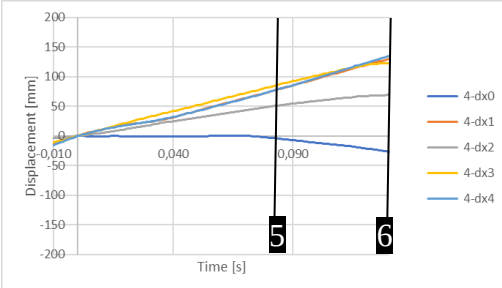

Figure 8. Plot of absolute displacement in x direction

Figure 4 shows the velocities at the 5 points. The signal is noisy and the measurements are expressed in the reference frame linked to the inclined plane. Figure 5 shows the same curves but the speeds are expressed in a reference frame linked to the pallet and the curve is smoothed (3 points average). As our study is aimed at understanding the load/pallet slip, we will work using the relative speed between the boxes and the pallet. In order to improve the reading, these curves will be the standard we will use to express the results, even if this type of smoothing attenuates a little the variations.
Figure 6 and Figure 7 show the detachment of the boxes and the pallet from the inclined plane carriage, and Figure 8 shows the displacement on x in the direction of movement and shows the beginning and end of the study area.

Motion analysis

The photos in Figure 9 are taken from the test number 4 and illustrate important phases of the movement.

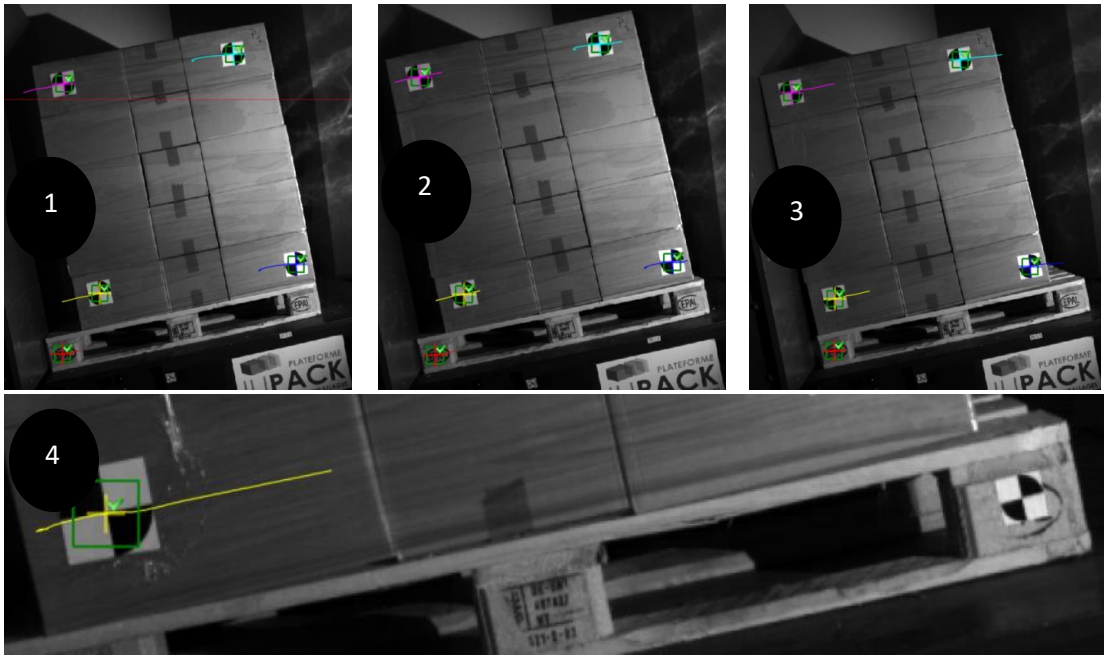

Figure 9. photos of trial 4 unfilmed pallet

The numbers of the steps below correspond to the numbers on the graphs in Figure 4, Figure 5, Figure 6, Figure 7 and Figure 8:
1: The pallet touches the wall, this is the beginning of the analysis phase (photo 1),
2: The columns of boxes tilt, the boxes start to lift, the contact area between the pallet and the boxes decreases,
3: All the columns have tilted, all the boxes have lifted, they are pressing on the front edge (photo 2 and photo 4),
4: The pallet tilts,
5: Pallet bounce: the carriage of the inclined plane comes into contact and bounces on the shock absorber,
6: The boxes of the top row touch the slope, this is the end of the analysis area: photo 3.

Set-up phase: between point 1 and point 3, the load moves, the boxes in contact with the pallet rise, first the right-hand column, then the center one and finally the left-hand one. Once the boxes have tilted, the columns tighten and the load starts to slide evenly. In this phase the load/pallet contact surface is constantly changing and decreasing. Moreover, the tilting of the load generates disturbances on the speed graph.
Sliding phase between point 3 and point 6: the boxes slide on the pallet. At point 4 the pallet lifts off the inclined plane, and from point 5 onwards the wooden pallet rises.
In this first part it appeared that the wrapping of the boxes to create a homogeneous load did not prevent the movement and tilting of the columns (figure 9, image 4, figure 10). This tilting causes a break in the box/pallet contact.

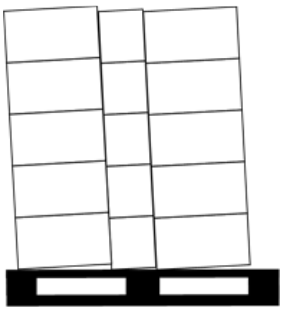

Figure 10. Illustration of the tilting of the columns during the test

For all the tests it will therefore be necessary to analyze the load application phase and the sliding phase separately.

Remarks

Graph readability

It can be seen from the graphs (figure 11) that points 2 and 3 (points located at the top of the pallet) have a similar behavior during the studied movement, the same is true (figure 11) for points 1 and 4 (points closest to the load/pallet connection). In the next graphs, in order to improve readability, we will only display one of the two points.

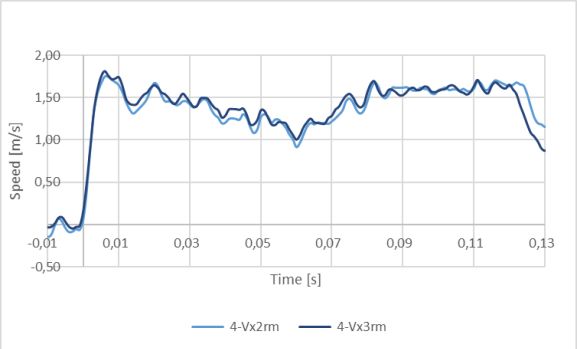

Figure 11. Comparison of point 2 and 3

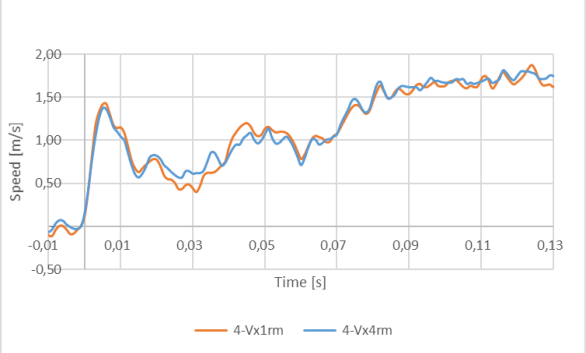

Figure 12. Comparison of point 1 and 4

Reproducibility study

Tests 1 and 4 were carried out using the same parameters, and it can be seen (Figure 13) from the curves for point 4 (left-hand graph) and point 1 (right-hand graph), which represents the relative velocity smoothed in x direction, that the results are transposable from one sample to the other. The results obtained in the two trials are comparable.

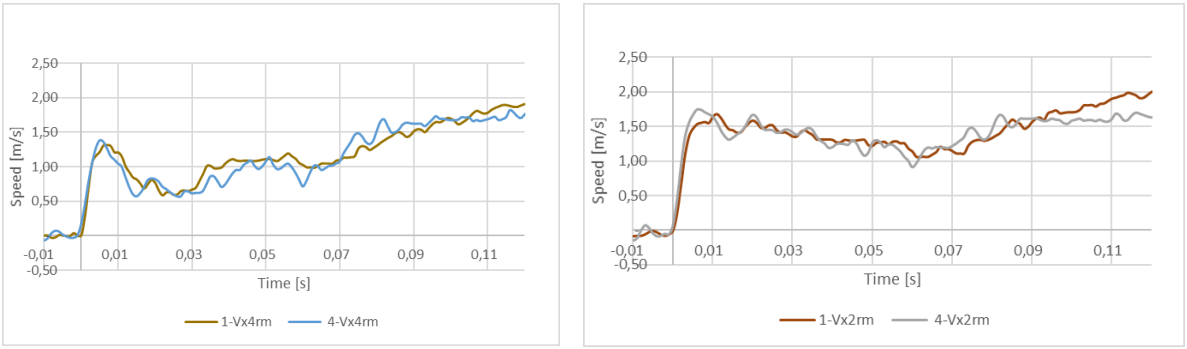

Figure 13. Relative velocity curves in x direction for tests 1 and 4

Effect of speed

In tests 2 and 4, the wrapping of pallets 2 and 4 was carried out with the same parameters, and only the impact speed varied.

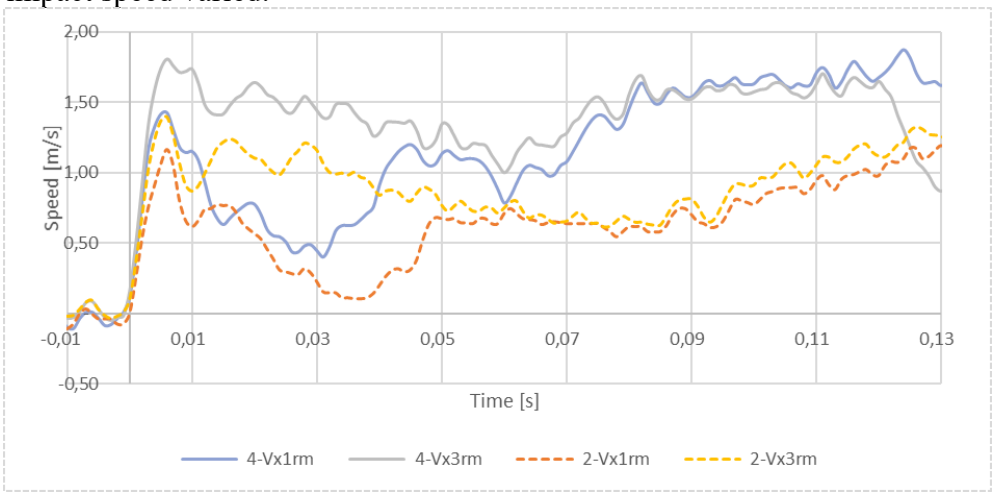

Figure 14. Plot of relative velocities on two tests performed at different speeds

In general, the behavior of the load in relation to the pallet is similar. It can be seen that the positioning and sliding phases are respected. The movement of the two logistics units is similar, but we can see that the duration of the different phases is inversely proportional to the speed.

Effect of Anti-Slip

Anti-slip increases the grip and friction in the load/pallet connection.
For our study we measured the coefficients of adhesion and friction for the different material pairs involved in the load/pallet connection:

	Coefficient of adhesion	Coefficient of friction
Wood pallet / Anti-slip	0,75	0,63
Box / Pallet	0,54	0,38
Box / Anti-slip	0,91	0,53

Figure 15. Coefficient of adhesion and friction

During the test, we observed that the anti-slip moves with the boxes, which was expected: the boxes/anti-slip sheet adhesion coefficient was higher than the pallet/anti-slip sheet coefficient.

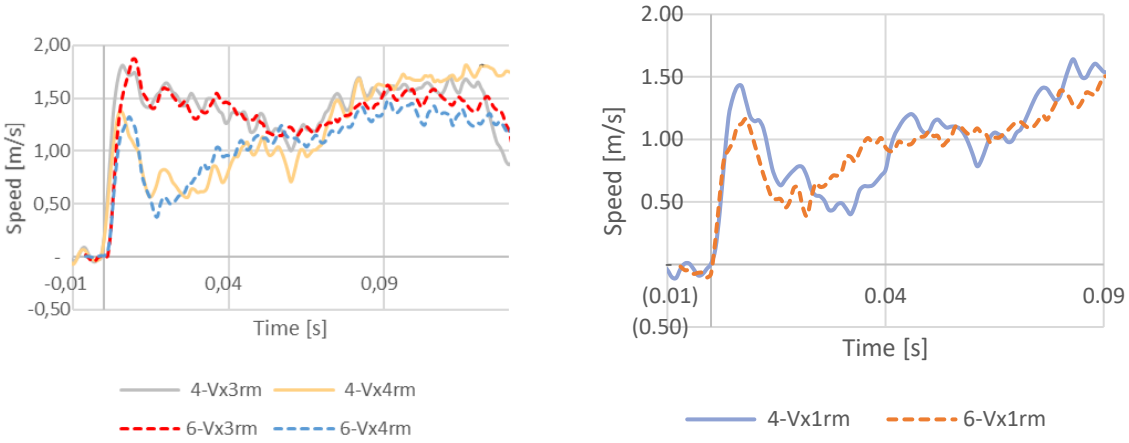

Figure 16. Relative velocity plot in smoothed x direction

The presence of anti-slip increases the adhesion, the friction in the load-pallet connection.
The set-up phase takes less time with the anti-slip, which shows that the columns tilt more quickly. Anti-slip minimizes the speed but especially at the end of the movement, when the load has stabilized.
The tilting of the columns affects the effectiveness of the anti-slip.

RESULTS AND ANALYSIS OF PALLET WITH PALLET WRAPPING

Effect of the number of turns

Increasing the number of stretch film turns at the bottom of the pallet is the classic response of manufacturers to the problem of cohesion of logistics units at the load/pallet link. We therefore compared the response to impact on the inclined plane of a pallet without stretch film (4), one with 4 turns of stretch film at the bottom (12) and one with 8 turns of stretch film at the bottom (14), to see the difference in response of the two stretch film systems.

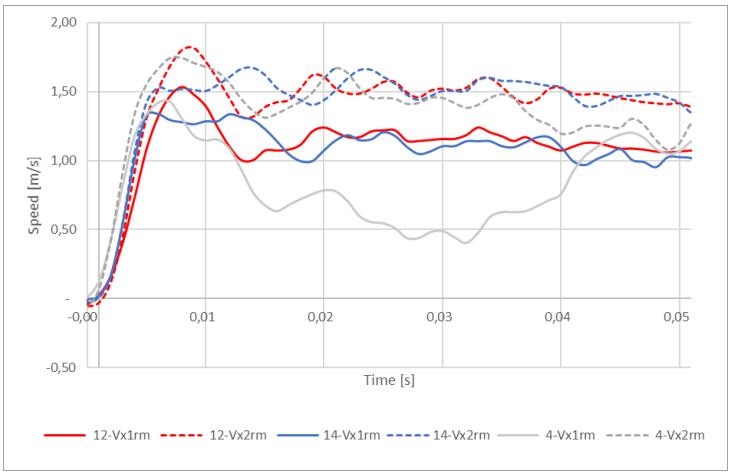

Figure 17. Comparative graph of relative speeds for logistics units with different number of turns at the bottom of the pallet

The set-up phase is very low in the case of stretch filmed pallets, due to the fact that the stretch film maintains contact between the boxes and the pallet. It can also be seen that the response curve of the test with the highest number of turns shows less oscillation. The more turns of the stretch film, the more the load remains homogeneous and flat on the pallet.

Effect of pre-stretching

The pre-stretching of the stretch film plastically deforms the stretch film, with a small variation in the width and therefore a variation in the thickness of the stretch film directly proportional to it. Pre-stretching minimizes the amount of stretch film used to shrink-wrap a logistics unit.

Figure 18 shows the response of Test 9 and Test 10, whose logistical units were performed with different pre-stretching. It can be seen that increasing the pre-stretch minimizes the duration of the setup zone it seems that pre-stretch minimizes the initial strength (different slope of the curves).

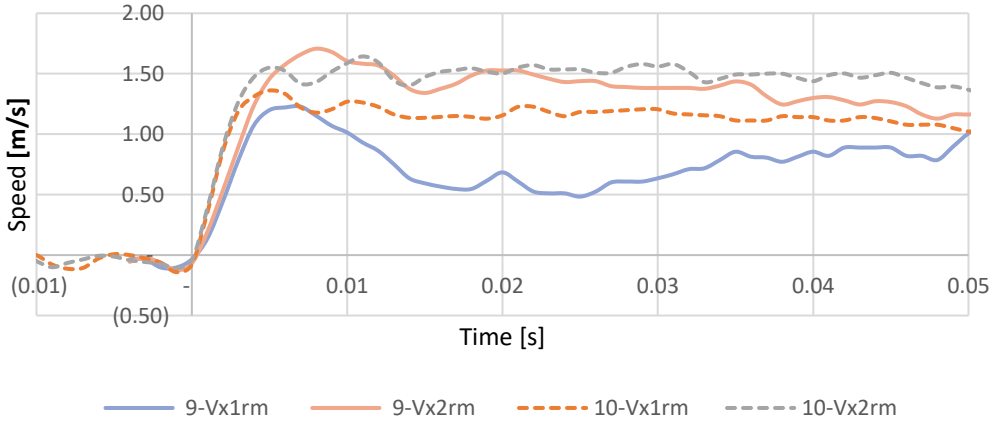

Figure 18. Plot of the smoothed relative velocity in two different pre-stretched cases

Effect of application tension

The application tension allows the stretch film to be stretched when wrapping.

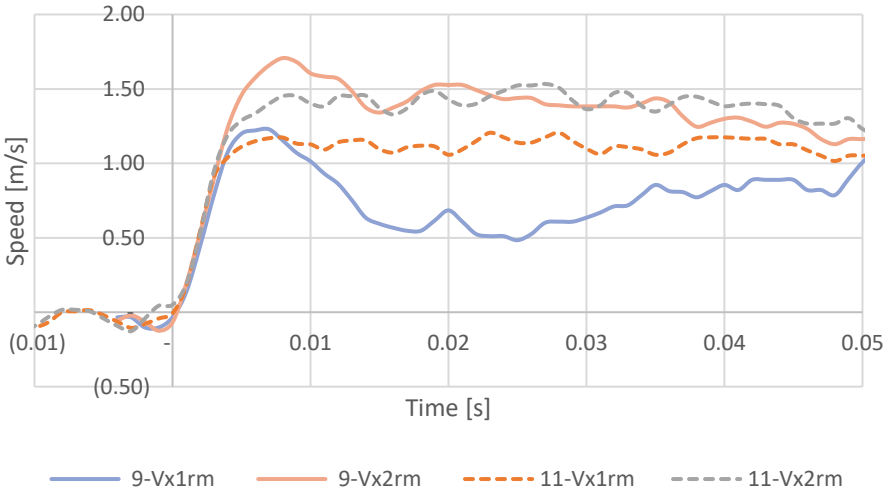

Figure 19. Relative velocity graph in x direction with evolution of the application tension

In the application phase the behavior of the stretch film is identical, however, the increase in the application tension allows the load to be homogenized. It can also be seen that the velocities are lower at the time of the beginning of the lifting of the boxes.
It can be seen that the curves for the top point 2 and the bottom point 1 are parallel, which shows that the load does not tilt very much, which is confirmed by the fact that the set-up phase is reduced. The response is more linear. The displacement phase is established much more quickly and therefore we have better slowing down of the load.

Comparative effect of application tension and pre-stretching

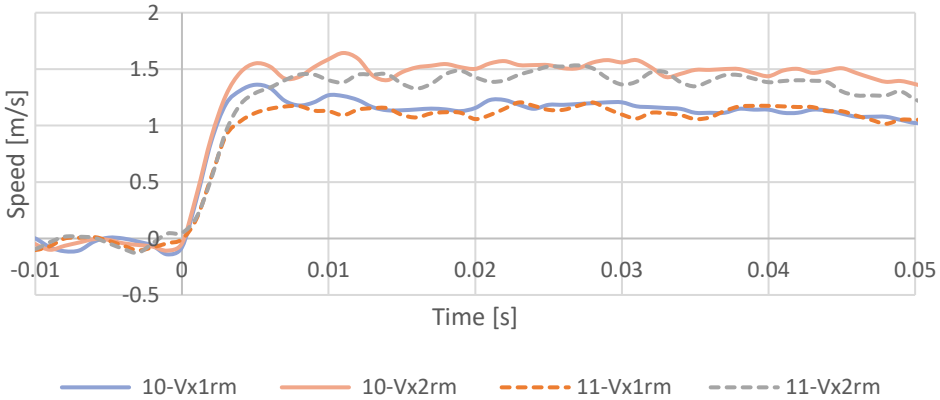

Figure 20: Relative velocity graph in x direction with evolution of the application tension and pre-stretching

It can be seen by comparing the effect of pre-stretching and application tension that in the case of the shock studied, both minimize the setting phase, but that application tension makes the system respond more continuously (curve with less oscillations) and limits the setting phase more. In the sliding phase the two solutions remain homogeneous (parallel curves).
It can be seen that both settings have a similar effect, with a decrease in set-up time, so it can be assumed that this is due to the improvement in load uniformity.

Cumulative effect of stretch film and anti-slip

Wrapping reduces the set-up time and keeps the boxes in place on the pallet, so we did a test to see if this would improve the effect of the anti-slip

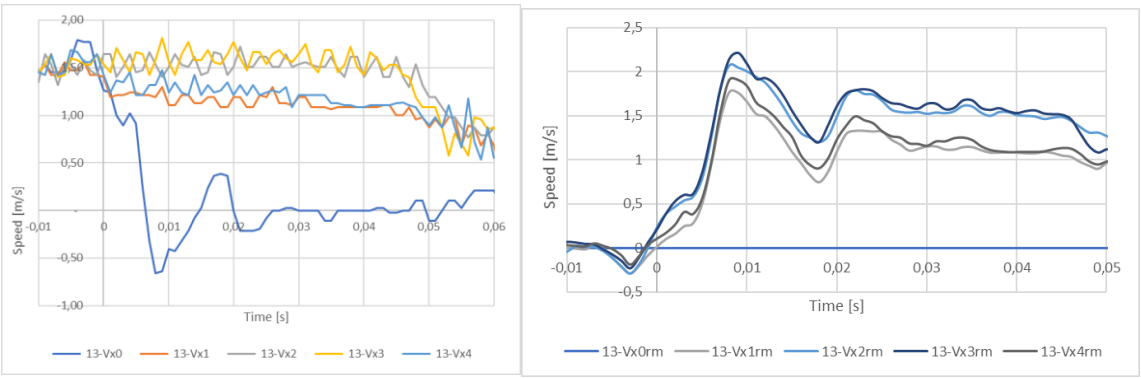

Figure 21: Plot of absolute velocities in x direction and velocity on a wrapped pallet with anti-slip

In this test, the tilting of the pallet at the moment of impact modifies the graph during the set-up phase, but not during the sliding phase. In Figure 21, it can be seen that the speed decreases progressively, and in this test, there was no tilting of the load in relation to the pallet, the stretch film kept the load pressed against the pallet and compared to the test with the use of anti-slip device alone (see paragraph 3.4), the deceleration slope is more significant.

CONCLUSION

It is clear from the observations made during this study that wrapping is an important factor in the load-pallet connection. We have seen that one of the key elements in the impact resistance of a logistics unit is to minimize the movement of the load in relation to the pallet, and that the stretch film perfectly fulfils this function. We have also seen that the tension of the stretch film and pre-stretching, contributes to limiting the sliding of the load in relation to the pallet, as much by the fact that it holds the load in place as by its own resistance. In addition, this study showed that the cohesion of the load is one of the key factors in maintaining the load-pallet connection.

The use of anti-slip is an interesting solution in the case of a problem of load slippage in relation to the pallet, but only if the cohesion of the load is well maintained and the load-pallet connection is good.

Following this study, it is clear that good wrapping must ensure that the load-pallet link is maintained throughout the logistics circuit, as this is one of the key elements of the stability of logistics units, and that we must try to have loads that are as homogeneous as possible.
The objective for the validation of the stretch film of the logistics units will be to validate that the stretch film ensures a good cohesion of the load, does not become loose and ensures the bonding during the whole distribution phase.
It also became apparent in this study that one of the functions of the stretch film was to maintain contact between the load and the pallet, and that the detachment of the boxes would have to be considered in order to produce a relevant model.

ACKNOWLEDGEMENTS

We would like to thank the Pierre Fabre company for its technical and financial support for this research project.

REFERENCES

[1] Bisha JV. Correlation of the elastic properties of stretch film on unit load containment (Doctoral dissertation, Virginia Polytechnic Institute and State University). 2012.
[2] Vanechuk L, ISTA transpack forum 2015: Dissecting Containment Force: compression, Stiffness, and their Roles stabilizing unitized goods
[3] Singh, J, Cernokus E, Saha K, Roy S. The effect of stretch wrap prestretch on unitized load containment. Packaging Technology and Science. 2014, 27(12), 944-961.
[4] Wyns J, Cook J, Dunno K. Post-Wrapping Behavior of High-Performance Stretch film, journal of Applied Packaging Research. 2018, Vol. 10: No. 3, Article 1.
[5] Park J, Horvath L, White M, Araman P, Bush RJ. The influence of stretch wrap containment force on load bridging in unit loads. Packag Technol Sci. 2018, 31, 701-708.
[6] Matyja T. Tilt test of a pallet load unit - simulation studies. Scientific Journal of Silesian University of Technology. Series Transport. 2020, 107, 107-117.
[7] Matyja T. Safety of transport operations performed using pallet load units. Scientific Journal of Silesian University of Technology. Series Transport. 2021, 112, 145-156.

DP-GO04

Statistical study on acceleration value data recorded on roundabout, curve, during a road trip to classify then in function of their impact on load stability

Baptiste Boutrige[1,2,3*], Victor Huart[1], Jean-Baptiste Nolot[3], Nicolas Krajka[1], Jérôme Pellot[1], Marie Le Baillif[2,3], Serge Odof[2,3] and Damien Erre[2,3]

[1]*R&D, Metropack, Reims, 51100, France*
[2]*ITheMM, Université de Reims Champagne-Ardenne, Reims, 51100, France*
[3]*R&D, ESIREIMS, Reims, 51100, France*

***Correspondence to:** Baptiste Boutrige. R&D, Metropack, 30-32 Rue du capitaine Georges Madon, Reims, 51100, France.*
E-mail: baptiste.boutrige@metropack.fr

ABSTRACT: During road trips by truck, in Europe, one accident out of four is related to a load stability problem. It is therefore important to investigate on what happens on the roads, and in particular what constraints are encountered on road trips.
Horizontal accelerations generated by turns, round-abouts, braking, etc, can affect the stability of a load. These event types are the root cause of pallet movement inside the truck, load sliding, total load tilting and in some cases, road accident. Moreover, these phenomena are very common during the distribution of goods, mainly in urban areas.
The shape of acceleration profiles generated by these different events are known. The characterization of curves, round-abouts according to their circumference, authorized speed, can constitute a severity indicator of impact of these events on the products stability.
In this work, to obtain this indicator, we have characterized and classed hundreds of horizontal events occurring during a truck transport. The impact of the different elements as round-about circumference, authorized speed, road curvature has been study and their impact on a load stability will be presented.

Keywords: Horizontal acceleration, Load stability, Round-abouts, Field measurement

INTRODUCTION

During transport, various events can have an impact on the loads being transported. Roundabouts, braking, etc. can generate horizontal accelerations that can affect the stability of a load. Transportation constraints are more and more investigated [1-10]. There are several tens of thousands of roundabouts in France. The impact of the roundabouts on the stability of a load is still poorly understood. The present study will investigate the effect of the roundabouts on the load stability according to their parameters. The relation between load stability and

acceleration has already been presented in previous work [11-12]. The acceleration undergone by the load will therefore be taken as stability criteria.

MATERIALS AND METHODS

Material

Transport tests were performed using two identical pallets made of partially loaded boxes and a 30m^3 truck. Details of the pallet loads are presented in Table 1 and figure 1. The pallets were equipped with two types of devices:

- 3 accelerometers 3D15 saver supplied by Lansmont (Monterey, United-States) were placed inside a box on top of each pallet and the last one on the truck's trailer floor. The recording was performed continuously at a sampling frequency of 50Hz.
- a 9XGPS saver supplied by Lansmont (Monterey, United-States) was used to record the travelled distance and the truck speed during the test. It was located on the passenger side seat.

Height	141.3 cm
Length	120 cm
Width	80 cm
Weight	247 kg

Table 1. Pallet load description.

Figure 1. Configuration in truck's trailer

Experiment

Two transport tests of one day each were performed. The first one consisted in a Reims – Soissons (France) turn / return trip, while the second one was a Reims – Troyes (France) turn / return trip. Details of both trips are presented in table 2. For both tests, the data from the accelerometer on the trailer's floor were associated with the GPS data in order to identify the adequate roundabout on the records. The data from the other accelerometers were used to record the acceleration undergone by the load itself.

	Test 1	Test 2
Total distance (km)	123	304
Number of roundabouts	89	93

Table 2. Trips details

The first test was performed in order to verify that both pallets underwent the same transport constraints. The second test studied the effect of ageing of the wrapped film on the load stabilization during transport. That for, one of the pallets was rewrapped with new wrapping film after the first transport test, while the second one was unchanged. Difference in recorded acceleration were again investigated while driving through roundabouts. In addition, correlations between roundabouts' parameters and recorded acceleration on the trailer's floor were investigated using both tests.

Figure 2 and 3 shows a typical signal recorded on a roundabout. Three steps are visible: the first corresponds to the entry into the roundabout (orange arrow on figure 2), followed by the taking of the curve of the roundabout (yellow arrow on figure 2) and finally the exit from the roundabout (green arrow on figure 2). For the present study, this signal was represented by two ramps around a plateau. The plateau was set at the optimum recorded value, in order to avoid underestimation of the signal. Figure 4 shows both recorded and simplified acceleration signals. The plateau was the main parameter investigated in the present study.

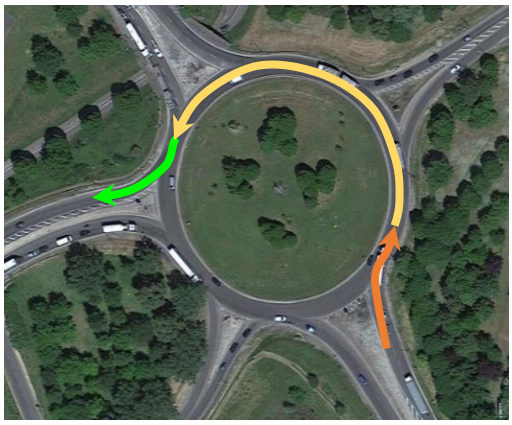

Figure 2. Different steps in roundabout.

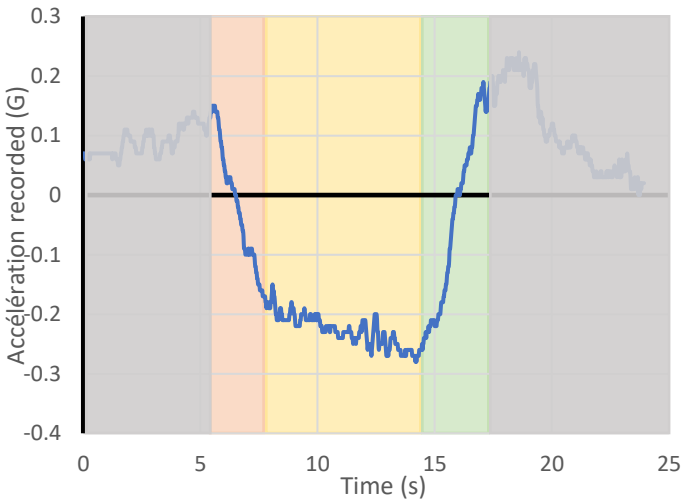

Figure 3. Acceleration recorded in function of the different steps.

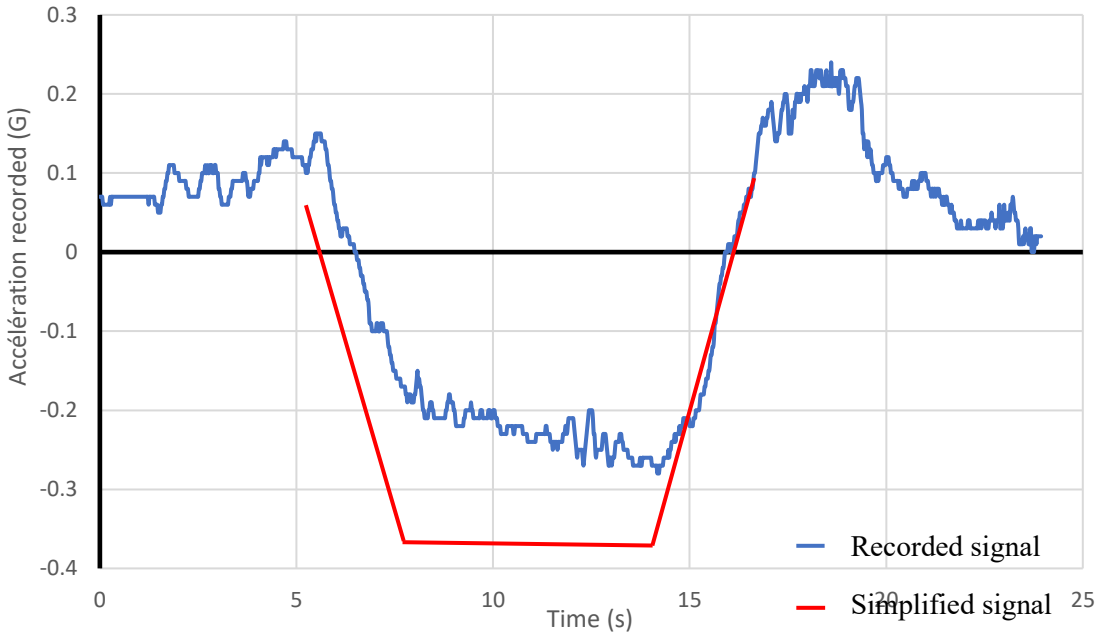

Figure 4. Recorded and simplified acceleration signals

RESULTS AND DISCUSIÓN

Roundabout characterization

182 roundabouts had been recorded during both tests, with different diameters. The distribution of these diameters is presented in Figure 5. Rice equation allowed to find the groups of roundabout diameters (see equation 1 where n the number of the group and N is the total of value we have.). According to the records, N was equal to 182, and a value of 11.33 was obtained for the number of groups. It was therefore decided to use 11 group in the present study.

$n = 2 \times \sqrt[3]{N}$ eq.1

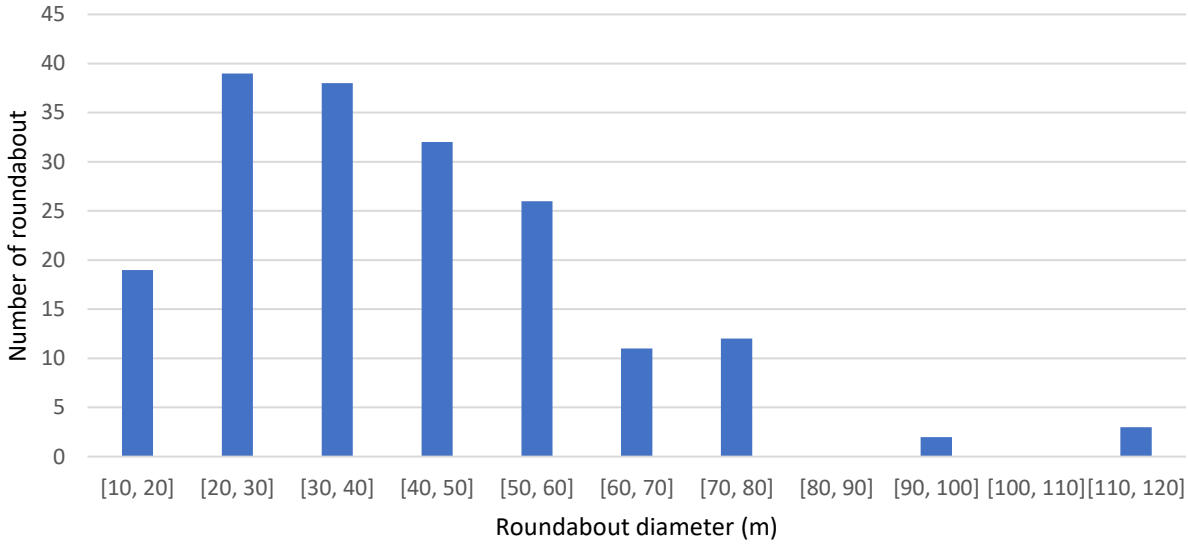

Figure 5. Number of roundabouts in function of the roundabout diameter

It can be observed most roundabouts had a diameter between 20 and 60 meters. In addition, all but 5 roundabouts had a diameter below 80 meters. It was decided that the records during these 5 events were not representative of typical transport conditions. They were therefore removed from the study which was then using only 7 groups of roundabouts.
Figure 6 presents the generated acceleration according to the roundabouts' diameter. One can note that several different values of acceleration was recorded for one given diameter. Acceleration was recorded from -0.05 to -0.35G for all diameters. No significant correlation can therefore be found between these two parameters.

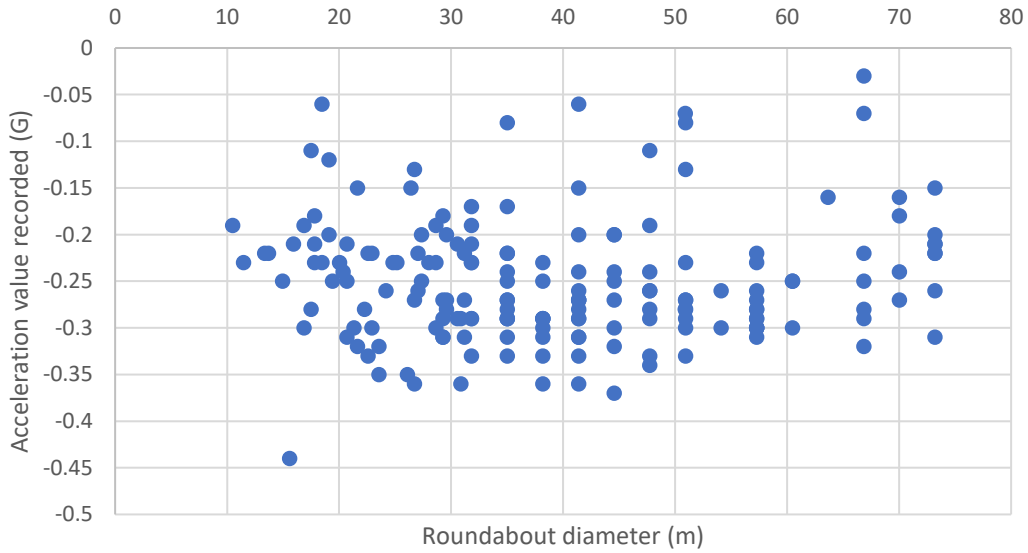

Figure 6. Acceleration value recorded in function of the roundabout diameter

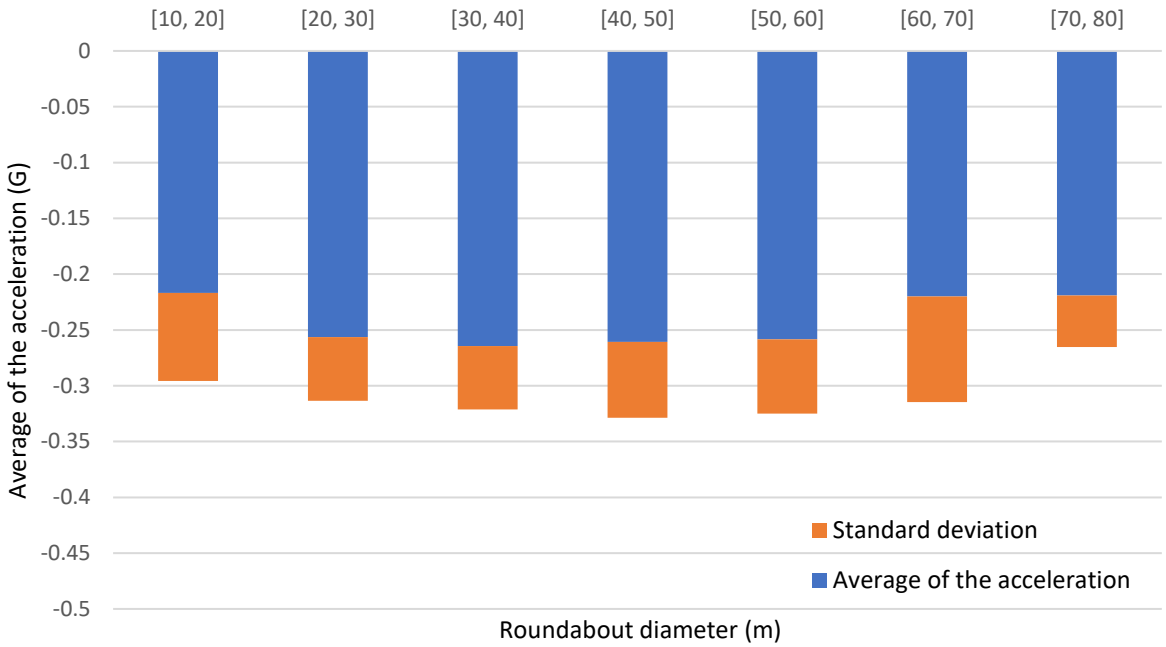

Figure 7. Average of the acceleration recorded in function of the roundabout diameter

Using the groups definition presented above, the average of maximum recorded accelerations and their standard deviations were calculated for each group. The results are presented in figure 7. The average of the acceleration was fairly constant, about -0.24G. No significant difference was found between the groups, confirming the results of figure 6.

The maximum speed during a roundabout was measured using the GPS data to occur at the end of the plateau. The average and the standard deviation (in orange) of the maximum speed were calculated for each group, and they are presented in figure 8. It can be observed that the maximum speed had a tendency to increase with the roundabout diameter. However, when a critical diameter about 50-60 meters was reached, the diameter had no further effect on the maximum speed which a value of about 33km/h.

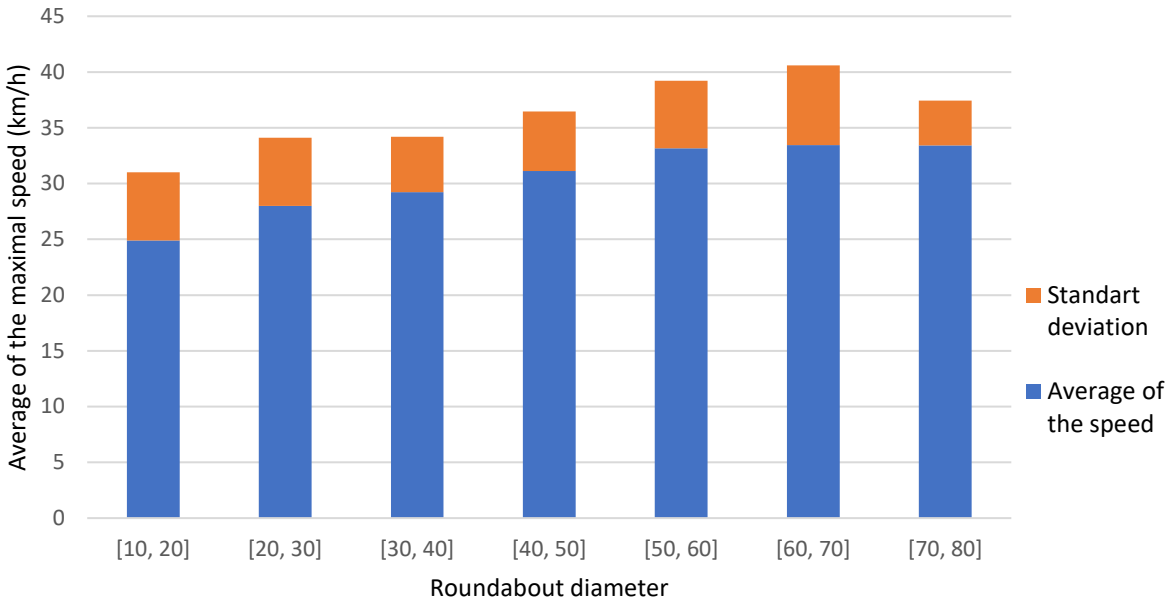

Figure 8. Average of the speed in the roundabout in function of the roundabout diameter

It can be concluded that the roundabout diameters affected the maximum speed but not the acceleration. The speed one may reach while driving through a roundabout is a function of the acceleration and its duration. For small roundabouts, the available distance and therefore the available time are not sufficient to reach the potential maximum speed one may use in a roundabout. However, when the critical diameter was reached, the potential maximum speed was reached. It might of interest to evaluate the effect of the roundabout diameter on the potential maximum speed. However, the records of the present study were not sufficient for such analysis. One may also consider the effect of the driving techniques of the driver which could affect the initial speed in the roundabout and therefore the acceleration recorded during such test. Such investigation could be the focus of further work.

Effect of acceleration on two identic pallets

The acceleration recorded on both pallets during test 1 are presented in figure 9. It can be observed that the recorded accelerations were almost identical for both pallets. It can therefore be concluded that they underwent identical transport constraints.

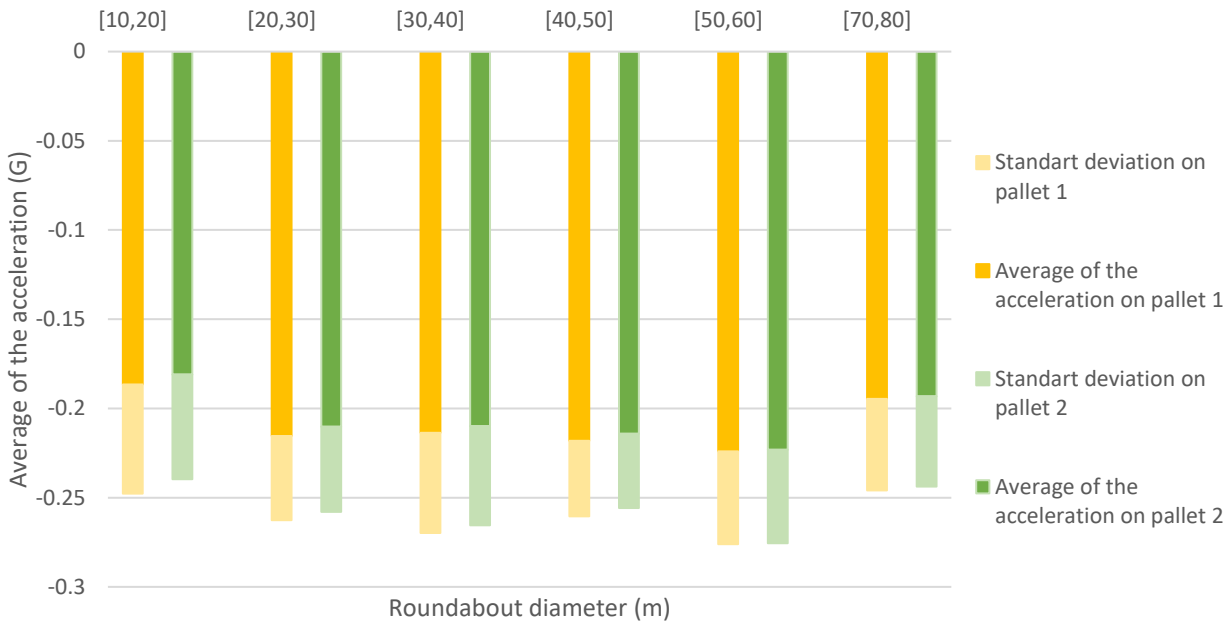

Figure 9. Acceleration recorded on both pallets during test 1 in function of the roundabout diameter

Effect of the ageing of the wrap film

Figure 10 presents the recorded acceleration of both pallets: pallet 1 with aged wrap film and pallet 2 with the renewed wrap film. Since it was proved above that both pallets underwent similar transport constraints, differences in recorded accelerations must be due to the ageing of the film. It can be observed that less intense acceleration was recorded for pallet 2 (new wrapping) than for pallet 1 (aged wrapping). Figure 11 present the accumulated recorded acceleration of both pallets during test 2. As for figure 10, the pallet with the new wrapping showed less intense accumulated acceleration than the pallet 1 with aged wrapping. It has been reported that wrapping application was performed at high extension level of the film, and out of its elastic deformation [13-14]. In addition, the transport caused stresses on the film that could be assimilated to fatigue. The obtained deformations were therefore most probably partly irreversible, leading to a lower ability of the film to maintain the load and absorb the kinetic energy resulting of the acceleration.

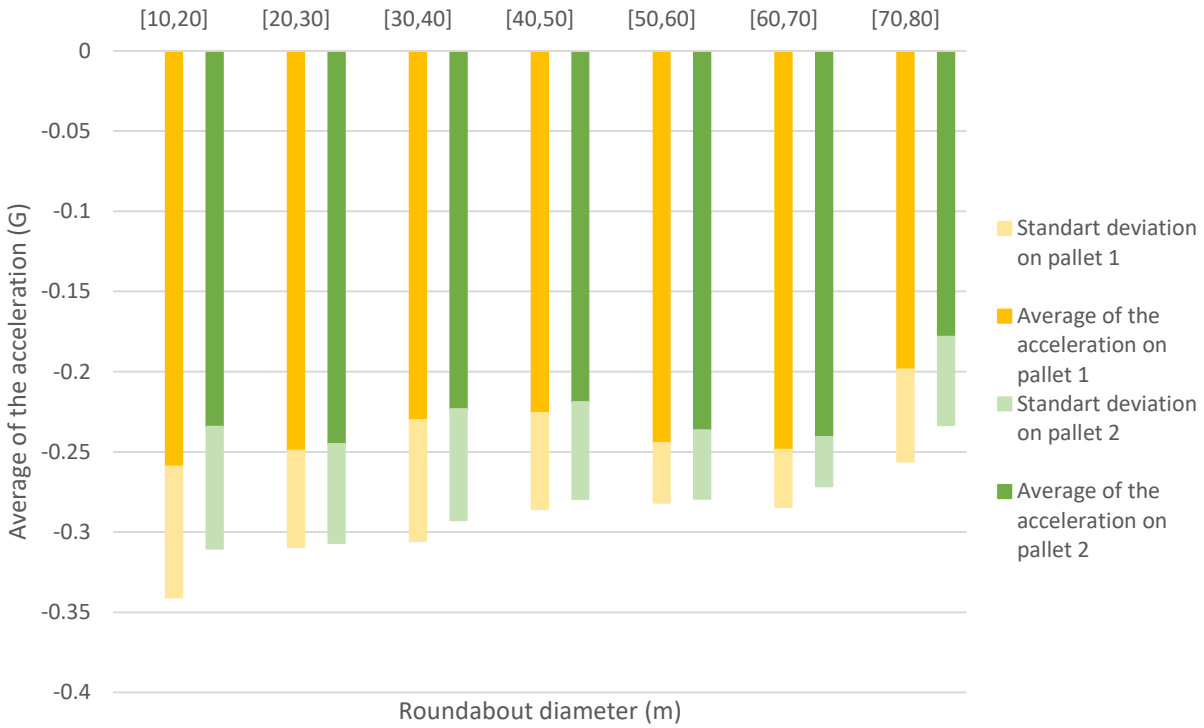

Figure 10: acceleration recorded on both pallets during test 2 in function of the roundabout diameter

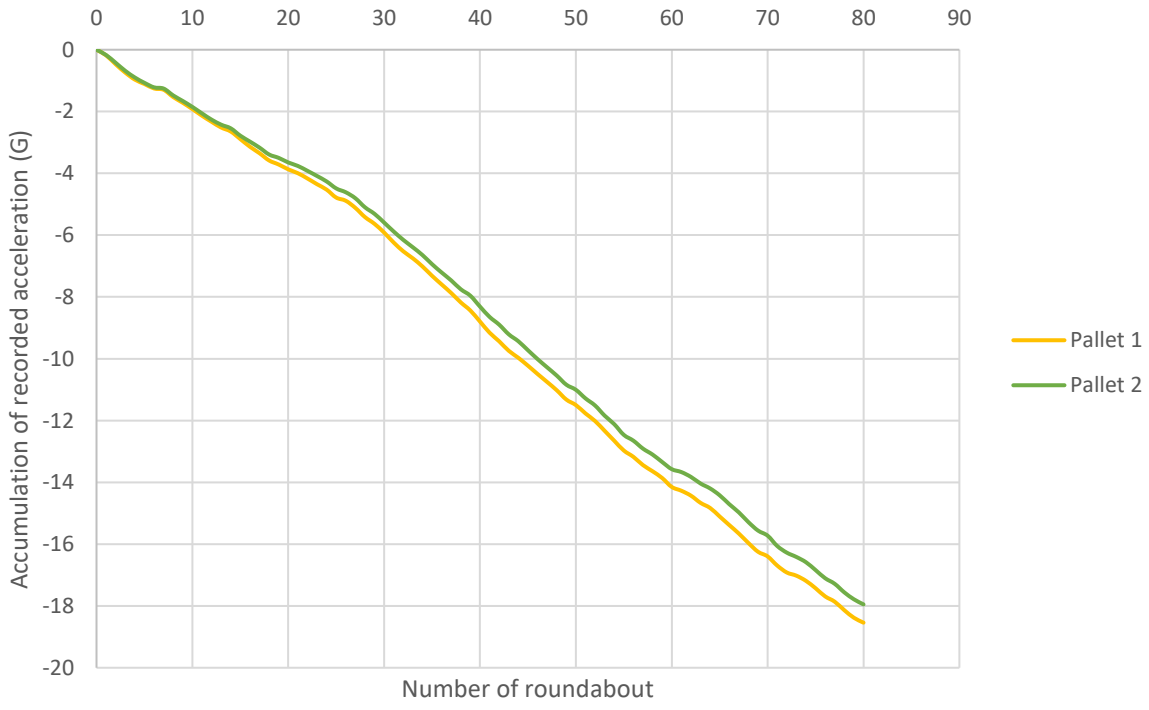

Figure 11. Accumulated recorded acceleration of both pallets during test 2

CONCLUSION

The roundabout is an unavoidable event during road trip. It was found in this study that there was no correlation between roundabout diameter and recorded acceleration. However, it was shown that the maximum speed was increasing with the diameter until a maximum value. The present work has proved that two pallets in the same truck underwent the same constraint history. It was also shown that the wrap film was ageing during transportation leading to a lower ability to absorb the kinetic energy generated during roundabouts. Further work could investigate the effect of driving techniques on recorded acceleration and maximum speed in a roundabout. It would also be of interest to study further the effect of fatigue on the ability of wrap films to absorb kinetic energy.

REFERENCE

[1] Huart, V., et al. "Check analysis of horizontal stresses in road transport", 27th IAPRI Symposium Conference on Packaging –Valencia 2015 SPAIN
[2] Rouillard V. Generating Road vibration test schedules from pavement profiles for packaging optimization. Packag Technol Sci. 2008.
[3] Kipp B. Environmental data recording, analysis and simulation of transport vibrations. Packag Technol Sci. 2008.
[4] Juwet M, Esprit E, Vanden Berghe G. On horizontal dynamic effects on palletized goods during road transport: measurement of horizontal dynamic effects. Packag Technol Sci. 2018.
[5] Kudarauskas N. Analysis of emergency braking of a vehicle. Transport. 2007.
[6] Nei D, Nakamura N, Roy P, et al. Wavelet analysis of shock and vibration on the truck bed. Packag Technol Sci. 2008.
[7] Kyle Dunno, Changfeng Ge – Characterization of low-acceleration, long-duration horizontal events using a spring suspension straight delivery box truck, 2021.
[8] Garcia-Romeu Manuel, de la Cruz Navarro Enrique – Effect of the sustained forces during transportation on the creep behavior of stretch film affecting unit load stability. Packaging Technology and Science. 2022.
[9] Kyle Dunno, Changfeng Ge – Field assessment of horizontal accelerations using air ride suspension trailers, 2022.
[10] Jean-Baptiste Nolot – Check analysis of horizontal stresses in road transport, 27th IAPRI Symposium Conference on Packaging – Valencia 2015 SPAIN
[11] Boutrige Baptiste – Determination of impact of the acceleration phenomenon on a load stability in packaging transport, 30th IAPRI Member Conference – Monterrey, Mexico, 2021.
[12] Boutrige Baptiste – Impact of the horizontal acceleration phenomenon duration on the tilt or toppling of the load, 23rd IAPRI Member Conference, Bangkok, Thailand, 2022.
[13] E. Leguebe – Effect of relaxation time, recovery time and extension speed during characterization of LLDPE wrap film properties – Packag Technol Sci, 2022;1-9.
[14] E.Leguebe - Determination of stretch film properties with hysteresis for freight transport applications - Conference paper, IAPRI Bangkok 2022

DP-GO05

Case study for optimisation and standardisation of packaging references improving its environmental behaviour

Marta Garrido[1], Jose Ignacio Garrigós[1], Patricia Navarro[1], Nuria Herranz[1], Francisco Javier Zabaleta[1]

[1]*ITENE (Packaging, Transport and Logistics Research Center), Valencia, Spain.*

ABSTRACT: Directive 94/62/EC focuses on minimizing the environmental impact of the packaging. These trends in manufacturing, compels designers to improve package design in order to standardise and optimize, by reducing the amount of package currently needed, to protect the product against distribution cycle hazards. Optimized and standardized packaging have environmental and cost benefits.
Companies, need to improve the distribution cycle efficiency by standardised and optimized packaging process, in order to reduce product damages, negative life cycle impacts and the costs associated to the packaging system and transport. For this purpose, it is necessary to carry out a packaging diagnosis that allows the identification of critical points from the technical, economic, and environmental points of view, from which the standardisation and optimization of the packaging system can be carried out. The resulting optimized packaging standards are then described through the design of technical specifications and packaging procedures that can be easily implemented in the companies.
The objective of this case study is to show the process of standardisation and optimization of the packaging eco-design process. As a result, the main Key Performance Indicators (KPIs) derived from the improvements achieved at logistic and environmental level were also shown and measured.

Keywords: Key Performance Indicators (KPIs), eco-design methodology, packaging optimization.

INTRODUCTION

According to Directive 2009/125/EC,1 eco-design is described as the design of packaging considering environmental criteria, some of the criteria that can be identified in relation to packaging are the reduction in weight or volume, increasing the recyclability of packaging, as well as a greater or better use of secondary raw materials obtained from the recycling of packaging waste.

It should be taken into consideration that a packaging system, even if it improves its environmental performance, must still fulfil its basic functions of containing and protecting the product from any risk that may occur during its distribution cycle.

Foam packaging solutions made of materials such as expanded polystyrene (EPS) and polyurethane (PUR), traditionally used to provide high protection against impacts, shocks, drops and vibrations, have been considered unsustainable packaging components because of their fossil-based and non-recyclable nature. Currently, more sustainable alternative solutions are being developed (recyclable and/or made from renewable materials), such as honeycomb cardboard structures as well as compostable or bio-based foams, to name but a few. Despite this environmental improvement, it must be noted that these materials do not have the same behaviour as traditional materials and it is necessary to validate their efficiency in packaging systems.

The aim of this study is to show the method of standardisation and optimisation of the packaging system – eco-design – developed by ITENE. To present the methodology, it has been worked on a real case study, a technical assistance project carried out by ITENE, which consists of the eco-design of a packaging system for electric bicycles shipped through an e-commerce distribution cycle, which allows the company to improve its packaging system towards a more sustainable solution, reducing damages. This project has been carried out for the bicycle supplier and distributor ORBEA located in Bilbao, Spain.

As validation of the working method, Key Performance Indicators (KPIs) have been developed to quantify the potential improvements achieved at a technical, economical, and environmental level.

METHODOLOGY AND EXPERIMENTAL DESIGN

The eco-design methodology developed by ITENE is based on the study and detailed analysis of the current situation, the search and development of packaging solutions according to technical, environmental, and economic criteria, and an exhaustive validation of the defined and designed solution.

The working method is common to any eco-design project, although it may be adapted according to the product, packaging, distribution cycle or the requirements or objectives of the company. The following sections describe the eco-design methodology:

Reference under study – Product and packaging

The product under study is a 25 kg electric road bike, shipped via an e-commerce distribution cycle to the customer; this reference has an intermediate degree of assembly, as the front wheel and handlebars are separate from the bike. Information on the packaging system, as well as a brief description of some of its key elements, is collected in Table 1.

COMPONENTS	
SHIPPING BOX **Design:** FEFCO 203. Manual assembly. **Dimensions (LxWxH):** 1710 x 205 x 860 mm. **Flute:** BC.	
INTERNAL SUPPORT - Air chamber inside the box **Design:** tailor-made for the product. Manual assembly. **Dimensions (LxWxH):** 2 380 x 215 x 1 145 mm. **Flute:** BC	
Views of the internal support:	 
PROTECTIVE AND POSITIONING ELEMENTS: Plastic components used for product positioning and surface protection (against friction or impact during the distribution cycle).	

1. PU foam	**2. PP elements.**	**3. EPS elementos**	**4. Cable tye**	**5. LDPE film and bubble wrap**
				

Table 1: Current packaging components system

According to the information collected in Table 1, it can be concluded that, in the current packaging system, cardboard elements are used at the structural level and plastic elements are used to fix and protect the surface of the product from possible abrasion during the distribution cycle due to vibrations and other associated risks.

Methodology

The following points describe the eco-design methodology in more detailed terms:
Initial diagnosis

After the product and the current packaging system identification, a diagnosis is carried out, including the analysis of the company's requirements and potential limitations. Table 2 shows some key aspects and a brief description of the information to be collected as a starting point for eco-design:

ASPECTS TO CONSIDER	INFORMATION TO BE COLLECTED
Product	Dimensions, weights, specification, properties and functions.
Packaging System	Data sheets and functionality of each component or element.
Packaging Process	Description and state of automation of the process, limitations for modification and/or previous solutions implemented.
Distribution Cycle	Delivery types (e-commerce), warehouse conditions, transport routes, type of transport, associated risks, intensity.
Product Damages	Quantified damages, types and ltheir level.
Other company-specific requirements:	Product protection, packaging, environmental, functional, cost and end-user requirements.
Objetives	What is expected from the eco-design project.

Table 2. Key aspects and information to be collected for an initial diagnosis

This diagnosis may be more or less exhaustive depending on the type of project, however, it is necessary to consider the importance of this analysis to identify opportunities for improvement, limitations, or key requirements, as well as to define the objectives of the project. These objectives can be the basis for generating monitoring KPIs to validate the results obtained in relation to the current situation.

Conceptual design

This phase focuses on identifying the way to achieve the objectives. For this purpose, work is done based on the diagnostic information, identifying solutions that respond to the requirements, limitations, and objectives. With this aim, the conceptual design is composed of the following actions:

Benchmarking

A search of commercial solutions for packaging components, as well as solutions applied by similar industries, is carried out, identifying developments, components or elements that meet the eco-design requirements. In order to evaluate these components, technical, environmental and economic information provided by suppliers is collected. In this way it will be possible to identify alternative materials and more sustainable and innovative solutions.

Conceptual design

Based on the information gathered in the benchmarking, and the diagnostic data, packaging designs are conceptually developed, these designs are modelled by computer using tools such as Siemens NX, a computer-aided design (CAD) software. In this way, visual design solutions are generated. This conceptual design must be validated by the company.

Detailed design

In this phase, the necessary specifications are generated to define the final solution. Some of the specification or tasks that can be performed include 2D drawings, technical sheets, assembly procedures, detailed 3D designs or physical prototypes, among others.

Validation

Verifying the feasibility of the developed solution is key to evaluate the success of the project. In this way, validation is considered a requirement of the methodology. Two key validations will be considered. The Functional Validation; exposing the new packaging solution to real working conditions, through transport simulation protocols, and the Environmental Validation, analysing the behaviour of the new eco-designed solution, through the Carbon Footprint (CF).

Monitoring KPIs

In order to validate the method developed, three of monitoring KPIs have been defined:

- **Technical KPI**: from the results obtained in the transport simulation protocols**.**
- **Environmental KPI**: considering the calculated FP.
- **Economic KPI**: based on the information obtained during the benchmarking stage and the packaging current cost.

DATA ANALYSIS AND RESULTS

The main data analysed, and results obtained from the eco-design method are described below:

Initial diagnosis

In this section, some key data obtained during the diagnostic stage are described:

Product Damages

Table 3 shows the main damages reported during a year. These damages correspond to 2% of the bicycles shipped in a year. The data includes all bicycle references and considers the different distribution cycles.

DAMAGE AREA	1. Gear system, and disc brakes	2. Bicycle frame	3. Handlebar and fork	
Damages	147	312	370	
	18%	38%	45%	
	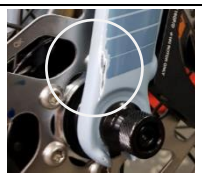			

Table 3: Reports of damages in product

As shown in table 3, the defects have been classified into 3 areas. The handlebar and fork were those with the highest number of damages. This information enables the identification of exposed areas to which special attention should be paid during eco-design process.

Distribution cycle

In order to characterise the distribution cycle, one of the company's e-commerce distribution routes has been monitored. This route between Bilbao and Germany was selected for its high damage probability.
For the route monitorisation, a Data Recorder (DR) has been installed inside the current packaging system with real product. The DR is a device designed and manufactured by ITENE, that records the linear accelerations, angular velocities, and shocks generated during the distribution cycle.
From this recorded information, it has been possible to generate ad-hoc, transport simulation protocol for the company. The simulation protocol is shown in Table 4.

Sequence	Test Category	Test Parameters	Test Level
1	Atmospheric Preconditioning	12 hours	23ºC y 50%RH
2	Shock: Rotational Flat Drop	Drop on edge 2-3 Drop on edge 3-4	Angle: 20º
3	Compression vertical	Face 2 down	Test weight x 3 current system weight
4	Multiaxial Random Vibration (Vertical + Pich & Roll)	Face 3 down. 105 min. Face 4 down. 105 min.	Test time according to "ISTA 3E Calculating Test Time"
5	Shock: Rotational Flat Drop	Drop on edge 3-5 Drop on edge 3-6	75 mm
6	Shock: Rotational Edge Drop	Drop on edge 2-3 Drop on edge 3-4	400 mm

Table 4. Transport simulation protocol.

This protocol is based on international standards,[2-7] with the advantage of including multi-axial vibration profiles and the real route severity. In order to validate the test protocol and its severity, the current packaging system has been tested. In conclusion, the protocol has been validated by the company, due to the fact that similar damages to those identified in real shipments - Table 3 – have been detected, as shown in Figure 1.

Figure 1. Pictures taken during the review of the current packaging reference after the testing protocol

The test protocol has subsequently been used as functional validation of the eco-designed packaging system.
El protocolo de ensayos posteriormente se ha utilizado como validación funcional del sistema de embalaje eco-diseñado.

Carbon footprint analysis

As an initial environmental diagnosis, the methodology based on Life Cycle Assessment (LCA) has been used to calculate the FP. [8-10] As a result of this calculation, a FP of 4.31 kg of CO_2 eq. was obtained, mainly generated by the raw materials that constitute the packaging system, so that the identification of more sustainable components may reduce the FP values obtained.

Conceptual design

After benchmarking and technical, economical, and environmental analysis of the identified components, 3D conceptual designs are carried out. The results of the 3D design, as well as the selected commercial components, are shown in Table 5.

3D DESIGN			
			
PACKAGING COMPONENTS			
Surface protection	**Shock/impact protection**	**Friction protection and immobilisation**	**Surface protection and fixing**
			
Corrugated cardboard	**Honeycomb cardboard**	**Corrugated cardboard**	**Kraft paper tape**

Table 5. Conceptual design of the eco-engineered packaging system

Detailed design

The key deliverables obtained at this stage are the physical prototype and technical drafts of the tailor-made cardboard blocking elements (this component has been designed using structural packaging design CAD programs and prototyping on a cutting plotter). Figure 2 and Figure 3 show images of the physical prototype.

Figure 2. Eco-designed packaging system and detail of frame protection

.

Figure 3. Protection and immobilisation components detail of the physical prototype

Technical and environmental validation

Two validation typologies of the eco-designed packaging system have been considered.

Functional Validation

The eco-designed packaging system has been validated through the transport simulation protocol (Table 3). Some pictures of the tests are shown in Table 6.

Rotational flat drop test	Compression, Vertical - Test	Multiaxial Random Vibration test	Rotational flat drop test	Rotational edge drop test
				

Table 6. Transport simulation test pictures - Eco-designed reference

The review carried out after the transport simulation tests shows that there is no damage to the product or the packaging system.

Environmental Validation

The FP of the new eco-designed packaging solution has been calculated, with a resulting value of 3.25 kg CO2 eq. This corresponds to an overall reduction of 1.06 kg CO2 eq. with respect to the current situation.

Validation – Monitoring KPIs

In this step, the monitoring KPIs were analysed with respect to the current situation:

- **Technical level:** Considering the results obtained after the test protocols conducted in the current situation as well as in the new eco-designed reference, it can be concluded that a reduction of damages is possible with the new packaging system.

- **Environmental level:** It has been possible to reduce the FP of the packaging system by 25% compared to the current situation.

	Current packaging system	**Eco-design packaging system**	**Reducción %**
kg de CO2 eq.	4.31	3.25	25 %

- **Economic level:** The cost of the packaging system has been reduced by 23.5% compared to the current situation.

	Current packaging system	**Eco-design packaging system**	**Reducción %**
Cost (€)	17.0	13.0	.5 %

CONCLUSIONS

The eco-design methodology has been a key tool to optimise the packaging system and achieve a balance between functionality and sustainability.

1. Through the diagnosis of the current situation, it is possible to identify opportunities and limitations for the development of the eco-design of the packaging system, as well as to set clear objectives, which will be considered throughout the steps of the methodology.
2. Benchmarking, as a phase of the conceptual design, allows the identification of market opportunities in terms of innovative components and key alternative solutions to be included or implemented in the conceptual development design, for which 3D design tools are essential to show the working process.

3. The detailed design allows to materialise the objectives and the working process carried out from the previous steps, the results obtained from this phase are key to identify the real viability of the solution.
4. Functional and environmental validations of the eco-designed packaging system make it possible to identify the eco-design operative and to check its efficiency under real conditions.
5. Analysing the monitoring KPIs, it is concluded that through the eco-designed packaging system, improvements have been obtained on a technical, environmental and economical level. On a technical level, a reduction a reduction of damages is possible with the new packaging system. At an environmental performance, the FP generated by the packaging system has been reduced by 25% and, finally, at economic level, the reduction has been 25.5%.

REFERENCES

1. The European parliament and the council of the European Union. Directive 2009/125/EC of the European Parliament and of the Council, of 21 October 2009.
2. ISTA. Ships in Own Container (SIOC) for Amazon.com Distribution System Shipment. ISTA 6 AMAZON Test Sequence Type B. Shock Tip/Tip Over. International Safe Transit Association.
3. ISTA. Ships in Own Container (SIOC) for Amazon.com Distribution System Shipment. ISTA 6 AMAZON Test Sequence Type B. Test in the intended shipping orientation or most stable orientation. Shock Tip/Tip Over. International Safe Transit Association.
4. ASTM. Standard Test Method for Random Vibration Testing of Shipping Containers; D4728-2017. American Society for Testing and Materials: West Conshohocken, PA, USA, 2022.
5. ISO. Packaging - Complete, filled transport packages and unit loads - Vertical random vibration test; ISO 13355:2016. International Organization for Standardization.
6. ISTA. Calculating Test Time; ISTA 3E. International Safe Transit Association.
7. UNE-EN. Packaging - Complete, filled transport packages and unit loads - Impact test by rotational drop UNE-EN 14149:2004.
8. UNE-CEN ISO/TS. Greenhouse gases - Carbon footprint of products - Requirements and guidelines for quantification and communication; ISO/TS 14067:2013.
9. ISO. Environmental management - Life cycle assessment - Principles and framework; ISO 14040:2006. International Organization for Standardization.
10. ISO. Environmental management - Life cycle assessment - Requirements and guidelines; ISO 14044:2006. International Organization for Standardization

DP-GO06

Optimal selection of the percentage of recycled material in plastic according to the risks of distribution cycle

Marta Garrido[1], Laura Esteban[1], Patricia Navarro[1], Nuria Herranz[1], Francisco Javier Zabaleta[1]

[1] *ITENE (Packaging, Transport and Logistics Research Center), Valencia, Spain*

ABSTRACT: Environmentally friendly packaging solutions have received greater attention in recent years due to the growing demand for sustainable developments. Legislation and customers are the main drivers to design for environment. Directive 94/62/EC focuses on increasing the life cycle and recovery of packaging, but also on minimizing the environmental impact of the packaging produced. These trends in manufacturing compels designers to improve package design in order to optimize, by reducing the amount of package currently needed, using recyclable materials, and increasing the % of recycled materials in the packaging composition, to protect the product against distribution hazards.

Companies, need to improve the distribution cycle efficiency by reducing product damage, negative life cycle impacts and the costs associated to the packaging system and transport. There is a widely recognized need for companies to find models, metrics, and tools for articulating sustainable development in recent years.

The final purpose of this case study is to develop a sustainable evaluation tool, with Key Performance Indicators (KPI), that needs inputs from the technical performance, environmental behavior, and packaging cost. The cases study, focus on a company in the phytosanitary sector, with primary plastic containers, in which the introduction of recycled material becomes an opportunity to improve compliance with environmental legislation, reducing environmental impacts and possibly costs. In order to implement the optimal recycling rate to maintain product protection, transport simulation tests and the determination of safety factors become a key environmental tool.

Keywords: Key Performance Indicators (KPIs), recycled content, validation methodology.

INTRODUCTION

The use of secondary raw materials in plastic containers is an increasingly common practice in the packaging industry. In particular, data from Plastics Europe show an increase of nearly 20% in the use of post-consumer recycled plastic in 2021 compared to 2020.[1] These changes are mainly motivated by legislative targets, such as those stated in Directive (EU) 2018/852 of the European Parliament and of the Council,[2] transposed in Spain through the Royal Decree 1055/2022 of 27 December, on Packaging and Packaging Waste.[3] This Royal Decree establishes minimum percentage objectives for recycled plastic content for the year 2030, with

a general target of 30% for non-compostable plastic packaging. In addition, a specific tax of 0.45 €/kg of virgin plastic content is established for single-use plastic (SUP) packaging.

These new legislative requirements make it necessary to identify measures, procedures, or methods for validating the new packaging solutions with recycled content, in comparison to the current references with 100% virgin plastic content.

The objective of this study is to generate an evaluation method to analyse the feasibility of introducing recycled material in packaging, the cost reduction due to the new economic rate and an optimal technical behaviour (environmental, economic, and technical feasibility). For this purpose, a case study has been developed to analyse the behaviour of the packaging in characterisation and transport simulation tests and to generate Key Performance Indicators (KPIs) capable of evaluating the selected solutions with respect to the current situation.

METHODOLOGY AND EXPERIMENTAL DESIGN

The methodology carried out has allowed characterising each reference individually, as well as generating comparisons that facilitate the customer's decisions when selecting the optimum packaging reference. The following sections describe the detailed experimental design carried out and the steps of the work method.

References under study

Three primary containers (1, 5 and 20 litres capacity) and three references of each container type (Current Reference, Supplier 1, and Supplier 2) were analysed for the study. Table 1 shows the characteristics of each type of primary packaging:

CONTAINER 1 – 1 LITRE CAPACITY

Reference	. Current Reference	. Supplier 1	. Supplier 2
Recycled content	0 %	50 %	50 %
Dimensions (LxWxH)	75 x 75 x 244 mm	75 x 75 x 244 mm	75 x 75 x 244 mm
Weight	120 g	120 g	120 g
Weight per litre of product	120 g/l	120 g/l	120 g/l
Figures			

CONTAINER 2 – 5 LITRES CAPACITY

Reference	Current Reference	Supplier 1	Supplier 2
Recycled content	0 %	50 %	50 %
Dimensions (LxWxH)	183 x 123 x 290 mm	183 x 123 x 290 mm	183 x 123 x 290 mm
Weight	200 g	200 g	200 g
Weight per litre of product	40 g/l	40 g/l	40 g/l
Figures			

CONTAINER 3 – 20 LITRES CAPACITY

Reference	Current Reference	Supplier 1	Supplier 2
Recycled content	0 %	50 %	50 %
Dimensions (LxWxH)	295 x 245 x 375 mm	295 x 245 x 375 mm	295 x 245 x 375 mm
Weight	1000 g	1000 g	1000 g
Weight per litre of product	50 g	50 g	50 g
Figures			

Table 1 Description of primary container references. Top: 1 litre capacity primary container. Middle: 5 litres capacity primary container; Lower: 20 litres capacity primary container

As shown in Table 1, the most significant difference between these three types of containers lies in the recycled content of their composition. For confidentiality reasons, the name of each supplier has been omitted and identified under a general reference name.
Concerning the secondary packaging, the 1 and 5-litre references were grouped in corrugated cardboard boxes according to the information given in Table 2. The 20 litres container references are placed directly on the pallet without grouping packaging.

GROUPING PACKAGING 1 – 1 LITRE CAPACITY			
Reference	**Cardboard box 1**		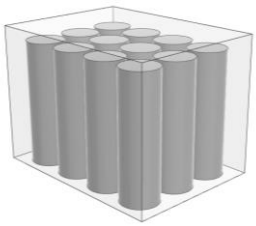
Carboard box dimensions (LxWxH)	370 x 275 x 270 mm		
1 litre containers	4 x 3 = 12 units		
Weight	430 g		

GROUPING PACKAGING 2 – 5 LITRES CAPACITY			
Reference	**Cardboard box 2**		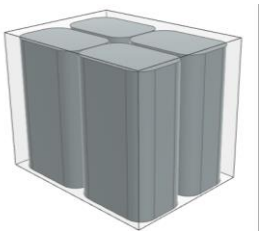
Carboard box dimensions (LxWxH)	380 x 285 x 300 mm		
5 litres containers	2 x 2 = 4 units		
Weight	450 g		

Table 2 Description of the grouping packaging references. Top: 1 litre capacity system. Lower: 5 litres capacity system

As shown in Table 2, the 1 and 5-litre references are palletised in carboard boxes of 12 and 4 units per pack respectively, and the 20-litre reference is not placed in grouped packaging. Table 3 shows the palletised system for the three types of references (1, 5 and 20 litres).

PALLETISED SYSTEM			
Reference	**1 LITRE PACKAGING**	**5 LITRES PACKAGING**	**20 LITRES PACKAGING**
Pallet dimensions (LxWxH)	1200 x 1000 x 1230 mm	1200 x 1000 x 1050 mm	1200 x 1000 x 900 mm
Weight	777.5 kg	815 kg	854 kg
Palletising pattern	Mixed pattern	Mixed pattern	Column
First palletising layer	4 – 4 –3 grouping packaging 	4 – 3 –3 grouping packaging 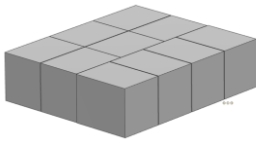	4 – 4 – 4 Not grouping packaging 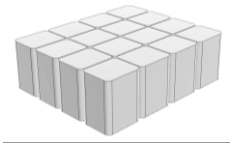
Pallet layers	4	3	2

			
Nº of grouping packaging	44	30	-
Nº of containers	528	120	32
Pallets stacking	1+1	1+1	1+1

Table 3 Description of the palletized system

After analysing the variables of the packaging systems, through the methodology described in the following section, the optimal solutions will be identified for each 1, 5 and 20 litres container reference.

Methodology

The method carried out to identify the optimal container is based on a practical analysis of the references under study.

Transport simulation tests

After a detailed analysis of the company's distribution cycle, the three current palletised systems (1, 5 and 20 litres containers) were subjected to a customised transport simulation test protocol. The tests included in the transport simulation protocols ad-hoc made for the company are described in Table 4:

TEST	STANDARD	INFORMATION
Atmospheric Conditioning Duration: 24 h	UNE-EN ISO 2233:2002	**Conditions:** 23ºC ± 2ºC / 50% HR ± 5% HR
Rotational Edge Drop	UNE-EN 14149:2004	**1st Drop:** 150 mm. Lift edge 5-3. **2nd Drop:** 75 mm. Lift edge 2-3.
Horizontal Impact	UNE-EN ISO 2244:2003	**Test Level:** 0.91 m/s **1st Impact:** Face 5 **2nd Impact:** Face 2
Vertical Random Vibration Duration: 4 h	UNE-EN ISO 13355:2016	**Random vibration spectrum** Spanish monitored route – DR ITENE. **Bandwidth:** 0.9 – 114.8 Hz **Overall RMS level (g):** 0.19

Table 4 Tests included in the transport simulation protocol ad-hoc for the company

The objective of testing the current packaging systems is to identify and characterise the current situation, thus enabling a comparison to be made with the new packaging solutions under study. After the results of these initial tests, the company set as an indispensable requirement for the selected packaging systems that the technical properties should be higher than or at least equal to those of the current packaging.

Box Compression Test

For the characterisation study of the primary packaging, Box Compression Tests (BCT) have been carried out, using testing machines according to the UNE EN ISO 12048:01[4] standard. This standardised test provides the load capacity of the container, in kg of force (kgf). The BCT statistical calculations have been made based on 5 replicates tested. The BCT is commonly used to evaluate cardboard boxes, however, by means of this test, it has been possible to characterise the maximum load capacity of these containers under real working conditions. Detailed information concerning the BCT tests carried out on the three types of containers (1, 5 and 20 litres), for each of the three references (Current Reference, Supplier 1 and Supplier 2), is given in section **3. Data analysis and results**.

Safety Factor

Once the results of the BCT tests had been obtained, the Safety Factor (SF) was calculated. The SF represents the relationship between the maximum capacity of a system (BCT) and the expected requirements it has to deal with (total weight to be supported).
In the SF formula [1], the BCT value corresponds to the results obtained from the Box Compression Test carried out in the laboratory, N is the number of pallet layers (including the stack), and W is the individual container weight:

$$SF = \frac{BCT}{(N-1) \times W} \qquad [1]$$

In order to maintain the integrity of the packaging system throughout the distribution cycle, the SF must be, based on the requirements set by the company and considering the simulation tests carried out, greater than or equal to the SF of the current packaging references.
Subsequently, and as described in the following sections, the transport simulation test protocol has been carried out once again to validate the containers selected by the company.

Monitoring KPIs

Results obtained from transport simulation test protocols, BCT characterisation tests and SF calculations are key to identify improvements of the selected containers at technical, environmental, and economic levels in relation to the current situation. In order to quantify these improvements, the following indicators have been generated:

- **Technical KPI:** by comparing the BCT of the new container selected with the current situation.
- **Environmental KPI:** considering the proportion of virgin and recycled plastic content.
- **Economic KPI:** by studying the variability of the rate set by the Royal Decree of 0.45 €/kg of virgin plastic by container.

DATA ANALYSIS AND RESULTS

According to the work method described in section **2. Methodology and experimental design**, and after the analysis of the tests carried out, the following results have been obtained:

Transport simulation test protocols

The test protocols have made it possible to identify and characterise the current situation of the three palletised packaging systems and to establish a comparative starting point to identify the possibility of improvement, setting these results as minimum requirements for the new references studied. The protocol tests are listed in Table 4.
As a result of these transport simulation tests, the three initial situations are considered as a PASS according to the acceptance criteria. None of the loads suffered collapse or apparent critical damage; in the case of the impact tests, the loads were aligned on the impact surface and the layers were slightly displaced.

Theorical and practical study

The information generated from the BCT tests on the primary containers, as well as the SF calculations for each case study, are shown in Table 5. It must be considered that the SF should be equal to or higher than the results obtained in the current references.

PRODUCT	1 litre		5 litres		20 litres	
	BCT (kgf)	**SF**	**BCT (kgf)**	**SF**	**BCT (kgf)**	**SF**
Current	131.16	16.73	64.7	2.49	360.88	5.73
Supplier 1	**162.05**	**20.67**	**89.06**	**3.43**	**422.33**	**6.70**
Supplier 2	100.46	12.81	46.07	1.77	334.24	5.31

Table 5: BCT and SF values calculated for the 1, 5 and 20 litres primary containers

The BCT and SF test results show that the three Supplier 1 container references have a higher resistance compared to the current and Supplier 2 containers. Consequently, it is therefore concluded that the three containers from Supplier 1 with a recycled content of 50% are optimal packaging solutions.

Validation – Transport simulation test protocols

Based on the previous transport simulation protocol and characterisation tests, it has been concluded that the optimum packaging solution with recycled content are those provided by Supplier 1. In order to evaluate and validate the performance of these new container references in a real working condition, transport simulation protocol tests have been carried out once again on the palletised packaging systems.
Considering the SF values and the amount of plastic per litre of product, as shown in Table 1 (120, 40 and 50 grams in each primary container of 1, 5 and 20 litres respectively), and taking into account that a lower plastic amount per litre makes it more probable that the change of material and the integrity of the system could be affected, only the 5 and 20 litres palletised systems have been tested. The transport simulation test protocols are described in Table 5.

Pictures of the validation protocol tests of the palletised references with the 5-litre and 20-litre Supplier 1 containers are shown in Table 6.

	Rotational Edge Drop	Horizontal Impact	Random Vibration	Final Review
5 L				
20 L				

Table 6. Pictures of laboratory tests conducted in the laboratory

During the review of the packaging systems, after the transport simulation test protocols, a leak was identified in one of the 20-litre containers in the first level of the palletised system, due to the perforation of the container by a steel nail from the pallet, for this reason the palletised system is considered as a FAIL. However, this failure was not related to the primary container performance and considering the good behaviour of both references (5 and 20 litres) in the transport simulation tests, it can be concluded that the primary containers of Supplier 1 are viable alternatives to the current container references.
With regard to the perforation in the 20-litre container, a more exhaustive control of the quality of the pallets is recommended in order to avoid damage to the containers on the first palletising

level, as well as using cardboard layers between the pallet and the first product level of the palletising system.

Validation – Monitoring KPIs

After the selection of the new references of 1, 5 and 20 litres for Supplier 1, the monitoring KPIs were analysed with respect to the current situation:

- **Technical level**: the BCT values obtained in the new reference compared to the current values are increased as follows:

Product	**1 litre**	**5 litres**	**20 litres**
BCT increase of the Supplier 1 container with respect to the current situation.	23.50 %	37.65%	17.00%

- **Environmental level**: the content of recycled material in the container is increased by 50% compared to the current situation in all three containers under study.

- **Economic level:** the virgin plastic content is reduced by 50% compared to the current situation, therefore the unit cost per kg of the tax is also reduced as follows:

Product	**1 litre (200 g)**		**5 litres (400 g)**		**20 litres (1000g)**	
Cost in €/kg due to the tax	**Current Reference**	**Supplier 1**	**Current Reference**	**Supplier 1**	**Current Reference**	**Supplier 1**
	0.054 €	0.027 €	0.09 €	0.045 €	4.50 €	2.25 €

CONCLUSIONS

Through the evaluation mechanism, it has been possible to study the viability of introducing recycled material into primary containers.

1. The transport simulation test protocols performed on current palletised references make it possible to define a comparative starting point on which to identify possibilities for improvement. The fact that the three systems PASSED the protocols, means that the selected systems must have the same or better performance than the current situation in order to ensure the integrity of the packaging system.

2. The BCT characterisation test results and the calculated SF for the primary packaging (1, 5 and 20 litres) allow a comparison between the performance of the current packaging and the new packaging solutions with recycled content.

3. The results of the transport simulation test protocols on palletised systems with the new primary packaging references selected (Supplier 1 with 50% recycled plastic) allow a final validation of the packaging solutions under real distribution cycle conditions.

   As a result of the perforation of the 20-litre container during the tests, it is recommended to check the quality of the pallets as well as to place cardboard sheets between the pallet and the first layer of the palletising system to prevent damage to the containers.

4. With respect to the monitoring KPIs for the evaluation of the results of the working method, it is concluded that on a technical, economic, and environmental level, an improvement is obtained by selecting the 1, 5 and 20 litres packaging references of Supplier 1 with respect to the current container references.

   On a technical level, the BCT is improved by 23.50%, 37.65% and 17.00% for the 1, 5 and 20 litres containers respectively, compared to the current situation. On an environmental level the recycled content is increased by 50% in all three scenarios and on an economic level, the tax applicable to virgin plastic is reduced by the recycled plastic content, so the cost of the tax will be reduced by 50%.

REFERENCES

1. Plastics-The Facts 2022. October 2022. PE-PLASTICS-THE-FACTS_FINAL_DIGITAL-1.pdf (plasticseurope.org)
2. Directive (EU) 2018/852 of the European parliament and of the council of 30 May 2018. L_2018150EN.01014101.xml (europa.eu) http://data.europa.eu/eli/dir/2018/852/oj
3. Royal Decree 1055/2022 of 27 December 2022, on Packaging and Packaging Waste. https://www.boe.es/eli/es/rd/2022/12/27/1055
4. ISO. Packaging - Complete, filled transport packages - Compression and stacking tests using a compression tester. 12048:1994. International Organization for Standardization.
5. ASTM. Standard Test Method for Determining Compressive Resistance of Shipping Containers, Components, and Unit Loads; D642-20. American Society for Testing and Materials: West Conshohocken, PA, USA, 2022.

DP-GO07

Evaluation of Maximum Pallet Deflection Under Dynamic Forklift Handling Conditions

Seth Capizzi[1], Laszlo Horvath[1], Yu Yang Huang[1], and Marshall S. White[1]

[1]*Department Of Sustainable Biomaterials, Virginia Tech; 1650 Research Center Dr. Blacksburg VA 24061, USA*

***Correspondence to**: Laszlo Horvath[1] [1]Department Of Sustainable Biomaterials, Virginia Tech; 1650 Research Center Dr. Blacksburg VA 24061*
E-mail: lhorvat@vt.edu

ABSTRACT: Industrial forklifts are used to move pallets safely and efficiently within warehouses and distribution centers, and previous studies have determined that the vibration stemming from forklifts can affect the stability of unbound unit loads. When pallets are supported by fork tines the maximum deflection values typically occur at the corners of the pallet, where the largest cantilever from the support condition is observed. Standard national and international pallet testing protocols (ISO 8611, ASTM D1185) contain recommended pallet deflection limits obtained from static testing procedures. However, the act of handling a pallet with a forklift is a dynamic process. This study evaluated the dynamic behavior and performance of unbound palletized unit loads, while focusing on dynamic pallet deflection and unit load stability.

To represent variations in the forklift handling of unit loads, the design of experiments included two load levels based on the static deflection limits in ISO 8611 (4.5 degrees and 20 mm) that were further classified by; fork tine angle (level and 4° tilt), and fork tine orientation (parallel and perpendicular to pallet length). For each of the nine different test combinations, three test replicates were completed. To simulate dynamic forklift handling conditions, fork tines supporting unit loads were mounted on a vibration table. A thirty-minute vibration profile measured from the fork tines on a forklift in operation was used during stability testing.

The results of these tests revealed that pallets experienced greater deflection during dynamic handing than in the static conditions simulated during the ISO testing. Additionally, fork tines were found to deflect and experience movement not reflected in the standardized test procedure. It was also found that unbound unit loads that were designed using the recommended ISO deflection limits showed signs of instability. These results indicate that the deflection limits in ISO 8611 could result in unstable, unbound unit loads.

Keywords: Forklift handling; pallet deflection; vibration; dynamic; ISO 8611

INTRODUCTION

Pallets have been an integral component of many supply chains since their invention in 1932 by Bill House and George Raymond, Sr [1]. As the backbone of transporting operations, the number of pallets in circulation continues to increase. In 2016, Nathan Gerber et al. estimated 839 million pallets were produced in the US including new pallets and used pallets[2]. Wooden pallets are most common. Of the companies surveyed in Modern Materials Handling annual pallet report, 97% reported using wooden pallets[3] . Of the companies surveyed, more than one third reported using plastic pallets[3]. Plastic pallet demand is also expected to increase from 2019 to 2024[4]. Multiple use, plastic pallets make up 81% of all plastic pallets in the US[5]. Multiple use plastic pallets are appealing to companies due to their material properties, cost, and reduced environmental impact[6].

Pallets are transported through supply chains using a variety of vehicles. Transportation of palletized unit loads can damage goods due to the effects of the vibration experienced during transit[7]. Vibration varies in different modes of transportation, and can be dependent on road condition, vehicle type, payload, and suspension[8] among other things. Research related to vehicle vibration is vast. Researchers have investigated components such as road condition[9,10], vehicle type[11,12], suspension type[13], and vehicle speed[14,15]. While vehicle vibration studies are extensive in these sectors, vibration studies involving forklifts are limited[16].

The most common method for transporting pallets in a warehouse is by a forklift[17], as 92% of respondents reported using forklifts to handle pallets[17]. The act of transporting a pallet with a forklift is a dynamic process, but the current standard to test pallets supported by forklifts involves a static testing procedure. Previous studies have revealed that forklift vibration is dependent on payload, vehicle type, speed, and road conditions[16]. It has also been found that the vibration stemming from a forklift amplifies pallet deflection[18]. Previous studies have revealed that vibration levels of forklifts are relatively low compared to over the road transportation values, but forklift handling supports less of the pallet compared to floor stacking conditions that are seen in transport. Several standard testing procedures have been developed to emulate forklift handling conditions, including ISO 8611[19,20], and ASTM D1185[21]. To test the performance of a pallet in forklift handling situations, the pallet is placed on rigid simulated fork tines and the deflection is measured as load is steadily applied. Additionally, deflection limits are reported in each standard to ensure the pallet does not exceed the prescribed maximum deflection limits during standardized test conditions.

Plastic pallets commonly experience more deflection due to their material properties. The stiffness of plastic pallets is commonly lower in comparison to wooden pallets. Therefore, in forklift handling scenarios plastic pallets will bend more than wooden pallets. They have a higher chance of reaching their maximum deflection limits under a lighter load than wooden pallets. The result of reaching a maximum deflection limit in a warehouse setting is the increased chance of unit load instability. Unit load stability refers to the unit load's ability to remain intact throughout various transportation and handling conditions.

Previous unit load stability studies, conducted on bound and unbound unit loads, supported by plastic pallets in forklift handling conditions, suggest that plastic pallets deflect differently in dynamic test settings than in the static conditions utilized by ISO 8611 and ASTM

D1185[18]. It was also revealed that in a dynamic test procedure, the fork tines themselves vibrate and deflect. Unbound unit loads displayed instability 58% of the time while bound unit loads remained stable through all dynamic tests. Furthermore, deflection values typically increased, for the fork tine and pallet, the further away the measurements are taken from the simulated forklift carriage[18]. However, in standard static testing procedures, simulated fork tines fully support the pallet and remain rigid for the entire test.

The objectives of this study were:
1. To measure pallet and fork tine deflection during vibrations associated with forklift handling of unit loads.
2. To correlate these deformations with the stability of unit loads.
3. To determine the applicability of ISO 8611 pallet deflection limits to create stable unit loads.

MATERIALS AND METHODS

Materials

Pallet

The single pallet used in this study was ta *40 in. x 48 in.* plastic pallet. The pallet measured 1219 mm. x 1016 mm. and weighed an average 11.2 kilograms. This pallet is primarily used for grocery distribution and is a non-reversible, nestable, block-class, 4-way entry pallet. Representative pictures of the pallet are found below (Figure 1).

Figure 1: Representative pictures of the 40 in. x 48 plastic pallet provided

Corrugated boxes

The two unit load designs tested in this study both contained regular slotted container (RSC) style corrugated boxes constructed using C-flute, single wall corrugated board with 5.6 kN/m nominal Edge Crush Test (ECT) value. The two unit load designs varied based off of payload.

A Kongsberg computerized cutting table (Esko, Miamisburg, Ohio, USA) was used to manufacture the boxes. The external dimension of the boxes was identical across the two unit load designs, measuring 203.2mm x 203.2mm by 254mm. The external dimensions of the boxes used in this study were carefully considered in order to create the most conservative test setup where the fork tines would not directly support the outside boxes. A total of four layers of corrugated boxes were placed on the top of each other on the pallet. The corrugated boxes were constructed to ensure that the center of gravity was maintained at half of the height of the box. To achieve this, two corrugated inserts were placed at the top and bottom of each corrugated box to secure evenly distributed wood pellets and achieve the necessary unit load payload determined using the ISO nominal fork tine test.

For the unit load designed using the static deflection limit of 4.5 degrees, the corrugated insert measured 195.3mm. x 190.5mm. x 69.9mm. and weighed 2.86 kg. to achieve a total payload of 343 kg. for the pallet. For the unit load designed using a static deflection limit of 20 mm, the corrugated inserts measured 195.3mm. x 190.52mm. x 82.6mm. and weighed 1.97kg. to achieve a total payload of 237.3 kg for each pallet. Figure 2 displays representative photos of the corrugated inserts used to maintain the center of gravity within each corrugated box. The top and bottom of the sealed using a 2 in. packaging tape (3M Corporation, Saint Paul, MN, USA).

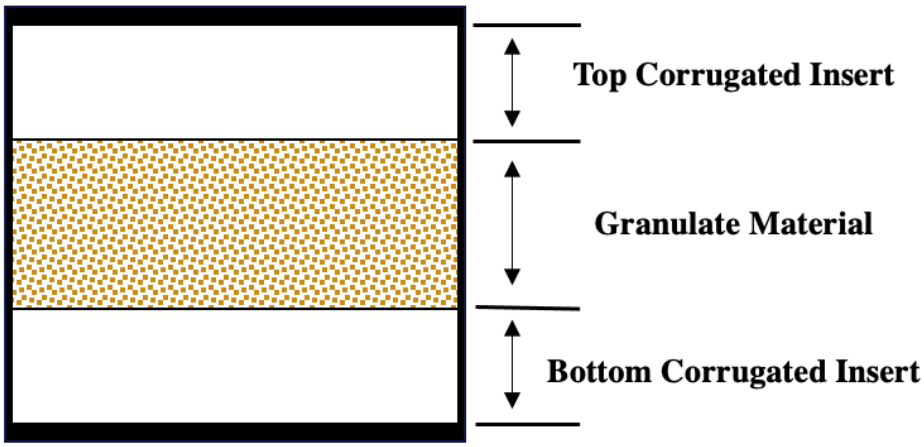

Figure 2: Representative internal layout of the corrugated boxes used for vibration testing including internal components used to achieve center of gravity.

Unit load

For each test repetition completed in this study a unit load was constructed of 120 total corrugated boxes (Figure 3). Each individual unit load consisted of four layers stacked in a column stacked pattern, including 30 boxes per layer. Each layer consisted of five rows of six boxes, where the six boxes remained parallel to the length of the pallet. Both bound and unbound unit loads were tested in this study. Bound unit loads were stabilized using linear low-

density polyethylene (LLDPE) stretch film purchased from U-line with the model number S-1524. The film was 80-guage thickness and had a width of 508 mm. The containment force used for the stretch wrap was 53.4 N, determined used a Highlight Film Force Pull Kit (PTC-919) based on the guidelines of ASTM D4649-03 (ASTM International, 2003). The film was pre-stretched 200% prior to application. Three top and bottom layers were applied, with a 40% overlap along the middle. The film force multiplier was 125%, and the carriage speed was set to 15% while the turntable was set at six RPM. A Highlight Synergy 4 stretch wrapper was used to apply the stretch film.

Figure 3: Representative photo of the unit loads used to conduct the dynamic fork tine support experiments in the parallel to the width orientation

Methods

Pallet load capacity

Pallet load capacity for the pallets used in this was study was determined using test 2a,b forklifting test presented in ISO 8611 Part 1 and Part 2 (ISO, 2011, ISO, 2021) testing standard. Pallets were tested in the static condition using Tinius Olsen (Tinius Olsen TMC, Horsham,

Pennsylvania) compression tester equipped with four 4,536 kg load cells. The testing procedures were previously reported by Yu Yang Huang[18]. The results of these static tests allowed us to design two unit loads, based off of payload. The pallet payload capacities were differentiated by different ISO static deflection limits. Using the data from the static tests, the pallet designed with a 4.5-degree (7.8% of the cantilever) static deflection limit had rated load capacity of 343 kg. and the pallet designed with a 20 mm static deflection limit had a rated capacity of 237.3 kg.

Dynamic unit load bending using fork tine support conditions

Dynamic testing was conducted using a custom simulated metal forklift support designed by Yu Yang Huang. The custom forklift support was designed to replicate a forklift carriage, where two 1066.8 mm fork tines (Atlas Companies, Atlas Forklift Forks) were used to support the load. The outside-to-outside span of the fork tines was 570 mm as prescribed in the ISO-8611 Part 1 (ISO 8611, 2021) test standard. The simulated forklift support was then secured to a vertical linear vibration table (Model 10000, Lansmont Corporation, Monterey, CA, USA) using bolts. The custom forklift support also used metal shims to simulate fork tines being initially level and inclined 4-degrees. The 4-degree incline was included because forklift drivers often tilt the fork tines upwards to stabilize the unit load during material handling. The maximum amount of tilt on most forklifts is 4-degree thus the authors wanted to simulate the most extreme scenario. Figure 4 provides a representative picture defining the components of the custom forklift support designed by Yu Yang Huang.

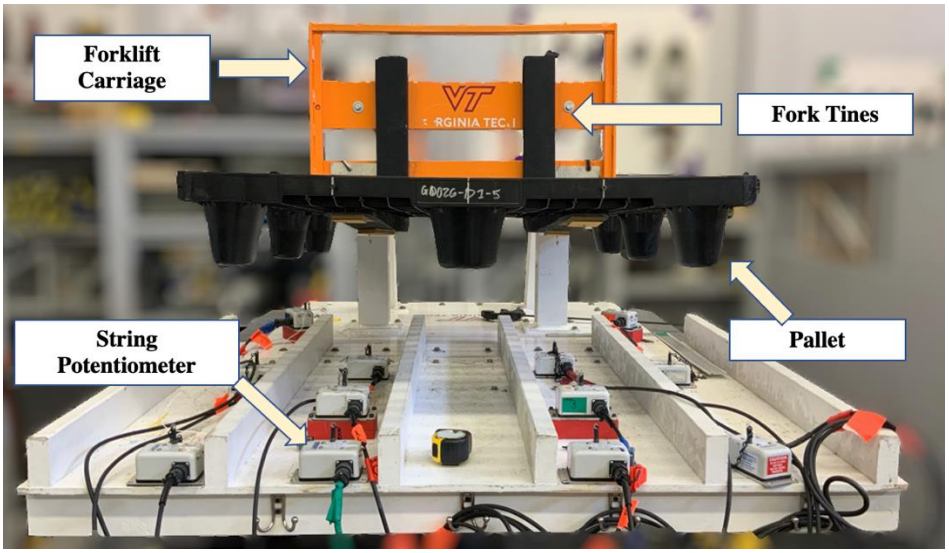

Figure 4: Custom forklift simulator designed by Yu Yang Huang

String potentiometers (P510-5-S10-NOS-30K, UniMeasure Inc., Corvallis, Oregon, USA) were used to capture the fork tine and pallet deflection that occurred throughout the

vibration test. The string potentiometers were secured to the top surface of the vibration table. Figure 5 displays the locations of the string potentiometers for the different setups.

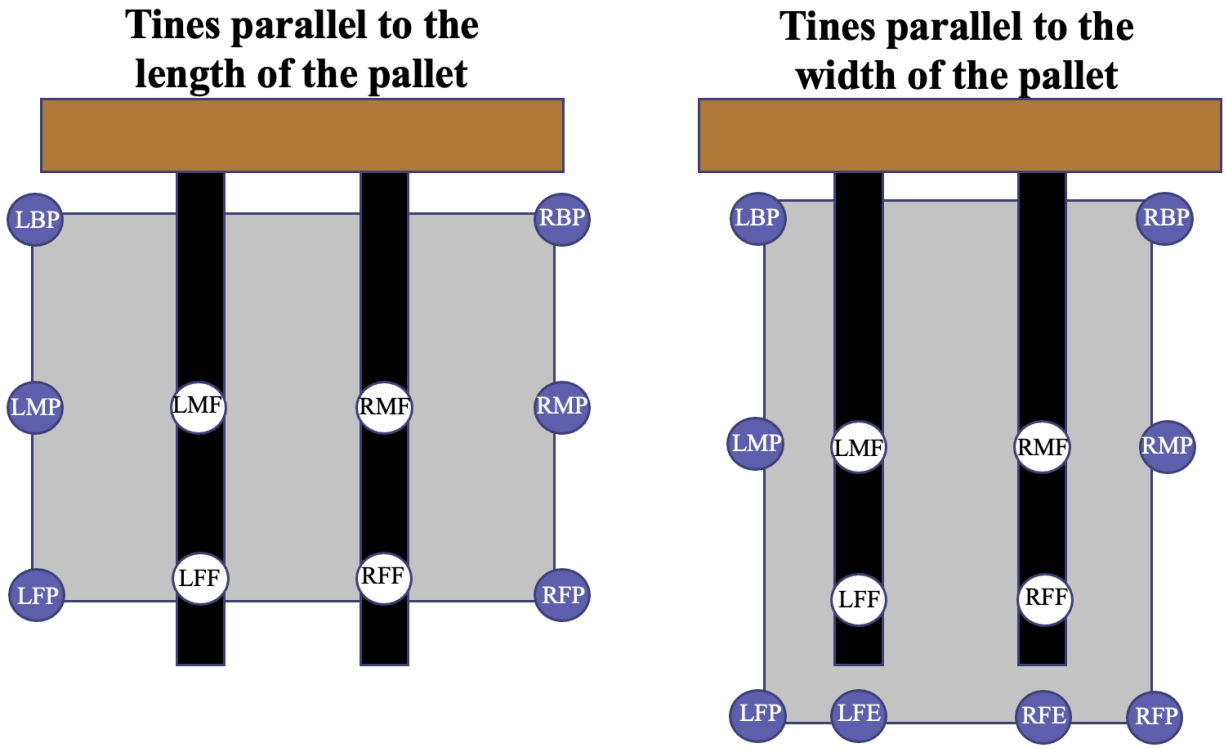

Figure 5: String potentiometer locations; **LBP** – Left back pallet, **LMP** – Left middle pallet, **LFP** – Left front pallet, **LMF** – Left middle fork tine, **LFF** – Left front fork tine, **RBP** – Right back pallet, **RMP** – Right middle pallet, **RFP** – Right front pallet, **RMF** – Right middle fork tine, **RFF** – Right front fork tine, **LFE** – Left fork tine extended (measured on pallet), **RFE** – Right fork tine extended (measured on pallet)

To emulate the vibration that occurs during forklift handling, a Power Spectral Density (PSD) profile representing a gas-powered forklift driven at 4.83 km./hour on asphalt carrying a load of 680 kg. was used[18]. The vibration profile previously collected by Yu Yang Huang was determined to be the most conservative vibration profile for the forklifts under the handling conditions tested. The pallets were exposed to up to 30 minutes of testing, In cases where unit load instability was observed, the vibration test was ended immediately. The 30 min. of vibration testing was selected to mimic the amount of time that the ISO 8611 defines for the creep testing. Although ISO 8611 requires another 30 min. of relaxation time without the payload the current study did not include the investigation of the effect of relaxation time on pallet performance thus the relaxation time was excluded from the study. Figure 6 displays the PSD profile used for dynamic testing.

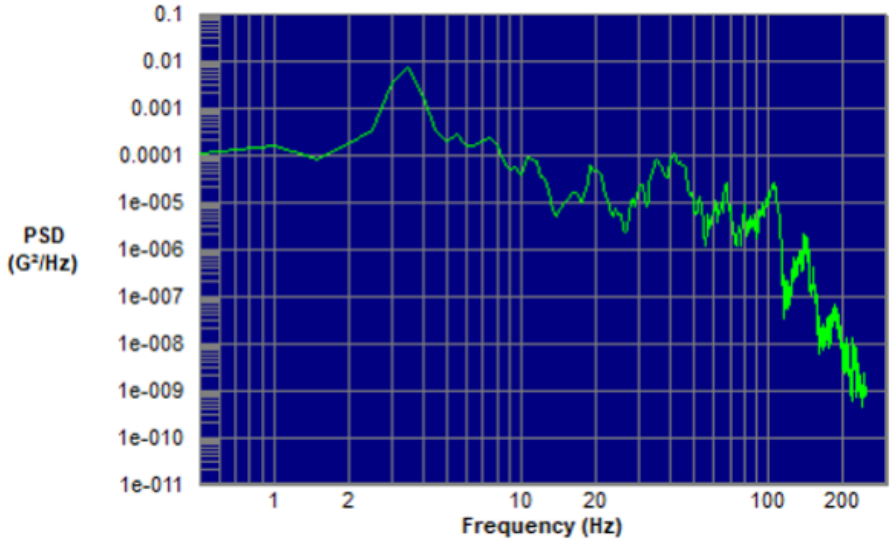

Figure 6: PSD vibration profile from a gas-powered forklift driven at 4.83 km./hour on asphalt carrying a unit load of 680 kg, measured at the carriage of the forklift

EXPERIMENTAL DESIGN

The experimental design of this project presented in Table 1, encompasses common material handling conditions commonly found during forklift handling of unit loads. Test scenarios included the effect of load stabilizers (bound and unbound), fork tine angle (initially level and a 4-degree incline), orientation of the pallet in relation to the fork tines (parallel to the width and parallel to the length), and unit load payload levels calculated using the static deflection limit reported in ISO 8611 (4.5 degree and 20 mm.). The resulting variable combinations consisted of nine different dynamic handling condition scenarios, and each handling condition was evaluated using three replicates.

Unit Load	Fork Tine Angle	Pallet Orientation	Static Deflection Limit	Test Replicates
Bound	Level	Parallel to the Width	4.5 degree	3
Unbound	Level	Parallel to the Width	4.5 degree	3
			20 mm.	3
		Parallel to the Length	4.5 degree	3
			20 mm.	3
	4 Degree Incline	Parallel to the Width	4.5 degree	3
			20 mm.	3
		Parallel to the Length	4.5 degree	3
			20 mm.	3

Table 1: Experimental design for each dynamic forklift handling condition combination.

DATA ANALYSIS

Pallet and fork tine deflection values were measured for each of the three test replicates conducted for the nine dynamic test scenarios. This resulted in 27 total data sets that were further analyzed for unit load stability, maximum deflection values, and dynamic movement. Deflection measurements were obtained in ten second intervals at three time ranges within each test. Initial deflection ("Initial Deflection") was calculated by processing the data points obtained within the first ten seconds after load was applied. The second time range occurred three minutes into the test ("At 3 min"), and the final time range occurred at the end of the 30-minute dynamic test or when unit load instability was first observed "At end of test").

Unit load stability was defined as the unit load's ability to remain intact for the full duration of the 30-minute vibration test. Resulting instability during any of the tests was measured at the first point that any box fell from unit load, and the time of that instability was recorded to compare the durability of unstable loads for each of the nine dynamic test scenarios. Unit load instability is reported in Table 2 as the number of replications that displayed instability before the 30-minute vibration was completed. Representative photos are provided for each of the nine test scenarios in which instability was observed.

Deflection values were recorded at three different time ranges in ten second intervals to acquire maximum, minimum, and average deflection measurements for each of the test scenarios. The values reported in the article were acquired using the "findpeak" function in MATLAB R2020b (Mathworks Inc, Natick, Massachusetts, USA) based on the work of Huang[18]. The maximum deflection values represent the ten highest peaks recorded during the respective ten second interval of time, with the minimum deflection values representing the ten lowest peaks recorded during the same ten second interval of time. The average deflection value represents the average of all the measurements obtained for that time interval. Measurements reported in this article were then derived as averages of the three test replicates for the nine different dynamic forklift handling scenarios. Additionally, for each of the nine test scenarios a representative graph has been provided that displays the continual deflection observed for the entire duration of the dynamic test.

Dynamic movement is characterized as the amount of undulation each location observed during the vibration sequence. This value was quantified as the maximum deflection value minus the minimum deflection value and then divided by two. Dynamic movement in millimeters was reported and represents half of the overall top-down movement each location experiences. The values reported in this article are averages of the individual calculations performed for each test replicate. How these values differentiate in regard to location, unit load design, and handling conditions is paramount to further compare them to the static test sequence currently used to test forklift support conditions.

RESULTS AND DISCUSSION

Results and discussion were grouped into the following measurement categories: unit load stability, dynamic movement, and deflection measurements.

Unit Load Stability

Unit Load instability was quantified as the percentage of three test replicates that did not survive the entirety of the 30-minute dynamic test for the nine test scenarios (Table 2). Bound loads remained stable for all test replicates; therefore, they were excluded from the stability analysis. The average time of instability for each test scenario was calculated by averaging the time of instability for each individual test replicate within each test scenario. The average time of instability for unbound unit loads designed using the static deflection limit of 4.5 degrees and 20mm was 11 minutes and 18 seconds and 15 minutes and 52 seconds, respectively. On average, the unit load designed using the static deflection limit of 20 mm. remained intact for four minutes and 32 seconds longer than the other unit load design. Of the twelve unit load replicates designed using the static deflection limit of 4.5 degrees, seven unit loads displayed instability. Only five unit loads designed using the 20 mm. static deflection limit displayed instability.

Unit Load	Fork Tine Angle	Pallet Orientation	Static Deflection Limit	Test Replicates	Unit Load Instability Rate	Average Time of Instability (min:sec)
Bound	Level	Parallel to the Width	4.5 degree	3	0/3	NA
Unbound	Level	Parallel to the Width	4.5 degree	3	3/3	5:58
			20 mm.	3	3/3	16:19
		Parallel to the Length	4.5 degree	3	2/3	8:11
			20 mm.	3	2/3	15:11
	4 Degree Incline	Parallel to the Width	4.5 degree	3	2/3	18:22
			20 mm.	3	0/3	NA
		Parallel to the Length	4.5 degree	3	0/3	NA
			20 mm.	3	0/3	NA

Table 2: Unit load instability rate and average time of instability for the nine different handling scenarios

Figure 7: Representative photos displaying unit load instability during vibration testing

Figure 7 displays representative pictures of unit load instability for all handling scenarios that experienced instability during testing. For unit loads designed using the 20 mm. static deflection limit, instability was observed only when the fork tines were initially level, of which only one unit load out of six unit load replicates remained stable for the entirety of the vibration test. As presented in Figure 1, unit loads tested with initially level tines commonly displayed instability towards the front of the pallet.

Of the twelve unit unbound loads designed using the static deflection limit of 4.5 degrees, seven total unit loads experienced instability. When this unit load design was tested using initially level fork tines, instability was commonly observed towards the front of the unit load. This is the same as previously found for unit loads designed using the static deflection limit of 20 mm. But, for unit loads tested with fork tines positioned at a 4-degree incline, instability was typically observed at the rear corners of the unit load, closest to the carriage of the simulated forklift support. This can be explained by the distribution of the load shifting towards the rear of the pallet when the fork tines are positioned at an incline.

Dynamic movement

Dynamic movement calculations quantified the undulation type movements that the pallet experienced through vibration while in a forklift transportation setting. Dynamic movement was observed for both the supported pallet and the supporting fork tines. This is in contrast to

current pallet testing procedures, where the pallet being tested and the supporting simulated fork tines remain static throughout the entire procedure.

Bound unit loads experienced far less dynamic movement than unbound unit loads that were tested using the same handling factors (level fork tines that were parallel to the width of the pallet) and unit load design (4.5-degree deflection limit). This handling scenario produced the most unit load instability for both unit load designs of unbound unit loads, while all bound unit loads remained stable for the entire test. When comparing the average maximum values that occurred during testing, bound unit loads experienced between 39% and 45% less dynamic movement than unbound unit loads. Additionally, bound unit loads experienced dynamic movement between 0.53 mm. and 1.96 mm. while unbound unit loads experienced between 0.24 mm. and 3.58 mm. This can be explained by the load bridging effect of load stabilizers, which increase the overall stiffness of the unit load[22] and decrease the opportunity for dynamic movement.

When dynamic movement is investigated in relevance to overall deflection, it was revealed that bound unit loads experience dynamic movement that is 27% of the total deflection on average. For unbound unit loads, dynamic movement is 10% of total deflection on average. While bound unit loads experienced more dynamic movement relative to deflection, all bound unit loads remained stable during vibration tests.

For unbound unit loads, dynamic movement was observed to increase from the back of the pallet towards the front of the pallet, likely due to the increased distance from the rigid support of the forklift carriage. Figure 8 provides a visual display of this phenomenon, where the width of the deflection line relates to dynamic movement. The back of the pallet experienced 70% less dynamic movement than the front of the pallet on average for unbound unit loads. This phenomenon was also observed for the fork tines, where dynamic movement increased from the middle of the fork tines to the tip of the tines. The middle of the fork tines experienced 46% less dynamic movement than the front of the tines on average for unbound unit loads.

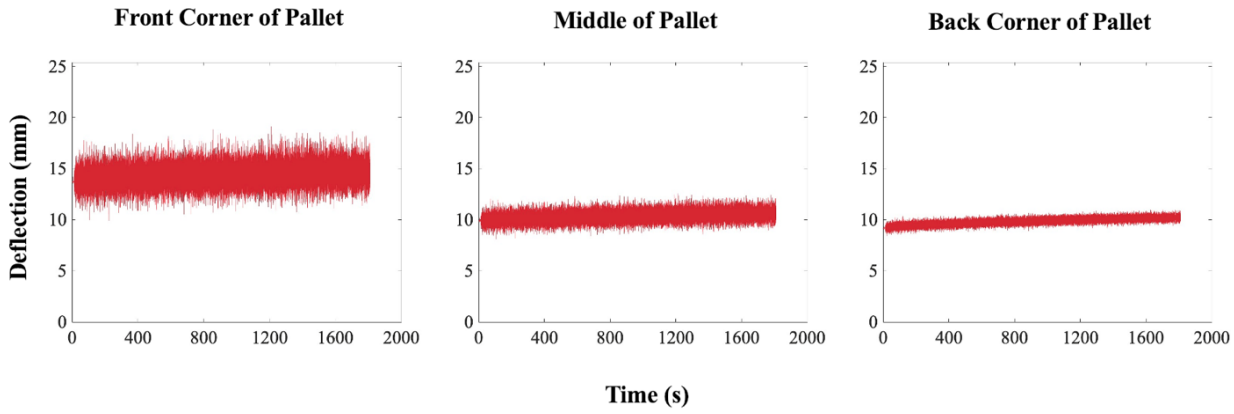

Figure 8: Representative dynamic movement during vibration testing for the front corner, middle, and back corner of the pallet

Dynamic movement is a representative characteristic in regard to material handling under forklift support conditions. Dynamic movement was observed for both the pallet and fork tines during vibration testing, meaning both components were experiencing up and down motion. This occurrence is in contrast with the current test procedure for pallets handled in forklift support conditions, where the simulated fork tines remain stationary for the entire test. Furthermore, dynamic movement is highly dependent on the location, as dynamic movement increased the further from the rigid forklift carriage. In comparison to the current testing procedure, the simulated fork tines are equally supported for their entire span.

Maximum Pallet Deflection

Deflection measurements were gathered for the full duration of the dynamic test sequence at ten different locations for unit loads racked with the simulated fork tines parallel to the width of the pallet and with two additional measurement locations for the unit loads racked with the simulated fork tines parallel to the length of the pallet. Figure 6 provides a visual representation of the locations used during testing. For each of the nine test combinations, an analysis of average maximum deflection measurements was performed. Deflection measurements reported in this article are averages of the three test replicates completed for each of the nine dynamic handling combinations. Table 3 summarizes the maximum average deflection for each handling scenario, defined by the location the measurement was observed. Additionally, correlating deflection angles were calculated to compare to the 4.5-degree static deflection limit reported in ISO 8611.

Unit Load Stabilizers	Handling Scenario	Static Deflection Limit	Time of Measurement	Maximum Avg. Deflection (mm.)	Angle	Location	Instability (#)
Bound	Level PTW	4.5 Deg.	Initial Deflection	4.67	0.83	FF	0
			At 3 Min.	6.07	1.07	MP	
			At end of test*	7.26	1.28	MP	
Unbound	Level PTW	4.5 Deg.	Initial Deflection	17.79	3.14	FP	3
			-	-	-	-	
			At end of test*	25.25	4.46	FP	
		20 mm	Initial Deflection	17.78	3.14	FP	3
			At 3 Min.	20.42	3.61	FP	
			At end of test*	22.04	3.89	FP	
	Level PTL	4.5 Deg.	Initial Deflection	13.34	3.43	FP	3
			At 3 Min.	18.34	4.72	FP	
			At end of test*	21.24	5.46	FP	
		20 mm	Initial Deflection	13.97	3.60	FP	2
			At 3 Min.	16.91	4.35	FP	
			At end of test*	18.12	4.66	FP	
	4 Deg. PTW	4.5 Deg.	Initial Deflection	16.75	2.96	BP, FP	2
			At 3 Min.	23.69	4.18	BP	
			At end of test*	33.33	5.88	BP	
		20 mm	Initial Deflection	17.78	3.14	BP	0
			At 3 Min.	19.91	3.52	BP	
			At end of test*	23.07	4.07	BP	
	4 Deg. PTL	4.5 Deg.	Initial Deflection	10.89	2.81	FP	0
			At 3 Min.	14.57	3.75	FP	
			At end of test*	16.82	4.33	FP	
		20 mm	Initial Deflection	13.97	3.60	FP	0
			At 3 Min.	16.11	4.15	FP	
			At end of test*	16.91	4.35	FP	

Table 3: Average maximum pallet deflection measurements and correlating deflection angle, location, and instability rate

Notes:
Instability represents the number of unit loads (out of three replicates) that became unstable during the vibration test.

Handling Scenario factors:
"Level" refers to unit loads that were supported by initially level fork tines
"4 Deg." refers to unit loads that were supported by fork tines that were inclined by 4 degrees.
"PTW" refers to unit loads that were supported by fork tines that were parallel to the width of the pallet.

"PTL" refers to unit loads that were supported by fork tines that were parallel to the length of the pallet.

Bound unit loads

Bound unit loads remained stable during all test replications. The maximum average point of deflection that occurred prior to starting the vibration ("Initial Deflection") was measured at the front of the right fork tine. The application of load caused a greater deflection to the fork tine than the pallet experienced because the effect of the stretch film greatly increased the stiffness of the unit load. The maximum average point of deflection that occurred at the three-minute time stamp and at the end of the test occurred in the middle of the pallet, along the width. This is also due to the effect of load stabilizers, that redistribute the load towards the middle of the pallet.

When comparing bound unit loads to unbound unit loads handled with the same factors and using the same payload, bound unit loads measured 71% less deflection at the end of vibration testing. For reference, all three unbound test replicates handled in this scenario and with the same payload became unstable 5 minutes and 58 seconds into the test, on average.

Unbound unit loads

Unbound unit loads experienced much greater deflection than bound unit loads, which consequentially increased the amount of instability observed from these test replicates. Of the unbound unit loads, 54% displayed instability. Instability was observed at angles ranging from 3.89 degrees to 5.88 degrees. Instability was commonly observed at the corners of the pallet, regardless of payload or handling factors. In all handling scenarios for unbound unit loads, the maximum average point of deflection was recorded at the corners of the pallet. Almost 74% of these points occurred at the front of the pallet, likely due to the increased cantilever from the rigid support of the simulated forklift carriage. The 26% of maximum average points of deflection that occurred at the back corner of the pallet occurred when unit loads were supported by fork tines that were inclined by four degrees and parallel to the width of the pallet. This handling scenario displayed maximum deflection at the back corner of the pallet due to both the incline of fork tines and length of the fork tines. The length of the fork tines is paramount to forklift support conditions, as unit loads supported by fork tines parallel to the length of the pallet overhang the tip of the fork tine. This also explains why unit loads supported by inclined fork tines that are parallel to the length of the pallet experienced maximum deflection at the front corners of the pallet.

The maximum average point of deflection that occurred in unbound unit loads occurred for unit loads designed with a 4.5-degree static deflection limit, handled by 4-degree inclined fork tines that were parallel to the width of the pallet. This value was 33.33 mm., which results in a deflection angle of 5.88-degrees. The average maximum point of deflection that occurred during the static portion of the test resulted in a deflection angle of 2.96. Therefore, the effects of vibration nearly doubled the amount of deflection this unit load experienced. As discussed before, the effects of vibration are not currently accounted for in pallet testing procedures.

CONCLUSIONS

The operation of transporting a unit load using a forklift is a dynamic procedure that involves some level of vibration. Current testing standards developed to replicate a forklift support scenario are static procedures, where the tested pallet is fully supported the entire length of the simulated fork tine. Replicating the dynamic behavior of a forklift and testing unbound unit loads on a simulated forklift with fork tines attached only to the carriage, the following conclusions were made:

- The operation of transporting palletized unit loads using a forklift includes a vibration interacting between the forklift tines and the pallet.
- During simulated movement of unit loads, pallet dynamic movement was 33% lower at the back of the pallet than the front on average. Dynamic movement increased 46% on average when moving from the middle to the front of the tine.
- Unbound unit loads, supported by pallets and tested to the ISO 8611 forklifting test deflection limits are unstable on level and inclined tines.
- Bound unit loads remained stable for all test replicates when subjected to dynamic test settings, and experienced 71% less deflection than unbound unit loads tested with the same handling factors at the end of the test.
- Considering these test results the ISO TC 51, "Pallets for unit load materials handling", technical committee, working group 2 "Pallet testing", should review the deflection limits in ISO 8611 part 2, Forklifting test 2.

REFERENCES

(1) Raymond, S. *History of the hand pallet truck*. https://raymondhandling.com/history-of-the-hand-pallet-truck/.
(2) Gerber, N.; Horvath, L.; Araman, P.; Gething, B. Investigation of New and Recovered Wood Shipping Platforms in the United States. *Bioresources* **2020**, *15* (2). https://doi.org/10.15376/biores.15.2.2818-2838.
(3) McCrea, B. *Annual Pallet Report: 2020's market evaluation*. https://www.mmh.com/article/annual_pallet_report_2020s_market_evaluation.
(4) *The Freedonia Group World Pallets*. www.freedoniagroup.com.
(5) Bugledits, D. *The Investigation of the Plastic Pallet Industry in the United States in 2018*; 2019.
(6) Bengtsson, J.; Logie, J. Life Cycle Assessment of One-Way and Pooled Pallet Alternatives. *Procedia CIRP* **2015**, *29*, 414–419. https://doi.org/10.1016/j.procir.2015.02.045.
(7) Chonhenchob, V.; Singh, S. P.; Singh, J. J.; Stallings, J.; Grewal, G. Measurement and Analysis of Vehicle Vibration for Delivering Packages in Small-Sized and Medium-Sized Trucks and Automobiles. In *Packaging Technology and Science*; 2012; Vol. 25. https://doi.org/10.1002/pts.955.

(8) Lamb, M. J.; Rouillard, V. On the Parameters That Influence Road Vehicles Vibration Levels. *Packaging Technology and Science* **2021**, *34* (9), 525–540. https://doi.org/10.1002/pts.2592.
(9) Marcondes, J. A.; Snyder, M. B.; Singh, S. P. Predicting Vertical Acceleration in Vehicles through Road Roughness. *J Transp Eng* **1992**, *118* (1), 33–49. https://doi.org/10.1061/(ASCE)0733-947X(1992)118:1(33).
(10) Zhou, R.; Yan, L.; Li, B.; Xie, J. Measurement of Truck Transport Vibration Levels in China as a Function of Road Conditions, Truck Speed and Load Level. *Packaging Technology and Science* **2015**, *28* (11), 949–957. https://doi.org/10.1002/pts.2176.
(11) Jarimopas, B.; Singh, S. P.; Saengnil, W. Measurement and Analysis of Truck Transport Vibration Levels and Damage to Packaged Tangerines during Transit. *Packaging Technology and Science* **2005**, *18* (4), 179–188. https://doi.org/10.1002/pts.687.
(12) Böröcz, P.; Singh, S. P. Measurement and Analysis of Delivery van Vibration Levels to Simulate Package Testing for Parcel Delivery in Hungary. *Packaging Technology and Science* **2018**, *31* (5), 342–352. https://doi.org/10.1002/pts.2327.
(13) Singh, J.; Singh, S. P.; Joneson, E. Measurement and Analysis of US Truck Vibration for Leaf Spring and Air Ride Suspensions, and Development of Tests to Simulate These Conditions. *Packaging Technology and Science* **2006**, *19* (6), 309–323. https://doi.org/10.1002/pts.732.
(14) Lu, F.; Ishikawa, Y.; Kitazawa, H.; Satake, T. Effect of Vehicle Speed on Shock and Vibration Levels in Truck Transport. *Packaging Technology and Science* **2010**, *23* (2), 101109.
(15) Garcia-Romeu-Martinez, M.-A.; Singh, S. P.; Cloquell-Ballester, V.-A. Measurement and Analysis of Vibration Levels for Truck Transport in Spain as a Function of Payload, Suspension and Speed. *Packaging Technology and Science* **2008**, *21* (8), 439–451. https://doi.org/10.1002/pts.798.
(16) Huang, Y. Y.; Horvath, L.; Böröcz, P. Measurement and Analysis of Industrial Forklifts Vibration Levels for Unit Load Testing Purposes. *Applied Sciences (Switzerland)* **2021**, *11* (7). https://doi.org/10.3390/app11072901.
(17) McCrea, B. *Annual Warehouse and Distribution Center Automation Survey: More automation, please*. https://www.mmh.com/article/annual_warehouse_and_distribution_center_automation_survey_more_automation.
(18) Huang, Y. Y.; Horvath, L.; Bouldin, J.; White, M. S. Evaluation of the Pallet Deflection That Occurs under Forklift Handling Conditions, Virginia Polytechnic Institute and State University, Blacksburg, 2021.
(19) Pallets for Materials Handling - Flat Pallets - Part 1. ISO 8611-1, 2011.
(20) Pallets for Materials Handling - Flat Pallets - Part 2. 8611–2, 2011.
(21) Standard Test Methods for Pallets and Related Structures-Employed in Materials Handling and Shipping, 2016.
(22) Park, J.; Horvath, L.; White, M.; Araman, P.; Bush, R. J. The Influence of Stretch Wrap Containment Force on Load Bridging in Unit Loads. *Packaging Technology and Science* **2018**, *31* (11). https://doi.org/10.1002/pts.2385.

DP-GO08

Effect of Wooden Pallets Characteristics on the Compression Strength of Palletized Plastic Pails with Double Overhang

Mary Paz Alvarez Valverde[1], Laszlo Horvath*[1]

[1] *Department of Sustainable Biomaterials, Virginia Tech, Blacksburg, VA, 24061, USA*

***Correspondence to**: Laszlo Horvath. Department of Sustainable Biomaterials, Virginia Tech, Blacksburg, VA, 24061, USA*
E-mail: lhorvat@vt.edu

ABSTRACT: The supply chain is made up of three key components: unit load stabilizers, packaging, and pallets. Understanding the interactions between these components is critical so that unit loads are designed in an efficient, sustainable manner. The interactions between corrugated boxes and wooden pallets have been widely investigated but there is a lack of studies on the effect of wooden pallets on the performance of plastic. The objective of this study was to understand the effect that deckboard thickness and pail location has on the plastic pail performance when the pail is supported on a single deckboard with a double overhang. The double overhang support condition is a critical condition for pails because the strength of the pail is the lowest with this support. Plastic pails were tested in two locations, the edge and the center of the pallet. These two locations were previously found to be the weakest and strongest support conditions for the pail, respectfully. Each location was tested using four different pallet deckboard stiffnesses and was compared to an additional rigid support condition. It was found that the pallet deckboard thickness and the location both had an impact on the pail compression strength and the pail deformation. The two support conditions led to different pail performances due to the asymmetrical and symmetrical support. The results of the study were compared to a previous pail study and found that the amount of support underneath the pail can impact the pail strength; increasing the amount of supported area can increase the pail compression strength.

Keywords: pallet; plastic pail; deckboard stiffness; unitload, compression strength

INTRODUCTION

In the American supply chain, 80% of packaged goods are shipped using pallets[1]. The supply chain is made of three physical components: unit load stabilizers, packaging and pallets[2]. With an estimated 839 million pallets in circulation in the United States[3], pallets and packaging have become an area of interest. Understanding how the pallets and packages interact with one another can lead to more cost effective, safe, and sustainable palletized unit loads. These interactions can be sorted into two categories, load bridging and pallet characteristic effects.

Load bridging was a phenomenon originally investigated by Collie[4] and Fagan[5]. They identified that when pallets are loaded with corrugated boxes, the compression stress was not uniformly distributed along the pallet but was being redistributed towards the supported ends. The load bridging effect was further investigated using palletized corrugated boxes by many researchers[4-10]. A correlation between the size of corrugated boxes and load bridging was identified. As the size of boxes increased more load was distributed towards the support reducing the bending of the pallet and increase the compression stresses on the corrugated boxes towards the stringers[6-8]. The box stacking pattern also had an impact on box performance as well as the performance of the pallet. It was found that column stacking was best for box strength while an interlocking stacking pattern was best to increase the performance of the pallet [9-11]. The containment forces during palletization was also found to impact behavior of the pallet[19].

Pallet characteristics also have an impact on packaging performance. Pallet deckboard gaps and thickness was found to have a significant impact on the performance of corrugated boxes. The relationship between pallet deckboard gaps and box compression strength was investigated by many researchers[12-14]. It was concluded that when pallet deckboard gaps were increased, which increased the unsupported box perimeter, there was a decrease in box compression strength. Pallet deckboard stiffness was investigated[15-18] and found to have an impact on corrugated box performance. Baker et al. found that pallet stiffness had a significant impact on boxes that are symmetrically supported on the pallet but only for scenarios where no pallet gap was present[15]. He also attempted to model this behavior using the principles of beam on elastic foundation[17]. He also hypothesized that this effect was due to the pallet deckboard rotating when supporting a single box on a pallet. In 2017, Phanthnousy conducted further experiments and instead found that the rotation of the deckboards has a negligible effect and would not impact the strength of corrugated boxes[16]. Other corrugated box and pallet interactions were found to have an impact on palletized boxes: asymmetrical loading[11], box overhang[12], and box location[15,16].

The interactions between packages and the pallet were further investigated by Quesenberry et al. who investigated the effect of deckboard stiffness on the performance of corrugated boxes when the box is asymmetrically loaded[22]. The investigation indicated that there when the stiffness of the deckboards increased the compression strength of pallets significantly decreased. This relationship can be utilized for holistic unit load design where designers can increase the deckboard thickness of a pallet and reduce the amount of material invested in corrugated boxes without decreasing the compression strength of the corrugated boxes. Quesenberry et al. conducted a preliminary financial analysis showing that this new design method can result in cost savings for the entire unit load. The effect of the proposed holistic unit load design method on the sustainability of the unit load was investigated by Kim et al.[23] He found that significant environmental benefits can be achieved by designing pallets and corrugated boxes using the proposed method by Quesenberry et al. Although, the relationship between pallets and corrugated box performance has been widely investigated, there is lack of studies that focus on the effect of pallets on the performance of plastic pails.

Plastic pails are primarily used to ship powders and liquids. The 5 gallon, cylindrical, HDPE pail is the most used[24]. Pails experience significant compression stress during use.

Similar to boxes, when plastic pails are loaded to failure the main mode of failure is wall buckling. Buckling is a physical phenomenon that occurs in shell elements where the strain experienced during compression[25]. The stored membrane energy of the shell element is converted into buckling energy to continue supporting load. The material, design, and method of compression impact the buckling of the shell element and the performance. Shells that experience axisymmetric, nonlinear buckling experience bifurcation buckling. Bifurcation buckling is considered a "post buckling" phenomenon since it takes place at the peak of the load vs. deflection curve[26]. Bifurcation buckling occurs when the shell element has load applied that exceeds the proportional limit and moves into the nonlinear buckling portion of the load-deflection curve. Cylindrical shell buckling has been investigated using finite modeling techniques[27-39], numerical techniques[40-44], digital image correlation[45-47], and physical testing[31,33,39]. Pinna and Ronalds[28] found that the support condition of the shell did have an impact on the bifurcation phenomenon and how it manifests on the cylindrical shell. However, there are no previous investigations on the impact of pallet support conditions on the cylindrical shell elements performance. Understanding the interactions between plastic pails, a cylindrical shell element, and a pallet support condition is important since it was found to have an impact on corrugated boxes.

The only study that was published on this topic was conducted by Alvarez et al. [21] She investigated the effect of various palletizing parameters such as deck board stiffness, pail location on the strength of plastic pails using a pallet simulator with a 3.5 in. pallet gap. It was found that the deckboard thickness and the location of the pail were both shown to have an impact on pail performance.

The lack of research knowledge on the interaction between plastic pails and wooden pallets was also identified by the wood pallet industry; therefore, the industry provided funding for this study through the Pallet Foundation. Further understanding of the interactions between pails and pallet will help pallet designers and packaging engineers to holistically design plastic pail unit loads by optimizing the cost of both pallets and plastic pails design efficiently.

OBJECTIVES

The main objective of the study was to investigate the effect of wooden pallet characteristics on the compression strength of plastic pails using a double overhang scenario.

The specific objectives of the study were the following:

1. Investigate the relationship between wooden pallet deckboard stiffness and plastic pail compression strength during a double overhang scenario.
2. Investigate the effect of asymmetrical loading due to the pail's location on the pallet and plastic pail compression strength during a double overhang scenario.

MATERIALS

Plastic Pails

The pails utilized in the study were 5-gallon, open headed, plastic HDPE pails (Uline.com, model S 7914). The pails were sealed using a pail lid (Uline.com, model S 9948). The pail lids were secured and sealed onto the pail with a rubber mallet. The pails were 14.5 in. tall with the lid, had a top diameter of 11.875 in., and a bottom diameter of 10.375 in. The wall thickness of the pails was 0.09 in. The pails were tested empty.

Load Applicator Jig

The tested pails had a wooden jig placed on top of the lid to ensure that the load was being distributed as if the pail was double stacked. The jig was created using the bottom 1.5 in. of a plastic pail and it was reinforced using two circular pieces of 0.75 in. thick plywood. The plywood pieces measured 10.25 in. in diameter to fit within the bottom of the pail.

Pallet Segment

The 23.5 in. x 36 in. small-scale pallet segment was created to simulate the support conditions on a wooden pallet. The small-scale pallet segment was made up of three stringers that measured 23.5 in. x 1.5 in. x 2.5 in. The three deckboards were measuring 36 in. x 5.5 in. To simulate different top deck stiffness scenarios, deckboards with four different thicknesses including 0.375 in., 0.5 in., 0.625 in., and 0.75 in. were used.

Both the deckboards and the stringers were made from defect free southern yellow pine. The deckboards were cut to length, to, width, and then planed down to the intended thickness. The stringers were cut to length and then width and planed on each face. A jig was created to ensure that the pallet would be built square when the deckboards were connected to the stringers. Two of the deckboards were placed on the end of the stringers and the third deckboard was placed in the center of the stringers length to ensure that there was a 3.5 in. gap in between the deckboards. The deckboards were fastened to the top and bottom of the stringers using three, #7, 2 in. long wood screws.

METHODS

Compression testing on a rigid surface

The compression tests using rigid surface were conducted using a MTS 322 universal testing machine (MTS System corporation, Eden Prairie, Minnesota, USA) that was equipped with a 5,000 lb. load cell. The pail was centered on a steel plate measuring 12 in. x 12 in. (Figure 1). The steel plate was secured to the MTS. The load applicator jig was placed on the top of the pail. The load was applied using a square, rigid wood load applicator that measured 14 in. x 14

in. The crosshead applied load at a rate of 0.5 in. per minute. The deformation of the pail was measured using the crosshead movement. The load was applied until the pail could no longer support additional load. The tests were conducted in laboratory ambient conditions.

Figure 1. Experimental setup for the pail compression testing on a rigid surface

Compression testing on a pallet segment

The compression test using flexible pallet segment tests were conducted using an MTS 322 universal testing machine (MTS System corporation, Eden Prairie, Minnesota USA) that was equipped with a 5,000 lb. load cell. The pallet segment was secured to the MTS using steel reinforcements. The deckboard deflections measurements were collected using Linear Variable Differential Transducers (LVDT) with ±1 in. stroke (Schaevitz 1000 HR-DC, Schaevtiz LLC Alliance Sensors Group, Bloomfiled Hills, MI, USA). Two LVDTs were used to collect measurements; their locations are presented in Figure 2. The LVDTs were connected to the pallet by placing a metal hook in the center of the deckboard span. The LVDT string was connected to the hook and ran through the roller which then went through a hole in the stringer.

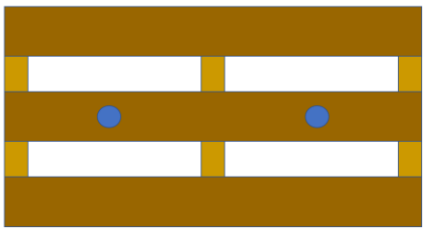

*Blue circles indicate location of LVDT deflection measurement

Figure 2. Locations of the deckboard deflection measurements using LVDTs during the compression testing

The pail was centered on the center deckboard between the center and outside stringers leaving a 2.44 in. overhang on both sides. The pail was loaded using the previously described load applicator jig and rigid wooden plate (Figure 3). The load was applied at a rate of 0.5 in. per minute. The crosshead movement, the amount of load applied, and the deflection of the pallet segment were collected by a computerized data collection system. The pails were crushed until they could no longer support the load. The pail deformation was calculated by subtracting the pallet deflection by the crosshead movement. The tests were conducted in laboratory ambient conditions.

Figure 3. Experimental setup for the pail compression testing on a flexible, pallet segment using the center support location

EXPERIMENTAL DESIGN

Effect of pail location on pail compression

Two pail locations on a pallet were investigated to understand the relationship between pail location and pail compression strength. Two locations included the edge of the pallet and the center of the pallet. These create two different loading conditions where the pail on the edge of the pallet experiences an asymmetrical support and the pail on the center of the pallet experiences a symmetrical support.

Effect of deckboard thickness on pail compression strength

Four pallet deckboard thicknesses and a rigid support condition were used to investigate the effect of pallet top deck stiffness on pail compression strength. The four thicknesses were 0.325 in., 0.5 in., 0.625 in., and 0.75 in. Each thickness weas used for both investigated pail locations. Ten replicate tests were conducted for each deckboard thickness and pail location combinations.

STATISTICAL ANALYSIS

An Analysis of Variance (ANOVA) was conducted to evaluate the effect of location and deckboard thickness on pail compression strength, pail deformation, and pallet deflection. The analysis for pail deformation, pail compression strength, and pallet deflection were conducted as separate models. The statistical model is presented in the following equation:

$y_{ij} = \mu + D_i + P_j + D_i P_J + \varepsilon_{ij}$

Where y_{ij} = response variable (pail deformation, pail compression strength, pallet deflection) m = overall mean, D_i = ith pail location, P_j = jth pallet deckboard thickness, $D_i P_J$ = interaction between the ith pail location and jth pallet deckboard thickness and ε_{ij} = random error.

A Tukey's HSD multiple comparison analysis with alpha = 0.05 was utilized to compare the measured means for each pail location and the pallet deckboard thickness levels.

LIMITATIONS

The following limitations apply to this study:

- The results only apply to the specific 5-gallon plastic pail used for the study.
- Only the performance of a single pail on the pallet deckboard was evaluated. Having multiple pails next to each other could interact with each other thus influence the testing results.
- Only ten replicate tests were conducted per pallet deckboard stiffness and location.

RESULTS

Pail placed on the center of the Pallet

The box compression and pail deformation results when the pail was placed in the center of the pallet are presented in Table 1. The result of the ANOVA analysis indicated that the deckboard stiffness was statistically significant ($p<.0001$) when analyzing the pail compression strength, the pail deformation at failure, and the pallet deflection. However, Tukey results revealed that the only significant difference for pail compressions strength was observed between the rigid condition and the flexible deckboard conditions. The compression strength of the plastic pail decreased by 30% when the pail was supported on the pallet segment compared to the rigid support. When the compression strength results were compared between the different deckboard stiffness levels, no significant differences were found. In 2022, Alvarez et al. also investigated the effect of pallet top deck stiffness on the strength of plastic pails in the presence of a 3.5 in. pallet gap[21]. Contrary to the results of the current study, Alvarez et al. observed an increase in the pail compression strength when pails evaluated on the pallet segment compared to the rigid support. In addition, Alvarez et al. observed a significant effect of the stiffness of the pallet top deckboard which is also different from the findings of the current study. The graphical comparison of the previous investigation and the results of the experiments are presented in Figure 4. When comparing the two sets of results the strength of

plastic pail is up to 47% lower when the pail is supported on the double overhang compared to the 3.5 in. pallet gap support. The cause of the decrease in pail compression strength could be explained with the increase of supported perimeter under the pail. When the pail is supported on the 3.5 in. deckboard gap it has 7.11 in. of unsupported perimeter which is only 22% of the total pail bottom. Meanwhile, when the pail is supported on double overhang, it has 21.14 in. of unsupported perimeter which is 65% of the total pail bottom. Therefore, similarly to corrugated boxes the amount of supported perimeter correlates to the compression strength of the pail

The pail deformation did show some dependence on the support conditions. However, the only substantial increase in pail deflection (50%) was only observed when the pail was supported on the thinnest (0.375 in.) deckboards compared to the rigid support condition. Previous results observed by Alvarez et al. did show a more consistent effect of pallet deckboards stiffness on pail deformation[16].

The pallet deflection measurements are presented Table 2. The deflection measurements were compared to the 0.75 in. deckboard thickness which was the most rigid. Deckboard deflection was statistically significant and indicates that the deckboard thickness does have a relationship with how much the board deflects. The difference in deflection between the thickest deckboard and the thinnest deckboard has a difference of 360%. Similarly, to the results obtained by Alvarez et al. there was no evidence that the failure of the pail occurring at a specific pallet deflection value.

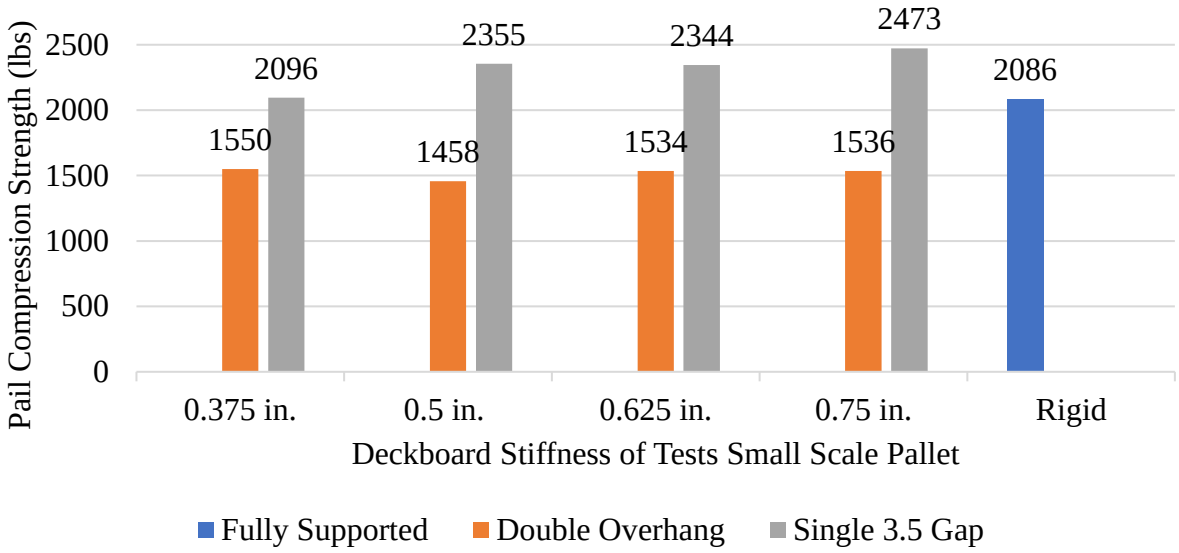

Notes:

Values from the single 3.5 in. gap study are derived from Alvarez Valverde et al.[21]

Figure 4. Comparison of the pail performance in terms of failure load when the pail is placed on the center of the pallet

Pail placed to the edges of the pallet

The box compression and pail deformation results when the pail was placed at the edge of the pallet support condition is presented in Table 3. The result of the ANOVA analysis indicated that the deckboard stiffness has a statistically significant effect ($p<.0001$) on the pail compression strength, pail deformation, and the pallet deflection. The results of the Tukey test revealed that the pail compression strength significantly decreased as the stiffness of the pallet top deckboards decreased. Pails supported on the 0.375 in. top deckboards had a 52% lower compression strength than pails supported on the rigid support. The results were also compared to the results obtained by Alvarez et al.[21] for pails supported on pallets with 3.5 in. pallet gaps. The trend observed in the current study is similar to the trend observed by Alvarez et al. who also observed that the reduction in pallet top deckboard stiffness results in a reduction in pail compression strength. Although the trend was the same, current results showed a much larger initial difference between the rigid support and the stiffest deckboard (37%) compared to the 9% reduction observed by Alvarez. The magnitude of the compression strength reduction as a function on the thickness of the top deckboards was in a similar range, 25% reduction for the current study compared to 32% reduction for Alvarez at al., when the pail compression strength values for the 0.75 in. and 0.375 in. deckboards were compared. The graphical comparison of the previous investigation and the results of the experiments are presented in Figure 5.

Contrary to the trend observed for the condition when the pail was centered on the pallet segment, the deformation of the pail decreased with the increase in pallet top deckboard stiffness. This trend was also different than the trend observed by Alvarez et al. who observed an initial increase then a decrease in pail deformation when the top deckboard stiffness decreased[21].

The trend observed for the deflection of the pallet during the experiment was in line with what was observed for the centered support and what was observed by Alvarez et al[21] (Table 4). The pallet deflection increased as the deckboard stiffness decreased; when comparing the 0.375 in. thickness to the 0.75 in. thickness, the deflection increased by 197%. This indicates that the pallet deflection is statistically significant but there can be no clear conclusions drawn on if there were a specific deflection limit that would cause pails to experience failure.

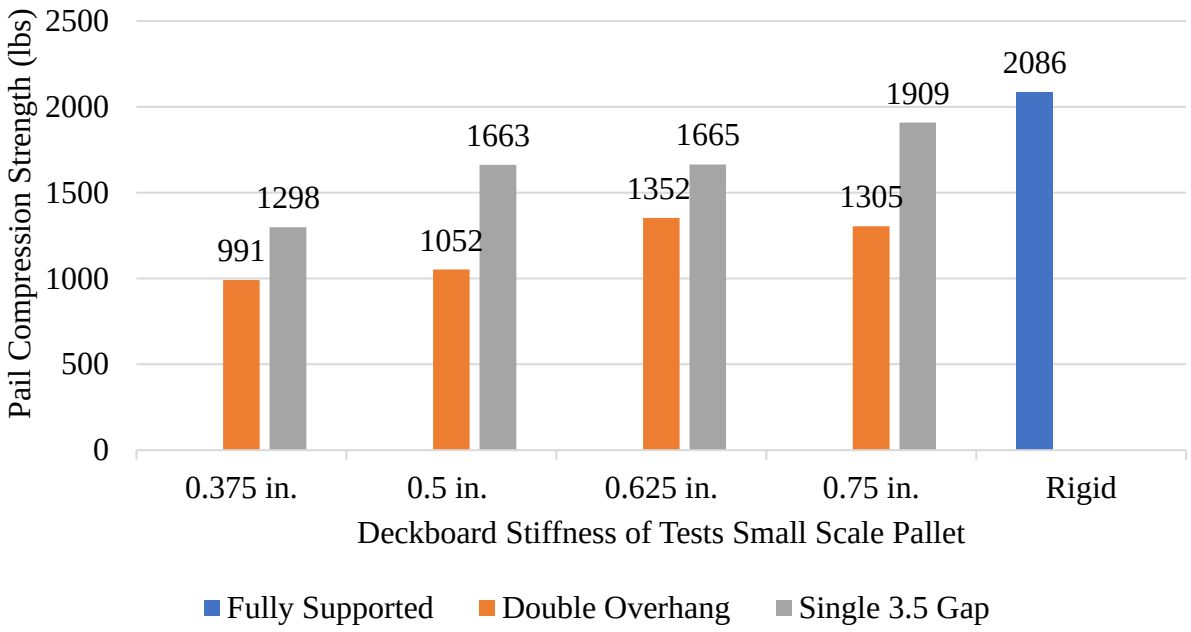

Notes:

Values from the single 3.5 in. gap study are derived from Alvarez Valverde et al.[21]

Figure 5. Comparison of the pail performance in terms of failure load when the pail is placed on the edge of the pallet.

The plastic pails are considered cylindrical shells and they experienced the two physical features of buckling when being compressed. The pails would first experience "elephant's foot" buckling where the plastic bulges across the bottom section of the pail. The second form of buckling under compression is called "bifurcation buckling" where the plastic shell converts membrane energy into buckling energy and the shell can no longer sustain load. When the pails failed, they all experienced bifurcation buckling. All the pail's buckling was seen at the lowest point of the sidewall shell towards the bottom diameter of the pail, this is due to the non-axisymmetric bifurcation buckling that the pail experienced. The failure location along the sidewall was different for the two investigated support conditions. The pails tested at the center of the pallet failed evenly on both sides of the pail and experienced bifurcation buckling where the deckboards were located and over the unsupported overhang (Figure 6b). When the pails were at the edge of the pallet the buckling was seen where pails were supported by the stringer and on top of the deckboard (Figure 6a). Both pail locations experienced pail failure where the stringer was located and where the deckboards were supporting the pail. The buckling trend indicates that the load that the pail was experiencing was being distributed towards the rigid stringers and forced the pail to buckle there since there was a concentration of stresses. This trend was also seen when the pails were tested using a 3.5 in. deckboard gap instead of a double overhang by Alvarez et al.[21]

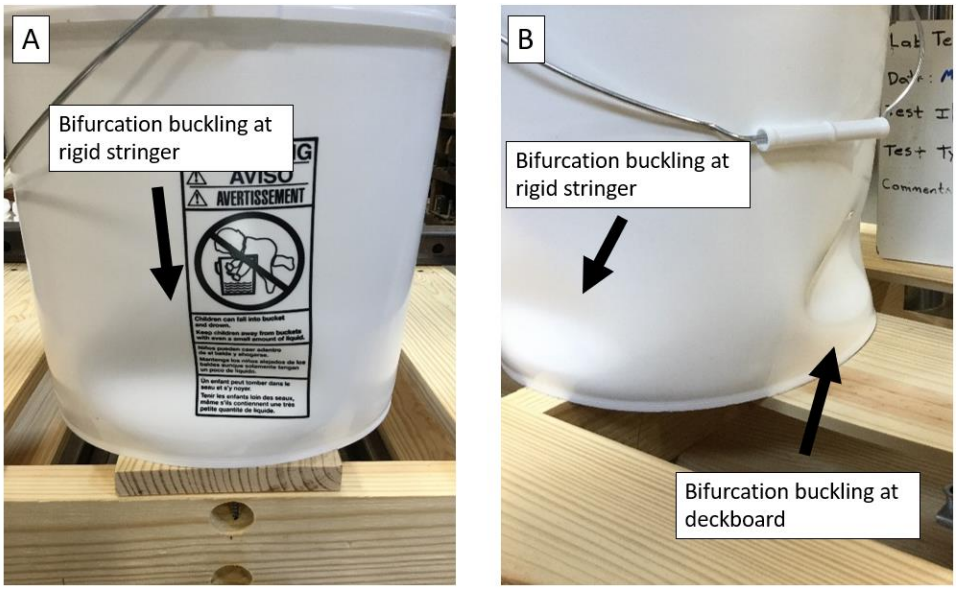

Figure 6. Representative pail failure modes: A) edge of the pallet and B) center of the pallet.

CONCLUSIONS

The main conclusions of the study are presented below:

- Pails supported on flexible wooden pallets allowing a 2.44 in. double overhang experienced a significant reduction in compression strength. Pails can have as much as 52% lower compression strength when stored on 0.375 in. thick pallet top deboards than pails stored on rigid support.
- The effect of the pallet top deckboard stiffness was only significant when the pails were tested at the edges of the pallet. The strength of pails can decrease as much as 24% when the pallet top deckboard thickness decreases from 0.75 in. to 0.375 in.
- There is no evidence that the failure of the pail occurs at a specific amount of pallet top deckboard deflection.
- The location of the pail on the pallet has a statistically significant effect on the compression strength of the pail. The compression strength is lowest when the pail is located on the edge of the pallet which produces an asymmetrical support condition. This phenomenon was also seen in a previous pail study.
- The compression strength of pails decreased up to 44% when supported at the edge of the pallet compared to the center of the pallet.
- It appears that the amount of the supported pail perimeter has a significant influence on the pail's compression strength. The compression strength of the pail can decrease up to 47% when the unsupported perimeter increases from 22% to 65%.

TABLES

.

	Deckboard Stiffness of Tested Small Scale Pallet				
	0.375 in.	**0.5 in.**	**0.625 in.**	**0.75 in.**	**Rigid**
Pail Compression Strength(lbs.)	1550 (7%) B	1458 (4%) B	1534 (3%) B	1536 (3%) B	2086 (6%) A
Change Compared to Rigid Setup	-26%	-30%	-26%	-26%	-
Pail Deformation at Failure (in.)	0.7175 (11%) A	0.4314 (7%) BC	0.4025 (3%) C	0.4848 (6%) B	0.477 (8%) B
Change Compared to Rigid Setup	+50%	-9%	-16%	+2%	-

Notes:
Values in parentheses are Coefficient of Variance values.
The different letters indicate that statistically significantly differences using $\alpha = 0.05$.

Table 1. Average pail compression strength and deformation results as a function of pallet top deck stiffness when the pails were placed to the center of the pallet

	Deckboard Stiffness of Tested Small Scale Pallet			
	0.375 in.	**0.5 in.**	**0.625 in.**	**0.75 in.**
Pallet Deflection at Pail Failure (in.)	0.2587 (12%) A	0.1513 (15%) B	0.1001 (6%) C	0.0562 (17%) C
Deflection Percent Difference Compared to 0.75 in. Thickness	+360%	+169%	+78%	-

Notes:
Values in parentheses are Coefficient of Variance values.
The different letters indicate that statistically significantly differences using $\alpha = 0.05$.

Table 2. Average pallet deflection at pail failure results as a function of pallet top deck stiffness when the pails were placed to the center of the pallet.

	Deckboard Stiffness of Tested Small Scale Pallet				
	0.375 in.	**0.5 in.**	**0.625 in.**	**0.75 in.**	**Rigid**
Pail Compression Strength(lbs.)	991 (5%) C	1052 (5%) C	1354 (6%) B	1305 (5%) B	2086 (6%) A
Change Compared to Rigid Setup	-52%	-49%	-35%	-37%	-
Pail Deformation at Failure (in.)	0.344 (19%) D	0.3286 (5%) CD	0.3816 (7%) BC	0.3947 (1%) B	0.477 (8%) A
Change Compared to Rigid Setup	-28%	-31%	-20%	-17%	-

Notes:
Values in parentheses are Coefficient of Variance values.
The different letters indicate that statistically significantly differences using $\alpha = 0.05$.

Table 3. Average pail compression strength and deformation results as a function of pallet top deck stiffness when the pails were placed to the edge of the pallet.

	Deckboard Stiffness of Tested Small Scale Pallet			
	0.375 in.	**0.5 in.**	**0.625 in.**	**0.75 in.**
Pallet Deflection at Pail Failure (in.)	0.3355 (10%) A	0.156 (8%) B	0.114 (14%) C	0.1131 (8%) C
Deflection Percent Difference Compared to 0.75 in. Thickness	+197%	+38%	+<1%	-

Notes:
Values in parentheses are Coefficient of Variance values.
The different letters indicate that statistically significantly differences using $\alpha = 0.05$.

Table 4. Average pallet deflection at pail failure results as a function of pallet top deck stiffness when the pails were placed to the edge of the pallet.

ACKNOWLEDGEMENTS

This research project was financially supported by the National Wooden Pallet and Container Association and The Pallet Foundation. Special thanks to Jordan Wells and Cameron Fischi for their support of the data collection.

REFERENCES

1. Raballand Gaël, Aldaz-Carroll E. How do differing standards increase trade costs? the case of pallets. *World economy*. 2007;30(4):685-702. doi:10.1111/j.1467-9701.2007.01009.x
2. White MS, Hamner P. (2005). Pallets move the world: The case for developing system-based designs for unit loads. *Forest Products Journal*, *55*(3), 8–16.
3. Gerber N, Horvath L, Araman P, Gething B. Investigation of new and recovered shipping platforms in the United States. *Bioresources.* 2020;15(2):2818-2838. Doi:10.15376/biores.15.2.2818-2838
4. Collie S. *Laboratory verification of pallet design procedures* [Master's thesis]. Blacksburg VA, USA:Virginia Polytechnic Institute and State University; 1984
5. Fagan G. *Load-support conditions and computerized test apparatus for wood pallets* [Doctoral dissertation]. Blacksburg, VA, USA: Virginia Polytechnic Institute and State University;1982.
6. Park J, Horvath L, White MS, Phanthanousy S, Araman P, Bush RJ. The influence of package size and flute type of corrugated boxes on load bridging in unit loads. Packaging technology & science. 2017;30(1-2):33-43.
7. Clayton AP, Horvath L, Bouldin J, Gething B. Investigation of the effect of column stacked corrugated boxes on load bridging using partial four-Way Stringer class wooden pallets. *Packaging Technology and Science*. 2019;32(9):423-439. doi:10.1002/pts.2438
8. Morrissette SM, Horvath L, DeLack K. Investigation into the Load Bridging Effect for Block Class Pallets as a Function of Package Size and Pallet Stiffness. *Packaging Technology and Science.*2020;34(1):51-69. doi:10.1002/pts.2539
9. Molina E, Horvath L, White MS. Investigation of pallet stacking pattern on unit load bridging. *Packaging Technology and Science*. 2018;31(10):653-663. doi:10.1002/pts.2406

10. Dunno K, Ge C, Rogers G, Johnson S. Influence of pallet pattern on top-to-bottom compression performance of unitized loads. *TAPPI Journal*. 2021;20(11):673-679. doi:10.32964/tj20.11.673
11. Rha, S. *Loss in Compression Strength of Corrugated Containers due to Offset and its Effect on Stability of Palletized Loads* [Master's thesis]. East Lansing, MI, USA: Michigan State University; 1996
12. DiSalvo, M. (1999). *Interactive effects of palletizing factors on fiberboard packaging strength* [Master's thesis]. San Jose, CA, USA: San Jose State University; 1999
13. Monaghan J., Marcondes J. Technical notes: overhang and pallet gap effects on the performance of corrugated fiberboard boxes. *Transactions of the asae*. 1992;35(6):1945-1947. doi: 10.13031/2013.28820
14. Baker M, Horvath L, White MS. Predicting the Effect of Gaps Between Pallet Deckboards on the Compression Strength of Corrugated Boxes. *Journal of Applied Packaging Research*. 8(3). doi: 10.14448/japr.08.0017
15. Baker M, Horvath L, White M. Effect of pallet deckboard stiffness on corrugated box compression strength. *Packaging Technology and Science*. 2016;29(4-5):263-274. doi:10.1002/pts.2201
16. Phanthanousy, S. *The Effect of the Stiffness of Unit Load Components on Pallet Deflection and Box Compression Strength* [Master's thesis]. Blacksburg, VA, USA: Virginia Polytechnic Institute and State University; 2017
17. Baker M, Horvath L, White MS, Scott M. Application of beam on Elastic Foundation to the interaction between a corrugated box and pallet deckboard. *Packaging Technology and Science*. 2017;31(5):377-385. doi:10.1002/pts.2338
18. Quesenberry C, Horvath L, Bouldin J, White MS. The effect of pallet top deck stiffness on the compression strength of asymmetrically supported corrugated boxes. *Packaging Technology and Science*. 2020;33(12):547-558. doi:10.1002/pts.2533
19. Park J, Horvath L, White M, Araman P, Bush RJ. The influence of stretch wrap containment force on load bridging in unit loads. *Packaging Technology and Science*. 2018;31(11):701-708. doi:10.1002/pts.2385
20. Alvarez Valverde MP, Horvath L, Bouldin J, Shahabi F. The effect of plastic pails on pallet deflection and pressure distribution for Stringer class wooden pallets. *Packaging Technology and Science*. 2021;34(7):423-434. doi:10.1002/pts.2571
21. Alvarez Valverde, M. P., & Horvath, L. (2022). Effect of wooden pallets characteristics on the compression strength of palletized plastic pails. Packaging Technology and Science, 35(10), 719–727. https://doi.org/10.1002/pts.2672
22. Quesenberry C, Horvath L, Bouldin J, White MS. The effect of pallet top deck stiffness on the compression strength of asymmetrically supported corrugated boxes. *Packaging Technology and Science*. 2020;33(12):547-558. doi:10.1002/pts.2533
23. Kim S, Horvath L, Russell JD, Park J. Investigation of the effect of pallet top-deck stiffness on corrugated box compression strength as a function of multiple unit load design variables. Materials. 2021;14(21):6613-6613. doi:10.3390/ma14216613
24. 5 gallon buckets. *ePackageSupply*. https://epackagesupply.com/buckets/5-gallon-buckets/.
25. Bushnell D. Buckling of Shells – Pitfall for Designers. *AIAA Journal*. 1981;19(9)

26. Bushnell D. Plastic Buckling. *Journal of Pressure Vessel Technology*. 1982;104(2): 51-72. doi:10.115/1.3264190
27. Ross CTF, Little APF. The buckling of a corrugated carbon fibre cylinder under external hydrostatic pressure. *Ocean engineering*. 2001;28(9):1247-1264. doi:10.1016/S0029-8018(00)00039-1
28. Pinna R, Ronalds BF. Buckling and postbuckling of cylindrical shells with one end pinned and the other end free. *Thin-walled structures*. 2003;41(6):507-527. doi:10.1016/S0263-8231(03)00006-5
29. Rahman T, Jansen EL. Finite element based coupled mode initial post-buckling analysis of a composite cylindrical shell. *Thin-walled structures*. 2010;48(1):25-32. doi:10.1016/j.tws.2009.08.003
30. Wang Y, Downes J, Wharton JA, Shenoi RA. Assessing the performances of elastic-plastic buckling and shell-solid combination in finite element analysis on plated structures with and without idealised corrosion defects. *Thin-walled structures*. 2018;127:17-30. doi:10.1016/j.tws.2018.01.030
31. Ozolins O, Kalnins K. An experimental buckling study of column-supported cylinder. *Procedia engineering*. 2017;172:823-830. doi:10.1016/j.proeng.2017.02.130
32. Ansari QM, Trinh LC, Zucco G, Weaver PM. Effect of elastic support on the linear buckling response of quasi-isotropic cylindrical shells under axial compression. *Engineering structures*. 2021;244. doi:10.1016/j.engstruct.2021.112796
33. Almroth BO, Holmes AMC. Buckling of shells with cutouts, experiment and analysis. *International journal of solids and structures*. 1972;8(8):1069-1068. doi:10.1016/0020-7683(72)90070-4
34. Papadrakakis M, Papadopoulos V. Finite-element analysis of cylindrical panels with random initial imperfections. *Journal of engineering mechanics*. 2004;130(8):867-876. doi:10.1061/(ASCE)0733-9399(2004)130:8(867)
35. Yu BH, Ma JJ, Liu Y, Selected, peer reviewed papers from the 2015 7th International Conference on Mechanical and Electrical Technology (ICMET 2015), July 1-2, 2015, Bali, Indonesia. Finite element analysis of cylindrical shell with a circular cutout using combination model of solid element and shell element. *Applied mechanics and materials*. 2015;799-800:739-745. doi:10.4028/www.scientific.net/AMM.799-800.739
36. Chen Q, Elwi AE, Kulak GL. Finite element analysis of longitudinally stiffened cylinders in bending. *Journal of engineering mechanics*. 1996;122(11):1060-1068. doi:10.1061/(ASCE)0733-9399(1996)122:11(1060)
37. Hagihara S, Miyazaki N. Finite element creep buckling analysis of circular cylindrical shell under axial compression taking account of creep damage. *Metals and materials*. 1998;4(3):295-298. doi:10.1007/BF03187780
38. Panda SK, Singh BN. Thermal post-buckling behaviour of laminated composite cylindrical/hyperboloid shallow shell panel using nonlinear finite element method. *Composite structures*. 2009;91(3):366-374. doi:10.1016/j.compstruct.2009.06.004
39. Kim M-H, Cho J-R, Bae W-B, et al. Buckling analysis of filament-wound thick composite cylinder under hydrostatic pressure. *International journal of precision engineering and manufacturing*. 2010;11(6):909-913. doi:10.1007/s12541-010-0110-4

40. Brodsky WL, Vafakos WP. Buckling analysis of ring-stiffened oval cylindrical shells. *Computers and structures*. 1974;4(6):1135-1158. doi:10.1016/0045-7949(74)90029-7
41. Grabovsky Y, Harutyunyan D. Scaling instability in buckling of axially compressed cylindrical shells. *Journal of nonlinear science*. 2016;26(1):83-119. doi:10.1007/s00332-015-9270-9
42. Batterman SC. Free-edge plastic buckling of axially compressed cylindrical shells. *J appl mech*. 1968;35(1):73-79. doi:10.1115/1.3601176
43. Franzoni F, Degenhardt R, Albus J, Arbelo MA. Vibration correlation technique for predicting the buckling load of imperfection-sensitive isotropic cylindrical shells: an analytical and numerical verification. *Thin-walled structures*. 2019;140:236-247. doi:10.1016/j.tws.2019.03.041
44. MALLET-PARET JOHN. Buckling of cylindrical shells with small curvature. *Quarterly of applied mathematics*. 1977;35(3):383-400.
45. Amarante RM, Pesce CP, Santiago RC, Ramos R, de Sousa José Renato M, Rabelo MA. Structural behavior assessment of a flexible pipe under axial compressive loads using digital image correlation. *Journal of the brazilian society of mechanical sciences and engineering*. 2018;40(9):1-12. doi:10.1007/s40430-018-1386-z
46. Wang Y, Downes J, Wharton JA, Shenoi RA. Assessing the performances of elastic-plastic buckling and shell-solid combination in finite element analysis on plated structures with and without idealised corrosion defects. *Thin-walled structures*. 2018;127:17-30. doi:10.1016/j.tws.2018.01.030
47. Zhao C, Niu J, Zhang Q, Zhao C, Xie J. Buckling behavior of a thin-walled cylinder shell with the cutout imperfections. *Mechanics of advanced materials and structures*. 2019;26(18):1536-1542. doi:10.1080/15376494.2018.1444225

DP-GP01

Predicting the Effect of Pallet Overhang on the Box Compression Strength

Saewhan Kim[1], Laszlo Horvath[*1], Eduardo Molina[1], Benjamin Frank[2], Steven Johnson[3], and Alonda Johnson[1]

[1]*Department of Sustainable Biomaterials, Virginia Polytechnic Institute and State University, Blacksburg, VA, 24061, USA*
[2]*Packaging Corporation of America, Mundelein, IL, 60060, USA*
[3]*West Rock, Carol Stream, IL, 60188, USA*

***Correspondence to**: Department of Sustainable Biomaterials, Virginia Polytechnic Institute and State University, 1650 Research Center Drive, Blacksburg, 24061, USA.*
E-mail: lhorvat@vt.edu

ABSTRACT: Unit loads, consisting of pallets and corrugated boxes, are widely used for storing and distributing packaged products. The corrugated box's compression strength can easily be affected by environmental parameters, such as pallet overhang, which reduces a box's effective compression strength (BCT). However, the effects of overhang on BCT remain poorly defined, prompting the corrugated industry to call for further research. The current study, aimed to investigate the effects of pallet overhang on BCT using four different sizes of corrugated boxes, made from two different board combinations, in order to compare existing values in the Fibre Box Handbook, in order to discover statistically significant factors, and to explore the possibility of developing a prediction model for the effects of pallet overhang. The boxes were examined in over a dozen single-side overhang configurations and five adjacent-side overhang scenarios. The average reduction in BCT was between -0.22% and -40.39%. These results indicated that the safety factors in Fibre Box Handbook fits well with adjacent overhang scenarios but overestimates single side overhang scenarios. The trend that BCT decreases as the magnitude of overhang increases was also observed, as expected. A range of multiple linear and nonlinear regression models, that provide the estimated change in a box's compression strength due to any overhang compared to a no-overhang scenario, were developed. These models showed great potential of using the model to predict the effect of pallet overhang on BCT through their high R2 values (0.82, 0.94, and 0.93). It was also able to learn from the models that the magnitude of overhang on the short and long side, whether overhang exists on a single side or adjacent side, box size, and board type are all statistically significant factors to the effect of pallet overhang on BCT. This work also indicated the need for further research refining the first-order model and extending it to other materials, box sizes, and box aspect ratios.

Keywords: Corrugated box, overhang, pallet, unit load, box compression strength, multiple linear regression

DP-PP01

Estimation of the degradation of strawberries during rail transport from knowledge and experiences made on roads trips

Jean-Baptiste Nolot [1*], Ellyn Dubecq[1,4], Sophie Annibal [4], Philippe Delloque [1], Victor Huart [3], Serge Odof [1,2], Mikael Meuret [1], Damien Erre [1,2]

[1]*ESIREIMS, Ecole Nationale Supérieure d'Ingénieurs de Reims, URCA University of Reims Champagne Ardenne, FRANCE*
[2]*ITheMM, Institut de Thermique, Mécanique, Matériaux – URCA University of Reims Champagne Ardenne, FRANCE*
[3]*METROPACK, Packaging Test Lab, Reims FRANCE*
[4]*CTIFL, Centre Technique Interprofessionnel des Fruits et Légumes, Rungis FRANCE*

***Corresponding author**:* Jean-Baptiste Nolot. *ESIREIMS, Ecole Nationale Supérieure d'Ingénieurs de Reims, URCA University of Reims Champagne Ardenne, FRANCE*
Email: jb.nolot@univ-reims.fr

ABSTRACT: The main harvests of fruits and vegetables are in southern Europe (Spain, southern France). The products must therefore be transported to Rungis (France near Paris) to supply the market. The Rungis market sells goods to wholesalers who redistribute them in Paris and northern Europe. The Rungis distribution platform is the world's leading fresh produce market. Arrivals break down as follows: Meat 15%, fruits & vegetables 71%, dairy products 9% and seafood 5%. They are gathered on 234 hectares (area equivalent to the state of Monaco). In 2019, 1,216,290 tons of fruit and vegetables were processed on the Rungis market for a turnover of €4,299 millions.

Transport is mainly operated by truck. Since 2021, a specialized logistics company has decided to restart an old railway line from the south of France (Perpignan) to Rungis (Paris). Each convoy consists of 12 wagons equivalent to 18 trucks. 500 pallets cross France daily. Today only 9% of goods freight is carried by rail against 90% by road. Ecology, fuel costs and road safety encourage our government to double the use of rail by 2030.

Sector professionals have asked the CTIFL (Interprofessional Technical Center for Fruits and Vegetables) to assess the impact of this logistical development on product quality. The harvesting, maintain good safety and measurement of the quality of plant products are the specialties of the CTIFL. CTIFL entrusted us with the study of rail & road logistics circuits. We must assess the impact of this change on an extremely fragile fruit : the strawberry.

Keywords: Fruits & vegetables, damaged strawberries, rail & truck environment recording, vertical vibration analysis, transport simulation, wooden crates, plastics crates, cardboard crates, tray of fruits.

INTRODUCTION

Our study concerns the measurement of several complete transport circuits from the fields to the display of the Rungis market. We placed data loggers (SAVER 3X90) on our pallets and measured these circuits.
We present in this work the comparison of rail & truck trips. The number of breaks in the supply chain is equivalent between the rail trip and the truck trip. The same types of shocks (Intensity, Duration, Velocity change) are measured. To differentiate rail & truck trips, we focused on the effect of vibrations.



Pallet specimens for truck data recording

Data Loger	SAVER 3X90 Lansmont
Sample rate	1000 Hz
Event duration	2,048 sec
Trigger	Signal (S) > 0.5G - Timer (T) = 2 min
Location	@ Bottom of the Pallet

From the vibration analysis of the truck trip (PSD, Distribution Grms, Duration), we built two vibrations tests protocols (Highway soft =0.228 Grms-86 min & Road hard=0.457 Grms-12 min + 0.409 Grms-51 min + 0.323 Grms-9 min) (see graph 1).

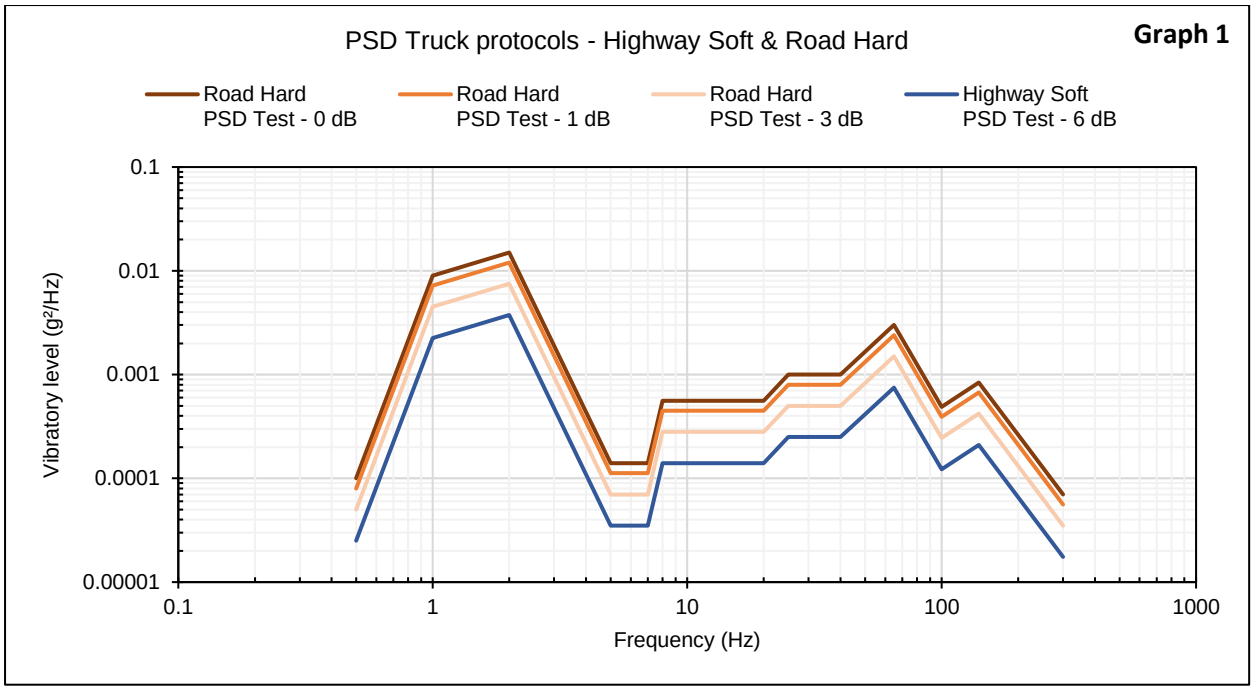

Graph 1

Following the latest rail recordings, a Vibration rail protocol (PSD, Distribution Grms, Duration) has been developed.

The two truck protocols were applied to fresh and fragile vegetable products (strawberries). We observed and quantified the damage produced on strawberries. From this knowledge, the objective is to calculate the probable damage produced by the rail protocol on strawberries.

STRAWBERRIES TRUCK TRANSPORT TESTING

Experimental assembly

The fresh strawberries are picked and placed directly in basket (250 grams). The boxes are stored in crates (16 x 250 gr = 4 kg). The crates are stacked in a column on a vibration table (SEREME). 3 types of crates are used by wholesalers: wooden crates, IFCO plastic crates (reused), cardboard crates.

Wooden crates, IFCO plastic crates, Cardboard crates

The vibratory behavior of the packaging was measured at 4 levels of stacking of the crates. Very small differences are measured between the different palletization floors. The baskets located in the center of the crates have a resonance @ 10 Hz 15 Hz regardless of the type of crates.
On the other hand, the amplifications are very different (see graph 2). The IFCO crate produces the strongest amplification: up to 10x more than cardboard and 5x more than wood.

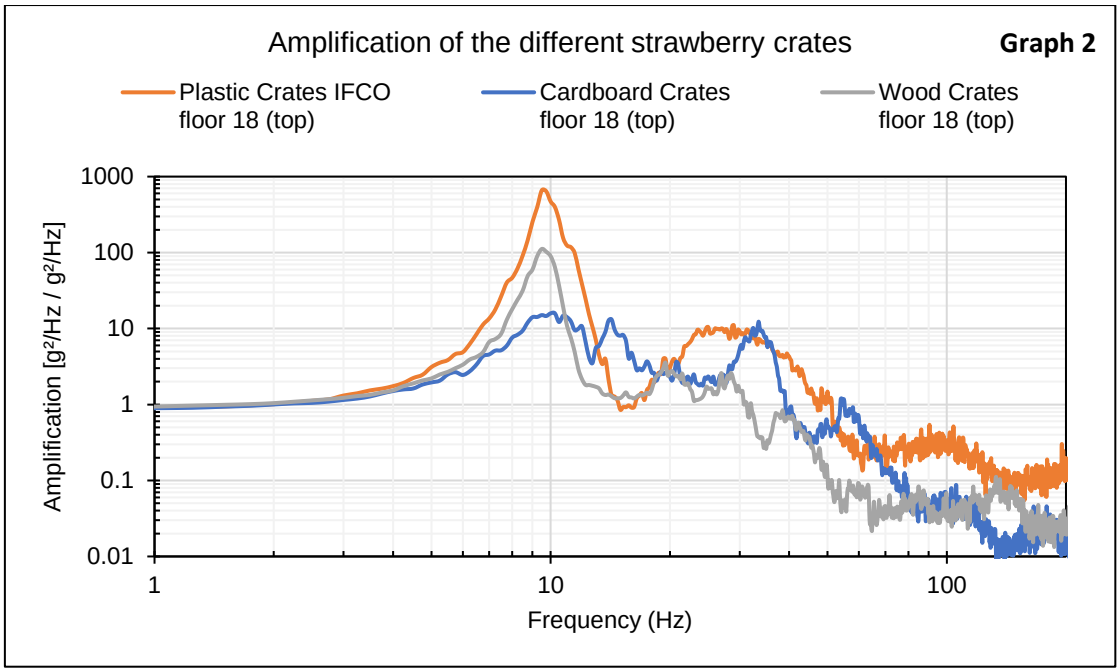

Graph 2

For budget reasons, we replaced strawberries with pebbles (same masses). Baskets with strawberries are placed in the center of the crates on floor 0 (bottom) – floor 6 – floor 10 - floor 14 and floor 18 (top).

Degradations and temporal monitoring

Two varieties of strawberries (Charlottes, Maras des bois) underwent these truck vibration protocols in our laboratory. The CTIFL constructed a fruit degradation index (DI) from the observations made at the end of the test. (Mildew, Number of wounds, Juice). Reference sample of strawberries is exempt from testing and protected for observation. Observations are carried out from Day 0 to Day+3. Strawberries are stored after testing in a climatic chamber under conditions [5°C - 80% RH].

The DI (degradation index) is calculated from levels of bruising Bx. A severity coefficient is applied to Bx to give more importance to high damage. This DI is calculated every 24 hours to follow the evolution of the degradation over time. Each strawberry contained in the basket is inspected daily.

Calculation of Degradation Index (DI) of strawberries from severity coefficient Bx
B0: No bruises (crush)
B1: Small bruises (< 5 affected achenes)
B2: From 5 to 10 affected achenes
B3: Pale pink, 10 affected achenes
B4: Pale pink, 15 affected achenes

B5: Pale pink, >15 affected achenes, moist crushing

$$DI = \frac{0 \times B0 + 1 \times B1 + 2 \times B2 + 3 \times B3 + 4 \times B4 + 5 \times B5}{Number\ of\ strawberry\ in\ the\ basket}$$

RESULTS

The control strawberries show less degradation than the tested strawberries.
The results present the degradation index difference between Day 0 and the Day+3 of observation : DI gap = (DI_3 - DI_0)

IFCO plastic crates cause more degradation than wooden crates.
The cardboard crate is the most effective way to protect the strawberries during transport.
The "Charlotte" strawberry variety is more resistant to vibrations than the "Maras des bois" variety.

DI (Degradation Index) after trucks tests									
Strawberries Varieties	Crates	Day 0		Day + 3		DI gap (DI_3 - DI_0)		Other dommages	
		Road Hard PSDs	Highway Soft PSD	Road Hard PSDs	Highway Soft PSD	Road Hard PSDs	Highway Soft PSD	Juice	Mildew
Charlottes	Plastic IFCO	0.22	0.19	1.88	1.49	1.66	1.3	Yes	No
	Wood	0.25	0.14	1.49	1.16	1.24	1.02	No	No
	Cardboard	0.09	0.11	0.91	0.92	0.82	0.81	No	No
Maras des bois	Plastic IFCO	0.59	0.5	2.15	1.95	1.56	1.45	Yes	No
	Wood	0.34	0.36	1.5	1.35	1.16	0.99	Yes	No
	Cardboard	0.38	0.35	1.44	1.07	1.06	0.72	Yes	Yes

CALCULATION OF THE PROBABLE DAMAGE PRODUCED BY THE RAIL PROTOCOL

Construction of a rail vibration protocol

To respond to environmental and governmental issues, the CTILF and its industrial partners have started a campaign to measure rail logistics circuits. We recorded a first trip (year 2022) from the south of France to the Rungis wholesale market (Paris).

The train travels 1000 km passing through the cities of Toulouse and Bordeaux. The Bordeaux-Rungis (Paris) railway line is characterized by a mild vibration environment. The Toulouse-Bordeaux railway line is worn out and vibrational levels are high.

We built a PSD's transport simulation protocol in accordance with the field. (PSD RAIL=0.599 Grms-5 min + 0.423 Grms-75 min). Our recording campaign resumed in 2023 to refine our protocol. (see graph 3)

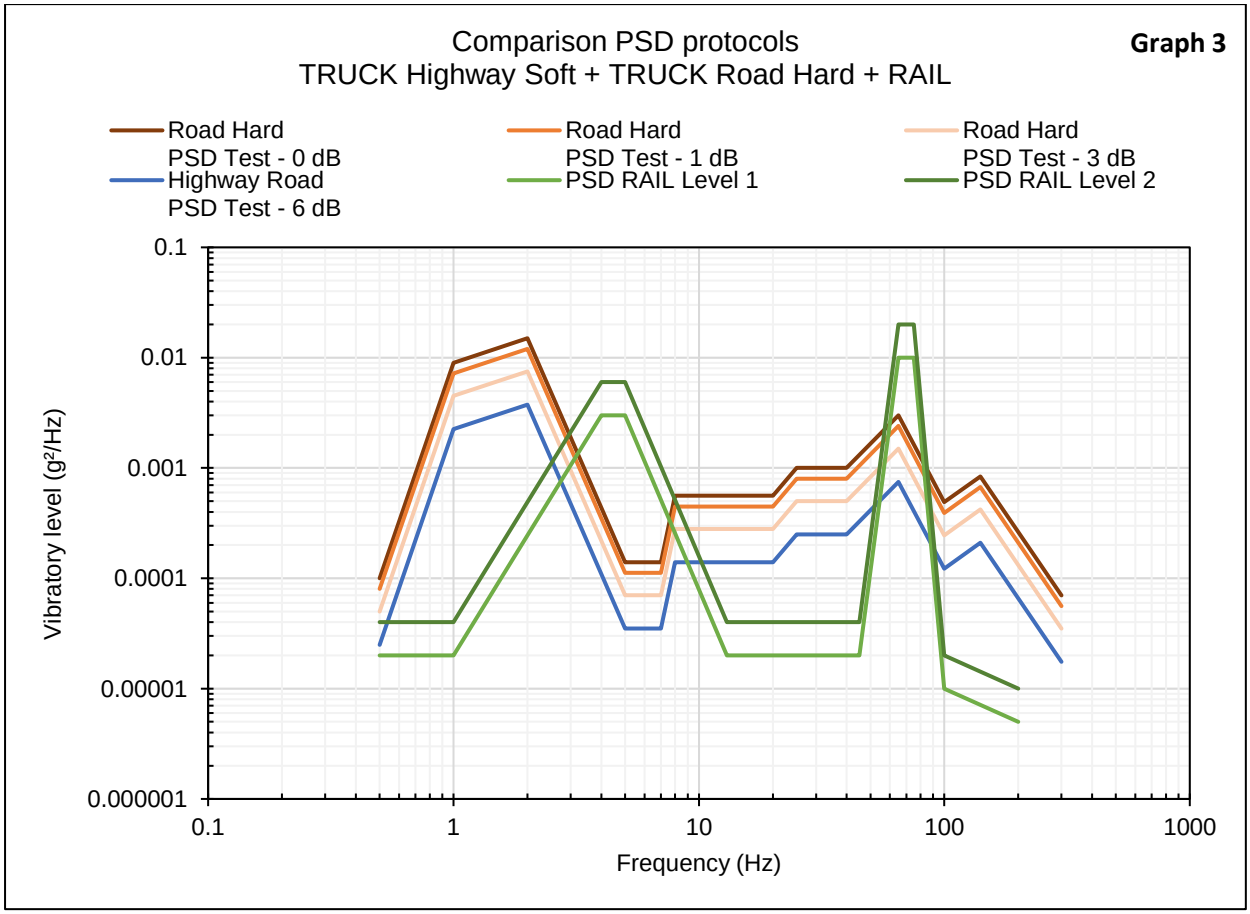

Graph 3

The analysis of the rail journey shows first vibration peak @ [4-5 Hz]. The second peak, centered @ [65-75 Hz], corresponds to the vibrations of the wagon cooling system.

Method of calculation of theorical DI with rail protocol

We base our reasoning on the following assumptions:

- The DI gap (DI_3-DI_0) for the plastic, wood, cardboard crates follow the order of the resonance peaks of these strawberry packages.
- So we can assume that damage on strawberries is produced by excitation at 10 Hz.
- We calculate the weighted sum (weighted by duration) of the vibration levels (g^2/Hz) @ 10Hz of each type of transport.
- The calculated vibration levels and the associated DI GAP for each crate and each variety are given in the results table.
- The DI GAP of the reference strawberries is given in this table.
- From these points we extrapolate the theoretical DI Gap produced by the rail transport.
- The calculations are based on a second order polynomial fit.

Results table DI Gap = (DI_3-DI_0)		Vibratory level @ 10Hz (g^2/Hz)	Plastic IFCO	Wood	Cardboard
Charlotte	Road Hard	0.000304	1.66	1.24	0.82
	Highway soft	0.00014	1.30	1.02	0.81
	RAIL	0.000085	1.02	0.83	0.70
	Reference sample	0	0.42	0.42	0.42
Maras des bois	Road Hard	0.000304	1.56	1.16	1.06
	Highway soft	0.00014	1.45	0.99	0.72
	RAIL	0.000085	1.19	0.85	0.64
	Reference sample	0	0.56	0.56	0.56

CONCLUSION

Different packagings are used to transport strawberries across Europe. The strawberries are gathered in basket, placed in crates and stacked on pallets. IFCO plastic, wood and cardboard crates do not produce the same damage to the strawberries.

Our experiments have shown that IFCO plastic crates destroy strawberries more than wooden crates and the wooden crate destroy strawberries more than cardboard crates. This observation is true for the two varieties of strawberries studied: “Charlotte" & "Maras des bois". We found that strawberries degradation is related to vibrations @10Hz.

Our calculations show that the degradation by rail transport should be [10-22%] lower than "truck highway soft" transport. For the most severe road transport (truck road hard), the

degradation decrease is [15-39%]. Future strawberry harvests will allow to experimentally verify these estimates.

REFERENCES

[1] A. Paternostera, S. Vanlanduitb, J. Springaela, J. Braeta, (2018)
Vibration and shock analysis of specific events during truck and train transport of food products
Food Packaging and Shelf Life
[2] Jarimopas B., Singh S. P., & Saengnil W. (2005).
Measurement and analysis of truck transport vibration levels and damage to packaged tangerines during transit.
Packaging Technology and Science
[3] V. Chonhenchob, S. Sittipod, D. Swasdee, P. Rachtanapun, S. P. Singh, and J. Singh (2009)
Effect of Truck Vibration during Transport on Damage to Fresh Produce Shipments in Thailand
Journal of Applied Packaging Research
[4] Böröcz P., & Singh S. P. (2016).
Measurement and analysis of vibration levels in rail transport in central europe.
Packaging Technology and Science

CONFERENCE PROCEEDINGS
LOGISTICS AND SUPPLY CHAIN

ORAL PRESENTATION

GENERAL STREAM

LS-GO01	How grocery retailers can utilize learnings from meal kit delivery services to optimize their supply chain
LS-GO02	Logistical Challenges to Deliver in the Last Mile for Consumer, Furniture, and Military including White Glove Services

LS-GO01

How Grocery Retailers can Utilize Learnings from Meal-Kit Delivery Services to Optimize their Supply Chain

Jay Singh[1*], Alex Yates-Robinson[1]

[i]*Packaging Program, Cal Poly State University, San Luis Obispo, CA 93407, USA*

***Correspondence to**: Jay Singh, Packaging program, Cal Poly State University, San Luis Obispo, CA 93407, USA.*
E-mail: jasingh@calpoly.edu

ABSTRACT: The COVID-19 pandemic surprised the collective US supply chain. Retailers, manufacturers, and distribution chains sought to meet a rapid increase in demand while facing their own shortages in materials and labor. Grocery retailers and meal-kit delivery services differ in many ways, but the major meal-kit delivery services did not endure the same consequence, in terms of supply or quality reduction, during the pandemic. While the meal-kit delivery services were initially set out to provide convenience and education, their major success and distinction came through their unique pre-pandemic supply chain optimization strategy. Traditional retailers do not and will never exclusively operate using the same supply chain model as meal-kit delivery services, but learnings can be applied help mitigate future supply chain disruptions. This research was carried out through analyzing peer-reviewed articles and conducting interviews with industry experts. Initial research focused on the modern supply chains, both in grocery and meal-kits. Research around the supply chains of each business model focused on how the current models operate, strengths and weaknesses within the models and the response to the COVID-19 pandemic. The results will be presented.

Keywords: Packaging, supply chain, COVID-19, meal-kit, retailers

INTRODUCTION

The collective supply chain was shocked by the COVID-19 pandemic, which resulted in retailers, manufacturers, and distribution chains struggling to meet a rapid increase in demand while dealing with their own shortages in materials and labor. While retailers have faced supply chain disruptions in the past due to wartime, natural disasters, and economic downturns, the enormity and impact of the COVID-19 pandemic was unique. Despite the supply chain having undergone significant changes over the past century, the guidance available for navigating COVID-19 was lacking [1].

In the weeks leading up to March 2020, consumers who shopped at grocery retailers may recall encountering progressively empty shelves and fellow shoppers filling their already full carts with more goods. Meal-kit delivery services, on the other hand, operate under

different constraints, consumer expectations, and supply chain models. The COVID-19 pandemic served as a test of the resilience and flexibility of both grocery retailers and meal-kit delivery services.

Table 1 highlights some of the key differences, discussed in this paper, between grocery retailers and meal kit delivery services

Comparison Chart: Grocery Retailer vs. Meal Kit Delivery Services

Grocery Retailers

Meal Kit Delivery Services

Grocery Retailers		Meal Kit Delivery Services
Business to Business (B2B)	Supply Chain	Direct to Consumer (D2C)
Push	Logistics Strategy	Pull
Consumer dictated qty	Purchase Qty	Pre-portioned
Multi-serving	Pkg Size	Single-serving
Fresh, some frozen	Protein Type	Frozen
Refrigerated and/or frozen	Transportation Conditions	Ambient
In-house network	Shipping Carrier	3rd party carrier
Varied by item	Shelf Life	7 days
Consistent	Demand	High variability

Table 1. Comparison between Grocery Retailers vs. Meal Kit Delivery Services

Grocery Retailers

Over the past century, the grocery retail industry has undergone significant changes due to supply chain optimizations and consumer demand for an abundance of choice. Prior to 1916, customers
provided their grocery lists to clerks who retrieved the requested items. However, the first self-service store, Piggly Wiggly, was opened in 1916, followed by the first supermarket, King Kullen, in 1930, which revolutionized the grocery business by uniting all food departments under the same roof [2]. Since then, innovations in the grocery retail industry have continued to evolve.

Innovations in subsequent decades include the invention of the shopping cart in 1937, the price scanner in 1974, and industry consolidation in the 1990s, with Walmart, Kroger, Costco, and SuperValu becoming major players [2]. Grocery retailers have developed complex supply chains to deliver a vast product offering to meet consumer expectations of full shelves, which requires ambient, refrigerated, and frozen distribution across domestic and international facilities. Most grocery chains use a *push* logistics strategy, in which inventory management

systems review historical purchase data to predict future demand and order products accordingly.

However, inventory issues can occur when there are unique and unanticipated fluctuations in demand, such as during the COVID-19 pandemic. Grocery retailers have adapted by providing new ways for consumers to shop and receive their groceries, such as through curbside pick-up and home delivery. These adaptations have allowed retailers to meet the needs of their customers during challenging times and ensure that they can continue to provide fresh produce and other products.

One of the biggest challenges faced by grocery retailers is food waste. Estimates suggest that 30-40% of the world's food is lost or wasted, and a study conducted by McKinsey & Company found that 16% of total food loss occurs upstream, while 14% occurs downstream [3,4]. Fruits and vegetables account for 28% of the negative environmental impact of food loss [5]. Food loss occurs primarily due to production surplus, produce not meeting specifications, and damage, while food waste is dependent on inventory management and consumer behavior.

The packaging of fresh produce plays a critical role in maintaining its quality and appearance during transportation and storage. Respiration, which is affected by temperature and humidity, is a major contributor to premature spoilage, and ethylene, a hormone associated with ripening, accelerates the process. Packaging must protect the produce from damage and minimize respiration during distribution. In addition, packaging must minimize pathogenic contamination and extend the shelf life of produce.

Corrugated trays have been found to be the most effective packaging for fresh produce, as they provide better overall quality and lower the risk of foodborne illnesses [6]. Grocery stores receive produce on pallets, either as a single unit or mixed pallet. Produce is packed into materials that extend its shelf life and mitigate the risk of crushing and premature spoilage. For example, fresh blueberries are packed into PET clamshell containers and then palletized into vented corrugated trays to prevent crushing and mitigate the risk of respiration [7].

The grocery retail industry has undergone significant changes over the past century, driven by supply chain optimizations and consumer demand for an abundance of choice. Innovations in subsequent decades include the invention of the shopping cart, the price scanner, and industry consolidation. Grocery retailers have adapted to meet the needs of their customers during challenging times, such as during the COVID-19 pandemic, by providing new ways for consumers to shop and receive their groceries. However, retailers still face challenges with food waste and the importance of packaging in extending the shelf life of perishable products. The packaging of fresh produce plays a critical role in maintaining its quality and appearance during transportation and storage, and corrugated trays have been found to be the most effective packaging for produce.

Meal-kit Delivery Services

Meal-kit delivery services have become increasingly popular in recent years due to their convenience and ease of use for busy individuals or those who are inexperienced in cooking. HelloFresh has gained popularity as a meal-kit delivery service due to its convenience and ease of use for busy individuals and those with limited cooking experience. Established in 2007, it is now the world's leading meal-kit

company. Customers select their meals ahead of time and receive pre-portioned ingredients and preparation instructions. Early adopters of meal-kits were typically young adults in urban areas who faced barriers to cooking for themselves.

Compared to traditional grocery retailers, HelloFresh has a shorter supply chain as it handles only raw ingredients. These ingredients are processed and transported to the company's three primary distribution centers in refrigerated trucks to minimize food spoilage. The distribution centers serve as warehouses, manufacturing facilities, and distribution centers. Raw materials are sorted, processed, and packed into meal-kits according to unique requirements for each recipe. The finished boxes are then shipped via a third-party shipping carrier, insulated to withstand ambient conditions for 48 hours prior to customer refrigeration.

HelloFresh offers 30-40 menu offerings per week, each containing 10-12 ingredients, for a total of 600 unique raw materials managed by the company annually [8]. To avoid over-inventorying, HelloFresh employs a pull logistics strategy and manages ingredients using an internal part numbering database.

HelloFresh strives to provide fresh and sustainable ingredients while minimizing food waste. To address the issue of premature spoilage, the company inspects produce multiple times and employs a dynamic forecasting system to minimize transportation distance. Less than 1% of ingredients are wasted, with the majority donated to local charitable organizations and food banks. Pre-portioning ingredients and using frozen protein helps to further reduce food waste [9].

HelloFresh's packaging is designed to withstand ambient conditions for 48 hours prior to customer refrigeration, utilizing a range of sustainable materials and optimized for each season (Figures 1 & 2). While some may criticize the packaging used by meal-kit companies, it is necessary to maintain product quality and HelloFresh continuously tests and optimizes their packaging to reduce waste [9].

Figure 1. Winter and Simmer Insulation for HelloFresh Meal-Kits

Figure 2: Examples of Contents and Components of a HelloFresh Meal-Kits

RESEARCH METHODOLOGY

The research methodology employed in this study involved analyzing peer-reviewed articles and conducting interviews with industry experts to gain insights into the modern supply chain for both grocery and meal-kit delivery [8-12]. The initial interviews focused on understanding the challenges faced by the meal-kit business model, the implications of the COVID-19 pandemic, and the sustainability of the business both financially and environmentally. Additional interviews were conducted with experts in the grocery retailer space to gain a better understanding of standard business practices and the impact of the pandemic on the industry. Peer-reviewed articles were used to examine supply chain disruptions, logistical challenges faced by both grocery retailers and meal-kits, and the sustainability of both businesses [1,2,13,14]. The research also explored the strengths and weaknesses of each business model's current supply chain operations and how they responded to the pandemic. Sustainability research focused on packaging usage, specifically the servings-to-volume ratio, and food waste. Overall, the study used a combination of qualitative and quantitative methods to provide insights into the supply chain and sustainability of grocery and meal-kit delivery businesses.

RESULTS

The meal-kit model differs greatly from the grocery model, which has successfully endured for over a century in the US despite undergoing consolidation, ingredient diversification, and various optimizations. However, the COVID-19 pandemic posed an unprecedented challenge that left a lasting impact on the grocery industry's business model. Though it is hoped that future supply chain crises will not be caused by a pandemic, it is crucial to explore how the grocery industry can learn from the meal-kit model to avoid significant shortages of essential items and continue delivering to customers.

Grocery Retailers and HelloFresh's Responses to COVID-19 Supply Chain Crisis

The COVID-19 pandemic caused a supply chain crisis for both meal-kit services and grocery retailers. Grocery supply chains were optimized for routine operations, not volatile settings. Panic buying from consumers led to an unexpected increase in demand, which the supply chain was not prepared or designed for, leading to shortages. Grocery retailers faced challenges managing rapidly fluctuating demand on specific items, making inventory management and demand planning complicated. With thousands of grocery chain networks, it became challenging to track inventory and reorder items. Purchase limits on certain items were put in place, and demand planners had to contend with which items were going to be in higher demand.

The pandemic was unpredictable in occurrence and scale, leading to inconsistent specific demand, making it a full-time job for procurement teams to keep track of high-demand items and move them between locations. The supply chain crisis highlighted the fragility of what was perceived as a robust supply chain, and increased variety of SKUs contributed to the challenges faced by grocery retailers. The pandemic was the first all-encompassing "natural disaster" affecting all parts of the country, leading to unpredictable demand, and making it challenging to manage the supply chain.

HelloFresh, a meal-kit company, was better positioned to weather the COVID-19 pandemic than grocery retailers due to their unique supply chain model. HelloFresh, unlike grocery retailers, orders in inconsistent quantities, dictated by menu offerings and customer preference, and customers are limited to three meals per week, making it difficult for them to overbuy. The menu offerings are planned 16 weeks in advance and finalized one week before assembly and delivery, giving meal-kits a significant advantage over grocery retailers in terms of procurement [8].

HelloFresh's supply chain was designed to meet the volatile demands of consumers and their meal-kit offerings, with supplier relationships that evolved into partnerships where both sides benefited financially. HelloFresh also has a 100% service level, ensuring that they get ahead of supply chain shortages, regardless of cost [10]. Their centralized inventory in a few distribution centers provides more visible transparency of in-stock items and easier movement of goods [8,10]. They justify "over-buying" raw materials to accommodate the week-to-week meal offerings and donate any excess ingredients. When the pandemic hit, HelloFresh diversified their suppliers, checked their raw material limitations and risks, and ensured that the flavor profiles of their meals were maintained. HelloFresh's supply chain was stable despite the instability occurring outside it due to their ability to manage demand, performance, and volatility.

Consumer Expectations and Perceptions

The expectations of grocery customers and meal-kit customers are similar but not the same. Grocery customers buy a wide variety of products, including produce, processed food, beverages, proteins, and numerous commodity items. In contrast, meal-kit customers

exclusively order meal-kit boxes, which contain produce and protein but not commodity items. Meal-kit customers don't expect a single meal-kit delivery to include all the necessary commodity items they buy from their local grocery store, nor do they expect the ability to choose between specific raw materials and ingredients. However, meal-kit customers expect a full box of necessary ingredients to prepare their selected meals.

The differences in expectations between the two models drive grocery stores to carry more than 30,000 items, increasing the complexity of inventory management [2]. Grocery customers see everything, including empty shelves and shortages, leading to negative perceptions of supply chain crises. In contrast, meal-kit customers only see the contents of their box, not the inventory challenges and "back house" work that goes into delivering the ingredients. As a result, meal-kits had a reliable supply chain that customers could trust, leading to their popularity during the pandemic. The expectations of each model must be considered when applying learnings from meal-kits to the grocery model.

Inventory Centralization

The pandemic affected the entire US simultaneously, unlike other disasters, making it impossible for grocery retailers to transfer items between distribution centers. HelloFresh's inventory centralization is a strength that eliminates the need to distribute to individual stores, and with only a few warehouses, it provides better inventory visibility and reduces food waste by delivering directly to customers' homes.

However, for grocery retailers, centralizing inventory to a few distribution centers would require a major overhaul of their model. They would need to reduce the number of distribution centers and expand key locations, which would result in the closure of existing stores. This is not a practical solution, especially since the current grocery model works well during regular business operations.

Curbside Model

Meal-kits have a significant advantage over grocery retailers because of their utilization of the *pull* method. Meal-kit customers order their boxes well in advance, which allows meal-kit companies to know exactly what their customers want before they buy it. Grocery retailers could learn from this model and implement a partial "pull" logistics strategy during times of profound crisis. This strategy would require customers to place orders for items three to five days ahead of time, with the concession that earlier orders have a higher likelihood of being fulfilled. To limit panic buying, restrictions on per-customer quantities would be put in place, and customers would have to be willing to accept substitutions. These substitutions could include different brands of the same product or similar produce.

Meal-kit companies use substitutions as a way to deliver full boxes to their customers. Although it is not ideal, it still allows customers to enjoy their meals without having to go to the grocery store. Providing customers with advance order options could come in the form of curbside pickup or delivery. Curbside pickup eliminates many of the costs associated with the last mile in grocery, but it does not offer the convenience of home delivery. Regardless of the

method chosen, both options remove the perception of empty shelves and instead focus on the availability of the items. This strategy would also eliminate or largely reduce the need for customers to travel from store to store looking for items that are unavailable at their local store.

Over-Buying

HelloFresh is driven by a single-minded mission of achieving a 100% service level, which enables them to purchase more inventory than necessary, regardless of the cost or potential for waste. Unlike meal-kits, grocery stores carry a vast array of products. However, in anticipation of supply chain disruptions, historical data could be used to identify which shelf-stable products are likely to experience increased demand. These items can be over-purchased to compensate for the spike in demand. Unlike frozen or perishable items, shelf-stable products require minimal handling and storage, making them easier to inventory. Nonetheless, the strategy would require significant storage space, which is a costly and time-consuming modification. To create more space, low-priority shelf-stable products may have their orders reduced or eliminated, allowing for higher-priority items to take up more space. However, this approach carries significant risk as grocery stores operate under a *push* model and must predict consumer demand and volume.

CONCLUSIONS

During the COVID-19 pandemic, both grocery retailers and meal-kits faced significant challenges in responding to rapidly changing demand. Despite having systems in place to protect their supply chains, grocery retailers faced shortages induced by consumer behavior, which was a rare occurrence for an industry that has consistently supplied shelf-stable and perishable items through numerous supply chain crises and natural disasters. This highlights the strength of the grocery chain, which has endured for over a century. However, it is important for grocery retailers to have an action plan and procedures in place in case of similar catastrophes.

On the other hand, meal-kit demand escalated during the pandemic, and their standard business model allowed them to respond accordingly. While grocery retailers cannot operate like meal-kits, they can still learn from them, particularly in areas such as demand planning and protein supply, which would help insulate their supply chain in the event of a similar crisis.

REFERENCES

[1] Aday, S., & Aday, M. S. (2020). Impact of COVID-19 on the food supply chain. Food Quality and Safety, 4(4), 167-180.

[2] Niemeier, S., Zocchi, A., & Catena, M. (2013). Reshaping retail: Why technology is transforming the industry and how to win in the new consumer driven world. John Wiley & Sons.

[3] Aull, B., Coggins, B., Kohli, S., & Marohn, E. (2022, August 15). The state of grocery in North America. McKinsey & Company. Retrieved March 23, 2023, from

https://www.mckinsey.com/industries/retail/our-insights/the-state-of-grocery-in-north-america-2022
[4] Borens, M., Gatzer, S., Magnin, C., & Timelin, B. (2022, September 7). Reducing Food Loss: What grocery retailers and manufacturers can do. McKinsey & Company. Retrieved March 18, 2023, from https://www.mckinsey.com/industries/consumer-packaged-goods/our-insights/reducing-food-loss-what-grocery-retailers-and-manufacturers-can-do
[5] Buzby, J. C., Farah-Wells, H., & Hyman, J. (2014). The estimated amount, value, and calories of postharvest food losses at the retail and consumer levels in the United States. USDA-ERS Economic Information Bulletin, (121).
[6] Siroli, L., Patrignani, F., Serrazanetti, D. I., Chiavari, C., Benevelli, M., Grazia, L., & Lanciotti, R. (2017). Survival of spoilage and pathogenic microorganisms on cardboard and plastic packaging materials. Frontiers in microbiology, 2606.
[7] U.S. Highbush Blueberry Council. (2022, April 26). Seasonality of Blueberries. Blueberry.org. Retrieved October 18, 2022, from https://blueberry.org/about-blueberries/seasonality/
[8] Jennings, R. Sr. Director, Procurement Operations. HelloFresh. (2022, May 6). Personal Communication
[9] Yorzyk, J. Sr. Director, Sustainability. HelloFresh. (2022, April7). Personal Communication
[10] Cicinelli, M. VP Operations and Technology. HelloFresh. (2022, June 3). Personal Communication
[11] O'Connor, J. Supply Chain Process Change Manager. Kroger (2022, April 18). Personal Communication
[12] White, N. (2022, May 5). Personal Communication
[13] Dolan, S. (2022, April 15). Last Mile Delivery Logistics explained: Problems & Solutions. Insider Intelligence. Retrieved April 15, 2023, from https://www.insiderintelligence.com/insights/last-mile-delivery-shipping-explained/#:~:text=As%20a%20share%20of%20the,partners%20to%20shoulder%20the%20cost.
[14] Heard, B. R., Bandekar, M., Vassar, B., & Miller, S. A. (2019). Comparison of life cycle environmental impacts from meal-kits and grocery store meals. Resources, Conservation and Recycling, 147, 189-200.

LS-GO02

Logistical Challenges to Deliver in the Last Mile for Consumer, Furniture, and Military including White Glove Services

S. Paul Singh, Ph.D.[1,2], Kevin D. Smith [1,3]

[1,2]*Professor Emeritus MSU, President PFA Inc.*
[2,3]*HQ Marine Corps, Installations & Logistics, Force Development Section*

***Correspondence to**:* Kevin D. Smith. *HQ Marine Corps, Installations & Logistics, Force Development Section*
E-mail: mgysgt.k.d.smith@gmail.com

ABSTRACT: This research will share "Last Mile" logistical challenges within the global Supply Chain caused by the COVID-19 pandemic. With the movement of consumer goods and military supplies, distribution of packaged goods, food, furniture, medical supplies, and pharmaceuticals, including White Glove Services. Therefore, innovative technologies and functions are required to provide end users with systems that enable successful delivery.

While transportation systems, autonomous delivery, and packaging methods have significantly improved. Truck, rail, ship, and aircraft movement of unitized loads as well as single parcel have significantly improved with continuous improvement in both cost and time efficiencies. Manufacturers and vendors can support their customers efficiently, employing a "Just-in-Time" coordination strategy referred to as the last mile. From delivering office electronics like servers and computers, home, or office furniture like beds, filing cabinets, medical and hospital equipment, as well as replacement and replenishment for military operations in an an active environment for the warfighter mat also require special handling expected of individuals delivering the products.

The physical and logistical challenges facing the last mile are complex for consumers and the military community. We will share why logistics and supply chain are critical to developing, designing, and delivering packaging products that meet the last mile supply chain system.

This paper discusses freight and delivery as well as services offered by companies called white glove and are expected by consumers or consignees. These are challenging conditions and include taxation as well as time spent by a delivery entity.

Goal: The speakers will cover a closer look at the challenges and where future research needs to cover a better understanding for the Transportation and Packaging companies.

INTRODUCTION

This paper provides challenges that face the fastest growing segment of the transportation and logistical companies. With a sharp growth in e-commerce both in the B2B and B2C customers, shippers are being faced with providing service in addition to just delivering a package or product itself across the front door. This clearly has set a higher demand for on-time delivery and in addition challenges companies face with taxation for e-shipments as well as assembly and minor installation. Therefore, there has been several hundred thousand companies that have been formed with a single delivery vehicle (truck or van) and 2-3 employees, one focusing on orders and the other two doing deliveries from groceries to appliances (refrigerators, washing machines, etc.) to furniture (beds, mattresses, dining tables, etc.) and this demand has sharply changed the way the old trucking companies and carriers have followed to provide this service with major shipping partners and building trust and loyalty with consumers.

While this type of high level service has existed before the last two years has shown a sharp growth and an increase in such service providers in the transportation environment in United States, Europe and Asia. Most of our work and presentation will share the trends, limitations and success of new enterprises, and a desire from the government and taxation agencies to impose sales and service tax on these operations, we will also share the last mile delivery in the military. With increased deployment of equipment globally with recent wars as well as major disasters from typhoon and earthquakes, shipments of replacement parts as well as humanitarian missions have challenged the US military to deliver in a harsh environment. These things range from blood and tissue in temperature controlled conditions and engines for a tank or helicopter in remote locations far from major distribution centers and help finish the installation and implementation of the product.

NEW TERMINOLOGY AND EMERGING TRENDS

While the terms such as “TRANSPORTATION” and “COMMON CARRIER” had existed for several centuries and were incorporated first incorporated into law in the United States over 200 years ago, new terms such as “last mile delivery” and “white glove delivery” have been more pronounced in the past two decades. So in this section we will cover these terms and their meaning as stated by various new businesses and what the US and state governments are interpreting.

One has to be careful not to consider two of the world’s largest trucking companies (FedEx and UPS) to be leaders of the last mile or white glove delivery. Both these companies are single parcel delivery companies that have grown exponentially since the 1990’s but while they have had or still operate smaller freight delivery services (FedEX Custom Critical, FedEx Freight) they truly deliver small packages weighing 150 lb. or less to the **doorstep or mailbox,** and their core parcel delivery business performs no assembly. They also do not cross the threshold of the front door to deliver, assemble and retrieve any packaging materials, as well as older or replaced product. The weights of products may range up to a 1000 lb. or more.

Listed below are key definitions and interpretations and the authors give credits to various new businesses and their blogs and white papers showing the distinction of these emerging markets.

Last Mile

In the business world, "Last Mile" refers to the last stage in a process, especially of a customer buying goods. When it is used in the context of transportation, supply chain, manufacturing, and retailing, the last mile is used to describe the **delivery of products the last leg of transportation.** This often means entering a home or office and for example delivering a mattress in the bedroom and also assembling the frame, placing the mattress on it, placing a head-board and finally removing all packaging as well as the old bed.

In supply chain management and transportation planning, the **last mile** is the last leg of a journey comprising the movement of people and goods from a transportation hub to a final destination. "Last mile" was adopted from the telecommunications industry which faced difficulty connecting individual homes to the main telecommunications network. Similarly, in supply chain management last-mile describes the difficult last part in the transportation of people and packages from hubs to final destinations. Last-mile delivery is an increasingly studied field as the number of business-to-consumer (b2c) deliveries grow especially from e-commerce companies in freight transportation, and ride-sharing companies in personal transportation. Some challenges of last-mile delivery include higher costs, ensuring complete visibility and transparency, increasing efficiency, and improving infrastructure with better equipment. Also the new players are regional usually serving major cities with large population density where both use of e-commerce purchases and use of personal vehicles for shopping and bringing goods home is scarce.

Due in part to demand on retailers and product manufacturers to provide expedited (same and next day) deliveries, tech-enabled last-mile technology platforms have emerged. Increased demand for last-mile fulfillment has put pressure on shippers to manage many types of delivery companies, which range from traditional parcel carriers, to couriers, to on-demand service providers that execute an "Uber for delivery" model utilizing contractors.

Matching the supply of delivery with the demand that has been created by shippers is a problem that is being addressed by several last-mile technology platforms. These companies connect shippers to delivery service providers to facilitate final mile deliveries. These last-mile technology platforms allow real-time data to be received by the shipper and the receiver which enables managers to act immediately when exceptions such as late delivery, address error, or product damage occurs.

As Amazon strengthens its last-mile logistics capabilities, competing retailers have become more interested than ever in last-mile technologies to compete. The fear of Amazon shutting it's parcel delivery relationship with FedEx and building its own fleet of delivery vehicles as well as intermodal containers and trucks has compelled CEOs of major transportation and logistics companies to seek alternative strategies.

The authors of this paper had presented previously in IAPRI Conference in China on the use of new transport technologies using drones and robots for both commercial and military applications for the last mile. So while the drones and robots may be more efficient in getting

products in remote and hard to reach places, they cannot deliver the final mile white glove service effectively as required by a sensitive consumer that also like removal of materials and old product, minor assembly and installation and accessing the entrance and delivering in a sensitive area like a kitchen, bathroom or bedroom. However, in general this delivery and service has increased the number of specialty robots and other delivery methods including drones.

Figure 1. A sidewalk robot made by Starship is shown delivering food to students at Oregon State University campus

A number of companies are actively using small delivery robots to do the last-mile delivery of small packages such as food and groceries just using the pedestrian areas of the road and travelling at speed comparable with a fast walking pace, companies actively delivering include

A **delivery robot** is an autonomous robot that provides "last mile" delivery services. An operator may monitor and take control of the robot remotely in certain situations that the robot cannot resolve by itself such as when it is stuck in an obstacle. Delivery robots can be used in different settings such as food delivery, package delivery, hospital delivery, and room service.

Being autonomous, the delivery robots primarily interact with the general public without the assistance of a human operator, in both positive and negative encounters. The delivery robot manufacturer Starship Technologies has reported that people kick their robots. However, the vast majority of human interactions are positive, and many people have anthropomorphized the robots due to their appearance. This has led to encounters where people feel a sense of caring towards the robots, assisting the robots when they are stuck, worrying for the robots on their journeys, or praising or thanking robots for their delivery service.

IMPORTANCE OF WHITE MILE (WHITE GLOVE AND LAST MILE) SERVICE

Sensitive shipments require extra care and detailed communication. Whether it's an important time-sensitive product launch of a new electronic device or phone, a critical medical equipment delivery to a hospital or a specialized home furniture or appliance delivery, ArcBest® offers customized final-mile services as a solution to complex **because the Final Mile is the Most Important.** Sensitive shipments require extra care and detailed communication. Whether it's an important time-sensitive product launch, a critical medical equipment delivery or a specialized home delivery, ArcBest® a division of ABF Freightways a major LTL company in the US offers customized final-mile services as a solution to complex shipping challenges. shipping challenges.

Difference between Last (final) Mile and White Glove Delivery

In terms of logistics, the "Last Mile" or "Final Mile" delivery service handles large and bulky freight during the last or "final mile" of the supply chain. "White Glove" refers to the handling and delivery of product into the home or office of a customer, including light assembly and experience.debris and packaging materials removal.

That's not easy when the final **mile is often the most expensive piece in** your transportation puzzle – as much as **53 percent of your transportation cost.**

"Logistics and delivery providers are trying to meet the growing demand for competitive omnichannel delivery services demanded by shippers and end customers, including same-day delivery, ship-from-store, and returns. These require greater speed, and agility, and often a restructuring of resources, technologies and operational processes," according to the **2022 State of Last Mile Logistics report.** Let's examine final mile logistics and final mile delivery more closely and identify solutions that can help improve the last mile stage in your freight transportation.

While final mile logistics and related shipping services have long been a staple of the modern transportation process, they are becoming more critical and in demand. Final mile delivery, or last mile delivery, is the final step in a freight shipment's journey to a customer. Demands on this last leg of a freight shipment journey are increasing, and so, too, is the complexity. You can attribute this uptick to several factors that are directly impacting commercial and residential final-mile delivery:

- The e-commerce shipping demands fueled by online purchasing increased significantly since 2020, driving up final-mile shipping demand exponentially.
- The demand for faster, more reliable tracking and monitoring of final-mile deliveries continues to increase with better **freight market insights.**
- Fears are decreasing around online orders delivered to home doorsteps or shipments that require set-up, installation, or other white-glove services.
- Direct-to-consumer shipping skips many of the usual intermediaries and has significantly impacted shippers' parcel management and final-mile logistics.
- More shippers are looking to improve brand image by shifting to more sustainable options such as final-mile tracking, load sharing, and local shipping services.

Best Suited for for Niche Markets

Today, final-mile delivery tracking and shipping optimization are integral to **supply chain visibility** and operations. Advances in final-mile handoffs promote increased access to multi-metric performance for the parcel, truckload, less-than-truckload (LTL), premium shipping services, final-mile number tracking, and more. Shippers can also enjoy an increase in overall shipping services, especially for those dealing with niche-focused shipping and highly-personalized shipping options.

E-commerce is transforming nearly every aspect of the shipping and logistics industries regarding the final mile. Because of this, the ability to pair custom last-mile delivery options with niche market needs and considerations is vital. Customer satisfaction is the top priority for shippers, and enhanced final-mile tracking and logistics make niche market management easier from start to finish.

Using Shipment Visibility To Improve Customer Experience

At the heart of improved delivery services lies enhanced data collection and analysis. Final-mile ***delivery tracking directly impacts customer experience*** and loyalty: stellar services and experiences mean return customers and a better reputation within the industry.

CONCLUSIONS

Speedy order fulfillment and distribution are no longer just part of shoppers' wish lists. The needs of consumers especially for B2C have changed especially after COVID-19 and online sales and e-commerce has expanded both product categories and services along with delivery and complete tracking visibility.

Consumers these days expect fast and reliable shipping every time they shop online. Even in B2B sales, customers are increasingly expecting the kinds of experiences they get from B2C channels. Retailers and last mile delivery companies need to provide consumers with multiple shipping options and affordable last mile delivery rates to combat the ever-looming threat of giants like Amazon Prime, AliBaba and Walmart.

In addition, there are new players in the block of last mile and white glove delivery that are regional and critical to a shipper or carrier.

ACKNOWLEDGEMENTS AND REFERENCES

The authors would like to thank over 200 reference blogs and white papers available on the web that were used to provide an insight into this fast growing segment and the California Board of Taxation and Revenue where Dr. Singh testified as an expert for a major e-commerce case on new tax laws for white glove delivery. For a list of references please contact the author due to the large number of reviews it will be electronically sent.

CONFERENCE PROCEEDINGS

PACKAGING FOR FOOD AND AGRICULTURE

ORAL PRESENTATION

GENERAL STREAM

PF-GO01

Use of waxes and rubbers to create SUPD-compliant coated packaging

Akansha Singh[1], Lauri K.J. Hauru[1], Mika Vähä-Nissi*[1]

[1]*VTT, Tietotie 4E, Otaniemi, Espoo, Finland - Finland*

***Correspondence to**: Mika Vähä-Nissi, Tietotie 4 E, FI-02150 Espoo, Finland.*
E-mail: mika.vaha-nissi@vtt.fi

ABSTRACT: The Single-Use Plastics Directive, or SUPD came into force on 3 July 2021 in the European Union in 2021. The main goal of the SUPD is to reduce the amount of plastic waste in the environment, especially the marine environment. SUPD restricts material choice in cotton bud sticks, cutlery, plates, straws, stirrers, sticks for balloons, cups, food and beverage containers. Synthetic polymers and oxo-degradable plastics are forbidden. This work was performed to create and assess SUPD-compliant natural options available to replace these plastics. Waxes and rubbers are some of the most common naturally available materials which impart water vapor and oxygen barrier properties. Different waxes - rice bran, carnauba, rapeseed, beeswax and rubbers - caoutchouc, guayule and chicle - and their combinations were tested in different ratios. They were coated on paperboard using different techniques like dispersion coating, hot melting coating in single and multilayer forms and their barrier properties were measured. The key target of this research was to identify the best options which can provide barrier properties, heat sealability and good printability. Out of the various options tested, rice bran wax provided a good moisture barrier whereas rubber helped in providing heat-sealability and a printable surface. A water vapor transmission rate (WVTR) in the range of 3-5 gm/m2/24 hr at 23 °C and 50% relative humidity was achieved with a multilayer product.

Keywords: barrier paper; multilayer structure; wax coating; rubber coating; water vapor barrier; oxygen barrier; cold sealing; coat weight

INTRODUCTION

Single-use plastic directive (SUPD) is legislation which aims to reduce the impact of plastic products on environment especially in the marine environment.[1] These include plastic straws, plastic cutlery, cotton swabs, balloon sticks, food, beverage containers made from expanded polystyrene and many more. The directive was passed on June 2019 and came into force on 3rd July 2021. Plastics are widely used in varied applications in food packaging. Due to their tendency to not biodegrade and poor recyclability, this has led to land and marine pollution.[2] SUPD sets limits on the alternatives which can be used as a replacement for the banned products. Either a monomeric or naturally polymerized items can be used to create an alternatives. There are several natural polymers available but very few of them provide the

required properties for the end use applications like strength, barrier, and optical properties. Natural waxes are non-polymeric mixtures of organic compounds mainly esters of fatty acids and fatty alcohols. They have been widely used in different applications like food, packaging, cosmetics, polishes etc.[3] However, utilization of waxes in packaging industry as a standalone product is very limited. The low melting point and lacking water vapor barrier properties have limited the use of waxes in packaging application. We have studied here the potential of the natural waxes and rubbers in packaging application specially with respect to water vapor transmission rate (WVTR) barrier properties. Natural waxes are widely available and can be potentially used in creating alternatives for plastic coated products.

METHODS

In this study we have studied different waxes and rubbers from varied sources and assessed their barrier properties with respect to creating a moisture barrier. Commercial waxes, both in solid and dispersion forms, were coated on a paper substrate. Beeswax, carnauba wax, anionic and cationic rapeseed wax, rice bran wax and four mixed wax products of proprietary composition (100, 200, RD22A and RD22B) were used. Two different coating methods were used in this study: dispersion coating and hot melt coating.

Dispersion coatings were done on 210 g/m2 paper board using an Erichsen coater (model no. 509/15). The commercial wax dispersion was coated on a paperboard substrate (Metsä Board Prime FBB Bright) at different grammages using a spiral drawdown rod (10-60 µm). The paperboards were then dried in oven at 120 °C for 5 mins for further analysis.

Hot melt coatings were done on the same paperboard using a spiral draw down rod (10-30 µm) in the heated environment of an oven. The temperature of the oven was kept at 120 °C. The paper was clamped to a metal plate and kept in the oven for heating at 120 °C along with the draw down rod. All the equipment was heated for 5 minutes in the oven. The melted wax was poured on the paper sheets and metered using draw down rod. The coated sheet was then brought at room temperature and allowed to cool down to create a coating layer on the paper.

Nanocellulose was made by enzymatic treatment followed by two passes of fluidization with Microfluidics Microfluidizer Processor M-110EH. Nanocellulose coating was done with Erichsen coater using a draw down rod (200 µm).

After the coating process, the coated paper samples were conditioned for 24 h at 23 °C and 50% RH. After conditioning, coating grammage, paper thickness and WVTR was measured. Water vapor transmission rate was measured using a Mocon device (MOCON PERMATRAN-W 3/34) at 23 °C and 50% RH.

RESULTS AND DISCUSSION

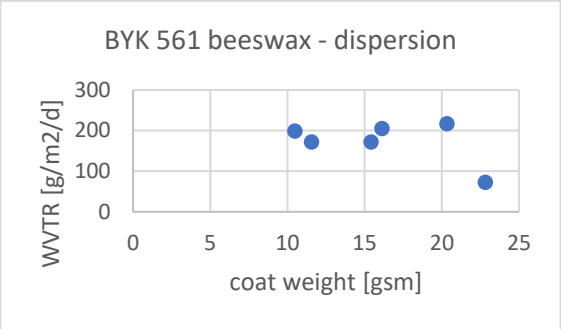

Figure 1 Bees wax

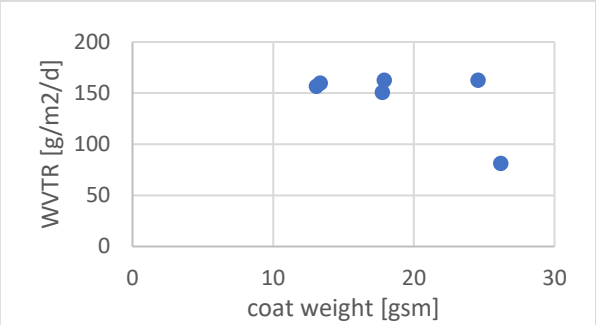

Figure 2 Carnauba wax

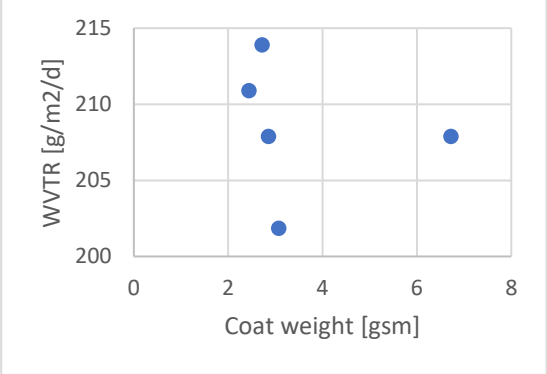

Figure 3 Rapeseed wax anionic emulsion

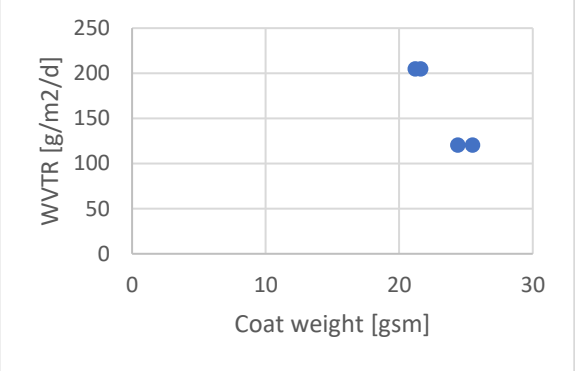

Figure 4 Rapeseed wax cationic emulsion

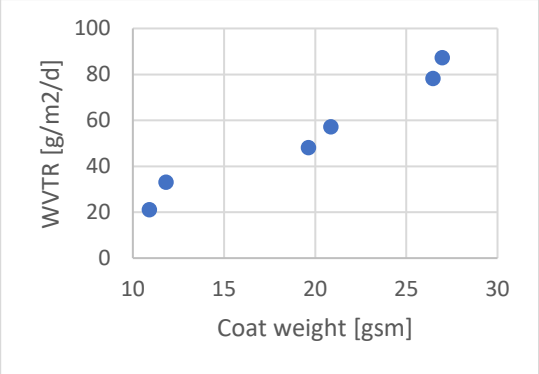

Figure 5 Proprietary wax 100

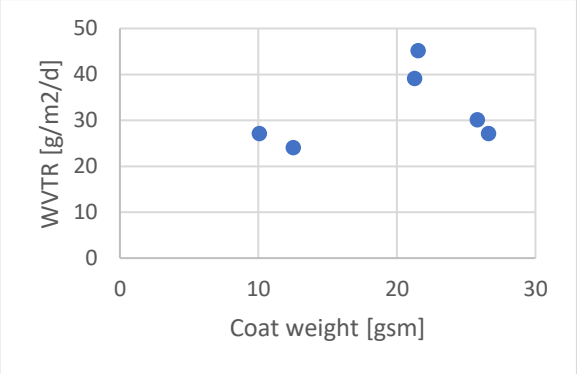

Figure 6 Proprietary wax 200

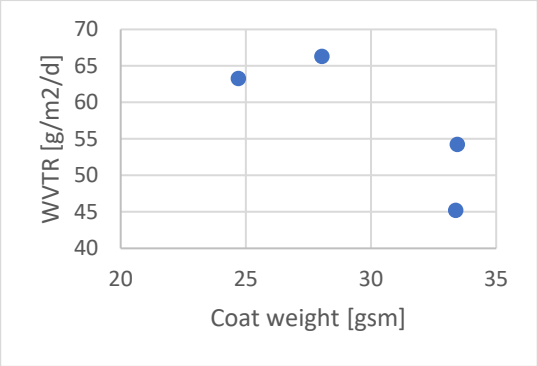

Figure 7 Proprietary wax RD22A

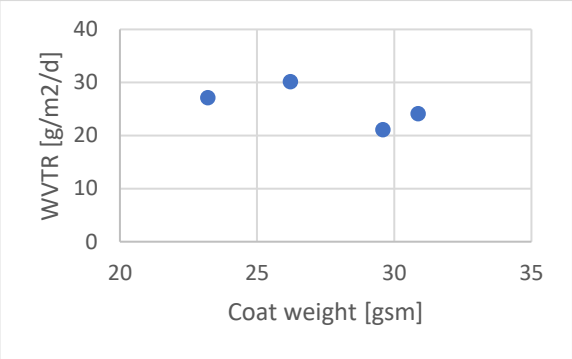

Figure 8 Proprietary wax RD22b

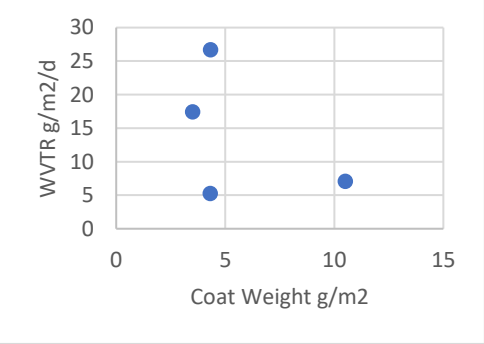

Figure 9 Rice bran wax

Beeswax, carnauba, rapeseed, rice bran and proprietary waxes coating showed different barrier water vapor barrier properties (Figure 1-8). Amongst all the waxes coated, the best properties were delivered by rice bran wax (Figure 9), followed by proprietary wax 100 and 200 (Figure 5 and Figure 6). Rice bran wax gave the best WVTR of 5 g/m2/d at a lowest coat weight of 5 g/m2, whereas proprietary wax 100 provided a good WVTR in the range of 20.25 g/m2/d. Beeswax (Figure 1), carnauba (Figure 2), rapeseed (Figure 3, Figure 4) and RD22A & RD22B (Figure 7 and Figure 8) provide a mediocre WVTR ranging between 60-220 g/m2/d. There was no obvious correlation in coat weight and water vapor barrier in general. This might be due to the low melting point of waxes which creates a sensitive coated surface which is prone to any surface damage. The coating was deformed with the slightest touch with proprietary waxes 100, 200, RD22A and RD22B.

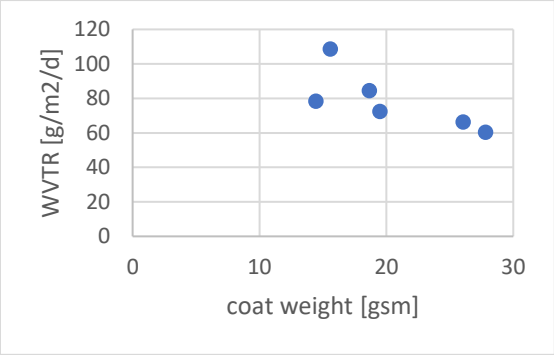

Figure 10 Rubber + wax (50:50)

Wax coated paper cannot be printed. Unvulcanized natural rubber is hydrophobic and sticky, which can enhance the surface properties when mixed with waxes. Proprietary wax 100 provided a good water vapor barrier and so it was selected to be mixed with rubber emulsion to see the impact on the barrier and printing properties. The wax and rubber were mixed in 50:50 ratio and coated on paper. The barrier measurements showed that with the addition of rubber emulsion, the water vapor barrier performance was reduced from 21 g/m2/day to 60 g/m2/d (Figure 10). Though the barrier properties achieved were mediocre, added rubber enhanced the surface properties and provided a printable surface along with a cold sealing property. Natural rubber (caoutchouc from *Hevea brasiliensis*) contains allergenic proteins, which render them unsuitable for the food and beverage packaging application.[4] However, these can be removed with a purification process such as the Vytex technology.[5] The rubber emulsion used in our experiments has been certified as non-allergenic and thus could be used in packaging applications for food and beverages.

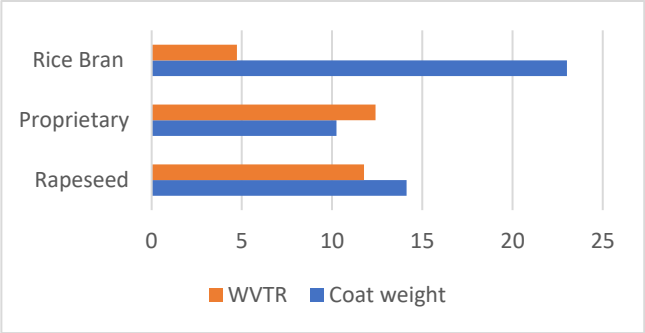

Figure 11 Comparison of the best hot melt coating results for each wax

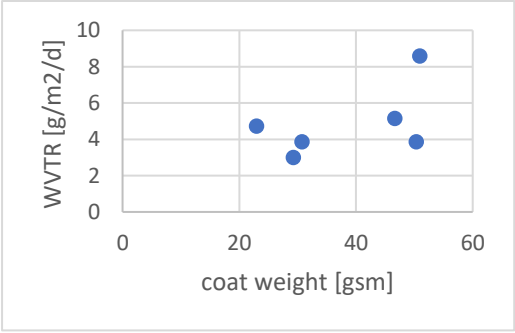

Figure 12 Water vapor transmission vs. coat weight for hot melt-coated rice bran wax

Hot melt coating provided comparatively better results when compared to their respective dispersions (Figure 11). At higher coat weights, the water vapor barrier performance can be seen deteriorating (Figure 12). This is due to the brittleness of film which has a higher to tendency to crack when the coat weight increases. This leads to creation of paths for gases to

penetrate, which reduces the barrier performance of film. Rice bran wax provides good water vapor barrier both in dispersion as well as hot melt coating at same coat weight.

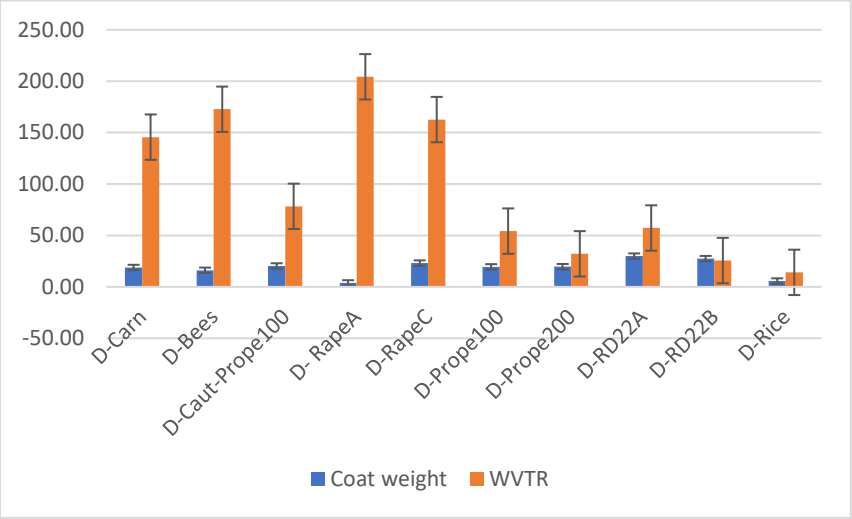

Figure 13 Comparison of different waxes as dispersion coatings

Different waxes provided different water vapor barrier properties at varied coat weight. The best performance was achieved from rice bran wax both in dispersion and hot melt coating of 5 g/m2/d at 5 g/m2 coat weight and 4.73 g/m2/day at 23 g/m2 (Figure 13), respectively. In general, the hot melt coatings provide better barrier properties in comparison to dispersion coating. It is difficult to achieve low coat weight by hot melt application, and at high coat weights the films tend to crack which makes it a challenging option. Dispersion coating is preferred for barrier application as it can provide a comparatively a lower coat weight and the film coated is less brittle compared to hot melt coatings.

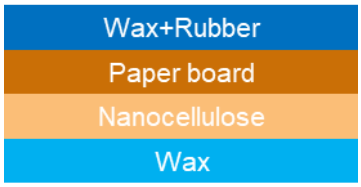

Figure 14 Multilayer structure

A multilayer structure was created to provide an overall moisture and oxygen barrier properties (Figure 14). It also had a printable top surface with a sealing strength. The top side of the paperboard was coated with a mixture of wax and rubber dispersion (50:50) which provides it a moisture barrier, a printable surface and sealing properties. The bottom layer of the paperboard was coated with nanocellulose to provide an oxygen barrier. Since nanocellulose is sensitive to moisture, it can be deteriorated by water, which reduces its oxygen barrier properties. Therefore, the nanocellulose was coated with wax as a protective layer for the moisture penetration.

CONCLUSION

Rice bran wax provides an excellent performance in providing a good water vapor barrier when compared to other natural waxes tested. It provides a good WVTR both in dispersion and hot melt coating in the range of 5 g/m2/day and 4.31 g/m2/day at coat weights of 5 and 23 g/m2, respectively. Generally, hot melt coatings provide a better water vapor barrier compared to dispersion coatings but achieving a lower coat weight is a challenge with hot melt coating. Higher coat weights do not improve the barrier properties in hot melt coatings. This is due to the brittleness of the film, which at high coat weight has a tendency to crack and create paths for gases to penetrate. Based on the properties achieved from rice bran wax, it could potentially replace plastic coating in cold food and beverage packaging solutions. The rubber and wax coating could also be used in packaging dry food as it provides good barrier, sealing and printing properties.

REFERENCES

1. European Union. Directive (EU) 2019/904 of the European Parliament and of the Council of 5 June 2019 on the reduction of the impact of certain plastic products on the environment. European Union. 2019.
2. Ritchie H, Roser M. Plastic pollution. https://ourworldindata.org/plastic-pollution
3. Krendlinger EJ, Wolfmeier UH. *Natural and Synthetic Waxes: Origin, Production, Technology, and Applications*. John Wiley & Sons; 2022.
4. Wagner S, Breiteneder H. Hevea brasiliensis latex allergens: current panel and clinical relevance. *International archives of allergy and immunology*. 2005;136(1):90-97.
5. Swansona M. Vytex® Natural Rubber Latex: An Eco-Friendly Alternative Raw Material.

PF-GO02

Microperforated PBAT/PLA Film with Enhanced Gas Transmission Rate for Packaging of Fresh Produce

Pichamon Sungdech[1], Vanee Chonhenchob[1], Charinee Winotapun[2] and Pattarin Leelaphiwat*[1]

[1]*Department of Packaging and Materials Technology, Faculty of Agro-Industry, Kasetsart University Bangkok, 10900 Thailand*
[2]*National Metal and Materials Technology Center, National Science and Technology Development Agency, Thailand Science Park, Pathum Thani, 12120 Thailand*

***Correspondence to:** Pattarin Leelaphiwat, Department of Packaging and Materials Technology, Faculty of Agro-Industry, Kasetsart University Bangkok, 10900 Thailand, pattarin.le@ku.ac.th*

ABSTRACT: Polybutyrate adipate terephthalate (PBAT), a biodegradable polymer with similar qualities to petrochemical-based polymers, is one of the promising material options for replacing single-use plastics. However, high production costs and poor mechanical qualities limit the application of this sustainable material. In this study, PLA (20 wt%) was blended with PBAT to increase mechanical characteristics and blown film processability. In addition, the PBAT/PLA film had a low gas transmission rate, limiting its use in packaging applications, especially for fresh produce. The laser microperforation technology was used to create a microperforated PBAT/PLA film with a wavelength of 10.2 μm, a laser frequency of 500 Hz, and a web speed of 10 m/min. The size and shape of holes on the PBAT/PLA film were observed using an optical microscope. The static method was used to measure the oxygen and carbon dioxide transmission rates of the films at 25 °C. Microholes were discovered to be formed at perforation thresholds of 92.4 J/cm^2. The microhole diameter increased from 84.82 to 209.74 μm as the laser density increased from 92.4 to 369.8 J/cm^2. The results showed that the gas transmission rates of the film increased with the number and diameter of microholes. The laser perforation appears to be a useful strategy for increasing the gas transmission rates of biodegradable film used for packaging fresh fruit.

Keywords: Polybutyrate adipate terephthalate; Polylactic acid; Microperforation; Gas transmission rate; Fresh produce

INTRODUCTION

Fruits are an important agricultural crop in Thailand's economy, earning significant revenue for the country. Thailand is the foremost producer and exporter of the most important and well-known tropical fruits in the ASEAN region. Fruit exports are frequently susceptible to various types of quality loss, such as decay. Internal factors, such as the respiration of the harvested

product, alter the flavor and expiration life of the produce. Changes in chemical composition and external factors such as temperature, gas composition in packaging, film permeability property, etc.

Consequently, packaging is critical for delaying produce deterioration, and polyethylene film is widely utilized in the sector since it allows gas to permeate well. The petroleum-based films, on the other hand, have insufficient gas permeability, especially for the high respiration rate produce. The oxygen within the package will be consumed and carbon dioxide will be produced by the produce, resulting in a lack of oxygen and carbon dioxide accumulation within the package, leading to anaerobic respiration and product deterioration. Furthermore, people are becoming increasingly concerned about the environment, which is contributing to a movement toward global conservation or environmentally friendly packaging. ~~Therefore, an enhanced gas tr~~ansmission rate for the packaging of fresh produce is necessary.

Microperforion is one technique for generating the equilibrium modified atmosphere (EMA), and micron-punctured technology is a useful technique that can improve the gas exchange of packaging films via single or multiple micron perforations that allow high-rate real-time gas exchange between the internal and external environments of the package[1]. Which avoids the formation of an anaerobic state. especially in produce with a high respiration rate. The factor affecting the gas permeability of microperforated film is the number and size of holes. The previous works revealed that an equilibrium modified atmosphere inside the package could be achieved in a microperforated film with 6 microholes (~50 μm diameter of each hole) for keeping the freshness quality of strawberries[2-3]. The levels of O_2 and CO_2 were equilibrated at 8% and 9%, respectively. The microperforated PET/PE film with a hole size of 113.5 μm could keep fresh-cut durian fresh. They found that the optimal amounts of 13% O_2 and 17% CO_2 inside the package were the best for preserving the freshness quality of durian for eight days at 8 °C. The appearance and firmness of the durian packed in the microperforated film were good throughout the storage duration. Subsequently, it was demonstrated that microperforated film could possibly be used as the packaging film for airfreighting fresh-cut durian from Southeast Asia to Europe[4]. Microperforated polylactic acid (PLA) and polybutylene succinate (PBS) films were used for modified atmosphere packaging of baby corn. Using a CO_2 laser, PLA and PBS films were perforated effectively, and gas permeabilities improved as the number of microholes increased. O_2 concentrations in neat PLA and PBS films without microholes decreased rapidly and were close to 0% after one day of storage, whereas CO_2 concentrations increased by up to 40%. The weight of unpackaged baby corn decreased by more than 10% by the second day of storage. When packed in all microperforated biodegradable films at 15 °C, the baby corn retained freshness attributes for more than 7 days, with acceptable weight loss of less than 5% throughout the storage period[5-6]. It has been demonstrated that laser perforation is an effective method for increasing the gas permeability of PLA and PBS films and tailoring the oxygen and carbon dioxide transmission rates by varying the number of micro perforations.

There is limited information from previous research regarding the microperforated films for the biodegradable composite, which should influence the laser energy absorption during perforation. For instance, polybutyrate adipate terephthalate (PBAT) is its main chain, which makes it strong, durable, readily moldable, and extremely flexible. Since polybutyrate

adipate terephthalate (PBAT) has similar properties to low-density polyethylene, it is widely used in the production of various forms of films. Food packaging film, as well as packaging film, agricultural film, etc. However, high production costs and poor mechanical properties limit the application of this sustainable material; consequently, it is frequently blended with other polymers, such as polylactic acid (PLA), which not only reduces production costs but also improves the properties of composite plastics. This study aims to improve the gas transmission rate of biodegradable blends of polybutyrate adipate terephthalate (PBAT) and polylactic acid (PLA) for fresh produce packaging applications.

MATERIALS AND METHODS

Film preparation

Blown film extrusion

The PBAT/PLA blend was fabricated at the different weight ratio of 80:20, 60:40, 40:60 and 20:80 using a blown film extrusion (Haake PolyLab OS RheoDrive 7 Model, Germany) with a screw diameter of 29 mm, 25 L/D and a compression ratio of 3: 1. The mold diameter was 35 mm and the mold gap was 1 mm. The polymer was squeezed through the ring mold at a screw speed of 60 rpm for PLA. The tank temperature (zones 1–3) and the set temperature (zone 4) were 150 °C, 155 °C, 160 °C and 160 °C.

Laser drilling

A CO_2 laser (Synrad, Ti60 Model, USA) with a wavelength of 10.2 μm, a laser frequency of 500 Hz, and a web speed of 10 m/min, respectively, was used to perforate the selected ratio of PBAT/PLA film based on their mechanical properties. Various laser fluences of 92.4 to 369.8 J/cm^2, related to pulse durations of 50–200 μs, respectively were used to irradiate the plastic film at the focusing area.

Film characterization

Mechanical properties

The mechanical properties of the non-perforated PBAT/PLA films at different weight ratios were determined for at least five samples using a universal testing machine (Model 5943, Instron, USA) with a 100 N loadcell, a crosshead speed of 500 mm/min, and a gauge length of 50 mm modulus. Young's tensile strength and elongation at break were verified in accordance with ASTM D882-02.

Fourier-transform infrared spectroscopy (FTIR)

To calculate the absorbance coefficient of the non-perforated PBAT/PLA film at the weight ratio of 80:20, the amount of laser absorbance was measured from the absorbance spectra in FTIR spectra. (FTIR 100, Japan) with frequencies from 4000 to 400 cm^{-1}. The frequency band at 980 cm^{-1} corresponds to a CO_2 laser wavelength of 10.2 μm and an absorption coefficient α (cm^{-1}) was evaluated as follows:

$$I = I_0 exp^{-\alpha z} \quad (1)$$

$$\alpha = -\frac{1}{Z} \text{In} \frac{I}{I_0} \quad (2)$$

Differential scanning calorimetry (DSC)

The thermal properties of the non-perforated PBAT/PLA film at the weight ratio of 80:20 were examined using DSC (DSC1, Mettler Toledo, USA) from -80 to 200 °C with a heating rate of 10 °C /min for 5–8 mg samples. Tested under nitrogen gas flow, the degree of crystallinity (Xc) of the film was calculated using Equation (3):

$$\% \text{ Crystallinity} = \frac{\Delta H_m - \Delta H_{cc}}{\Delta H^\circ_m} \text{ x } 100 \quad (3)$$

where ΔHm, ΔHcc and ΔH°m is the enthalpy of melting. Enthalpy of cold crystallization and the melting enthalpy of 100% crystallinity, respectively. At least three samples were analyzed.

Thermogravimetric analysis (TGA)

The thermal degradation of the non-perforated PBAT/PLA film at the weight ratio of 80:20 was examined using TGA (TGA2, Mettler Toledo, USA). 8–10 mg samples were tested at a heating rate of 10 °C /min under a nitrogen gas flow from 30 °C up to 800 °C for three replications.

3D laser scanning confocal microscope

The surface morphology and polymer surface profile of the microholes on the film surface were observed using a laser scanning confocal microscope (LEXT OLS4100, Olympus, Japan), recording the microhole size, width, and volume loss. Volume loss describes the amount of material lost on the film surface during drilling for a single microhole. At least three samples were studied.

Gas transmission rate

The oxygen and carbon dioxide transmission rates of the microperforated PBAT/PLA (80:20) films were determined using static methods at 25 °C and 60% RH as described by micro level. A cylindrical acrylic container (test film area 103 cm^2) was set as the top lid of a cylindrical acrylic container (capacity 1,610 cm^2). An acrylic ring was placed on top of the film and clamped. Chamber with two gas valves (inlet and outlet for gas flushing) are regulated. A gas

mixture of 21% CO_2, 0% O_2 and 79% N_2 is introduced into the acrylic chamber with a gas flow rate of 250 cm^3/min for 6 hours to remove residual gas Then the inlet and outlet valves are closed. Gas samples were taken from a 6 cm^3 cylinder after 1 day by a gas analyzer (CheckMate II, MOCON Inc., USA). The oxygen and carbon dioxide values of gas transmission rates were calculated [7].

Statistical analysis

Data were presented as average ± standard deviation (n = 3) and calculated using Minitab software for Windows, version 21 by one-way analysis of variance (ANOVA) and post-hoc Tukey tests, with significant difference set at $p \leq 0.05$.

RESULTS AND DISCUSSION

Mechanical properties of non-perforated films

The mechanical properties of the non-perforated PBAT/PLA films were determined following ASTM standard D882-02. In Table 1, it is found that the PBAT/PLA film at the weight ratio of 80:20 had the highest tensile strength and elongation due to the addition of PLA which is formable using blow-film extrusion at 150/155/160/160 °C and a screw speed of 60 rpm.

Formulation	Tensile Strength (MPa)	Elongation at break (%)	Young's Modulus (MPa)
PBAT: PLA (80:20)	31.9 ± 2.9	377.3 ± 20.2	273.7 ± 21.1
PBAT: PLA (60:40)	25.6 ± 0.5	237.0 ± 21.8	394.1 ± 44.7
PBAT: PLA (40:60)	32.3 ± 1.4	9.4 ± 1.6	1009.9 ± 71.3
PBAT: PLA (20:80)	42.9 ± 2.3	3.1 ± 0.03	1375.1 ± 43.3

Table 1. Mechanical properties of the non-perforated PBAT/PLA films with different weight ratios.

Fourier-transform infrared spectroscopy (FTIR)

Because 10.2 μm is a relatively long wavelength, a photo-thermal mechanism including melting, decomposition and vaporization of the polymers was the main process. The absorption characteristics of PBAT/PLA films were analyzed using an FT-IR spectrometer, with the frequency band at 980 cm^{-1} attributed to the CO_2 laser wavelength of 10.2 μm. Fig. 1 shows the FTIR spectra of PBAT/PLA (80:20) films with a thickness of 30 μm. Based on the results, the absorbance at 980 cm^{-1} from the FTIR spectra was used to investigate the absorption coefficients of PBAT/PLA films using Eq (2). as 0.077247 cm^{-1}, respectively. These results suggested that PBAT/PLA (80:20) films absorbed the CO_2 laser in this region, resulting in thermal processes such as melting, decomposition and vaporization.

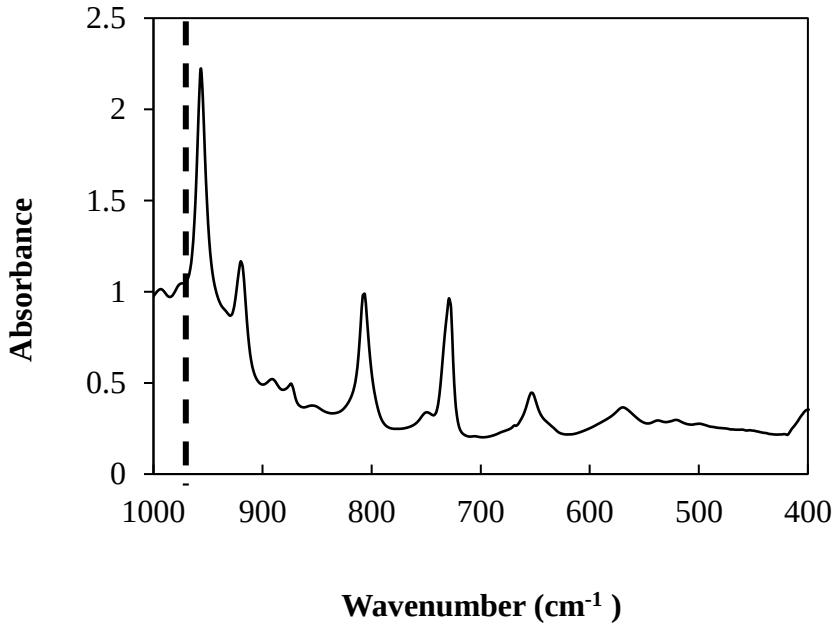

Figure 1. FTIR spectra of polybutyrate adipate terephthalate (PBAT)/ polylactic acid (PLA) (80:20)

Thermal properties (DSC and TGA)

Table 2. shows DSC thermograms of PBAT/ PLA (80:20) film presented as glass transition temperature (T_g), crystalline melting temperature (T_m) and cold crystallization temperature (T_{cc}). Thermal transition of PBAT/ PLA (80:20) film at 58 ± 33, 114 and 105 ± 9 °C and the crystallinity percentage (%) (△Hcc) using Eq (3). was 24 ± 3%.

Film	Glass transition temperature Tg (°C)	Cold crystallization temperature Tcc (°C)	Melting temperature Tm (°C)	Crystallinity percentage (%)	Decomposition temperature 5% loss (°C)
PBAT/ PLA (80:20)	58 ± 33	105 ± 9	114	24 ± 3	359 ± 5

Table 2. Thermal properties and calculated absorption coefficients of PBAT/PLA (80:20) film.

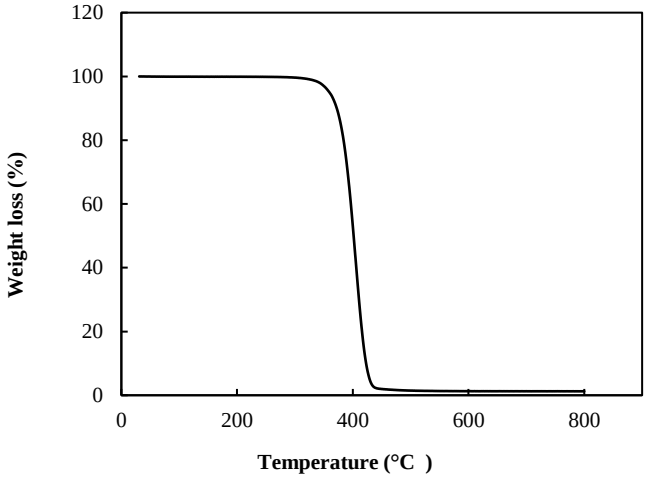

Figure 2. TGA thermogram of the polybutyrate adipate terephthalate (PBAT)/Polylactic acid (PLA) (80:20) film.

The TGA results showed that 5% weight loss of the initial mass occurred when the decomposition started. This value was observed in all samples at an average temperature of 359 °C as shown in Fig. 2.

Surface morphologies of microhole on the PBAT/PLA *film surface*

A microhole was initially detected on the PBAT/PLA (80:20) film surface at a laser fluence of 92.4 J/cm^2. Hole diameter and area increased with laser fluence. The polymer absorbed energy from the laser and melted as the surface temperature increased due to thermal conduction. Therefore, microhole diameter increased with increasing laser fluence. When laser irradiation on the PBAT/PLA (80:20) film increased from 92.4 to 369.8 J/cm^2, the microhole area on the PBAT/PLA (80:20) film surface increased from 7,720.66 ± 673.27 to 46,420.85 ± 3,854.11 μm^2.

The microhole appeared initially as an elliptical shape. The diameter of the microhole in the machine direction (MD) and transverse direction (TD) was determined, with results shown in Table 3. The aspect ratio (MD/TD) of hole diameter was higher than 1 with an increase in laser fluence because film web speed was run at 10 m/min while the laser head was fixed. The heat-affected zone on the focused film surface caused continuous heating in the film's moving direction, resulting in an elongated microhole. At a high laser fluence of 369.8 J/cm^2, equivalent to a pulse duration of 200 μs, the aspect ratio of the microhole was 1.33 while at a low laser fluence of 92.4 J/cm^2, corresponding to a pulse duration of 40 μs was 1.14, aspect ratios of microholes on the surface of the PBAT/PLA (80:20) film.

Energy density (J/cm^2)	Pulse duration	Hole area (µm^2)	Diameter in TD (µm)	Diameter in MD (µm)	Aspect ratio (MD/ TD)	%Volume loss
92.4	50	7,720.66 ± 673.27 ^{D}	84.82 ± 2.30 ^{D}	98.03 ± 2.90 ^{D}	1.15	1,112,849.80 ± 804812.21 ^{C}
184.9	100	19,374.53 ± 804.39 ^{C}	133.76 ± 3.83 ^{C}	181.07 ± 8.74 ^{C}	1.35	4,422,216.48 ± 197777.50 ^{BC}
277.4	150	31,709.34 ± 4,497.97^{B}	174.94 ± 23.92 ^{B}	223.18 ± 4.26 ^{B}	1.27	6,348,613.51 ± 1184642.26 ^{B}
369.8	200	46,420.85 ± 3,854.11^{A}	209.74 ± 8.93 ^{A}	280.16 ± 14.49 ^{A}	1.33	16,574,039.62 ± 2892282.80 ^{A}

Table 3. Hole area, diameter of microhole in the machine direction (MD) and transverse direction (TD), aspect ratio and %volume loss of the PBAT/PLA (80:20) film under various laser fluences.

Gas transmission rates

The oxygen and carbon dioxide compositions within the acrylic jar for the microperforated PBAT/PLA (80:20) films with 1 hole 100 pulse, 1 hole 150 pulse, 1 hole 200 pulse, 3 hole 200 pulse and 5 hole 200 pulse were obtained from the model under static method test conditions at a temperature of 25 °C. It was found that the oxygen and carbon dioxide transmission rates of the films increased with the number and diameter of microholes (Table 4 and 5). The highest gas transmission rate of the microperforated PBAT/PLA film was investigated for a 5 hole 200 pulse at the OTR of 1,530 ± 16 (cm^3/d) and CO_2TR of 1,430 ± 80 (cm^3/d), followed by a 3 hole 200 pulse, 1 hole 200 pulse, 1 hole 150 pulse and a 1 hole 100 pulse, respectively. Therefore, it can be concluded that increasing the duration of the pulse and the number of holes can enhance the gas transmission rate of the PBAT/PLA film. Typically, the beta value of fruit with a significant respiration rate is less than 1. However, the current market film has a beta of 3, which is unsuitable for fresh produce, whereas the beta of the microperforated PBAT/PLA films in this study ranges from 0.82 to 1.01. This indicates that the oxygen transmission rate was higher than the carbon dioxide transmission rate, making it adequate to be used to extend the shelf life of fresh produce.

Number of microhole	Pulse duration (μs)	Energy density (J/cm^2)	Average through-microhole area and diameter		
			MD (μm)	TD (μm)	Area (μm^2)
Control	-	-	-	-	-
1	100	184.9	180.43± 7^B	150.82±23^A	21,104.65±669^C
	150	277.4	214.12±12^B	172.65±7^A	35,005.51±1,717^B
	200	369.8	266.71±5^A	211.48±3^A	44,660.62±1,176^A
3	200	369.8	270.67±13^A	196.18±21^A	46,540.27±2,069^A
5	200	369.8	264.34±22^A	211.46±47^A	46,554.13±3,937^A

Table 4. Hole area, diameter of microhole in the machine direction (MD) and transverse direction (TD), aspect ratio and %volume loss of PBAT/PLA (80:20) films under various laser fluences.

Number of microhole	Pulse duration (μs)	Energy density (J/ cm^2)	Microholes		
			25 °C		
			OTR/ hole (cm^3 / d)	CO_2TR/ hole (cm^3 / d)	CO_2TR/OTR
Control	-	-	284 ± 11^B	226 ± 5^B	0.86
1	100	184.9	381 ± 18^A	356 ± 43^A	1.01
	150	277.4	582 ± 30^A	571 ± 83^A	0.98
	200	369.8	1296 ± 91^A	1068 ± 28^A	0.82
3	200	369.8	1309 ± 85^A	1231 ± 44^A	0.94
5	200	369.8	1530 ± 16^A	1430 ± 80^A	0.93

Table 5. Gas transmission rates of PBAT/PLA (80:20) films with various numbers of microholes.

CONCLUSION

The PBAT/PLA (80:20) films were effectively perforated using a CO_2 laser with a 10.2 μm wavelength and pulse fluences of 92.4 to 369.8 J/cm^2 corresponding to pulse durations of 50-200 μs, respectively. At higher laser fluences, the hole diameter and area increment increased. The thermal properties of materials and the absorption coefficients of the biodegradable film influence the formation of microholes. At a film web speed of 10 m/min, laser irradiation on the film surface generated heat in the moving direction of the film, resulting in the formation of an elliptical microhole. The results indicated that the gas transmission rates of the film increased as the number and diameter of microholes increased. Laser perforation appears to be an effective method for enhancing the gas transmission rates of the biodegradable composite film used to package fresh produce.

ACKNOWLEDGEMENT

The authors would like to thanks Department of Packaging and Materials Technology, Kasetsart University and The Graduate School, Kasetsart University for financially support.

REFERENCES

[1] Winotapun, C., Aontee, A., Inyai, J., Pinsuwan, B., Daud, W. Laser perforation of polyethylene terephthalate/polyethylene laminated film for fresh produce packaging application. Food Packag. Shelf Life 2021; 28, Article. 100677.
[2] Xanthopoulos, G., Koronaki, E., & Boudouvis, A. Mass transport analysis in perforation-mediated modified atmosphere packaging of strawberries. Journal of Food Engineering 2012; 111(2), pp. 326–335.
[3] Winotapun, C., Watcharosin, U., Kerddonfag, N., Chinsirikul, W., Takarada, W., & Kikutani, T. Microhole formation behavior of polypropylene film using CO2 laser irradiation. Journal of Fiber Science and Technology 2017; 73(10), pp. 240–250.
[4] Boonthanakorn, J., Daud, W., Aontee, A., & Wongs-Aree, C. Quality preservation of fresh-cut durian cv. 'Monthong' using micro-perforated PET/PE films. Food Packaging and Shelf Life 2020; 23, Article 100452.
[5] Winotapun, C., Aontee, A., Inyai, J., Pinsuwan, B., Daud, W.,. Laser perforation of polyethylene terephthalate/polyethylene laminated film for fresh produce packaging application. Food Packag. Shelf Life 2021; 28, Article 100677.
[6] Winotapun, C., Issaraseree, Y., Sirirutbunkajal, P., Leelaphiwat, P. CO2 laser perforated biodegradable films for modified atmosphere packaging of baby corn.Food Packag. Shelf Life 2023; 341, Article 111356.
[7] Wihodo, M., & Moraru, C. I. Physical and chemical methods used to enhance the structure and mechanical properties of protein films: A review. Journal of Food Engineering 2013; 114(3), pp. 292-302.

CONFERENCE PROCEEDINGS

PACKAGING FOR HAZARDOUS AND DANGEROUS GOODS

PEER-REVIEWED

PH-GP01

How to measure the angle of repose of hazardous substances in the test centres for dangerous goods packagings

Eva Schlick-Hasper[1], John Bethke[1], Thomas Goedecke[1]

[1]*Federal Institute for Materials Research and Testing (BAM), Unter den Eichen 44-46, Germany - 12203*

***Correspondence to**: Eva Schlick-Hasper. Federal Institute for Materials Research and Testing (BAM), Unter den Eichen 44-46, Germany – 12203*
E-mail: eva.schlick-hasper@bam.de

ABSTRACT: The flow properties of a powdery or granular filling material of a dangerous goods packaging are safety-relevant, both in terms of mechanical safety and safety against the release of hazardous substances. To specify the flow properties, the angle of repose is measured in the recognized test centres for dangerous goods packagings in Germany. Previous investigations on non-hazardous substances revealed that some of the methods currently used in the test centers have disadvantages for certain filling goods.

The objective of this work is to extend the investigations to measurements on real hazardous substances and to further concretise the assessment. For this purpose, the angle of repose is measured using four methods (ISO 4324, funnel test, plate method plexiglass, plate method mineral glass) on five hazardous substances (sodium nitrate, ammonium bicarbonate, Biathlon 4D (herbicide), Cantus (fungicide) and Pergafast (color developer)).

Another goal is to investigate the influence of different pre-conditioning and thus a different water content of the bulk material on the angle of repose. For safety reasons, however, these tests are carried out on three non-hazardous substances.

The findings are that for each of the five hazardous substances, the results of the four methods differ significantly. Only for sodium nitrate, the four measurement methods provide comparable values. Overall, the measured values for the ISO method have the smallest scatter (max. coefficient of variation c_(v,max): 5%), for the funnel test the largest (c_(v,max): 25%).

Pre-storage of the three non-hazardous goods in three different controlled atmospheres leads to significantly different measurement results for the angle of repose for the most fine-grained substance investigated.

Only the ISO method is suitable for measuring the angle of repose of real hazardous substances in terms of applicability, repeatability and occupational safety. It is also important, especially with finely powdered filling goods, to carry out controlled preconditioning.

PH-GP02

Improved criteria for evaluating impact targets in regulative drop tests of dangerous goods packagings

Nikolaos Lengas, Karsten Müller, Eva Schlick-Hasper, Marcel Neitsch, Sergej Johann, Manfred W. Zehn

Federal Institute for Materials Research and Testing (BAM), Unter den Eichen 44-46, Germany - 12203

***Correspondence to**: Eva Schlick-Hasper. Federal Institute for Materials Research and Testing (BAM), Unter den Eichen 44-46, Germany – 12203*
E-mail: eva.schlick-hasper@bam.de

ABSTRACT: According to the international dangerous goods regulations, design type tests are used for the approval of dangerous goods packagings. Within this framework, complete, filled transport packages are subjected to free fall drop testing to assess their resistance to mechanical damage. To this end, the impact surface must be considered essentially unyielding. Leading regulations like ADR/RID require that the impact surface shall be part of a foundation structure that has a mass at least 50 times that of the heaviest package to be tested. The problem is that many manufacturers do not possess impact targets that satisfy the required 50 times mass ratio for regulative recurrent drop tests during series production. Therefore, an investigation of the dependency between impact target characteristics, e.g., mass ratio, and the assessment of a packaging's ability to withstand damage is highly relevant for industrial application. The objective of this work is to verify existing and define improved criteria for impact target structures based on systematic experimental investigations and numerical analyses. Previous evidence in this context highlights the relevance of other parameters in addition to the mass ratio. For instance, the energy amount in target motion during impact, and the mechanical response of the packaging should be considered. For this purpose, two packaging design types with significantly different mechanical response were examined, namely steel drums and fibreboard boxes. As model impact targets for the drop test, steel plates of different thicknesses were used to achieve mass ratios of 1:15, 1:30, and 1:50. Their connection to the ground was simulated using a bedding of high strength spring elements. Two different drop test series were carried out. In the first one, the 50 % failure drop height was determined for both packaging types. The results for the different model impact targets were statistically inconclusive. In the second drop test series, many parameters such as drop height, mass ratio, and target eigenfrequency were varied. The results were then enhanced with numerical analyses to describe the interactions of packaging and target properties during impact. Thereby, an evaluation model with an approximation quality of over 95 % was developed.

Based on the findings, new essential evaluation criteria are introduced which are applicable in drop test scenarios comparable to the examined steel impact pad. Firstly, the value of the square root of the surface area of a target (given by the product of its length and width) must be at most 50 times as large as its thickness. Secondly, a new comprehensive formula is provided to determine if the deformation energy of a package relative to the total impact energy is greater than 98 %. This energy percentage threshold was analytically derived in previous work. The combination of these two further developed criteria can be used instead of the generalized requirement of the 1:50 mass ratio. In practice, these results lead to great advantages in the evaluation of already installed impact targets for dangerous goods packagings.

CONFERENCE PROCEEDINGS

PACKAGING MACHINERY AND SYSTEMS

ORAL PRESENTATION

GENERAL STREAM

PA-GO01 Developing a design method and tool for producing customizable forming shoulders

PA-GO01

Developing a design method and tool for producing customizable forming shoulders

Ellen Lucas[1], Ilknur Ilhan*[1], Roland ten Klooster*[1]

[1]*Faculty of Engineering Technology, Department of Design Engineering, Chair Packaging Design and Management, University of Twente, Enschede, 7522 NB, The Netherlands*

***Correspondence to:** Ilknur Ilhan. Department of Design Production and Management, University of Twente, De Horst (Building 20), Room W251. Drienerlolaan 5, Enschede, 7522 NB, The Netherlands.*
E-mail: i.ilhan@utwente.nl

ABSTRACT: Forming shoulders have a key role in folding the film in the flow packaging process. The shoulder is the part that guides the film from a planar state into a tunnel shape. It is typically used in Form Fill Seal (FFS) machines. The shape of forming shoulders is important for creating packaging with the right quality. Because, if the surface of the shoulder has irregularities this can be seen in the final packaging. For each product, a unique forming shoulder is needed. Most of the forming shoulders as seen in the market are handmade with traditional manufacturing methods, like sheet metal forming and it is unknown how the shape of the sheet metal is decided. The result of the manual production of the forming shoulders is that the forming shoulders for the same product are not exactly the same. Only the smallest difference in the forming shoulder can cause the packaging to come out completely different. This research aims to overcome the gap between theory and practice. It provides a comparison of the methods in literature and discusses which one is most suitable for integrating into a reproducible context. A method from the literature concerning the developable surface is used as a reference. Based on this literature mathematical descriptions that describe the shoulder surface are generated. Then, based on parametric modelling a CAD model is generated. The CAD model is linked to a tool which can be used to adapt the variables of the mathematical descriptions and makes the method reproducible. The gap between theory and practice is bridged by this result.

Keywords: Forming shoulder, bending curve, developable surface, form fill seal machines, CAD model, packaging machinery

INTRODUCTION

Forming shoulder is part of a flexible film packaging machine by which the film is guided from a planar web into a tube shape which eventually will form flexible bags.[1,2] Forming shoulders are typically used in two types of Form Fill Seal (FFS) systems which are Horizontal

Form Fill Seal (HFFS) and Vertical Form Fill Seal (VFFS). The machines in HFFS systems are often referred to as Flow Packers and the ones in VFFS systems are referred to as Trans Wrappers.

The geometry of forming shoulders changes based on the product dimensions, packaging design, and the type of forming system. Product dimensions determine the size of the cross-section of the shoulder. Package design on the other hand can dictate the symmetry of the shoulder depending on the type and placement of the longitudinal seal on the packaging as well as the placement of the gusset areas. If the seal is in the center, the forming shoulders are symmetric, otherwise asymmetric. Centro symmetry of the shoulder cross section can change as well to provide more design options.[3] When it comes to creating gusseted bags, butterfly-shaped shoulders are used.[4] The final aspect influencing the shape of the forming shoulder is the type of FFS system. For example, the VFFS machines usually have a forming shoulder with a round cross-section, also referred to as round shoulders while the HFFS machines have shoulders with rectangular-shaped cross-sections.[1] Having the right and faultless geometry has a crucial impact on the quality of the final package. Slight variations or irregularities in the shape and surface of the shoulder can result in wrinkles, misalignment, runnability and seal integrity issues. The settings of the machine can be modified based on the shoulder but this does not solve all problems.[5]

There are many methods suggested in literature to produce forming shoulders. In industry, shoulders are generally manufactured by using traditional methods such as metal sheet processing and milling.[6,7] These methods can also include some hand work which limits the accuracy of the shoulder surface. Although computer-aided designs assist the production of shoulders, the adaptability of these designs to various packaging requirements is questionable. Additionally, the methods used for creating the digital models of forming shoulders are unclear. When forming shoulders are digitally created, additive manufacturing or numerical controlled processes can be used to produce the shoulder. This results in more accurate forming shoulders. Also, it allows for the creation of exact copies or adapted versions and decreases the production time once a method is defined.

To produce various types and shapes of shoulders through additive manufacturing and numerical controlled processes, easily adaptable CAD models are needed. However, defining the modeling method for the forming shoulder proposes some issues. First, it is hard to precisely capture the shape of a forming shoulder with basic CAD modeling. This is due to the double curved surfaces that depend on many factors like the size of the cross-section. To precisely capture the double curved surface mathematical descriptions are needed next to the basic CAD modeling techniques. Also, the method needs to be easily adaptable and reproducible without having to create mathematical descriptions all over again for each new forming shoulder to account for different product dimensions. An easily adaptable and reproducible method helps to integrate the method into the production environment of companies.

This paper aims to investigate the methods proposed in literature for the digital modeling of forming shoulders. Based on this investigation, it creates an adaptable digital model which can be used for producing various types and shapes of shoulder. Therefore, it starts by comparing the methods used in literature. Then, it determines the most suitable

method to a reproducible, adaptable context and applies it to a case study focusing on forming shoulders for Flow Packers. Additionally, it develops a tool to help an easy transition from product dimensions and design requirements to a customized digital model of the forming shoulder. First, provided literature search on the digital modelling methods, then application of chosen method to a case study and finally created tool helps manufacturers with designing forming shoulders for their applications.

LITERATURE RESEARCH

Search strategy

Forming shoulders is not a highly researched topic. Most of the accessible research about the geometry of forming shoulders is gathered from Scopus, SciFinder, Web of Science and Google scholar databases. The related articles are searched through a combination of the keywords "forming shoulder", "forming collar", "shoulder geometry", "form fill seal", and "packaging machine" and their synonyms. The result is a list of papers about all aspects of forming shoulders. For this research, only the papers that mention the mathematical description and digital modeling of forming shoulders are included. These papers are filtered from the list, which results in a list of 13 papers that explain how forming shoulders can be modeled.

Modelling methods

The literature on the design of forming shoulders is limited. Though, the research that has been done shows that there are multiple ways to create a digital model as given in Table 1. The methods having similar strategies are grouped under 4 larger overlapping methods. Each one of the 4 methods has its way of defining the shoulder surface. Method 1 defines it by using known developable shapes. Methods 2 and 3 use the generator lines, and method 4 creates lines based on the finite element methodology. The main features of these overlapping methods are explained in the following subsections.

No	Method Name	Research articles	Cross section type
1	Developable surface	Mot, E., 1972	Round and superellipses
		Zhou Y.J et all, 2004	Rhomb shape
		Zhou Y.J et all, 2006	Non-centrosymmetric shapes
		Zhou Y.J et all, 2008	Round
		Zhou Y.J et all, 2010	Butterfly shape for gusset bags
2	Differential geometry	Molenaar, J. 1989	Round
		Boersma, J. et all, 1995	Round and conical
		McPherson, C. J. et all, 2004	Round
		McPherson C. J. et all, 2005	Round and rectangular
		Hicks, B. et all., 2007	Round
		Matthews J. et all, 2011	Round
3	B-Splines	Fanni, M. et all, 2000	Round
4	Finite elements method	Deoski, A. et all, 2010	Round

Table 1. The four digital modelling methods.

Developable surface method

The first method relies on the preservation of the developable surface using known developable shapes. Mot provides the basis upon which the other authors continued. He creates formulas to describe certain distances in the 2D and 3D surfaces. Through equating both distances, descriptions for parameters linked to the shoulder can be created. Mot shows that the collar of a round shoulder consists of one flat triangular region and two truncated cones with intersecting apexes. By equating the length of the circumference of the round cross-section to superellipses, rectangular cross-sections can also be achieved. However, the article doesn't explain how the changing cross-section influences the angles and cones of the collar.[1]

Zhou et all provide formulas to define the shoulders having various types of cross sections such as trapezoid, triangle, round, butterfly and rectangle-shaped shoulders based on developable surface.[3,4,7,8] Instead of superellipses, the authors use four straight lines which connect four arcs having the same radius to switch from one cross-section type to another easily.[3] This method gives more design possibilities compared to superellipses. Zhou et all also create a 3-D model of a round shoulder using CAD software, though they fail to mention which features to use. This model focuses on creating the offset bending curve to accurately locate the metal shoulder parts before welding.[7]

Differential geometry method

The second method also relies on the developable surface of the forming shoulder. However, the authors describe it through differential geometry. They all use the method of Mot as a basis and extend it by using differential equations to describe the generator lines laying on the surface. Molenaar and Boersma make the initial differential description of a concave bending curve and take a step to fully describe the collar surface of the shoulder with a planar triangle in which the vertex lays on the peak point of the bending curve. They additionally generate differential equations to describe a conical shoulder in which all the generator lines of the collar surface interact at the apex of a single cone. This type of shoulder does not contain a planar triangle at the backside. Instead, its collar surface overlaps with the surface of the cone.[9]

Although most of the authors who use the differential geometry method focus on round shoulders, McPherson et all also provide a way to translate the round cross-section to a rectangular one. The authors divide the circular shoulder into quadrants at 90º intervals. Then they add planar regions to two sides and the back of the shoulder with a desired length to create a rectangular cross-section with rounded edges.[10] However, for each forming shoulder having a different type of cross-section, new equations for the generator lines must be created. So, the full method must be rewritten. Besides, a certain degree of adaptability can be achieved solely based on the round cross-section. Therefore, Hicks et all create an adaptable integrated CAD-CAM process that guides the designers to select feasible input parameters to design a round forming shoulder for VFFS machines. Since the digital model does not include the seal area, this area is added after the shoulder profile is produced by a computer numerical control (CNC) machine.[11]

B-splines method

In the third method, Fanni and Shabara expand the second method by stating that the bending curve can be modeled through B-splines and Non-Uniform Rational B-splines (NURBS). B-splines provide the flexibility to create various shapes of cross sections without having to create the equations all over again for each new forming shoulder. The authors start by defining several conditions that must be fulfilled to make a correct bending curve. Then, they systematically apply computer-aided geometrical design to obtain a simplified and flexible mathematical description of the B-spline curve. With this new approach, authors achieve to generate bending curves that give comparable results with the measured existing shoulders.[12] However, for this method, the authors only consider the round forming shoulders. To model the various forming shoulders with CAD software additional research is needed to gather and list the points that define the B-splines.

Finite elements method

The fourth and final method does not take the full forming shoulder as basis. Instead, it divides the shoulder as a collar and a tube. Since the geometry of the tube is fully defined, it simulates only the collar which freely bends around the bending curve. Desoki et all determine how the film should bend from flat into a tunnel, within certain deformation limits by applying the Finite Element Method (FEM). The surface of the film is divided into quadrilateral and triangular elements to track the changes during enforced displacement. In this method, a flattened collar is connected to the final bending curve with connecting nodes. As one of the contributions to the literature, the authors incorporate fin and lap seal configurations into their model while determining the final bending curve. They also fix the flat triangle of the planar edge as a boundary before the curved collar is gradually formed. Once the location of each element is known the ruling lines on the collar surface can be obtained. This model with the straight ruling lines can directly be transferred to a CNC machine to generate the collar surface.[13] However, to import the model into CAD, special FEM-compatible software might be needed. Because the authors only define the surface for round forming shoulders, a new bending curve needs to be calculated for different types of cross-sections.

CASE STUDY

Methodology

As the methodology, initially, the design requirements of the adaptable forming shoulder are determined for the case. Then the most suitable digital modeling method that satisfies the requirements is chosen based on the literature research presented in the previous section. As a result, an adaptable digital model is created. Via prototyping, boundary parameters were determined which results in a feasible shoulder. These boundaries are incorporated into a tool that assists the designers to generate various shapes of working forming shoulders.

Design requirements

The design requirements of the shoulder and the tool are determined considering the current working shoulders, the literature, and the packaging process in which the shoulder is going to be used. First of all, the shoulder should fold the film into the desired packaging shape without excessively stretching or causing wrinkles. It should have a planar leading edge to lead the film smoothly toward the bending edge. The film should make full contact with the bending edge of the shoulder. The shoulder should fit in the flow packer and be mounted on the currently used mounting system. Then, the digital model should be easily adaptable, therefore the tool should calculate all the parameters of the shoulder for a given packaging size, film width, and a minimum number of input parameters. The tool should also suggest how to model the shoulder based on the calculated parameters and boundaries. The obtained 3D model should be suitable for modern manufacturing methods such as 3D printing, and it should not require additional modifications which decrease accuracy.

Finding the most suitable modelling method

There are some common features explained in the literature research. First, all the authors divide the forming shoulder in the same way: the collar and the tube. The film first touches the shoulder at its leading edge or planar edge at the end of the collar. The curvature of the collar manipulates the film into a tunnel shape. All authors use the bending edge to describe the connection between the tube and collar. The bending edge is the starting point of the folding and the shape of the bending edge determines the curvature of the forming shoulder. So, the performance of the forming shoulder relies on the shape of the bending edge. The authors also mention the main geometrical parameters such as the back angle (θ), the height (h), and the radius of the circular cross-section (Rc) which directly influences the functioning of the shoulder. Most of the papers indicate that these shoulder parameters are interdependent. This means, if one of the parameters is chosen, it becomes apparent that the other parameters are restricted. For example, if the h:Rc ratio is set, the back angle (θ) can only be moved within a certain interval, without forcing the material. These relationships are important to know for a customizable concept and they are best shown by McPherson et all among the existing research.[14] The main features and parameters of a forming shoulder can be seen in Figure 1.

To create an easily customizable model of the forming shoulder, the mathematical description of a bending edge should be able to define various types of cross-sections by simply changing the input. Most authors develop their methods for round forming shoulders. The case discussed here focuses on HFFS machines in which rectangular cross-sections are preferred. Therefore, the chosen method needs to provide the translation from a round cross-section to a rectangular cross-section and possibly other non-centrosymmetric shapes.

The rounded rectangle is one of the techniques which helps to switch from a round to a rectangular cross-section. The formulas of rounded rectangles are described by Zhou et all.[3] This technique readily gives a wide range of design possibilities for changing the shoulder geometry. It starts with assigning four straight lines and four arcs having the same radius to the cross-section which creates a base for further calculations. The literature proposes two

other techniques to work with a rectangular cross-section. The use of a superellipse is one of them. With this technique, an actual rectangle cannot be created, since the lines are not touching but

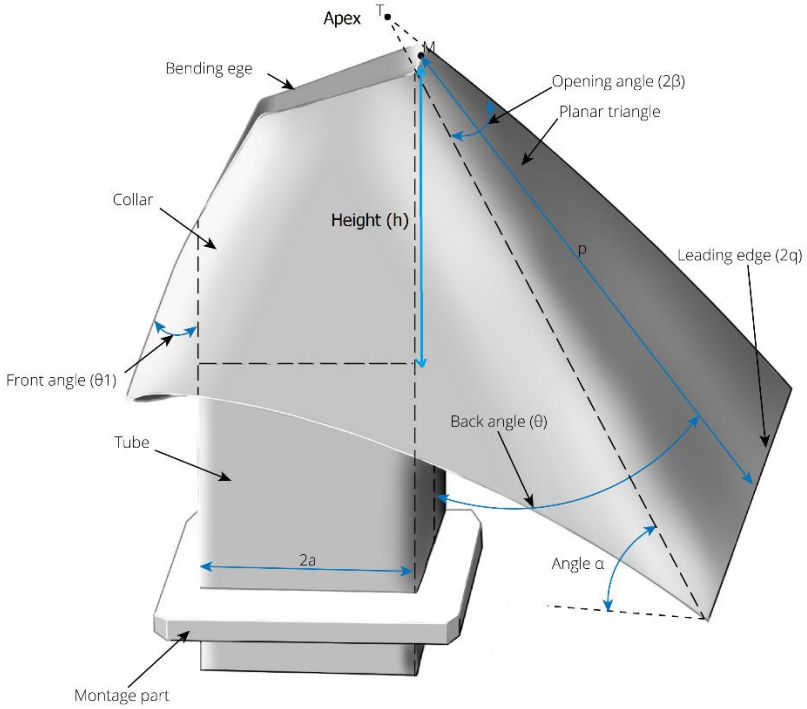

Figure 1. Main features of the forming shoulder.

only approaching the rectangular frame. Besides that, the mathematical description of a superellipse is complicated and not easy to work with. The last technique is adding planar regions where first a round shoulder is modeled and then it is cut into four sections and planes are added in between. This method has some issues since only the radius of the corners belong to cross-section of the initial shoulder design are known. This leads to small forming shoulders at first. These three different cross-section transition techniques are visualized in Figure 2. For this case study rounded rectangle technique is chosen.

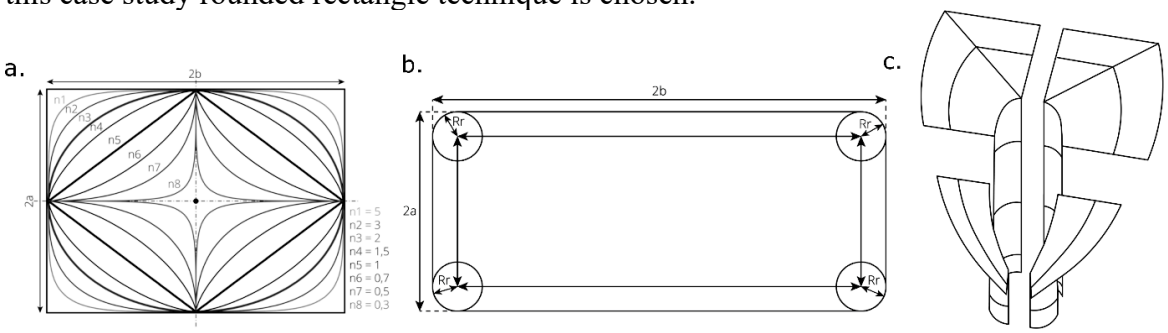

Figure 2. Methods to create rectangular cross-sections; a. superellipses, b. rounded rectangle, c. planar regions. (Figures are adapted from [1,3,10])

The rounded rectangle technique (Figure 2.b.) is only used by the researchers using the developable surface method for creating their digital model. Therefore, the developable surface method proposes a solution on how to easily produce rectangular forming shoulders for HFFS machines where the other options mainly considered round forming shoulders. Additionally, it can be easily integrated into a tool because it uses parameters. Thus, the developable surface method appeared to be the best suited for this case study.

Results

Digital model

To create the digital model the mathematical descriptions given for the developable surface method must be validated. This is done by checking if the presented formulas line up with the geometry of a legitimate forming shoulder. Additionally, the formulas that could not be obtained from literature are derived purely based on geometrical relations. During the application of the chosen method, the method is expanded and adapted where needed.

In this case study a CAD modeling program Autodesk Inventor is used for 3D modeling. Mathematical descriptions are transferred to Inventor by using the parametric modeling function. A parametric model is dimensioning a model with parameters to make it more adaptable. In Inventor, the 'Parameters' option opens a table with all the dimensions in the model. Each dimension in this overview can be renamed to the name of a parameter. One can also link an Excel sheet with parameters to the dimensions in the CAD model. If the parameters are changed in the Excel sheet, this can be automatically imported into the 3D model by which creating new types of shoulders becomes easier.

To deconstruct the shoulder into parameters the first step is tuning the method. The forming shoulder is divided into features and parameters are linked to each feature. This shows how the features of the shoulder can be mathematically described by parameters and how they can be linked to each other and the shoulder geometry. The inputs for modeling the forming shoulder are set as the film, the product, and the shoulder. Through literature, it was found that the back angle and the opening angle must be chosen as inputs of the shoulder otherwise the other parameters cannot be calculated. The method should be extended to find the descriptions of parameters that are not given in literature but are part of the deconstructed model. The digital model should also incorporate the fin seal. Therefore, mathematical descriptions are updated by including seal margins to the film width. Once the full shoulder is defined based on parameters the second stage, the modeling of the forming shoulder can start. The calculations of method 1 are applied to model the bending edge and fringe curve, the outer edge of the shoulder. When these edges are set the tube and collar can be created with basic CAD modeling features.

Prototyping

To test and improve the CAD model, prototypes are produced via 3D printing. These prototypes helped to correct the errors and decision-making along the way. The prototyping

showed that the accuracy of modeling and export settings highly influence the model produced. A developable surface has a Gaussian curvature of zero.[15] Therefore, in the CAD program, the Gaussian curvature of the surface over which the film runs should be checked. If this is not zero it is known that the shoulder does not work. Besides that, zebra stripes can be used to make the curvature of the surface visible. This also shows if there are any disruptions on the surface. If these checks are done before the production, simple issues can be discovered and the shoulder can immediately be improved, and valuable prototyping time can be saved.

Via prototyping certain improvements are made step by step. For example, the fin seal guide should be modelled such that it distributes the force on the film and better guide the film. Also, the bending edge should be adapted such that it can be printed, so its thickness should be increased. Finally, the length of the mounting slot should be adapted. Besides, the prototypes helped to determine and narrow down the boundary values of the shoulder parameters. The back angle is changed gradually to see its influence on functionality of the shoulder. It has been shown that circular cross-section provides a narrower range for back angle (θ) than rectangular cross-sections. Also, it is proven that the force required to be applied to pull the film along the shoulder increases by decreasing θ confirming the literature.[2] Therefore, it should be taken into account that if the back angle is too small the film might get damaged during the process. In the early prototypes, the film came loose from the front surface of the shoulder. To improve the tracking of the film over the front part of the shoulder the front angle (θ1) should be increased. Since the front angle is dependent on other parameters, it can be adapted by making θ or p smaller (see Figure 1).

Tool

For easy customizing, a tool linked to a CAD model is introduced. This tool can translate the inputs to outputs that serve as input for the parameters of the CAD model. In the insert page of the tool, first, some of the independent variables such as the dimensions of the product which is going to be packaged, the fin seal width (k), and film width (Wf) are entered. When these entries are put to the insert page one by one another page calculates the outputs including boundaries of the following input variables. While determining the boundaries, outcomes of prototyping and testing, available information in the literature, geometrical constraints and physical constraints imposed by the machine. The following input variables include the main features of the shoulder such as back angle (θ), height of inflow plane (p), height of shoulder (h), and opening angle (2β). The calculations first determine the dimensions of the tube. Then the calculations determine the dimensions of the collar of the shoulder, though the height of the shoulder and the opening angle are determined based on the suggested boundaries. The calculations are top-down so first the values on the top need to be filled in and calculated before the others can be calculated. When all input variables are entered the summary screen creates a list of all the parameters and the needed information to input into Inventor. Since the tool is linked to Inventor through the parameter option and all the parts are dimensioned based on formulas, the new 3D model can be generated with one click.

Production

For production additive manufacturing was found to be the most suitable technique. Computer-controlled milling also takes away manual labor but has many implications on the design of forming shoulders which restricts their geometrical freedom. 3D printing has an easy setup, requires few manhours, and results in highly accurate models, with only a small limitation on the maximum print size. The two most suitable 3D printing techniques are FDM (Fused Deposition Modelling) and SLS (Selective Laser Sintering) whereas SLS provides the best opportunities. Although prototyping is done via FDM technique, SLS technique might be preferable for production since it gives more geometric freedom, printing needs no support, and there are no leftovers from broken-off supports, so the surface is smoother.

Workflow

As an overview, the workflow starts with knowing the film and product dimensions. Additionally, the margins for the seal area are determined based on the product requirements and packaging design. These independent variables are entered into the insert page of the excel tool. Then the main variables of the shoulder are filled observing suggested minimum and maximum values. Since the outputs of the tool are linked to the CAD model via parametric modeling, the digital model can easily be updated for given product dimensions. The model is exported as a .stl file. One should consider the orientation of the geometry such that few supports are needed for 3D printing. Finally, customized forming shoulders with various shapes and sizes are created via the chosen type of 3D printing technique. These steps are represented in Figure 3.

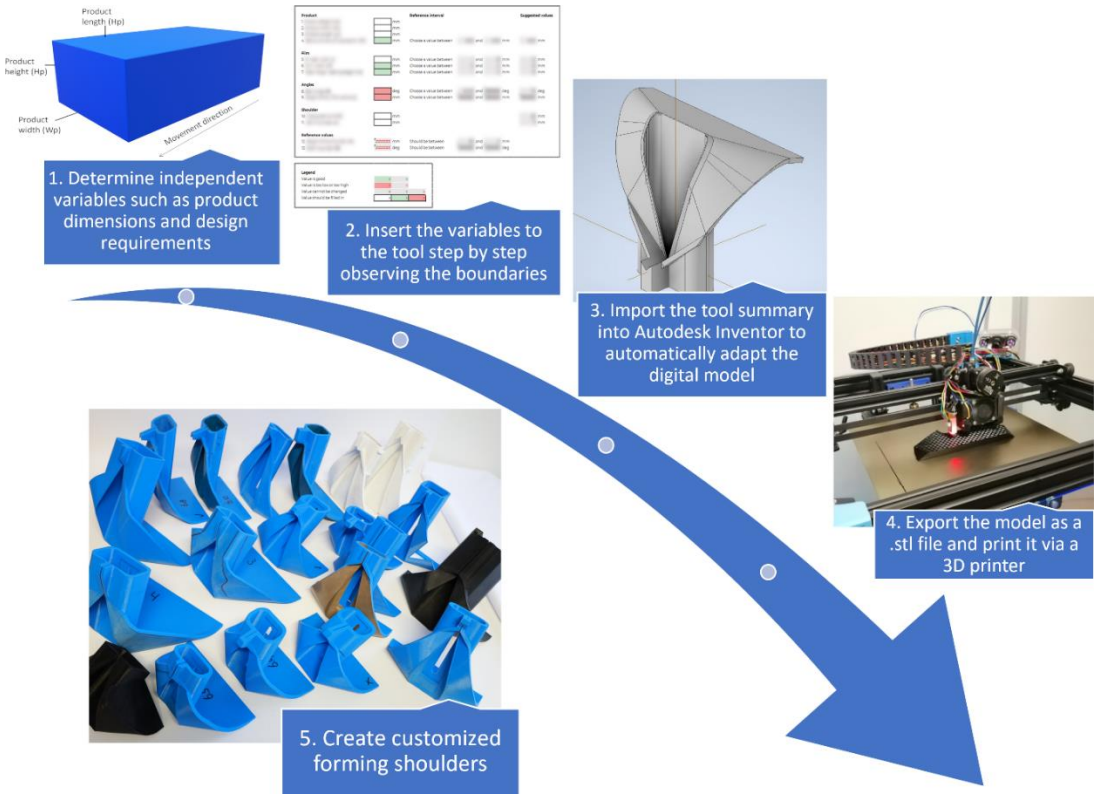

Figure 3. Creating customized forming shoulders step by step.

Improvement points

Forming shoulders is a complex subject and there are still many parts left to be researched. During prototyping, some issues and improvement points are recorded. These issues and points are discussed in this section.

First, the tests of the prototypes mainly showed the influence of the film properties on the performance of the shoulders. For example, in film A the shoulder works well but in film B it does not work anymore. To overcome these issues the method should take the type of film into account. However, while determining the boundaries, the film thickness is ignored since the dimensions are in mm and the thickness of the film is in micron. Additionally, the friction forces between the shoulder surface and the film surface are ignored. The factor that can improve the forming shoulders the most is the inclusion of the film in the method. Matthews et all present that different coefficient of friction values between each type of flexible film material and the shoulder surface can influence the functioning of the shoulder. Therefore, the lowest bound for the design choice of the back angle (θ) needs to be determined based on the coefficient of friction, the elastic limit for the material, and the web tension generated by FFS machine.[2] As the next step, an input section can be integrated into the tool to enter the values related to film-shoulder interaction. Then the suggested boundaries can be calculated accordingly.

The second issue is related to the placement of the cones. In literature, the collar of a standard round shoulder is defined using two symmetrical cones connected with the planar triangle. The position of the apex of the cones (T) intersects at the same spot in these types of shoulders.[7] Yet, the literature does not clarify how this position changes when the cross-section is switched from round to rectangle. In the shoulders with rectangular cross-sections, 4 different cones are used for defining the collar surface as two symmetrical cones on the front and 2 symmetrical cones at the back. During prototyping, it has been decided to keep all the apexes in the same spot laying at the top of the planar triangle adhering to what is stated in the literature. However, for some design configurations, lack of curvature of the front part gives issues with the printing of the shoulder. The size and shape of the collar curvatures are depending on the placement cones' apexes. Therefore, it should be investigated if moving the apexes of the cones is a way to solve this issue. The top of the front cones cannot be simply moved because this results in torsion in the surface and disrupts the developable surface. To move the top of the cones the bending edge and fringe curve equations should be rewritten. When these are implemented and inserted into Inventor a new model can be created with the apexes of the front cones in another spot.

As next, it is examined that some of the legitimate forming shoulders from the industry contain a rim around the bending edge. This rim removes the developability of the shoulder surface since it is added on top of the bending edge. However, it might have a positive influence on functioning. Therefore, it was decided to make a copy of this rim and add it to some of the prototypes. In fact, the rim lightened the damage on the film and improved the tracking of the film along the bending edge. However, it did not eliminate the issues. The role and the necessity of the rim should be researched further.

Finally, during the tests of the prototypes, their durability was not tested. The film did not run over the prototypes longer than 10 minutes. Still, when checking the forming shoulders after, it could be noticed that there was already some wear on the forming shoulders. Different surface finishing options should be considered to make the shoulder more resistant to wear and decrease excess frictions which might cause issues in film forming.

CONCLUSION

This paper defines an adaptable method based on literature that can capture the shape of a forming shoulder in CAD software. Among 4 different methods, it chooses the developable surface method for digital modelling since it provides an easy transition from round to rectangular cross sections. To make the method reproducible for customized shoulders it introduces a tool that translates the general inputs to inputs for the CAD model. The tool guides the designers via suggesting boundaries to create a functioning shoulder for defined product and packaging requirements. With that, the paper makes the gap between theory and practice smaller. It should be noted that small changes in the geometry or settings of the machine results in larger changes in the performance of the shoulder. Therefore, further research is needed to improve the accuracy and functioning of the shoulder, and further narrow down the boundaries of the tool especially considering the surface interactions between the film and the collar.

AKNOWLEDGEMENT

The study has been executed as a master thesis for a company.

REFERENCES

1. Mot E. The “shoulderproblem” of forming, filling and closing machines for pouches. *Applied Scientific Research*. 1973;27(1):1-13. doi:10.1007/BF00382472/METRICS
2. Matthews J, Hicks BJ, Mullineux G, Goodwin J, Burke A. Modelling the Material Flow and Web Tension in the Vertical Form–Fill–Seal Packaging Process. *Packaging Technology and Science*. 2011;24(8):435-450. doi:10.1002/PTS.949
3. Zhou YJ, Qian XM. Non-centrosymmetric section forming shoulders in packaging machines. *Packaging Technology and Science*. 2006;19(2):97-104. doi:10.1002/PTS.712
4. Yi-Jie Z, He-Ping C. Study on Forming Shoulders with Butterfly section in Packaging Machines. Published online 2010.
5. Merabtene M, Tanninen P, Varis J, Leminen V. Heat Sealing Evaluation and Runnability Issues of Flexible Paper Materials in a Vertical Form Fill Seal Packaging Machine. *Bioresources*. 2022;17(1):223-242. doi:10.15376/biores.17.1.223-242
6. Mcpherson C, Hicks B, Berry C, Medland T, Mullineux G. *UNDERSTANDING MACHINE-MATERIAL INTERACTION FOR IMPROVED DESIGN METHODS*.; 2005.
7. Zhou YJ, Zhang QJ. CAD application on manufacture of forming shoulder for packaging machines. *Key Eng Mater*. 2009;392-394:161-165. doi:10.4028/www.scientific.net/kem.392-394.161
8. Zhou YJ, Wang ZW. Study on rhomb shoulders in packaging machines. *Packaging Technology and Science*. 2004;17(5):287-294. doi:10.1002/PTS.664
9. Boersma J, Molenaar J. Geometry of the shoulder of a packaging machine. *SIAM Review*. 1995;37(3):406-422. doi:10.1137/1037084
10. McPherson CJ, Mullineux G, Berry C, Hicks BJ, Medland AJ. Design of forming shoulders with complex cross-sections. *Packaging Technology and Science*. 2005;18(4):199-206. doi:10.1002/PTS.691
11. Hicks B, Mullineux G, Matthews J, Medland T. Towards an integrated CADCAM process for the production of forming shoulders with exact geometry. *Proc Inst Mech Eng B J Eng Manuf*. 2007;221(10):1521-1531. doi:10.1243/09544054JEM896
12. Fanni MAM, Shabara MAN. A New Method for Designing the Shoulder of Packaging Machines. *MEJ Mansoura Engineering Journal*. 2021;25(2):1-11. doi:10.21608/BFEMU.2021.157985
13. Desoki A, Morimura H, Hagiwara I. General design of the forming collar of the vertical form, fill and seal packaging machine using the finite element method. *Packaging Technology and Science*. 2011;24(1):31-47. doi:10.1002/pts.919
14. McPherson CJ, Mullineux G, Berry C, Hicks BJ, Medland AJ. The performance envelope of forming shoulders and implications for design and manufacture. *http://dx.doi.org/101243/0954405041485993*. 2005;218(8):925-934. doi:10.1243/0954405041485993
15. Developable Surface -- from Wolfram MathWorld. Accessed February 25, 2023. https://mathworld.wolfram.com/DevelopableSurface.html

CONFERENCE PROCEEDINGS

PACKAGING MATERIALS

ORAL PRESENTATION

GENERAL STREAM

PM-GO01	Biochar composites for sustainable thermal packaging applications
PM-GO02	Effect of Consecutive Extrusion Process on the Properties of Recycled Polyethylene Terephthalate (rPET)
PM-GO03	Sugarcane as a source to produce paper in Mexico. Study to evaluate the feasibility for Mexican Industry
PM-GO04	Effect of wrapping parameters and transport constraints on stretch film properties for freight transport applications

PEER-REVIEWED

PM-GP01	Seal materials in flexible plastic food packaging: a review
PM-GP02	Effect of food simulants on CuONP stability in bionanocomposite food packaging film

POSTER PRESENTATION

PM-PP01	Release of Vanillin, trans-Cinnamaldehyde, and Citral from Poly(butylene succinate) Films Containing Lignin Nanoparticles

PM-GO01

Biochar Composites for Sustainable Thermal Packaging Applications

Madan M. Manipati[1], Cassidy R. Draper[2], Kathleen T. Draper[3], Thomas A. Trabold[3] and Carlos A. Díaz[4*]

[1]*Golisano Institute for Sustainability, Rochester Institute of Technology, Rochester, New York 14623, USA*
[2]*Department of Biomedical Engineering, Rochester Institute of Technology, Rochester, New York 14623, USA*
[3]*Cinterest LLC, East Rochester, New York 14445, USA*
[4]*Department of Packaging Science, Rochester Institute of Technology, Rochester, New York 14623 USA*

***Correspondence to:** Carlos A. Díaz. Department of Packaging Science, Rochester Institute of Technology, Rochester, New York 14623 USA.*
E-mail: cdamet@rit.edu

ABSTRACT: Biochar materials are derived from pyrolysis of organic biomass, often for the purpose of producing soil amendments. However, there is also significant potential for utilizing biochar in developing sustainable insulation materials, because it is known that certain types of biochar combined with biomass-based substrates can generate composites with high porosity and low thermal conductivity. In this study, we have explored combinations of biochar materials with a sustainable bio-based binder as a potential alternative to expanded polystyrene (EPS) for high-value products that require low temperature during transport, such as vaccines and selected food items. EPS is known to have negative environmental impacts and few options exist for re-use or recycling, and thus there is an immediate market need for new materials that reduce greenhouse gas (GHG) emissions and other impacts while simplifying end-of-life handling. Our research has focused on understanding the impacts of different types of biochar, produced using various feedstocks over a range of temperatures, on key properties of composite insulation panels, including density, compressive strength, thermal conductivity and R-value. We have identified several combinations of biochar and organic binder that provide performance comparable to EPS, and in one case achieve about a 10% lower thermal conductivity than that measured for EPS, in close agreement with values reported in literature (~0.038 $Wm^{-1}K^{-1}$). Through application of in-house characterization methods including scanning electron microscopy (SEM), universal testing machine (UTM), compression testing machine and Fourier transform infrared spectroscopy (FTIR), we have identified key properties of the biochar-binder matrix that enhance thermal insulation properties.

Keywords: biochar; binder; expanded polystyrene; thermal conductivity; R-value

INTRODUCTION

Biochar is a stable form of carbon produced by thermochemical conversion of biomass under reduced oxygen conditions. The conventional use of biochar has been as a renewable soil amendment, but there is growing interest in applying biochar in a wide range of other environmental and industrial applications, in some cases as an alternative to fossil fuel-derived carbon black or activated carbon. It is our expectation that waste-derived biochar (where the feedstock is low-cost or "free") could have great potential in regards to both cost reduction and carbon sequestration [1]. For example, Zimmermann and co-workers developed a carbon-based foam with potential use as thermal insulator [2], and these preliminary results suggest the possibility of insulating panels made completely from renewable resources that could displace expanded polystyrene (EPS). EPS is known to have negative environmental impacts and few options exist for re-use or recycling, and thus there is an immediate market need for new materials that reduce greenhouse gas (GHG) emissions and other impacts while simplifying end-of-life handling.

High porosity and low thermal conductivity (i.e., 0.0355 $Wm^{-1}K^{-1}$) was achieved by Zimmermann et al. using a wood precursor followed by pyrolysis. However, the samples were small and significant shrinkage happened during carbonization. Carbon aerogels have shown very low thermal conductivity due to their nano-sized pores and particle structure; thus, they are promising for high thermal insulation applications [3]. Lazzari and co-workers investigated the direct inclusion of biochar to make cellulose based aerogels. Thermal conductivity down to 0.024 W $m^{-1}K^{-1}$ was obtained. Again, the samples were small and the process required the sublimation of ice for 70 hours in a freeze dryer [4], and this could challenge pilot- or industrial-scale production. Segovia and co-workers developed wood fiber thermal insulation boards using a bio-based adhesive as a binder with acceptable thermo-mechanical properties (i.e., 0.064 $Wm^{-1}K^{-1}$) [5]. The Segovia et al. paper identified wood-based fibers as natural, local materials that are nontoxic, recyclable, and can provide good thermal insulation properties.

Based on the literature review, a thermal insulating panel made with biochar and a bio-based binder hasn't been reported previously and could potentially simplify the fabrication and facilitate the scale-up of the technology. Biochar feedstock type, particle size and shape, and biochar mass loading might impact parameters related to the insulating and mechanical stability properties of the mixture. Insulating panels can be effectively "tuned" to produce new materials suitable for temperature-controlled packaging and to develop a fabrication process and engineering prototypes for biochar-based composite materials for thermally insulated packaging. These sustainable and potentially carbon-negative materials can be used as a replacement for expanded polystyrene and other carbon intensive packaging systems, to access the rapidly expanding market in temperature-controlled shipping, especially for food, vaccines, pharmaceuticals, etc. In this study, we have therefore explored combinations of biochar materials with a sustainable bio-based binder as a potential alternative to expanded polystyrene (EPS) for high-value products that require low temperature during transport.

MATERIALS AND METHODS

Biochar from two different feedstocks was procured from commercial sources. A wood-based biochar in two shapes, coarse (BC1) and fine (BC2) (Aries Green™ manufactured by Aries Clean Energy, Franklin, TN), and a crop by-product biochar (BC3) (Glanris™ commercial). Both BC1 and BC2 had a low aspect ratio while BC3 had a slender rod-like shape. Figure 1 illustrates the structure of biochars used in this research for the preparation of composite panels. Bausch & Lomb Stereo Zoom-5 microscope was used to capture the images.

A bio-based binder was used as a matrix for the composites. This naturally occurring polymer was modified to allow gelling and crosslinking. A control sample with no biochar is labeled BC-0. Figure 2 shows an array of samples, from left to right of expanded polystyrene (EPS), and panels containing BC0, BC2, and BC3.

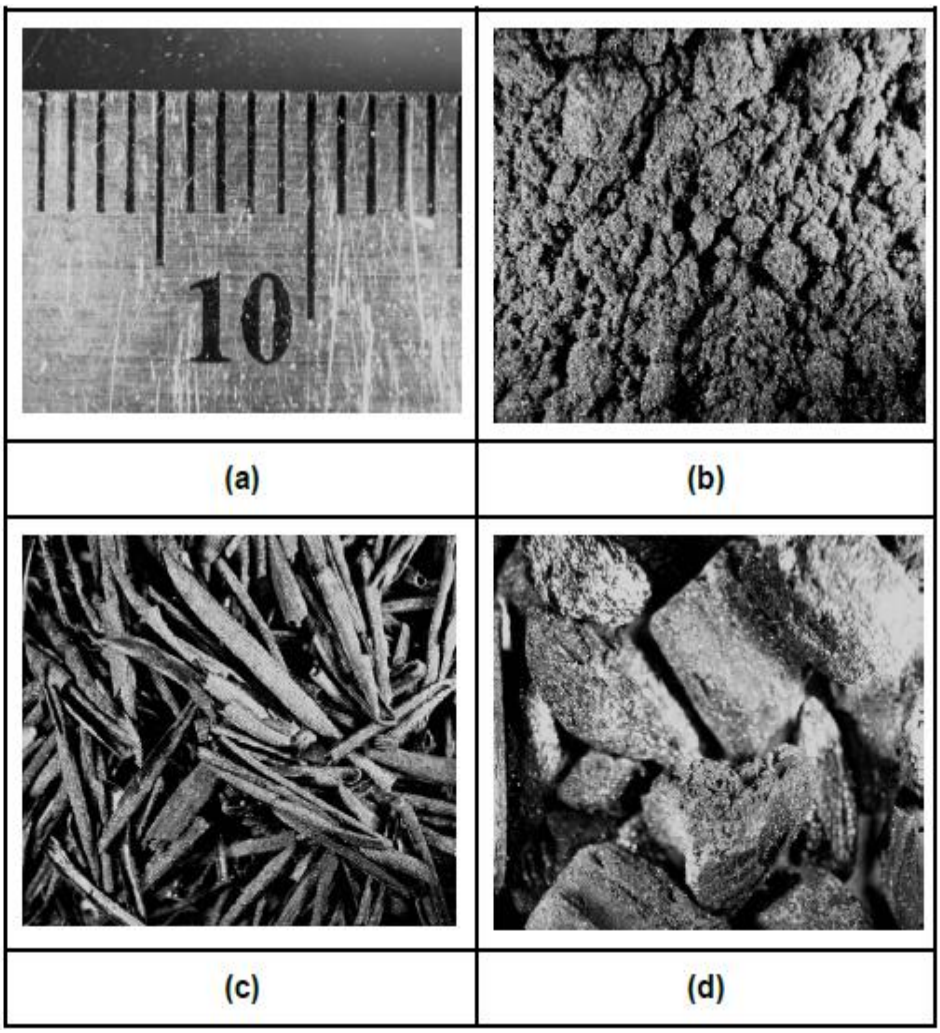

Figure 1. Bausch & Lomb Stereo Zoom-5 microscope images: (a) mm scale; (b) fine wood biochar (BC2); (c) crop residue biochar (BC3); (d) coarse wood biochar (BC1)

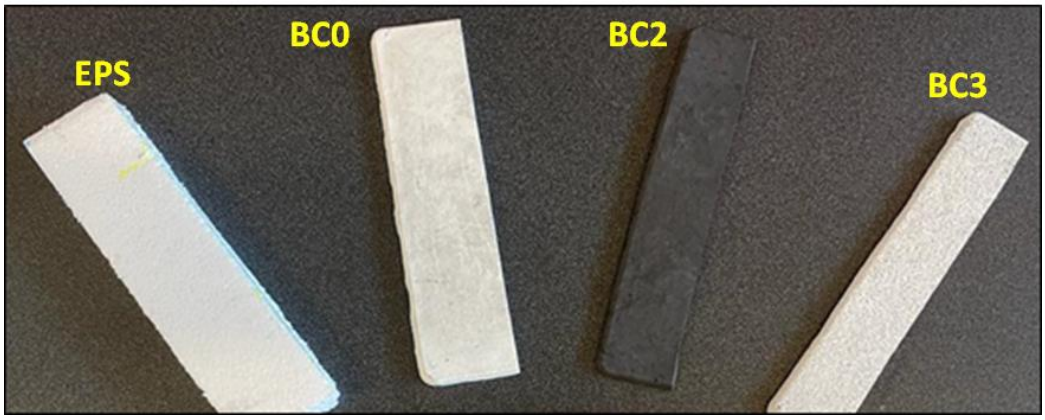

Figure 2. Different panel compositions

Sample preparation

The fabrication of thermal packaging prototype panels was done by blending biochar with bio-based binder and then forming the mixture into rectangular panels using a silicone mold. The binder is water activated. The BC1-33 (i.e., composite comprised of 1/3 BC1 by mass and 2/3 bio-binder) panel was prepared by combining 50 grams of biochar with 100 grams of bio-binder and 400 ml of water. The sample was mixed manually until visually homogeneous and the mixing time was kept under 60 seconds. The paste was transferred to a silicon mold and air dried for one hour. The samples were then removed from the silicone mold and placed in a freeze drier (HarvestRight^{TM} pharmaceutical freeze drier HRFDL) at -30 °F for 35 hours (See Figure 3). The freeze drier step was used to prevent warping that was observed during initial runs conducted with conventional oven drying. It in envisioned that industrial scale production will use a continuous process with a stepwise drying to avoid warping. All samples were prepared in a similar manner where the biochar and bio-binder content amounted to 150 grams. The nominal planar dimensions of the panels were 21 cm by 18 cm, with a thickness of 7.7 mm.

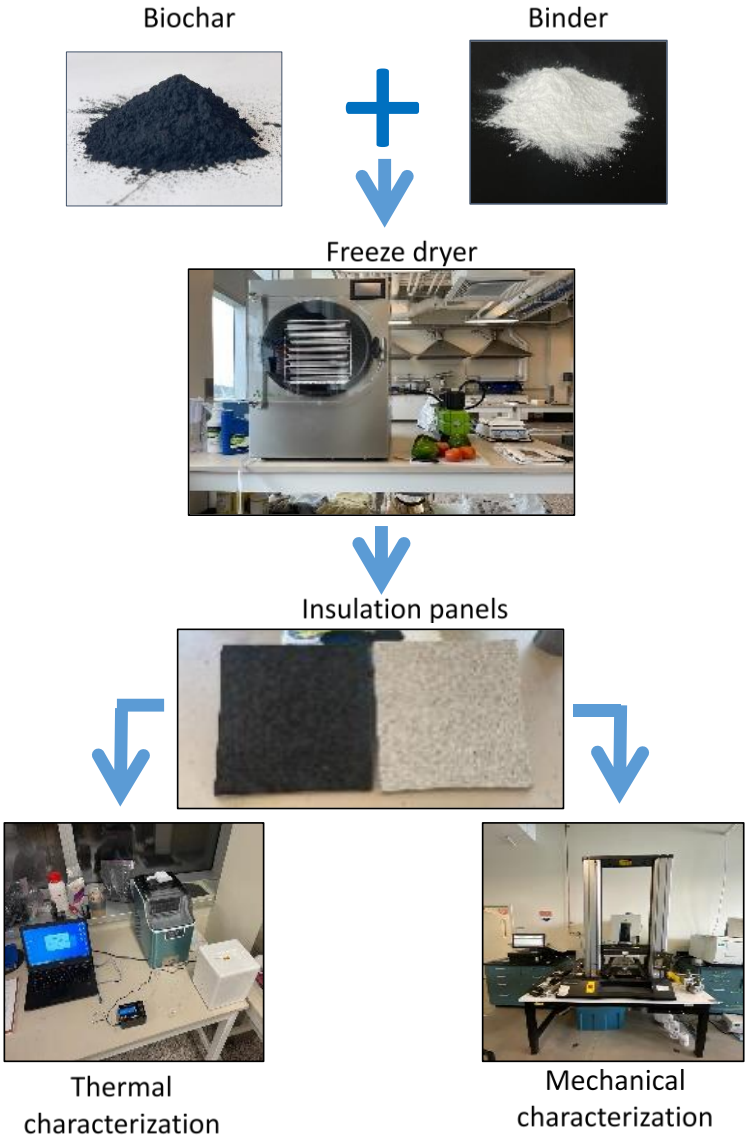

Figure 3. Experimental process of thermal insulation panel fabrication and characterization

Thermal conductivity characterization

Thermal conductivity was obtained using a heat flux sensor from FluxTeq^{TM} (PHFS-09e heat flux sensor; Blacksburg, VA, USA). This sensor directly measures heat flow which is then used to compute R-value. An EPS cooler was used to create a constant internal temperature using ice filled slightly above half of the available volume. This was similar to the method developed by Burgess [6]. The top panel of the cooler was replaced with the fabricated panels containing biochar. To ensure a hermetic seal, petroleum gel (Vaseline) was used at the interface of the cooler and the sample panels. The test was run for 6 hours and the thermal conductivity values below were calculated from the average of discrete measurements acquired from 3 to 6 hours

(see Figure 4). The heat flux sensor was mounted on the inside of the cooler using heat sink paste. The initial start-up of the test (0 to 3 hours), during which the system was reaching thermal equilibrium, was not considered in computing thermal conductivity via Equation 1:

$$k = \frac{Qd}{A\Delta T} \quad (1)$$

where:

k = thermal conductivity [$Wm^{-1}K^{-1}$]
Q = heat flow through the material [W]
d = panel thickness [m]
A = heat transfer area [m^2]
ΔT = temperature difference [K]

ΔT was measured by the thermocouples connected to the FluxTeq instrument and d was measured separately for each panel. To validate the values obtained from the FluxTeq, the test was performed on a commercially procured EPS panel. The values were in close agreement with those reported in literature (~0.038 W $m^{-1}K^{-1}$) [7].

Mechanical characterization

Mechanical characterization of composite panels was performed on a universal testing machine (Instron™ of Illinois Tool Works, Model No. 5567). Flexural test (3-point bend test) was conducted following standard ASTM D790. Rectangular samples were cut from insulating panels and the test was conducted with a supporting span of 65 mm.

Edge crush test was conducted on the composite panels according to TAPPI standard T 839 om-02, on a compression tester made by Testing Machines Inc. (TMI™), Model 17-76-00-0001.

Scanning electron microscopy (SEM)

Structural analysis was conducted using the scanning electron microscopy (SEM) system of TESCAN™ with in-built software VegaTC. SEM images were captured at 1000x magnification for four material composition, as presented below in Figure 9: (a) Binder + Biochar (BC2); (b) Binder + Biochar (BC3); (c) Binder + Biochar (BC1); and (d) EPS.

All SEM imaging was applied with a beam intensity of 10 keV, with samples prepared by first gold sputtering for 90 s. Cross sections were obtained using a blade and the samples were mounted on the stand with carbon tape.

RESULTS AND DISCUSSION

Table 1 provides a list of all the samples fabricated and measured properties. Figure 4 plots the computed thermal conductivity values collected between 3 and 6 hours of testing. Generally small variations were observed as a function of time, except for BC3-50 which displayed a distinct drop in thermal conductivity after 5 hours of testing. This may be attributed to an external factor, such a sudden change in outside temperature during testing, although no such change was independently verified. All the samples have measured average thermal conductivities in the range of 0.035 to 0.065 Wm-1K-1. The sample with only bio-binder (BC0) showed the highest thermal conductivity, whereas the sample with 33% BC3 displayed the lowest thermal conductivity among the compositions fabricated in this experimental campaign.

Code	Number of panels	Density* [gcm^{-3}]	Thermal conductivity* k[$Wm^{-1}K^{-1}$]	Flexural stress [MPa]		Modulus (Automatic Young's) [MPa]		Edge Force [Nmm^{-1}]	Crush
	N	mean	mean	mean	s.d.	mean	s.d.	mean	s.d.
EPS	2	0.012	0.039	0.100	0.010	1.510	0.070	51.977	1.946
BC0	2	0.465	0.064	1.380	0.170	119.900	7.260	97.116	26.013
BC1-33	1	0.227	0.053	0.310	0.040	13.280	-	75.478	0.936
BC1-50	1	0.231	0.057	0.230	0.040	6.390	-	55.025	1.174
BC2-50	3	0.380	0.041	0.790	0.170	63.180	19.440	47.954	3.041
BC3-33	3	0.300	0.037	0.340	0.010	33.460	5.560	37.739	3.920
BC3-50	1	0.278	0.050	0.240	0.021	31.260	3.804	26.602	0.218

Note: *These properties showed a standard deviation of approximately ±5%

Table 1. Results of characterization of seven different panels. Standard deviations (s.d.) are based on triplicate measurements. For cases with a single fabricated panel (N=1), multiple specimens were obtained from the single panel.

To analyze the different effects of biochar type, biochar mass content and biochar shape (coarse vs. fine), the average properties were plotted individually along with the density for comparison. Figure 5 shows the thermal conductivity of the different panels. All the samples have thermal conductivity in the range of 0.03 to 0.07 $Wm^{-1}K^{-1}$. The panel containing BC3 showed a lower thermal conductivity than that with BC1, despite having slightly higher density.

In general, it is expected that the density would vary inversely proportional with the thermal conductivity [8]. This statistically significant difference observed in Figure 5 demonstrated the influence of biochar type on the thermal conductivity. Comparing samples with 33% biochar vs. 50% biochar showed an increase in thermal conductivity for both types of biochar derived from wood waste and crop residues.

Since BC0 has the highest thermal conductivity, a U-shape in the relationship between thermal conductivity and biochar content can be observed. This suggest that there is an optimum biochar concentration that will yield the lowest thermal conductivity, and should be further studied. Comparing panels made with coarse and fine biochar (BC1 vs. BC2), the results suggest that finer biochar (BC1) favors lower thermal conductivity. This might be due to more air-filled pores trapped in the structure because of the smaller particle size. This effect is also evident despite the increase in density. BC3-33 showed a similar thermal conductivity to EPS. This might be due to the high aspect ratio structure of BC3, which helped to trap even more air than BC1, thereby providing further decreased thermal conductivity.

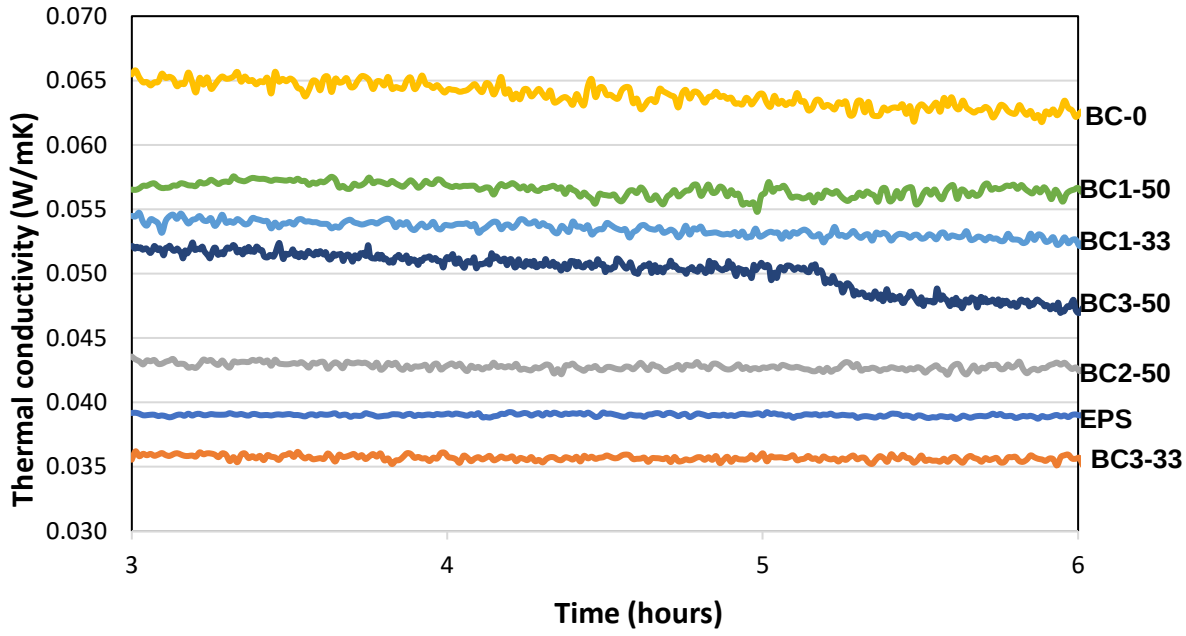

Figure 4. Temporal variation in measured thermal conductivity of panels tested

Figure 6 shows the edge crush force of the different panels. For comparison, the density is also plotted. All the samples have edge crush force in the range of 20 to 100 Nmm^{-1}. The sample with only bio-binder showed the highest edge crush force, with suggests that the matrix is providing most of the load bearing capacity. Biochar type and content have a significant effect on edge crust force. Increasing amounts of biochar lowered the edge crush force, 33% vs. 50%. Also, the high aspect ratio biochar (BC3) weaken the panels even below the EPS

benchmark. When comparing panels made with coarse and fine biochar, the coarse has a slightly higher strength, despite the increase in density (BC1-50 vs. BC2-50).

Figure 7 shows the flexural stress of the different panels. For comparison, the density is also plotted. All the samples have flexural stress values higher than the EPS in the range of 0.2 to 0.8 MPa. BC2 showed a better flexural stress than BC1 and BC3. It is evident that fine biochar panel (BC2) is showing better performance of flexural stress than coarse biochar panels. The results show the sensitivity of the flexural strength to the particle size. This can be attributed to a better compaction (higher density), and improved stress transfer between the matrix and the particles [9].

Figure 8 shows the modulus of elasticity which relates to the stiffness of the panels. This property strongly correlates with the density of the panels which is also plotted. All the samples have modulus values in the range 10 to 70 MPa, greater than EPS. Similar to the flexural strength, BC2 modulus values are higher than BC1 and BC3. This indicates that formulations with coarse biochar show lower modulus values than those with fine biochars. Clearly, particle size and aspect ratio have significant effects on the modulus of elasticity, with finer particles and higher aspect ratios yielding improved stiffness of the composite panels.

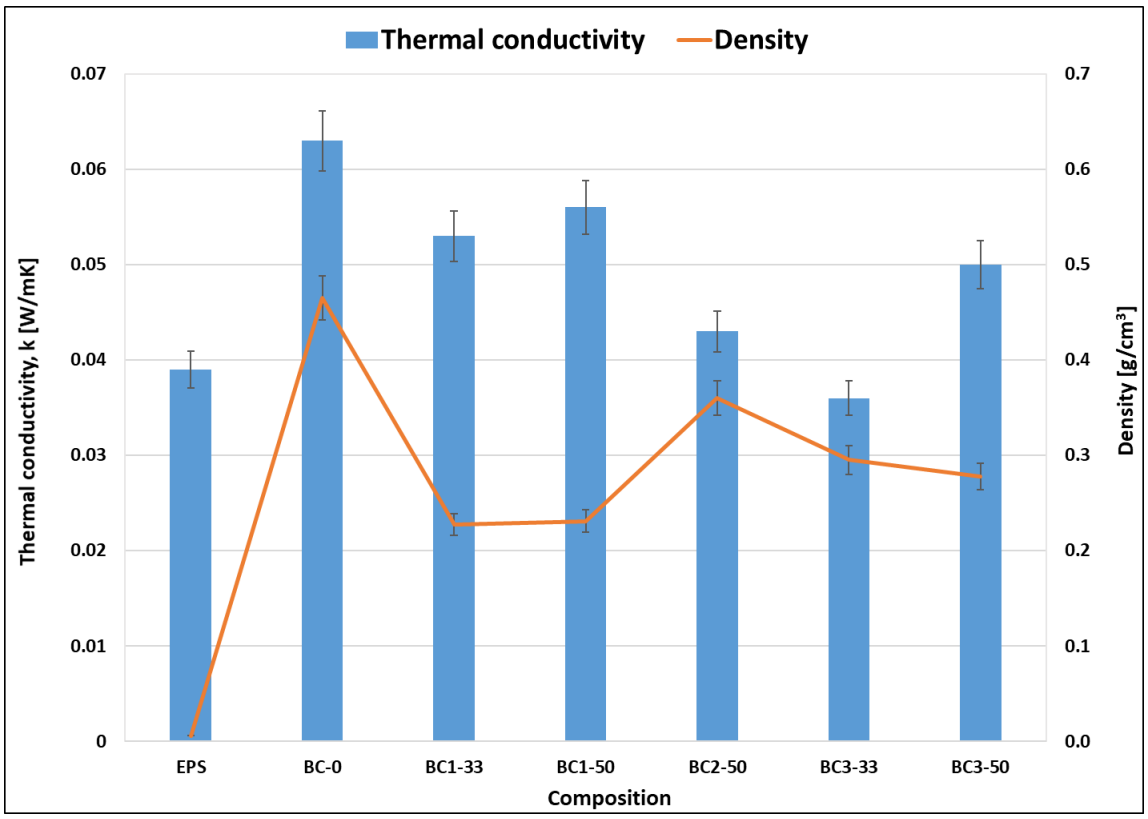

Figure 5. Average thermal conductivity vs. density

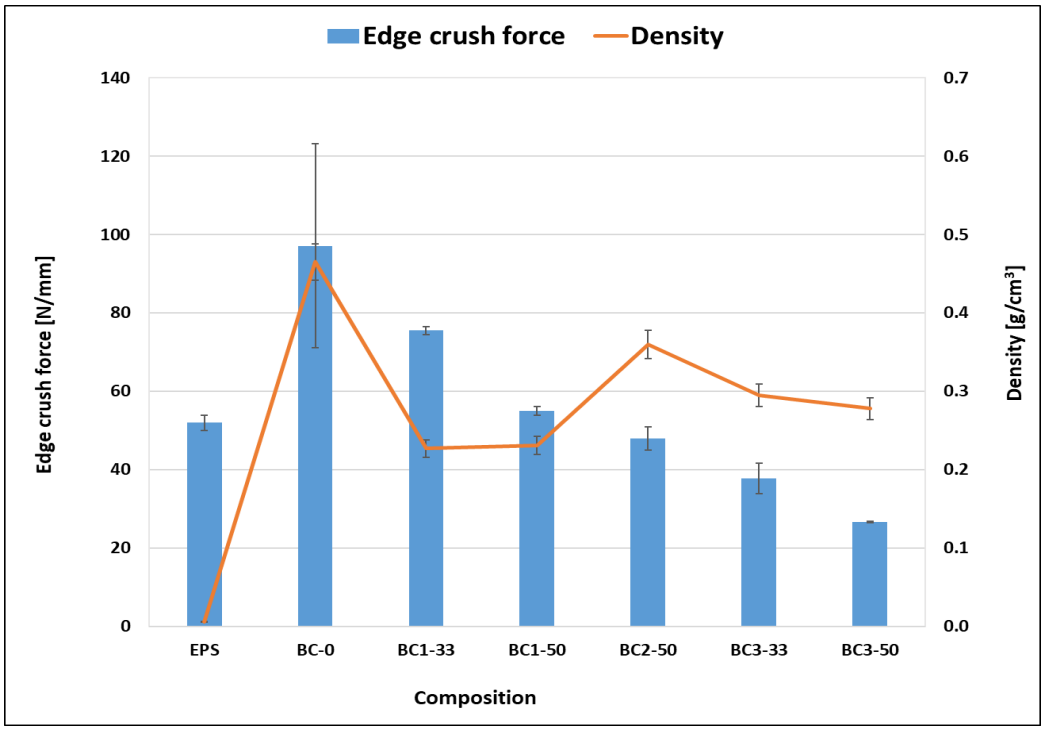

Figure 6. Average edge crush force vs. density

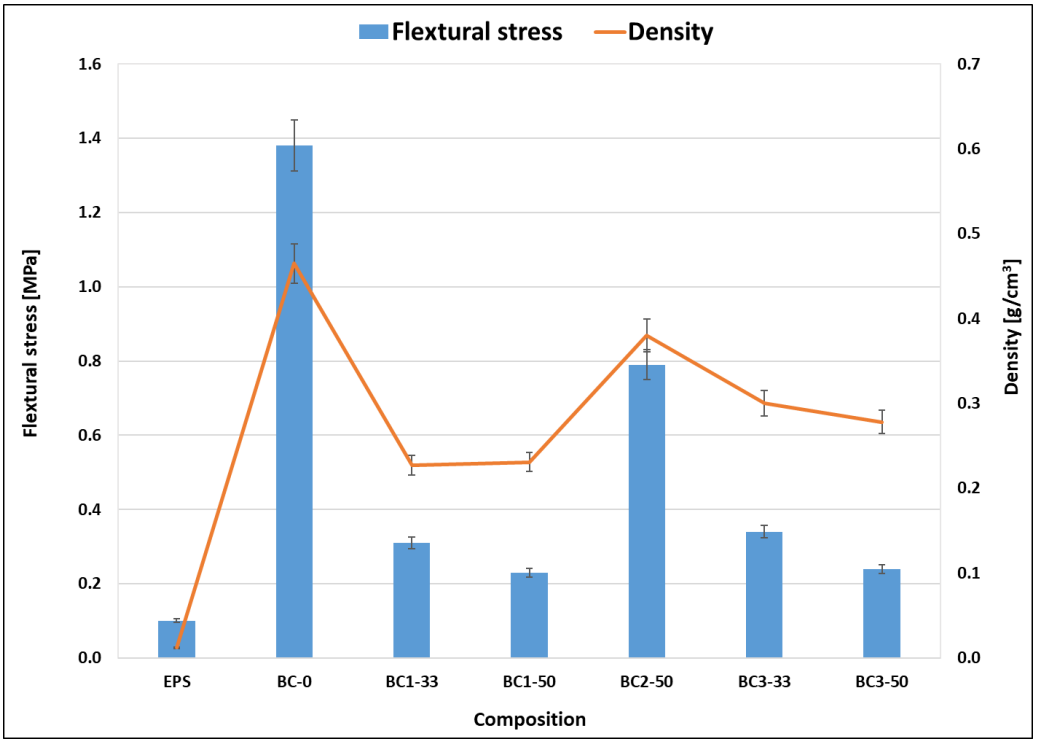

Figure 7. Flexural stress vs. density

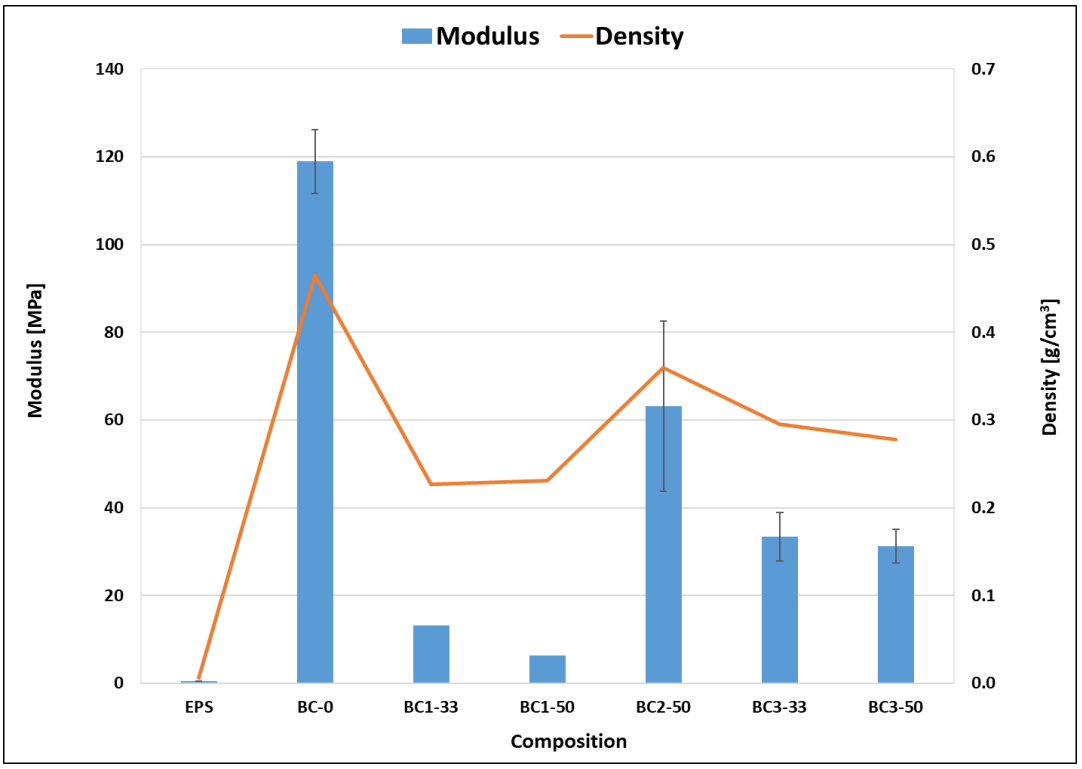

Figure 8. Flexural modulus of elasticity vs. density

Figure 9 shows SEM images of selected samples. Fine biochar (BC2, Figure 9a) is dispersed in the binder and shows a similar structure to BC0 (not shown). Porous structures at the material interfaces might enable reduction in thermal conductivity. The larger particles (BC1, Figure 9c) have less interface area and most of the porosity comes from within the honeycomb-like biochar structure. The high aspect ratio biochar (BC3) has more of a sheet-like structure that can curl and trap pores in a different way. Figure 9d shows EPS for comparison, however the micrograph displays a distorted cell structure because of the method for exposing the cross section (i.e., blade cut). This microstructure analysis give some insight into the mechanisms of heat transfer in the panels and should be further explored in future work.

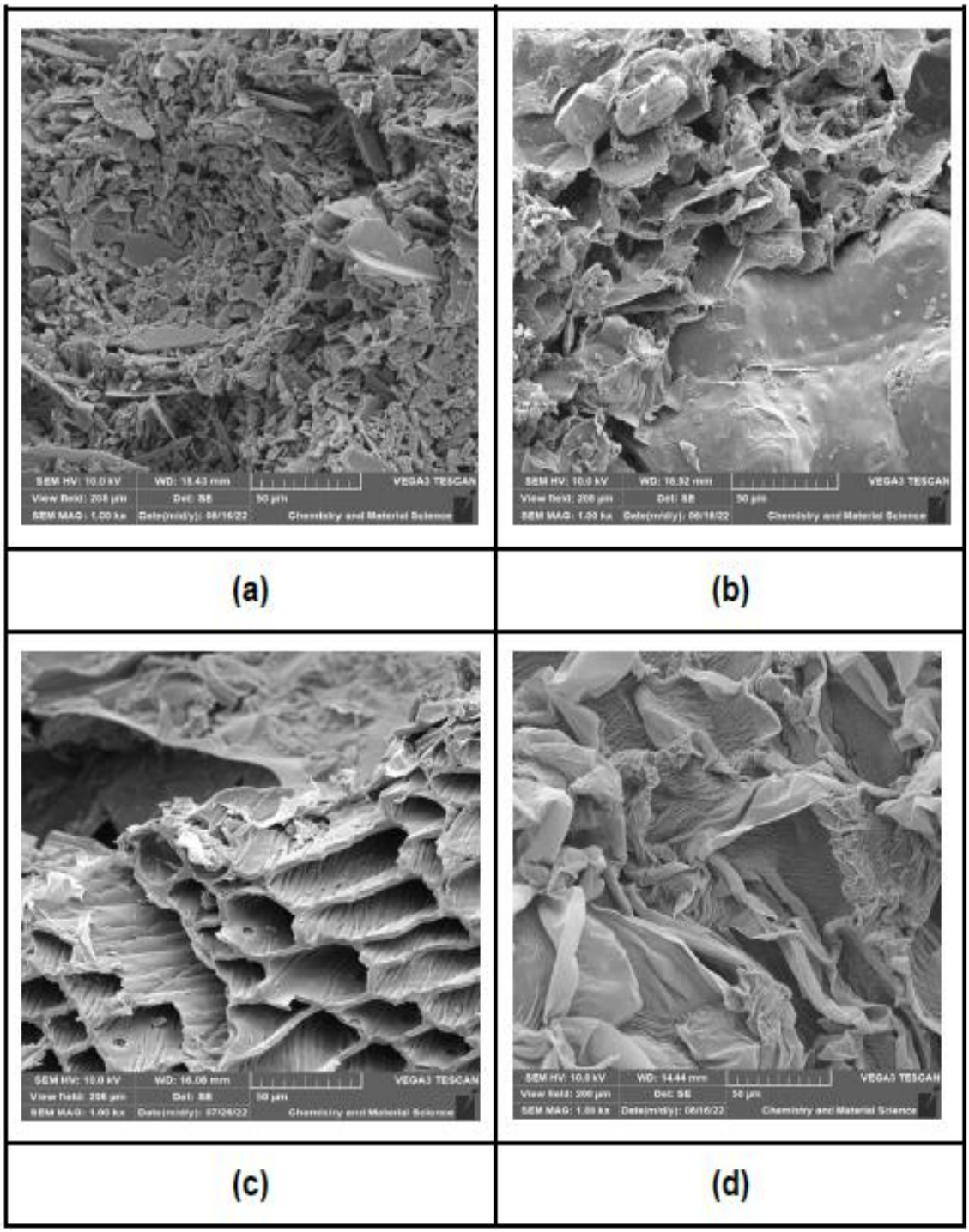

Figure 9. SEM images at 1000x magnification: (a) Binder + Biochar BC2-50; (b) Binder + Biochar BC3-33; (c) Binder + Biochar BC1-33; (d) EPS

CONCLUSIONS

Thermal insulating panels made with renewable resources, bio-binder and biochar, were fabricated in various compositions, with some achieving insulating properties comparable to those of expanded polystyrene (EPS). The biochar feedstock type, mass content, particle size and particle aspect ratio all played a role in the thermal and mechanical performance of the panels. Additionally, the different compositions affected the density, flexural strength and modulus, and the edge crush strength.

Biochar type showed a significant effect in improving the thermal insulation of the panels. The biochar with high aspect ratio produced panels with the lowest thermal conductivity, slightly lower than that measured for EPS. It is worth mentioning, however, that this comes with a considerably higher density compared to EPS. The results presented in this work demonstrate the potential for future alternative thermal insulation packaging that is fully bio-based**.**

REFERENCES

[1] D. Woolf, J. E. Amonette, F. A. Street-Perrott, J. Lehmann, and S. Joseph, "Sustainable biochar to mitigate global climate change," *Nat. Commun. 2010 11*, vol. 1, no. 1, pp. 1–9, Aug. 2010.

[2] M. V. G. Zimmermann, D. Perondi, L. K. Lazzari, M. Godinho, and A. J. Zattera, "Carbon foam production by biomass pyrolysis," *J. Porous Mater. 2020 274*, vol. 27, no. 4, pp. 1119–1125, May 2020.

[3] L. Hu, R. He, H. Lei, and D. Fang, "Carbon Aerogel for Insulation Applications: A Review," *Int. J. Thermophys.*, vol. 40, no. 4, pp. 1–25, Apr. 2019.

[4] L. K. Lazzari, D. Perondi, V. B. Zampieri, A. J. Zattera, and R. M. C. Santana, "Cellulose/biochar aerogels with excellent mechanical and thermal insulation properties," *Cellul. 2019 2617*, vol. 26, no. 17, pp. 9071–9083, Aug. 2019.

[5] F. Segovia, P. Blanchet, N. Auclair, and G. G. E. Essoua, "Thermo-Mechanical Properties of a Wood Fiber Insulation Board Using a Bio-Based Adhesive as a Binder," *Build. 2020, Vol. 10, Page 152*, vol. 10, no. 9, p. 152, Sep. 2020.

[6] G. Burgess, "Practical thermal resistance and ice requirement calculations for insulating packages," *Packag. Technol. Sci.*, vol. 12, no. 2, pp. 75–80, 1999.

[7] Nuclear Power, "Thermal Conductivity of Expanded Polystyrene." [Online]. Available: https://www.nuclear-power.com/nuclear-engineering/heat-transfer/heat-losses/insulation-materials/thermal-conductivity-of-expanded-polystyrene/. [Accessed: 28-Apr-2023].

[8] B. J. Brinkworth, "Thermal Diffusivity of Non-metallic Materials," *Nat. 1964 2014926*, vol. 201, no. 4926, pp. 1309–1309, 1964.

[9] S. Audu Seth, I. Suleiman Aji, and A. Tokan, "Effects of Particle Size and Loading on Tensile and Flexural Properties of Polypropylene Reinforced Doum Palm Shell Particles Composites ," *Am. Acad. Sci. Res. J. Eng. Technol. Sci.*, vol. 2313, pp. 231–239, 2018.

PM-GO02

Effect of consecutive extrusion process on the properties of recycled polyethylene terephthalate (rPET)

Rizka Try Gustina[1], Amporn Sane[1], Piyawanee Jariyasakoolroj[1], Busarin Chongcharoenyanon[1]*

[1]*Department of Packaging and Materials Technology, Faculty of Agro-Industry, Kasetsart University, Bangkok 10900, Thailand*

***Correspondence to**: Busarin Chongcharoenyanon, Department of Packaging and Materials Technology, Faculty of Agro-Industry, Kasetsart University, Bangkok 10900, Thailand.*
E-mail: busarin.cho@ku

ABSTRACT: The present study aims to investigate the effect of the consecutive extrusion process on the physical, mechanical and barrier properties of polyethylene terephthalate (PET) and determine the overall migration of substances from the materials. A twin-screw extruder was used to melt virgin PET (vPET) pellet and recycled PET (rPET) with a screw speed of 130 rpm at the temperature range of 120-280 ℃. The melting process of PET pellets was held from 1 to 6 cycles to imitate rPET processing. The results showed significant variations in the mechanical and physical properties of rPET with the consecutive extrusion processes carried on. The thermal properties and morphology of vPET and rPET were investigated on the pellet while the tensile properties, barrier properties and overall migration were investigated on the sheet. Increasing the number of consecutive extrusion processes affects the significant result in the mechanical and physical properties of rPET. Chain cutting due to hydrolysis, thermal and oxidation degradation were considered responsible for the decrease in the quality of rPET. Chain cutting results in shorter chains and therefore higher free volume. The results show that the processability of rPET was lower as the number of consecutive recycling processes increased. According to the Commission Regulation (EU) 10/2011, the overall migration result of PET from R0 to R6 was less than 10 mg/dm² which complied with the regulation.

Keyword: PET, Recycling, Physical properties, Mechanical properties, Barrier properties, Overall migration

INTRODUCTION

Polyethylene terephthalate (PET) is a thermoplastic belonging to the polyester family. It is a semi-crystalline polymer with excellent chemical resistance, and good mechanical and barrier properties[1]. PET has a high melting temperature (T_m) of around 255 ℃ and a glass transition temperature (T_g) of around 70℃[2]. Due to the increasing concern about the environmental issue, recycling PET (rPET) attracts great interest. However, along the recycling processes, PET goes

through hydrolytic and thermal degradation causing molecular weight reduction and resulting in the properties of rPET. A consecutive extrusion process can decrease the physical and mechanical properties of plastics. The decomposition of the polymer chain reduces the molecular weight and causes changes in chemical properties. The changes can also result in chemical diffusion or migration of substances from plastics when in contact with foods. There are many causes of the properties degradation of rPET such as thermo-mechanical degradation of the polymer chains, the deterioration of thermo-oxidative as well as hydrolytic scission[2]. The chemical release of PET can be affected by storage time and surroundings. The sun exposure test revealed the PET degradation products on the outer surface of the bottle. The released substances include terephthalate monomers and dimers[3]. Furthermore, in long-term storage, water in bottles showed higher levels of formaldehyde and acetaldehyde[4]. One of the most effective ways to manage a PET recycling stream is the bottle-to-bottle recycling process. The post-consumer recycled (PCR) PET bottles are reassembled into new PET bottles. However, there is a risk of the misused container for storage of household cleaners or garden chemicals can enter the stream. The hazardous compounds may be absorbed into the polymer. The effective recycling process is applied to ensure that the contamination is removed from the packaging polymer to avoid the migration of the contaminants to packed food[5].

This study aims to investigate the effect of the consecutive extrusion process on the properties of PET (physical, mechanical, and barrier properties) as a function of the consecutive extrusion process and to determine chemical migration substances from rPET.

MATERIALS AND METHODS

Preparation of rPET resin and rPET sheet by consecutive extrusion process

The virgin PET (vPET) pallet from a local factory in Bangkok, Thailand was dried at 160 ˚C for 6 hours before the melting process[6]. The sample of vPET (R0) was fed to a twin-screw extruder (LTE-20-40, Labtech Engineering, Thailand). The processing temperature was set at 120-280 ℃ and a screw speed of 145 rpm. The extrudates were cut into pellets (R1) by a strand pelletizer (LZ-120, Labtech Engineering, Thailand). The pellets were the stock for the next recycling process. The extrusion process was repeated five times to produce resin samples R2 to R6.

The vPET and rPET pellets were used to prepare the sheet sample. The pellets were fed to the twin-screw extruder (LTE-20-40, Labtech Engineering, Thailand) connected with a 10 cm sheet die. The temperature of the extruder barrel and the cast sheet extruder was 220-275 ℃. These consecutive **extrusion processes mimicked the** PET recycling process resulting in the vPET sheet (R0) and rPET sheet (R1-R6).

Properties of vPET resin and rPET resin determination

Moisture content

The moisture content was measured via the thermogravimetric approach stated in the Association of Official Analytical Collaboration (AOAC)[7]. The empty moisture can was dried in an oven at 105 ˚C for 3 hours and transferred to a desiccator to cool. Three grams of the resin samples were weighed in the moisture can and recorded. The resin in the moisture can and lid were dried in the oven at 130 ˚C for 30 minutes. Then, the moisture can was transferred with a partly covered lid to the desiccator to cool. Reweigh the moisture can and the dry resin sample. The moisture content was calculated.

Melt flow index

The vPET and rPET pellets were dried in the oven at 160 ˚C for 6 hours, to reduce the moisture content before Melt flow index (MFI) measurement. The melt flow index of the samples were determined according to the American Standard Testing and Material (ASTM D1238-10) standard test method for melt flow rate of thermoplastics by extrusion plastomer[8]. A Melt Flow Indexer (MFI-203, Custom scientific, USA) with a load cell of 2.16 kg, a time interval of 6 min. The temperature was set at 285 ℃ with a preheating time of 7 min. MFI were determined in triplicate and reported as mean ± SD in g / 10 minutes.

Differential scanning calorimetry (DSC)

The differential scanning calorimeter (DSC1 STARe, Mettler-Toledo, Switzerland) was used to determine the sample's physical properties and thermal transition. According to the American Standard Testing and Material (ASTM D3418) Standard Test Method for Transition Temperatures and Enthalpies of Fusion and Crystallization of Polymers by Differential Scanning Calorimetry[9]. The samples were weighed in an aluminum pan and placed in a DSC instrument together with a reference pan. The temperature range analyzed was 30-290 ˚C. A heating and cooling rate of 10 °C/min was used with a nitrogen atmosphere around the sample, the nitrogen flow rate of 10-50 mL/min ± 5%. TA Universal Analysis software was used to analyze the recorded thermograms.

Fourier transform infrared (FTIR)

Fourier transform infrared (FTIR) spectra of samples were recorded with an attenuated total reflectance (ATR) mode using an FTIR spectrometer (Bruker Tensor 27, Bruker Corporation, Germany). The spectra were recorded from 4,000 - 400 cm^{-1}.

Properties of vPET sheet and rPET sheet determination

Color

The color measurement was done in the CIELAB color space with a colorimetry (CQXE, Color Global Co., Ltd., Thailand) calibrated by a white tile and the standard black card. The results were reported as color-space coordinates; L* (lightness), a* (position between green and red) and b* (position between yellow and blue).

Tensile properties

The tensile properties of vPET and rPET sheets were tested using a universal testing machine (Instron 5900, USA) according to the standard method of the American Society for Testing and Materials (ASTM D882) Standard Test Method for Tensile Properties of Thin Plastic Sheeting[10]. The sample strips of the uniform width and thickness of 2.5 x 5 cm and range of thickness of sheet 0.50 ± 0.01 mm to 0.75 ± 0.01 mm were used. The sample sheets were stored at 25 °C and 50 ± 2% relative humidity for 48 h. The machine was manipulated with a 5 kN load cell at a speed of 500 mm/min under 23 ± 2 °C and 50 ± 10 % relative humidity.

Impact test

The prepared vPET and rPET sheets were examined for impact strength properties. First, the sample was cut to a square of 10 cm. After that, the sheet's impact strength were tested per ASTM D3420 Standard Test Method for Pendulum Impact Resistance of Plastic Film[11]. The samples were tested by an Impact Testing Machine (FIT-01, Jinan Languang Mechanical and Electrical Technology, China). The testing area had a diameter of 60 mm. The result was reported with an average of the three replicates.

Water vapor permeability determination

The vPET and rPET sheet sample were assessed for the water vapor transmission rate (WVTR) by WVTR test machine (PERMATRAN-W® MODEL 398, Mocon, USA). The test was done followed the American Society for Testing and Materials (ASTM 1249) Water Vapor Transmission Rate Through Plastic Film and Sheeting Using a Modulated Infrared Sensor[12]. The sheets were cut into 10 cm^2. The thickness of the sheet samples was measured using a film thickness gauge. The temperature of each test was recorded.

Overall migration testing

The overall migrations of the vPET sheet (R0) and the rPET sheet (R1-R6) were determined by the gravitational method according to the European Union Commission Regulation No. 10/2011[13] and the amendment Commission Regulation (EU) 2020/1245[14]. The sample sheets were cut and exposed to food simulant B (3% acetic acid) and food simulant C (50% ethanol).

The overall migration test was achieved under the standard testing condition overall migration 2 (40˚C/10 days) and the standard testing condition overall migration 3 (70℃ for 2 hours). The overall migration was determined and compared with the overall migration limit of 10 mg/dm^2 or 60 mg/kg to declare compliance with the Regulation.

RESULT AND DISCUSSION

Physical properties of vPET and rPET

The appearance of pellet and sheet

The virgin PET pallet (R0) was referred to as a control sample. The consecutive extrusion process of the R0 resulted in the rPET pellets (R1-R6). The appearance of the pellets was shown in figure 1. Increasing the number of consecutive extrusion processes affects the color of the pellets as they became more yellow. The sizes of the pellets from each cycle were gradually smaller due to the processability of the polymers. The sample R4 to R6 were non-uniformed and tangled which indicated the quality reduction.

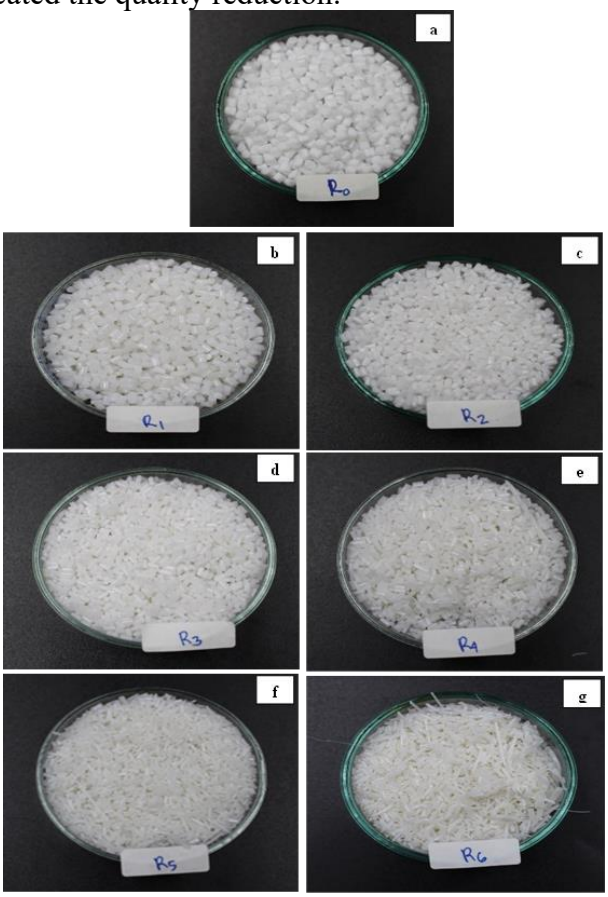

Figure 1. The appearance of vPET and rPET. (a) virgin PET pellet, (b - g) rPET pellet from the consecutive extrusion process 1 to 6

The quality reduction is also shown in the rPET sheet samples after the consecutive extrusion process. The sheets were smaller in width (cross-direction). The sheets could not form in even thickness as shown in figure 2.

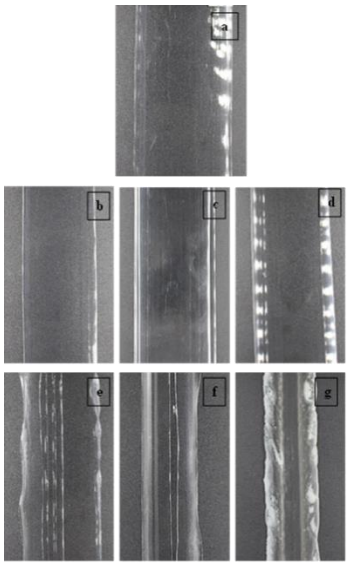

Figure 2. The appearance of vPET and rPET. (a) virgin PET sheet, (b - g) rPET sheet from the pellet of the consecutive extrusion process 1 to 6

During the consecutive extrusion process, thermal degradation produces various types of end groups in the polymer chain. First, the molecular weight of PET decreases due to the break of the ester bond chain. This breaking can occur randomly of the ester bond or at the end of the chain which increases the carboxyl end group. One chain cleavage takes one water molecule and forms one hydroxyl end group and one carboxyl end group. With the chain cutting procedure, the polymer chains are shortened i.e., reduce in molecular weight, which causes a great decrease in mechanical properties resulting in a decrease in the quality of pellets and sheets compared to vPET samples[15,16].

The color measurement was carried out using HunterLab CIELAB colorimeter, and the measurement was converted by the instrument to CIELAB color-space coordinates as shown in table 1.

Samples	L*	a*	b*
R0	38.30 ± 0.75	0.03 ± 0.07	-2.25 ± 0.10
R1	40.10 ± 0.88	-0.05 ± 0.03	-2.29 ± 0.12
R2	39.57 ± 0.31	0.01 ± 0.03	-1.54 ± 0.26
R3	39.25 ± 0.58	0.06 ± 0.03	-1.22 ± 0.05
R4	43.68 ± 2.65	0.02 ± 0.04	-0.86 ± 0.24
R5	42.16 ± 1.41	0.03 ± 0.10	-0.83 ± 0.42
R6	45.28 ± 3.66	-0.19 ± 0.03	-0.65± 0.27

Table 1. The color values of vPET and rPET sheet according to CIELAB

The lightness of the sample is indicated by the L* value which is crucial to indicate the quality of rPET. The lower L* value expressed the darkness of the samples. The sample R0 (control sample) has an L* value of 38.30. The more consecutive extrusion processes are carried out, the higher the L* value in the sample. The more negative a* indicated a slight green. In addition, for b* values, rPET samples showed negative values in the range of -0.6 to -2.2. The results of b* show that, with the increase of consecutive extrusion or the recycling process of rPET, the appearance turned yellow. According to James, D. E. and L. G. Packer (1995)[17], the yellowing of PET is caused by thermal degradation. Throughout the thermal processing of PET above its melting temperature, thermal cleavage of the PET ester bonds results in shorter chains. Then acid and vinyl ester end groups form. The thermal processing is intense in repeated recycling which generates more carboxyl end groups in PET and causes more oxidation[18]. The higher b* value exhibited the yellowness of the rPET sample which experienced repeated heat processing. The color shifting caused by chain-cutting reactions and subsequent morphological changes[19,20]

Density of pellet

The density results of vPET (R0) and rPET (R1-R6) were in the range of 1.30 – 1.42 g/cm³ as shown in figure 3. vPET has the highest density and the rPET from the consecutive extrusion R1 to R5 were comparable while the R6 gave the lowest density of rPET. The variation in the density is caused by the amount of free volume among the polymer chains. Short-chain polymers form more free volume than long-chain polymers[21,22]. While the polymer got through the screw of the extruder, the polymer chains incision, oxidation, hydrolysis and thermal degradation occurred. These reactions resulted in short chain polymers, so the density was lower. During the manufacture and processing of rPET, polymers subjected to high temperatures melt and process enough polymer to cause chain cutting (thermal breakdown). Every chain scission consumes one water molecule, creating one carboxyl and one hydroxyl end group. The polymer chain shortens (reduced molecular weight) with the chain scission process. The molecular weight dependence follows the molecular weight dependence of density and is thus easily understood via the free-volume concept. Higher molecular weight polymers give fewer chain ends, which will have less free volume, higher T_g, and higher density, and vice versa[23].

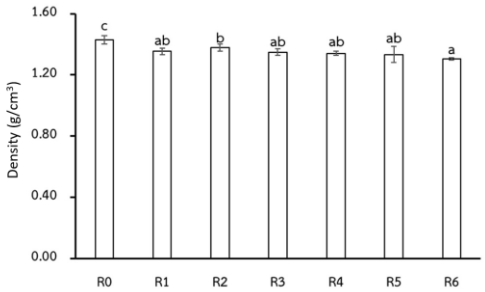

Figure 3. The density of vPET and rPET. The data is reported as mean ± SD. The different small letters indicate a significant difference at $p < 0.05$ (Duncan's new multiple range test).

The melt flow index (MFI)

The MFI was determined using Melt Flow Indexer (MFI-203, Custom Scientific, USA) according to the American Society for Testing and Materials (ASTM 1238-10) with a load cell of 2.16 kg at a temperature of 285˚C. The MFI of vPET (R0) and rPET (R1-R6) were in the range of 44.18 to 298.15 g/10 min (figure 4). The samples that passed more cycles of the consecutive extrusion processes had more MFI. The MFI relates to the viscosity which is reflected by the molecular characteristics of each polymer. The increase in cycle brings the shorter chain with lower molecular weight and leads to the decrease in viscosity. An increase in the number of consecutive extrusion processing causes an increase in the degree of degradation, as indicated by an increase in the concentration of the carboxyl end groups and the melt flow index. In addition, the relation between molecular weight and viscosity. The decrease in the molecular weight (chains break) leads to a reduction in viscosity, i.e., a reduction in the resistance to flow that causes an increase in the melt flow index[24].

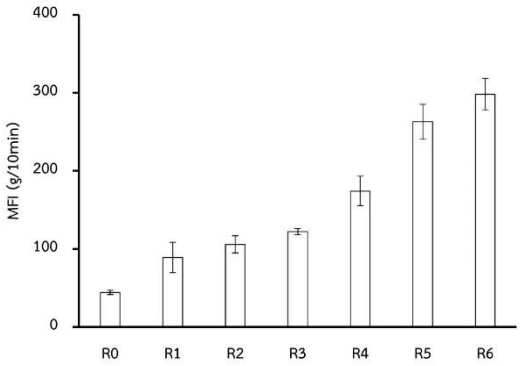

Figure 4. Melt flow index of vPET and rPET. The data is reported as mean ± SD. The different small letters indicate a significant difference at $p < 0.05$ (Duncan's new multiple range test).

The moisture content of pellet

Figure 5 shows the moisture content value of vPET and rPET. The data is reported as mean ± SD. The results were higher than the previously reported value of 0.02% or less[25]. High moisture content and high temperatures trigger the hydrolysis degradation in rPET in the consecutive extrusion process. The condition decreases the crystallinity of rPET which arise the amorphous component and water content of the polymer[21,26-29].

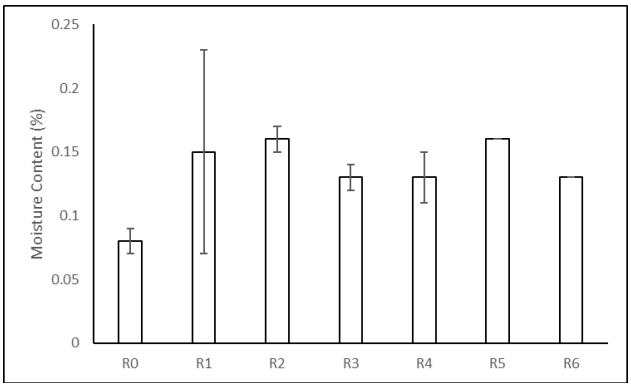

Figure 5. The moisture content of vPET and rPET

Fourier transform infrared spectroscopy

The functional groups for polymers in vPET and rPET were determined by Fourier transform Infrared (FTIR) Spectroscopy in the wavelength range of 4,000-400 cm^{-1} as shown in figure 6. The specific spectra of vPET and rPET are not different. The characteristics are as follows: a peak appears at wave number 1,711 cm^{-1} indicated the stretching vibration of the C=O bond of the carboxylic group. The peak at wave number 1,233 cm^{-1} represents the C-O stretched vibration of carboxylic groups[30-34]. The peak at wave number 1,090 cm^{-1} represents the symmetric stretching vibrations of $O–CH_2$ of the ethylene glycol group. The gauche conformation laid within the PET amorphous region. The peak at wave number 718 cm^{-1} represented the bending vibrations of C–H and C–C of the benzene group. Increasing the number of extrusion cycles had no significant effect on the specific spectra of PET, in other words, the chemical functional groups of the decomposed PET were not different from those of vPET.

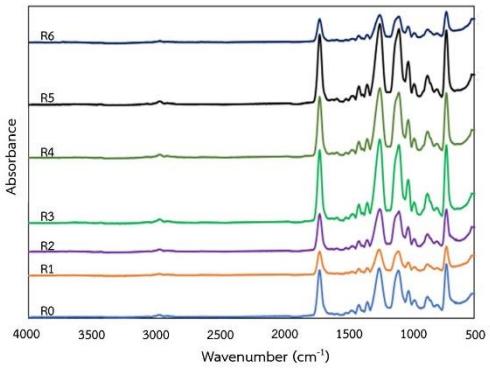

Figure 6. The spectrum of FTIR of vPET and rPET

Mechanical properties of vPET and rPET

Tensile properties of sheet

Figure 7 shows a decrease in tensile strength and elongation at break of the rPET through the consecutive extrusion process. It was found that vPET had a tensile strength of 77.0 MPa, elongation at break of 5.1% and Young's modulus of 1,259.2 MPa. Through the consecutive extrusion process, the mechanical properties tend to decrease. The rPET samples from the early cycles (R1-R3) had tensile strength and the elongation at break decreased in the range of 65.5-71.4 MPa and 4.6-5.0%, respectively. The results significantly decreased in the later cycles (R4-R6). However, Young's modulus was not significantly changed. Along the consecutive extrusion process, the deterioration of the polymer structure is attributed to the decline of tensile properties[35]. Mechanical recycling with an extruder installs physical forces which lessen the tensile properties of the polymers. To enhance the quality of materials, vPET is added to the rPET input e.g., the ratio of vPET:rPET is 70:30 for PET bottle recycling[2].

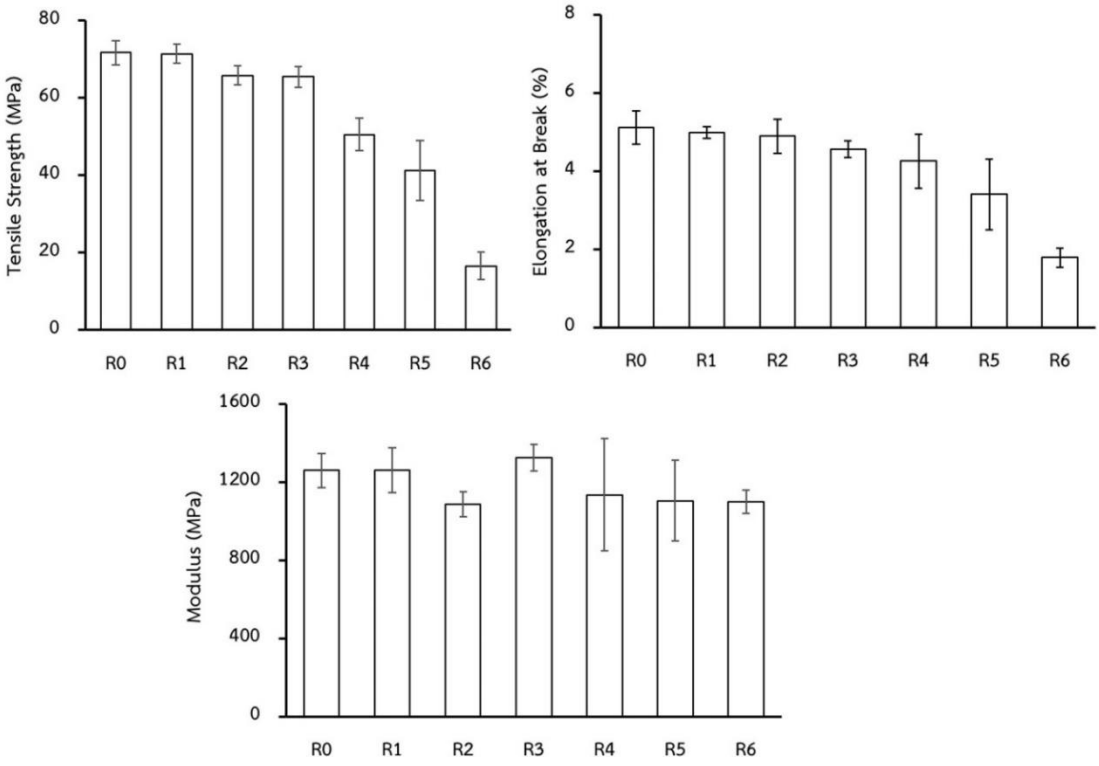

Figure 7. (a) Tensile strength, (b) Elongation at break, (c) Young's modulus of vPET and rPET

Impact test

Figure 8 shows the effect of the consecutive extrusion process on the toughness of the vPET and rPET sheets. The impact test indicates the total energy the sheet absorbed to the rupture

point of the material. It shows the ability to resist the impact of the sheet. The sample from the consecutive extrusion process R0-R4 can be tested but the sample R5 and R6 were too small for the testing apparatus. The sample of vPET (R0) had an impact strength of 2.4 Joules. After the 1–3 extrusion cycle (R1–R3), the impact strength decreased slightly in the range of 2.0–2.4 Joules. However, after 4 cycles of extrusion, the impact resistance was reduced to only 0.6 joules. The reduction of the molecular weight of the polymer results in a decrease in the impact resistance[35,36] which is consistent with the results of tensile property testing.

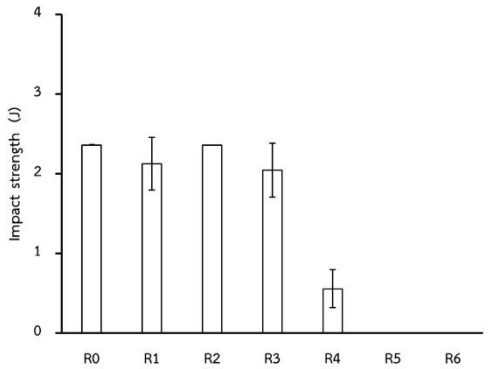

Figure 8. Impact test of vPET and rPET

Thermal properties of vPET and rPET

Differential scanning calorimetry (DSC) analysis

The results of the thermal properties determined by Differential Scanning Calorimetry (DSC) estimated by the second heating scan of vPET and rPET are shown in Table 2. Considering the sample vPET (R0), the glass-transition temperature (T_g) was 73.7 °C and the melting temperature (T_m) was 243.9 °C. After the consecutive extrusion process, the T_g and T_m of rPET (R1-R6) were 74.8–81.4 °C and 251.3–253.4 °C, respectively. The crystallinity of vPET and rPET was calculated from the endothermic energy at the T_m position of PET (ΔH_m). The crystallinity of vPET (R0) was 60.0%. After extrusion, it was found that the crystallinity of rPET (R1-R6) decreased in the range of 15.5–43.7%. The consecutive extrusion process caused the degradation of the polymer chain resulting in shorten polymer chain and adecrease in the amount of crystallinity[37-39].

Sample	T_g (°C)	T_m (°C)	ΔH_m (J / g)	ΔH_c (J / g)	% Crystallinity
R0	73.66	243.91	-60.50	0.69	60.01
R1	79.62	252.00	-54.30	54.30	15.54
R2	79.41	251.33	-32.27	0.35	32.02
R3	74.84	252.57	-35.96	0.69	35.47
R4	80.78	251.89	-44.18	0.63	43.73
R5	81.35	253.36	-42.45	1.15	41.63
R6	79.08	253.43	-16.25	0.25	16.07

Table 2. Differential scanning calorimetry of vPET and rPET

Barrier properties of vPET and rPET

Water vapor permeability (WVP)

The WVP of PET sheets are shown in Figure 9. The vPET sheet (R0) has a WVP of 4,500 g.mil/m^2.day.atm. Along the consecutive extrusion process R1 to R5, the WVP increased in the range of 6,633–13,102 g.mil/m^2.day.atm. Moreover, the WVP of the R6 sheet was significantly increased to 48,897 g.mil/m^2.day.atm. The short-chain polymer and low crystallinity allowed more water vapor to diffuse through the sheet[40].

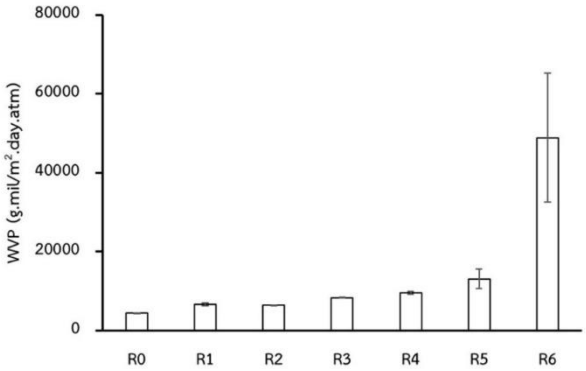

Figure 9. The water vapor permeability of vPET and rPET

Overall migration

The overall migration (OM) test was carried out using food simulant B (3% acetic acid) and food simulant D1 (Ethanol 50%) under the standard testing condition for overall migration 2 (OM2) at 40˚C for 10 days and the standard testing condition for overall migration 3 (OM3) at 70℃ for 2 hours. The results are shown in figure 10.

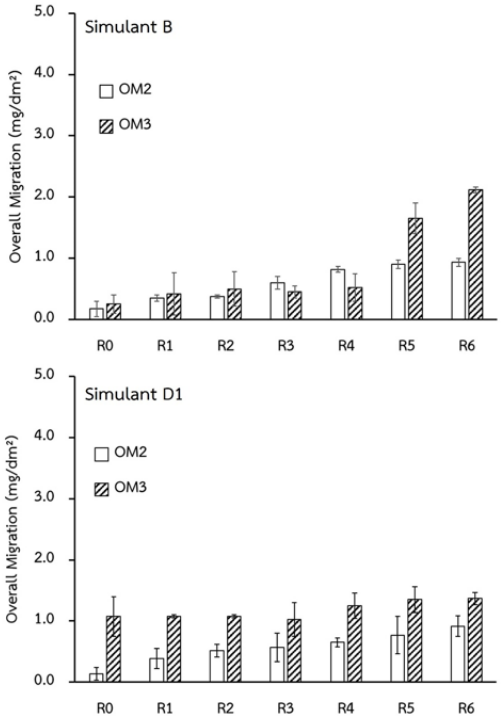

Figure 10. Overall migration of vPET and rPET in food simulant B and food simulant D1

Samples were extracted in food simulant B (3% acetic acid) which was assigned to simulate the foods that have a hydrophilic character with pH below 4.5 and food simulant D1 (50% ethanol) which represents the foods with oil in water emulsions and food with alcohol content higher than 20%. The extraction was conducted under the standard testing conditions OM2 which represented the worst foreseeable contact conditions of the storage at ambient temperature or lower temperature. This condition includes the hot-fill process condition or heating at the range of 70-100 °C for a maximum of time equal to 120/2^((T-70)/10) minutes. The OM of vPET extracted in food simulant B and food simulant D1 were 0.2 mg/dm^2 and 0.1 mg/dm^2, respectively. The OM of rPET was increased by the consecutive extrusion process to the range of 0.4–0.9 mg/dm^2 in both simulants. The samples were also tested under the testing condition OM3 which represented the worst foreseeable contact conditions of the hot-fill process condition or heating at the range of 70-100 °C for a maximum of time equal to 120/2^((T-70)/10) minutes, which are not followed by long-term room temperature or refrigerated storage. The OM of vPET (R0) was 0.3 mg/dm^2 in food simulant B and 1.1 mg/dm^2 in food simulant D1. The consecutive extrusion process R1 to R3 slightly increased the OM while R4 to R6 significantly increased the OM. In comparison, the OM result obtained under the OM3 testing condition was higher than the result obtained under the OM2 testing condition. The high temperature close to the glass transition temperature of PET results in higher diffusion of the substances from the materials. The OM in food simulant B was higher than that of simulant D1 because acetic acid hydrolyzed PET. However, the OM of all samples were still lower than the

overall migration limit (OML) of 10 mg/dm^2 which complies with European regulations regarding food packaging [41].

CONCLUSIONS

The consecutive extrusion process was employed to imitate the mechanical recycling process of PET. The process decreased crucial properties of rPET such as appearance, mechanical properties, and processability. The high temperature, moisture in the material, and force under the screw of the extruder destroyed the structure of the polymer which led to the polymer chains incision, oxidation, hydrolysis, and thermal degradation. These reactions highly affected the rPET from the 4th consecutive extrusion process and later (R4-R6). The overall migration results for food simulant B and food simulant D1 under the standard testing condition OM2 and OM3 complied with European Regulations. The addition of vPET and other additives to improve the quality of rPET in multiple recycling are essential for the processability and quality of the rPET recyclate.

REFERENCES

1. Alexander P. *Encyclopedia of agriculture and food systems.* Elsevier; 2014.
2. Schyns ZOG, Shaver MP. Mechanical Recycling of Packaging Plastics: A Review. *Macromolecular Rapid Communications.* 2021;42(3):2000415.
3. Schmid P, Kohler M, Meierhofer R, Luzi S, Wegelin M. Does the reuse of PET bottles during solar water disinfection pose a health risk due to the migration of plasticisers and other chemicals into the water? *Water Research.* 2008;42(20):5054-5060.
4. Lugwisha E, Mahugija JA, Mwankuna C. Levels of formaldehyde and acetaldehyde in selected bottled drinking water sold in urban areas in Tanzania. *Tanzania Journal of Science.* 2016;42(1):1-14.
5. Welle F, Franz R. Migration of antimony from PET bottles into beverages: determination of the activation energy of diffusion and migration modelling compared with literature data. *Food additives & contaminants Part A, Chemistry, analysis, control, exposure & risk assessment.* 2011;28(1):115-126.
6. Duarte IS, Tavares AA, Lima PS, et al. Chain extension of virgin and recycled poly(ethylene terephthalate): Effect of processing conditions and reprocessing. *Polymer Degradation and Stability.* 2016;124:26-34.
7. Horwitz W. *Official methods of analysis of AOAC International. Volume I, agricultural chemicals, contaminants, drugs/edited by William Horwitz.* Gaithersburg (Maryland): AOAC International, 1997.; 2010.
8. ASTM International. ASTM D1238-10 Standard Test Method for Melt Flow Rates of Thermoplastics by Extrusion Plastometer. In:2013:16.
9. ASTM International. ASTM D3418-21 Standard Test Method for Transition Temperatures and Enthalpies of Fusion and Crystallization of Polymers by Differential Scanning Calorimetry. In:2021:8.

10. ASTM International. ASTM D882-18 Standard Test Method for Tensile Properties of Thin Plastic Sheeting. In:2018:12.
11. ASTM International. ASTM D3420-21 Standard Test Method for Pendulum Impact Resistance of Plastic Film. In:2021:5.
12. ASTM International. ASTM F1249-20 Standard Test Method for Water Vapor Transmission Rate Through Plastic Film and Sheeting Using a Modulated Infrared Sensor. In:2020:6.
13. The European Commission. Commission Regulation (EU) No 10/2011 of 14 January 2011 on plastic materials and articles intended to come into contact with food. In: EUR-Lex, ed: Official Journal of the European Union; 2011:89.
14. The European Commission. Commission Regulation (EU) 2020/1245 of 2 September 2020 amending and correcting Regulation (EU) No 10/2011 on plastic materials and articles intended to come into contact with food. In: Official Journal of the European Union; 2020:17.
15. Flynn JH. Chapter 14 - Polymer degradation. In: Cheng SZD, ed. *Handbook of Thermal Analysis and Calorimetry.* Vol 3. Elsevier Science B.V.; 2002:587-651.
16. Pan J, Chen X. 2 - Modelling degradation of amorphous biodegradable polyesters: basic model. In: Pan J, ed. *Modelling Degradation of Bioresorbable Polymeric Medical Devices.* Woodhead Publishing; 2015:15-31.
17. James DE, Packer LG. Effect of Reaction Time on Poly(ethylene terephthalate) Properties. *Industrial & Engineering Chemistry Research.* 1995;34(11):4049-4057.
18. Bikiaris DN, Karayannidis GP. Chain extension of polyesters PET and PBT with N,N′-bis (glycidyl ester) pyromellitimides. I. *Journal of Polymer Science Part A: Polymer Chemistry.* 1995;33(10):1705-1714.
19. Badia JD, Strömberg E, Karlsson S, Ribes-Greus A. The role of crystalline, mobile amorphous and rigid amorphous fractions in the performance of recycled poly (ethylene terephthalate) (PET). *Polymer Degradation and Stability.* 2012;97(1):98-107.
20. La Mantia FP. *Recycling of plastic materials.* ChemTec Publishing; 1993.
21. Al-Azzawi F. *DEGRADATION STUDIES ON RECYCLED POLYETHYLENE TEREPHTHALATE*: POLYMER SCIENCE AND ENGINEERING, LONDON METROPOLITAN UNIVERSITY; 2015.
22. Venkatachalam S, Shilpa GN, Jayprakash VL, Prashant RG, Krishna R, Anil KK. Degradation and Recyclability of Poly (Ethylene Terephthalate). In: Hosam El-Din MS, ed. *Polyester*. Rijeka: IntechOpen; 2012:Ch. 4.
23. Attwood J, Philip M, Hulme A, Williams G, Shipton P. The effects of ageing by ultraviolet degradation of recycled polyolefin blends. *Polymer Degradation and Stability - POLYM DEGRAD STABIL.* 2006;91:3407-3415.
24. Romão W, Franco MF, Corilo YE, Eberlin MN, Spinacé MAS, De Paoli M-A. Poly (ethylene terephthalate) thermo-mechanical and thermo-oxidative degradation mechanisms. *Polymer Degradation and Stability.* 2009;94(10):1849-1859.
25. Awaja F, Pavel D. Recycling of PET. *European polymer journal.* 2005;41(7):1453-1477.

26. Fernando S, Christensen P, Egerton T, et al. Carbon dioxide formation during initial stages of photodegradation of poly(ethyleneterephthalate) (PET) films. *Materials Science and Technology.* 2009;25:549-555.
27. Hosseini SS, Taheri S, Zadhoush A, Mehrabani-Zeinabad A. Hydrolytic degradation of poly(ethylene terephthalate). *Journal of Applied Polymer Science.* 2007;103(4):2304-2309.
28. Negoro T, Thodsaratpreeyakul W, Takada Y, Thumsorn S, Inoya H, Hamada H. Role of Crystallinity on Moisture Absorption and Mechanical Performance of Recycled PET Compounds. *Energy Procedia.* 2016;89:323-327.
29. Thumsorn S, Yamada K, Wei Leong Y, Hamada H. Effect of pellet size and compatibilization on thermal decomposition kinetic of recycled polyethylene terephthalate/recycled polypropylene blend. *Journal of Applied Polymer Science.* 2012;124(2):1605-1613.
30. Chen Z, Hay JN, Jenkins MJ. FTIR spectroscopic analysis of poly(ethylene terephthalate) on crystallization. *European Polymer Journal.* 2012;48(9):1586-1610.
31. Coates J. Interpretation of Infrared Spectra, A Practical Approach. In: *Encyclopedia of Analytical Chemistry.*2006.
32. Pearce EM, Bulkin BJ, Ng MY. Fourier Transform IR Spectroscopy for the Study of Polymer Degradation. In: *Polymer Characterization.* Vol 203. AMERICAN CHEMICAL SOCIETY; 1983:571-593.
33. Smith BC. *Infrared Spectral Interpretation: A Systematic Approach (1st ed.).* Boca Raton: CRC Press; 1998.
34. Stuart BH. *Infrared Spectroscopy: Fundamentals and Applications.* John Wiley & Sons, Ltd; 2004.
35. Wu H, Lv S, He Y, Qu J-P. The study of the thermomechanical degradation and mechanical properties of PET recycled by industrial-scale elongational processing. *Polymer Testing.* 2019;77:105882.
36. Candal MV, Safari M, Fernández M, et al. Structure and Properties of Reactively Extruded Opaque Post-Consumer Recycled PET. *Polymers.* 2021;13(20):3531.
37. Demirel B, Yaraş A, Elçiçek H. Crystallization behavior of PET materials. *Balıkesir Üniversitesi Fen Bilimleri Enstitüsü Dergisi.* 2011;13(1):10.
38. Liu RYF, Hu YS, Schiraldi DA, Hiltner A, Baer E. Crystallinity and oxygen transport properties of PET bottle walls. *Journal of Applied Polymer Science.* 2004;94(2):671-677.
39. Mohammadi S, Taremi FA, Rafizadeh M. Crystallization conditions effect on molecular weight of solid-state polymerized poly(ethylene terephthalate). *Iranian Polymer Journal.* 2012;21(7):415-422.
40. Cocca M, Lorenzo MLD, Malinconico M, Frezza V. Influence of crystal polymorphism on mechanical and barrier properties of poly(l-lactic acid). *European Polymer Journal.* 2011;47(5):1073-1080.
41. Masmoudi F, Alix S, Buet S, et al. Design and Characterization of a New Food Packaging Material by Recycling Blends Virgin and Recovered polyethylene terephthalate. *Polymer Engineering & Science.* 2020;60(2):250-256.

PM-GO03

Sugarcane as a source to produce paper in Mexico. A study to evaluate the feasibility for Mexican Industry

Cristina Guzman-Siller[1*], Alexia D.L. Martinez[2], Valeria Montemayor-Garza[2], Alisson Villareal-Hurtado[2], Ma Guadalupe Paredes[2], and Carlos Escamilla-Alvarado[3]

[1]*Industrial Design, Univ. de Monterrey, San Pedro Garza Garcia, N.L. 66238, México*
[2]*Engineering School, Univ. De Monterrey, San Pedro Garza Garcia., N.L. 66238, México*
[3]*Faculty of Chemistry, Univ. Autónoma de Nuevo Leon, San Nicolas G, N.L. 64290, México*

***Correspondence to:** Cristina Guzman-Siller. Industrial Design, Univ. de Monterrey, San Pedro G.G., 66238, México.*
E-mail: cristina.guzman@udem.edu

ABSTRACT: Environmental impacts have persuaded the industry to look for new material resources or to implement new technologies, to generate biodegradable or composted materials. Spain introduced sugarcane into the Veracruz area in the year 1522. Now, Mexico is the sixth producer of sugarcane in the world, with 4.6% of the global production, 59,333,988 million tons a year[2]. The production is concentrated in 51 sugar factories in the country. Veracruz state is the biggest producer, with 37.6 % of its 22 sugar factories.
India, South Africa, Colombia, and Argentina are the only four countries that had developed the commercial production of paper based on sugarcane.[3]. Paper from sugarcane has demonstrated to be a more sustainable option because it doesn't use chemistry in its process.
Mexico does not have wood forests to produce paper, most of the Mexican paper is recycled from imported paper and cardboard, producing low-quality cardboard. Therefore, this project starts by asking: Why not use another material source with longer fibers to improve Mexican cardboard?
This study has two objectives, review the 4 countries producing paper based on sugarcane and analyze their process and the quality of their papers. After this review, the target will be to develop the best process to produce this type of paper in Mexico.

Keywords: bagasse sugar cane, sugarcane paper, biodegradable materials, composted materials, sugarcane pulp

INTRODUCTION

The research started by studying the production of sugarcane in Mexico and looking for a source of bagasse sugarcane to start to know the product and make the first analyses of the material. It was not easy because the largest companies are using the material to produce energy. At the same time, we investigated paper factories to see who was working with bagasse,

and surprisingly we found that most of the companies are not using bagasse in their line of production since 2020. One of the companies told us that they stopped using bagasse because the support from the government was cut-off. In order to continue to understand the reasons better, interviews with the industry will be continued.

The bagasse of sugar cane began to be used in Mexico 150 years ago, and the National Chamber of Cellulose and Paper Industry, reported in 2001, from the year before, the production of 199,755 tons of white chemistry cellulose from bagasse representing 34.3% of paper production [1]. In 2010 the Mexican paper industry leveraged 4.7 million of Mg recycled fiber which represented 87% of the fiber material used per year [2].

The process to obtain the bagasse requires 36 hr of natural dry, which goes into the mill to reduce the size and then is sieved to separate in sizes between 180 to 850 mm to be used and tested [3]. The bagasse is a residue of the production of sugar or alcohol, in industrial processes can reach around 26% to 29% of the processed sugarcane [4]. Other authors, such as Bantacut [5] and Guerra [6] sustain that 30-40% can be reached, depending on factors, such as harvest time, agronomic practices, soil conditions, and milling operations [7]. Rao [8] recommends storing the bagasse for two months to improve processability at the paper machine, destroy the sugar residues, and destroy foaming. To produce the pulping the use of soda and low temperature is a common process, and the use of dioxide or ODEPD for bleaching is better to reduce water production than traditional Chlorine and hypochlorite [9].

Sugarcane bagasse has attracted attention as a substitute for non-wood raw materials and many researchers are studying the possibilities of the pulp of sugarcane [10], but nowadays a small portion is used because it is hindered by its short fibers producing low strength [11]. Varshney [12] pointed out that the use of bagasse makes the products lightweight, flexible, and microwaveable which prevents leakage and can be relevant to produce packages and other products.

The need to replace plastic is a worldwide trend. With bioplastics based in natural fibers, or paper pulped, some are large producers of sugarcane such as Brazil, India, Thailand, China, Mexico, Colombia, and Australia as well other countries with less production such as the Philippines, Iran, Egypt, and England. The research is focused on micro and nanofibers studying their structural behavior and diverse applications [2]. Bagasse is not the only fiber that has been studied, others like bamboo, coconut, avocado, coffee, banana, agave, pineapple, potatoes, oil palm castor oil plants had been tested and some had been combined to mix their characteristics [11, 13, 7, 14]

Importance

The use of plastic for packaging has been rising in the last decade, because of their low cost, low weight, long lasting life and suitable for diverse applications. Nevertheless the residues and contamination from plastic packaging had a harmful effect on the environment as well the production of them

There are a few studies related to the life cycle assessment (LCA) on bagasse pulp and most of them, in mold products to test their biodegradable aspect or compare sugarcane bagasse pulp vs polystyrene (PS) [15].

Nowadays, packaging products manufactured from renewable materials, fiber base, represents only 2% of the market [15]. When the waste of many products could be transformed into a source of raw material to develop eco-friendly packages.

In the case of Mexico, the secondary fibers is a source that is strongly used; Mexico is placed on the top ten collectors of recycled paper world wide with an index of 46.7%, and the third place of recycling secondary fiber with an index of 78.6%, but the secondary fibers are degradable with the uses reducing their quality, therefore the use of natural fibers non-wood materials could enrich their properties [16]. This research is based on the statement of low quality of paper produced in Mexico, which becomes recycled corrugated cardboard with low resistance.

The ultrafiltered biopulping of sugarcane bagasse has the potential to decrease the demand of chemicals, and strengthen the quality of the paper and be environmentally sustainable [17].

As Sibali points out, only 10% of global paper production uses non.wood lignocellulosic material, which has short growing cycles and low lignin content reducing the consumption of energy and chemicals in the pulping process [18].

Objectives

The objectives of this study are three. The first goal is presented in this paper.

1) To determine the characteristics of the sample and get familiar with the fiber material to see the favorable characteristics and the complicated elements that form part of the fibers.
2) Research about the paper industry, the role and history of sugarcane bagasse in the paper industry and review the industry and the products that are produced from natural fibers.
3) Investigate the process used to treat the fibers, whitening, and evaluate them from their impact to the environment, water treatments, soil contamination and residues management process. (this goal is not presented in this paper)

MATERIALS AND METHODS

The bagasse sample was collected at Panuco Veracruz, a sugarcane factory which belongs to the group PANTALEON, a Guatemalan firm. Veracruz is the state which produces 37.6% of sugarcane in Mexico. The fiber was collected at the mill, transported to Monterrey and naturally dried for a month. Latter was sieved to separate in three sizes large, medium and powder and was stored in a plastic bag. For the lab test the powder was used.

Prior to the determination of a methodology for the pulping and bleaching of the sugarcane bagasse, the material was analyzed regarding its composition (lignin, cellulose, holocellulose, total solids and volatile solids content); the sample of sugarcane bagasse used had a size of less than 210 µm.

The experimental development took place in the Center for Biotechnology and Nanotechnology Investigation following their procedures (Monterrey, Nuevo Leon, Mexico).

Determination of the total solids (TS) and volatile solids (VS) content

First, in an analytical balance, the porcelain crucible (W0) was weighed. The balance was tare and approximately 0.2500 g of sugarcane bagasse sample was added to the crucible, obtaining the weight of the sample (S). Then, the crucible with the sample was taken to a drying oven where it remains at a temperature of 105°C until the weight is constant (3 hours). After removing it from the oven, it is weighed again on the analytical balance (W1). Then, the sample is calcined in a muffle furnace for 3 hours at a temperature of 550°C and weighed again (W2). Finally, to calculate the content (%) of total solids (TS) and volatile solids (VS) the following equations were used:

$TS=FW1-W0S*100$ ***(1)***
$VS=W1-W2W1-W0*100$ ***(2)***

Determination of lignin content

Approximately 0.2000 g of sugarcane bagasse sample (S) are weighed on an analytical balance. Then, the sample was inserted into a test tube with a lid and, using a precision pipette (1 ml), 2 ml of H2SO4 at 72% were poured into the test tube. After agitating the tube to mix its contents, the test tube was heated using a water bath at a temperature of 40°C for 1 hour to create a digestion process. Then, the contents of the test tube were poured into an Erlenmeyer flask (125 ml) as well as 56 ml of water by first pouring it into the test tube and then the flask. After covering the top of the flask with aluminum foil, the flask was placed in a water bath and boiled for 2 hours at a temperature of 80-90°C. Then, using a Gooch crucible with filter paper (previously weighed-W0) and a vacuum filtration flask connected to a vacuum, the contents of the flask were filtered using distilled water when necessary to ensure all the contents were filtered. After this, the crucible was taken to a drying oven at a temperature of 105°C until the weight was constant. After it was removed from the oven and weighed (W1), it was taken to a muffle furnace for 3 hours at a temperature of 550°C. Then, the crucible was removed and weighed (W2). To calculate the lignin content the following equation was used:

$Lignin\ content=W1-W2S*100$ ***(3)***

Determination of cellulose content

A piece of paper, around 0.1000 g of the sample was weighed on an analytical balance (S) . Then, the sample was inserted into a test tube with a lid and, using a precision pipette (1 ml), 2 ml of distilled water and 1 ml of nitric acid were poured into the test tube. Then 8 ml of acetic acid were poured into the tube. After agitating the tube to mix its contents, the test tube was placed in a water bath and boiled for 2 hours at a temperature of 80-90°C. After removing the test tube, using a Gooch crucible with filter paper (previously weighed-W0) and a vacuum filtration flask connected to a vacuum, the contents of the tube were filtered using distilled water when necessary to ensure all the contents were filtered. Then, the test tube was taken to

the drying oven where it stayed at a temperature of 105°C until the weight was constant. Then, the crucible was taken out and weighed (W1). After this, it was taken to a muffle furnace for 3 hours at a temperature of 550°C. Then, the crucible was removed and weighed (W2). Finally, to calculate the cellulose content the following equation was used:

*Cellulose=W1-W2S*100* ***(4)***

Determination of holocellulose content

A piece of paper, around 0.1000 g of the sample was weighed on an analytical balance. Then, the sample was inserted into a test tube and 15 ml of bleach (Cloralex) were added. After agitating the tube to mix its contents, the bleach was left to proceed with the bleaching process until the sample was bleached. Then, using a Gooch crucible with filter paper (previously weighed-W0) and a vacuum filtration flask connected to a vacuum, the contents of the tube were filtered using distilled water when necessary to ensure all the contents were filtered. Then, the test tube was taken to the drying oven where it stayed at a temperature of 105°C until the weight was constant. After this, the crucible was taken out and weighed (W1). Then, it was taken to a muffle furnace for 3 hours at a temperature of 550°C. Then, the crucible was removed and weighed (W2). Finally, to calculate the cellulose content the following equation was used:
*Holocellulose=W1-W2S*100* ***(5)***

RESULTS

Test #	**W0 (crucible weight) (g)**	**S (material weight) (g)**	**W1 (g)**	**TS (%)**	**W2 (g)**	**VS (%)**
1	9.3254	0.2501	9.5622	94.6821	9.3715	80.5321
2	9.2014	0.2614	9.4481	94.3764	9.2463	81.7998
3	10.2159	0.3256	10.5230	94.3182	10.2752	80.6903
Average				94.4589		81.0074

Table 1.- Total Solids and Volatile solids

Test #	W0 (Gooch crucible + filter weight) (g)	S (material weight) (g)	W1 (g)	W2 (g)	% Lignin
1	29.5478	0.2024	29.6309	29.5715	29.3478
2	34.0547	0.2176	34.1427	34.0811	28.3088
3	21.4798	0.2088	21.5593	21.5039	26.5326
Average					28.0631

Table 2.- Lignin Percents

Test #	W0 (Gooch crucible + filter weight) (g)	S (material weight) (g)	W1 (g)	W2 (g)	% Cellulose
1	20.3347	0.1325	20.3899	20.3522	28.4528
2	25.8385	0.1241	25.8869	25.8523	27.8807
3	23.4687	0.1078	23.5122	23.4816	28.3859
Average					28.2398

Table 3.- Cellulose Percent

Test #	W0 (Gooch crucible + filter weight) (g)	S (material weight) (g)	W1 (g)	W2 (g)	% Holocellulose
1	25.3473	0.1017	25.4061	25.3616	43.7561
2	24.7358	0.1020	24.7937	24.7492	43.6275
3	21.5251	0.1029	21.5833	21.5390	43.0515
Average					43.4784

Table 4.- Holocellulose results

	Sugarcane Bagasse
Total Solids	94.46%
Volatile Solids	81.01%
Lignin	28.06%
Cellulose	28.24%
Holocellulose	43.48%

Table 5. Average composition of the Sugarcane bagasse

DISCUSSION

For this chemical characterization four main components were analyzed, which were the following: total solids and volatile solids, lignin, cellulose and holocellulose. From the three tests, the average lignin content was 28.06%, which compared to literature reviews was considerably high. In different studies, lignin content would range from 5.70 to 23.33%. Lignins are seen as natural impurities, and are undesirable in a finished paper product, which is why lower values are preferable. The average cellulose content was 28.24%, lower than the values reported in other studies, which range from 29.80% to 54.87%. Resano et al. (2021) reported a cellulose content of 29.80% for non-industrial bagasse, which is prepared by artisans, but was still considered an anomaly. The average holocellulose content was 43.62%, also lower than that found in other studies. Values would range between 50.00% and 78.60%.

Reference		Lignin	Cellulose	Holocellulose
19	Prado-Martínez et al. (2012)	19,98%	-	73,24%
20	Hurter (2001), as cited in Prado-Martínez et al. (2012)	19-24%	-	59-76%
21	Gil-López et al. (2019)	23,15 ± 0,32%	35,44 ± 0,69%	-
22	Vázquez et al. (1999), as cited in Singh et al. (2021)	15%	40%	-
9	Bhardwaj et al. (2019)	19-24%	32-44%	-
4	Resano et al. (2022); sample "BS2A" (industrial bagasse obtained from the top of the storage pile)	9,74%	42,91%	-
4	Resano et al. (2022); sample "BT1" (artesanal bagasse)	5,70%	29,80%	-
23	Murphy (2017), as cited in Resano et al. (2022)	20,50%	41,82%	-
3	Rodríguez et al. (2016); bagasse marrow	30%	-	60,30%
24	Agnihotri, Dutt & Tyagi (2010)	17,70%	-	78,60%
25	Rezende et al. (2011)	22,20%	35,20%	-
26	Almeida et al. (2000), Anselmo and Badr (2004), Hoareau et al. (2004), as cited in Guimarães et al. (2009)	19-25%	32-55%	50-84%
27	Guimarães et al. (2009)	23,33%	54,87%	71,39%
This study		**28.06%**	**28.24%**	**43.62%**

Table 6. Lignin, cellulose and holocellulose content of sugarcane bagasse in literature compared to this study

CONCLUSIONS

As we saw in table 6 the sample of Mexican bagasse sugarcane presented the highest percentage of lignin. Some authors consider that high lignocellulosic biomass is not recommended to produce paper, but it has good characteristics to produce bioethanol. Maybe that's the reason why the Panuco factory uses their bagasse sugarcane to produce energy to

supply the factory and the extra production goes to the supply network of the National Commission of Electricity. On the other side different authors are studying the properties of lignin as a dispersant, adhesives and antioxidants in plastics or to develop bioplastics, opening new perspectives for sugarcane bagasse.

The lowest percentage of cellulose in the sample carries out the fact that this sample of fiber material, does not represent the best material to produce paper. But more studies need to be done, because the sugarcane bagasse has different properties depending on the ground and agriculture practices.

Hollocelulose in the study, presents the lowest percentage of the cases studies. Therefore, knowing that holocellulose is composed of cellulose and hemicellulose, the low percent of cellulose confirm this result. Eventhow, the uses of holocellulose are diverse and important for different industries such as animal feed, pharmaceutical, textile, and others.
This first phase was not positive for paper production, but the experiments were done just with the powder and not with the fibers itself. More studies need to be done with the actual sample, and with at least other samples from a different location.

The second objective is to review the industry and the products that are produced from natural fiber to evaluate different options and products that can be made with Mexican bagasse of sugarcane.

REFERENCES

[1] Quiñones, J. a. D., Hernández, J. L., De Jesús Vargas Radillo, J., & Dueñas, R. S. (2016). Propiedades de resistencia de una pulpa kraft de pino mezclada con médula del bagazo de caña de azúcar. Madera y Bosques, 8(2), 17–26. https://doi.org/10.21829/myb.2002.821298

[2] Robles, F. M. N., Saucedo, R. C. A., Delgado, F. E., SanjuáN, D. R., & Turrado, S. (2018). EFECTO DE LAS MICROFIBRAS DE CELULOSA SOBRE PAPEL CON ALTO CONTENIDO DE FIBRA RECICLADA. Revista Mexicana De Ciencias Forestales. https://doi.org/10.29298/rmcf.v5i24.320

[3] Rodríguez, E. C., Fernández, V. L., De La Caridad Montano Pérez, A., & Ramírez, D. D. (2016). Caracterización de residuos agroindustriales con vistas a su aprovechamiento. Revista Centro Azúcar, 43(4), 27–35. https://biblat.unam.mx/hevila/Centroazucar/2016/vol43/no4/3.pdf

[4] Resano, D. R., Guillen, O. M., Ubillús, F., & Barranzuela, J. L. (2022). Caracterización fisicoquímica del bagazo de caña de azúcar industrial y artesanal como material de construcción. Información Tecnológica, 33(2), 247–258. https://doi.org/10.4067/s0718-07642022000200247

[5] Bantacut, T., Romli, M., Noor, E., 2018. Biomass by-product from crystal sugar production: a comparative study between Ngadirejo and Mauritius sugar mill. EES (Ecotoxicol. Environ. Saf.) 141 (1), 12009.

[6] Guerra, S.P.S., Denadai, M.S., Saad, A.L.M., Spadim, E.R., da Costa, M.X.R., 2020. Sugarcane: biorefinery, technology, and perspectives. In: Sugarcane Biorefinery, Technology and Perspectives. Elsevier, pp. 49–65.

[7] Singh, S. P., Jawaid, M., Chandrasekar, M., Senthilkumar, K., Yadav, B., Saba, N. & Siengchin, S. (2021). Sugarcane wastes into commercial products: Processing methods, production optimization and challenges. Journal of Cleaner Production, 328, 129453. https://doi.org/10.1016/j.jclepro.2021.129453
[8] Rao, M. (1997). Industrial Utilization of Sugar Cane and Its Coproducts. ISPCK Publishers and Distributors: New Delhi, India.
[9]. Bhardwaj, N. K., Kaur, D., Chaudhry, S., Sharma, M. R., & Arya, S. (2019). Approaches for converting sugarcane trash, a promising agro residue, into pulp and paper using soda pulping and elemental chlorine-free bleaching. Journal of Cleaner Production, 217, 225–233. https://doi.org/10.1016/j.jclepro.2019.01.223
[10] Hemmasi, A. H., Samariha, A., Tabei, A., Nemati, M., Khakifirooz, A., & Branch, A. (2011). Study of Morphological and Chemical Composition of Fibers from Iranian Sugarcane Bagasse. American-Eurasian Journal of Agricultural and Environmental Science, 11(4), 478–481.
https://www.cabdirect.org/cabdirect/abstract/20123093982?q=(au%3a%22Hemmasi%2c+A.+H.%22) accessed February 2023.
[11] Liu, C., Luan, P., Li, Q., Cheng, Z., Sun, X., Cao, D. & Zhu, H. (2020). Biodegradable, Hygienic, and Compostable Tableware from Hybrid Sugarcane and Bamboo Fibers as Plastic Alternative. Matter, 3, 2066–2079. https://doi.org/10.1016/j.matt.2020.10.004
[12] Varshney, R. (2020). Ayodhya-based CHUK is turning sugarcane waste into sustainable cutlery for Indian Railways, Google, Amazon. Athena Information Solutions Pvt. Ltd. galelinkgalecom.udemproxy.elogim.com/apps/doc/A647061996/STND?u=udem&sid=ebsco&xid=953e54e1.
[13] Hamid, L., Elhady, S., Abdelkareem, A. & Fahim, I. (2022). Fabricating Starch-Based Bioplastic Reinforced with Bagasse for Food Packaging. Circular Economy and Sustainability, 2, 1065-1076.
[14] Faubla, F. I. B., & Troya, A. B. C. (2021). Bagazo de caña de azúcar (Saccharum officinarum) y almidón de yuca (Mianihot esculenta) como sustituto de poliestireno en la elaboración de platos biodegradables.
[15] Fangmongkol, K. (2020). Life cycle assessment of biodegradable food container from bagasse in Thailand. https://www.semanticscholar.org/paper/Life-cycle-assessment-of-biodegradable-food-from-in-Fangmongkol-Gheewala/5250edba3434778d3b2dcca6950c798d951a05c4
[16] García, T. E., Murillo Vázquez, R. N., Rodríguez Rivas, A., Anzaldo Hernández, J. & Rivera Prado, J. J. (2015). Obtención de celulosa blanqueada de Ricinus communis L. mezclada con fibra industrial para fabricar papel bond. Redalyc.org. http://www.redalyc.org/articulo.oa?id=63442133008
[17] New Environmental Pollution Study Findings Recently Were Reported by Researchers at Kurukshetra University (Ultrafiltered Biopulping Strategy for the Production of Good Quality Pulp and Paper From Sugarcane Bagasse). (2020). Documento - Gale Academic OneFile. link.gale.com/apps/doc/A640919227/AONE?u=udem&sid=ebsco&xid=3166e20e.

[18] Sibaly, S., & Jeetah, P. (2017). Production of paper from pineapple leaves. Journal of Environmental Chemical Engineering, 5(6), 5978–5986. https://doi.org/10.1016/j.jece.2017.11.026
[19] Prado-Martínez, M., Anzaldo-Hernández, J., Becerra-Aguilar, B., Palacios-Juárez, H., Vargas-Radillo, J. & Rentería-Urquiza, M. (2012). Caracterización de hojas de mazorca de maíz y de bagazo de caña para la elaboración de una pulpa celulósica mixta. Madera y Bosques 18(3), 2012:37-51.
[20] Hurter, W.R. 2001. Nonwood plant fiber uses in papermaking. Hurter Consult Incorporated. Extracted from "Agricultural Residues", Tappi. 1997. Non wood fibers short course notes, updated and expanded.
[21] Gil-López, D. I. L., Lois-Correa, J. A., Sánchez-Pardo, M. E., Domínguez-Crespo, M. A., Torres-Huerta, A. M., Rodríguez-Salazar, A. E. & Orta-Guzmán, V.N. (2019). Production of dietary fibers from sugarcane bagasse and sugarcane tops using microwave-assisted alkaline treatments. Industrial Crops & Products, 135, 159–169. https://doi.org/10.1016/j.indcrop.2019.04.042
[22] Vazquez, A., Dominguez, V.A., Kenny, J.M., 1999. Bagasse fiber-polypropylene based composites. J. Thermoplast. Compos. Mater. 12 (6), 477–497.
[23] Murphy, R. (2017). Sugarcane: production systems, uses and economic importance, Nova Publishers, ISBN: 978-1-53610-898-9, New York, USA
[24] Agnihotri, S., Dutt, D., & Tyagi, C. (2010). Complete characterization of bagasse of early species of saccharum officinerum-Co 89003 for pulp and paper. ResearchGate. https://www.researchgate.net/publication/282321508_Complete_characterization_of_bagasse_of_early_species_of_saccharum_officinerum-Co_89003_for_pulp_and_paper_making
[25] Rezende, C. A., De Lima, M. M., Maziero, P., deAzevedo, E. R., Garcia, W., & Polikarpov, I. (2011). Chemical and morphological characterization of sugarcane bagasse submitted to a delignification process for enhanced enzymatic digestibility. Biotechnology for Biofuels, 4(1). https://doi.org/10.1186/1754-6834-4-54
[26] Almeida, J.M.R., Boynard, C.A. & Monteiro, S.N. (2000). Effect of chemical treatments on the surface morphology of sponge gourd (Luffa cylindrica) fibers. In: Mattoso, L.H.C., Leão, A.L., Frollini, E. (Eds.), Natural Polymers and Composites (3rd International Symposium - ISNaPol 2000). Publishers: Embrapa Agricultural Instrumentation, São Paulo University (USP), São Paulo State University (UNESP),, Sao Carlos, SP, Brasil.
[27] Guimarães, J., Frollini, E., Da Silva, C. G., Wypych, F., & Satyanarayana, K. G. (2009). Characterization of banana, sugarcane bagasse and sponge gourd fibers of Brazil. Industrial Crops and Products, 30(3), 407–415. https://doi.org/10.1016/j.indcrop.2009.07.013

PM-GO04

Effect of wrapping parameters and transport constraints on stretch film properties for freight transport applications

Elora Leguebe*[1,2,3], Victor Huart[1], Nicolas Krajka[1], Jérôme Pellot[1], Marie Le Baillif [2,3], Damien Erre[2,3]

[1]*R&D, Metropack, Reims, 51100, France*
[2]*ITheMM, Université de Reims Champagne-Ardenne, Reims, 51100, France*
[3]*ESIREIMS, Reims, 51100, France*

***Correspondence to:** Elora Leguebe. R&D, Metropack, 30-32 Rue du capitaine Georges Madon, Reims, 51100, France.*
E-mail: elora.leguebe@metropack.fr

ABSTRACT: Currently, ecology has become a major issue for the world. In the field of packaging, the eco-design of the film is desired for a lower mass of plastic on the pallet, while maintaining the stability of the load. This is how this morphological study of stretch film to know its capacities and limits. This study will focus on the effect of different parameters of wrapping and transportation on the stretch film properties. Investigation was focused on different morphology tests in order to analyze the damage caused by wrapping process and transport constraints. Characterization included DSC (Differential Scanning Calorimetry) and infrared. Effect of wrapping speed, wrapping pattern and acceleration in transport were investigated. The morphology was found to be affected by the wrapping process, showing changes in crystallinity. The present study shows the importance of wrapping parameters for the morphology of the stretch film on the pallet and therefore for the load stability.

Keywords: stretch film; wrapping film; stretch film behavior; morphology; transport.

INTRODUCTION

Major portions of linear low-density polyethylene (LLDPE) films are used as flexible packaging [1]. Resistance to failure and tensile properties are important physical performance criteria for stretch films. It is generally recognized that molecular orientation is essential for the performance of LLDPE stretch film in wrapping applications [2]. Despite its importance, relation between film properties, processing conditions and polymer structure are still poorly understood.

The present study was focused on the effects of different parameters of wrapping and transportation on the stretch film morphology and properties. The effect of testing parameters such as the speed wrapping, the fatigue and the acceleration of transport on the measured film properties were investigated.

MATERIALS AND METHODS

The materials used were performed using cast co-extruded LLDPE stretch films (Resinex 581 grade machine wrapping and LC2 grade manual wrapping) supplied by Embal'Vit company (Reims, France). Reference specimens of LLDPE were prepared according to IS 14995 standards [3]. The polymer films were set between two sheets of paper prior cutting to avoid catching by the cutting machine blade. Specimens were cut according to standards in transverse (TD) and longitudinal directions (LD) prior tapping on a cardboard frame (Figure 1).

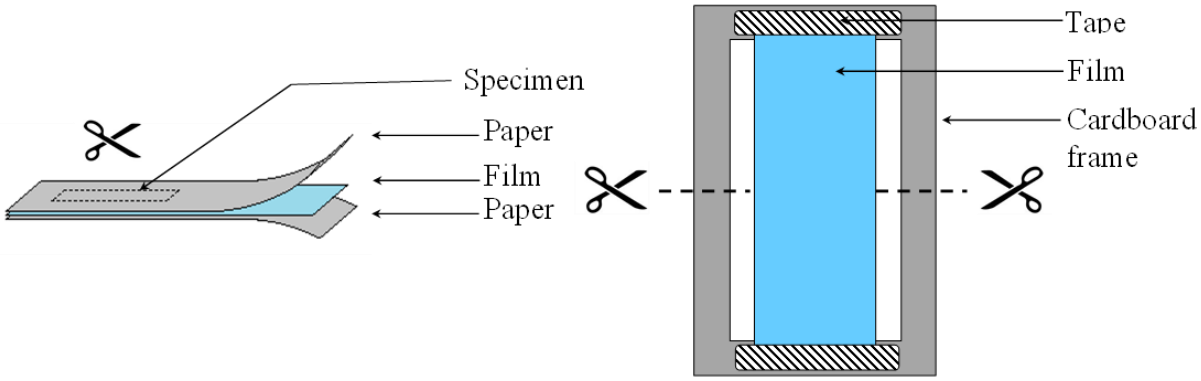

Figure 1 Assembly and cutting of test specimens

Simulation of wrapping applications was performed on some reference specimen by using hysteresis tests. First hysteresis test (hysteresis cycle 1) corresponds to the test described in ASTM D882 [4]. The second hysteresis test (hysteresis cycle 2) is similar to the first one except the extension speed which was increased from 127 mm/min to 450 mm/min as presented in previous work [5]. The hysteresis tests were performed using MTS tensile testing machine.
Reference materials were compared with wrapped pallets films with and without transportation stresses. The wrapping of pallet was performed using a turntable wrapping Rotoplat 708 supplied by Embal'Vit company (see Figure 2). The specimens were recovered by directly tapping the cardboard frame on the wrapped pallet film. The specimens were the carefully cut around the frame in order to obtain same dimension as for the reference materials.

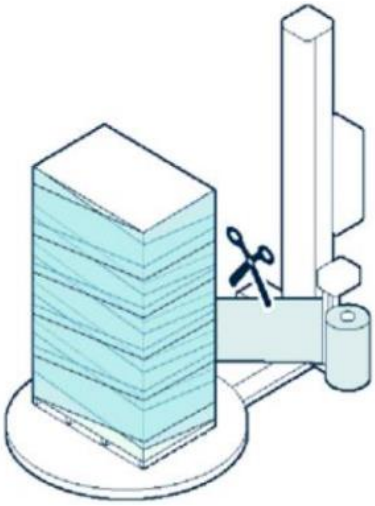

Figure 2 Turntable wrapping Rotoplat 708

The transportation stresses considered in the study were 5 simulated accelerations, and 100 fatigue cycles (hysteresis cycle 2). The accelerations were simulated using an acceleration bench (see Figure 3) according to EUMOS 40509:2020 standard [6].

Figure 3 Acceleration bench [7]

The fatigue cycles were performed using MTS tensile testing machine, by running the hysteresis 2 cycle on specimens. All specimens were conditioned at room temperature 23°C (73.4°F) and 50% of humidity at least 24 hours prior testing. Table 1 resumes all test specimens.

Name	Origin	Stress
Ref	Roll	None
Ref-1H1	Roll	Hysteresis cycle 1
Ref-1H2	Roll	Hysteresis cycle 2
Wrap	Wrapped Pallet	None
Wrap-acc	Wrapped Pallet	5 accelerations
Wrap-100H2	Wrapped Pallet	100 Hysteresis cycle 2

Table 1 Summary of specimens of LLDPE stretch film characterized

CHARACTERIZATION

Differential Scanning Calorimetry was performed using DSC 204 F1 Phoenix to investigate the morphology of the polymer films. Samples of about 5,5g were analyzed under N_2 atmosphere. The temperature profile used consisted in two heating-cooling cycles from 25°C to 145°C with a heating and cooling speed of 3°C/min. The polymer crystallinity was calculated using equation 1 (where ΔH is the melting enthalpy of the samples and ΔHm° the reference melting enthalpy for 100% crystalline polyethylene: 293 J/g [8]).

$$Xc\% = (\Delta H / \Delta Hm^\circ) \quad \text{(Eq.1)}$$

Infrared absorbance data were obtained using a PerkinElmer Spectrum Two FT-IR spectrometer. Spectra were obtained in a 450-4000 cm^{-1} range. All the IR scans were corrected for baseline effects. Characteristic bands for PE are referred to be [9]:

- 2926 cm^{-1}: C-H bond, antisymmetric stretching.
- 2852 cm^{-1}: C-H bond, symmetric stretching.
- 1455 cm^{-1}: C-H bond, deformation shear.
- 720 cm^{-1}: rocking.

The absorbance around 720 cm-1 for LLDPE has also been referred to supply information on the crystalline morphology of the polymer. The absorbance is reported to be the result of three contributions: amorphous phase, a-axis crystalline phase and b-axis crystalline phase as presented in Figure 4.

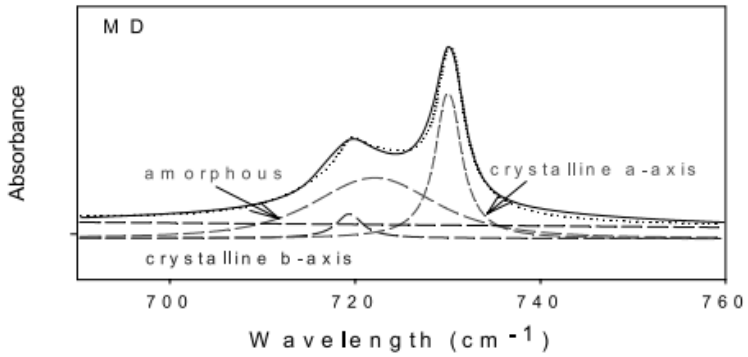

Figure 4 LLDPE curve into a-axis, b-axis, and amorphous phase contributions [10]

RESULTS AND DISCUSSIONS

Differential Scanning Calorimetry

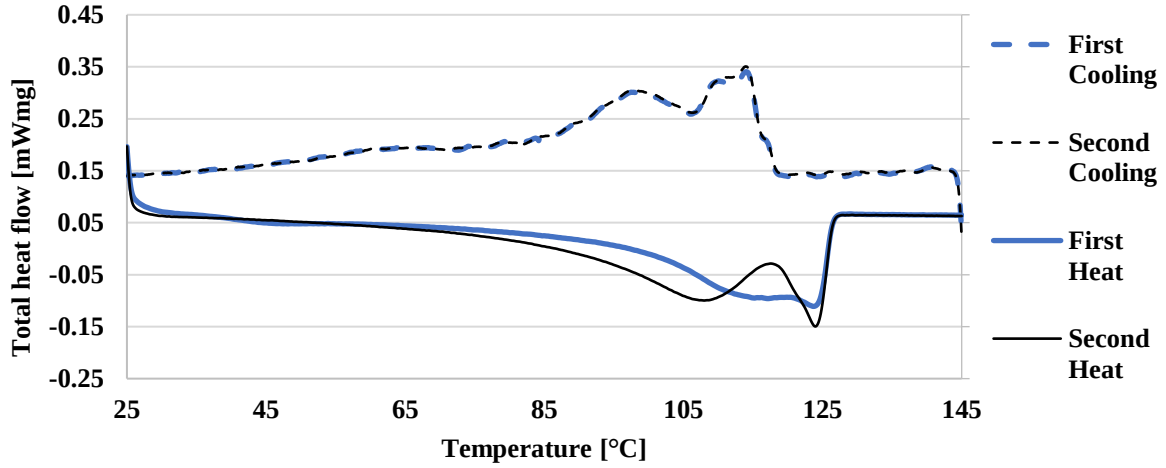

Figure 5 DSC curves of Ref specimen

Figure 5 shows a representative curve obtained by DSC for the reference material. The first heat showed a broad, melting curve with a single peak maximum at 123.7°C, which indicates the presence of various crystal sizes in the polymers [11].

The total heat of fusion associated with this peak was 103.8 J/g, which corresponds to 35.4% of crystallinity. The cooling curve showed crystallization peaks at 99, 109, 114 and 117°C and a total heat of crystallization of 128 J/g. The second heating shows two melting peaks with a maximum at 108 and 124.1°C and a total heat of fusion and % crystallinity of 118.4 J/g and 40.4% respectively. The difference between both heating been due to thermal history of the material. Similar results have been presented in the literature [12].

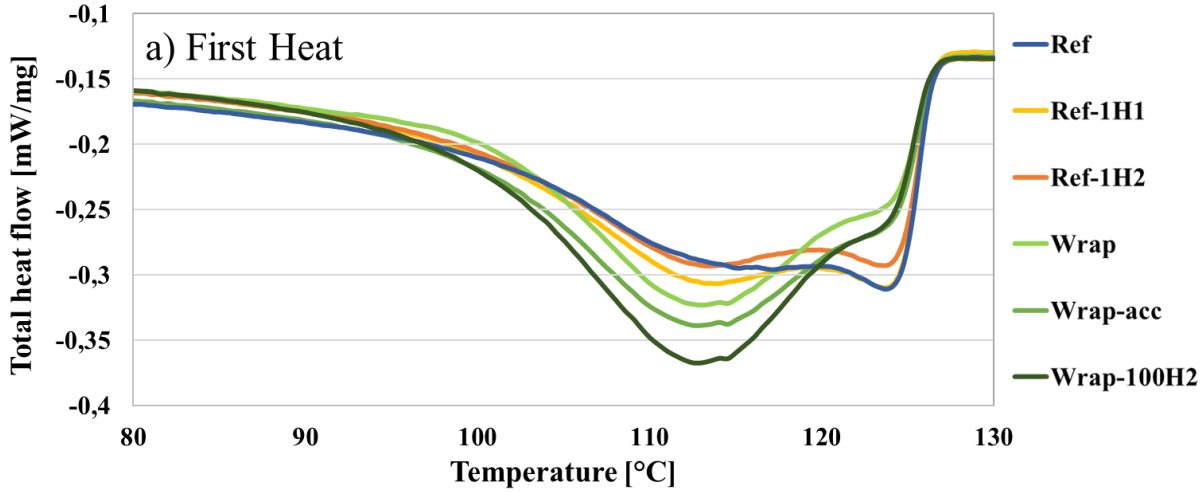

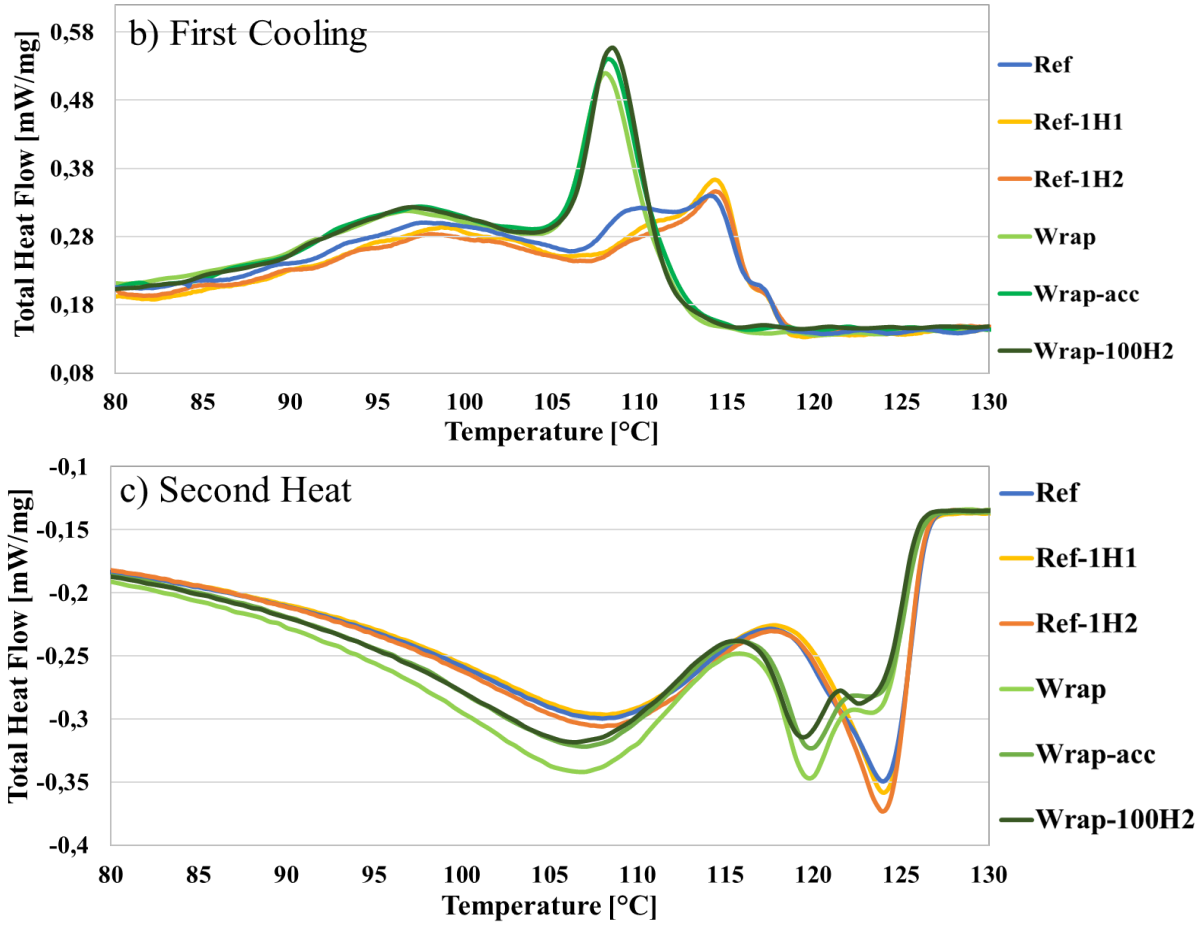

Figure 6 DSC curves of all materials: (a) first heating, (b) first cooling, (c) second heating

Figure 6 presents the DSC curves of all materials and Table 2 their related calculated properties. One can see that all reference material showed very similar DSC curves. Only slight increase of intensity on the broad shoulder around 112°C with increased stretching speed can be observed. However, this difference completely disappeared on the second heating, meaning that no significant morphological change had occurred due to the hysteresis cycles.
All wrapped films showed similar behaviors, whereas different from the reference materials. The broad melting peak around 112°C was more intense for wrapped materials than for reference materials, while the intensity of the peak around 124°C was significantly lower for wrapped, than reference materials.

All materials showed the same broad crystallization peak around 98°C. While reference material showed thin, multiple peaks of medium intensity at 110°C, 114°C and 117°C, wrapped films showed an intense unique thin peak around 109°C. This is probably due to a drastic change in morphology during the wrapping. This morphological change, which can be considered as a degradation, was confirmed by the second heating where wrapped materials showed three melting peaks while only two were visible for reference materials [13]. One may

note that both transport stresses increased the intensity of the degradation initially caused by the wrapping.

Sample	ΔH_m(J/g)	X_c(%)
Ref	73.43	25.06
Ref-1H1	81.30	27.74
Ref-1H2	82.45	28.14
Wrap	74.18	25.32
Wrap-acc	83.54	28.51
Wrap-100H2	90.95	31.04

Table 2 Crystallization and melting process parameters of LLDPE stretch film.

The degree of crystallization was measured for all materials to be from about 25 to 31%, which corresponds to values in the literature [14]. The wrapping did not significantly change the degree of crystallization. However, it can be noted that all stresses on reference materials or wrapped materials caused an increase of the degree of crystallization. This might be explained by an increase of the alignment of the polymer chains due to the stresses. The stretching speed, accelerations in transport and fatigue cycles, seem therefore to have affected the morphology of the polymer film.

Infra-red analysis

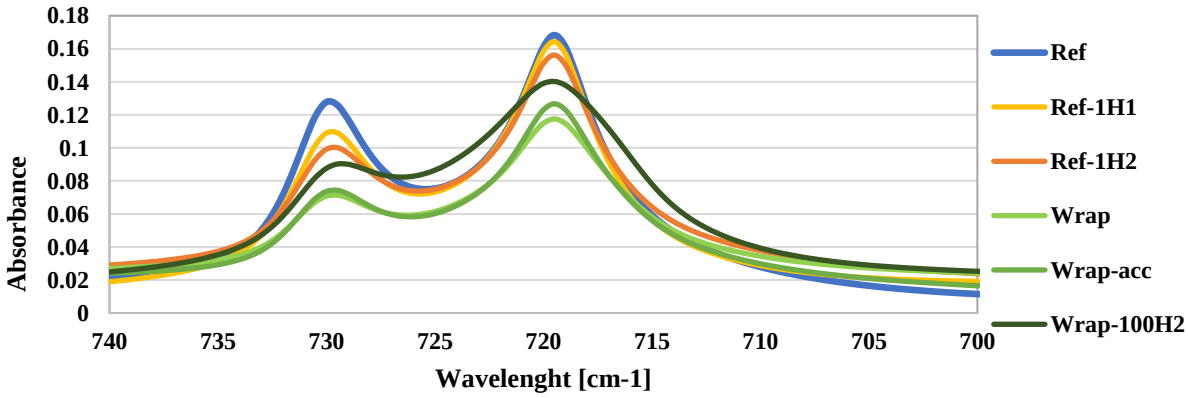

Figure 7 Absorption spectrum of LLDPE stretch film with constraints at 700-740 cm^{-1}

Figure 7 shows the infrared spectra of all material. The characteristic band for polyethylene at wavelength 720 cm^{-1} is referred to be present only if more than $4CH_2$ follow each other, which was the case in our study [15].

The stresses caused by hysteresis cycles seemed to have cause a decrease of the absorbance intensity and a slight increase of the broadness of the peak for reference materials. This could be coherent with a decrease of the crystallinity, which contradicts the DSC results. The wrapped materials showed a lower intensity of absorbance than reference materials. The acceleration did not seem to have had any effect while the fatigue seemed to increase the peak intensity.

It is probable that two mechanisms occurred simultaneously. On one hand, stretching due to stresses or wrapping might align the polymer chains. On the other hand, the mechanical stresses and especially the wrapping might degrade the film thought chain scissions. The wrapping is a process during which the film is stretched at severe stress that do not allow the material to adapt and therefore may cause polymer degradation as chain scission [16]. The differences in FTIR results might not be sufficient to be significant. They would require to be confirmed by the other tests as Gel Permeation Chromatography (GPC) in order to obtain more accurate information on the molecular weight distribution.

CONCLUSIONS

The present study was focused on stretch film used in tertiary packaging and its ability to maintain the stability of a pallet during transport. The effect of parameters such as wrapping or transport constraints on the morphology of the stretch film were investigated using reference material taken directly from the roll and the same film after wrapping on a pallet. Multiple stresses were applied in order to simulated real application: hysteresis and acceleration simulation. The specimens' morphology was analyzed by DSC and FTIR. Wrapping was found to cause changes in morphology clearly visible on DSC results. Additional stresses were slightly increasing these changes. It was proposed that two mechanisms occurred simultaneously: an alignment of the polymer chain with stretching that increased the crystallinity and a chain scission of the polymer due to fast and intense stretching. The FTIR did not allowed to confirm these results and further investigations would be required in order to obtain more information on the polymer molecular weight distribution.

REFERENCES

[1] K. Osborn –Plastic Films– Technology and Packaging Applications, Lancaster, Technomic Publishing (1992).
[2] R. Krishnaswamy –The influence of solid-state morphology on the impact strength of linear low-density polyethylene blown films- Chevron Phillips Chemical Company.
[3] IS 14995 (2001): Stretch Cling Films [PCD 12: Plastics]
[4] ASTM D882-18: Standard Test Method for Tensile Properties of Thin Plastic Sheeting.
[5] E. Leguebe – Effect of relaxation time, recovery time and extension speed during characterization of LLDPE wrap film properties – Packag Technol Sci, 2022;1-9.
[6] Eumos 40509 :2020 standards, eumos.eu/quality-standards/
[7] https://www.rycobel.com/fr/produits/trumotion-acceleration-test-systems-unit-load-stability-system.

[8] B. Wunderlich - Macromolecular Physics; Crystal nucleation, growth, annealing - Academic Press: New York, 1976.
[9] D. Czarnecka – Films LDPE/LLDPE made from post-consumer plastics: processing, strcuture, mechanical properties – Advances in Science and Technology Research Journal, Volume 12, No.3, Septembre 2018, p134-142.
[10] X. Zhang – Oriented structure and anisotropy properties of polymer blown films: HDPE, LLDPE and LDPE – Polymer 45(2004) 217-229. Science Direct 2003.
[11] S. Auksornhul - Effect of the blow-up ratio on morphology and engineering properties of three-layered linear low-density polyethylene blown films - Journal of Plastic Film & Sheeting 2018, Vol. 34(1) 27–42.
[12] L. Thomas – Characterization of melting phenomena in linear low-density polyethylene by modulated DSC – TA Instruments Publication No. TA-227.
[13] A. Ghaneh-Fard – Effects of film blowing conditions on molecular orientation and mechanical properties of polyethylene films - Journal of Plastic Film & Sheeting 1999, Vol. 15.
[14] D. Li – Effect of crystallinity of polyethylene with different densities on breakdown strength and conductance property – Materials 2019,12,1746: doi:10.3390/ma12111746.
[15] G. McNally – The effect of polymer properties on the mechanical behavior and moprphological characteristics of cast polyethylene film for stretch and cling film applications – Journal of plastic film & sheeting, sage publications, 2005,21(1), pp.39-54.
[16] J. V. Bisha - Correlation of the Elastic Properties of Stretch Film on Unit Load Containment - Ph.D. thesis, Virginia Polytechnic Institute and State University, 2012.

PM-GP01

Seal materials in flexible plastic food packaging: a review

Bram Bamps[*1], Mieke Buntinx[1], Roos Peeters[1]

[1]*Hasselt University, imo-imomec, Materials and Packaging Research & Services, Wetenschapspark 27, 3590 Diepenbeek, Belgium*

[*]***Correspondence to**: Bram Bamps, Hasselt University, imo-imomec, Materials and Packaging Research & Services, Hasselt 3500, Belgium.*
E-mail: bram.bamps@uhasselt.be

Abstract: Flexible packaging has many advantages in the food industry, arising from low weight, formability, multilayer complexity and cost. Heat sealing is a very efficient technique to close flexible food packaging. Currently, many thermoplastic materials are used in seal layers. A seal can be formed when these materials are heated and brought into contact, thereafter polymer chains diffuse across the seal interface and entangle. Hydrogen bonds, polar and ionic interactions are molecular forces that can come into play, depending on the thermoplastic materials that are used in the seal layer. Bonds between identical polymers, referred to as autohesion, are formed in pouch applications (e.g. horizontal and vertical form-fill-seal packages). In lidding applications, the flexible film is sealed to a rigid cup, tray or bottle, whereby bonds can be formed between non-identical polymers because the materials are often provided by different suppliers. All heat seal technologies imply heating of seal layers but differ in the heating principle. In the food industry and in most scientific seal studies, the seals of mono- and multilayered packaging are mainly formed by conductive heating. Recently, the use of emerging technologies, such as ultrasonic and laser heating, are increasingly described in recent papers. Applied seals are characterized by strength after a specified cooling time. Immediately after heating, this strength is referred to as hot tack. A good seal performance is crucial to guarantee food safety and quality. Besides strength, tightness is important to prevent food degradation, caused by microorganisms and external gases; and to keep aromatic gases inside the package. This review aims to give a literature overview which can support stakeholders in the food industry to improve and optimize the material selection in flexible packaging, in order to obtain seals with desired tightness and strength. Heat seal studies on materials and seal technology of flexible food packaging, such as pouches and lidding films, are considered. Scientific data is categorized from a materials' perspective, based on chemical structure, which is revealed by chemical and thermal analysis. A majority of the seal studies is categorized in a first section on polyolefins as seal layers. The following sections describe the seal functionality of i) ethylene copolymers, such as ionomers, and ii) polyesters, such as poly(ethylene terephthalate), pol(lactic acid) and poly(butylene succinate). The role of plasticizers, fillers and other additives in the seal performance is also described. Finally, material properties, such as chain length and melting temperature (Tm), as underlying causes of seal performance, are summarized.

Keywords: heat sealing, flexible food packaging, heat seal materials, seal strength, hot tack.

PM-GP02

Effect of food simulants on CuONP stability in bionanocomposite food packaging film

Nattinee Bumbudsanpharoke[1*], Busarin Chongcharoenyanon[1], Nathdanai Harnkarnsujarit[1], Seongyoung Kwon[2] and Seonghyuk Ko[2]

[1]Department of Packaging and Materials Technology, Faculty of Agro-Industry, Kasetsart University, 50 Ngam Wong Wan Rd., Latyao, Chatujak, Bangkok, 10900, Thailand
[2]Laboratory of Nano-Enabled Packaging and Safety, Department of Packaging, Yonsei University, 1 Yonseidaegil, Wonju-si, Gangwon-do, 26493 Republic of Korea

***Correspondence to**: Nattinee Bumbudsanpharoke. [1]Department of Packaging and Materials Technology, Faculty of Agro-Industry, Kasetsart University, 50 Ngam Wong Wan Rd., Latyao, Chatujak, Bangkok, 10900, Thailand*
E-mail: nattinee.bu@ku.ac.th

ABSTRACT: Addition of copper oxide nanoparticles (CuONPs) to poly(butylene-adipate-co-terephthalate) (PBAT)/thermoplastic starch (TPS) biopolymer blend produced bionanocomposite films with improved mechanical and oxygen barrier properties, as well as enhanced other benefits including light blocking and antimicrobial activity. In this study, the PBAT/TPS-CuO bionanocomposite films with varying CuONPs contents (0.05, 0.5, 1, and 2%) were challenged by food simulants (10% ethanol and 3% acetic acid) according to European Regulation 10/2011. CuONPs in the bionanocomposite films demonstrated good stability when exposed to 10%ethanol; however, it was dissolved in 3% acetic acid. The X-ray diffraction and the energy dispersive spectroscopy results showed that CuONPs in the film were complete lost after acid exposure, whereas CuONPs in the films exposed to 10%EtOH were preserved. The maximum overall migration value was 5.0 mg/dm2. Inductively coupled plasma optical emission spectroscopy was used to confirm the presence of Cu in the simulants. The highest soluble Cu value of 12.39 mg/kg detected from PBAT/TPS-CuO2%, while migration value decreased as concentration ratio in film was decrease. Although both values were within the threshold limits established by current legislation for non-specific migration limit substances in food contact materials, the properties of bionanocomposite were altered. The mechanical properties of a post-migrated PBAT-TPS/CuO films taken from acidic conditions were reduced by 22% in tensile strength and 53% in elongation at break due to holes and micro-cracks on the film surface observed by scanning electron microscope. The average sealing strength of all bionanocomposite films decreased by about 25% after acid exposure. The oxygen permeability, on the other hand, was significantly improved, with a 16.3% reduction. Because the film had lost all of its active agent, film was unable to inhibit Escherichia coli growth. While 3% acetic acid caused dissolution of CuONPs and significant changes in properties of PBAT/TPS-CuO film, 10% ethanol caused very minor to no changes in bionanocomposite film properties.

PM-PP01

Release of Vanillin, trans-Cinnamaldehyde, and Citral from Poly(butylene succinate) Films Containing Lignin Nanoparticles

Pathtamawadee Nuamduang[1], Rafael Auras[2], Charinee Winotapun[3], Pattarin Leelaphiwat*[1]
[1]Department of Packaging and Materials Technology, Faculty of Agro-Industry, Kasetsart University, Bangkok 10900, Thailand
[2]School of Packaging, Michigan State University, East Lansing, Michigan 48824-1223, United States
[3]National Metal and Materials Technology Center, National Science and Technology Development Agency, Thailand Science Park, Phathum Thani 12120, Thailand

Correspondence to: Pattarin Leelaphiwat. [1]Department of Packaging and Materials Technology, Faculty of Agro-Industry, Kasetsart University, Bangkok 10900, Thailand.
E-mail: pattarin.le@ku.ac.th

ABSTRACT: This work evaluates the effect of extraction solvents to measure the concentration of compounds on developed biodegradable films of (poly(butylene succinate) - PBS) incorporated with spherical lignin nanoparticles (LN) and natural agents (NA), such as vanillin, trans-cinnamaldehyde, and citral as an antimicrobial packaging. Composite films of PBS/LN, PBS/LN/10%NA, and PBS/10%NA were manufactured via conventional blown film melt-extrusion. The composite films containing lignin appeared brownish, while the films containing each natural agent showed a milky color. Two different solvent extractions, ethyl acetate: hexane (1:1) and water: methanol (1:1), were used to evaluate each natural agent's remaining contents on the PBS-based film compared to the thermogravimetric analysis (TGA) method. According to the solvent extraction results, ethyl acetate: hexane solution was suitable for use as a solvent for extracting natural agents from the PBS-based film. PBS/LN/NA composite film shows a higher remaining content of each NA than PBS/NA, and the extraction concentration was similar to the thermogravimetric method. The diffusion coefficients of each natural agent in the liquid phase were determined from PBS-based films diffusing in water and 10% ethanol solutions at 23 °C. The diffusion coefficients of each natural agent from PBS and PBS/LN-based films in water were between 1.00 x 10^{-12} to 8.14 x 10^{-16} m^2/s while the diffusion coefficients of each natural agent in 10% ethanol were 1.20 x 10^{-15} to 9.99 x 10^{-17} m^2/s. The highest release rate of cinnamaldehyde from the PBS-based film was found in both water and 10% ethanol.

Keywords: lignin nanoparticles, natural agents, solvent extraction

INTRODUCTION

Sustainable packaging has gained attention from the food industry, consumers, and governments to reduce packaging waste. This type of packaging material is made of bioplastic polymers that are derived from renewable biomass sources. Poly(butylene succinate) – PBS - is a biodegradable aliphatic polyester synthesized by condensation of succinic acid and 1,4-butanediol. This compostable home plastic has processability and mechanical properties close to those of commercially available polyethylene (PE) and polypropylene (PP), and PBS's ester bonds can be chemically degraded by water, making PBS desirable for many biodegradable packaging applications. So, PBS can be a potential material to replace single-use plastic. However, PBS resin is expensive, creating technical and market feasibility barriers. Adding bio-renewable and biodegradable fillers into the biopolymeric matrix is a promising choice to maintain the composite biodegradability, lower the PBS cost, and provide active functions, including antimicrobial and antioxidant properties. Lignin is an interesting, sustainable, and low-cost alternative to non-renewable, toxic fillers in polymers. Aside from its abundance and low cost, lignin is favorable for numerous attractive properties, including biodegradability, antioxidant and antimicrobial activity, high carbon content, high thermal stability, and stiffness in food packaging materials. Large lignin particles might not be suitable for applications of flexible film. However, the developed spherical lignin nanoparticles offer several advantages, including compatibility with host polymers.

Antimicrobial packaging is part of active packaging that provides active protection in which the packaging, the product, and the environment interact. Antimicrobial agents, both synthetic additives and natural agents, provide the antimicrobial function to have either biocidal effects or biostatic abilities. However, natural antimicrobial agents have received increasing attention due to their antimicrobial properties and is generally recognized as safe (GRAS) by the USFDA. Natural antimicrobial agents like essential oils contain a complex compound mixture. Thus, volatile natural agents have been effective against various foodborne pathogens. The mode of action of natural antimicrobial agents incorporated into the package can be achieved by direct or indirect contact systems, which are influenced by the controlled, constant release onto the food surface. To measure the mass transfer profile of volatile natural agents, the first step to analysis is to know the compounds' real concentration after processing using methods such as solvent extraction. The concentration extraction from plant material is influenced by various parameters such as solvent polarity, particle size, extraction procedures, and conditions. The reasoning for selecting an extraction solvent or solvent mixture in addition to the extraction procedure is frequently not well studied and/or not clearly documented. Most previous studies typically used dichloromethane as the solvent for extraction. However, this may cause a GC column to get stuck due to the high molecular weight of the polymer in the injected solution. This work aimed to develop a systematic approach for extracting compounds from a polymer matrix and to determine the diffusion rate of the compounds in simulated solutions.

OVERALL

This research aimed to study the effect of extraction solvents by comparing the extraction efficiency of water: methanol (1:1) and ethyl acetate: hexane (1:1) using extraction techniques to measure the actual concentration and diffusion coefficients of compounds on the developed biodegradable PBS films by incorporated with spherical lignin nanoparticles (LN) and natural agents (NA), such as vanillin, trans-cinnamaldehyde, and citral as antimicrobial packaging.

MATERIALS & METHODS

Development of PBS antimicrobial films containing lignin nanoparticles and natural agents - vanillin, trans-cinnamaldehyde, and citral

The PBS blend films containing natural agents were prepared by adding a PBS masterbatch containing lignin and each natural agent to the PBS resins. Composite films of PBS/LN, PBS/LN/10% (nominal) NA, and PBS/10% (nominal) NA were manufactured via conventional blown film melt-extrusion (Thermo Scientific^{TM} HAAKE Rheomex for the HAAKE PolyLab OS torque rheometer platform, Karlsruhe, Germany) connected with a 19 mm diameter annular die to form a film. The temperatures of the feeding zone, the compression zone, and the metering zone and die were 150, 155, 160, and 160 °C, respectively. The rotation rate of the feeder was fixed at 60 rpm. Thickness (30±5 mm) was determined using a micrometer (Mitutoyo, Japan) with at least 5 replicates at different film positions. A neat PBS was prepared as a control. The proportions of PBS, lignin, and natural agents were mixed, as shown in Table 1.

No	Abbreviation	Natural agent	PBS (wt.%)	Lignin (wt.%)	Natural agent (wt.%)
1	PBS	-	100	-	-
2	1LNP	-	99	1	-
3	P10VL	vanillin	90	-	10
4	P1LN10VL	vanillin	89	1	10
5	P10CN	trans-cinnamaldehyde	90	-	10
6	P1LN10CN	trans-cinnamaldehyde	89	1	10
7	P10CT	citral	90	-	10
8	P1LN10CT	citral	89	1	10

Table 1 Proportion of poly(butylene succinate) - PBS, lignin - LN, and natural agents – vainilin (VL), trans-cinnamaldehyde (CN), and citral (CT).

Determination of the remaining natural agent content

To quantify the remaining contents of each natural agent in the film after processing, they were evaluated by solvent extraction. The sample film weighed around 30 mg. Then, it was placed in a 20 mL screw thread vial containing 10 ml of different solvent extractions (ethyl acetate:

hexane (1:1) and water: methanol (1:1)) at 23 °C for 24 h and kept in the dark. After conditioning, the extracted solution was sampled 100 µL from the aliquot at 0.25, 0.5, 0.75, 1, 2, 3, 6, 12, and 24h and put into the 250 µL insert vial. The extracted solution of 1 µL was injected into a gas chromatography 7890A model coupled with a 5975C inert XL MSD with Triple-Axis detector (GC-MSD) (Agilent Technology, Santa Clara, CA, United States). The gas chromatography conditions were 1.0 mL.min^{-1} of helium flow rate, and the temperature program was set from 40 to 320 °C at 40 °C.min^{-1}. compounds were analyzed using the A VF-5ms column (40 m length, 0.25 mm diameter, and 0.25 mm film thickness) (Agilent Technology, Santa Clara, CA, United States). The concentration of each natural agent released in the liquid phase was calculated from the external standard curve. Standard solutions of each natural agent in dichloromethane were prepared and used to construct the calibration curve. The experiments were performed in triplicate.

Determination of diffusion coefficients

The diffusion coefficient of each natural agent in the liquid phase was studied following ASTM 4754-98 with some modifications. Sample films were cut into 4×4 cm and then inserted into a 40 mL screw cap amber glass vial containing 30 mL each of distilled water as a neutral food simulant and 10% ethanol as an alcoholic food simulant and kept at 23±2 °C for a designated period of time until equilibrium was reached. The total amount of compounds in the polymer blend films was determined using the gas chromatography 7890B model coupled with a 7010B Triple Quad mass spectrometric detector (GC-MSD) (Agilent Technology, Santa Clara, CA, United States). The gas chromatography conditions were 4.0 mL.min^{-1} helium flow rate, and the temperature program was set from 40 to 90 °C at 30 °C.min-1, followed by 90 to 110 °C at 5 °C.min^{-1}, 110 to 165 °C at 40 °C.min^{-1}, 165 to 180 °C at 5 °C.min^{-1}, and 180 to 320 °C at 40 °C.min^{-1}. The VF-5ms column (30 m length, 0.25 mm diameter, and 0.25 mm film thickness) was used to analyze the compounds. The concentration of each natural agent released in the liquid phase was calculated from the external standard curve. The diffusion coefficient of each natural agent in packaging films in the liquid phase was based on the Fick's second law. The analytical solution can be described as follows:

$$\frac{M_t}{M_\infty} = 1 - \sum_{n=1}^{\infty} \frac{1\alpha(1+\alpha)}{1+\alpha+\alpha^2+q_n^2} exp\left[-\frac{Dq_n^2 t}{L^2}\right] \qquad (1)$$

where M_t is the concentration of natural agent diffused into the food simulant at time t; M_∞ is the concentration of natural agent diffused into the food simulant at equilibrium; q_n^2 is the non-zero positive roots of $tan\ q_n = -\alpha q_n$ where $\alpha = V_f/K_{p,f}V_p$; V_f is the volume of food; V_p is the volume of membrane; $K_{p,f}$ is the partition coefficient where $K_{p,f} = C_{p,\infty}/C_{f,\infty}$ where $C_{p,\infty}$ is the concentration of the natural agent in the membrane at equilibrium; and $C_{f,\infty}$ is the concentration of the natural agent in the food simulant at equilibrium. D is the diffusion coefficient of the natural agent; L is the thickness of the membrane containing the natural agent.

RESULTS

Amount of natural agents

Two different polar-nonpolar solvent extractions, ethyl acetate: hexane (1:1) and water: methanol (1:1) were used to evaluate each natural agent's remaining contents on the PBS-based film as shown in Figure 1. According to the solvent extraction results, the hexane solution was suitable for use as a solvent for extracting natural agents from the PBS-based film. Ethyl acetate: hexane mixture has a higher ability to extract nonpolar components when considering the precision of the replication of the results.[1] All the compounds extracted with ethyl acetate-hexane solution showed a smoother baseline than water: methanol. However, the highest yield for extractable substances was achieved by polar solvents like water: methanol.[2] This is because low molecular-weight high-density solvents like methanol have a higher vapor volume for the same injection volume and head pressure compared to high molecular-weight low dense solvents like hexane. Then, an expansion of the solvent beyond the volume of the liner could result in back flashes and contaminated spectra. From this point, the extraction with water: methanol solvent can cause noise, and this will affect the overestimation of the value of the compounds even when integrated with the same range. The loss of compounds caused by the evaporation of natural agents in the film processing, especially direct adding the natural agents to the film without any encapsulation or protection would lead to the decline of the antibacterial ability of the composite film. The PBS/LN/NA composite film shows a higher remaining content of each NA than PBS/NA; results are presented in Table 2.

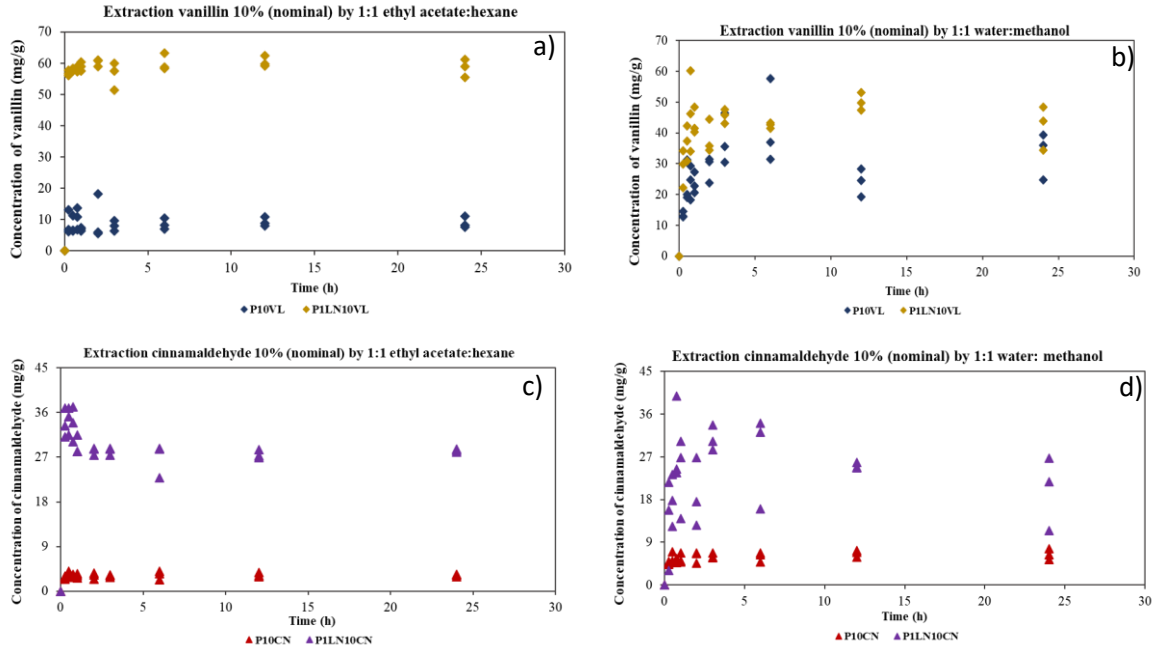

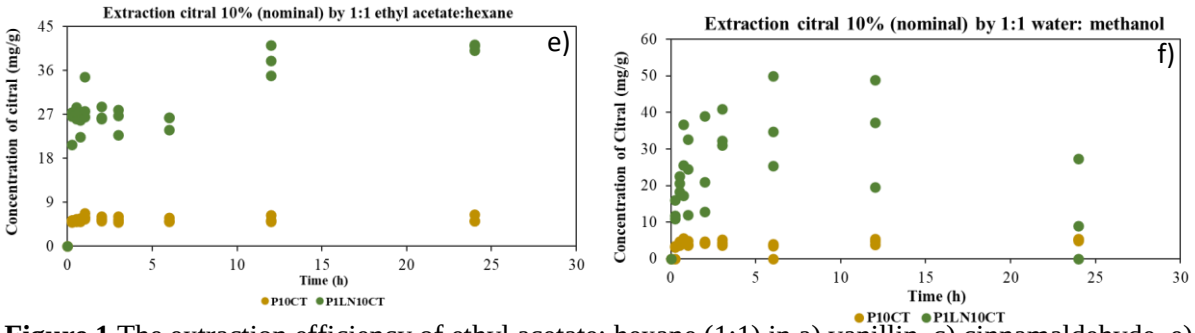

Figure 1 The extraction efficiency of ethyl acetate: hexane (1:1) in a) vanillin, c) cinnamaldehyde, e) citral and extraction efficiency of water: methanol (1:1) in b) vanillin, d) cinnamaldehyde, f) citral using extraction techniques in PBS blends films

Time (h)	Vanillin concentration (mg/g)				Trans-cinnamaldehyde concentration (mg/g)				Citral concentration (mg/g)			
	Ethyl acetate: Hexane		Water: Methanol		Ethyl acetate: Hexane		Water: Methanol		Ethyl acetate: Hexane		Water: Methanol	
	P10VL	P1LN10VL	P10VL	P1LN10VL	P10CN	P1LN10CN	P10CN	P1LN10CN	P10CT	P1LN10CT	P10CT	P1LN10CT
0.00	0.00 ± 0.00a	0.00 ± 0.00a	0.00 ± 0.00a	0.00 ± 0.00a	0.00 ± 0.00a	0.00 ± 0.00a	0.00 ± 0.00a	0.00 ± 0.00a	0.00 ± 0.00a	0.00 ± 0.00a	0.00 ± 0.00a	0.00 ± 0.00a
0.25	8.64 ± 3.86b	56.88 ± 0.79bc	13.41 ± 0.94bc	28.81 ± 6.07b	2.74 ± 0.26c	33.80 ± 2.92c	4.64 ± 0.34bc	13.48 ± 9.45bc	5.24 ± 0.21c	24.98 ± 3.55b	2.23 ± 1.95b	12.88 ± 2.73b
0.50	8.11 ± 2.72b	57.86 ± 0.50bc	23.43 ± 6.86cd	36.89 ± 5.71bc	3.29 ± 0.60c	34.54 ± 2.77c	5.59 ± 1.23cd	17.79 ± 5.49cd	5.31 ± 0.27d	27.34 ± 1.22bc	4.27 ± 0.54cd	20.52 ± 2.08cd
0.75	10.52 ± 3.52b	58.16 ± 0.81bc	24.11 ± 5.51cd	46.85 ± 13.11cd	3.07 ± 0.31c	33.78 ± 3.50c	5.19 ± 0.47bcd	29.34 ± 9.13d	5.33 ± 0.37c	25.25 ± 2.61bc	5.13 ± 0.69d	26.54 ± 9.76d
1.00	6.93 ± 0.57b	58.94 ± 1.40bc	23.58 ± 3.37cd	43.44 ± 4.33cd	3.09 ± 0.46c	29.33 ± 1.91b	5.55 ± 1.05cd	23.71 ± 8.64cd	6.18 ± 0.62c	29.66 ± 4.50c	4.19 ± 0.64cd	23.03 ± 10.41cd
2.00	9.95 ± 7.17b	60.19 ± 1.15c	28.61 ± 4.22de	38.17 ± 5.40bc	3.11 ± 0.68c	28.27 ± 0.70b	5.99 ± 1.18cd	18.97 ± 7.26cd	5.66 ± 0.44c	27.05 ± 1.35bc	4.44 ± 0.25cd	24.28 ± 13.37cd
3.00	8.01 ± 1.58b	56.32 ± 4.39b	37.52 ± 8.17ef	45.47 ± 2.26cd	3.05 ± 0.27c	28.33 ± 0.75b	6.07 ± 0.53cd	30.84 ± 2.67d	5.52 ± 0.54c	25.88 ± 2.74bc	4.45 ± 0.84cd	34.73 ± 5.34cd
6.00	8.66 ± 1.76b	60.10 ± 2.63c	42.02 ± 13.89f	42.47 ± 0.84cd	3.22 ± 0.89c	26.80 ± 3.41b	5.99 ± 1.05cd	27.40 ± 9.94d	5.38 ± 0.46c	25.54 ± 1.49bc	2.56 ± 2.23bc	36.68 ± 12.34bc
12.00	9.32 ± 1.45b	60.51 ± 1.71c	24.04 ± 4.52cd	50.15 ± 2.87d	3.26 ± 0.49c	27.64 ± 0.84b	6.63 ± 0.73d	25.12 ± 0.66cd	5.60 ± 0.73c	38.12 ± 3.11d	4.73 ± 0.86d	35.25 ± 14.71d
24.00	9.02 ± 1.86b	58.55 ± 2.87	33.33 ± 7.62def	42.22 ± 7.16cd	3.20 ± 0.27c	28.38 ± 0.27b	6.43 ± 1.12d	19.94 ± 7.81cd	5.67 ± 0.79c	40.86 ± 0.59d	5.22 ± 0.25d	27.40 ± 13.98d
Double extraction[2]	0.00 ± 0.00a	1.04 ± 0.13a	4.02 ± 0.04ab	4.21 ± 0.37a	1.12 ± 0.97b	1.38 ± 0.02a	3.71 ± 0.55b	3.23 ± 0.04ab	1.14 ± 0.99b	3.46 ± 0.45a	0.00 ± 0.00a	0.00 ± 0.00a

[1]a-c letters indicate significant differences between time on the same treatment. Data were analyzed for multiple comparisons by analysis of variance (ANOVA) with Duncan's multiple range test at a significance level of $p \leq 0.05$.
[2]Double extraction is making an extraction with sample films again to make sure that the selected compounds can completely extracted the compound from the films.

Table 4 Comparison of extraction yields at 23 °C using various solvents (ethyl acetate: hexane (1:1) and water: methanol (1:1)

Determination of diffusion coefficients

Release on water

The release profile of vanillin (Figure 2), cinnamaldehyde (Figure 3), and citral (Figure 4) in sample films into the water can be observed. In the case of PBS/10% (nominal) NA, the release of compounds reached equilibrium faster than PBS/LN/10% (nominal) NA. The diffusion processes of PBS/10% (nominal) VL and PBS/10% (nominal) CN reached equilibrium after approximately 3 minutes and took longer for all PBS/LN/10% (nominal) NA films. This vanillin result is in accordance with Razaei et al. report that vanillin showed a burst release in the first 5min due to the release of surface-loaded vanillin. Then, the release increased gradually with time to reach an equilibrium.[3] However, the addition of lignin increased the mass transfer step of the natural agent in the PBS/LN/10% (nominal) NA film by desorption of some parts of the natural agent from the surface of lignin into the PBS matrix. The PBS/LN/10% (nominal) NA film could prolong each natural agent release to achieve sustained release. The slow release of antimicrobial agents can be an advantage by constraining the microbial growth of food during storage.[4] The diffusion coefficients were calculated with the equation 1 method and presented in Table 2.

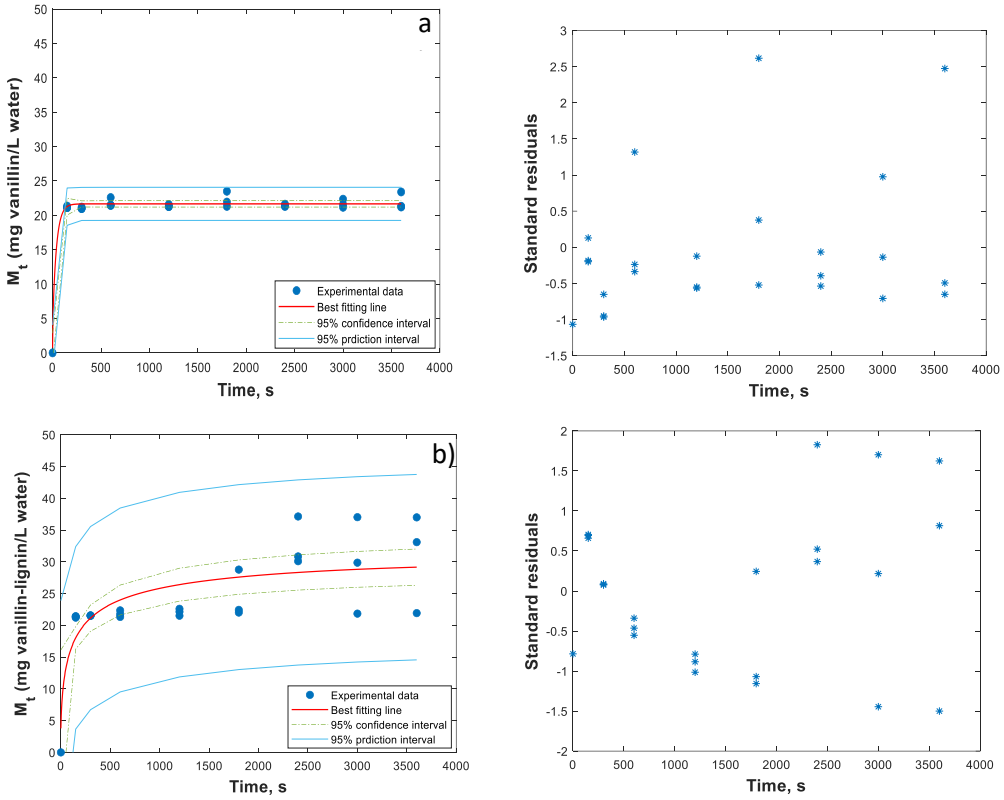

Figure 2 Experimental and predicted release of vanillin from a) PBS/VL and b) PBS/LN/VL into the water at 23 °C as a function of time. The associated standard residual plot for each graph is shown on the right.

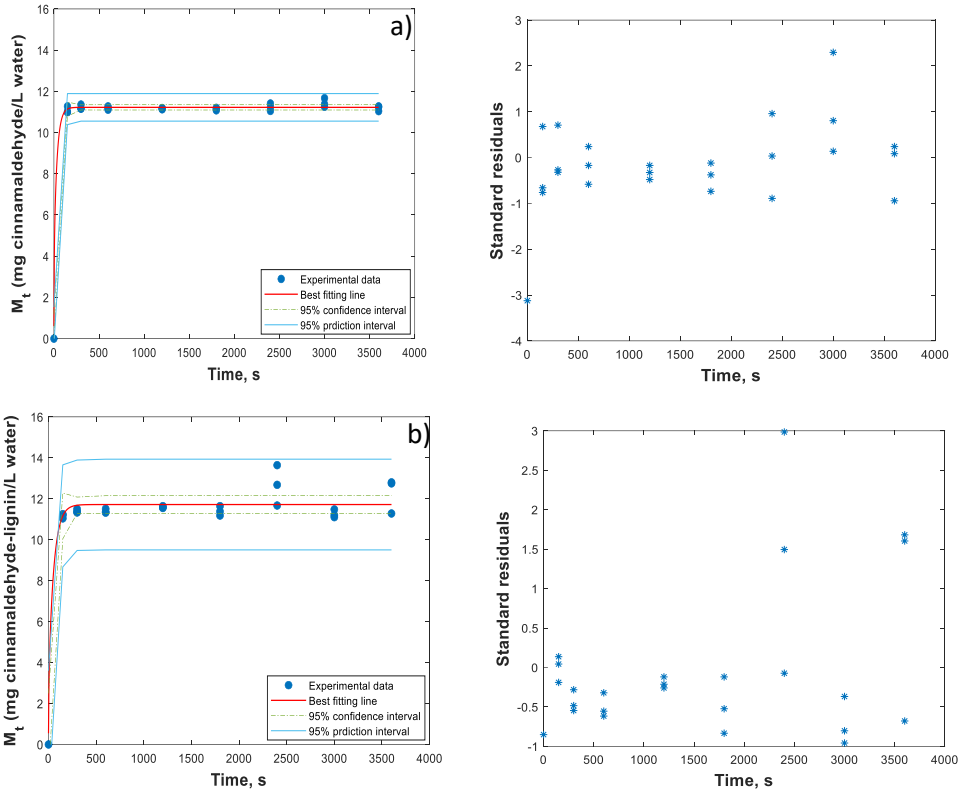

Figure 3 Experimental and predicted release of cinnamaldehyde from a) PBS/CN and b) PBS/LN/CN into the water at 23 °C as a function of time. The associated standard residual plot for each graph is shown on the right.

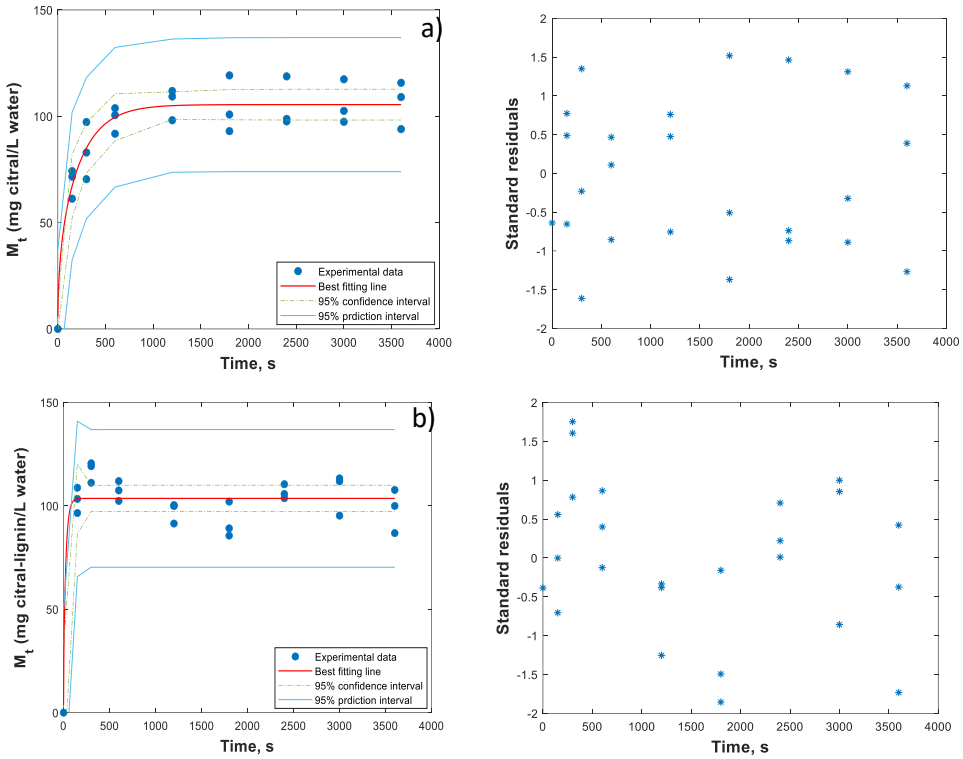

Figure 4 Experimental and predicted release of citral from a) PBS/CT and b) PBS/LN/CT into the water at 23 °C as a function of time. The associated standard residual plot for each graph is shown on the right.

Release on 10%EtOH

The release profile of vanillin, cinnamaldehyde, and citral in sample films into 10%EtOH can be observed in Figure 5 to Figure 7. The release profiles of natural agents from PBS-blend films in most of the treatments took longer to reach equilibrium except in PBS/LN/10% (nominal) CN films. Cui et al. found that the cinnamaldehyde released from the PLA film and the PLA with carbon nanotube film reached about 52.7% and 33.4% in methanol solution, within the first 7 days. After that, the cumulative release of cinnamaldehyde in the film showed a relatively steady upward trend and finally stabilized.[5] The fastest release of cinnamaldehyde from the PBS-based film (PBS/CN) was found in both water and 10% ethanol. The diffusion coefficients and other parameters of each compound released in 10%EtOH are presented in Table 3.

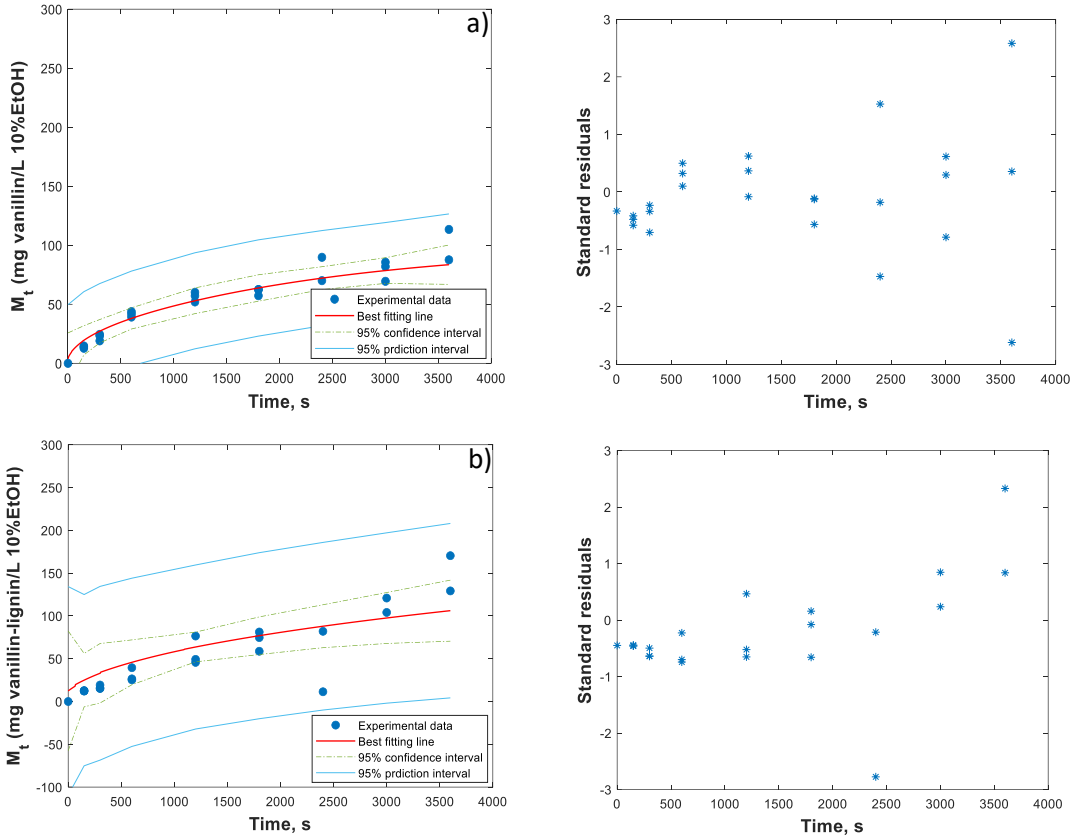

Figure 5 Experimental and predicted release of vanillin from a) PBS/VL and b) PBS/LN/VL into the 10% EtOH at 23 °C as a function of time. The associated standard residual plot for each graph is shown on the right.

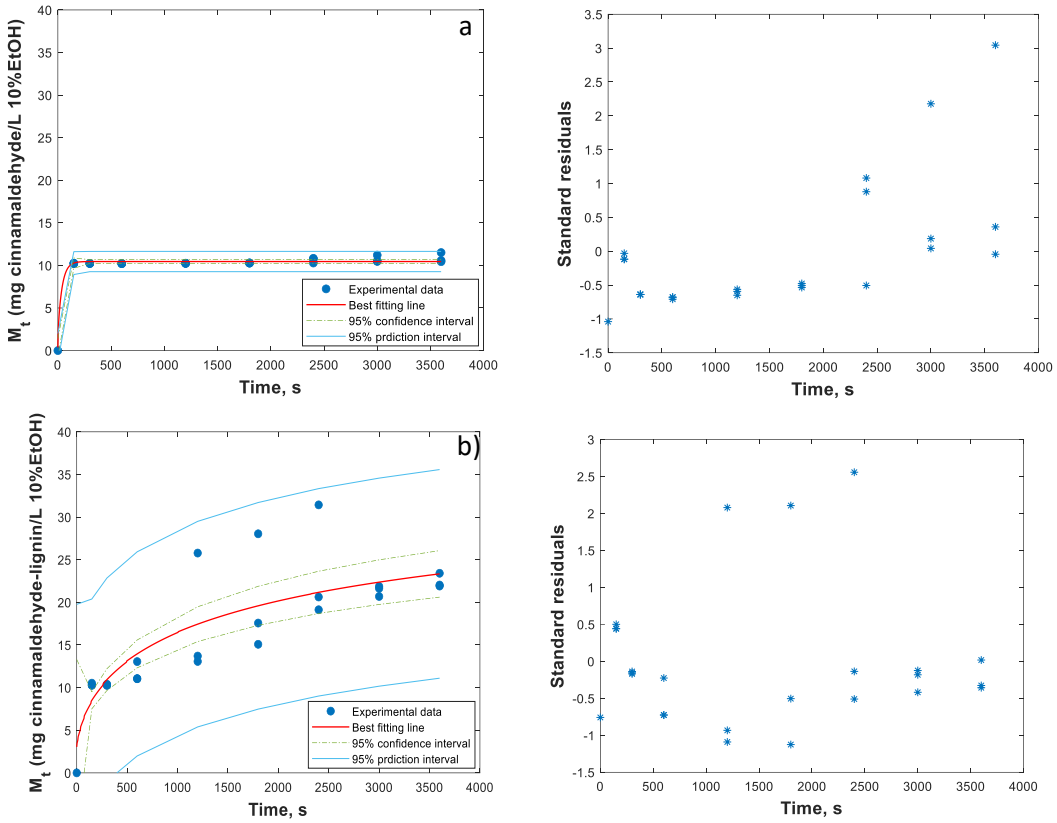

Figure 6 Experimental and predicted release of cinnamaldehyde from a) PBS/CN and b) PBS/LN/CN into the 10%EtOH at 23 °C as a function of time. The associated standard residual plot for each graph is shown on the right.

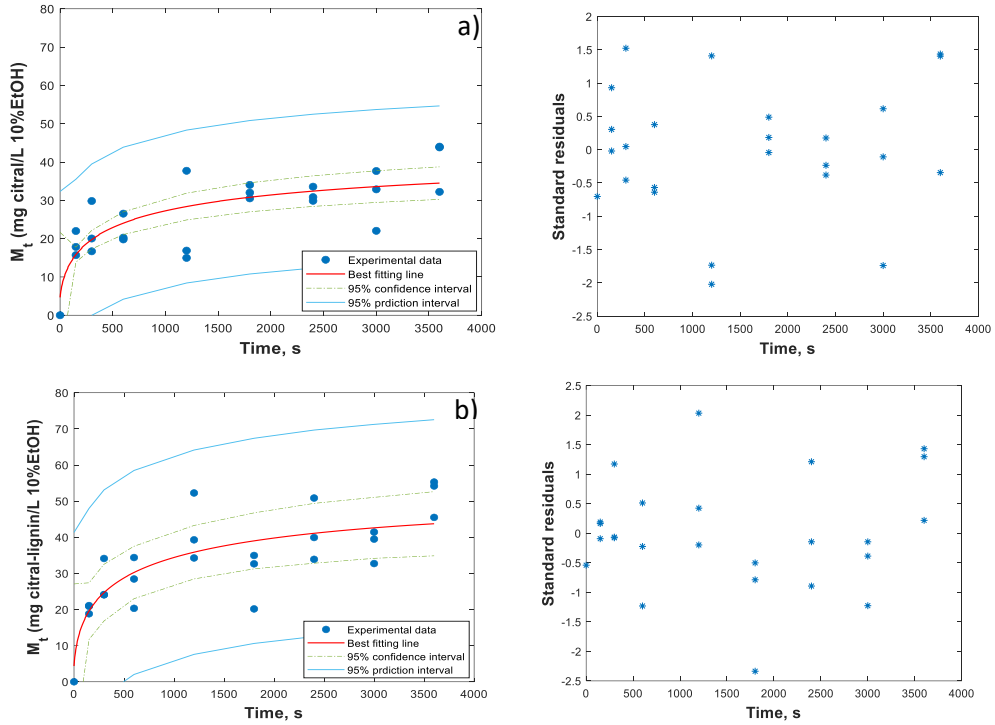

Figure 7 Experimental and predicted release of citral from a) PBS/CT and b) PBS/LN/CT into the 10%EtOH at 23 °C as a function of time. The associated standard residual plot for each graph is shown on the right.

Treatment	WATER				10%ETOH			
	Diffusion coefficient (cm^2/s)	Mt∞	α	RMSE	Diffusion coefficient (cm^2/s)	Mt∞	α	RMSE
10VL	1.60×10^{-7}	2.17×10^{-12}	4.21×10^{-12}	0.701	2.50×10^{-9}	1.01×10^{-11}	7.40×10^{-13}	11.571
P1LN10VL	1.14×10^{-9}	3.00×10^{-12}	1.18×10^{-14}	4.822	3.41×10^{-10}	2.75×10^{-11}	2.93×10^{-13}	27.584
10CN	1.10×10^{-7}	1.12×10^{-12}	8.73×10^{-14}	0.195	1.62×10^{-7}	1.05×10^{-12}	4.33×10^{-12}	0.346
P1LN10CN	9.21×10^{-8}	1.17×10^{-12}	2.56×10^{-13}	0.644	2.43×10^{-10}	3.24×10^{-12}	2.17×10^{-14}	4.011
10CT	1.65×10^{-8}	1.05×10^{-11}	1.10×10^{-13}	9.080	3.64×10^{-10}	4.04×10^{-12}	1.42×10^{-14}	6.632
P1LN10CT	2.42×10^{-7}	1.04×10^{-11}	1.40×10^{-12}	9.689	1.05×10^{-9}	4.75×10^{-12}	2.49×10^{-14}	8.062

Table 3 Comparative analysis of diffusion coefficient and concentration of compounds at equilibrium, alpha, and root mean square error of natural agents at 23 °C.

ACKNOWLEDGEMENT

The authors would like to thank Department of Packaging and Materials Technology, Kasetsart University, School of Packaging, Michigan State University, and Mass Spectrometry and Metabolomics Core, Michigan State University for the machine used in this research.

REFERENCES

[1] López, A., Rico, M., Rivero, A., & Suárez de Tangil, M. (2011). The effects of solvents on the phenolic contents and antioxidant activity of Stypocaulon scoparium algae extracts. *Food Chemistry*, *125*(3), 1104-1109. https://doi.org/10.1016/j.foodchem.2010.09.101

[2] Taha, S. M., & Gadalla, S. A. (2017). Development of an efficient method for multi residue analysis of 160 pesticides in herbal plant by ethyl acetate hexane mixture with direct injection to GC-MS/MS. *Talanta*, *174*, 767-779. https://doi.org/10.1016/j.talanta.2017.06.080

[3] Rezaei, A., Nasirpour, A., Tavanai, H., & Fathi, M. (2016). A study on the release kinetics and mechanisms of vanillin incorporated in almond gum/polyvinyl alcohol composite nanofibers in different aqueous food simulants and simulated saliva. *Flavour and Fragrance Journal*, 31(6), 442-447.

[4] Stroescu, M., Stoica-Guzun, A., & Jipa, I. M. (2013). Vanillin release from poly(vinyl alcohol)-bacterial cellulose mono and multilayer films. *Journal of Food Engineering*, *114*(2), 153-157. https://doi.org/10.1016/j.jfoodeng.2012.08.023

[5] Cui, R., Jiang, K., Yuan, M., Cao, J., Li, L., Tang, Z., & Qin, Y. (2020). Antimicrobial film based on polylactic acid and carbon nanotube for controlled cinnamaldehyde release. *Journal of Materials Research and Technology*, 9(5), 10130-10138.

CONFERENCE PROCEEDINGS

NOVEL PACKAGING

ORAL PRESENTATION

GENERAL STREAM

NP-GO01	Pilot-scale processing and functional properties of compostable thermoplastic gliadin/poly(ε-caprolactone) blend films
NP-GO02	Fluorescent markers for bioplas tics from encapsulated algae chlorophyll

NP-GO01

Pilot-scale processing and functional properties of compostable thermoplastic gliadin/poly(ε-caprolactone) blend films intended for food packaging

Alejandro Aragón-Gutiérrez[1], Pedro Francisco Muñoz-Gimena[2], Miriam Gallur[1], Rafael Gavara[3,4], Daniel López[2,4] and Pilar Hernández-Muñoz[3,4]

[1]Grupo de Tecnología de Materiales y Envases, Instituto Tecnológico del Embalaje, Transporte y Logística, ITENE, Unidad Asociada al CSIC, calle de Albert Einstein 1, 46980 Paterna, Valencia, Spain;
[2]Instituto de Ciencia y Tecnología de Polímeros, ICTP-CSIC, calle Juan de la Cierva 3, 28006 Madrid, Spain.
[3]Instituto de Agroquímica y Tecnología de Alimentos, IATA-CSIC, calle del Catedrático Agustín Escardino Benlloch 7, 46980 Paterna, Valencia, Spain.
[4]Interdisciplinary Platform for "Sustainable Plastics towards a Circular Economy" (SusPlast-CSIC), 28006 Madrid, Spain

***Correspondence to**: Alejandro Aragón-Gutiérrez, Instituto Tecnológico del Embalaje, Transporte y Logística, ITENE*
E-mail: alejandro.aragon@itene.com

ABSTRACT: Gliadins are the major component of wheat gluten. These proteins present excellent properties to consider their use in food packaging applications. Some of these properties are their film forming behaviour, great adhesively to other surfaces, biodegradability, and capability to deliver bioactives. Recent concerns about the excessive waste generated by conventional non-biodegradable plastics used in packaging applications makes interesting to continue exploring the potential of gliadins in this technological area. The applicability of gliadins in industrial environments present some challenges related to their processability in conventional plastic transformation equipment. In this study, films of thermoplastic gliadins (TPG) blended with poly(ε-caprolactone) (PCL) were obtained in a pilot-scale extruder and characterized by means of structural, morphological (SEM), thermal (DSC and TGA), mechanical (tensile test), and barrier properties (oxygen and water vapor permeability) aiming to determine their suitability for food applications. Finally, the compostability of the films was assessed to determine the influence of gliadins on the biodegradation and disintegration rate of PCL under home-composting conditions. Transparent and flexible films of PCL/TPG were obtained, and the presence of gliadins reduced the oxygen permeability at 0% and 50% relative humidity values. In addition, gliadins accelerated the biodegradation and disintegration rate under home-composting conditions of blend films with respect pristine PCL, showing the potential interest of the developed materials for packaging applications.

Keywords: poly(ε-caprolactone); thermoplastic gliadins; extrusion; polymer blends; film properties; compostability; sustainable food packaging.

INTRODUCTION

During the last few years, the production and use of plastic materials have increased enormously and contributed to the problem of waste disposal. The concerns about solid waste, and its volume, has generated some alternatives to minimize the problem created in the environment, being the biodegradable polymers one of them to replace traditional materials, especially in the packaging sector [1,2]. Among others, poly(ε-caprolactone) (PCL) has gained great attention in recent years due to its great stretchability, low glass transition temperature, T_g = −60°C, and good miscibility and compatibility with other polymers. Moreover, PCL can decompose into carbon dioxide, methane, water, inorganic compounds, and biomass by the enzymatic action of both, aerobic and anaerobic microorganisms [3–5]. However, some of its characteristics, e.g., non-biobased nature, high price or low melting point limit a broader application of this polymerin more fields. PCL-food hydrocolloid blends have been studied as an encouraging approach to enhance PCL functionalities. Although starch has been the preferable choice to prepare PCL- based films, several authors have also reported the benefits of using proteins such as zein or wheat gluten as an alternative to improve the performance of PCL-based films, increase the renewable content of material and reduce the final cost of the formulation [6,7]. In this line, some research studies on gluten proteins have established that the two components present ingluten, gliadins and glutenin, can be employed individually to expand their range of application. Following this strategy, this work aimed to use gliadins extracted from wheat gluten in the preparation of PCL-plasticized gliadin blends by conventional film-extrusion process. The performance of films of PCL and PCL incorporated with 30 wt.% and 50 wt.% of plasticized gliadins was assessed and the end of life of the films was evaluated under home-composting conditions.

SAMPLES PREPARATION

The gliadin-rich fraction was extracted from wheat gluten according to the method described by Balaguer et al. [8]. In brief, wheat gluten was dispersed in 70% (v/v) ethanol/water mixture, stirred overnight at room temperature, and centrifuged at 5000 rpm for 20 min at 20 °C. The supernatant containing the gliadin-rich fraction was collected and used as the film-forming solution. Glycerol was added as plasticizer at 25% (g/100 g of dry protein) and the solvent was allowed to evaporate at 37 °C for one day. The obtained material was powdered by using a cutting mill. Then, blend film formulations were prepared in a pilot-scale co-rotating twin screw extruder Brabender TSE 20/40. PCL pellets were fed through the main hopper employing a gravimetric feeder while plasticized gliadins (TPG) were introduced inside the extruder in powder form through a side feeder. Films of PCL, and PCL containing 30 wt.% (PCL-TPG30) and 50 wt.% (PCL-TPG50) of plasticized gliadins were obtained using an extrusion calender line as shown in Figure 1.

Figure 1 Illustrative picture of the film-extrusion process of PCL-TPG30 reference

RESULTS AND DISCUSSION

Structural and morphological characteristics

The successful physical blending of both components, PCL, and thermoplastic gliadins, was confirmed by Fourier transformed infrared spectroscopy analysis. The spectra of PCL-TPG blends showed the appearance of the stretching vibration of amide I and the bending vibration of amideII characteristic of gliadin proteins. On the other hand, the morphological study of the cross- sections of the films revealed a smooth and clean surface for PCL sample (see Figure 2), while in the binary blends, random-ordered conglomerates of particles could be detected, suggesting a lack of miscibility between plasticized gliadins and PCL.

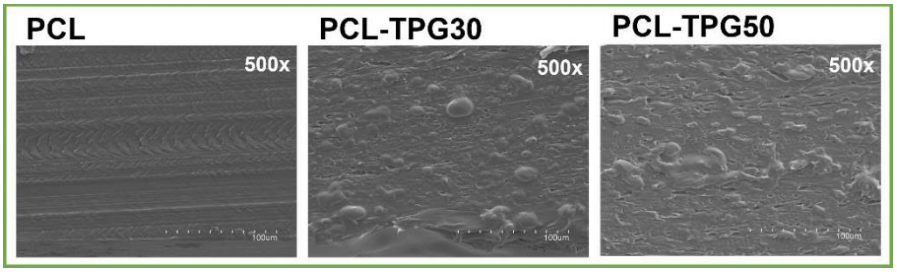

Figure 2 SEM micrographs of PCL-based films at 500x magnification

Thermal properties

Differential scanning calorimetry (DSC) was employed to study the melting (T_m) and crystallization (T_c) temperatures of PCL-based films as well as to investigate the crystallinity degree of the extruded samples (Table 1). Pristine PCL presented during the first and second heating scan, endothermic peaks at 61°C and 57°C, respectively, associated with the melting

process of PCL [9]. With respect PCL-TPG blends, the presence of gliadins did not significantly modify the melting temperature of PCL, whereas the crystallinity degree calculated from the first heating thermogram after normalizing the PCL amount in the blend, shifted from 57.1% for PCL to 65.6% and 83.1% for PCL-TPG30 and PCL-TPG50, respectively, indicating a nucleating effect of gliadins over the PCL polymer matrix. Moreover, the crystallization temperature during the cooling scan slightly decreased by the addition of plasticized gliadins, suggesting a heterogeneous nucleation of PCL provoked by the presence of gliadins.

Formulation	Tm (°C)	Xc (%)	Tc (°C)	Tm (°C)
PCL	61	57.1	31	57
PCL-TPG30	59	65.6	29	57
PCL-TPG50	59	83.1	27	56

Table 1 DSC thermal parameters obtained during first heating scan, cooling, and second heating scan.

The influence of plasticized gliadins over the thermal stability of PCL was evaluated by thermogravimetric analysis (TGA). Figure 3 displays the thermograms of the different formulations. PCL presented an onset degradation temperature (calculated at a 5% weight loss) of 369°C, and the maximum decomposition temperature was located at 408°C.

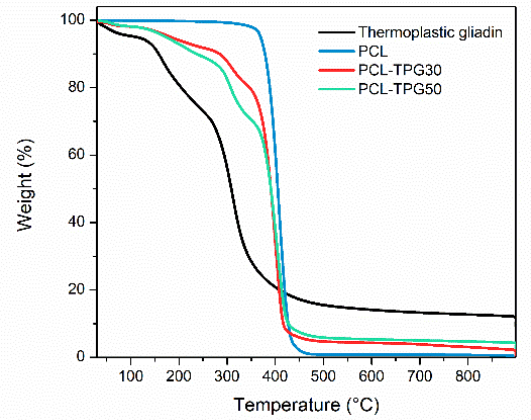

Figure 3 TGA curves of plasticized gliadins, and PCL-based films

On the other hand, PCL-TPG blends showed three main degradation stages associated with the loss of glycerol used as plasticizer for gliadins, followed by the decomposition of gliadins and the final the degradation stage of PCL polymer matrix.

Mechanical properties

Tensile tests were conducted in accordance with the the standard ISO 527-3 and the results in terms of Young's modulus (E), stress at yield (σy), stress at break (σB) and elongation at break

(εB) were obtained from the stress-strain curves (Figure 4) [10]. PCL film presented a Young Modulus, a stress at yield and a stress at break of 318 ± 45 MPa, 10.2 ± 1.3 MPa and 31.5 ± 2.9 MPa, respectively.

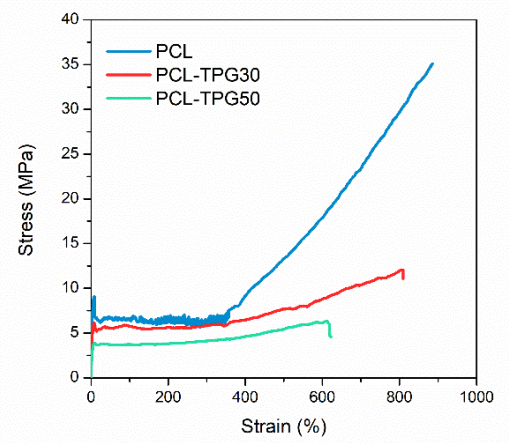

Figure 4. Stress-strain curves of PCL and PCL-TPG films

In the binary blends, the tensile test curves illustrated that the yield point and the Young Modulus decreased as the concentration of gliadins increased in the formulations. PCL-TPG film, as well as pristine PCL film, showed a strain-hardening phenomenon, caused by the orientation of polymer chains. Finally, the addition of up to 50 wt.% of plasticized gliadins in PCL-based films did not affect the high stretchability characteristic of PCL, presenting all films elongation at break values above 600%.

Barrier properties

Due to the relevance of barrier performance of flexible films intended for food applications, the oxygen and water vapor permeability coefficients of all samples were determined, respectively, following the standards F1927-20 and ASTM F1249-20 [11,12].

Reference	**Oxygen permeability (m^3 m/ m^2 s Pa) ×10E^{19}**			**WVP [(g mm)/(m^2 day mmHg)]**
	0% RH	50% RH	75% RH	50% RH
PCL	76.8 ± 2.4	80.3 ± 2.5	82.7 ± 2.0	0.33 ± 0.01
PCL-TPG30	40.7 ± 0.8	55.2 ± 1.1	96.7 ± 2.7	0.36 ± 0.01
PCL-TPG50	22.6 ± 2.4	38.9± 4.7	93.8 ± 10.3	0.49 ± 0.03

Table 2 Oxygen and water vapor permeability coefficients of PCL-based films

Oxygen permeability tests were conducted at room temperature and at three different relative humidity values: 0%, 50%, and 75% RH. As shown in Table 2, the variation in the relative humidity values did not significantly affect the oxygen permeability of PCL, presenting values in the range of 76.8×10^{-19} to 82.7×10^{-19} (m^3 m)/ (m^2 s Pa). Interestingly, the incorporation of 30 wt.% and 50 wt.% of gliadins resulted in an evident reduction in the oxygen permeability at 0% and 50% RH. Nevertheless, as gliadins are sensitive to moisture, the increase in the RH to 75%, led to oxygen permeability values above the one obtained for control PCL film. With respect water vapor permeability, the tests were carried out at room temperature and at 50% RH. The value of water vapor permeability of polycaprolactone film was 0.33 ± 0.01 (g mm)/(m^2 day mmHg). The WVP increased slightly with the incorporation of 30 wt.% of gliadins to a value of 0.36 ± 0.01 (g mm)/(m^2 day mmHg), while blending PCL with up to 50 wt.% of TPG increased the WVP of the film by 48%. This result was ascribed mainly to the increase in the hydrophilicity of the films owing to the high content of amide groups in gliadins [13].

Home-compostability assessment

The end of life of the developed films was assessed by conducting the home-compostability test following the French standard NF T 51-800 [14]. The first stage consisted of determining the ultimate aerobic biodegradation of the films. In this work, the aerobic biodegradability of all samples was calculated by measuring the amount of evolved carbon dioxide following the standard ISO 14855-1:2012 [15]. Microcrystalline cellulose was used as positive reference material, and, according to the standard, the relative biodegradation is demonstrated if the conversion of carbon into carbon dioxide from the samples is at least 90% of the conversion of carbon to carbon dioxide from the reference material in a period no loner than 365 days. As shown in Figure *5*.a., plasticized gliadins had a faster biodegradation profile than cellulose, reaching a plateau with a maximum of 90% biodegradation (110% with respect to cellulose) just after 60 days. In contrast, pristine PCL sample showed an initial lag period of around two weeks followed by the degradation phase which progressed up to reaching a percentage biodegradation (%B) with respect to MCC of 40% after 210 days of test. With regard PCL/TPG blends, the presence of plasticized gliadins promoted an accelerated biodegradation rate with respect pure PCL, showing an intermediate behavior between PCL and gliadin samples. Specifically, PCL-TPG30 and PCL-TPG50 reached, respectively, a %B after 210 days of test of 89% and 96% with respect to cellulose, confirming the positive effect of gliadins over the biodegradability of PCL-based films. The next stage of the home-compostability test was the evaluation of the disintegration of the films under controlled conditions. Figure 5.b. illustrates the qualitative evaluation of the PCL and PCL-TPG films at different times. It could be observed that after 71 days of exposure to home-composting conditions, films lost their transparency and acquired a brownish tonality. Moreover, PCL-TPG blends started to break into fragments, suggesting that the presence of plasticized gliadins promoted a higher disintegration rate compared to pristine PCL film. Finally, after 180 days of test, all film samples presented a satisfactory complete decomposition, confirming their suitability for home-composting end of life.

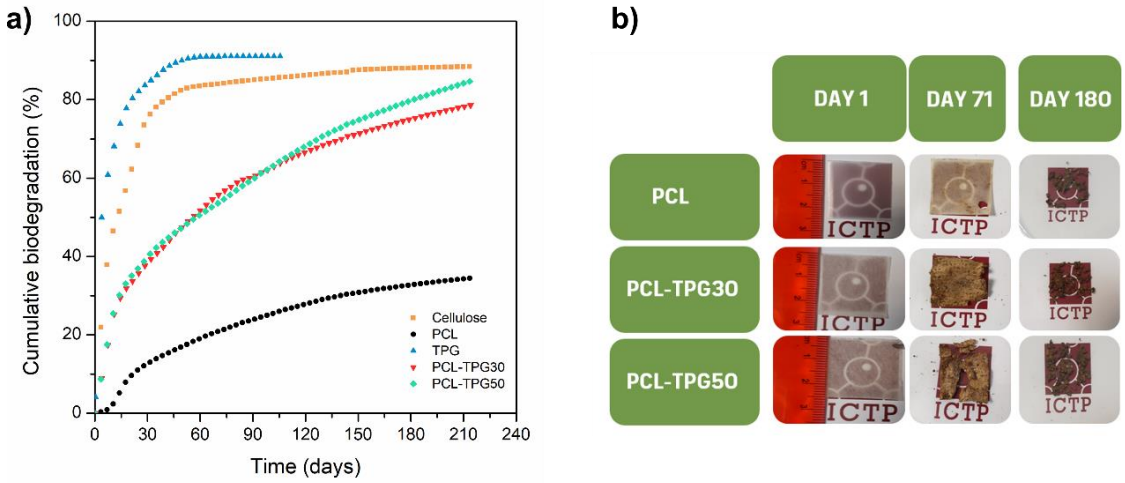

Figure 5 Cumulative biodegradation (a) and disintegration (b) of PCL and PCL-TPG blend films under homecomposting conditions.

CONCLUSION

In the present work, novel PCL-based films containing up to 50 wt.% of plasticized gliadins wereprepared by melt extrusion processing in a twin-screw extruder and fully characterized. The results described in this work show the feasibility of the employed method to obtain sustainableflexible and home-compostable films by industrial processing extrusion technique with enhanced functionalities.

REFERENCES

1. Mariani, P.D.S.C.; Neto, A.P.V.; da Silva, J.P.; Cardoso, E.J.B.N.; Esposito, E.; Innocentini-Mei, L.H. Mineralization of poly(ε-caprolactone)/adipate modified starch blend in agricultural soil. *J. Polym. Environ.* **2007**, *15*, 19–24, doi:10.1007/s10924-006-0044-1.
2. Pucciariello, R.; D'Auria, M.; Villani, V.; Giammarino, G.; Gorrasi, G.; Shulga, G. Lignin/Poly(e-Caprolactone) Blends with Tuneable Mechanical Properties Prepared by High Energy Ball-Milling. *J. Polym. Environ.* **2010**, *18*, 326, doi:10.1007/s10924-010-0212-1.
3. Taherkhani, S.; Moztarzadeh, F. Fabrication of a poly(ε-caprolactone)/starch nanocomposite scaffold with a solvent-casting/salt-leaching technique for bone tissue engineering applications. *J. Appl. Polym. Sci.* **2016**, *133*, 19–21, doi:10.1002/app.43523.
4. Mahieu, A.; Terrié, C.; Agoulon, A.; Leblanc, N.; Youssef, B. Thermoplastic starch and poly(ε-caprolactone) blends: Morphology and mechanical properties as a function of relative humidity. *J. Polym. Res.* **2013**, *20*, doi:10.1007/s10965-013-0229-y.
5. Gajdosova, V.; Strachota, B.; Strachota, A.; Michalkova, D.; Krejcikova, S.; Fulin, P.; Nyc, O.; Brinek, A.; Zemek, M.; Slouf, M. Biodegradable Thermoplastic

Starch/Polycaprolactone Blends with Co-Continuous Morphology Suitable for Local Release of Antibiotics. *Materials (Basel).* **2022**, *15*, doi:10.3390/ma15031101.
6. Corradini, E.; Mattoso, L.H.C.; Guedes, C.G.F.; Rosa, D.S. Mechanical, thermal and morphological properties of poly(ε-caprolactone)/zein blends. *Polym. Adv. Technol.*
7. **2004**, *15*, 340–345, doi:https://doi.org/10.1002/pat.478.
8. Mohamed, A.; Finkenstadt, V.L.; Gordon, S.H.; Biresaw, G.; Palmquist Debra, E.; Rayas- Duarte, P. Thermal properties of PCL/gluten bioblends characterized by TGA, DSC, SEM, and infrared-PAS. *J. Appl. Polym. Sci.* **2008**, *110*, 3256–3266, doi:10.1002/app.28914.
9. Balaguer, M.P.; Gómez-Estaca, J.; Gavara, R.; Hernandez-Munoz, P. Functional Properties of Bioplastics Made from Wheat Gliadins Modified with Cinnamaldehyde. *J.Agric. Food Chem.* **2011**, *59*, 6689–6695, doi:10.1021/jf200477a.
10. Monteiro, M.S. de S.B.; Tavares, M.I.B. The Development and Characterization of Polycaprolactone and Titanium Dioxide Hybrids. *Adv. Nanoparticles* **2018**, *07*, 11–27, doi:10.4236/anp.2018.71002.
11. *ISO 527-3:2018 Plastics — Determination of tensile properties — Part 3: Test conditionsfor films and sheets*; 2018;
12. ASTM F1927-20; Standard Test Method for Determination of Oxygen Gas Transmission Rate , Permeability and Permeance at Controlled Relative Humidity Through Barrier Materials Using a Coulometric Detector 2020, 1–6.
13. ASTM F1249-20; Standard Test Method for Water Vapor Transmission Rate Through Plastic Film and Sheeting Using a Modulated Infrared Sensor. *ASTM Int.* 2020.
14. Balaguer, M.P.; Cerisuelo, J.P.; Gavara, R.; Hernandez-Muñoz, P. Mass transport properties of gliadin films: Effect of cross-linking degree, relative humidity, and temperature. *J. Memb. Sci.* **2013**, *428*, 380–392, doi:10.1016/j.memsci.2012.10.022.
15. NF T51-800; Plastics - Specifications for plastics suitable for home composting 2015.
16. UNE-EN ISO 14855-1:2013; Determinación de la biodegradabilidad aeróbica final de materiales plásticos en condiciones de compostaje controladas. Método según el análisis de dióxido de carbono generado. Parte 1: Método general. 201

NP-GO02

Fluorescent markers for bioplastics from encapsulated microalgal pigments

Hector Torres-Pierna,[a] Alejandro Aragón,[a] Ana Compadre,[b] Gatien Fleury,[b] Soraya Sanchez.[a] M. Gallur[a]

[a]*Packaging, Transport, & Logistics Research Institute (ITENE), C/ Albert Einstein,1. Parque Tecnológico. Paterna, Spain. hector.torres@itene.com, alejandro.aragon@itene.com, soraya.sanchez@itene.com, miriam.gallur@itene.com*
[b]*CEA MicroAlgae Processes Platform, F-13108 St Paul Lez Durance, France. acompadre@luma-arles.org, gatien.fleury@cea.fr*

ABSTRACT: Fluorescent markers based on natural pigments were designed to improve the recyclability of bioplastics. A mixture of chlorophyll a, chlorophyll b and carotenoids were extracted from microalgal cultures. These pigments were encapsulated into layered double hydroxides (LDH) to generate heat-resistant fluorescent markers. The markers were incorporated by twin screw compounding into polylactic acid (PLA) and polybutylene succinate adipate (PBSA) matrices to produce fluorescent specimens to achieve an improved identification and sorting of bioplastic waste in the recycling process.

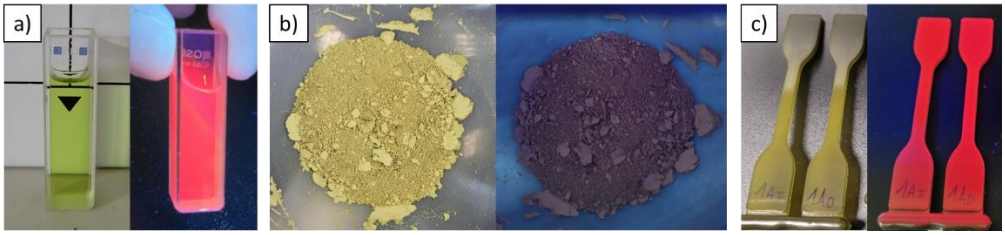

Pigments extract (a), stabilized into LDH (b) and fluorescent nanocomposite specimen obtained from it (c) under visible and UV (365 nm) light.

INTRODUCTION

Half of the global plastic waste is mismanaged, neither recycled nor composted, it ends up as landfilling or leaks into nature, mostly aquatic environments [1]. A promising solution for plastic waste and accumulation in nature is the use of biobased and biodegradable plastics. Commercial biopolymers or bioplastics solutions are still limited to certain applications. The current state of maturity of PLA and PBSA production technology cannot compete with standard thermoplastic grades (such as PET, PE, PP…), therefore, the coexistence of bioplastics with conventional plastics in packaging is to be foreseen.

Proper identification and sorting techniques of plastics are needed to solve this industrial and ecological challenge. IR spectroscopy is currently used at waste sorting facilities to automate the identification and separation of plastics of different natures. However, limitations still exist for closely related grades, such as recyclable, home compostable, and industrial compostable blends of polymers. Fluorescent markers have been proposed as

promising additives to identify and discriminate fractions of plastics difficult to differentiate by classic spectroscopic methods [2].

Many biological organic pigments such as chlorophyll present fluorescent, which could be used as a biobased marker. However, such dyes often have poor thermal and light stability, yielding them unsuitable for polymer extrusion techniques and outdoor applications [3]. Herein, biobased fluorescent markers for biopolymers are presented. Inspired by previous works [4], these markers consist of pigment extracts from *Chlorella vulgaris* microalga encapsulated in nanoclays, such as montmorillonite (MMT) and layered double hydroxides (LDH). Our objective is to achieve superior thermal stability of the Chlorella pigments to withstand the harsh conditions of extrusion compounding processes. The obtained biobased fluorescent markers were incorporated into biodegradable nanocomposites by twin-screw melt compounding. These specimens were then analysed in terms of thermal properties and recyclability.

EXPERIMENTAL SECTION

Materials

The fluorescent markers were prepared using two kinds of nanoclays, Montmorillonite (**MMT**), a cationic clay (Cloisite 116, BYK), and the Layered Double Hydroxide (**LDH**) hydrotalcite, an anionic clay (Pural MG63-HT, Sasol). Absolute ethanol (Sigma Aldrich, 32205-M) was used for the extraction of the algal pigments, and ethanol 96% v/v (Sharlau, ACS, Reag. Ph Eur) and concentrated hydrochloric acid 37% (Sharlau, ExpertQ®, ACS) were used for the swelling of the nanoclays.

Extraction of pigments from algal biomass

The fluorescent pigments were extracted from **Chlorella vulgaris NIES227** grown in standard conditions (25°C, 150 µE/m²/s 20 h per day, 2% CO_2 in air at 200 L_N/h) in a Flat Panel Airlift (FPA) reactor of 25 L (Subitec, Germany) with a modified Beijerinck Medium, with ammonium replaced by nitrates (with equivalent molarity). Once a density of 6 g_{DW}/L (grams of dry weight per litre) was reached, the Chlorella vulgaris NIES227 was harvested from the reactor before to be centrifuged at 7000 rpm (Beckman Coulter Avanti J-26S XP, JLA 8.100) to discard the culture medium. The pellets were collected and stored at -20°C during several weeks before the pigment extraction. The biomass was extracted with absolute ethanol in the darkness at 60°C. The operation was repeated three times on the same biomass sample, to remove most of the pigments, with a ratio of about 0.5 g of dried biomass per mL of ethanol. The Figure 1 shows the extraction scheme and characterization procedure followed for the fluorescent pigment's extraction.

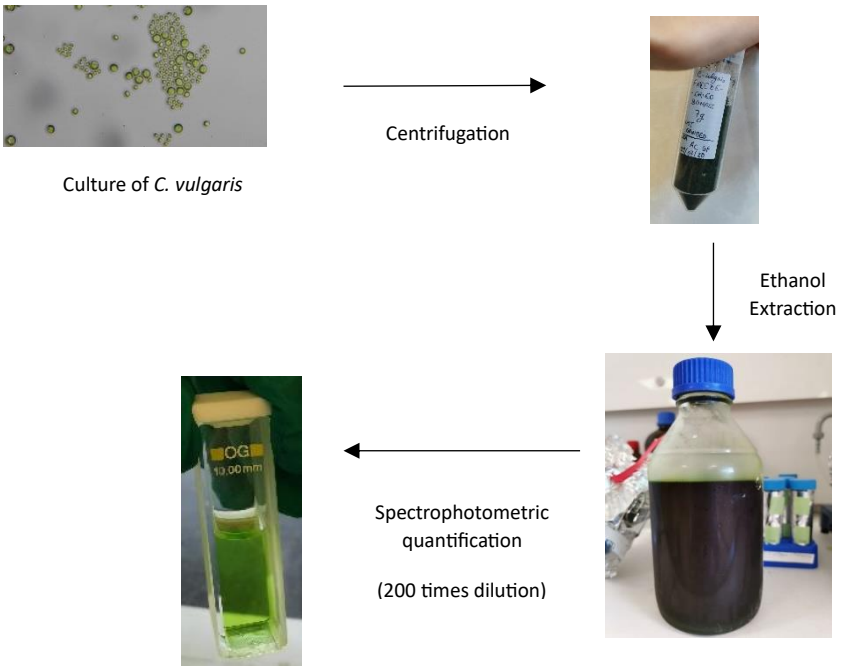

Figure 1 Extraction and quantification steps of the fluorescent pigment mix from Chlorella vulgaris culture

After a 200-fold dilution, the pigments of the extract were quantified with a 1 nm resolution spectrophotometer (Biotek Epoch 2) with the equations proposed by Lichtenthaler [5].

$$Chl_a = 13.36\, A_{664.2} - 5.19 A_{648.6} \quad Equation\ 3$$
$$Chl_b = 27.43\, A_{648.6} - 8.12 A_{664.2} \quad Equation\ 4$$
$$Carotenoids = \frac{1000 A_{470} - 2.13 Chl_a - 97.64 Chl_b}{209} \quad Equation\ 5$$

The stability of the provided extracts containing chlorophyll a, chlorophyll b and carotenoids was checked before integration into their nanoclay thermal protections.

Synthesis of nanoclay fluorescent markers

To improve the thermal resistance of the microalgal dye upon the compounding process, nanopigments were generated according to the method described by Micó-Vicent [4], based on the intercalation between clay platelets.

Briefly, 6.25 g of nanoclay (MMT or LDH) were dispersed into 250 mL of water/ethanol mixture (50 vol.%) over 24 hours at 1500 rpm with a mechanical stirrer (IKA, RW20 Digital) at pH 4.5. After this period, 67.5 mL of the pigments extract are added, and the agitation is maintained for 24 hours more before the dye-load clay is isolated by centrifugation at 8000 rpm and dried in the dark at room temperature. The supernatant was collected and measured by UV-vis spectroscopy to calculate the payload and the encapsulation efficiency.

Bionanocomposites preparation

The encapsulated compounds were introduced into two different biopolymers using a conical compounding equipment (Xplore MC15, Miniextruder DSM). Once processed at identified temperature, time and processing speed, the molten formulation was transferred to a small injection molding machine to inject standardized specimens used to evaluate the final properties of the developed composites. The biopolymers used as matrices were polylactic acid (PLA LX175 from TotalEnergies Corbion) and poly(butylene succinate-co-butylene adipate) (PBSA FD92) with 30% of thermoplastic starch as an additive). The processing temperatures were 190ºC and 165ºC respectively, both at 100 rpm mixing rate.

Characterization techniques

Differential scanning calorimetry (DSC). DSC was employed to calculate the main transition temperatures as well as their corresponding enthalpies. The measurements were carried out using a DSC Q-2000 calorimeter (TA Instruments, New Castle, DE, USA). Thermograms were generated during the first heating of the sample from 0 °C to 200°C/min at a heating rate of 10°C/min in nitrogen atmosphere, and then a cooling step from 200°C to 0°C at the same rate. The typical mass of the sample was 4 mg. Indium was used to calibrate the temperature and enthalpy reading.

Thermogravimetric analysis (TGA). TGA was carried out by dynamic measurements with TGA Q-500 thermogravimetric equipment at a constant heating rate of 10°C/min under nitrogen atmosphere to avoid any thermo-oxidative degradation. The maximum degradation temperatures (T_{max}) of the different degradation stages were calculated from the first derivative (DTG) of the TGA curves. The onset degradation temperature was calculated at a 5 % weight loss ($T_{5\%}$) from the TGA curve.

Qualitative Fluorescence determination. The samples containing fluorescent markers were exposed to UV light from a mercury lamp (Vilber Lourmat, VL-6.L, 365 nm) in a dark room. Fluorescence was visually confirmed when present (photography).

Encapsulation Efficiency (E.E.). The amount of microalgal extract encapsulated in the nanoclays was determined by difference from the liquid residue of the synthesis. After the filtration of the nanopigments, the filtrate was collected and adjusted to a known volume. The concentration of each pigment type in this filtrate was determined by UV-vis spectroscopy (Jasco, V-630), as commented in the previous point 3.3.3.1. This is a measure of the efficiency of the encapsulation process.

RESULTS AND DISCUSSION

Characterization of pigments from microalgal biomass

In Chlorella vulgaris NIES 227, the main fluorescent pigments are chlorophyll a, chlorophyll b and a pool of carotenoids mainly composed of β-carotene, Lutein, Neoxanthine, Violaxanthine and Zeaxanthine. UV-vis spectroscopy was used to confirm that the main pigments in *chlorella* strains are the chlorophylls, indicated by strong absorption in the blue and red wavelength ranges. The results are shown in Table 1. After the third extraction, the total pigment content in the biomass corresponds to about 4 % of the biomass dry weight and the pigment ratio is about 80 % of chlorophylls and 20 % of carotenoid. In total, 700 ml of ethanol extract containing 570 mg of pigments were obtained. The corresponding absorption spectrum and pigments profile are plotted in the graphs of Figure 2.

	Chl_a (µg/mL)		**Chl_b (µg/mL)**		**Carotenoids (µg/mL)**	
	Diluted	**Concentrated**	**Diluted**	**Concentrated**	**Diluted**	**Concentrated**
Average	2.6964	**539.3**	0.6738	**134.8**	0.6561	**131.2**
SD	0.0005	0.1	0.0012	0.2	0.0010	0.2

Table 1 Quantification of the main pigments in the ethanol extract of C. vulgaris NIES227

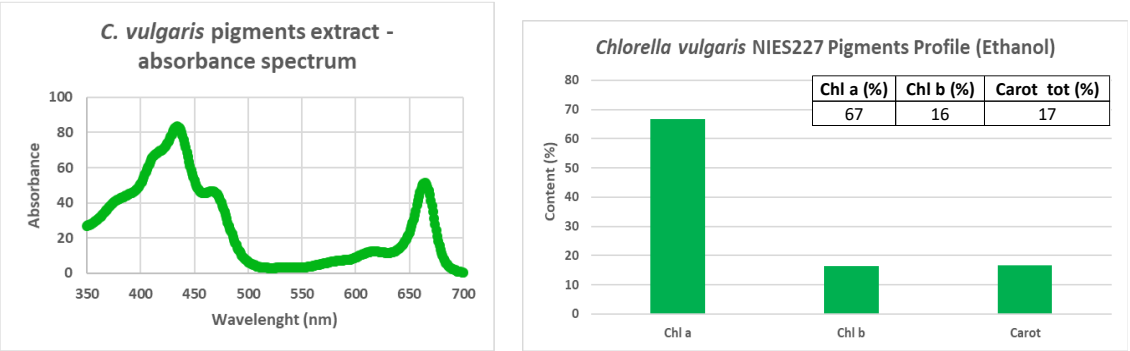

Figure 2 (left) Absorption of the extract of Chlorella vulgaris NIES227 and (right) corresponding pigments content in the ethanol extract.

Chlorella extract nanopigments

The obtained nanopigments were exposed to UV light from a mercury lamp (265 nm), and reddish fluorescence was observed in both cases, as can be observed in Figure 3 and Figure 4, with LDH nanoclays having a higher brightness than MMT. This agrees with the encapsulation

efficiency (E.E) determined by UV-vis spectroscopy, which in the case of MMT was approximately 75 % on weighted average for chlorophyll A, B and the carotenoids. Encapsulation efficiency determined by UV-vis spectroscopy, was around 95 % in the case of the LDH nanoclay.

E.E. Chl A (%)	E.E. Chl B (%)	E.E. Carot (%)
77.4	64.1	78.3

Figure 3 Visual aspect, and fluorescence and E.E of the different pigments with MMT clay.

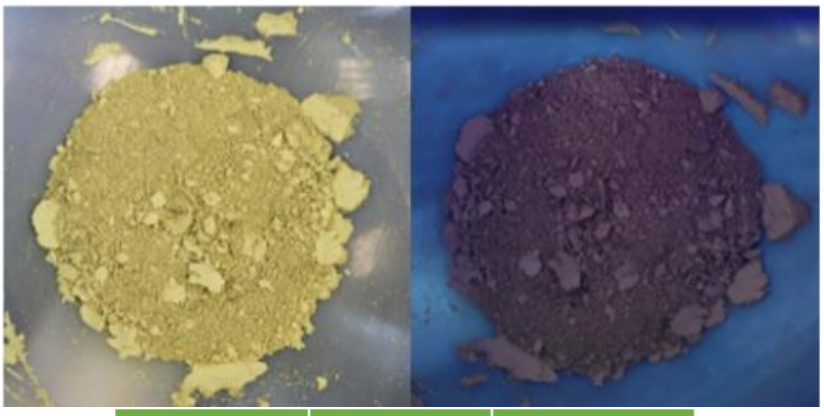

E.E. Chl A (%)	E.E. Chl B (%)	E.E. Carot (%)
96.8	90.6	94.1

Figure 4 Visual aspect, fluorescence and E.E. of the different pigments with LDH clay.

Biobased nanocomposites

These encapsulated fluorescent systems were then compounded with both PLA and PBSA at different content ratios, using a MC15 (Mini-extrusor/injector DSM Xplore). The fluorescence of the MMT based encapsulation was only observed when loaded into PBSA at 3 wt.% (Figure 5). On the other hand, the LDH encapsulated compounds gave fluorescent specimens at all the concentrations tested in PLA (Figure 6) and when compounded with PBSA, both with and without adding thermoplastic starch (Figure 7). As a side note, fluorescence from both the PLA

and PBSA control samples was also observed with blue-white emission, easily distinguish from the chlorophyll red emission.

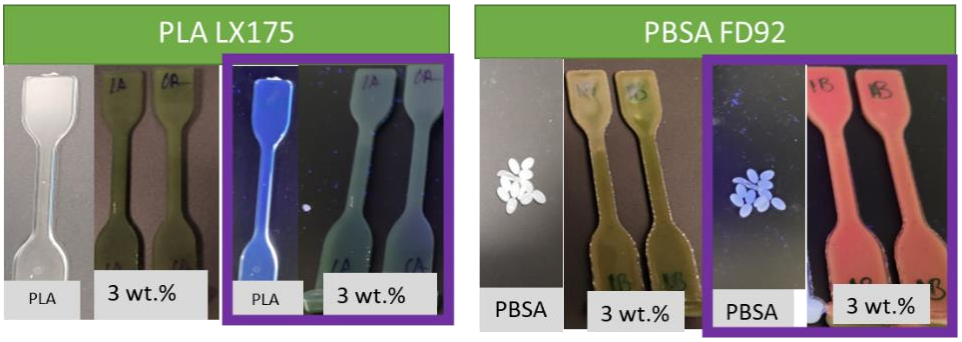

Figure 5 Injected specimens of MMT nanopigment with PLA and PBSA at 3 wt.%, and blanck samples for control

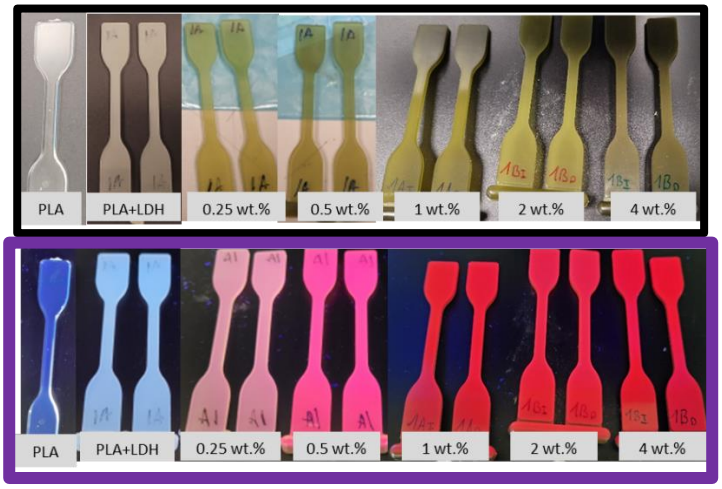

Figure 6 Injected specimens of LDH nanopigment compounded with PLA LX175.

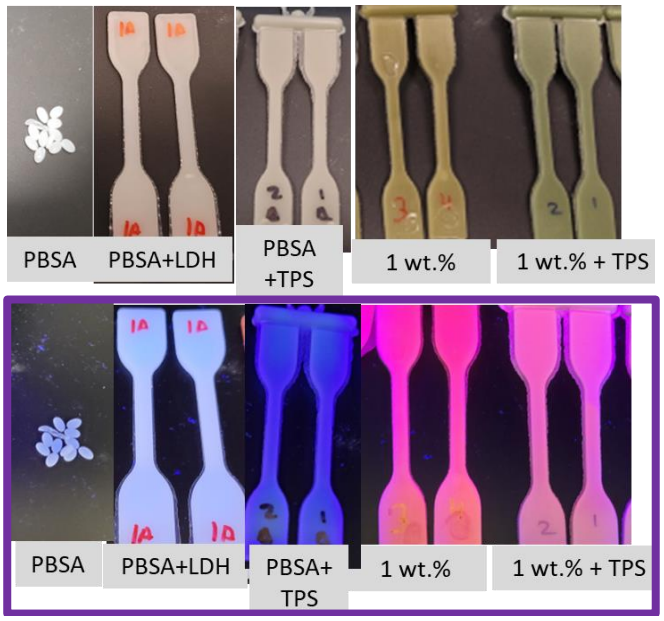

Figure 7 Injected specimens of LDH nanopigment compounded with PBSA FD92 at 1 wt.%, with and without starch.

Thermal characterization

It was also observed by DSC and TGA that the thermal properties of the specimens were not significantly different from the relative control samples containing only the LDH clay (Table 2 and Table 3).

Reference sample	$T_{5\%}$ (°C)	Residue (wt.%)
PLA Blank	351	1.1
PLA + LDH 1%	314	2.3
PLA + F-LDH 1%	333	2.4
PBSA Blank	382	2.5
PBSA + LDH 1%	347	4.4
PBSA + F-LDH 1%	349	3.4

Table 2 TGA analysis of PLA and PBSA samples with LDH clay and fluorescent marker

Reference sample	T_g (°C)	T_{cc} (°C)	T_m (°C)	T_c (°C)
PLA Blank	54.4	-	149	
PLA + LDH 1%	55.9	109	152	
PLA + F-LDH 1%	55.3	109	152	
PBSA Blank	-	-	87.5	61.5
PBSA + LDH 1%	-	-	86.4	58.6
PBSA + F-LDH 1%	-	-	87.0	59.2

*T_g: Glass transition temperature / T_m: Melt temperature / T_c: Crystallization temperature / T_{cc}: Cold Crystallization temperature.

Table 3 DSC analysis of PLA and PBSA samples with LDH clay and fluorescent marker

Recyclability test

The viability of these fluorescent markers as indicators for recyclable biobased materials was tested by reprocessing the material comprising it three times. PLA containing 1% of the LDH fluorescent marker was processed at 190 °C, with a residence time in the twin-screw compounder of 4 minutes and the extruded to air. The sample presented the characteristic fluorescence of the chlorella extract marker (Figure 8, sample 0). This sample was subsequently cut into small pellets of about 3 mm length and feed into the extruder to obtain a sample recycled for the first time (Figure 8, sample 1). This process was repeated further for 2 more times (Figure 8, sample 2 and sample 3). After these 3 cycles of melting and extrusion, the fluorescence observed from the samples was still maintained, with a constant emission color. However, the intensity of the emitted light was decreasing after each step.

This trial indicates that the recycling of PLA incorporating the fluorescent marker is feasible. Further development including stabilizers and/or refreshing the amount of marker would be needed for a successful recyclable industrial application.

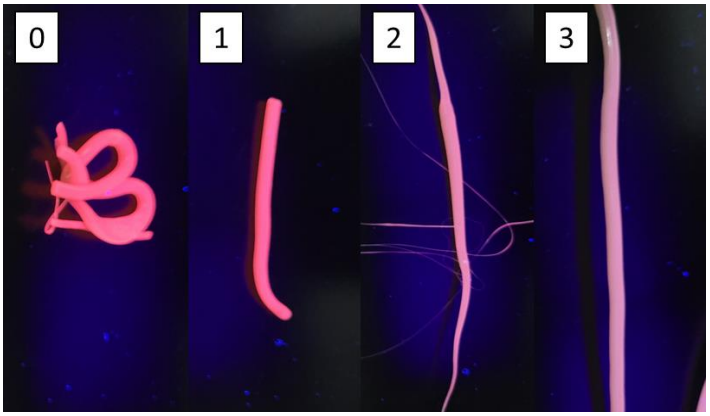

Figure 8 Recycling of PLA including fluorescent markers

CONCLUSION

Fluorescent pigments, Chlorophyll a, Chlorophyll b and a pool of carotenoids mainly composed of β-carotene were successfully extracted from algal biomass with ethanol. High thermal resistance biobased fluorescent markers were successfully obtained by encapsulation process into nanoclays MMT and LDH. The Encapsulation efficiency of the natural pigments in the LDH was determined by UV-vis spectroscopy to be above 90%. These markers were introduced into PLA and PBSA through twin-screw compounding and obtained fluorescent specimens. No appreciable modification of the thermal properties of the unmarked polymers was observed. PBSA doped with thermoplastic starch gave higher fluorescence than PLA. The clay concentration ranged from 0.25 to 3 wt.% with increasing fluorescent signal.

No degradation of the fluorescent pigment was observed after the compounding process. The thermal properties of the material obtained did not change with respect to the control samples additivated with virgin LDH, suggesting little to no migration of the pigments into the polymers. When trying to qualitatively optimise the amount of marker in the formulation, 1% of LDH marker yielded the best fluorescent performance with the minimum amount of marker. Three cycles of melt compounding and extrusion processing were performed with PLA as matrix to demonstrate the resistance of these markers to the recycling process. The fluorescence was maintained after each cycle, although with visible decrease of the fluorescent signal.

The use of these markers in biobased matrices can be used for the separation of biobased polymers from conventional ones, and to discriminate between closely formulated mixtures of biopolymers. This will improve plastic-waste management, allowing to better identify the end-of-life of the final products at sorting facilities, rather it be recycling, home composting or industrial composting.

REFERENCES

1 Global Plastics Outlook: Policy Scenarios to 2060. OECD. https://www.oecd-ilibrary.org
2 Olscher, C., Jandric, A., Zafiu, C. Part, F. *Polymers.* **2022**, *14*, 3074.
3 Hsiao, C. et al. *Food Chemistry*. **2020**, *306*, 125300
4 Micó-Vicent, B. et al. *Polymers* **2020**, *12*, 2508
5 Lichtenthaler, H.K., Buschmann, C. *Curr. protoc. food anal. chem.* **2001**, *1*, 1.

CONFERENCE PROCEEDINGS

PACKAGING SUSTAINABILITY

ORAL PRESENTATION

GENERAL STREAM

PEER-REVIEWED

POSTER PRESENTATION

PS-GO01

Research after an innovative way to determine designs of squeeze bottles with the least leftovers

Zoë Menting[1], Sanne van der Molen[1], Roland ten Klooster[*1]

[1]*Department Design, Production and Management, University of Twente, Drienerlolaan 5, Enschede, 7522NB, Netherlands*

***Correspondence to:** Department Design, Production and Management, University of Twente, Drienerlolaan 5, Enschede, 7522NB, Netherlands.*
E-mail: r.tenklooster@utwente.nl

ABSTRACT: This research focuses on the sustainability of top down squeeze bottles for sauces. An important issue that came out of the analysis is that the bottles cannot be emptied completely. Leftovers are problematic for sustainability because it is food waste. Therefore, research was done on how the amount of left overs could be reduced for mayonnaise by design of top down squeeze bottles.
To reduce the stickiness of mayonnaise to PET bottles, bottles are often oil coated on the inside with an edible oil. A test method is developed to test the amount of leftovers in different top down squeeze bottles available on the market. The method is based on vertical movements and a defined amount of shocks. The results show that the shoulder area has a significant effect on the amount of leftovers in the bottle for oil coated as well for bottles without oil coating. Designs are made of shoulders based on theoretical design rules like the used radius, the sharpness of rings, the slope of the shape. The designs are gathered in a field with the size of a thermoform sheet. A 3D printed mould is made with 6 designs, including the current design, to be able to test the designs in the right material in a fast and cheap way. The opening of the bottle is made by hand by cutting of the top. The shoulders are filled with mayonnaise and then tested with the defined method. For oil-coated models, slightly reducing the size of the shoulder area is enough to ensure that the product flows through the shoulder much better, for bottles without oil coating, the smaller the shoulder area the less leftovers are found.
The research shows an innovative way of testing many designs of shoulders of top down PET bottles on leftovers in a fast and cheap way.

Keywords: reducing leftovers, PET top down squeeze bottle, prototyping, test method.

INTRODUCTION

PET squeeze bottles for sauces cannot be emptied completely [1]. This causes annoyance at consumers and is not sustainable because it produces food waste. Therefore, research is executed how leftovers in top down squeeze bottles can be reduced. A choice has been made

for mayonnaise as being a viscous product that sticks to the bottle and that can be exemplary for other sauces.

The influence of design and material choice for the bottles is investigated. Squeezing is experienced by consumers as convenient. Upside down bottles were introduced during the nineties of previous century to be able to empty the bottle better and caps with good dosing possibilities were the next step. Heinz was not the first with an upside down bottle, but they are an important brand in the market and they introduce the upside down bottle in 2002 [2]. With a cap with a nozzle dosing can be done well and a viscous product like mayonnaise comes out of the bottle fast when operated in the right way. Testing new designs is nevertheless hard because to get understanding of the effect of the design, a bottle in the right material and shape should be available. This cost time and quite some money and there is hardly any research to be found on this issue. An option would be to produce a 3D-printed model of the design but this does not give a proper judgement of emptying because used materials have different characteristics which influence among others stickiness and squeezability of the bottle. The focus of the research is on finding a way to test new designs of PET bottles in an easy way, meaning faster and cheaper than by making metal moulds and blowing bottles. A preform mould is not needed, because preforms can be acquired on the market.
The research question is therefore: what is a proper method with which designs of squeezable PET bottles for viscous products can be tested on leftovers in an easier way than producing a bottle by using metal moulds?

LEFT OVERS IN PET BOTTLES

The squeeze bottle that is the focus of this research is made of polyethene terephthalate polyester (PET), a slightly polar material. The polarity causes the water in the mayonnaise to be attracted and easily stick to the walls of the bottle. To prevent this, in the current situation a layer of oil is sprayed into the bottle before filling. This oil layer ensures that the walls of the bottle stay clean and the product flows to the opening.
A simple way to test how well PET bottles with sauce can be emptied is to smash it on the table one time, and empty it by squeezing. After this leftovers still can be seen, and therefore the procedure can be repeated. To standardize this a procedure to empty bottles in the same way is defined as follows: emptying the bottles by squeezing, when there is no product above the valve, bottles are tapped on a workbench in vertical direction three times followed by squeezing and repeating this five times. This procedure is used to empty several sauce bottles.

Squeeze bottles of 4 different brands with their original mayonnaise are taken from the market. One has an oil layer inside, the others not. Next, 6 bottles of different brands are emptied, cleaned and filled with the same mayonnaise. Two bottles of the same design are provided with different caps that have the same screw thread, filled with the same mayonnaise, to get understanding of the influence of the cap. Two bottles with almost the same design, but with different dimensions of the openings are tested with mayonnaise and ketchup. At last 5 persons have been testing the same four different bottles to compare the results after the test procedure. None of the bottles was emptied completely and the amount of left overs was rather comparable. Clearly could be seen that the product accumulates in the shoulder area.

To be sure the same procedure is used for emptying bottles with and without oil on the inside, bottles are tested by the same person. Two bottles of each have been tested. In the bottle without oil sprayed on the walls leftovers could be seen all over the bottle, in the bottle with oil sprayed on the walls, most of the left overs can be found in the shoulder area. The amount of leftovers on the oil coated bottles is getting close to the amount in the shoulder area. Ketchup gives less leftover than mayonnaise which is more viscous and sticky. The company does not want to publish the figures of leftovers because of confidentiality, and it is irrelevant in view of this research topic. The focus of the research is to investigate the influence of the shoulder area. It is decided to do this for both bottles; with and without oil coating on the inside. For some sauces a coating of oil on the inside causes colour change of the product, which is not always wished. Nevertheless, results for both situations are of importance.

The shoulder area is shown in the circle in figure 1. Design parameters are the bottle opening, shoulder diameter, the cap design (the diameter), the flatness and dimensions of the shoulder, edges on the shoulder that often are used for stiffness of the design, the squeezability of the bottle that also is related to the before mentioned edge. If the bottle is too flexible it will fold and cannot be emptied very well.

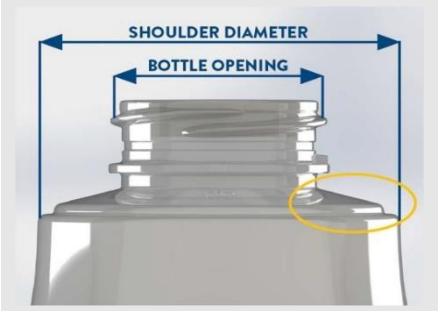

Figure 1 Shoulder area of bottle

Figure 2 A shoulder with conical design

DESIGNING THE SHOULDER

The cap plays a role in the design. If the angle of the shoulder surface is adjusted to a more conical design, as shown in Figure 2, the cap must be made higher to create a soft transition in the design and needs more material. Caps are standardized. Choosing an existing cap design from a supplier is a preferred choice from perspective of costs, quality and functionality.

Reducing the shoulder diameter and enlarging the bottle opening is an option to try to reduce cumulation of product in the shoulder. In Figure 3 four concepts with reduced shoulders surfaces are shown.

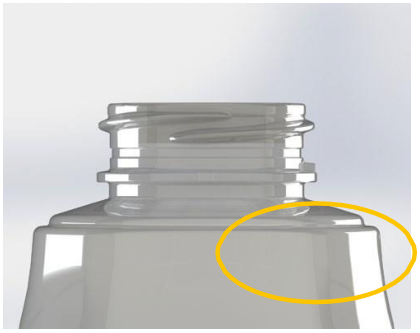 Smaller shoulder surface – step 1	 Smaller shoulder surface – step 2
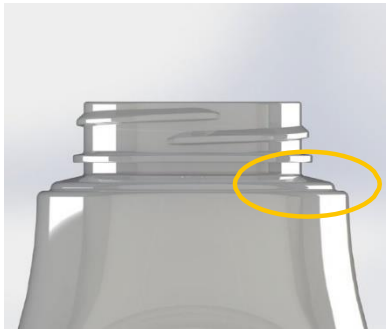 Smaller shoulder surface – step 3	 Smaller shoulder surface – minimal shoulder design, no extra edge

Figure 3 Four examples of reducing the shoulder surface

For the design with the minimal shoulder surface the use of a double-walled cap is not feasible. This also would cause that the cap becomes this small that the top-down function will be more critical. Besides that, a single wall cap might need a diameter of the opening of the bottle that requires extra material for the bottle neck design.
In the current shoulder an edge is taken up. The edge is part of the design and it is considered as being part of the iconic shape. Therefore the edge is retained in all concepts except one, to investigate whether this element affects the amount of leftovers.

TESTING POSSIBILITIES

The effect of the designs of the shoulder areas on leftovers can only be determined by testing. One possibility to test this would be to model the complete bottles in a 3D software package

and simulate the product flow in the bottle. However, the necessary knowledge to do this and the simulation software are lacking although some attempts have been made [3]. It would take quite some time to set this up and before that the way of working has to be validated.

Another possibility to test the designs is to create prototypes of the concepts. However, it is rather expensive to create prototypes of the entire bottles because metal moulds have to be produced. The biggest wins can be reached to focus on the shoulder areas and it is decided to focus on making models of the shoulders only.

First, a plan is made on how to create these shoulder models and determine the important factors. Then a test method is set up. And finally the models are tested and the results are analysed.

For proper testing the material should be PET. The dimensions of the shoulders approximate the shape of the designed concepts as closely as possible. Preferably this accounts for the inside dimensions of the shoulder bottle designs because this is the part where the product flows.

To accomplish this, a Computer-Aided Design (CAD) model was created of the inside of the current bottle and of the concepts. Of the current bottle, only the outside dimensions of the bottle and the diameter of the inside of the neck finish are known because this determines the surface of the mould. For the neck finish part the internal dimensions are known as well. The wall thickness below the finish can differ slightly because of the production process, injection stretch blow moulding. For the model, it is decided to use the known diameter of the opening and to count 1 mm of material thickness for the shoulder area. In practice the thickness from the neck finish towards the body of the bottle will decrease, but it is assumed that if this way of modelling is taken for the concepts as well, the difference with practice will not be large.

3D printing of the designs can be used to produce models, but not with PET. The material will be different and the surface can have a structure depending on the chosen resolution of the 3D printing process.

3D printing is often used for production of moulds. By using the 3D designs of the shoulder parts, PET shoulder designs can be made with thermoforming. For this reason the CAD models were 3D printed in polyurethane hard foam, brandname Prolab. The designs that are made are taken up in Table 1. The parameters that are considered are neck finish diameter (mm), shoulder diameter (mm), shoulder surface area length (mm), presence of edge in shoulder (yes/no), tested amount of shoulders (a number).

With thermoforming of a PET sheet the designs can be produced in the same way so the characteristics will be more or less the same. The 3D printed models are positioned and fixed to a surface so they create one mould all together. A PET sheet of 1 mm thickness is positioned over the shoulder designs and by positive thermoforming with vacuum the outside of the designs is reproduced in PET to represent the inside of the made designs. The opening of the

	DESIGN	TESTED SHAPE	NECK FINISH	SHOULDER DIAMETER	SHOULDER AREA	EDGE IN SHOULDER	TESTED AMOUNT
1	Current		30 mm	50 mm	10 mm	Yes	3
2	Concept 1		30 mm	48 mm	9 mm	Yes	3
3	Concept 2		38 mm	50 mm	6 mm	Yes	3
4	Concept 3		38 mm	48 mm	5 mm	Yes	3
5	Concept 4		38 mm	48 mm	5 mm	No	3
6	Concept 5		38 mm	41 mm	1.5 mm	Yes	3

Table 1 Shoulder design concepts

shoulders is a closed surface on top of the bottles after thermoforming. By cutting off this part of every shoulder that is formed openings are created. The shoulder designs are separated from the sheet by cutting by hand. An example of a PET model is shown in Figure 4.

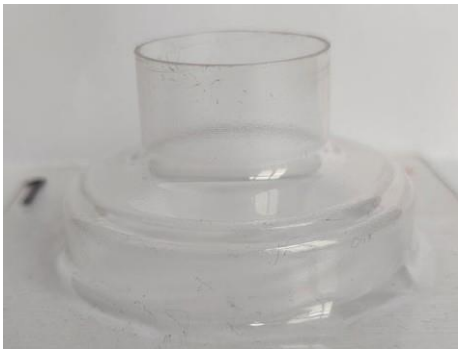

Figure 4 Photo of one shoulder

TEST METHODS

The purpose of the test is to investigate whether the design of the shoulder area has an effect on the leftovers. To accomplish this, a stepwise approach has been set up.
To determine the weight of leftovers, the weight of the empty model must be known. If oil is used the weight of the model with oil is of importance as well. The amount of oil must be within a certain range and therefore the models are weighed again if they are applied with oil.

It is not of importance to know the amount of product in the model because in practice the shoulder will be filled for 100% with product. It is of importance to determine how much product stays behind after executing a procedure that reflects practice of emptying a sauce bottle, to be able to judge the difference between the designs.
The openings are larger than with a cap. In fact the leftovers that normally would stay behind in the cap are not included in this way. The test can show the influence of the bottle design. In practice the cap will have influence on the total amount of leftovers but with the models the leftovers related to the bottle design can be tested. And in this way the influence of the design parameters as taken up in the table can be considered.

In order to perform the test efficiently and in the same way for each model, a wooden tray is made to hold the models, as shown in Figure 5. The models cannot be filled while standing in the tray on a scale it is decided to fill the models after placing them in the tray. The top surface of the closure is standing on the table where the product is filled. The models are filled to the top. The amount of product will not be the same in each model as mentioned earlier. In addition, the surface are of the different designs also differ; for some models there is more surface area for the product to stick to because the opening is larger.
As product mayonnaise is chosen because it is sticky, causes quite some leftovers in practice compared with other sauces like ketchup, and because it does not flow on its own very well.

Figure 5 The wooden plate with six models for testing

To reflect practice a few issues have to be taken into account. Normally the user squeezes the bottle, creating pressure for the product to flow. The opening is normally a silicon valve and the product does not flow on its own to the outside. For determining leftovers it is of importance to understand that the flow of the product to the valve is of importance because when the product accumulates above the valve, it can be squeezed out. This is justified by the observation that leftovers mainly can be found on the inside surface of the shoulder. The free flow of the product inside the shoulder can be simulated by lifting the tray. Lifting will cause the product to flow through the opening to the outside.

When there is no product above the valve, and users have the idea that bottles are not empty, they will shake the bottle or tap it on the table. This extra effort is simulated with sauce bottles by tapping the bottle on a workbench three times, then squeezing it again and repeating this five times, as described before.
This is not possible for the models, but shaking can be simulated by tapping the edges of the tray on the workbench 3 times, waiting 3 seconds, and then repeating this five times. The models are weighed when the product stops leaking from the models for 3 seconds. This is needed because the mayonnaise dries out quickly because it is exposed to the air in an open area. The drying out of the mayonnaise affects the flow through the models. Therefore, weighing is performed as quickly as possible. After the models are weighed, they are placed back in the holder to simulate the additional effort as described. After finishing the tapping the models are weighed again to determine the final amount of leftovers.

Overview of the test method
1. Weighing the models
2. For the models with oil: applying an even layer of oil coating within chosen margins
3. For the models with oil: Weighing of the models including oil coating
4. Placing of the models in the tray on the workbench
5. Filling of the models with mayonnaise
6. Lifting the tray to allow the product to flow through
7. Weighing of the models when dripping of the mayonnaise has stopped for 3 seconds
8. Tapping of the tray 3 times, waiting 3 seconds and repeating this up to 5 times as long as there is a reasonable amount of mayonnaise dripping from the models
9. Weighing of the models to determine the final leftovers

TEST RESULTS

In this study, the test was performed three times with coating and three times without coating. The individual values are shown as lines and the bandwidth between the highest and lowest values are accentuated by a light background in Figure 7.

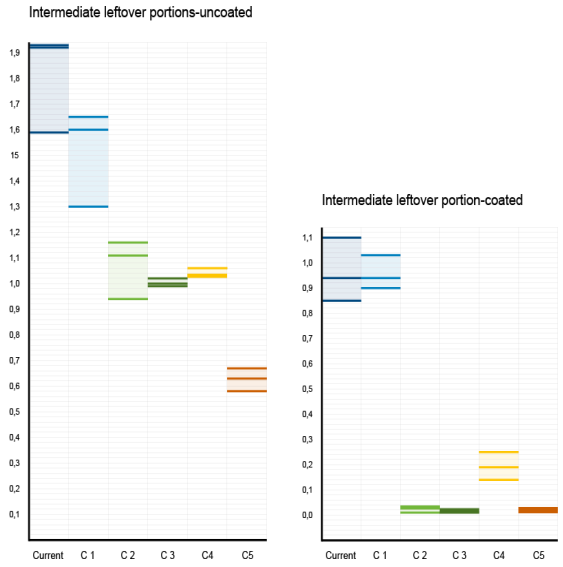

Figure 6 Results of weighing when dripping stopped for 3 seconds, without oil coating (left), with oil coating (right)

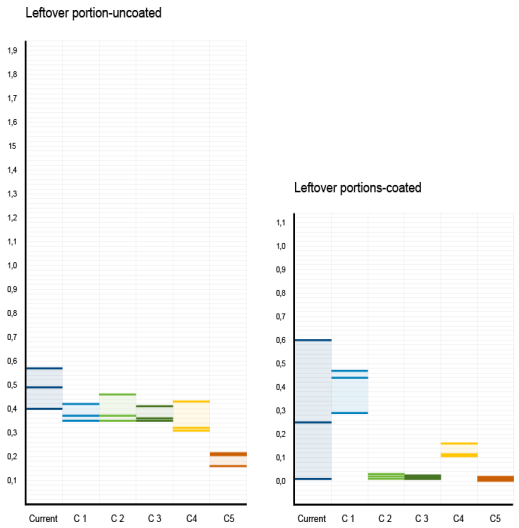

Figure 7 Results of weighing after the complete test procedure, without oil coating (left), with oil coating (right)

The following observations are made:

- Bottles with a narrow opening have more leftovers than the bottles with a wide opening.
- There is even difference between the amount of left overs between a shoulder area of 5 and 6 mm, although the differences are not large for bottles with oils, but without oil coating on the inside the difference is quite large.
- The differences are larger for the intermediate weighted leftovers than for the final weighted leftovers; so extra effort helps to let more product flow through the opening.
- The total amount of leftovers is ca. halve of the amount for oiled bottles compared to bottles without oil coating, showing the shoulder area as being an important part of the bottle where leftovers are caused.
- In addition, it is notable that in the concept where the edge is removed from the shoulder design more leftovers is found than at the similar concept with the edge.
- For the oil coated bottles, the product runs almost directly through design concepts 2, 3 and 5, thus, for the bottles in which an oil coating is provided, these designs are suitable to minimize the amount of leftovers.
- For the uncoated bottles, leftovers remain in all designs, however, the smaller the shoulder area the fewer the leftovers.

DISCUSSION

Filling the mayonnaise to the top of the plate results in an uneven amount of product in each model. Filling everything with the same amount is more difficult because the use of a piping bag is preferred so that the product is touching all the walls. Weighing the models while filling

them with a piping bag was not possible because of the size of the tray. This tray was necessary to easily test them all in the same way and mimic shaking of the bottle.
Testing in the tray is not the best way because the product does not flow through the different models at the same speed. Thus, for some of the models, the product does not flow for a while when the weighting starts. Weighing a specific model earlier than others is difficult because the other models also have to be kept in focus. In addition, during the intermediate weighing moment, the product still flowed out, which is difficult to prevent for models without a cap. However, this test is about what remains after a certain time and this way of testing ensures that all models have had the same test duration.

CONCLUSIONS

A method is developed to test leftovers in PET bottle designs. Shoulder designs are made and are created in PET by positive thermoforming shoulders on base of a mould made by 3D printing in polyurethane hardfoam of several designs. In this way the inside shape of shoulders of bottles is reproduced. On base of a developed test, the way of working was discriminating in the designs. The method is rather fast and cheap. Comparing the amount of leftovers with the amount of leftovers in the original PET bottles showed that the method is representative for the amount of leftovers in the shoulder area.

AKNOWLEDGEMENTS

This research is part of a master thesis executed at a sauce producing company. The final design results are confidential.

REFERENCES

[17] Hans C. Mayer; Bottle Emptying: A Fluid Mechanics and Measurements Exercise for Engineering Undergraduate Students, Department of Mechanical Engineering, California Polytechnic State University, San Luis Obispo, CA 93407, USA; Fluids 2019, 4(4), 183; https://doi.org/10.3390/fluids4040183
[18] Yolanda Salcedo-Sillesa; The Age Of The Squeezable Heinz Ketchup Bottle: A Look At Its History Evolution And Status As An Iconic Symbol; https://havenhillcuisine.com/the-age-of-the-squeezable-heinz-ketchup-bottle-a-look-at-its-history-evolution-and-status-as-an-iconic-symbol/ visited April 20, 2023
[19] Turaga, V., Bhavi, S., Soppin, M. and Srinivasa, V. (2021) “Fluid Structure Interaction (FSI) Simulation of Flow through a Squeeze Bottle”, The International Journal of Multiphysics, 15(4), pp. 389-396. https://doi:10.21152/1750-9548.15.4.389

PS-GO02

The position of refill systems in the future of supermarkets

Emmilie Kuks[*1], Esther Koopmanschap[*1], Bjorn de Koeijer[1]

[1]*Department of Design, Production and Management, Faculty of Engineering Technology, University of Twente, 7522 NB Enschede, The Netherlands*

***Correspondence to**: Emmilie Kuks or Esther Koopmanschap, Department of Design, Production and Management, Faculty of Engineering Technology, University of Twente, Drienerlolaan 5, 7522 NB Enschede, The Netherlands.*
E-mail: e.m.a.kuks@student.utwente.nl or e.s.t.koopmanschap@student.utwente.nl, or Bjorn de Koeijer: b.l.a.dekoeijer@utwente.nl

ABSTRACT: The significance for retail to take a pro-active position within the sustainability-related discourse is increasing at a rapid pace. The role of physical brick and mortar stores is changing, influenced by an acceleration of the significance and consumer acceptance of online alternatives, the impact of a global pandemic, and the progression from single-use packaging to reusable or refillable options. Within these developments, refill and packaging reuse systems show to be promising concepts for future-proof retail. This research focuses on the future of physical supermarkets, and investigates the position of refill systems with product-packaging combinations as the central point of interaction.
Future forecasting is presented as a research method to define different themes based on historical trends, the current state of retail, and predictive literature. This approach leads to a detailed perception of future-proof retail, and the definition of design challenges. Subsequentially, prospects are created, which describe in detail what the future of in-store refill systems and the role of packaging within that could look like. These prospects are based on future themes, observations of current refill systems, the current customer journey, and identified success factors.
This research demonstrates future forecasting as a valuable method to support the development and testing of future concepts. The prospects reveal trends in future forecasting: technological developments, digitalization, consumer tailoring, and supply chain collaboration. Designing according to consumer needs (ease-of-use, price-driven, and social aspects) is crucial for the success of future concepts. With these interventions, the research provides developers with the tools to design product-packaging concepts fit for future retail systems, and to increase the success rate of these concepts.

Keywords: sustainability, future forecasting, reusable packaging, refill systems, design tool

INTRODUCTION

With a rapidly changing retail environment, and increased significance and consumer acceptance of online alternatives, the impact of a global pandemic, and the progression from

single-use packaging to reusable or refillable options comes the urge for retail to act pro-actively. A key focal point for future-proof retail innovation relates to refill and packaging reuse systems, and the sustainability-related potential linked to that [1-3]. In this article, we present a design research approach towards the development of refill system prospects, which describe in detail what the future of in-store refill systems and the role of packaging within that could look like. As an intermediate intervention, this research presents a future forecasting framework. These findings are based on future themes, observations of current refill systems, the current customer journey, and identified success factors. This research provides value for product-packaging and retail developers, by means of these interventions – these can act as tools to design product-packaging concepts fit for future retail systems, aiming to increase the success rate of these concepts. The scope of this research covers the current Dutch retail environment.

Approach

In the initial research stage, insights were collected on the recent historical developments of supermarkets. Furthermore, the current state of supermarket environments, including the position of product-packaging combinations within that, was analyzed, and literature addressing the future development of supermarkets was collected. The findings were combined to define trends within the supermarket landscape throughout the years. These trends have been converted into a future forecasting framework (outcome 1) which visualizes the observed changes and aims to predict future trends for ten different themes. The framework also indicates three main threads that can be marked as time-independent, constant factors. The future forecasting framework and observations on refill systems as they are currently designed form the basis for an iterative design process that results in four prospects (outcome 2), outlining a number of situations that are likely to occur when considering the position of refill systems in future supermarket environments. The research approach is visualized in Figure 1.

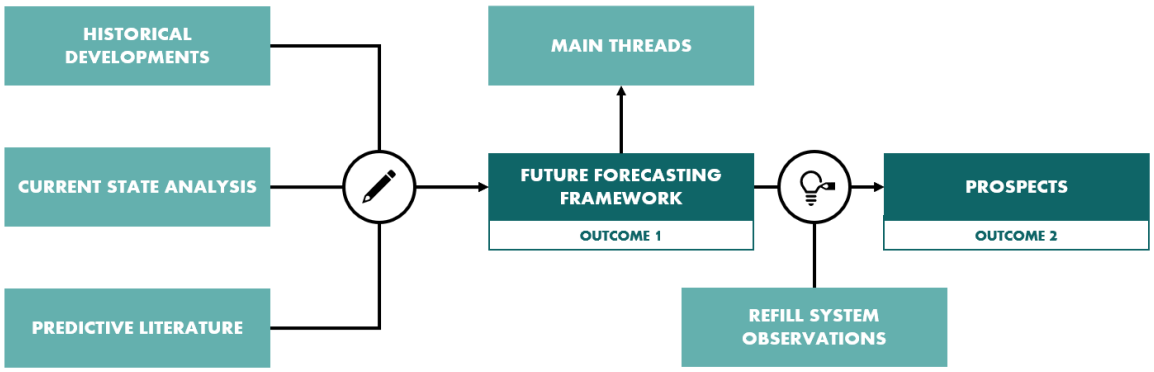

Figure 1 Research approach: steps and elements

ANALYSIS

Supermarket history

To understand the environment that consumers encounter when going into a supermarket nowadays, it is crucial to understand where the origins can be found that initiated changes in the supermarket landscape. While the contemporary supermarket allows consumers to purchase all daily or weekly goods at once – whether one needs a new bottle of shampoo, or aims to purchase the ingredients for an extraordinary dinner – the old-fashioned grocery store was a neighborhood establishment where consumers could primarily buy dry (bulk) foods. The grocer received items from the wholesaler in bulk packages and weighted them on the counter in the desired amount using a scale [4, 5]. Additionally, a milkman came to each home once a week to swap emptied milk bottles for new full ones, and consumers went to the bakery to purchase freshly baked bread. In recent decades, multiple developments occurred, including pre-packing, pre-pricing, increased governmental regulations, branded goods, and the application of discounts to influence the consumers' purchasing behavior [5]. Nowadays, the combination of physical (brick and mortar) stores and e-commerce-based options constructs the supermarket landscape [6].

Supermarket state-of-the-art

By means of a customer journey definition, insights into the stages consumers experience when visiting a supermarket are analyzed. These stages range from reasonings behind the consideration of purchasing goods to selecting a payment method at the counter or arranging transportation. Business strategies [7, 8] shed light on the various factors influencing what modern supermarkets characterize and how they conveniently service customers. The customer journey and business strategies highlight that supermarkets previously placed a strong emphasis on low prices, wide choice, effective marketing, slim margins, and a finely balanced, expertly managed chain [7, 9].
The progression from the historic retail situation and environment to the current supermarket setup are hypothesized to include predictive value for future developments (Figure 2). The traditional grocery store where customers brought their reusable jars and bottles has been replaced by a centralized supermarket with single-packed goods. Extrapolating to upcoming developments, the initiation of a transition can be identified once more. Driven by sustainable ambitions, this shift aims to reduce single-use packaging, attempts to reuse packaging, and buy locally produced goods to cut down on product transportation [1, 2].

Future supermarkets

Trends that are expected to occur in the future can be identified in literature [2]. The increase of technology integration, including digitalization, algorithm use, and customer-specific experiences based on data collection, is the most frequently discussed issue when it comes to future supermarkets. Packaging refill systems and an increased focus on retail in online environments are indicated as key directions for development. Overall, academic literature on

retail environment developments shows to be limited – therefore, these indicative findings have mostly been collected in other streams of information.
Although it is challenging to predict retail developments for the coming decades, we can assume that physical supermarkets will never completely disappear, despite the expansion of e-commerce (online supermarkets and delivery services) [6, 10, 11] and consumers having the option to buy groceries without any location-based dependencies. Supermarkets can also serve as a social space where people interact, a micro-community with a significant impact on local societies.

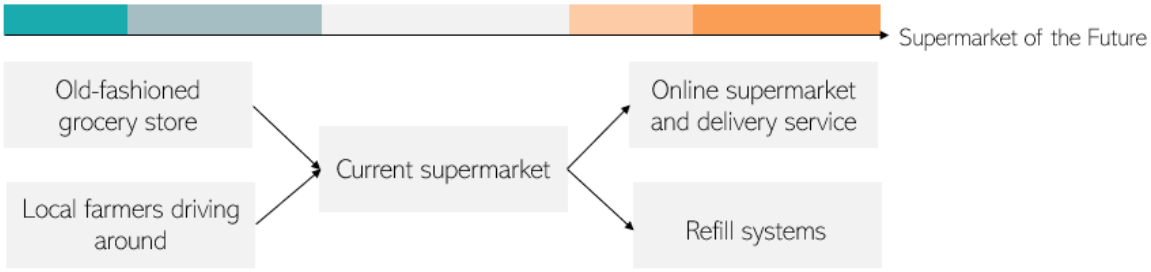

Figure 2 Systematic changes in grocery shopping

Reuse and refill systems developments

Sustainability transitions have encouraged the initiation to switch from single-use packaging to reusable and refillable packaging. One of the promising concepts that is noticed in recent inventive developments are refill systems within the context of the physical supermarket [1, 3]. From a theoretical standpoint, refill and return product-packaging systems can be categorized in four types [1, 3, 12], with primarily a consumer-focused distinction. However, in practice these four reuse categories do not demonstrate a clear-cut division since some of the current developments could be categorized under multiple types of models, depending on how consumers handle the packaging. In addition to the theoretical substantiation and categorization of reuse models, academic research into the current state of practical implementation and potential future of refill systems is limited. This can be explained by the potential competitive advantage for retail chains provided by the large-scale rollout of reuse systems in retail environments.
In current in-store refill systems, different technologies are trialed and implemented that cause multiple differences. The in-store refill systems differ in type of dispensing [per package/per quantity], payment system [deposit/one-time buy], packaging ownership [(online) supermarkets/food brands/customer], the way the product is weighed [integrated weighing system/weighing done by customer], and location in the supermarket [dedicated refill corner/at relevant product category] [13-18]. The combination of the technology, the actions the consumer has to perform, and the user interfaces lead to many different effects on the understandability and ease-of-use for the consumer. This in turn has an effect on the foundation of sustainability. Incorrect usage by the customer can lead to system inefficiency and profit decrease, due to unfinished transactions and food waste, affecting the sustainability. Continuous innovation of the system is required to simplify interactions, and to improve the technology and customer experience. In addition, new systems require customers' attention and

willingness to learn. Implementing a refill system also has its effect on the distribution and stocking of food in supermarkets [13]. Food is transported in bulk, which could have the potential of reducing primary and secondary packaging, since it requires less packaging per volume of food. Also, at the consumer side the system could potentially decrease package and food waste. Pursuing continuous innovation, cross-sector collaboration, sustainable advantages, standardization, and profitability for the businesses are essential for the success of refill systems [1, 19, 20].

DESIGN PROPOSITIONS

Future forecasting framework

Based on the addressed insights, a future forecasting framework is proposed, which aims to define future scenarios for developments related to supermarket environments (Figure 3). The framework lists multiple themes, by order of certainty. Furthermore, some main recurring threads can be identified – these are expected to remain of high importance within future developments:

- Ease of use: customers want to put little effort and attention into grocery shopping;
- Price-driven: customers seek for affordable products and are sensitive to financial benefits;
- Social aspect: customers value the social interaction facilitated through grocery shopping.

Prospects

Based on the various themes from the future forecasting framework, four promising prospects have been developed, which outline what the future of refill systems potentially include (Figure 4). Each theme's future expectations were distributed among the four prospects in accordance with their occurrence probability. The observations of current developments helped to understand the complexity and challenges of these systems, in relation to their future manifestation.

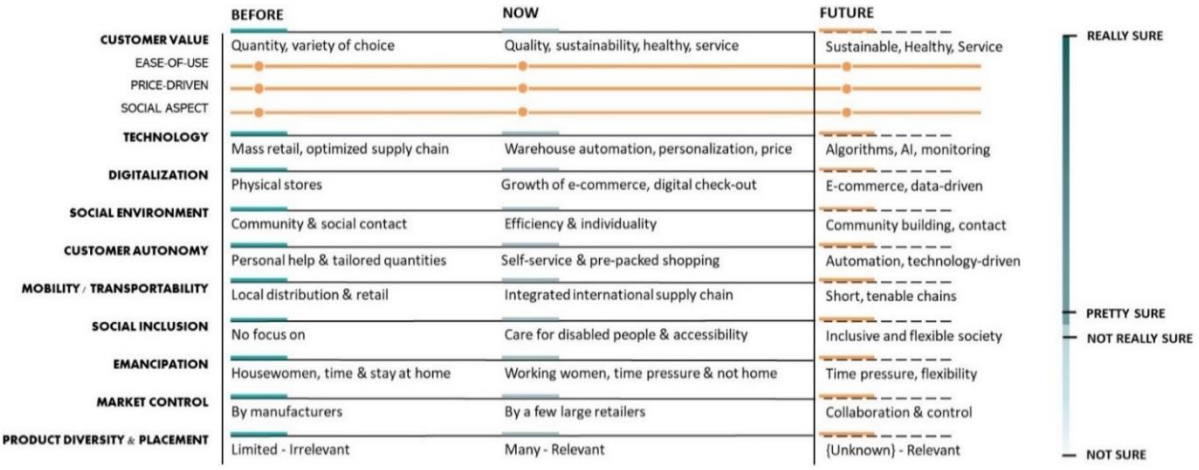

Figure 3 Future forecasting framework of supermarket developments

Prospect 1: Smart shopping

This prospect is based on high-tech technologies, link with e-commerce and data collection and use. Smart in-store sorting systems are created by high-end technologies. This system collects data from reusable packaging. It is possible to gather information about how frequently customers refill a package at a store and how frequently they bring it back after a single use. Also, it makes it simpler to track packages and count returned packages. The reusable packaging is available for purchase both in-store and online, and customers can either get it picked up or return it to a store. Eventually, the manufacturer will receive the packages back and clean and refill them. The grocery shopping experience will not change dramatically, but it must be considered that all packages must be returned, which requires consumers' behavior change.

Prospect 2: Automated shopping

Grocery stores will eventually be completely automated because of new developments. The physical store is no longer a walk-through area but consists of multiple counters where the grocery items are not fully visible to the customer. A customer can fill out their shopping list on a screen, deliver it to a desk attendant or place an online order from home. The standardized packages get filled with the right product and amount via the automated system. In this prospect, marketing and in-store product placement have little to no impact on consumers' buying behavior. The buyer can only see the product through a catalogue or screen, leaving out the appearance and feel of the package and products. The packaging of grocery items is standardized which makes it possible to use one type of packaging for many different foods and brands. Business collaboration between farmers, producers, wholesalers, and retailers is intensified for the usage of packaging and the supply chains are shortened and the steps from production to customer are minimized.

Prospect 3: Fast flexible shopping

To facilitate a fast and flexible shopping experience for consumers, it should be possible to always offer new reusable containers within the store to meet the needs of consumers who will visit the store with limited available time and possibly forget their reusable container(s). Therefore, this system offers the possibility to borrow reusable packages from the supermarket where needed. Moreover, by utilizing the e-commerce logistics & return system for the collection of reusable containers, consumers also have the possibility to hand in their containers from home with little effort. Given that, the possibility to also bring one's own reusable container to the supermarket illustrates the high flexibility of the system depending on the personal preferences of consumers and fitting to their specific needs. In the back end, this system can only be realized with high flexibility in the food supply logistics, aligned to multiple and altering packaging types. Close collaboration between manufacturers, wholesalers and grocery stores is therefore crucial to reach a flexible chain.

Prospect 4: Personalized shopping

Inclusivity has become highly important, resulting in the tailoring of grocery shopping to a customer's personal circumstance. Every customer is different and therefore customers hand in information of their situation (mobility, price affordance, frequency of shopping, household details, etc.) to a national, independent organization. A personal (digital) shopping and retail plan is created based on the personal conditions of a customer, based on that this organization will recommend which stores the buyer must visit. For example, for some customers it is suggested to have their groceries delivered due to their (limited) mobility. However, because of the existence of the physical store and tailored shopping advice, the influence of product presentation by retailers is still significant on consumer's purchasing decisions. The product placement is therefore highly relevant for the success of brands.

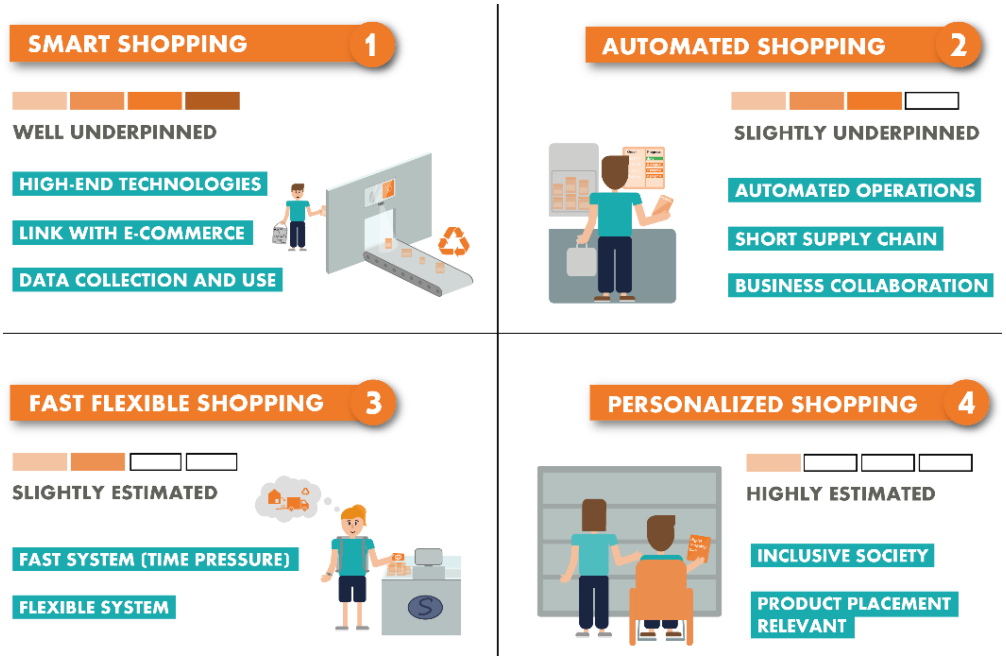

Figure 4 Refill system prospects and their characteristics

CONCLUSIONS

This research proposes a future forecasting framework for the future of supermarkets, which acts as the basis for the development of four prospective development scenarios. With this, we demonstrate both the added value of the design research approach, and the potential value of the framework and the prospects for product-packaging and retail developers when developing product-packaging concepts fit for future retail systems. The design research approach demonstrates options to handle uncertainty in relation to future developments: combining the findings from the past and current state with future assumptions and current trends provides options to fill initial development gaps, and to offer a clear view on future situations.
The developed forecasting framework and the outcomes of the applied technique on the role of refill systems supports developers in designing for the future by applying the different expected

directions presented in this research as a starting point. Furthermore, the research outcomes reveal the current challenges and complexities within the researched field, which can be used for future optimization of product-packaging combinations and in-store refill systems, contributing to their success rate. Overall, it can be said that in-store refill systems are a promising concept for future supermarkets to support in solving multiple packaging-related challenges and complexities that are being faced right now.

DISCUSSION

This research provides insights into both the development direction of retail environments, and the application of a design research approach for this, by means of the future forecasting framework and the refill system prospects. A key point of discussion is the link between the themes mentioned in the future forecasting framework and the building of the prospects. The future forecasting themes are combined based on their occurrence. The combination of two to three themes provided a proper foundation on which to build the prospect. The possibility that combining more themes could have finally led to a stronger foundation was not further explored. However, combining more themes into building one prospect does say more about the total system, since developments always result from a mix of factors, they never emerge from just one – substantiating the decision to not develop a prospect for each theme. This research is an initial impression of the use of themes in prospect building, but it is important to delve deeper into how those themes are exactly handled in prospect building. The prospects are created as a method to visualize uncertain future situations. Although the prospects differ from each other and offer distinct directions for future developments, trends can be observed that emerge in each prospect. The presence of these trends in every single prospect may be a tentative indication of the likelihood that these trends will actually play a role in the future of the researched field. The trends observed for the future role of refill systems are technology & digitalization, consumer tailoring, and importance of collaboration. Furthermore, the future forecasting framework reveals the existence of three main threads that show to be constant over time, which indicates that the role of these main threads is likely to remain prominent.

There are many factors influencing the possible success of refill systems, such as customer understanding and ease-of-use. Human-centred design improvements are crucial for the success of these systems in the future. The researchers could not find significant academic research on these new developments yet, likely because newly developed in-store refill systems are currently being tested by commercial parties. More research should be done on the development and practical implementation of in-store refill systems, to create a better understanding of what possibilities there are for the future and how to overcome the complexities. Keeping an eye on new innovations is important for business value, as some of these provide the groundwork for future success. A key limiting factor in this research, in addition to the novelty of the knowledge, is the scope. The collection of information and the following design research approach as presented in this research, was primarily focused on the Dutch market and retail environment. Follow-up research can be directed towards a more international view on this topic, both as comparative exercise and to understand the sensitivity of the findings. With this, the development directions can be further solidified for internationally operating product-packaging and retail developers, such as large brand owners.

REFERENCES

[1] De Koeijer B, Ten Klooster R, Hesseling I, Huijben C. Designing reusable packaging: tool development, validation, and implications. 23rd IAPRI World Packaging Conference, Bangkok, Thailand, 2022.
[2] Kramer P, Meinema W, ter Berg J. Kansen om Nederlanders en Nederlandse supermarkten in beweging te krijgen om herbruikbare verpakkingen te gebruiken en introduceren. 2021.
[3] Megale Coelho P, Corona B, ten Klooster R, Worrell E. Sustainability of reusable packaging–Current situation and trends. Resources, Conservation & Recycling: X (6), 2020, DOI: 10.1016/j.rcrx.2020.100037.
[4] Muller C. Delivering Food to the Front Door: A New, Or Very Old, Convenience? 2015. https://www.bu.edu/bhr/2015/02/01/780/ (accessed: 24 February 2023).
[5] LevensmiddelenKrant. Geschiedenis huidige supermarktformules. 2008. https://www.levensmiddelenkrant.nl/geschiedenis-huidige-supermarktformules (accessed: 24 February 2023).
[6] Eikelmann S, Hoogenberg M, Langkammer J, Starke F, Worm M, Pujol J. The future of grocery shopping. strategy&, PwC, 2022.
[7] Loss Prevention Magazine. New Research Finds Supermarkets' Business Model is on the Knife Edge. 2021. https://losspreventionmedia.com/new-research-finds-supermarkets-business-model-is-on-the-knife-edge/ (accessed: 24 February 2023).
[8] Bruijnes C, Diepenmaat H, ten Klooster R, van Soest JP, Langeveld G, Balk V. The State of Sustainable Packaging. 2020.
[9] Magretta J. Why Business Models Matter. Harvard Business Review (80), 2002, p. 86-92.
[10] Sheth JN. Combining insights from the environmental and behavioural sciences to understand what is required to make reusable packaging mainstream. Journal of Strategic Marketing (29), 2021, p. 598-607, DOI: 10.1080/0965254X.2021.1891128.
[11] Van Giesen R, Leenheer J. Towards more interactive and sustainable food retailing - An empirical case study of the supermarket of the future. International Journal of Retail & Distribution Management (47), 2019, DOI: 10.1108/IJRDM-11-2017-0280.
[12] Ellen MacArthur Foundation. Reuse – Rethinking Packaging. 2019.
[13] Netherlands Institute for Sustainable Packaging (KIDV). Reusable packaging: learnings from the United Kingdom for the Dutch market. 2022.
[14] SmartVrac. The First Automated Bulk Solution. https://www.smartvrac.fr/ (accessed: 25 November 2022).
[15] MIWA. Easy shopping experience. https://www.miwa.eu (accessed: 25 November 2022).
[16] Purcell. Simplified refill solutions. https://www.purcell.eco (accessed: 25 November 2022).
[17] Algramo. Technology-led innovation to revolutionize the way we consume. https://algramo.com (accessed: 25 November 2022).
[18] Lidl. Introducing our brand-new no spill laundry detergent refill stations. https://www.lidl.co.uk/about-us/lidl-changes-for-the-better/refill (accessed: 25 November 2022).
[19] Megale Coelho P, Corona B, Worrell E. Reusable vs single-use packaging - A review of environmental impacts. 2020.
[20] Long TB, Looijen A, Blok V. Critical success factors for the transition to business models for sustainability in the food and beverage industry in the Netherlands. Journal of Cleaner Production (175), 2018, p. 82-95, DOI: 10.1016/j.jclepro.2017.11.067.

PS-GO03

Microfibrillated cellulose as reinforcement in PLA based packaging materials: Dry or wet addition in extrusion processes?

S. Sánchez[a], P. Albaladejoa[a], R. Sáncheza, J[a]. M. Alonsoa[a], M. Gallura[a]

Packaging, Transport, & Logistics Research Institute (ITENE), C/ Albert Einstein,1. Parque Tecnológico. Paterna, Spain.

***Correspondence to**: soraya.sanchez@itene.com, pilar.albaladejo@itene.com, rafael.sanchez@itene.com, jose.alonso@itene.com, miriam.gallur@itene.com*

ABSTRACT: The aim of this study was the use of liquid feeding as innovative alternative to additivate microfibrillated cellulose (MFC) to a biobased polymeric matrix, polylactic acid (PLA), during compounding processes. To reach a proper dispersion of the MFC into the PLA matrix and avoid its well-known agglomeration problems, the MFC was chemically modified in order to confer it hydrophobicity to improve its compatibility with PLA. PLA/MFC nanocomposites were obtained through both wet and dry compounding process, and their final properties were compared. The use of a plasticizer has been evaluated in wet compounding process. The results exhibited an improvement of the mechanical and barrier properties, reducing the oxygen permeability up to 13% and the water vapor permeability up to 11%, in the PLA-based composites produced by wet compounding process. These results indicate the potential of these new materials with good barrier properties for packaging applications.

INTRODUCTION

The concept of biobased materials in the field of polymers aims to use alternative sources such as biomass instead of petrol-based sources to produce new materials. Polylactic acid (PLA) is one of the most attractive biobased polymers due to its excellent strength and biodegradability properties. However, its brittleness and poor heat resistance restrict its use in many applications. Therefore, the use of nanofillers have been proposed as alternative to obtain nanocomposites with improved properties.

Microfibrillated cellulose (MFC) has a great potential as nanofiller because of its natural abundance, biodegradability, as well as its good mechanical strength and high surface area. MFCs are originally produced in aqueous suspension. However, nanofillers are usually desired to be in dried form for compounding processes. MFC cannot be directly dried by simple evaporation process since an irreversible agglomeration of the fibres, called hornification [1], can be occurred, hindering the dispersion of the MFC into the nanocomposite. Therefore, other alternatives, such as spray-drying, are proposed to preserve the fibrillar structure of the MFC without hornification. Nevertheless, some issues such the high cost of this technique and the difficult feeding of the dried MFC into the extruder, due to its tendency to aggregate, have not been solved yet.

As an alternative to cellulose nanofibers drying, wet compounding is proposed to validate a sustainable and feasible method to improve the dispersion of the cellulose fibers in hydrophobic polymer matrix as PLA, avoiding the cost of drying the MFC suspension gel with high water content. However, the feeding of aqueous suspensions into the melt compounding process could be problematic. To solve this problem, solvent exchange, and dispersion of the MFC into a plasticizer matrix was proposed [2].

EXPERIMENTAL SECTION

Materials

Eucalyptus cellulose provided by *Ence Energía y Celulosa, S. A. (ENCE)*. The reagents used in this work were: octadecylamine, ODA (Sigma Aldrich, C 99%), reagent grade ethanol (Sigma Aldrich); glutaraldehyde, GA (Scharlau, 25% w/w aqueous solution), Epoxidized soybean oil, ESBO (Glentham Life Sciences).

Extraction of microfibrillated cellulose from woody sources

The eucalyptus cellulose was disintegrated to reduce the size of the fibers up to micrometric size. The disintegration process was carried out with a grinder (Super Mass colloider, Masuko Sangyo, Japan) with two specific stones; a static and a rotating grinding stone, this combination facilitates the breakdown of the cell-wall structure of the fibres. The cellulose at 2%wt. solid content was fed into the grinder and subjected to several passes between the stone section, which was set to 1500 rpm, until a gel consistency is obtained.

Modification of microfibrillated cellulose

The modification of the MFC was done by a simple, facile, and environmentally friendly procedure. The modification process was performed following the procedure described elsewhere [3]. MFC solutions in DI water were prepared and vigorously stirred with a magnetic stirrer for 15 min to form a homogeneous dispersion. At the same time, 10 wt% ODA (in ethanol) solution was prepared separately by vigorous stirring of the mixture for 30 min until the solutions become transparent. Then the above ODA solution was added sequentially into the dispersed MFC suspension and kept stirring for another 1 h. Next, GA solution (12.5 wt%, diluted in water) was added slowly to the MFC/ODA solution with continuous stirring for 4 h at 55ºC to complete the linkage between the two reactants. After that, the solutions were vacuum filtered and washed with enough water followed by large amount of ethanol to remove the unattached ODA and GA from the MFC surface. Subsequently, the MFC-ODA was conditioned by two methods for the biocomposites production. Part of the MFC-ODA was dried by spray drier to obtain it in powder state. The obtained powder was then kept in a sealed aluminium foil until its use in the wet compounding process. Other part of the MFC-ODA was prepared by solvent exchange from water to acetone and then, a processing additive (PA) was added, and the remaining solvent was evaporated to obtain the MFC-ODA in liquid state ready to use in wet compounding process.

Biocomposites preparation

The polylactic acid was conditioned prior to processing in order to eliminate humidity, avoiding possible degradation of the polymer during processing. The drying stage was carried out at 90°C for 5 hours. After the drying step, the biocomposites were processed at ITENE facilities at laboratory and pilot scale.

Laboratory trials were carried out using a Miniextruder DSM Xplore, with maximum mixing volume of 15 cc, using a co and contra-rotating screws. Once processed at identified temperature, time and processing speed, the molten formulation was transferred to a small injection molding machine in order to injected standardized specimens used to evaluate the final properties of the developed composites.

Pilot scale trials were carried out using a co-rotating twin screw extruder, model Brabender DSE 20/40, with a diameter of 20 mm and a L/D ratio of 40. The co-rotating twin screw extruder was equipped with a main gravimetric feeder for pellets, Maguire MGF-8-41. To produce the biocompounds, the PLA was fed by the main feeder, while the MFC-ODA was incorporated by the side feeder.

For dosing the additives two different side feeders were used. A side volumetric feeder, Brabender MT1-1, for dosing the additives in powder state (dry compounding process) and a side volumetric feeder, eco-PEN600 Preeflow, connected to a pressurized vessel 6110 Sagola, which allows the additivation of high viscosity solutions for the wet compounding process.

Characterization techniques

Fourier Transformed Infrared Spectrophotometer analysis (FTIR)

The FTIR spectra of the MFC samples were recorded on an instrument (Bruker, Tensor 27 with ATR, Specac) in the range of 500–4500 cm^{-1} with a resolution of 4 cm^{-1}.

Thermogravimetric Analysis (TGA)

A Thermal Gravimetric Analyzer (Q500 IR, TA Instrument) was used to characterize the thermal stability of the unmodified and modified MFC samples. Approximately 3-6 mg of each sample was heated from 25ºC to 900ºC at a heating rate of 20ºC/min. All of the measurements were performed under a nitrogen atmosphere with a gas flow of 20 ml/min. Finally, the atmosphere was changed to oxygen and an isothermal for 10 minutes at 900ºC was performed.

Mechanical properties

The mechanical properties of the dog bone specimens produce by injection moulding were evaluated in terms of elastic modulus (E); tensile stress (TS), and strain at break ("B%) by submitting the specimens to stress–strain tests in a universal tensile test machine Testometric M350–20CT (Rochdale, UK), according to the standard UNE EN ISO 527-2:1997 with a feed rate of 20 mm/min and a distance between jaws of 50 mm.

Permeability analysis

The oxygen permeability assessment was conducted in an OX-TRAN 2/21 and OX-TRAN 2/22 (Mocon, Inc., Minneapolis, MN) equipment, in accordance with ASTM D3985-17. The results are expressed in the form of permeability with the correction of the sample thickness in each case.

The water vapour permeability assessment was conducted on a PERMATRAN-W Model 3/33 (Mocon, Inc., Minneapolis, MN) equipment, in accordance with ASTM F1249-13.

RESULTS AND DISCUSSION

MFC chemical modification

FTIR Analysis

FTIR analysis were performed with the aim to confirm that MFC was successfully modified with ODA. Unmodified MFC is employed as reference material. ATR-FTIR spectra of MFC and MFC-ODA are reported in Figure 1.

The FTIR spectrum of unmodified MFC showed the typical absorption bands of cellulose. After modification several interesting changes were noticed. The reaction between cellulose and ODA was accomplished through glutaraldehyde (GA) assisted coupling reaction. Therefore, the aldehyde groups in GA were simultaneously crosslinked with the -OH groups of cellulose through the formation of acetal and ether linkages and the amino groups of ODA through the imine linkage. The most significant changes in the FTIR spectrum of MFC-ODA samples were the large intensity increase for the C-H stretching and deformation peaks which appeared at 2850 y 2930 cm^{-1}. The successful reaction of the GA with MFC, resulting in the hemiacetal structure, would suppose a change to the absorption spectrum below 1200 cm^{-1}, since is overlapped with the typical cellulose signals.

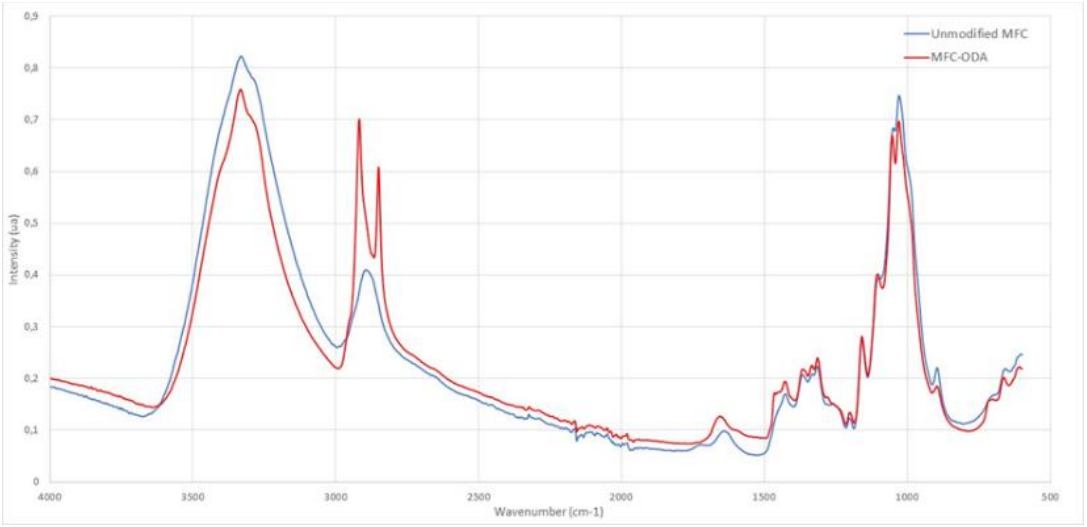

Figure 1 Spectra comparison of unmodified MFC and MFC-ODA

Thermogravimetric Analysis (TGA)

Thermal stability is an essential property of the MFC considering its final use in this study as reinforcement of PLA in compounding processes. In order to better understand the thermal stability and behavior of the MFC, the thermal properties of unmodified and modified MFC-ODA were analysed by thermogravimetric analysis (TGA). The thermogram (TG) and 1st derivative thermogram (DTG) curves of MFC and MFC-ODA are compared in Figure 2.
Both samples showed a small mass loss around 100ºC associated to residual moisture evaporation. A single weight loss step above 334°C was observed for unmodified MFC, while the MFC-ODA present a single weight loss step above 348ºC. The modification of MFC leads to an improvement of thermal stability. Regarding onset temperature, unmodified MFC is around 285ºC, while MFC-ODA is around 291ºC. Thermal degradation of MFC during compounding process is one the challenges to use successfully the MFC as reinforcement in polymeric materials. It should be remarked that the onset temperatures of both unmodified and modified MFC are above to the processing temperature of the polymer selected, thus no degradation are expected for them, during their processing.

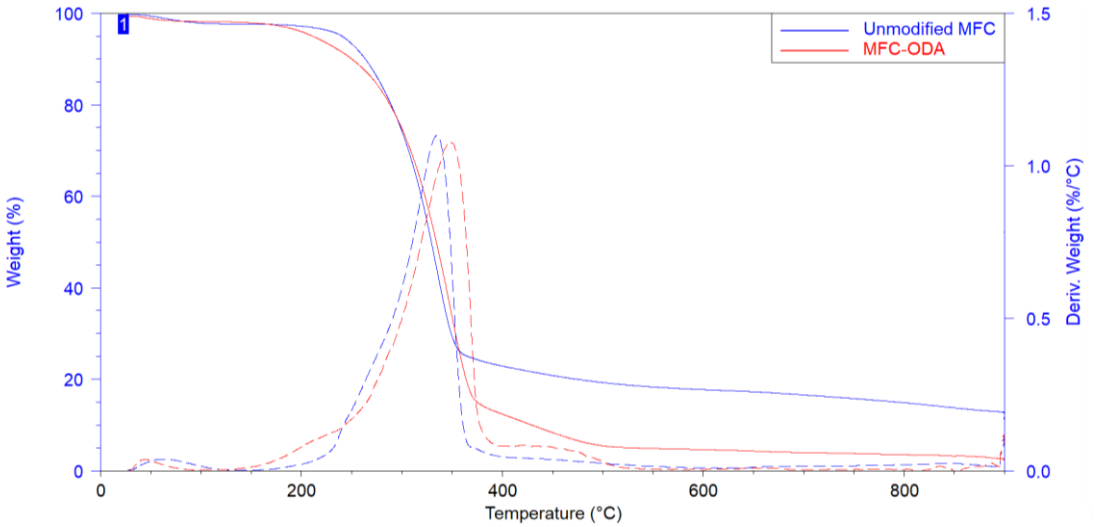

Figure 2 Comparison of the TG and DGT curves of unmodified MFC and MFC-ODA.

Biocomposites preparation

The PLA/MFC based composites were produced at laboratory and pilot scale by using the two routes proposed in this study, wet and dry compounding process. The formulations produced are reported in Table 1.

	References	Lab scale	Pilot scale
	Base matrix	PLA	PLA
Dry compounding process	Unmodified MFC	PLA + 1% MFC	-
		PLA + 3% MFC	-
	Modified MFC-ODA	PLA + 1% MFC-ODA	-
		PLA + 3% MFC-ODA	-
Wet compounding process	Processing additive (PA)	PLA + 10% PA	PLA + 10% PA
	Unmodified MFC	PLA + 1% MFC + 10% PA	PLA + 1% MFC + 10% PA
	Modified MFC-ODA	PLA + 1% MFC-ODA + 10% PA	PLA + 1% MFC-ODA + 10% PA

Table 1 PLA based formulations produced.

The production of the PLA/MFC based composites were carried out by compounding process using a co-rotating twin-screw extruder. The microcompounding process at laboratory scale was carried at 190 ºC and 200 rpm for a residence time of 4 minutes. The temperature profile of the extruder during the compounding process and the processing parameters used to produce the formulations at pilot scale are reported in Table 2 and Table 3, respectively.

Zone 1	Zone 2	Zone 3	Zone 4	Zone 5	Zone 6	Zone 7	Zone 8	Zone 9	Die
190 ºC	190 ºC	195 ºC	195 ºC	195 ºC	200 ºC	200 ºC	200 ºC	200 ºC	205 ºC

Table 2 Temperature profile used at pilot scale to produce the PLA/MFC based composites.

References	Extrusion speed (rpm)	Lateral dossification (mL/min)	Production (kg/h)
PLA (Blank)	300	-	16
PLA + 10% PA	600	-	12
PLA + 1% MFC + 10% PA	600	16	12
PLA + 1% MFC-ODA + 10% PA	600	16	12

Table 3 Processing parameters used at pilot scale to produce the PLA/MFC based composites.

Mechanical properties

The mechanical properties obtain from the stress-strain curves of the PLA/MFC based composites produced at laboratory and pilot scale are reported in Table 4 and Table 5, respectively.

References	TS (MPa)	E (GPa)	Eb (%)
PLA (Blank)	75 ± 2	3.3 ± 0.1	4.1 ± 0.1
PLA + 1% MFC	71 ± 1	3.3 ± 0.0	4.2 ± 0.5
PLA + 3% MFC	62 ± 2	3.2 ± 0.1	4.4 ± 0.6
PLA + 1% MFC-ODA	73 ± 1	3.3 ± 0.1	3.2 ± 0.2
PLA + 3% MFC-ODA	69 ± 3	3.4 ± 0.1	3.8 ± 0.4
PLA + 10% PA	63 ± 4	3.0 ± 0.1	3.1 ± 1.0
PLA + 1% MFC + 10% PA	63 ± 2	3.1 ± 0.0	5.6 ± 2.8
PLA + 1% MFC-ODA + 10% PA	58 ± 2	3.0 ± 0.0	4.0 ± 1.7

* Tensile strength (TS), Elastic modulus (E), and elongation at break (Eb).

Table 4 Mechanical properties of the injected specimens produced at laboratory scale.

No significant changes on the elastic modulus values were observed for the samples processed at laboratory scale by dry compounding process. It was observed that the incorporation of the MFC led to a decrease of the tensile strength compared to pure PLA. This decrease is less pronounced for the MFC-ODA. In addition, a strong decrease of the tensile strength values is observed by increasing the concentration of the MFC and MFC-ODA in the biocomposites due to their poor dispersion and subsequent chain restriction movement of the polymer.

On the other hand, the use of a plasticizer (PA) slightly reduces the stiffness of the biocomposites, as can be observed from the elastic modulus values. Besides, the plasticizer also enhances the ductility of the PLA matrix favouring plastic deformation, as evidenced by the increment of elongation at break [4]. However, the little difference observed in the elongation at break values of the PLA + 10% PA is an indication that the additivation of the plasticizer (PA) at laboratory scale was not carried out properly. More information was obtained from the samples processed at pilot scale in which the additivation of the plasticizer (PA) was controlled with a volumetric feeder.

References	TS (MPa)	E (GPa)	Eb (%)
PLA (Blank)	64 ± 3	2.9 ± 0.1	5.5 ± 0.1
PLA + 1% MFC	67 ± 1	3.3 ± 0.1	3.5 ± 0.3
PLA + 1% MFC-ODA	65 ± 1	3.3 ± 0.1	2.5 ± 0.1
PLA + 10% PA	52 ± 4	2.7 ± 0.2	127 ± 43
PLA + 1% MFC + 10% PA	55 ± 2	2.8 ± 0.2	23 ± 10
PLA + 1% MFC-ODA + 10% PA	44 ± 2	2.8 ± 0.1	16 ± 2

* Tensile strength (TS), Young modulus (E), and elongation at break (Eb).

Table 5 Mechanical properties of the injected specimens produced at pilot scale.

For dry compounding process it can be observed an increase of the stiffness by incorporation of both the MFC and the modified MFC (MFC-ODA). This effect can be also evidenced by the decrease in the elongation at break values. No significant changes compared to the neat PLA matrix were observed for the tensile strength results.

By comparison, for the wet compounding process, the addition of a plasticizer to the PLA matrix not only strongly increases the elongation at break compared to neat PLA, but also a decrease of the elastic modulus was observed indicating that the material becomes more flexible. The MFC addition counterbalanced this effect by increasing the rigidity of the material, evidenced by a slightly increase of the elastic modulus.

On the basis of the mechanical properties obtained, by underlining the importance of the use of a plasticizer (PA) to avoid the costly drying step of the MFC, the wet compounding process is posed as a promising alternative for the production of MFC biocomposites.

Permeability analysis (P_{oxygen}, $P_{water\ vapor}$)

The values of oxygen permeability (P_{oxygen}) and the water vapour permeability ($P_{water\ vapor}$) and the improvement percentage compare with the neat PLA matrix for the PLA/MFC based composites produced at laboratory and pilot scale are tabulated in Table 6 and Table 7, respectively.

References	P_{oxygen} (cc·µm/m²·dia)	% Improvement	$P_{water\ vapor}$ (g·µm/m²·dia)	% Improvement
PLA (Blank)	27645 ± 3215	—	8041 ± 594	—
PLA + 1% MFC	27641 ± 2160	0.01	7642 ± 217	4.96
PLA + 1% MFC-ODA	23098 ± 3933	16.45	7718 ± 143	4.01
PLA + 3% MFC-ODA	28815 ± 593	Not improved	7797 ± 351	3.03
PLA + 10% PA	33562 ± 1807	Not improved	8250 ± 291	Not improved
PLA + 1% MFC + 10% PA	34289 ± 11483	Not improved	7559 ± 90	8.38
PLA + 1% MFC-ODA + 10% PA	29577 ± 1006	11.87	8435 ± 363	Not improved

Table 6 Barrier properties (P_{oxygen} and $P_{water\ vapor}$) of the injected specimens produced at laboratory scale.

The addition of MFC to the PLA matrix did not produce any improvement of the oxygen barrier properties of the samples produce through a dry compounding process, while an enhancement of nearly 5% was observed for water vapor permeability. However, it should be noted the improvement in barrier properties observed for the modified MFC (MFC-ODA), reaching a decrease of the oxygen permeability higher than 16% and up to 4% for the water vapor permeability.
On the other side, as observed for the mechanical properties, no conclusions can be drawn from the results obtained for the samples produced by wet compounding process. A deeper evaluation of the permeability results is done below for the samples produced at pilot scale.

References	P_{oxygen} (cc·µm/m²·dia)	% Improvement	$P_{water\ vapor}$ (g·µm/m²·dia)	% Improvement
Blank PLA	19455 ± 174	—	7121 ± 77	—
PLA + 10% PA	23840 ± 5032	Not improved	7923 ± 1618	Not improved
PLA + 1%MFC + 10% PA	20717 ± 92	13,10	6978 ± 23	11,93
PLA + 1% MFC-ODA + 10% PA	25772 ± 238	Not improved	7493 ± 77	5,43

Table 7 Barrier properties (P_{oxygen} and $P_{water\ vapor}$) of the injected specimens produced at pilot scale.

Only the permeability measurements of the samples processed by wet compounding process were carried out. The results show a marked increase in oxygen and water vapor permeability by addition of the plasticizer (PA). The incorporation of the plasticizer lead to an increase of PLA chains mobility producing greater free volume in the matrix which allow the movement of oxygen and water vapor molecules through the polymeric matrix. Nonetheless, it should be noted that the incorporation of the MFC to the matrix strongly improves the barrier properties against oxygen and water vapor. No noticeable improvement was observed for the modified MFC.

CONCLUSION

Production and modification of MFC was carried out successfully for the reinforcement of PLA matrix. In order to overcome the well-known MFC agglomeration drawback and at the same time reduce processing, the addition of the MFC in liquid (wet compounding process) was evaluated. For comparison, PLA/MFC and PLA/modified MFC biocomposites were obtained by dry and wet compounding process and their final mechanical and barrier properties were evaluated. The study was carried out at laboratory and pilot scale to evaluate the feasibility of the process to be up scaled. Before wet compounding process the water from the MFC was removed by solvent-exchange and dispersed in a plasticizer to enhance its dispersion into the PLA matrix. In general, an increase of the mechanical properties was observed, while a strong improvement of the barrier properties was noticed for the PLA/MFC biocomposites produced by wet compounding process. No noticeable improvement in the final properties of the PLA/MFC-ODA biocomposites was observed compared to the net PLA.

REFERENCES

1 Laivins GV, Scallan AM (1993) The mechanism of hornification of wood pulps. Proc 10th Fundamental Research Symposium, PIRA International, Oxford, UK: 1235-1260.

2 Herrera N, Mathew AP, Oksman K. Plasticized polylactic acid/cellulose nanocomposites prepared using melt-extrusion and liquid feeding: Mechanical, thermal and optical properties. Compos Sci Technol. 2015;106:149-155. doi:10.1016/j.compscitech.2014.11.012.

3 Referencia: Roy, S., Zhai, L., Van Hai, L., Kim, J. W., Park, J. H., Kim, H. C., & Kim, J. (2018). One-step nanocellulose coating converts tissue paper into an efficient separation membrane. *Cellulose*, *25*, 4871-4886. DOI:10.1007/s10570-018-1945-6.

4 Molinari, G.; Gigante, V.; Fiori, S.; Aliotta, L.; Lazzeri, A. Dispersion of Micro Fibrillated Cellulose (MFC) in Poly(lactic acid) (PLA) from Lab-Scale to Semi-Industrial Processing Using Biobased Plasticizers as Dispersing Aids. Chemistry 2021, 3, 896–915. https://doi.org/10.3390/chemistry3030066

PS-GO04

New sustainable inks for the packaging printing industries

Jesús Palenzuela*[1], Inmaculada Lorente[1], Aimie Pichon[1]

[1]*Centro Tecnológico del Embalaje, Transporte y Logística (ITENE), Paterna 46980, España.*

*__Correspondence to:__ *Dr Jesús Palenzuela, Head of Additives, Printing technologies and Functional surfaces Unit, ITENE. Jesus.palenzuela@itene.com*

ABSTRACT: Along the recent years, we have witnessed an increase of the policies and administration strategies to improve the sustainability of plastic, packaging, waste management, and their interaction with the environment. This policy pressure has found positive synergies with the industry, which is aiming to produce and invest in greener and sustainable solutions. Nowadays, packaging companies are more willing to move towards sustainable solutions with improved environmental impact, aiming to reduce the carbon footprint and aiming, for example, to employ inks with more bio-based content with smaller amounts of volatiles and/or avoiding the employ of organic solvents. In this context, sustainability in the packaging could be tackled by the following means:
1) By developing sustainable inks.
2) By working on the packaging material.
3) By implementing new control systems, such as intelligent labels.
Among other strategies, one of the solutions proposed by ITENE in order to reduce the environmental impact of packaging, it is the development of bio-based inks, to reduce the dependence of petrol derivative products and increase the sustainability of the packaging. ITENE is presenting, four biobased coulored inks: cyan, magenta, yellow and black for the flexographic printing completely formulated with biobased components, which could be applied in the packaging industry. The inks have been tested at industrial level, showing good compatibility with the plastic and cellulosic-based substrates. The bio-based content of these inks has been characterised, showing a high bio-based carbon content using radiocarbon analysis (circa > 94%). Besides, these bio-based inks are aiming to be biodegradable and compostable, so they could be used in compostable and sustainable packaging.

Keywords: Ink; sustainable packaging; bio-based ink; flexography; printing industry; plastic; paper: cardboard

INTRODUCTION

Sustainability in packaging is currently the driving force to fuel further demand in the market. Sustainable packaging moved a market size of USD 258.35 billion in 2020 and an estimated growth to USD 385.35 billion in 2028, exhibiting a CAGR of 5.3 % in the mentioned period.[1] Sustainable packaging (or green packaging) reduces the use of energy and minimises the pernicious environmental effects of the materials employed in the packaging fabrication. In

contrast to traditional packaging, green packaging also shows a lower carbon footprint, which improves human and ecological sustainability in the long term. Sustainable packaging also implements strategies for reducing the amount of waste and pollution produced during the manufacturing process[2]. One of the market biggest driving factors in the green packaging is an increasing awareness of environment protection and sustainable living. This new paradigm, together with public policies and new government legislation[3] in favour of the environmental sustainability, pushes the industry to the employ of renewable resources in new development processes[4].

During the last years and since the coronavirus pandemic, the interest for the sustainable packaging has increased along with a dramatically increase in the demand for food packaging, healthcare goods and e-commerce transportation. However, interest decreased for industrial, luxury, and some B2B-transport packaging. The impact on packaging players relied on their portfolios and their exposure to specific markets, substrates, and packaging end-users.

As sustainability is currently the driving force to fuel further demand in the market, bio-based inks play an important role in the development of sustainable packaging. Bio-based inks are very attractive because they do not rely on fossil resources and they contribute to the packaging sustainability, as they are designed with pigments, resins, and other additives from natural raw materials and renewable sources, avoiding the dependency of other resources such as petrol, and keeping away from the petrol prices fluctuations. Additionally, when bio-based inks are formulated with water, these inks also contribute to improve even further the sustainability, avoiding the emissions of volatile organic compounds, which is also on benefit of the health and safety of the ink manipulators during the ink fabrication and following printing processes. Currently, there are in the market, inks with the "OK Compost" label, certified by TÜV Austria.[5] These inks could be employed in the compostable and sustainable packaging, however, due to the fact that the current certified inks are not fully biodegradable, the amount of ink that it can be printed on the packaging, it is limited to the indications given by the ink manufacturer, and at any case, it must not exceed the 1% in weight of the total packaging amount.

Bio-based, biodegradable, and compostable inks could allow the printing without weight limitation, facilitating the printing designs while keeping the compostability of the final packaging. Besides, these inks promote the reduction of the carbon footprint, the non-emission of volatile organic compounds and the non-dependency of fossil resources. Within this new ink paradigm, ITENE Technological Centre has developed new solutions of bio-based sustainable inks able to be printed on the packaging itself or on for example, on a label. These inks can provide a solution to the needs of the nowadays society demands. ITENE, in the framework of the Generalitat Valenciana financed BIOSURFINK project[6,7] has developed bio-based inks for the flexographic and gravure printing in the colours of cyan, magenta, yellow and black (CMYK).

MATERIAL AND METHODS

Bio-based inks. The cyan, magenta, yellow and black inks developed by ITENE were prepared according to the following pigments origins:

Cyan	Vegetal based pigment
Magenta	Animal based pigment
Yellow	Vegetal based pigment
Black	Vegetal based pigment

Table 1 Origin of the CMYK pigment bio-based sources

The pigments were employed in the range of 5% to 25% (weight) and in some cases, it needed some chemical modifications in order to improve the stability and compatibility of the pigment with the binder and the solvent. The pigments are added upon stirring to favour the pigment wetting in the solvent. The consequent pigment dispersion in the solvent was achieved under vigorous stirring. Milling of the particle was achieved in wet milling up to the desired particle size in approx. 3 hours, measured with a laser diffraction technique, Mastersizer 3000 (Malvern Instruments Ltd., UK).
The pigments were incorporated in the bio-based inks varnishes which included the following binder, solvent, and additives families:

Binder	Vegetal derivative from renewable sources
Solvent	Water or bio-based solvent
Additives	Bio-based promoters to improve the adhesion, dispersion, and colour intensity.

Table 2 Origin of the CMYK ink bio-based sources

Binder study. The bio-based polymers employed as binders were carefully chosen, and its compatibility with the solvent studied. Once the pigment were selected, different polymers from vegetal sources were employed in the selected relation to increase the solution viscosity able to be printed by flexography and gravure printing techniques. The binder was prepared mixing the polymer in a concentration between 6% to 25% (weight), depending of the colour ink. The final concentration was adjusted according to the desired final printing requirements and measured with the Ford cup No. 4 method, in the range of 22 – 24 seconds. The binder was mixed with the solvent upon stirring and in some cases, temperature up to 60 °C was applied.

Time stability. Stability analysis of solutions and emulsions was possible with the LUMIFuge® developed by LUM GmbH (Germany). This type of analysis is performed on the ink samples produced.

Printing trials. Printing tests were carried out on the QD printer from Harper (USA) which allows flexographic printing. The printing tests were carried out on several substrates. These prints were made at a speed of 20 m/min. The anilox has an ink volume per cell of 17.00 cm^3/m^2 and a number of cells per inch of 120. The pressure between the printing roller and the substrate could not be modified and no information on this value was communicated by the supplier.

Colour evaluation. Colour was measured by spectro-densitometer SpectroDens from TECHKON (Germany). Measuring conditions were illuminant D65 observer 10°. Thus, each print previously made was measured in four points of the printed area. The average of these results is kept.

From these values, the chroma C* can be calculated. It is the relative saturation of the analysed hue. A value of chroma as high as possible is sought in order to obtain a satisfactory intensity of the colour.
This value is calculated as follows:

$C^* = \sqrt{a^{*2} + b^{*2}}$ *(Equation 1)*

RESULTS AND DISCUSSION

Particle size

The particle size is analysed for each of the formulations made with the different colouring materials, binders, additives, ultrasonic treatment conditions and concentrations. The average range of results obtained can be seen at the table below:

	Dx (50) (µm)	**Dx (90) (µm)**
Cyan	13.00 – 3.50	28.00 – 15.40
Magenta	9.73 – 6.00	41.80 – 24.40
Yellow	4.51 – 2.05	16.10 – 5.02
Black	5.70 – 0.17	62.3 – 2.12

Table 3 Particle size characterisation of the different inks

The particle size analysed by the Mastersizer shows that some of the measured values, especially for the magenta ink, are slightly too large regardless the conditions of mixing, milling and the additives added. Indeed, Dx (90) is between 24 and 42 µm. Nevertheless, it is worth mentioning the remarkably small size of the particles in the black ink in terms of Dx (90) 2.12 µm after milling and ink stabilisation.

Time stability

Time stability performs physically accelerated, direct and efficient stability testing and ranking of formulations. It examines the physical stability of the samples through means of an optical stability analyser that accelerates physical destabilization by centrifugal force. The LUMiFuge® measurements was done at 2,300 × g for 4 hours at 25 °C. Lower instability index values indicate better emulsion stability. A value of 1 means that a component is very unstable, and a value of 0 means that it is very stable. This type of analysis is performed on the four

coloured ink samples produced. The instability index obtained ranged between 0.003 for inks developed with water-based solvent, to 0.211 for inks developed with vegetal-based binder and bio-based solvents.

Bio-based content characterisation

The Carbon bio-based inks were analysed under the following standard and reported. These standards analyse the measuring of the $^{14}C/^{12}C$ and $^{13}C/^{12}C$ isotopic ratios. The results can be seen at the next table:

	C Bio-Based content	**Standard**
Cyan	94 %	ASTM D6866
Magenta	100 %	EN 16640
Yellow	100 %	EN 16640
Black	100 %	ASTM D6866

Table 4 Bio-based content and the standard followed

Printing trials

The developed inks were printed at laboratory scale employing the mentioned printer in the Material and Methods section. The substrates employed were PLA, PET, polyolefins, paper, and cardboard.

Figure 1 Colour obtained after printing on PLA (each colour left) and cardboard (each colour right).

Colour characterisation

The obtained colours were printed and the colorimetric analysis of the printing trials collected. The results obtained was the average of four values taken at four different printing positions. We observe that in general, the higher the dye concentration, the higher the chroma, which was expected. As well, the smaller the particles size, the higher the colour intensity. An example of a colour characterisation can be seen next:

	L	**a***	**b***	**C***
Cyan	75.53	-8.03	-17.32	19.09
Magenta	67.16	31.64	-9.57	33.05
Yellow	89.67	-4.69	44.98	45.22
Black	36.64	1.88	4.95	5.29

Table 5. Colour characterisation of the different inks

CONCLUSIONS

An interesting set of four bio-based inks in the colours of cyan, magenta, yellow and black has been developed at ITENE. These inks offer a promising and alternative solution to conventional inks fabricated from petrol derivatives and non-renewable resources. As they have been able to be printed on different substrates (PLA, PET, PP, PE, paper and cardboard), they are suitable for general applications but especially relevant for those applications related to sustainable packaging and sustainable content. The bio-based content has been evaluated in terms of ^{14}C and ^{13}C ratios versus ^{12}C, showing ranges of bio-based carbon from 94 to 100%, depending of the ink. The colour tonality was difficult to adjust due to the limitation offered by the natural and renewable pigments, however these four colour inks show a large potential and could be of interest for many applications and commercial purposes.

REFERENCES

[1] Green Packaging Market Size | Global Report [2021-2028] (fortunebusinessinsights.com)
[2] L. Bautista, L. Molina, S. Niembro, J. M. García, J. López, A. Vílchez, Chapter Eight - Coatings and Inks for Food Packaging Including Nanomaterials; Micro and Nano Technologies, Emerging Nanotechnologies in Food Science, Elsevier, 2017, 149-173,
[3] www.un.org/sustainabledevelopment/sustainable-development-goals/
[4] Y. Goh, S. Lauro, S. T. Barber, S. A. Williams, T. A. Trabold; Cleaner production of flexographic ink by substituting carbon black with biochar; Journal of Cleaner Production; 2021; 324; 129262,
[5] www.tuv-at.be/green-marks/certifications/ok-compost-seedling/
[6] www.itene.com/casos-de-exito/biosurfink-tintas-tratamiento-superficies/
[7] www.itene.com/casos-de-exito/biosurfink-2022-tintas-sostenibles-tratamiento-superficies-envases/

PS-GO05

Recycled Polymers: Improving recycled high density polyethylene properties through reactive extrusion

Alejandro Guillem[a], Octavio Ortega[a], José Alonso[a], Miriam Gallur[a]

Packaging, Transport, & Logistics Research Institute (ITENE), C/ Albert Einstein,1 Parque Tecnológico, Paterna, Spain

ABSTRACT: The use of plastic materials has increased during the last decade due to their wide variety of properties and structures. Rigid and flexible plastic packaging sector represent around 44% and 39% of the global and the European plastics consumption by application, respectively. However, these packaging solutions present issues to be classified and/or recycled (heterogeneity of waste, separation difficulties, degradation, contamination, etc.), with the potential loss of resources, as well as problems in the management of packaging wastes. There is a huge interest to facilitate the recyclability of HDPE packaging applications because they represent almost half of global HDPE consumption. From those packaging examples, extrusion blow molding applications represent a suitable target to be improved and increase their recycling uses. The objective of this research is to provide a suitable route to improve properties of post-consumer recycled HDPE (PCR HDPE).

A suitable approach for improving such properties in a cost-effective manner can be achieved through the reactive extrusion technology. Reactive extrusion consists of promoting a reaction within the extruder while the recycled polymer is in melting state. With the use of specific initiators, additives and fillers, properties of PCR HDPE were enhanced to a great extent reaching similar values as those reported for virgin HDPE grades. To evaluate the results of reactive extrusion technology, different characterization methodologies such as online rheology, tensile properties and environmental stress cracking resistance (ESCR) tests have been applied. Recent trials carried out at ITENE have reported a remarkable 4-fold increase in ESCR tests while improving at the same time the ductility of the polymer without significantly affecting its strength. Therefore, the research showed that reactive extrusion can be considered a suitable technique for the improvement of PCR HDPE properties.

INTRODUCTION

The consumption of plastics has been increasing in recent decades due to the versatility in terms of properties of this family of materials (lightness, ease of transformation or low cost), reaching a demand of 50.3 million tons in Europe in 2021 (data from [1]). Of these 50.2 million tons, 39.1% were demanded by the packaging sector.

However, continuous growth of the plastic industry has also led to a continuous increase in the amount of waste generated. In 2021, 29.5 million tons of post-consumer plastic waste were collected in Europe, and only 35% of the total plastic packaging waste was recycled [1]. This is mainly due to separation difficulties, high susceptibility to degradation, presence of contaminants and heterogeneity in properties of recycled plastics.

This current situation is still far from the targets set by the European Plastics Strategy, Directive (EU) 2018/852 on packaging and packaging waste, and the Waste and Contaminated Soil Law. Among these targets, it highlights as targets to achieve by 2030 a plastic recycling rate of 55% and 100% of packaging reusable, recyclable or compostable.

In order to solve these problems and fulfil with the different requirements set by European legislation, it is necessary to look for new packaging solutions to improve the properties of polymeric matrices, especially recycled ones.

In this sense, one of the most demanded materials is high density polyethylene (HDPE), characterised by low cost and good mechanical and chemical properties for rigid packaging applications (mostly extrusion blow moulding). However, when considering recycled HDPE, its heterogeneity, lower processability, melt strength and mechanical properties due to material degradation and the presence of contaminants limit their use in high added value applications such as packaging of cleaning products [2]. In addition, for this kind of applications, high resistance to stress cracking, i.e., cracking in the presence of active media, is usually required. Such resistance is critical in the industry, as it has been estimated that 15% of premature and in-service failures are due to stress cracking [3].

Since the aforementioned properties are largely influenced by the configuration of the polymer at the molecular level, the development of new processes is required to affect the structure of the material and restore its properties. Conventional additive and compounding strategies are generally insufficient due to the degradation of recycled HDPE and the presence of other fractions or contaminants in its composition.

For this purpose, reactive extrusion (RE) is presented as a suitable technique to carry out this modification. RE allows the recycled HDPE to be chemically modified during the extrusion process. In this way, the incorporation of new functionalities in the polymer or an improvement of the present ones may be achieved by modifying its molecular structure.

To design these reactive extrusion processes for recycled HDPE, the main characteristics are molecular weight, molecular weight distribution, branching and chain distribution. These will have a significant influence on the properties of the polymer in both solid and molten states and, therefore, on its processability and final properties.

In order to modify the molecular structure, it is proposed to insert secondary chains into the backbone by branching, combining their distribution and length, to obtain an adequate balance of stiffness, resistance to stress cracking and rheological properties.

For this purpose, the most common modification reaction of polyethylene was taken as a starting point, which is the grafting of new functional groups onto the main chain [4].

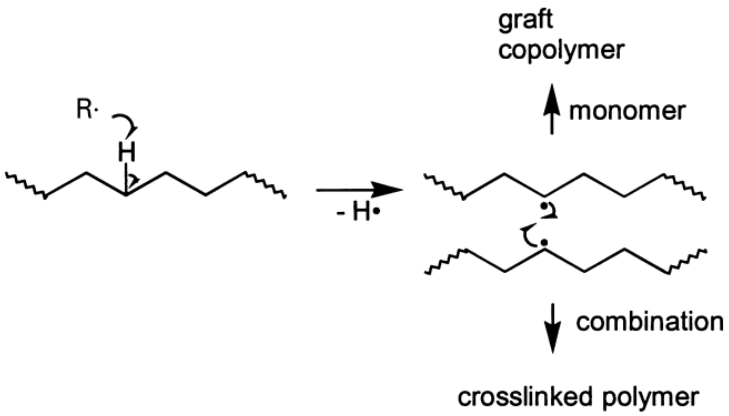

Figure 1 Reaction mechanism by grafting.

This process involves the reaction of molten polyethylene with a polymerizable monomer in the presence of a free radical initiator. Inadequate control of the process parameters can lead to uncontrolled reactions such as cross-linking, cleavage of the main chain, shear degradation or homopolymerization of the monomer. Therefore, it is of vital importance to control these parameters, as well as a proper selection of initiating agent and functional groups to be introduced into the polyethylene main chain.

The use of online control measures of the reactive extrusion process, such as online rheology is of paramount importance to evaluate the reaction extent. This technique allows the measurement of two different types of viscosities. The first one corresponds to shear viscosity, and it may be related to the molecule size and thus to the size of the branches and the three-dimensional structures of the polymer in the molten state formed by a cross-linking reaction. The second one is the elongational viscosity and it may be related to the branching of the polymer chains within the polymer matrix and can therefore give an indication of the number of secondary chains formed in the main chain.

MATERIALS AND METHODS

Materials

A postconsumer recycled HDPE grade was supplied by IBER RESINAS. It consists of a macroscopically heterogeneous mixture of recycled postconsumer HDPE. Different initiators based on peroxides (peroxide_1 and peroxide_2), an organic additive based on olefins (olefin) and an inorganic filler (functionalized double layered hydrotalcite – LDH) were also selected. A virgin HDPE grade, Lotrene Q5202BN, supplied by QCHEM was selected as a reference material.

Reactive extrusion

The reactive extrusion process was carried out in a twin screw extruder ZSE 27 Maxx (Leistritz, Germany) with a screw diameter of 28.3 mm and a L/D ratio of 60 and an online rheometer

(LDR 11, Leistritz GmbH) was placed just before the exit die of the extruder. Below it is included a table with the different formulations considered. In case of peroxide_1, three different concentrations were tested.

REFERENCE	FORMULATION
rHDPE	Recycled HDPE
rHDPE_1	Recycled HDPE + peroxide_1_concentration_1 + olefin
rHDPE_2	Recycled HDPE + peroxide_1_concentration_2 + olefin
rHDPE_3	Recycled HDPE + peroxide_2 + olefin
rHDPE_4	Recycled HDPE + peroxide_1_concentration_3+ olefin + LDH

Table 1 References processed by reactive extrusion.

Characterization techniques

Online rheology

The online rheometer (LDR 11, Leistritz GmbH) deviates part of the polymer flow through a slit die with two different width channels connected by a hyperbolic transitional section which generates a constant elongational flow. Pressure transducers record the pressure of the melt along the rheometer channel and viscosities are calculated from this data and the geometry channel. Flow rate and consequently shear and elongational rates are controlled by the pump speed.
Two different types of viscosities were measured with this device varying the melt pump speed from 0 to 35 r.p.m at the melt temperature measured by the extruder, shear viscosity and elongational viscosity. The first one was measured by the pressure loss between the entrance section and the exit of the constant section channels. The second one was measured by the pressure loss in the transitional section or hyperbolic flow.

Melt flow index

In addition to online rheological measurements, which enabled a study of the rheological behaviour, it was evaluated the melt flow index (MFI), parameter commonly used in the plastics industry, and compared with the reference material. MFI was measured on a Goettfert MI-3 melt flow indexer according to the ISO 1133-1 standards. The temperature was set at 190 °C, previously heated for 5 minutes, and a weight of 21.6 kg.

Environmental stress cracking resistance

Environmental stress cracking resistance (ESCR) was measured based on ASTM D1693. The test consists of exposing a series of U-shaped bent specimens with a notch to an active medium, mainly Igepal CO-630 diluted at 10%. Values are given as the cracking time of a minimum of 5 specimens out of a total of 10.

To do this, first, plates of the different formulations and the reference material were prepared according to the D4703 standard. The plates were obtained with a moulding

temperature of 177□C and a cooling ramp of 15 ± 2□C/min to 76□ºC. The plate thickness was within the range of 1.84-1.97 mm and was taken as a reference from ASTM D1693.
Once plates were produced, the specimens were cut and notched. Subsequently, a centred notch was made in each specimen with a depth of 0.3-0.4 mm and specimens were bent to reproduce the same bending force on each of the specimens. Once bent, the specimens were transferred to the specimen holder with the use of the gripping forceps, introducing the holder into the test tube with the 10% Igepal CO-630 solution.

Three replicates of each reference were placed inside a thermal bath at 50ºC, and visually inspected every 4-8h.

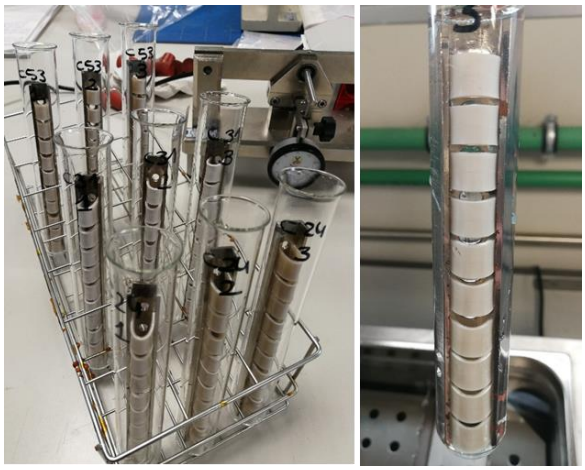

Figure 2 Environmental stress cracking resistance test.

Mechanical properties (tensile)

Sheets for tensile testing were obtained by cast extrusion in a stand-alone single-screw extruder KE 30/32 (Brabender) with an L/D 25. The thickness was set to obtain 350 microns. In addition to rHDPE formulations, vHDPE was also processed by this technique to obtain specimens for mechanical testing.

Tensile tests were performed according to the ISO 527 on a Universal testing machine model M350-20CT on the cast sheets. Specimens were conditioned at 23 °C and 50% humidity for at least 24 h, and at least 5 specimens were tested for each formulation.

RESULTS

Online rheology

The reactivity of the reactive agents as well as the type of reactions between the olefinic additive and the recycled HDPE matrix were evaluated by the measurement of the viscosity of the formulations. As mentioned above, the online rheometer calculates two types of viscosities, the shear viscosity and the elongational viscosity. The results of the shear and elongational viscosity measurements are shown below:

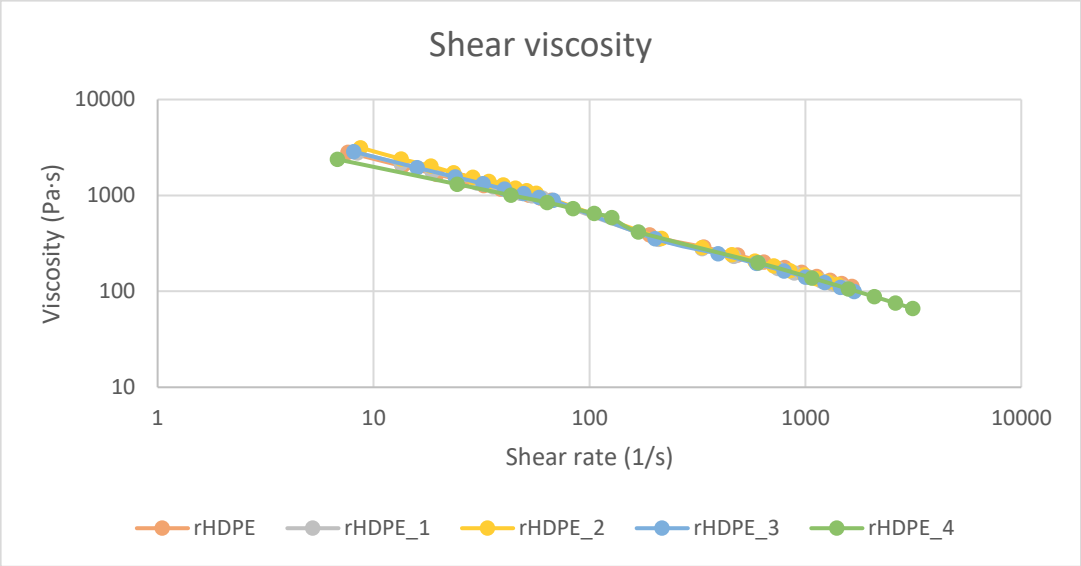

Figure 3 Shear viscosity of the different formulations

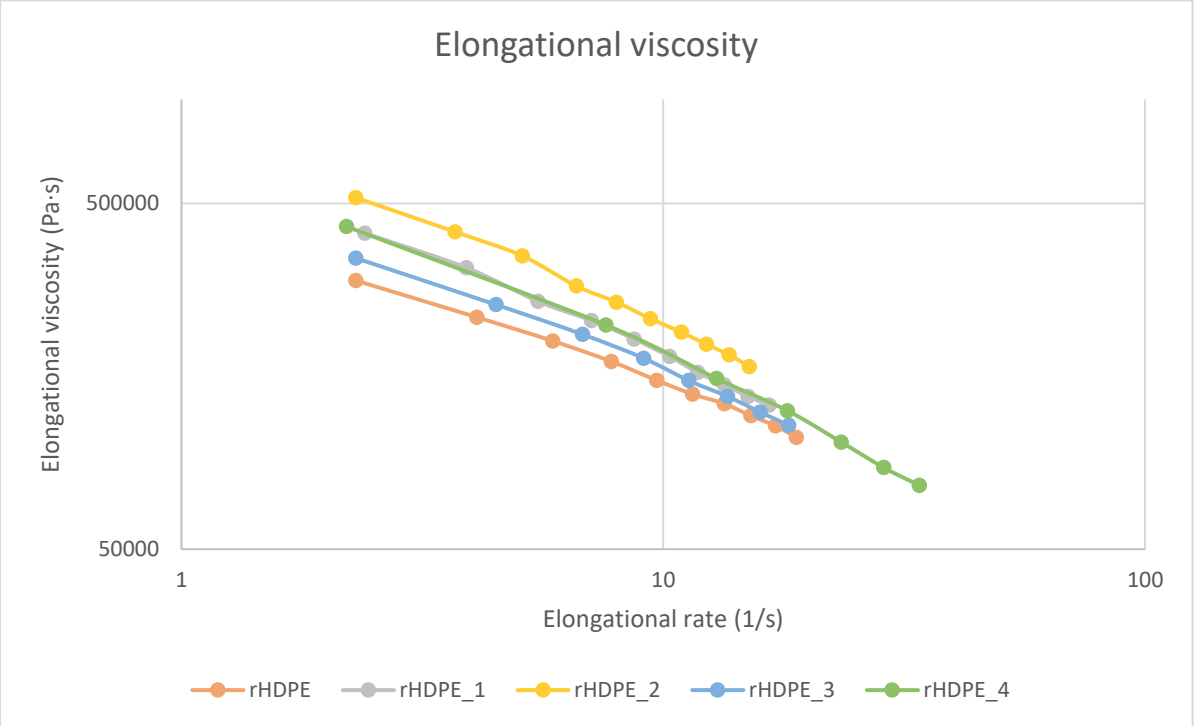

Figure 4 Elongational viscosity of the different formulations

The shear viscosity of the material showed very slight differences with respect to the unmodified rHDPE matrix (rHDPE), so that in principle it could be stated that the crosslinking reactions in the rHDPE matrix have been minimal or even non-existent.

In terms of elongational viscosity, appreciable differences were observed compared to unmodified rHDPE. Formulation rHDPE_2 showed the greatest improvement. From these

results it could be extracted that the reactions that took place in the extruder corresponded mainly to branching reactions.

Melt flow index

The MFI values for the different formulations are shown in Table 21.

Ref.	MFI (g/10min)
vHDPE	33*
rHDPE	45,8 ± 0,7
rHDPE_1	34,2 ± 0,5
rHDPE_2	19,1 ± 0,8
rHDPE_3	40,2 ± 0,7
rHDPE_4	37,3 ± 0,8

*Data from the technical data sheet (TDS).

Table 2 MFI results for the different recycled HDPE formulations

As it was confirmed in the online rheology measurements, the reactive modifications of the rHDPE produced an increase in the viscosity of the material, leading also to a reduction of the melt flow index. Values similar to the reference material or even lower were achieved.

Stress cracking resistance

The results obtained in the evaluation of the stress cracking resistance of the most promising recycled HDPE formulations are shown in Table :

REF.	Stress cracking resistance (h)
vHDPE	50*
rHDPE	<24
rHDPE_1	55
rHDPE_2	110
rHDPE_3	45
rHDPE_4	90

*Data from the TDS.

Table 3 Stress cracking resistance results

The different reactive extrusion routes carried out on recycled HDPE led to an improvement in the resistance to stress cracking, exceeding in most cases the reference virgin HDPE and even twice in case of rHDPE_2 and rHDPE_4.

Mechanical properties (tensile)

The results obtained in the tensile test are presented below:

REF.	Tensile strength (MPa)	Strain @ break (%)	Yield stress (MPa)	Yield strain(%)
vHDPE	23,4 ± 0,9	671,4 ± 186,3	23,4 ± 0,9	10,7 ± 0,2
rHDPE	26,1 ± 0,4	73,3 ± 20,9	26,1 ± 0,4	10,9 ± 0,3
rHDPE_1	21,6 ± 0,4	1094,3 ± 374,4	21,6 ± 0,4	12,3 ± 0,3
rHDPE_2	20,4 ± 1,2	789,3 ± 314,3	20,4 ± 1,2	12,2 ± 0,6
rHDPE_3	21.0 ± 0.3	1216.1 ± 369.2	21.0 ± 0.3	12.3 ± 0.6
rHDPE_4	23.3 ± 0.3	590.2 ± 215.1	23.3 ± 0.3	11.3 ± 0.5

Table 4. Tensile test results

By means of reactive extrusion, the ductility of recycled HDPE was improved, as it can be seen from the increase in elongation. In fact, even the elongation at break of the reference HDPE was exceeded, reaching values of up to 1216% in the case of the rHDPE_3 formulation. Likewise, this same formulation together with rHDPE_1 provided the highest increase in yield point elongation, achieving values of 12.3%. This is because of the formation of different branches on the polymer backbone, which result in a higher ductility.

CONCLUSIONS

Reactive extrusion processes were studied for the chemical modification of the molecular structure of a postconsumer recycled HDPE to insert secondary chains into the main chains and improve their performance for extrusion blow moulding applications.

The modifications of the recycled HDPE by reactive extrusion were confirmed by online rheological measurements, observing no relevant changes in shear viscosity and an increase in the elongational viscosity, which may be related to branching reactions. Formulation rHDPE_2 showed a sharper increase in the elongational viscosity, which also led to a lower MFI.

These formulations were analysed in terms of mechanical and chemical properties. Mechanical properties were enhanced in terms of ductility, observing a closer behavior to the reference material. Finally, chemical properties were tested by means of environmental stress cracking resistance tests with a 10% Igepal CO-630 solution at 50ºC. A 4-fold improvement in stress cracking resistance was observed, reaching values of up to 100h in case of references rHDPE_2 and rHDPE_4. These values were twice as high as those of the reference material.

REFERENCES

[1] P. Europe, “Plastics The Facts - 2022,” 2022.

[2] H. McGeough, “The Chemical Engineer - Challenges for recycled polymers in Europe,” [Online]. Available: https://www.thechemicalengineer.com/features/challenges-for-recycled-polymers-in-europe/.

[3] R. Al-Zubi, D. A. Brent Strong and M. Lampson, *Understanding Environmental Stress Crack Resistance (ESCR) in Rotomolded Polyethylene Tanks.*

[4] G. Moad, "The synthesis of polyolefin graft copolymers by reactive extrusion," *Progress in Polymer Science*, vol. 24, no. 1, pp. 81-142, 1999.

PS-GO06

A trend-based analysis of packaging material amounts per capita per day in The Netherlands

Roland ten Klooster[*1], Bjorn de Koeijer[1]

[1]*Department of Design, Production and Management, Faculty of Engineering Technology, University of Twente, 7522 NB Enschede, The Netherlands*

***Correspondence to**: Roland ten Klooster. [1]Department of Design, Production and Management, Faculty of Engineering Technology, University of Twente, 7522 NB Enschede, The Netherlands*
E-mail: r.tenklooster@utwente.nl

ABSTRACT: The focus of the research is on the relation between the amount of packaging material used per capita per day (pcpd) and trends influencing these figures, which provides indications of the key parameters. Based upon the yearly figures of the Dutch Waste Fund the amount of waste per capita per day in the Netherlands has been analyzed from 2013 to 2021 in four material categories: paper/board, metal, glass, and plastics. The amount raised from 394 grams in 2013 to 414 grams in 2021 pcpd. COVID caused an increase in the amount of paper and board because of home delivery in 2020 but this decreased the year after. An investigation into trends was executed to get insight in the developments. Packaging materials for dinner is an important cause of the use of packaging material as shown in an earlier study. In contrast, many packaging types have been reduced in weight, e.g., glass bottles, PET bottles, metal food cans, beverage cans, etc. Despite this reduction on the level of product-packaging combinations there is an increase in the amount of packaging material used pcpd.
The causes can be found in several trends like shorter time to prepare food from 55 minutes in 1965 towards less than 20 minutes in 2019, freshly packed products with modified atmosphere, recipes with other origin which leads to more packs etc. which means more packaging material. Time advantaged in grocery shopping is also a cause. More portioning to reduce food waste is also influencing the amount of used packaging material. It is hard to conclude if the increase in amount of packaging is more or less sustainable because leftovers, food waste, damage figures also should be involved for the total overview.
Conclusion is that to reduce the amount of packaging material pcpd behaviour and awareness of accepting new package concepts with the consequences are important parameters.

Keywords: packaging design, packaging material, design brief, sustainability, key figures, benchmarking, trends

INTRODUCTION

In 2017 a study (Ten Klooster, Koeijer, & Lange, 2017) [1] on key figures regarding the amount of packaging material used per person per day in the Netherlands was published. Several approaches were used to get insight in daily packaging material amounts used. The first approach covers figures from a Dutch national research institute about consumption patterns and it is used to calculate the amount of packaging material based on what Dutch citizen eat per day looking at the most lightweight package option and the heaviest solution found in the market. Secondly, a number of consumers have been weighing their packaging waste for several weeks. The third approach is an attempt to find a way to buy the 'regular' groceries with both the most savings on packaging material and the highest use of packaging materials. Finally, the annually published waste figures by the Dutch waste fund (Afvalfonds Verpakkingen) [2] were used and divided by the average number of Dutch inhabitants for the year. The figures of the waste fund are part of the extended producer responsibility policy that is active in the Netherlands.

All scenarios to determine the amount of packaging material have a lot of unknowns and uncertainties. The figures by the waste fund are considered as being reliable figures. Companies that put more than 50.000 kgs of packaging material on the market have to register their figures of used packaging materials. Two independent research activities cover the other companies on base of figures of reviews of more than 4000 companies. By extrapolating and scaling on base of figures of the chamber of commerce registration, the final figures are determined. The mentioned research on key figures also showed that the main part of used packaging materials in the Netherlands is caused by preparing dinner, consuming beverages, and the consumption of dairy products [1].

The figures of the waste fund [2] are followed since 2013 up to now and they show the amount of packaging material per capita per day over the years. Published figures like those of the Section Organization Wine (Koninklijke Vereniging van Nederlandse Wijnhandelaren; KVNW) [3] in the Netherlands show a decrease of the average weight of wine bottles over the years. The amount of material pcpd is increasing while individual packaging concepts are decreasing in weight. This raises questions. The research question therefore is: what are the causes that people use or need more packaging material per day and what are developments influencing this?

This research sets societal trends against functional needs and continuous improvements and innovations in the field of packaging. The start of the period of time that is considered is aligned with the use of more packaging material which started around 1950. This is also the period that plastics were introduce, used at larger scale, and used for packaging. Focus area will be the Netherlands. The final goal is to get understanding of possible drivers that influence the current needed amount of packaging material. This can be used to set up activities to reduce the amount of packaging material per person per day and to feed discussions in this field.

DEVELOPMENT OF PACKAGING USE

An overview of several trends that influence the use of packed food since the sixties up to now is presented. The research after amount of packaging material per person per day showed that

dinner has an important share in the total amount of used packaging material. One focus therefore will be on developments of preparing food and their influence on the use of packaging material.

Amount of packaging material per capita

Figure of the waste fund show that the amount of packaging per capita has grown from 394 grams in 2013 towards 414 in 2021. The use of metal and glass is rather stable, while paper and board and plastics are the cause of the increase. The growth is close to 0.5 % per year.

Gram per capita per day	2013	2014	2015	2016	2017	2018	2019	2020	2021
Glass	88	86	81	81	80	80	80	80	80
Paper and Board	196	190	198	202	202	198	211	228	217
Plastics	76	77	80	81	82	83	83	87	85
Metal	33	36	33	33	35	34	33	32	32
Total	394	389	392	397	399	395	407	428	414

Table 1. Amount of packaging material per capita per day 2013-2021

Preparing meals in the Sixties

The traditional menu was bread, boiled potatoes, seasonal vegetables, and meat (Wijn & Staveren, 1980) [4]. One out of ten households had a refrigerator [5]. Daily shopping therefore was a need. Daily food was bought at small supermarkets [4]. Potatoes ask quite some time to prepare; they have to be peeled and then boiled for ca. 20 minutes. In the 30's a housewife was busy in the kitchen for 2 ½ hours per day preparing food, in the 60's this was reduced to 1 hour (Jobse van Puten, 1995) [6]. Moreover families ate soup out of a can or made out of a pouch on Saturdays, to relieve the housewife. Chinese food like Nasi and Bami were introduced in cans and was a big success [7]. Up to the sixties most dairy desserts were prepared at home. The use of fridges made it possible to store dairy desserts prepacked in glass bottles and cartons. Milk was sold in glass bottles by the milkman, but also in plastic bags (Stichting Historie der Techniek, 2000) [5]. The first margarine brand that used a plastic one-way tub to replace paper wrappers was Bona. The introduction was a great success [7]. In 1960 a questionnaire showed that 15% of the Dutch sometimes eat 'outside', meaning in a restaurant. Twenty years later this was 75%. In 1960 in the Nederlands there were 225 Chinese restaurants, in 1970 the figure was 618, and in the beginning of the 80's almost 2000 (Montijn, 1991) [8]. Both households and restaurants used canned foods [6].

Preparing meals and eating out in the Seventies

Visits to restaurants were still limited. Chinese restaurants had a large share in the total number of restaurants [4]. Menus at home still contained mainly Dutch traditional food: potatoes, meat, and vegetables [6]. Very slowly, foreign influences entered the kitchens like Italian-inspired food, French onion soup with cheese, Chinese/Indonesian nasi goreng, and Mexican chili con carne. Standard dessert was yoghurt or custard. In weekends Bourbon or Saroma pudding was

made, both brand names and both from powder out of a pouch. Potatoes were 8% of the energy input in 1950 and went down to 5% in 1975 [4]. Prepacked food slowly entered the kitchens. The growth of fridges in households went from 10% in 1960 to 93% in 1974 and 98% in 1980 [9] and made storage of vulnerable products easier.

Preparing meals and eating out in the Eighties

The number of single-person's households increased and with this the need for easy to prepare individual meals. The market introduction of the microwave makes heating of food easy and fast. The market acceptance of the microwave went up very fast to almost 80% of households in the nineties. Moreover ready-to-eat (microwavable) meals, entered the market [7]. Figure 1 shows that market acceptance of the microwave was faster than of the tumble dryer and dishwasher. Going out for dinner became moreover a culinary adventure with the introduction of Greek, Mexican, and Balkan restaurants.

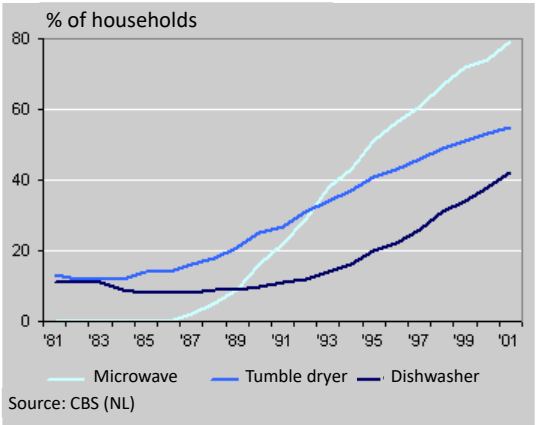

Figure 1. Use of household equipment (CBS) [10]

Preparing meals and eating out in the Nineties

A generation of star cooks change the way of preparing dinner. The television studio became their furnace and they showed that everybody can prepare a quality dinner. In the Netherlands cooks like Braakhekke and Spijkers, in the UK Jamie Oliver probably was the most popular cook at the end of the 90's with his program 'The Naked Chef' [7]. An important development in the field of packaging was the large-scale application of modified atmosphere packaging for meat, fish, and poultry improving food safety and freshness, especially for those products that previously had to be bought on a daily base. Later coffee, nuts, and bakery products were gas packed. A mixture of Asian and Western influences became popular; fusion cooking with variation in cooking techniques. And at the end of the decennium food with names like 'carpaccio of … beetroot, tuna fish', 'on a bed of … rucola, sea salt', 'timepiece of … sea bass, mushrooms', were served [7].

Other societal trends throughout the years

Time savings

The time spent in the kitchen to prepare food reduced drastically from more than two hours in the thirties [6], towards 55 minutes in the sixties [8], 45 in the eighties [4] and an estimated 18 minutes currently. Bags with seven different types of prepacked salad, washed and ready to serve are exemplary of time-saving quality products. By adding tomatoes the salad is ready to be served. A lot of products are processed so that preparing time is reduced – like preboiled or baked potatoes, partly prepared meat, etc. The introduction of technical equipment for the kitchen shows the importance of time savings like the rate of households that used a refrigerator, the use of the high-pressure cookers that reduced the time for boiling potatoes, and the introduction of the microwave.

Portioning to avoid food waste

As indicated by Williams (Williams, Lindström, Trischler, & Wikström, 2020) [12], portioning of food is of high importance for food waste reduction, in many cases this accounts as being more important than the used amount of packaging material, in relation to environmental impacts. This can mean that the packaging material amounts used are increasing, while the total environmental burden is decreasing.

Consciousness in choosing packed products

Online and on social media many guides can be found to reduce or avoid the use of plastics, not to buy prepacked food, how to reduce packaging material, etc. Some reuse and refill initiatives were accepted by consumers in the Netherlands, like Pieter Pot, a company refilling glass jars with products and distributing them across the Netherlands. Statistics about the effect of trends like these are not present. Refill systems for primary packaging attract a lot of media attention, but making them economical beneficial is not easy.

Birth rate and participation of women on the labour market

In 1935 on average a woman delivered 2.5 children and this figure slowly decreased to 1.7 in 1995 and is stable since then [10]. A steady growth of female participation on the labour market since 1950 can be identified [10]. In the fifties the share was 35%, in the eighties 50% and grew steadily towards over 65% in 2013, and is still growing. Figure 2 gives an overview of the trend from 1950 towards 2007. Sources mention that innovation is partly driven on base of time savings in a household [8] [13] and in this occasion related to preparing food.

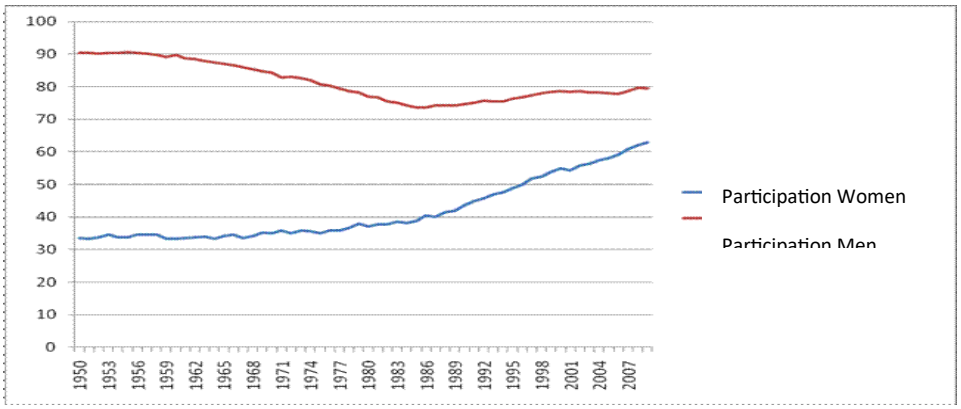

Figure 2. Participation of men and women on the labour market [10]

COMBINING TRENDS AND DEVELOPMENTS

From this small historical overview on base of a lot of trends, it can be concluded they fit into developments towards reductions in time required to prepare dinner. Important parameters are the growth of the number of households with a fridge, the use of kitchen equipment like microwaves, packaging concepts that keeps products fresh for longer times, less available time for preparing food. Figure 3 present the parameters against the average time used to prepare dinner.

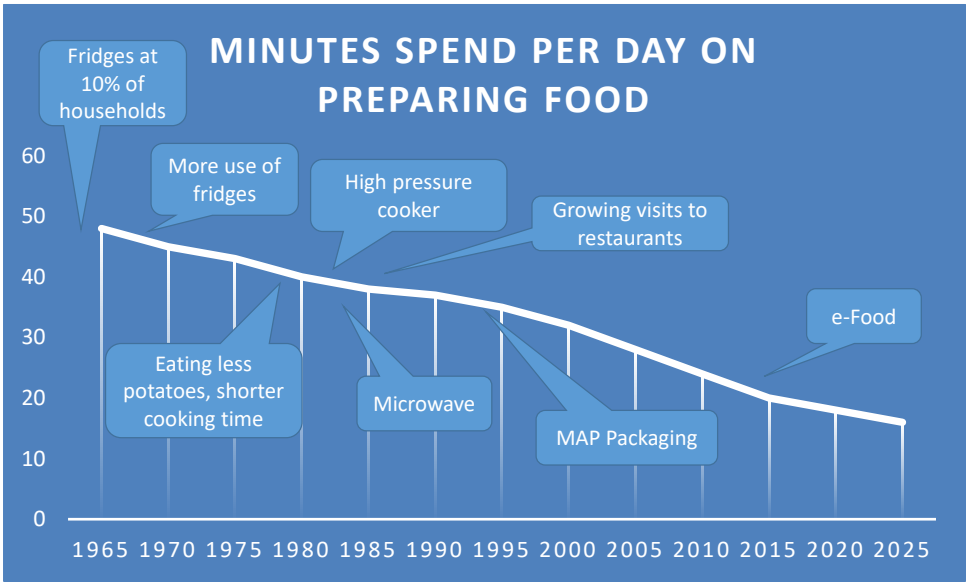

Figure 3. Time spent to prepare food over the years

It can be concluded that related to packaging people were eating out of home more often, variation in recipes was growing, more ingredients were used, and also shorter time to prepare dinner was accepted. Except for eating in a restaurant, this means using more packaging material.

CONTINUOUS IMPROVEMENT OF PACKAGING ITEMS

Throughout the years, individual packaging has become lighter and weight reduction is still going on. Continuous improvement, better control of processes, sometimes innovations, all with costs as the key driver, make it possible to reduce weight. The producer that can offer the same function fulfiller for less money can get orders.
According to Transparency Market Research (TMR) data, a decrease in unit weight has been observed across all packaging types of the 29 that have been analyzed over the period 1990 to 2015 [14]. Figure 4 presents the reduction with an average of 26% in unit weight. The minimum reduction of these 29 items over 25 years was 8% for paper bags and sacks and the maximum was 58% for PET water bottles. Older packaging types like paper bags probably are closer to the minimum needed amount while newer packaging types like PET bottles could be improved more. There are limits to material efficiency, but also innovations can speed up the process again. A good example is the introduction of metallocene polyethylene in 1992 by which the yield went up and the thickness of PE films for the same purpose decreased.

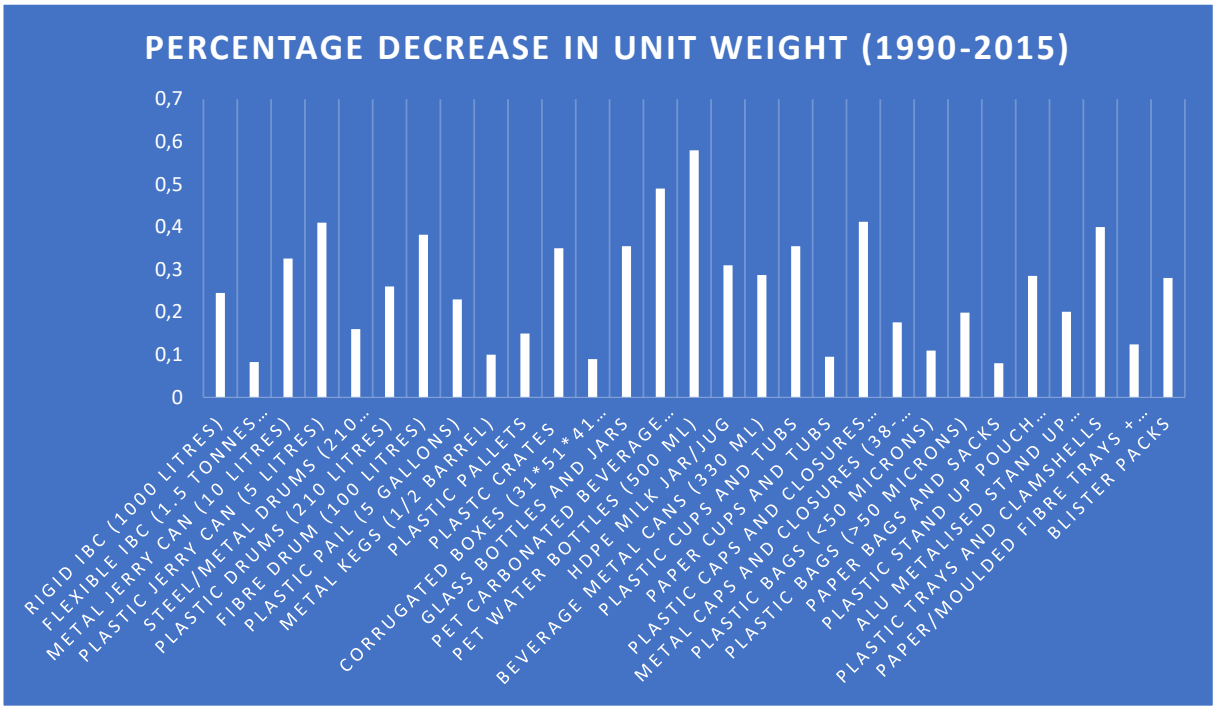

Figure 4. Relative reduction in weight of single packaging items

The presented figures are in line with some analyses executed in the Netherlands. In the eighties of previous century, the so-called APO reusable beer bottle had a weight of 360 grams. The bottle that replaced the APO in 1986, the BNR bottle that is still used by some brand nowadays, has a weight of 260 grams. Newer reusable bottles have a weight of 240 grams or even less.
One of the sectors is the Dutch organization of wine sellers. Annually, this organization determines the average weight of used bottles on base of research executed by an external

agency. In 2014 the average weight per liter is 520 grams. An overview over the years is presented in Figure 5. Based upon this study, the branch has set targets to reduce the average weight of glass bottles for wine by 1% per year.

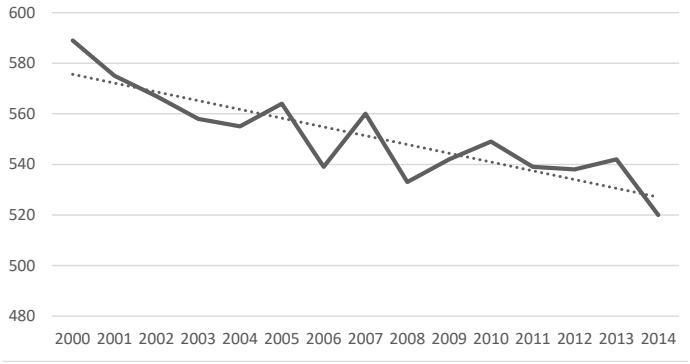

Figure 5. Average weight of glass bottles on base of weight per liter with trend line [Sector Innovation Plan Wine [20] [g/liter]

If a brand has decided to change the structural packaging design, a step is made towards the use of less material according the newest production techniques and then it will take many years before the following step is made. A return on investments period is mostly determined by the high investments for the packaging line and the tooling for the packaging. Moving towards another structural packaging design can be supported by a marketing campaign which involves costs as well. So steps are made over certain periods of time, but on average every company is doing this, so the average weight of single items goes down over the years.
Looking at the figures a careful conclusion can be that on average single packaging items reduce in weight with ca. 1% per year.

OVERVIEW OF DEVELOPMENTS THAT INFLUENCE THE TOTAL AMOUNT OF USED PACKAGING MATERIAL

Developments over time that reduce the use of packaging materials are taken up in an overview, just as developments and trends that increase the use of packaging material.

Developments and trends that reduce the amount of packaging material	Developments and trends that increase the amount of packaging material
Continuous improvement of single packaging items save on average 1% on weight per year	More use of home appliances that can store food better (fridge), that can heat up food faster (microwave) that enhances using prepacked and prepared food
Consumer behaviour: consciousness in choosing packed food, avoiding the use of plastic	More prepared and prepacked food means time savings for preparing dinner
	Prepacked, MAP packed, longer shelf life, means time savings for doing shopping
	More different ingredients over the years based on other recipes from foreign countries means more use of (smaller packed) additional ingredients
	More women participating on the labour market, meaning less overall time to do shopping and to prepare dinner
	Better portioning of food to avoid food waste

Table 2. Overview developments influencing the used amount of packaging material

CONCLUDING REMARKS

Figures show that the amount of packaging material per person per day is slowly growing with ca. 0.5% per year. The reduction of weight of single items is about 1% per year. This shows that other trends and developments currently influence the use of packaging with ca. 1.5% per year.

Trends that influence the use of packaging materials show that this growth is probably partly related to time reduction for doing shopping and preparing dinner. It can be concluded that if a reduction of the total amount of packaging material is wanted, it would be a good strategy to focus on solutions that are in line with this. Another option could be to work on awareness, for example by showing how investing time in shopping and preparing dinner can lead to using less packaging material per person per day and be more sustainable. Looking at the drivers behind the use of the current amount of packaging material, it is not to be expected from companies prepacking food that the total amount of packaging material used per person per day will reduce.

REFERENCES

[1] Klooster R. ten, B. de Koeijer, J. de Lange, "Towards a generic set of packaging material keyfigures," in *28th IAPRI Symposium on Packaging*, Lausanne, Switzerland, 2017.

[2] Afvalfonds Verpakkingen, [Online]. Available: www.afvalfondsverpakkingen.nl. [Accessed 2023 March 2023].

[3] Brancheplan Duurzaam Verpakken 2018-2022, Stichting Wijnfonds (KVNW), Den Haag, 2019.

[4] Wijn, J.F. de, W.A. van Staveren, De voeding van elke dag, 2e herz. dr., Bohn Scheltema & Holkema, 1980.

[5] Stichting Historie der Techniek, Techniek in Nederland in de twintigste eeuw, deel III, Landbouw en Voeding, Walburg Pers,, 2000.

[6] Jobse - Van Puten J., Eenvoudig maar voedzaam: cultuurgeschiedenis van de dagelijkse maaltijd in Nederland, Nijmegen, Nederland: SUN, 1995.

[7] Trends in eating and drinking in the years 60, 70, 80, and 90, [Online]. Available: https://www.myhappykitchen.nl/nostalgie-en-geschiedenis/. [Accessed 23 March 2023].

[8] Montijn I., Aan tafel! Vijftig jaar eten in Nederland., Utrecht/Antwerpen, Nederland/België: Uitgeverij Kosmos, , 1991.

[9] CBS, Statistisch Zakboekje, CBS, s Gravenhage, 1982.

[10] Centraal Bureau voor de Statistiek, CBS, [Online]. Available: https://www.cbs.nl/nl-nl/nieuws/2003/16/magnetron-verovert-nederlandse-keuken. [Accessed 23 March 2023].

[11] Centraal Bureau voor de Statistiek (National Statistical Service), [Online]. Available: https://www.cbs.nl/. [Accessed 23 March 2023].

[12] Williams Helen, Lindström, Annika; Trischler, Jakob; Wikström, Fredrik, "Avoiding food becoming waste in households – The role of packaging in consumers' practices across different food categories," *Journal of Cleaner Production*, no. https://doi.org/10.1016/j.jclepro.2020.121775, p. 14, 2020.

[13] Baudet H., Een Vertrouwde Wereld. 100 Jaar Innovatie in Neder, Amsterdam: Uitgeverij Bert Bakker, 1986.

[14] Eunomia Research & Consulting Ltd, COWI, Milieu, Arcadis, "Assessment of options for reinforcing the Packaging and Packaging Waste Directive's essential requirements and other measures to reduce the generation of packaging waste," EUROPEAN COMMISSION Environment DG Directorate B — Circular Economy Unit B.3 – From Waste to Resources, Brussels, 2021.

PS-GO07

A review of sustainable packaging trends globally and in India with changes in regulatory & consumer requirements

Saurabh Vasant Narawade[1], Prasad Balan Iyer*[1]

[1]*SIES School of Packaging, SIES campus, Plot No.1C, Sector-5, Navi Mumbai - Navi Mumbai, India*

***Correspondence to**: Prasad Balan Iyer. SIES School of Packaging, SIES campus, Plot No.1C, Sector-5, Navi Mumbai - Navi Mumbai, India*
E-mail: sopdirector@sies.edu.in

Abstract: For over a decade sustainability in packaging is a mega trend shaping packaging industry. Some companies have focused on quick gains, some have greenwashed their deeds while some have overpromised and under-delivered. Packaging has an emotional connect with consumers & has a lot to do with branding. Any packaging material or design change has implications on branding strategy. All companies are aware of this fact & hence super cautious while bringing any change in packaging. It is unfortunate that the discussion, debates & brainstorming over packaging sustainability majorly boils down to replacing / banning plastics & find 'green' alternatives. While the topics like sourcing of raw materials, energy requirement for conversion operations & most importantly, emission footprint in all processes from sourcing to disposal get conveniently side-lined. This paper has reviewed the trends in packaging sustainability globally and specifically in India based on primary & secondary data of research surveys, market reports, review articles, project reports, organizational goals/ objectives, and their sustainability reports.

This paper has reviewed the trends in packaging sustainability globally and specifically in India based on primary & secondary data of research surveys, market reports, review articles, project reports, organizational goals / objectives, and their sustainability reports. The analysis of this existing data brings forth striking differences in consumption patterns, consumer preferences & their opinions pertaining to packaging sustainability in developing and the developed world. It also shows how large number of companies have sustainable packaging commitments but lack clear sustainability metrics and inadequate upskilling of their employees towards achieving their goals.

The objective of the paper is to shed light on how consumer perception & behaviour changes with regards to packaging sustainability based on the economic background of the region. And how governments, companies & society are responding to this need of the hour to make sustainable living a common place.

INTRODUCTION

World population is expected to reach 8.5 billion by 2030 & 9.7 billion by 2050. With burgeoning population comes burgeoning demand for food, medicines, products for personal

care, home care & cosmetics. With products come packaging, whose role is multifunctional, including but not limited to containment, preservation, protection & brand promotion. Skyrocketing e-commerce has further widened the scale of packaging waste problem. Packaging waste at the end of life of products is one of the most visible wastes at any site of landfill or dump yard. This brings inevitable & unending blame for packaging & thereby packaging community. To tackle this humungous problem of packaging waste & to disburden landfills, there is an increasing demand for expediting path of sustainable packaging.
As per widely accepted & popular notion, sustainable packaging is the packaging which is *recyclable and safe for people and the environment, lessening our ecological footprint and environmental impact*.

WHAT IS SUSTAINABLE PACKAGING?

As per the criteria suggested by Sustainable packaging coalition, sustainable packaging is the packaging solution which,[1]
A. Is beneficial, safe & healthy for individuals and communities throughout its life cycle.
B. Meets market criteria for performance and cost.
C. Is sourced, manufactured, transported, and recycled using renewable energy.
D. Optimizes the use of renewable or recycled source materials.
E. Is manufactured using clean production technologies and best practices.
F. Is made from materials healthy throughout the life cycle.
G. Is physically designed to optimize materials and energy.
H. Is effectively recovered and utilized in biological and/or industrial closed loop cycles.

It is practically not possible to design & develop packaging that would conform to all the parameters laid down in above definition. But packaging material or process which ticks maximum boxes of above parameters can very well be considered as sustainable packaging. Companies aiming for sustainable packaging generally have short term & long-term actions. Short term actions include:

1. Downgauging (Reducing thickness of individual films in laminates, elimination of one or two layers in multilayer films, reducing bottle thickness, lightweighting of bottle, reducing bottle/cap height for e.g., increasing use of low-rise caps for tubes)
2. Size reduction (reducing size of sachets, reducing label size)
3. Removal of tinting & Masterbatches: For e.g., Transparent PET bottles are one of the most recycled plastics. But PET bottles with coloured MBs makes recycling difficult. Hence companies are opting for transparent PET bottles with shrink sleeves.
4. Synchronization across family: Single MB across family of products e.g, single colour caps for entire range of shampoo & conditioner.

Whereas long term actions include:

1. Mono-material based packaging (bottle, caps, labels from same material which saves the time & efforts for sorting & segregation during end of life of product)
2. Exploring alternatives for existing packaging substrates. (Shifting to paper-based substrates, water-based coatings)

For packaging to be truly sustainable, consumers & regulatory authorities need to understand difference between compostable, industrially compostable, recyclable, bio based and biodegradable. Out of total plastic consumed, only 9% gets recycled as per OECD report [2]. Rest of others either incinerated, end up in oceans or landfills. Flexible films & laminates are most difficult to recycle and hence most often not recycled at all. Recycled plastics has challenges in terms of cost and availability. Collection, sorting, treatment of scrap & conversion operations- all these factors contribute to the cost of PCR resins. Issues with PCR: obnoxious odour, lack of availability, impurities, absence of control over quality.

Discussion based on various studies and surveys

Regulatory landscape

There has been a general awakening on the issue given that 29 out of 30 countries studied have started to discuss and implement sustainable-packaging regulations.[3] As expected, these regulations are intended to enforce new requirements with the principal aim of limiting the negative impact of packaging on both the environment and on human health.
Countries have mostly embarked on their sustainability journey by addressing the start and the end of the flow—that is, the restriction of certain materials and a focus on waste management via extended producer responsibility (EPR). Regulations include bans and restrictions, taxes and levies, and waste management measures to enhance disposal, encourage reuse and recycling, and promote alternatives to plastic products. Plastic bags, disposable single use plastic items, and microbeads are three important sources of plastic pollution with plastics being described as the most used packaging substrate worldwide.[4] In business-to-consumer applications, plastic packaging is mostly single-use, and most of it is discarded the same year it is produced. Most countries in the world have separate laws for packaging of food, pharma, cosmetics & hazardous goods. Packaging-waste management is subject to the highest number of regulatory measures worldwide.
Below are the points which help to have a bird eye view of regulations across the globe.

Plastic packaging: In the past three years, sustainable-packaging regulations have tended to focus primarily on plastic packaging (versus other substrates). Eighty-three percent of the legal measures relating to sustainable packaging worldwide has focus on plastics—with a total of 147 measures identified. The European Union and Asia have the highest number of regulations focusing on plastics, with France and India being the top countries in this respect.

Beverage packaging: Regulations worldwide tend to have a relatively higher focus on beverage packaging than on other categories such as food and home, personal-care packaging. However, there are noticeable regional differences:

- The European Union and North America focus more on beverages, with 50 to 60 percent of their regulatory measures having a specific end-product scope targeting beverages.
- Latin America and the Middle East focus more on food packaging.

- In the European Union and Asia, an emerging trend aims to tackle packaging across multiple product categories, reflecting a more holistic approach beyond a single focus area (such as beverages) to encompass a broader spectrum of end-use areas.

Primary versus secondary packaging: Regulations tend to focus on primary packaging all over the world, but a focus on secondary and tertiary packaging is more prevalent in Asia:

- Worldwide, nearly 90 percent of legal measures with a specific scope of packaging type tackle primary packaging alone or together with other packaging types (secondary, tertiary).
- China, India, Vietnam, and the Philippines are proposing regulatory measures that focus on secondary and tertiary packaging, while India has the most measures focusing on secondary and tertiary packaging. China has also shown an increasing focus on regulations around e-commerce packaging to minimize waste and leakage.

Taxes on plastic packaging:
Organisations like OECD believes that plastic packaging tax has the potential of reducing plastic packaging waste & giving impetus to recycling infrastructure. Reducing consumption of plastic in packaging, inculcating the habit of reuse & recycle & collection of funds for creating waste management infrastructure are the primary reasons for sates implementing plastic packaging taxes. The UK's plastic packaging tax, or PPT, applies at a rate of £200 per tonne for companies that manufacture or import filled or unfilled plastic packaging greater than 10 tonnes per year. As part of the European Union's Green Deal and Covid recovery package, in 2021 the EU also introduced a plastic tax. The EU's "tax" is actually a contribution rather than a tax and is levied on EU member states in proportion to the non-recycled plastic packaging waste produced by each state.

Many of the countries that have chosen to impose a plastic tax are in Europe. Developing countries have shown a greater willingness to implement outright bans. China is another developing country that has outlawed certain types of plastic packaging. India has also passed new tax laws facilitating a plastic ban.
The United States still lacks country-wide bans or taxes on plastic bags, although some states have implemented such laws.

Regulatory vehicle for change: Data [3] reveals that financial penalties (versus subsidies) represent the main and preferred regulatory vehicle for sustainability change in the packaging industry: approximately 45 percent of legal measures implying a defined financial fallout refer to penalties—and these are generally related to taxes, fines, and fees. For example, France uses incentives the most to encourage change in packaging sustainability.

Regulatory landscape in India

India produces about 3.5 million tons of plastic waste per year. While some 60 percent of the waste is currently collected through informal channels and "recycled," most of that plastic is either "downcycled" into materials that cannot be further reused and recycled or transformed into a furnace oil via pyrolysis (high temperature heating), a non-environmentally friendly

process. Neither of these solutions offer truly sustainable forms of recycling in the circular economy sense. The new regulations like EPR rules, PWMR, single use plastic ban is changing that.

EPR rules
Using a phased-in approach, producers, importers, and brand owners of plastic packaging in India will be required to meet minimum targets for collecting and recycling their plastic waste starting in April 2024. Plastic packaging is classified into 4 categories. EPR rules include specifications for reuse, recycling, use of recycled plastic content, and end-of-life disposal of non-recyclable plastic packaging.
Categorisation under EPR includes: [5]

Category I:	Rigid package plastic
Category II	Flexible plastic packaging of single layer or multilayer (more than one layer with different types of plastic)
Category III	Multi-layered plastic packaging (at least one layer of plastic and at least one layer of material other than plastic)
Category IV	Plastic sheet or like used for packaging as well as carry bags made of compostable plastics

The requirement starts at 30 percent for "category I" plastics (PET plastic bottles and other rigid coloured plastic containers) and gradually scales up to 80 percent by 2027. Moreover, starting in April 2025, the same companies will be required to demonstrate that at least 30 percent of this same category of plastic packaging is manufactured using post-consumer recycled ("PCR") content.
In other words, brand owners will no longer be allowed to downcycle their plastic waste or use only virgin plastic in their packaging. They must show that it is made from, in part, recycled plastic. Any companies that fail to meet these targets will have to pay "environmental compensation" penalties that will be used to offset the costs of collecting their waste.
The recycling obligation for producers will be 50% for rigid plastics in 2024-25, 60% in 2025-26, 70% in 2026-27, and 80% from 2027-28 onwards.

Environmental compensation: Any companies that fail to meet these targets will have to pay "environmental compensation" penalties that will be used to offset the costs of collecting their waste. This penalty shall be levied based upon polluter pays principle, with respect to non-fulfilment of EPR targets by producers, importers, and brand owners, for the purpose of protecting and improving the quality of the environment and preventing, controlling and abating environment pollution.

Single use plastic ban: At the United Nations Environment Assembly in 2019, India piloted a resolution on addressing single-use plastic products pollution. Ministry Of Environment Forest

And Climate Change has notified the Plastic Waste Management Amendment Rules, 2021.These rules prohibit specific single-use plastic items which have "low utility and high littering potential.

A. Consumer perception & demands:

Sustainability is the key topic for packaging value chain. Marine litter is top in minds of consumers of Europe & Japan, while pollution is the top concerns for Asian consumers. But study suggest that most consumers disagree on which type of packaging is the most sustainable. Companies end up making bold & sometimes impractical commitments owing to downstream pull from consumers and companies responding to regulatory push. Companies continue to innovate new packaging formats & respond to regulatory pressure & meet targets of own.[6] Out of which inclusion of PCR is the most common. Better labelling on packaging, explaining its sustainability attributes and increased availability would encourage consumers to buy products with sustainable packaging. Replacing plastic packaging is top of mind choice for most brands as they look to switch out to materials that offer better environmental footprint.

Demography, consumption & disposal patterns of consumers in develop & developing countries varies greatly. As per survey report by McKinsey & company, topmost concern for consumers in developed countries like US, UK & Japan include marine litter, while consumers from developing world concerns are air & water pollution due to packaging waste. To find a better & sustainable packaging solution, companies need to understand how consumers are at local levels are using & disposing their packaging. In all countries surveyed, the overwhelming majority of respondents claim to be willing to pay more for sustainable packaging across end-use areas. In food service, for example, highest willingness to pay is in China, where 86 percent of consumers say they are willing to pay "a lot" or "a bit more" for sustainable packaging, followed by Indonesia, the United States, and Brazil (75 percent, 68 percent, and 66 percent, respectively). In Germany, Italy, India, and the United Kingdom, around 56 to 59 percent say they are willing to pay "a lot" or "a bit more" for sustainable food-service packaging.[6] But there's a need to interpret this data with a pinch of salt. Willingness to pay more may not always translate into actions, especially for consumers developing economies. Markets in South Asia are extremely price sensitive & even slight price that too because of packaging can bring in shift of consumer base to alternate brands. Moreover, consumers may not always know what they exactly want & what is the most feasible solution possible in given price range with respect to packaging. As suggested by study conducted in European countries by European Institute of Innovation & technology, lack of knowledge about food packaging is hindering its effective disposal, indicating more consumer education is needed to reduce packaging waste.

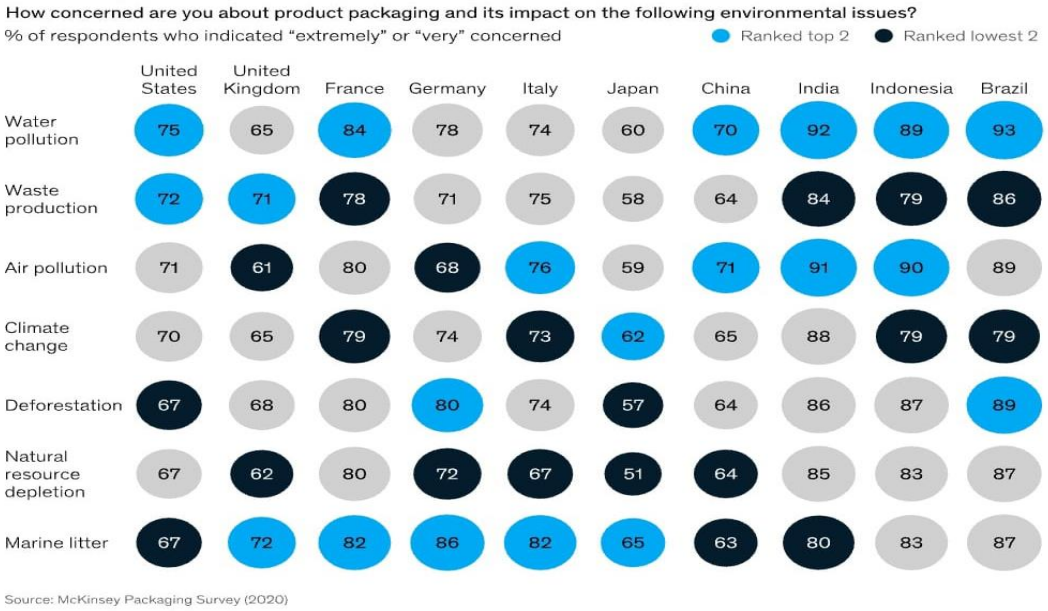

Consumer perception around the world is less aligned on what packaging substrates are most sustainable but more aligned on the least sustainable options.

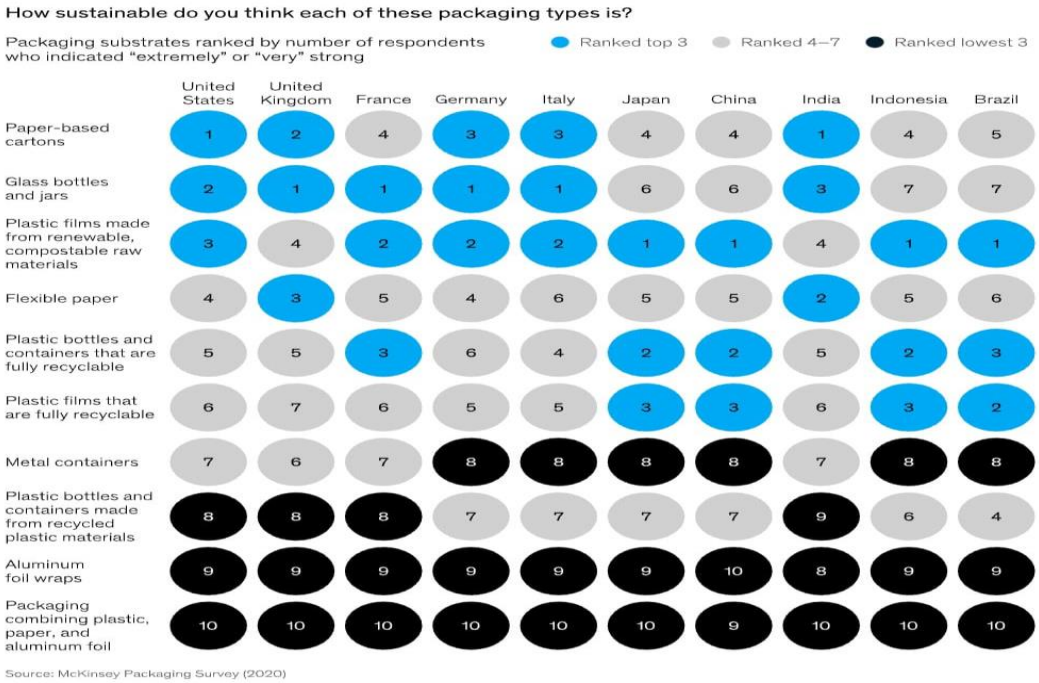

Source: Sustainability in packaging | McKinsey

Paths taken by companies

Led by the Ellen MacArthur Foundation, in collaboration with the UN Environment Programme, the Global Commitment has united more than 500 organisations behind a common vision of a circular economy for plastics. Driven by the goal of tackling plastic pollution at its source, companies representing 20% of all plastic packaging produced globally have committed to ambitious 2025 targets to help realise that common vision. More than 100 commitments by 24 MNCs across the world[9,10].

Key progress metrics:

Ensure 100% of plastic packaging is reusable, recyclable, or compostable
Committed by all signatories.
Reason for slow progress: Diverse packaging portfolios. Signatories with high usage of flexibles likely to miss targets.

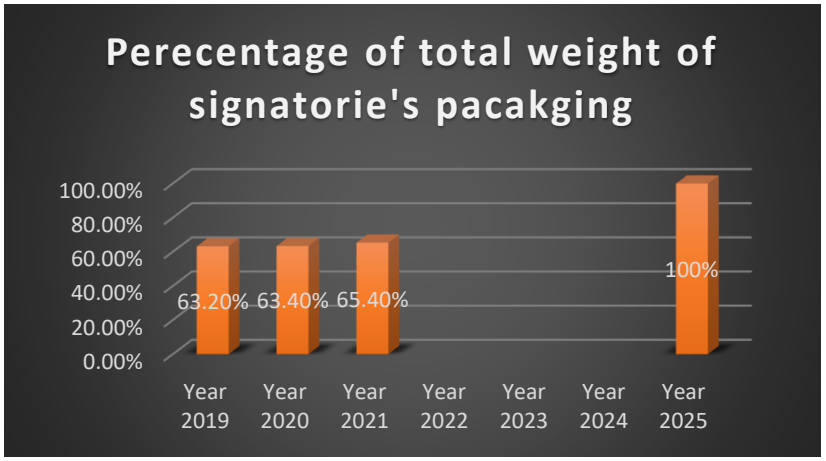

Increase the share of post-consumer recycled content target across all plastic packaging used
Percentage (of total weight) of post-consumer recycled (PCR) content in brand and retail signatories' plastic packaging.
PCR commitments by companies vary from 2% to 100%.

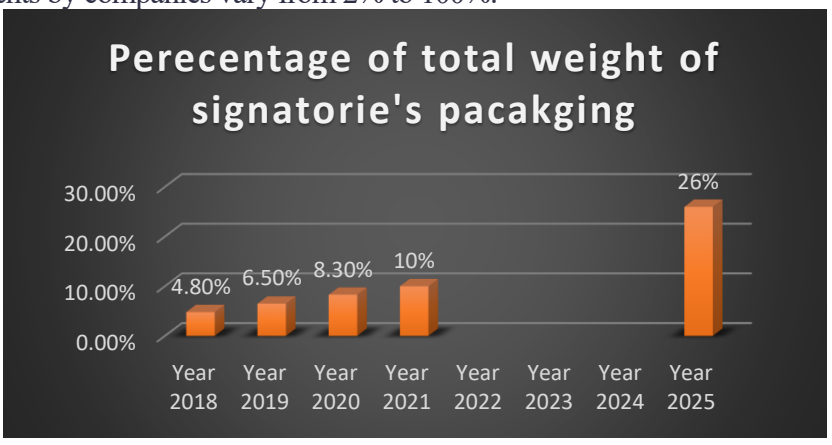

Progress: Only 23% of signatories are on the track to achieve targets by 2025.

Decrease the use of virgin plastic in packaging.
Weight of brand and retail signatories' virgin plastic packaging in million metric tonnes (MMT). This commitments by companies vary from 0.5% to 100%.

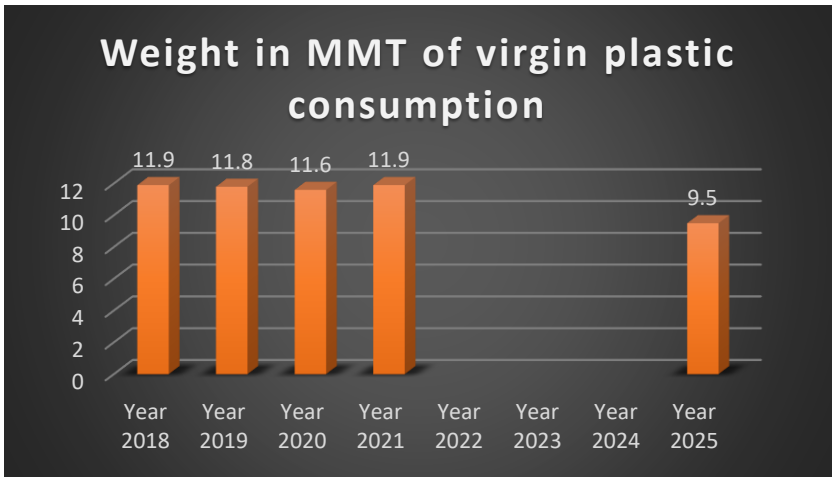

Reducing usage of virgin plastic usage is brought in by either inclusion of PCR or by shifting to other materials mostly paper-based substrates.
59% signatories have reduced usage of virgin plastic & the companies that have charted this path are some of the biggest converters & users of plastic packaging.

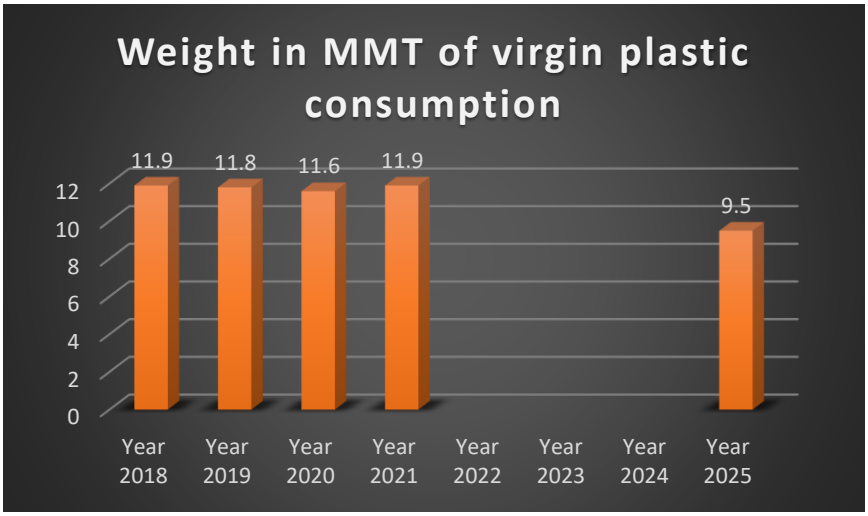

Take action to move from single use towards reuse models where relevant
Percentage (of total weight) of brand and retail signatories' plastic packaging that is reusable.

This step involves installation of refill stations at supermarkets, introducing refillable packaging, refill pouches. This commitments by companies vary from 0.5% to 100%. This action has great scope for B2B and bulk buying with options such as returnable crates, drums & jerry cans.

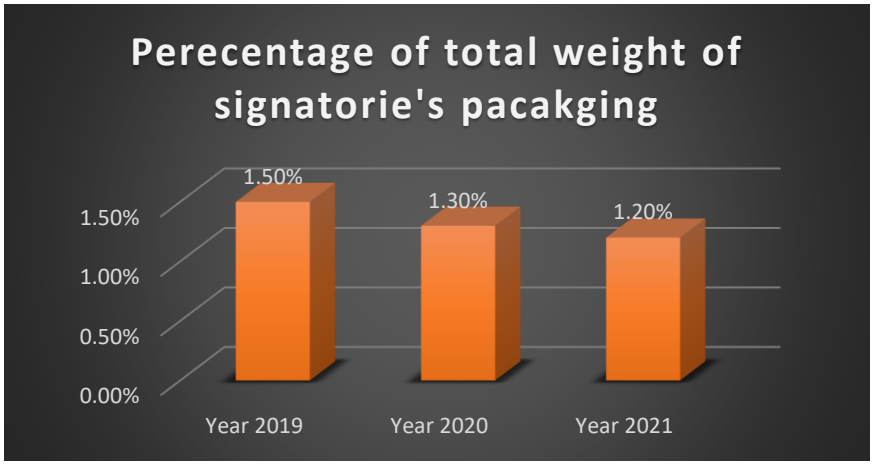

Eliminate problematic or unnecessary plastic packaging

Total number of elimination examples for 2020 and 2021 reported by packaging producer, brand, and retail signatories with percentage of elimination examples by method in 2021 highlighted (as reported by packaging producer, brand, and retail signatories). This action is taken majority by material change instead of elimination. This step is extremely crucial especially for e-commerce services.

CHALLENGES

As per report: SUSTAINABLE PACKAGING TRENDS: A Survey of Packaging and Sustainability Stakeholder [7], below are the challenges for Purchaser, Importers, Brand Owners (PIBOs) for packaging sustainability:

1. The infrastructure that PIBOs need do not exist (i.e., recycling facilities).
2. Consumers are not willing to pay for the available solution.
3. Retail outlets are not set up to handle changes (i.e., returnable packaging, refill stations).
4. Current sustainable packaging options are far too expensive.
5. Regulations and compliance for packaging is a moving target that is hard to plan for.
6. Too much hype around potential solutions and no practical option.
7. Sustainable packaging options are not scalable.
8. The problem is so complex one doesn't know where to start.
9. All the options are unproven, so one finds it difficult to commit and invest.
10. Not facing any challenges.
11. Other.

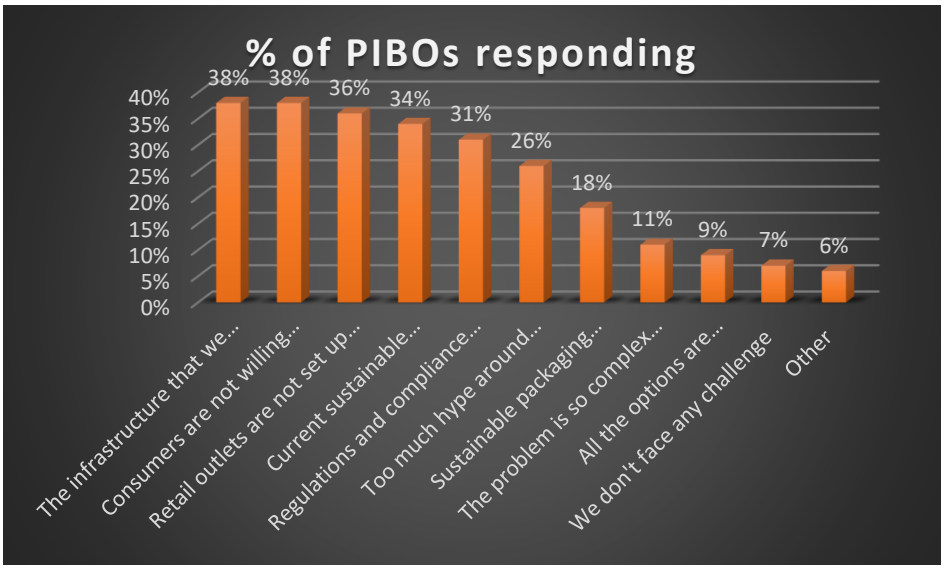

Analysis of the above data suggests that although strong progress has been made in some areas, majority of the companies are most likely to miss 2025 targets set as per their voluntary commitments. Overpromising, shifting goalposts or dropping commitments altogether are the most popular tactics employed by companies. To greenwash their deeds, companies arrange beach clean-up drives, tree plantation drive that too with expensive tie-ups with celebrities. Hence experts believe that time-bound action plans with proper checkpoints, backed by regulatory mandates are better to hold organisations accountable.

The prospect of not meeting 2025 targets reinforces the urgency for businesses to accelerate actions particularly around reuse, flexible packaging and decoupling business growth from packaging use.

CONCLUSION

Consumer sentiments seem to be shifting continuously. Understanding consumers' sentiments and preferences around sustainability at a granular level will be a key early indicator for the value chain as to future regulatory pressure and instances where large packaging-substrate shifts could occur. Proactively identifying these sentiments and potential shifts could allow packaging suppliers to stay on top of trends as they develop and to become a thought partner by supporting customers in revamping their packaging portfolio. Packaging suppliers should take a strategic look at their portfolios and assess them with three key questions in mind:

1. What is the substrate shifts you can foresee in your focus markets based on anticipated consumer perception and regulatory changes?
2. What is the resulting value at stake (that is, where are you most exposed given this and your market position)?
3. What are the potential growth opportunities for which you would be uniquely positioned to provide winning solutions?

Answering these three questions will help to create an actionable fact base. Based on this, packaging suppliers should update and enhance their product- and technology-strategy road map with relevant sustainability narrative.

REFERENCES

1. Complete Definition of Sustainable Packaging August 2011
2. The current plastics lifecycle is far from circular - OECD.
3. Sustainability in packaging: Global regulatory development across 30 countries | McKinsey
4. Legal limits on single-use plastics and microplastics | UNEP - UN Environment Programme
5. Centralized EPR Portal for Plastic Packaging (cpcb.gov.in)
6. Sustainability in packaging | McKinsey
7. sustainable-packaging-survey-report.pdf (jabil.com)
8. Sustainability_Packaging_Trends-2022_Survey_Report.pdf (jabil.com)
9. The Global Commitment 2022 (ellenmacarthurfoundation.org)
10. Global Commitment 2022 Progress Report | Shared by New Plastics Economy (thirdlight.com)
11. Sustainable packaging: Five key levers for impact | McKinsey
12. https://mohua.gov.in/pdf/627b8318adf18Circular-Economy-in-waste-management-FINAL.pdf
13. https://www.mckinsey.com/industries/paper-forest-products-and-packaging/our-insights/the-drive-toward-sustainability-in-packaging-beyond-the-quick-wins
14. https://www.mckinsey.com/industries/paper-forest-products-and-packaging/our-insights/sustainability-in-packaging-investable-themes
15. https://www.mckinsey.com/industries/consumer-packaged-goods/our-insights/creating-good-packaging-for-packaged-goods
16. https://www.teriin.org/sites/default/files/2021-12/Circular-Economy-Plastics-India-Roadmap.pdf

PS-GO08

Accelerating the Biodegradation of Poly(lactic acid) at Mesophilic conditions by Biostimulation

Pooja Mayeka[r1], Anibal Bher[1], Rafael Auras[*1]

School of Packaging, Michigan State University, East Lansing, MI 48824, USA

***Correspondence to:** Dr. Rafael Auras, School of Packaging, Michigan State University, East Lansing, MI 48824, USA.*
E-mail: aurasraf@msu.edu

ABSTRACT: Poly(lactic acid) – PLA – has garnered much interest due to its low environmental footprint and ability to replace conventional polymers and be disposed of in industrial composting environments. Although PLA is compostable when subjected to a suitable set of conditions (i.e., aerobic thermophilic conditions for an extended period), its wide acceptance in industrial composting facilities has been affected adversely due to longer degradation timeframes than the readily biodegradable organic fraction of waste mostly made of cellulose and starch. PLA's requirement to be fully exposed to thermophilic conditions for prolonged periods to biodegrade has restricted its adoption and hindered its acceptance in industrial composting facilities. Furthermore, PLA has not been certified as home compostable conditions due to the lower temperature range of the overall degradation process. Thus, PLA's biodegradability was investigated in a compost matrix under mesophilic conditions at 37 °C for 180 days by biostimulating the compost environment with skim milk, gelatin, and ethyl lactate to enhance the different stages of PLA biodegradation. The biodegradation of PLA involves chemical hydrolysis, enzymatic hydrolysis, bioassimilation, and mineralization. The evolved CO_2 was measured using an in-house direct measurement respirometer system, and the number average molecular number (M_n) was tracked by size exclusion chromatography. Compost biostimulated with skim milk and gelatin enhanced the mineralization of PLA by 35.7% and 13.0%. It improved the reduction in M_n by 53.2% and 61.7%, respectively, compared to PLA without any interference from any biostimulants, which did not show any degradation by the end of 180 days.

Keywords: microorganisms, pla, biostimulant, mesophilic, enzymes.

INTRODUCTION

Polylactic acid (PLA) is famous for its biodegradability and biocompatibility, and it is a potential alternative to reroute organic contaminated plastic waste from landfills to composting facilities. PLA is known to undergo chemical hydrolytic degradation under composting, which produces a significant reduction in its molecular weight and decline in properties [1].This reduction in molecular weight precedes the assimilation by microorganisms and final mineralization to CO_2. However, it is difficult for PLA to degrade in lower temperatures

(environment backyard/ home composting) because of its dependence on high temperatures (*c.* 60 °C) to undergo chemical hydrolysis. Additionally, PLA degradation in natural environments (usually associated with lower temperatures) is slow due to the sparse distribution of PLA-degrading microbes compared to other more aggressive degradable environments such as industrial compost.

Biostimulation and bioaugmentation techniques are included under the bioremediation domain and are planned to eradicate hazardous pollutants/waste materials which are toxic to the environment. These techniques use enhanced settings or biological workers/microorganisms to eliminate pollutants and are designed to make up for the lack of factors that can speed up the removal process in an environmentally friendly way. Biostimulation is an eco-friendly approach that addresses limiting factors such as nutrients (in the form of enzyme inducers) [2,3], electron donor or acceptor compounds [4,5], nitrogen supplying compounds [6,7], and compounds that can activate the biochemical processes, by providing necessary resources or chemicals to stimulate the environment [8,9].

Thus, this study aimed to investigate the effectiveness of biostimulating the compost environment with selected compounds by tracking CO_2 evolution and changes in number average molecular weight (M_n), molecular weight distribution (MWD) and crystallinity (X_c) of PLA degradation with and without biostimulants.

MATERIALS & METHODS

Materials

PLA Ingeo™ 2003D resin, with L-lactic acid content of 96%, was obtained from NatureWorks LLC (Minnetonka, MN, USA). Skim milk powder was procured from the local Walmart store (Lansing, MI, USA). Gelatin was purchased McCormick & Co., (Hunt Valley, MD, USA) via Amazon. Ethyl lactate was procured from Sigma Aldrich™ (St. Louis, MO, USA).

Elemental analysis of PLA and Biostimulants

The carbon, hydrogen, and nitrogen content of PLA, skim milk, gelatin, and ethyl lactate were determined using CHNS/O Elemental Analyzer, PerkinElmer 2400 Series II (Shelton, CT, USA) and is presented in Table 1.

Material	% Carbon	% Hydrogen	% Nitrogen
PLA	49.72 ± 0.19	5.72 ± 0.04	0.11 ± 0.07
Skim milk	41.28 ± 0.13	6.33 ± 0.03	5.75 ± 0.06
Gelatin	44.79 ± 0.32	7.05 ± 0.08	16.44 ± 0.09
Ethyl lactate	31.93 ± 0.98	5.46 ± 0.34	0.05 ± 0.03

Table 1 Carbon, hydrogen, and nitrogen content of the materials tested.

Biodegradation test in compost and tracking on thermal and physical properties

The biodegradation of PLA and the effect of the addition of biostimulants on the degradation of PLA were evaluated under aerobic mesophilic conditions using an in-house direct measurement respirometric (DMR) system by analysis of evolved CO_2 under simulated composting conditions [10–12]. The system was supplied by a non-dispersive infrared gas analyzer (NDIR) Li-COR® LI-820 (Lincoln, NE, USA) which measures the CO_2 concentration. The temperature, relative humidity, and air flow rate of the chamber were maintained at 37 ± 2 °C, 50 ± 5% RH, and 40 ± 2 cm^3/min respectively. Detailed information about the DMR chamber, the compost, and bioreactor preparation can be found elsewhere [13]. Manure compost was obtained from Michigan State University (MSU) Composting Facility (East Lansing, MI, USA). Ethyl lactate, skim milk, and gelatin were added at 8 g individually per bioreactor and mixed with compost matrix thoroughly with the PLA pellets to ensure uniform distribution. CO_2-free air (< 30 ppm) was supplied to each bioreactor, and the CO_2 evolved was measured for a specific time. Mineralization, the total amount of carbon converted to CO_2 molecules, was calculated according to equation (1).

$$Mineralization\ \% = \frac{(CO_2)_t - (CO_2)_b}{M_t\ x\ C_t\ x\ \frac{44}{12}}\ x\ 100 \qquad (1)$$

The weight average (M_w), number average (M_n) molecular weight, and molecular weight distribution (MWD) of the PLA for each treatment with the biostimulants was measured using the SEC instrument from Waters Corp (Milford, MA, USA). PLA samples were retrieved at specific time intervals and dissolved in tetrahydrofuran (THF) solvent in the ratio of 2:1. The unit was equipped with an isocratic pump (Waters® 1515), an autosampler (Waters® 717), a series of Styragel® columns (HR4, HR3, HR2) and a refractive index detector (Waters® 2414) and a temperature of 35 °C with a flow rate of 1mL/min was maintained. The Mark-Houwink constants of K = 0.000174 dL/g and α = 0.736 were used to determine the M_n and M_w of PLA samples. The data was analyzed using Waters Breeze™2 software.

A differential scanning calorimeter (DSC), model Q100 (TA Instruments, New Castle, DE, USA) was used to determine the glass transition temperature (T_g), melting temperature (T_m), crystallization temperature (T_c), and X_c for the PLA samples retrieved from biostimulated compost. Samples weighing between 5-10 mg were sealed in aluminum pans and subjected to a heating cycle to understand the evolution of crystallinity. The samples were cooled down to -5 °C and then heated to 210 °C at a ramp rate of 10 °C/min. The cooling was achieved using a nitrogen cooling system, maintaining the purge flow rate at 70 mL/min. The thermogram was analyzed using the software Thermal Universal Analysis 2000, V4.5 (TA Instruments). The degree of X_c was calculated using equation (2).

$$\chi_c\ \% = \frac{\Delta H_m - \Delta H_c}{\Delta H_m^0}\ x\ 100 \qquad (2)$$

RESULTS AND DISCUSSION

The CO_2 evolution of PLA samples was tracked over a test duration of 180 days to understand the biodegradation behavior at mesophilic temperature. **Figure 1**, **2,** and **3** show the biodegradation of CO_2 evolved and % mineralization of cellulose, skim milk, gelatin, ethyl lactate, PLA, cellulose-skim milk, PLA-skim milk, cellulose-gelatin, PLA-gelatin, cellulose-ethyl lactate, and PLA-ethyl lactate in compost at 37 °C. To be concise, only the biostimulant effect of skim milk on PLA degradation is discussed in detail. Figures and tables have been provided for gelatin and ethyl lactate, but the discussion will be presented in a future paper.

Effect of skin-milk on cellulose and PLA degradation

Figure 1a and **b** show the CO_2 evolved and % mineralization of cellulose, skim milk, PLA, cellulose-skim milk, and PLA-skim in compost at 37 °C. Cellulose evolved around 37 g of CO_2 and reached a mineralization of ~88%, whereas skim milk showed around 39 g of CO_2 evolution and attained over 100 % of its carbon conversion after 180 days. A priming effect is observed in skim milk due to the over-degradation of the indigenous carbon in the compost.

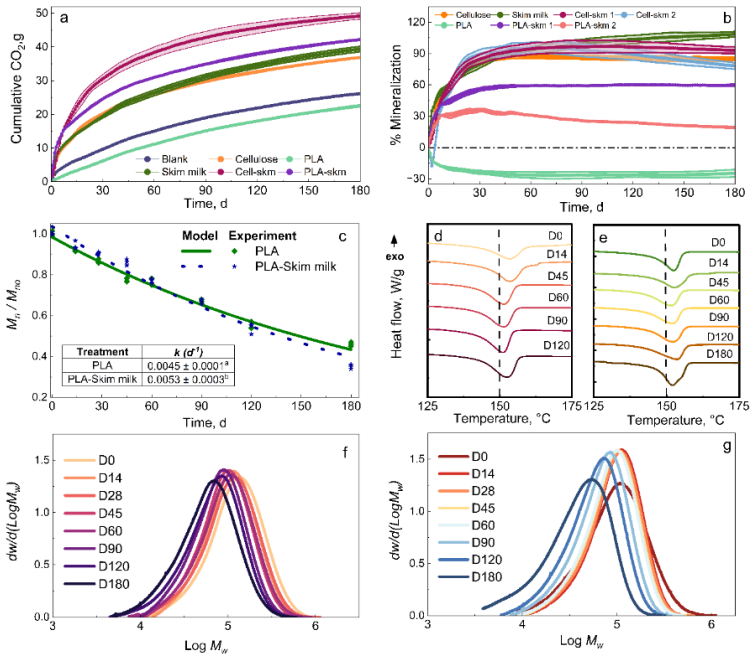

Figure 1. Cumulative CO_2 evolution (a) and Mineralization (b) of blank, cellulose, PLA, skim milk, cellulose + skim milk (Cell-skm), PLA + skim milk (PLA-skm) in compost at 37 °C. (c) represents the normalized M_n reduction as a function of time for PLA in control compost and compost biostimulated by skim milk. The experimental data was fitted using a first-order reaction of $M_n / M_{no} = e^{(-kt)}$, where M_{no} is the initial M_n, k is the rate constant, and t is the time. The inset shows the k fitted values. Values in the column with different lowercase letters are statistically different ($\alpha = 0.05$ Tukey-Kramer Test). (d) and (e) depict DSC thermograms for PLA and PLA in compost biostimulated by skim milk. (f) and (g) shows the MWD of PLA in compost and compost biostimulated with skim milk.

Since skim milk and cellulose are readily biodegradable and can be easily utilized as a carbon source by the microorganisms present in the compost, no lag phase was evident. Skim milk was added to the compost to induce the protease activity of the microbes present since serine protease (3.4.21.112), belonging to peptidases, is the class of extracellular enzymes able to hydrolyze the peptide bonds linking to the amino acids in the protein structure. The structure of skim milk comprises lactose, casein, and whey protein, making it a good precursor for the protease enzymatic activity by the microorganisms in the compost. Since both cellulose and skim milk constitutes a good carbon source when both are present in the compost, they are expected to show a much higher CO_2 evolution. The CO_2 evolution of the bioreactor containing both cellulose and skim milk (Cell-skm 1) is only around 49 g which is not far off from the CO_2 evolution of cellulose and skim milk and show ~97% biodegradation. To better understand the interaction and isolate the degradation behavior of cellulose in the presence of skim milk (Cell-skm 2), we estimate the mineralization value wherein the background signal from the bioreactor containing skim milk is subtracted. As seen, the mineralization % depicting the degradation behavior of cellulose reaches a maximum value of 96%. The value is higher than cellulose alone, as skim milk and cellulose are easily accessible to microorganisms. PLA pellets in compost show around 22.5 g of CO_2 evolution, whereas blank produces around 26 g of CO_2, implying that no carbon from PLA was degraded. In a blank bioreactor, the microbes can easily utilize the organic matter in the compost, whereas in a bioreactor containing PLA, the presence of PLA leads to a reduction in the working efficiency, which translates to reduced carbon conversion as a collective. We do not see any mineralization in the case of PLA owing to the low temperature of 37 °C. These values are very low when compared to the degradation of PLA in thermophilic temperatures [14,15].The negative mineralization values are generated as an artifact and indicate that the blank bioreactors produce more CO_2 than the bioreactors containing PLA samples. The bioreactor containing PLA and skim milk (PLA-skm 1) shows CO_2 evolution of around 42 g and maximum mineralization of ~60% by the end of the test duration. This shows improved mineralization when compared to PLA alone where no mineralization is observed. To isolate the degradation behavior of PLA in the presence of skim milk, mineralization PLA-skm 2 (subtracting blank + skim milk) is calculated as mentioned earlier. We see positive mineralization indicating the enzymatic degradation of PLA due to the presence of skim milk. To further corroborate the biostimulation activity of skim milk, samples of PLA were retrieved at specific time intervals from the bioreactor and evaluated.

The reduction in M_n of PLA was tracked until the end of the test as seen in **Figure 1c**. When treated with skim milk, the kinetic reduction rate of PLA was higher as compared to PLA in compost, which was not biostimulated by any treatment. There was a significant difference in the degradation rates for PLA alone and PLA treated with skim milk as seen in k value shown in **Figure 1d** inset (PLA k = 0.0045 ± 0.0001 and PLA-skim milk k = 0.0053 ± 0.0003). The PLA samples were also evaluated to understand crystallinity's degradation and evolution at 37 °C. The X_c increased from 28.3% to 31.4% for PLA, and from 28.3% to 39.7% for PLA samples biostimulated with skim milk, as seen in **Figure 1d** and **e**. The significant difference between the two indicates the degradation of samples occurring in the presence of skim milk. **Figure 1f** and **g** present the MWD for PLA in compost and compost biostimulated with skim milk. The peak amplitude for PLA in **Figure 1f** remains approximately the same throughout the test duration. No broadening of the peak and negligible shift indicates that the chemical hydrolysis

proceeds slowly at a mesophilic temperature of 37 °C. Whereas for PLA biostimulated with skim milk, a significant shift and broadening of the peak are observed in **Figure 1g** depicting the change in crystallinity and reduction in M_n. The presence of skim milk initiates the protease activity and the concurrent occurrence of chemical hydrolysis, producing a significant peak shift.

Effect of gelatin on cellulose and PLA degradation

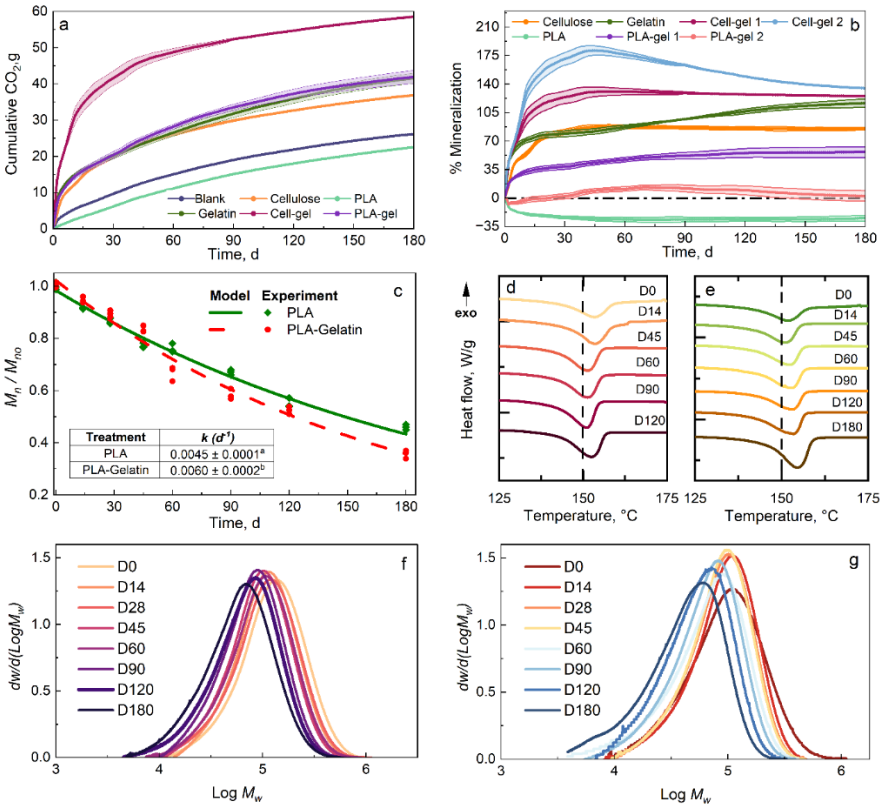

Figure 2. Cumulative CO_2 evolution (a) and Mineralization (b) of blank, cellulose, PLA, gelatin, cellulose + gelatin (Cell-gel), PLA + gelatin (PLA-gel) in compost at 37 °C. (c) represents the normalized M_n reduction as a function of time for PLA in control compost and compost biostimulated by gelatin. The experimental data was fitted using a first order reaction of the form $M_n / M_{no} = e^{(-kt)}$, where M_{no} is the initial M_n, k is the rate constant, and t is the time. The inset shows the k fitted values. Values in the column with different lowercase letters are statistically different ($\alpha = 0.05$ Tukey-Kramer Test). (d) and (e) depict DSC thermograms for PLA and PLA in compost biostimulated by skim milk. (f) and (g) shows the MWD of PLA in compost and compost biostimulated with gelatin.

Effect of ethyl lactate on cellulose and PLA degradation

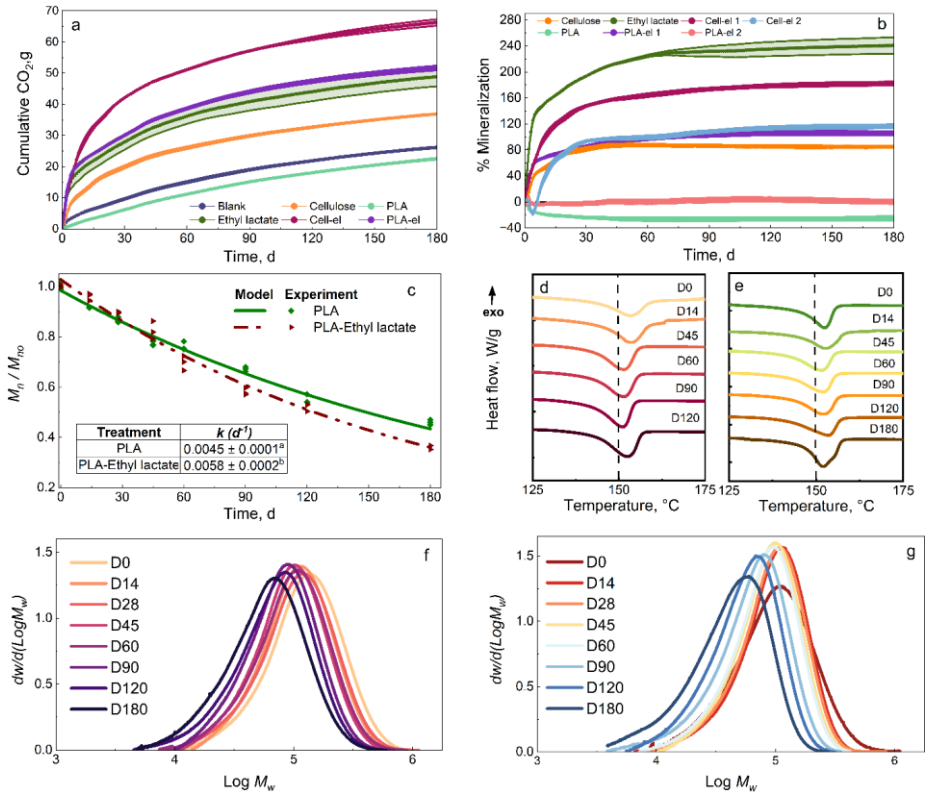

Figure 3. Cumulative CO_2 evolution (a) and Mineralization (b) of blank, cellulose, PLA, ethyl lactate, cellulose + ethyl lactate (Cell-el), PLA + ethyl lactate (PLA-el) in compost at 37 °C. (c) represents the normalized M_n reduction as a function of time for PLA in control compost and compost biostimulated by ethyl lactate. The experimental data was fitted using a first order reaction of the form $M_n / M_{no} = e^{(-kt)}$, where M_{no} is the initial M_n, k is the rate constant, and t is the time. The inset shows the k fitted values. Values in the column with different lowercase letters are statistically different ($\alpha = 0.05$ Tukey-Kramer Test). (d) and (e) depict DSC thermograms for PLA and PLA in compost biostimulated by skim milk. (f) and (g) shows the MWD of PLA in compost and compost biostimulated with ethyl lactate.

CONCLUSION

This study investigated the biodegradation behavior of PLA using biostimulation treatment under an aerobic simulated mesophilic setting. Different compounds were used to study the biostimulation effect by targeting different steps in PLA biodegradation. A long lag phase is observed for PLA without any treatment, indicating a slow hydrolysis phase. This is depicted as negative mineralization over the test duration of 180 days. Improved CO_2 evolution was observed for PLA when the compost was amended with the addition of skim milk, gelatin, and ethyl lactate. Crystallinity's evolution and molecular weight changes further corroborated this.

REFERENCES

[1] H. Tsuji, "Hydrolytic degradation," in *Poly(lactic acid) : synthesis, structures, properties, processing, and applications*, New Jersey: John Wiley & Sons, Inc, 2022, pp. 467–519.
[2] H. Pranamuda, Y. Tokiwa, and H. Tanaka, "Polylactide Degradation by an Amycolatopsis sp," *Appl. Environ. Microbiol.*, vol. 63, no. 4, pp. 1637–1640, Apr. 1997.
[3] A. S. Al Hosni, J. K. Pittman, and G. D. Robson, "Microbial degradation of four biodegradable polymers in soil and compost demonstrating polycaprolactone as an ideal compostable plastic," *Waste Manag.*, vol. 97, pp. 105–114, Sep. 2019.
[4] D. B. Watson *et al.*, "In Situ Bioremediation of Uranium with Emulsified Vegetable Oil as the Electron Donor," *Environ. Sci. Technol.*, vol. 47, no. 12, pp. 6440–6448, 2013.
[5] Q. I. Yang, H.-T. Shang, X.-L. Wang, H.-D. Li, and J.-L. Wang, "Anaerobic Degradation of Tetrachloroethylene Using Different Co-substrates as Electron Donors ," *Biomed. Environ. Sci.*, vol. 19, pp. 73–76, 2006.
[6] S. Simpanen *et al.*, "Biostimulation proved to be the most efficient method in the comparison of in situ soil remediation treatments after a simulated oil spill accident," *Environ. Sci. Pollut. Res.*, vol. 23, no. 24, pp. 25024–25038, 2016.
[7] Y. Boonluksiri, B. Prapagdee, and N. Sombatsompop, "Promotion of polylactic acid biodegradation by a combined addition of PLA-degrading bacterium and nitrogen source under submerged and soil burial conditions," *Polym. Degrad. Stab.*, vol. 188, 2021.
[8] L. Cosgrove, P. L. McGeechan, P. S. Handley, and G. D. Robson, "Effect of biostimulation and bioaugmentation on degradation of polyurethane buried in soil," *Appl. Environ. Microbiol.*, vol. 76, no. 3, pp. 810–819, Feb. 2010.
[9] P. Tribedi *et al.*, "Bioaugmentation and biostimulation: a potential strategy for environmental remediation," *J. Microbiol. Exp.*, vol. 6, no. 5, pp. 223–231, Nov. 2018.
[10] ASTM International, "ASTM D5338-15(2021) : Standard Test Method for Determining Aerobic Biodegradation of Plastic Materials Under Controlled Composting Conditions, Incorporating Thermophilic Temperatures," in *ASTM Standards*, 2021, pp. 1–7.
[11] International Standard ISO/FDIS 14855-1:2012, "Determination of the ultimate aerobic biodegradability of plastic materials under controlled composting conditions - Method by analysis of evolved carbon dioxide, Part 1: General method," 2012. .
[12] T. Kijchavengkul, R. Auras, M. Rubino, M. Ngouajio, and R. Thomas Fernandez, "Development of an automatic laboratory-scale respirometric system to measure polymer biodegradability," *Polym. Test.*, vol. 25, no. 8, pp. 1006–1016, 2006.
[13] E. Castro, "Design And Construction Of A Medium-Scale Automated Direct Measurement Respirometric System To Assess Aerobic Biodegradation Of Polymers," 2013.
[14] E. Castro-Aguirre, R. Auras, S. Selke, M. Rubino, and T. Marsh, "Insights on the aerobic biodegradation of polymers by analysis of evolved carbon dioxide in simulated composting conditions," *Polym. Degrad. Stab.*, vol. 137, pp. 251–271, Mar. 2017.
[15] P. C. Mayekar, E. Castro-Aguirre, R. Auras, S. Selke, and R. Narayan, "Effect of nano-clay and surfactant on the biodegradation of poly(lactic acid) films," *Polymers (Basel).*, vol. 12, no. 2, pp. 1–16, 2020.

PS-GP01

Life cycle assessment of multiple dispensing systems used for cosmetic product packaging

Shambhavi Rathore*[1], Breanna Schuler[1], Jonghun Park[1]

Toronto Metropolitan University, 350 Victoria Street, Toronto, ON, M5B 2K3, Canada

***Correspondence to**: Shambhavi Rathore. Toronto Metropolitan University, 350 Victoria Street, Toronto, ON, M5B 2K3, Canada*
E-mail: shambhavi.rathore2000@gmail.com

ABSTRACT: Worldwide, the packaging industry for consumer product goods, including personal care and beauty products, generates over $25 billion in sales. An extremely high environmental impact follows the large demand in the industry. Almost 70% of the plastic waste generated in the cosmetics market is not recyclable. Sustainability in the beauty industry is complex and multifaceted, requiring an evaluation of all factors. Packaging plays an important role in the cosmetics market, and considering the amount of waste it generates, it is essential to understand packaging dispensing systems from an environmental perspective. This study investigated the environmental impacts of three dispensing systems commonly used for cosmetic product packaging: the general dip-tube pump, the airless pump and the bag-in-bottle format. A cradle-to-grave life cycle assessment (LCA) was performed to quantitatively analyse the environmental burden of those three different dispensing systems, using a facial cream as a test case. The LCA analysed the environmental impacts generated by the packaging materials and incorporated the environmental impacts created by the facial cream residue left behind in each dispensing system. The system boundary of this LCA included the material production, intermediate processes, distribution, use and end-of-life phases of the packaged facial cream products. The LCA complied with the ISO standards, 14,040:2006 and 14,044:2006, and LCA software SimaPro v 9.0 was used to analyse the results. The life cycle inventories used in this LCA included US-EI 2.2, USLCI and Ecoinvent 3. TRACI 2.1, including ten mid-point life cycle impact categories, was chosen as the life cycle impact analysis method. Comparative and contribution analyses were conducted to interpret the LCA data. The comparative analysis demonstrated that the airless pump packaging system had less environmental burden than the other two packaging systems for all the life cycle impact categories. The bag-in-bottle alternative had the highest environmental impact for eight of the ten impact categories. The contribution analysis results revealed that the packaging material production phase most contributed to the environmental burden of all three packaging formats, followed by the lotion residue.

Keywords: Cosmetic product packaging, Life cycle assessment, Packaging sustainaility.

PS-PP01

Sustainable Development of Single-Use Paper Cups for Beverage Packaging in Thailand

Supawadee Theerathammakorn*[1], Todsaporn Khongthong [2]

[1,2] *School of Science and Technology, Sukhothai Thammathirat Open University, Nonthaburi, Thailand*

***Correspondence to:** Supawadee Theerathammakorn, Sukhothai Thammathirat Open University,*
E-mail: s_thee49@yahoo.com or supawadee.the@stou.ac.th

ABSTRACT: The goal of this study was to investigate the demand for single-use paper cups in beverage packaging in order to reduce the use of single-use plastic cups in accordance with Thailand's Roadmap. By asking 100 customers who frequent well-known coffee shops in five Thai provinces online and in-person questions. This includes a preliminary internet search for Thai stores and businesses selling paper cups. According to the findings, the consumers were made up of an equal number of men and women, mostly between the ages of 21 and30, who preferred coffee over tea and chocolate. More than half of the drinking cups were made of both paper and plastic, with the majority of them holding cold drinks. Plastic cups, nearly all consumers agreed, are harmful to the environment and should be replaced with paper cups. However, 6 percent opposed the use of paper cups due to durability concerns and preferred reusing the cups. Furthermore, the aforementioned stores were discovered to use three types of single-use paper cups to contain beverages: PE-coated paper cups, PLA-coated paper cups, and PBS-coated paper cups. Each type of paper cup requires its own collection and disposal method. As a result, in light of the concept of sustainable development, it should be more aware of how such materials are disposed of and what types of paper cups truly contribute to sustainable development.

Keywords: sustainable development, paper cup, single-use cups, coating, beverage packaging

INTRODUCTION

According to plastic pollution's impact on marine species, biodiversity, ecosystems all over the world, the effect can lead to human health through the food chain and polluted environment of oceans and beaches contaminated with microplastics and chemical additives used in the plastic items [1]. According to Pollution Control Department, Ministry of Natural Resources and Environment [2] reported that there would be about 2.76 million tons of plastic waste after use or about 11 percent of the total waste in 2021. Such plastic waste has only about 20 percent of its capacity to be recycled. The remainder was single-use plastics such as plastic bags, plastic

cups, plastic straws, plastic boxes, and foam food containers, which were managed by landfills and incinerated in incinerators, some are used as waste fuel (Refuse Derived Fuel, RDF). Only 3 percent of plastic waste was left in the environment and was not managed. Most plastic waste was disposed of in landfills and combined with other solid waste. Plastic garbage often has a low bulk density and is robust. It affects the waste disposal budget and landfill area since it takes up more space in the landfill than other types of waste and takes a long time to disintegrate. Additionally, dumping plastic waste in the environment will clog city sewers, leading to flooding issues, particularly during heavy downpours. The problem of rubbish floating in the canals and some flowing into the sea can cause the problem of plastic waste and microplastics. Therefore, Thailand's roadmap on plastic waste management for 2018-2030 with the vision of moving towards sustainable plastic management through the circular economy was established. Two targets were set for the vision. The first target is to reduce and replace some single-use plastic by using environmentally friendly products. In this target, it is intended to stop using single-use plastic packaging by 2022, especially plastic cup less than 100 microns in thickness. The second target is to convert all plastic waste to the circular economy by 2027, which focuses on recycling waste materials after consumption and repurposing them in manufacture [3]. Using bioplastic and paper cups is an option that has been used to reduce plastic waste, especially single-use plastic cups in cafes, from the COVID-19 epidemic until now [4]**.** Therefore, in this study, the researcher is interested in single-use paper cups for beverage packaging now in terms of whether or not they are consistent with Thailand's roadmap and move the country toward sustainable development.

GOAL OF THE RESEARCH

This research aims to investigate the demand for single-use paper cups in beverage packaging in order to reduce the use of single-use plastic cups in accordance with Thailand's Roadmap and concerning sustainable development, as shown in Figure 1.

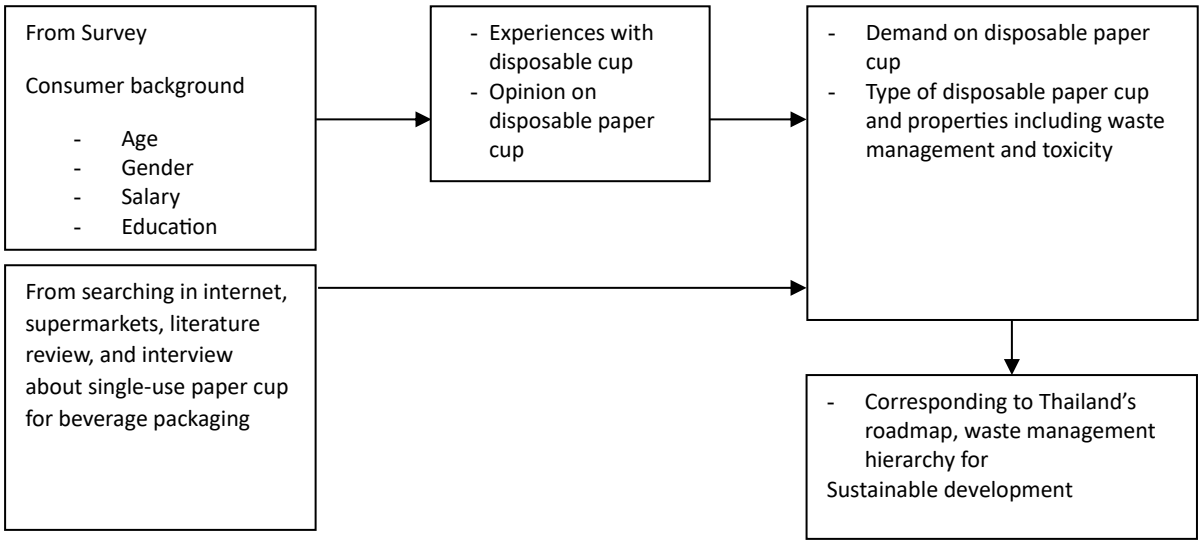

Figure 1. Conceptual framework of the research

EXECUTION OF THE RESEARCH

To find out demand for single-use paper cups

In order to survey 100 consumers, a questionnaire made on a Google Form link was used, and in the event that participants had problem with the internet link, interviews were done after the questions in the questionnaire. The questions came in three parts. Consumer background was covered in the first section, including gender, age, income, and education. The second part contain information about paper drinking cup, including: 1) experience with coffee or tea use in terms of beverage types, frequency of consumption, and cost, 2) cup types that typically encountered when purchasing a beverage; 3) drinking cup experience regarding which drink types (hot or cold), agreement or disagreement regarding switching from a plastic cup to a paper cup, and explanation. The final section dealt with more recommendation. The one hundred customers who buy a drink in coffee shops in five Thai provinces (Chonburi, Uttaradit, Phichit, Phra nakhon Si Ayutthya, and Bangkok) by purposive sampling. The collected data was evaluated by percent and chi-square.

To determine whether single-use paper cups for beverage packaging meet Thailand's roadmap or not

A preliminary online search was done for Thai stores and businesses selling paper cups was conducted. This study also includes a survey of Nonthaburi supermarkets, a review of many research papers on single-use paper cups for beverage packaging (SPBP), and interviews with two recognized companies. The gathered information was assessed in light of Thailand's Roadmap and the waste management hierarchy in terms of reuse, recycling, and disposable. In order to achieve sustainable development dimension, human toxicity and cost were factors. the

RESULTS AND CONCLUSIONS

Demand of disposable paper cup for beverage packaging

According to the 100 consumers' backgrounds consisting of an equal number of men and women, mostly between the ages of 21 and 30, who preferred coffee over tea and chocolate, as shown in Table 1, the results in Table 2 reveal that more than half of the drinking cups were made of both paper and plastic, with the majority of them holding cold drinks. Moreover, the findings show nearly all consumers agreed (94 percent) that plastic cups are harmful to the environment and should be replaced with paper cups. However, 6 percent opposed the use of paper cups due to durability concerns and preferred reusing the cups. The results present the idea of replacing disposable paper cups for beverage packaging with less environmentally impactful materials, which corresponds to Thailand's roadmap target 1, in order to reduce the use of single-use plastic cups.

With a p-value of less than 0.01, Chi-square analysis shows that subgroups within each category of drink type and frequency of buying a drink, price, cup type, drink group, and plastic impact concern are significantly different.

Due to the fact that 100 consumers surveyed were not asked about bioplastic used for drinking cups, the information about bioplastic in terms of environmentally friendly materials might lead to misunderstandings. This is because the plastic cups mostly used for cold drinks in cafés such as Amazon, Starbucks, and Intanin are made of polylactic acid or PLA [4].

Items	Percent
Gender	
- male	48.0
-female	52.0
Age	
- below 20	10.0
- 21-30	35.0
- 31-40	23.0
- 41-50	18.0
- above 50	14.0
Salary	
- below 15,000 baht	15.0
- 15,001-20,000 baht	27.0
- 20,001-40,000 baht	31.0
- above 40,001	27.0
Education	
- below bachelor	18.0
- bachelor degree	72.0
- master degree	10.0

Table 1 Percent of the 100 consumers from the 5 provinces in Thailand in terms of background information

Items	Percent
Drink type	
- coffee	37
- tea	20
- chocolate	21
- juice	9
- milk	8
- carbonated drink	5
Frequency of buying a drink	
- everyday	23
- 2-3 times per week	60
- once a month	17
Price	
- below 50 baht	31
- 50-80 baht	39
- 81-110 baht	18
- above 110 baht	12
Cup type	
- plastic	34
- paper	2
- both	64
Drink group	
- cold	47
- hot	15
- both	38
Plastic impact concern and substitution with paper cup	
- agree	94
- disagree	6

Table 2 Percent of the 100 consumers from the 5 provinces in Thailand in terms of drinking cup information

	drink type	Frequency of buying a drink	price	cup type	drink group	plastic impact concern
Chi-Square	42.800[a]	32.540[b]	18.000[c]	57.680[b]	16.340[b]	77.440[d]
df	5	2	3	2	2	1
Asymp. Sig.	.000	.000	.000	.000	.000	.000

Remark: a. 0 cells (0.0%) have expected frequencies less than 5. The minimum expected cell frequency is 16.7.
b. 0 cells (0.0%) have expected frequencies less than 5. The minimum expected cell frequency is 33.3.
c. 0 cells (0.0%) have expected frequencies less than 5. The minimum expected cell frequency is 25.0.
d. 0 cells (0.0%) have expected frequencies less than 5. The minimum expected cell frequency is 50.0.

Table 3 Chi-square results of drinking cup information of the 100 consumers

Result of web searching, supermarkets surveys, and company interviews

Variety of Single-use paper cup discovered in Thailand

Three different varieties of SPBP have been identified, according to online searches on the topic and surveys conducted at Nonthaburi supermarkets includin Top Supermarket and Lotus: paper lining with polyethylene [5], polybutylene succinate (PBS) [4][5], and PLA [6].

Remarkable Properties of SPBP found including waste management and toxicity

The ability to cover the paper surface is important to SPBP as it helps the resulting paper cup have a good heat sealability during cup forming. This study discovered that the coating abilities of PLA and PBS are limited due to theirs hydrobicity. Then they easily penetrates into the paper fiber's moisture-favorite substrates, including its heat-resistant during extrusion coating [7], which leads to uneven coating and a higher coating weight than that of PE lining in order to create a sufficient amount of coating and to facilitate adhesion [8]-[12] as shown in Table 4. For example, PLA is brittle and cracks easily at low temperatures and low heat distortion temperatures (HDT) prevents resins from forming when subjected to high temperature or hot drink packaging. It also causes necking during the extrusion coating, which causes the coating to be uneven, resulting in good enough non-adhesion as mentioned above. However, the properties of PLA and PBS have been improved to achieve better sealability for extrusion coating by blending other polymers [13] such as PP, EVA [7].

Waste management concern: the results reveal that SPBP with PE lining should be recycled, but due to the difficulty of separating the PE lining from the paper cup, the waste paper cup waste is disposed of in landfills 14][15]. This has an effect on the environment, especially because of microplastics. Paper cups coated with PLA and PBS can be disposed of by compostable fertilizers, provided they are in proper condition at temperatures up to 60 º C. Improper handling will contribute to plastic pollution [15]. PBS is a bioplastic that is recyclable and compostable. It decomposes more easily than PLA because it can be digested at a lower temperature at an ambient temperature of 30 º C [15], which is the landfill disposal method in suitable conditions until it becomes fertilizer. Considering the waste hierarchy, the sequence of

waste management puts recycling and composting in the same order [16]. However, the amount of paper cup waste that must be disposed of as fertilizer should be separated into compostable plants. If numerous people are being misled, they can typically be thrown away and used as fertilizer by landfills. Animals that consume plastic suffer injury if there are not enough microbes to completely degrade it. Additionally, it contributes to the depletion of wood resources, which is the first factor to be taken into account the waste management hierarchy [17]. When composted in the proper facilities, compostable cups are a good alternative, and recycling is a method of disposal that helps reduce the impact of global warming as well as the use of resources by reusing them [18].

Bioplastics such as PLA and PBS are still expensive materials compared to petroleum-based plastic PE, which leads to a higher cost of SPBP. In addition, the coating properties of PLA and PBS are not good, causing the need to use a greater amount of coating. As a result, the cost is even higher.

All three lining types can be hazadous to both people and ecosystems, as shown in Table 4. PE coatings were found to contain heavy metals and microplastics in hot water at 80-95 ° C soaked in paper cups for just 15 minutes [19], which can affect human health. However, according to the Thai Industrial Standard for paper cups for beverage (TIS-1141-2022)[20], the hot water used for the test was set at 100 ºC $\pm$ 1 ° C for 15 minutes, which is higher temperature than the condition described by Ranjan et al. [19]. In addition, paper cups with any plastic coating produced in Thailand must be inspected for quality in accordance with test standards as specified in Notification of the Ministry of Public Health (No. 435), B.E. 2565 (2022), issued under the Food Act, B.E. 2522 (1979), Re: Determination of Quality or standards of plastic containers [21], which cover chemical contamination and heavy metals.

As for bioplastic, it was found that there were chemical contaminants in composting. This is due to the combination of ingredients to improve PLA and PBS properties [22], which may have an impact on the ecosystem.

Items	PE lining	PLA lining	PBS lining
Density (g/cm3)	**0.922 [23]**	**1.98 [8]**	**1.26 (BioPBS™ FZ79AC) [24]**
Maximum temperature used (degree C)	**100 (one side for hot drink) [12]**	**n.d.**	**95 (two side for hot drink) [10]**
Coating ability	**Smooth coating and less coating weight for seal strength [8]**	**Hydrophilic property requires more coating weight to improve seal strength and water resistance when compared to PE lining [8]**	**Hydrophilic property requires more coating weight need to improve seal strength and water resistance when compared to PE lining** Heat sealable problem and less flexibility [9] (Kamolsuwan, personal communication, April 28, 2023)
Coating weight (g/m^2)	**13±2 (on base paper weight 190±8 g/m^2) [11]** Cold beverage – 2 side coating [11] Hot bev- one side coating [12] **less than PLA coating weight (on solid beached sulfate paperboard weight 165 g/m^2) [8]**	**Higher than PE coating weight (density PLA- 1.98 g/m^3 on solid beached sulfate paperboard weight 165 g/m^2) [8]**	**19±5 (on base paper weight 190±8 g/m^2) [10] Two side coating for hot beverage [10] Lower coating thickness than PLA [25]**

Table 4 Density, maximum temperature used, coating ability, coating weight, shelf life, waste management, cost, and toxicity of the three types of SPBP

items	PE lining	PLA lining	PBS lining
Shelf life	12 months [11][12]	**6 months [26]**	**8 months [10]**
Waste management	**Recyclable (but hard to separate then push to landfill) [14][15]**	**Compostable in compostable plant under condition, temp 60 ° C [15]**	**Compostable in compostable plant under condition, temp 60, 30 ºC, faster compostable or recyclable [15]**
cost	**Cheaper than PLA and PBS (Kamolsuwan, personal communication, April 28, 2023)**	**Higher cost than petroleum polymer [15] Moderate cost less than PBS (Kamolsuwan, personal communication, April 28, 2023)**	**Most Expensive compared to PLA and PBS [9] (Kamolsuwan, personal communication, April 28, 2023) then mixing with natural fiber can reduce cost and increase flexibility [9]**
toxicity	**Microplastic and heavy metal found from paper cups were transferred to hot water (80-95 ºC left for 15 mins [19]** Thai Industrial Standard, TIS 1141-2022 requires hot water at 100±1 ºC for 15 minutes [20]	**Toxicity from chemical substances found in similar to conventional plastic due to adding chemical substances during manufacturing process. [22]**	**Toxicity from chemical substances found in similar to conventional plastic due to adding chemical substances during manufacturing process. [22]**

Table 4 Density, maximum temperature used, coating ability, coating weight, shelf life, waste management, cost, and toxicity of the three types of SPBP (continued)

CONCLUSION

According to the results, consumers are demanding beverage cups with consideration for their impact on the environment by reducing plastic waste. A paper cup might be one of alternatives. The study found that there are paper cups coated with petroleum-based plastics (PE), and bioplastic (PLA and PBS). The usage of bioplastics has a drawback in that they are more expensive than petroleum-based ones, especially those with regard to cup adhesion. The three different varieties of paper cups' toxicity is another issue. The paper cups now in use don't appear to address all three facets of sustainable development.

RECOMMENDATIONS

In keeping with Thailand's Roadmap for Sustainable Development's goals of decreasing plastic waste and its negative effects on the environment. To attain the best properties of good adhesion with less coating content and cheaper cost, research and development to improve the properties of PLA and PBS would be a very challenging task. In order to consider the effects on the environment as well, green chemicals should also be employed. To decrease the usage of paper resources, which are recyclable materials, appropriate disposal techniques, such as recycling, may need to be taken into account on SPBP. For decomposition into fertilizer, such waste should be separated for composting. The fertilizers should be inspected for safety in accordance with the rules before being used; otherwise, they will pose a toxicity risk to the ecosystem and humans in the food chain.

REFERENCES

1. Tekman, M. B., Walther, B. A., Peter, C., Gutow, L. and Bergmann, M. (2022). **Impacts of plastic pollution in the oceans on marine species, biodiversity and ecosystems,** 1–221, WWF Germany, Berlin. Doi: 10.5281/zenodo.5898684
2. Pollution Control Department, Ministry of Natural Resources and Environment. (2022). **Thailand State of Pollution Report 2021**. Bangkok: AP Connex Co.,Ltd.
3. Pollution Control Department, Ministry of Natural Resources and Environment. (2021). **Thailand's Roadmap on Plastic Waste Management 2018-2030.** Retrieved April 4, 2023 from
4. https://www.pcd.go.th/wp-content/uploads/2021/10/pcdnew-2021-10-19_08-59-54_995414.pdf
5. PTT Oil and Retail Business Public Company Limited. 2017. **Amazon Bio Cup (BioPBS coated paper cup).** Retrieved April 4, 2023 from https://www.cafe-amazon.com/csr-detail.aspx?Lang=EN&C=5
6. https://th.pandocups.com/compostable-paper-cups/double-wall-compostable-cups/8oz-double-wall-pla-cup.html
7. ThaiKK Company Limited. (2023). **Coated paper for cup and bowl**. (in Thai). Retrieved April 28, 2023 from https://www.thaikk.co.th/label-bu/food-packaging-paper/cup-bowl-coated-paper/
8. GoodWill Retail Company Limited. (2023). **Paper cup/Lid for paper cup.** (in Thai). Retrieved April 29, 2023 from https://goodwillretail.co.th/paper-beverage-cup-lid-for-paper-cup/
9. Sakdadetrit, S., Saedan, M. and Suttiruengwong, S. (December 6-7, 2013). Improved heat distortion temperature (HDT) and impact strength of Polylactic acid (PLA) by blending with Polypropylene (PP) and Polyethylene-co-vinyl acetate (EVA). **Proceedings i**n the 10th National Kasetsart University Kamphaeng Saen Conference, Naknopatom, 346-354. (in Thai).
10. Rhim, J.W. and Kim, J.H. (2009). Properties of Poly(lactide)-Coated Paperboard for the Use of 1-Way Paper Cup. **Journal of Food Science**, 74(2), 105-111.
11. Rafiqah, S.A., Khalina, A., Harmaen, A.S., Tawakkal, I.A., Khairul Zaman, K., Asim, M., Nurrazi, M.N., and Lee, C.H. (2021). A Review on Properties and Application of

Bio-Based Poly(Butylene Succinate). **Polymers** 2021, 13, 1436, 1-28.
12. Research and Development (KK) Section, ThaiKK Group. (2020a). **Technical Information, Product name: 2 Side PBS Cup Stock Paper.** Retrieved April 28, 2023 from https://www.thaikk.co.th/wp-content/uploads/2021/08/C1PBSC-080720.pdf
13. Research and Development (KK) Section, ThaiKK Group. (2020b). **Technical Information, Product name: 2 Side PE Cup Stock Paper.** Retrieved April 28, 2023 from https://www.thaikk.co.th/wp-content/uploads/2021/08/C2PEC-080720-2.pdf
14. Research and Development (KK) Section, ThaiKK Group. (2020c). **Technical Information, Product name: 1 Side PE Cup Stock Paper.** Retrieved April 28, 2023 from https://www.thaikk.co.th/wp-content/uploads/2021/08/C1PEC-080720.pdf
15. Wacker Chemie AG. (n.d.). **VINNEX® Resins for paper coating; Improved Processing and Performance of Biopolyesters in Paper Coating.** Retyrieved April 29, 2023 from https://www.wacker.com/h/medias/7130-EN.pdf
16. Genovesi, A., Aversa, C., Barletta, M., Cappiello, G., and Gisario, A. (2022). Comparative life cycle analysis of disposable and reusable tableware: The role of bioplastics. **Cleaner Engineering and Technology**. 6, 100419, 1-9.
17. Triantafillopoulos, N. and Koukoulas, A.A. (2020). The Future of Single-use Paper Coffee Cups: Current Progress and Outlook. **BioResources**. 15(3). 7260-7287.
18. EPA United State Environmental Protection Agency. (n.d.). **Sustainable materials Management: Non Hazardous Materials and Waste Management Hierarchy**. Retrieved April 23, 2023 from https://www.epa.gov/smm/sustainable-materials-management-non-hazardous-materials-and-waste-management-hierarchy
19. Suskevice, V. and Grönman, K. (2019). Single-Use Paper Cups Circularity Improvement and Environmental Impact Mitigation Measures for Lappeenranta University of Technology Campus. **Proceedings**, 16, 58; doi:10.3390/proceedings2019016058, 1-6.
20. Durrell, K. (2019). Huhtamaki LCA study: **Paper cups have lower carbon footprint than reusable options when recycled**. Retrieved April 30, 2023 from https://www.packaginginsights.com/news/huhtamaki-lca-study-paper-cups-have-lower-carbon-footprint-than-reusable-options-when-recycled.html
21. Ranjan, V.P., Joseph, A, and Goel, S. (2021). Microplastics and other harmful substances released from disposable paper cups into hot water. **Journal of Hazardous Materials.** 404, part B, 15, 124118.
22. Thai Industrial Standard Institutes. (2022). **Paper Cups for Beverage, TIS. 1141-2022.** Ministry of Industry. (in Thai).
23. Ministry of Public Health. (2022). **Notification of the Ministry of Public Health (No.435), B.E.2565 (2022)** issued under the Food Act B.E. 2522 (1979) Re: Determination of quality or standards of plastic containers. (in Thai).
24. Zimmermann, L., Dombrowski, A., Völker, C., Wagner, M. (2020). Are bioplastics and plant-based materials safer than conventional plastics? In vitro toxicity and chemical composition. **Environmental International.** 145, 106006. 1-11.
25. Westlake Polymer LLC. (2022). **TRUCOAT® EC479: Technical Data Sheet.** Retrieved April 28, 2023 from https://www.westlake.com/sites/default/files/EC479%20TDS%2007-06-22_0.pdf

26. PTT MCC Biochem.Company Limited (n.d.a). **BioPBS™ FZ79AC Technical Data Sheet.** Retrieved April 29, 2023 fromhttps://productsandsolutions.pttgcgroup.com/files-products/pdf/packaging/TDS_FZ79AC.pdf
27. Mitsubishi Chemical Europe GmbH. (2023). **Coated Paper.** Retrieved April 30, 2023 from https://www.mcpp-global.com/en/mcpp-asia/applications/segment/packaging-coated-paper/
28. Going Green Solution Pty Limited. (2023). **Compostable Cup PLA 360 ml.** Retrieved April 29, 2023 from https://goinggreensolutions.com.au/pla-biocup-360-ml.html

31st iapri MEMBERS' CONFERENCE

Mumbai | May 22-25, 2023

SILVER SPONSOR

IMA SAFE P.G.

mespack
A DURAVANT COMPANY

PACKFORA
MAKE YOUR PACKAGING SHINE

YOGESHWAR PLASPAX

Godrej | CONSUMER PRODUCTS

REGISTRATION SPONSOR

ecobliss

LOGISTICS SPONSOR

WRAPTECH
Engineered To Excellence

ACCOMMODATION PARTNER

PACOPACK INDUSTRIES
CORRUGATED BOXES

MEDIA PARTNER

PrintWeek

WhatPackaging?